PARTIALLY PRESTRESSED CONCRETE

INTERNAL SQUARE PANEL

by

HOKE SAI LAI

A thesis presented in fulfilment of the requirements

for the Degree of Doctor of Philosophy

Department of Civil Engineering

The University of Leeds

February 1986

To my parents

ABSTRACT

This work is concerned with the general behaviour of an internal panel in a column supported multi-bay floor structure, under the influence of various prestressing tendon arrangements. The prestressing effects are studied with the help of a finite element package (PAFEC), representing the prestressing forces by equivalent vertical loads. From a variety of possible spacing arrangements, the distribution of prestressing moments is shown to be most effective in counteracting the moments due to externally imposed load when the tendons are narrowly banded in the column vicinity.

The effects of tendon arrangement on slab behaviour are further investigated by means of an experimental programme comprising three series of ten tests of 1.5m span partially prestressed panel with typical span to depth ratio, levels of loading, levels of prestress and geometry of tendon profiles.

The models were fixed along the edges to simulate the continuity of an internal panel in a multi-panel slab system. Post-tensioned tendons were arranged in various patterns, as currently employed in construction practice, to induce either a medium or a low level of prestress in the test panel, conforming to the design recommendations of a number of codes of practice.

Test results indicated that the serviceability behaviour of the slabs with a low level of prestress was strongly influenced by

the tendon distribution and the amount of non-prestressed reinforcement. Slabs with tendons banded closely in the column area exhibited a higher cracking load and were stiffer after cracking.

The flexural strength of the test slabs was found to be greater than that predicted by yield line theory and the increase was attributed to membrane action. The experimental values of tendon stress at ultimate load and of punching shear were compared with those obtained by various design methods.

ACKNOWLEDGEMENTS

I gratefully acknowledge the facilities provided for this investigation by Professor A.R.Cusens, Head of Civil Engineering Department at the University of Leeds.

I am particularly indebted to Dr.E.W.Bennett and Dr.J.Harrop for their constructive criticism, encouragement and constant guidance throughout the course of this research.

I would like to extent my thanks to the technical staff of the department for their ready assistance in the preparation of tests; Dr.K.Y.Chu and Mr.W.K.Hui for their helps during the experiment; Mr.R.Duxbury for taking some of the photographs and Mrs.R.Duxbury for typing the equations and symbols of this thesis.

I would also like to acknowledge my sincere thanks to Dr.K.H.Lee for his useful discussions and ready assistance from the tests to the preparation of this thesis.

I am greatly indebted to the members of my family who have been, and will always be, a constant source of love, encouragement and support.

I would also like to express my deep gratitude to a special friend Miss Y.F.Lee for her invaluable help and exhilarating companionship throughout this period.

Finally, the studentship provided by the University of Leeds is also gratefully acknowledged.

Notation

a	deflection, generally
a_c	maximum elastic deflection in a test panel
a_m	maximum elastic deflection in an internal panel
a_p	maximum elastic prestressing camber
A_c	area of concrete section
A_d	area of tendon duct
A_p	area of prestressing steel
A_s	area of non-prestressed steel
b	width of section, generally
b_{crit}	width of critical section
b_1, b_2	shorter and longer widths of column strip of a rectangular panel
c	column side length
d	effective depth of total tension reinforcement
d_p	effective depth prestressing steel
d_s	effective depth of non-prestressed steel
D	flexural rigidity
e	eccentricity of tendon, generally
e_{OB}	eccentricity of tendon at the column
E_c	modulus of elasticity of concrete
E_s	modulus of elasticity of steel
f_c	concrete stress at extreme fibre
f_c'	concrete compressive strength (cylinder)
f_{cp}	concrete compressive stress at mid-depth due to prestressing
f_{cpe}	concrete stress at tendon level
f_{cu}	concrete cube strength

f_{pb}	tendon stress at failure of slab
f_{pe}	effective prestress in tendon
f_{pu}	characteristic strength of tendons
f_{py}	yield stress of tendon
f_s	stress in non-prestressed steel
f_t	modulus of rupture
f_t'	split cylinder tensile strength of concrete
f_y	yield stress of non-prestressed steel
h	overall slab depth
I_{cr}	second moment of area of cracked section
I_e	effective second moment of area
I_g	second moment of area of gross section
L	side length of slab, generally
L_x, L_1	shorter span of a rectangular panel
L_y, L_2	longer span of a rectangular panel
M	bending moment, generally
M_{cr}	moment required to crack a section
M_o	moment necessary to produce zero concrete stress (reference moment)
M_p	prestressing moment, generally
M_{sec}	secondary prestressing moment
M_n	ultimate moment of resistance
P	prestressing force, generally
P_e	effective prestressing force
P_o	prestressing force under M_o (reference force)
P_{pb}	prestressing force at failure of slab
P_{pu}	ultimate prestressing force
P_s	effective force in non-prestressed steel

u_{crit}	length of critical perimeter
v	shear stress, generally
v_c	ultimate shear stress (Concrete Society)
v_{cw}	ultimate shear stress (ACI)
V	column axial load or punching shear force, generally
V_{cw}	punching shear capacity (ACI)
V_c	punching shear capacity (Concrete Society)
V_p	vertical components of effective prestressing forces within a perimeter of h/2 from the column face
x	neutral axis
W	load intensity, generally
W_{bal}	transverse equivalent prestressing load
W_u	ultimate load intensity
z	lever arm
u, v, w	displacement components
x, y, z	coordinates
α	distribution coefficient
α_e	modular ratio of steel to concrete
β	ratio of tendon eccentricity at the support and at mid-span
θ_n	rotation of yield line
$\theta_x, \theta_y, \theta_z$	section rotation components
λ	distance ratio of the inflection point in tendon to the span of the slab
ν	Poisson's ratio
ξ	shear enhancement factor for thin slab
ρ^*	equivalent reinforcement ratio (Concrete Society = $\frac{f_{pu}}{fy} \rho_{ps} + \rho_s$)

ρ_e equivalent reinforcement ratio (Cleland = $\frac{f_{pb}}{f_y}\frac{d_p}{d}\rho_{ps}+\rho_s$)

ρ_{ps} ratio of prestressed reinforcement ($\frac{A_{ps}}{bd}$)

ρ_s ratio of non-prestressed reinforcement ($\frac{A_s}{bd}$)

ω_e equivalent reinforcement index (= $\rho_e\frac{f_y}{f_{cu}}$)

δ arbitrary unit displacement

Definitions:

Column line: Imaginary beam running over the columns with a width of column size plus slab depth.

Middle width: Imaginary beam whose width is taken as the difference between the width of the panel and that of the column line.

Column strip: Imaginary beam running over the columns with a width equal to one half of the width of the panel.

Middle strip: Imaginary beam whose width is taken as the difference between the width of the panel and that of the column strip.

ABBREVIATIONS

ACI	American Concrete Institute
ASCE	American Society of Civil Engineers
BS	British Standard
CEB	Comite Euro-Internationale du Beton
CP	Code of Practice
FIP	Federation Internationale de la Preconstrainte

LIST OF TABLES

LIST OF PLATES

TABLE OF CONTENTS

Page

PART 1

GENERAL INTRODUCTION AND REVIEW OF PREVIOUS WORKS

CHAPTER ONE

Introduction

1.1 Partial Prestressing

Although Freyssinet first succeeded in prestressing concrete with high strength steel in the late 1920's, the major development of prestressed concrete did not take place until the second half of the twentieth century, and it was also in this period that the concept of partial prestressing began to arouse widespread interest. The original design criterion had been to permit no tensile stress in the concrete, but around 1940's, first Emperger and then Abeles proposed an alternative design philosophy whereby limited tensile stress or even hair cracks could be permitted. For this Abeles had devised the term "partially prestressed concrete" to distinguish it from "fully prestressed concrete".

The idea of partial prestressing was strongly opposed by many engineers, but it remained alive despite of the "all or nothing" approach of Freyssinet who insisted that, relative to a given load, a structure either was or was not prestressed and no cracking of the section should be allowed. The use of partially prestressed concrete thus remained in controversy for some 20 years. Nevertheless, research activities brought about an improved knowledge of materials and a better understanding of the structural behaviour of partially prestressed members in the ultimate condition, and under fatigue and sustained loading,

including their performance under service load and durability. Today, partial prestressing is accepted world wide, at least implicitly, in most codes of structural engineering design and it is generally recognised that its range covers the complete spectrum between full prestressing at one extreme and conventional reinforced concrete at the other.

1.2 Classification of Concrete Structures

In the British Code CP110 (1), which is based on the CEB Recommendations (2), prestressed concrete structures are classified as follows on the basis of the stress condition of the concrete under service load:

Class 1 : Prestressed concrete in which no tensile stresses are permitted in concrete under service load (commonly termed "Full Prestressing").

Class 2 : Prestressed concrete in which limited tensile stresses less than the concrete flexural tensile strength are permitted under service load (sometimes termed "Limited Prestressing").

Class 3 : Prestressed concrete in which flexural cracking in the tension zone is permitted under service load (termed "Partial Prestressing").

In this class of structure non-prestressed reinforcement must be provided to give the tension resistance required at ultimate load, as well as to control the width (< 0.2 mm) and spacing of the cracks.

A further class of structure not found in CP110 is introduced in the CEB-FIP Recommendations (2), vis,

> Class 4 : Conventional reinforced concrete without prestressed reinforcement in which cracks of limited width are permitted under service load.

In the present study, the main emphasis is on Class 3 structures.

1.3 Partial Prestressing in Building Slabs

Under dead and live loading, the largest bending moments in a multi-panel slab system are found over the intermediate supports. In ordinary reinforced concrete, these large moments can only be resisted with a high concentration of reinforcement which can create significant difficulties in construction. On the other hand, the moments in the middle strips are only about one quarter of the magnitude and are well within the capacity of ordinary reinforcement. It is therefore logical to introduce partial prestressing in these regions of high bending moments, since the contribution of the high strength steel tendons to the ultimate

moment will reduce the total reinforcement requirement thereby resulting in considerable economy over reinforced concrete in the total cost of steel, and permitting a less congested layout in the region of the supports.

The non-prestressed or passive reinforcement contributes to the ultimate strength and increases the ductility of the slab, thus avoiding sudden failure. This feature is of particular value in design for seismic conditions. The reinforcement also helps to control the crack distribution and to limit the width of the cracks. The behaviour of a partially prestressed slab will actually be improved compared with that of a reinforced concrete slab as the concrete is generally uncracked or the cracks remain closed under the permanent dead load and are only likely to be visible on the rare occasions when the loading approaches the full service design load. Well-distributed hair cracks are usually considered harmless in prestressed structures.

Slabs in which the live to dead load ratio is high are particularly well suited to the application of partial prestressing over the supports. A fully prestressed solution would involve excessive prestress in the spans with the inherent problem of excessive camber, whereas with a partially prestressed solution in which the total or a proportionally larger number of tendons in a panel are located in the column area, it is possible to reduce the peak moments without introducing an uneconomically high degree of prestress into the other parts of the slab.

1.4 Bonded or Unbonded

Both bonded and unbonded systems have been used in construction but prestressing with unbonded tendons is more commonly adopted in most countries with the exception of Australia and New Zealand. Factors in favour of post-tensioning using unbonded tendons are generally:

(a) maximum possible tendon eccentricities. This is of special importance in thin slabs.

(b) simple and rapid placing of tendons

(c) elimination of grouting operation

(d) low losses of prestressing force due to friction, particularly if a lubricant is used

(e) prestressing steel is adequately protected against corrosion by the metal sheaths or plastic tubes, and sometimes also by an anti-corrosive lubricant

(f) the system is generally more economical.

The arguments for post-tensioning with bonded tendons are:

(a) increased ultimate moment and

(b) unlike unbonded tendons local failure of a tendon has only a limited effect in a slab.

In partially prestressed slabs improved control of crack width is achieved with a combination of tendons and ordinary reinforcement; under which conditions unbonded tendons are entirely satisfactory in performance.

1.5 Purpose of Research

This investigation was an attempt to study the general behaviour of an internal square panel subjected to various tendon arrangements. A square panel was chosen so that large bending moments are produced over the support under vertical loading.

The investigation was carried out in two phases. In phase 1, the distribution of prestressing moments induced by a given prestressing force in an internal square panel was studied by varying the amount of prestress, hence the proportion of the total number of tendons, in the column and middle strips. For tendon distribution purposes, two different column strip widths were used namely L/10 and L/2. The study was carried out with the help of a finite element package (PAFEC).

In phase 2, an experimental programme of ten tests of partially prestressed square panels with various tendon arrangements was carried out. A square panel with a centre column was fixed at the edges in order to simulate the boundary conditions along the mid-panel lines of adjacent internal panels in a multi-panel slab structure. Two general levels of prestress were used representing a medium and a low value according to design practice as represented in a number of codes. The serviceability and the ultimate load behaviour were studied and where appropriate, predicted values from these codes were compared with the experimental results.

1.6 Method of Experimental Investigation

The majority of the experimental investigations of slab behaviour had been made by means of tests of a representative single panel of a complete slab system. For an internal panel, it has generally been assumed that the line of contraflexure under pure vertical loads extends to approximately 0.2L from either side of the column centre lines. Many models have therefore been simply supported along this line of contraflexure and loaded carefully through the column. With regards to the study of the flexural behaviour of post-tensioned slabs, this simple model is considered unsatisfactory for the following reasons:

(1) the lack of continuity at the boundary makes it difficult to reproduce the deformation which would develop in a real structure and consequently the load-deflection relationships of such models are not meaningful.

(2) In continuous indeterminate structures, secondary moments are generated due to prestressing. These effects, which are by no means secondary in importance, will affect the column reactions and in a statically determinate model are completely absent. Even if the prestressing tendons in the model are placed to represent the actual profiles in a real structure, restraints are required in order to produce the simulated effects but in doing so, the contraflexure position will be shifted, thus violating the basic

assumption.

(3) Complete distribution of prestress cannot take place over the relatively short span of the simple model and the prestressing effects will be exaggerated.

(4) Unbonded tendon stress increase due to flexural deformation is much higher in this model due to its short span.

(5) Compressive in-plane forces as well as redistribution of moments which occur in real structures cannot develop due to the lack of continuity.

These disadvantages have also been noted by Clark (3) and Franklin (7).

Long and Masterson (4) recognising the importance of boundary conditions on the behaviour of slabs had attempted to simulate the behaviour of a real structure by employing models which extended to mid-span between the columns. A carefully designed system of restraints which allowed realistic boundary conditions to occur under pure shear or combined loading was incorporated in the model. The basic assumptions of the test, the loading setup and the function of the restraining system are shown in Figs.1.1, 1.2 and 1.3 respectively. A slightly improved system was used later by Gilbert (5), Cleland (6), and Franklin (7) in a series of tests to investigate the punching behaviour of edge and internal columns of reinforced and post-tensioned slabs. Their results indicated that there were considerable differences from those obtained using simpler models. The sophisticated model allowed compressive membrane action to develop and redistribution of moments to occur

and its ultimate punching capacity was enhanced.

In view of the shortcomings of a simple model in simulating the behaviour of an actual internal panel, the model adopted in the investigation was therefore basically similar to that used by Long et al. The restraining system was, however, simplified on the basis of symmetry of loading of the panel. The slab dimensions, test arrangement and discrepancies in the model are discussed in detail in Chapters Five and Six.

1.7 Outline of Thesis

The thesis is divided into three parts. Part 1 consists of a general introduction in Chapter One and a review of previous research and current design practice of unbonded post-tensioned slabs in Chapter Two.

Chapters Three and Four form the contents of Part 2 and are devoted to the study of prestressing effects induced in a typical internal square panel under various tendon arrangements. Different aspects of the finite element package (PAFEC) and the transformation of prestressing forces into transverse vertical loads using the load-balancing idealisation are presented in Chapter Three. The results of the study are discussed in Chapter Four in which advantages of adopting a closely banded tendon arrangement in the column region are shown.

Part 3 consists of Chapters Five to Nine and is concerned with the experimental study of the serviceability and ultimate

load performance of ten square panels.

The experimental programme including materials and fabrication of slabs is described in detail in Chapter Five.

In Chapter Six, the discrepancies between the results obtained with the present model and test arrangement and the flexural behaviour of an actual internal panel are discussed.

The theoretical calculation of ultimate flexural strength of the test slabs is considered in Chapter Seven.

In Chapter Eight, the behaviour of the slabs under test is described and discussed. Experimental measurements of the prestressing effects are verified with theoretical values and comparisons made between experimental and computed deflections using the equivalent frame method of computation. The short-term and long-term deflections at mid-panel in the internal panels are extrapolated from experimental values and the influence of different tendon distribution patterns on the deformation of the slabs are discussed. The flexural strength calculated as in Chapter Seven and the punching shear strength, computed using various recommended methods are also compared with experimental results and discussed.

The conclusions of the investigation described in Parts 2 and 3 are presented in Chapter Nine and suggestions for further research are made.

CHAPTER TWO

Review of Previous Works and Current Design Practice

2.1 Development of Unbonded Post-tensioned Flat Slabs

Post-tensioned flat slabs have become increasingly popular with structural engineers over the past 25 years resulting in their current widespread use, especially for floor and flat roof construction. The popularity of this form of construction can be generally attributed to:

(a) a better understanding of the principles involved in prestressing flat slabs, leading to simplification of design techniques.

(b) The availability of high strength steel and concrete and the development of improved prestressing equipment.

(c) The demand for longer spans and high-rise construction.

(d) The improvement in field methods which makes prestressed slabs little more difficult for contractors to construct than conventional reinforced slabs.

Most prestressed slabs are built in the United States and European countries with unbonded tendons. Post-tensioned slabs have also been used increasingly in Australia and New Zealand but there bonded systems predominate. Whether one-way or two-way structural action is used in the design, a span/depth ratio of 40-45 is quite typical in the construction of residential apartments, offices, parking structures and hotels. It has been

claimed that a 30% reduction of the thickness required for a reinforced concrete slab can be achieved by post-tensioning, thereby reducing the slab dead load significantly.

In addition to economic advantages, the upward forces created by draping the post-tensioned tendons which normally carry 70%-100% of the slab dead load, can be utilised to reduce the resultant deflections due to loading and a nearly deflectionless final surface can be achieved. This minimises the possibility of cracking in partitions and is particularly advantageous when there is the possibility of the penetration of cracks by corrosive elements.

The early practice in design was to provide practically no non-prestressed bars or wires in the critical sections of maximum moment. Over the last 25 years, however, the trend has been to allow tension in the concrete at service load, allowing the service moment to be fairly close to the cracking moment in local areas where bonded reinforcing steel is used in conjunction with unbonded tendons. Indeed, the bonded reinforcement is no longer treated as just 'extra steel' but is designed to contribute actively to the serviceability and ultimate behaviour of the slabs.

2.2 Review of Previous Works

2.2.1 Tests of Multi-panel Slab System

In order to trace the development of the design and

construction of post-tensioned flat slabs, it will be instructive to review some of the important tests on full size and scale models of multi-panel slab system. These will be used to trace the evolution of the design practice which has now been summarised in the recommendations of the current codes.

The first reported test on an unbonded post-tensioned slab was conducted by Scordelis, Pister and Lin (8) in 1956. The specimen was a full size 4.27m * 4.27m * 127mm thick square concrete slab prestressed in two directions. Prestressing was accomplished by means of unbonded tendons axially placed and uniformly distributed in both directions in order to produce an average prestress of 2.80 N/mm^2 in each direction. The slab was simply supported at the four corners to simulate a lift slab and was loaded uniformly by means of air pressure in a plastic bag. Experimental deflections and strains were checked against classical elastic theory and good correlations were obtained. The slab developed a classical yield line pattern although bonded steel was not used.

In 1958, Scordelis, Lin and Itaya (9) tested a four-panel structure with a span/depth ratio of 28. The specimen was supported on 9 columns. Draped parabolic tendons equally spaced in both directions furnished an average prestress of 1.03 N/mm^2 in the slab. On the basis of the results, the authors concluded that the behaviour of the prestressed slab loaded within the elastic conditions could be satisfactorily predicted using plate theory.

At about this time, reports of tests on prestressed slabs

were also received from Australia.

In 1964, Gamble (10) published the results on tests of a 76.2mm thick slab having two spans each 3.65m wide in one direction and three spans each 2.74m wide in the other direction. Light weight concrete was used. The slab was unusually highly prestressed, ranging from 3.45 N/mm^2 in the long span and 2.69 N/mm^2 in the short span, by using tendons evenly spaced in both directions. The tendons were axially placed in the slab and did not therefore reflect the usual practice in construction. The tests, however, yielded useful data for shear strength evaluation.

In 1967, a long-term testing programme was conducted by Brotchie and Beresford (11) on a large scale prestressed slab. The overall dimensions of the structure were 17.92m * 13.72m and 76.2mm thick with the supporting columns spaced on a 3.67m * 2.74m grid. The resulting span/depth ratio was 48 and 36 in the long and short span respectively. The tendon profiles were draped to follow the overall panel moment profiles and tensioned to essentially balance these moments at the sustained load. The resulting average prestress was 2.33 N/mm^2 in the long span and 1.21 N/mm^2 in the short span. It was possibly the first reported test on a full size slab where the tendons were banded in the column and middle strips. In addition to its self weight, the structure was subjected to a sustained uniform loading of 3.7 kN/m^2 for a period of over 30 months and was finally tested under incremental uniform loading to failure. It was found that both the long-term and short-term behaviour were satisfactory despite the

high span/depth ratio of 48 in the slab. Although non-prestressed steel was not included in the test slab the authors, nevertheless, recommended its use in order to increase the ductility and toughness of the slab.

Back in the United States, there followed an increase in research activities to study the elastic and post-elastic behaviour of prestressed concrete slabs. The effects on slab behaviour by different tendon arrangements and the provision of non-prestressed reinforcement over the column area were under close scrutiny. In addition, the validity of designing prestressed slabs using the equivalent frame method, newly incorporated into the ACI 318-71 Code (12), was also investigated.

In 1976, four small scale models were tested by Nawy and Chakrabarti (13). The specimen was 1.5m square and 35mm thick and was a four-panel continuous structure simply supported along the edges and at the centre by a column. The prestressing force was furnished by unbonded tendons draping parabolically in both directions. The tendons were both uniformly arranged and banded in the test series and the resulting prestress was 1.80 N/mm^2 in each of the two directions. In one of the specimen (designated RP-2), 67% of the tendons were banded and distributed in the column strip width (L/2) in each direction. A closely banded arrangement of the tendons in the column vicinity in one-direction and uniformly distributed in the other orthogonal direction was also investigated (RP-3). The deflection of the slabs computed using the equivalent frame method showed good correlation with the test

results. Mild steel reinforcement over the column in one of the specimens (RP-4) was found to control cracking effectively.

At the University of Texas in the late 1960's and early 1970's an extensive testing programme was carried out under the supervision of Burns. The programme included a series of tests on isolated panels and the conclusions were later incorporated in several multi-panel slab tests. The isolated panel tests will be described in section 2.2.2. The tests on multi-panel slab system consisted of two nine-panel and one four-panel scale models. Some of the provisions of the design recommendations from ACI-ASCE Committee 423 (1974) (14) were an outgrowth of this testing programme.

The two nine-panel scale models were conducted by Burns and Hemakom (15,16) and were designated as Slab I and Slab II.

Slab I (15) was a 1/3 scale model of a prototype structure. The overall dimensions were 9.91m square and 74mm thick and the model had three spans each 3.05m wide in both directions. The tendons were parabolically draped and arranged with 70% in the column strip and 30% in the middle strip in each direction. Using the equivalent frame method, the prototype of this model was designed with 100% of the slab dead load balanced by the tendons resulting in an average prestress of 2.31 N/mm^2 in both directions. The area of non-prestressed steel was 0.15% of the column strip area. This bonded reinforcement was used as top steel in the slab and was placed in the immediate column region to control cracking. The slab behaved elastically and carried an imposed service load

of 3.35 kN/m^2 without any cracking being observed. However, some inelastic behaviour was evident as soon as localised column cracking had taken place. Cracking was absent from the positive moment regions at service load level and it only became extensive at failure. The ultimate behaviour of the slab was described as ductile and it was able to carry an applied load of up to 9.58 kN/m^2 when yield line patterns developed. However, the slab ultimately failed by secondary punching shear in one of the internal columns.

Slab II (16) was a 1/2 scale model which made use of a banded tendon arrangement in practice. It was the first reported test of a multi-panel structure where the tendons were fully banded in the column vicinity in one direction and uniformly distributed in the other direction. The overall dimensions of the model were similar to Slab I above, but the spans for the prototype were only one third as great and the average prestress was 1.03 N/mm^2 as compared with 2.31 N/mm^2 in Slab I. The prototype structure was designed for tendons to carry about 70% of the slab dead load. Despite the unconservative design of prestress and the unusual tendon arrangement, Slab II was found to perform satisfactorily up to service load and it almost reached the factored load (i.e. 1.4 DL + 1.7 LL). It was also found that the symmetrical behaviour of the slab was not affected by the tendon layout.

The testing of the third multi-panel structure, Slab III, was conducted by Kosut, Burns and Winter (17) and it was designed to study the behaviour of external column/slab connections. .The

structure, a 1/2 scale model, was a four-panel structure of overall dimensions of 6.1m square and 70mm thick and with columns spaced at 3m centres. The tendon arrangement was similar to Slab II but the prestressing wires were tensioned to give an average prestress of 1.24 N/mm^2 in each direction. From the observations made in Slab II, the minimum amount of bonded steel in accordance with the ACI Code (1977) (18) provisions (0.75% of the area of the span for each direction) was placed between lines 1.5h from either side of the column faces. The placement of this reinforcement was closer to the column than in Slab II. Behaviour of Slab III was completely elastic at all possible arrangements of the service load on the slab and it was found to have a load capacity greater than the factored ultimate load. A yield line pattern developed at the final applied load of 10.06 kN/m^2.

From the above discussion, several features in the development of post-tensioned slab design and construction can be summarised as follows:

(a) Prior to the 1970's, most post-tensioned slabs were constructed without any supplementary bonded reinforcement.

(b) The load-balancing approach in conjunction with the equivalent frame method appears to be the most widely adopted design method.

(c) 100% of the slab dead load is usually balanced by the tendon forces which results in an average prestress level of 1.20 N/mm^2 to 2.30 N/mm^2.

(d) The viable span for this type of construction appears to

be in the region of 7.0m or greater and span/depth ratio between 40-45 is generally adopted.

(e) The tendon arrangement is predominantly that of 70-30% distribution in the column and middle strips as recommended by the ACI-ASCE Committee 423 (1974). Other patterns of layout are also used to a limited extent.

(f) The recommended minimum area of non-prestressed reinforcement is only required over the columns.

(g) This amount of bonded reinforcement generally ensures a flexural type of failure followed by a secondary punching shear.

(h) There is little experimental data on the flexural behaviour of prestressed slabs with the unbonded tendons laid in other alternative patterns e.g. those used in European practice.

(i) Although slabs prestressed with 70% of the dead load balanced are found to perform satisfactorily at the service and ultimate state, there is as yet little experimental data to justify the use of a very low prestress level in prestressed slab construction.

The tests on multi-panel slab systems indicate that the column area should receive special consideration in detailing and design of reinforcement. This is because the slab column connection is a location of both shear and bending moment and is very susceptible to a sudden punching type of failure which can sometimes initiate a progressive collapse throughout the structure (19). For this reason, the behaviour of post-tensioned slabs in

the critical column area has always been of great concern to designers. Fortunately, guidelines are available in the various codes of practice but the provisions in the codes are generally derived from tests based exclusively on the use of specimens which represent a sub-system of a complete slab structure. The research activities in this area will now be considered.

2.2.2 Tests of Single-panel Slab System

In 1958, Scordelis, Lin and May (20) investigated the ultimate shear strength of reinforced and prestressed slabs constructed by the lift slab method. The tests consisted of 15 slab/column specimens, 12 of which were prestressed with unbonded tendons. All specimens were 1.83m square and had a thickness of 150, 200 or 250mm. The slabs were supported along all four edges and centrally loaded. Major variables were concrete strength, amount of reinforcing steel and prestressing (ranged from 1.70 to 3.45 N/mm^2). In all the prestressed slabs, bonded reinforcement was not provided in the immediate column vicinity. The results of the test series were accurately predicted by the following equation:

$$\frac{V}{bdf_c'} = 0.175 - 0.035f_c' + 0.0001\rho_{ps} f_{pe} d \quad \text{--- Eqn. 2.1}$$

In 1967, Grow and Vanderbilt (21) tested 10 light-weight concrete slabs of 0.91m square overall and 76mm thick. The amount of prestress was the main variable and this was ranged from 0.04 N/mm^2 to 4.52 N/mm^2. They found that there was a linear increase in shear strength with an increase in either the effective initial

prestress or the ultimate tendon force. Two empirical formulae were proposed to predict the shear strength of the test series:

$$\frac{V}{bd} = 2.48 + 0.30\ f_{pe} \qquad \text{--- Eqn. 2.2}$$

and

$$\frac{V}{bd} = 1.33 + 0.53\ f_{pb} \qquad \text{--- Eqn. 2.3}$$

where f_{pe} = average effective prestress immediately after post-tensioning

f_{pb} = average ultimate prestress immediately prior to failure

It was also found that the expressions derived by Moe (22), Hognestad et al (23), Yitzaki (24), Scordelis et al (20) also gave reasonably good agreement with the test results eventhough some of the expressions were developed on the basis of ordinary reinforced concrete slabs. Grow and Vanderbilt, nevertheless, stressed the importance of testing models which more closely simulated real structures than the simpler models of the previous investigators.

In 1971, Gerber and Burns (25) reported results from tests conducted in 1965 which involved 10 post-tensioned flat slab specimens of 3.7m square overall, simulating both lift slab (6 specimens) and cast-in-place (4 specimens) construction. The slab was supported on a 300mm square precast column at the centre. Unbonded tendons providing an average prestress of 1.72 N/mm^2 in each direction were laid to prototype slab parabolic profiles. The tendons were distributed with two from each direction passing over the column in the cast-in-place specimens and over the lifting

collars in the lift slab specimens. The only other variable was the amount and types of supplementary bonded reinforcement placed over the column. It was found that the shear design of prestressed slabs using equation 2.1 was conservative, providing factors of safety of the order of 3 to 4.5. This was assumed because the equation did not include the effects of bonded reinforcing steel. The authors concluded that the reinforcing steel helped to control cracking and increased the ductility of the structure and that tendons passing over the column greatly increased the reserve capacity of the connection and improved the ability to transmit load to the column after failure.

Smith and Burns in 1974 (26) reported a series of three tests on simple isolated models (1/3 scale) extending to mid-span of the prototype and loaded along the line of contraflexure. The specimens were 2.74m square and 70mm thick and were supported by a single column stub at the centre. Unbonded tendons, laid to the same profiles as in the actual slab, were distributed in a ratio of 70%-30% in the column and middle strips respectively. The average prestress was 2.24 N/mm^2 in each direction. The main variable was the amount of bonded reinforcement over the column which ranged from 0.15% (Slab 2), and 0.24% (Slab 3) of the cross sectional area of the column strip. Slab 1 contained no reinforcing steel. All slabs failed in a combination of flexure and shear with the actual failure mode occurring as punching shear. The ultimate shear strength was found to exceed slightly the values predicted by equations 11-22 in the ACI-ASCE Committee 423 (1974) recommendations. This was assumed because the equation

(similar to Eqn.11-13 in the ACI 318-83 Code (27)) was based on beam action instead of two-way slab behaviour. The presence of bonded reinforcement was found to improve the flexural behaviour and was effective in distributing cracks and controlling crack widths in the column area.

The conclusions from these tests were later applied to the scaled multi-panel tests described earlier. Based on the observations in Slab I and II, Burns and Hemakom (15,16) recommended that the minimum area of non-prestressed steel should be placed within a zone bounded by lines 1.5h on either side of the column in order to ensure that ultimate shear strength of the column connections exceeded that predicted by the ACI Code. In general, it was also recommended that the banded tendon arrangement in Slab II should be used in construction because the localised prestress at the exterior columns increased the flexural cracking capacity and enhanced the shear strength.

Hawkins (28) in 1981 reported the results on testing (carried out in 1976) of six full size post-tensioned slab specimens, four of which were internal column model subjected to moment transfer and the other two simulated a lift slab internal connection and an edge column. In addition to the moment to shear ratio, the tendon layout was varied and cyclic loading was applied to simulate the seismic response of the specimens. The minimum area of bonded reinforcement was used over the column in all the specimens. It was found that all reinforcement, bonded or unbonded, within lines 1.5h on either side of the column was effective for moment

transfer to the slab and that the shear capacity of regions subject to moment transfer was increased by concentrating the tendons through the column.

Most of the research activities described above were carried out in the United States. In Britain, the punching behaviour of edge and internal column connection of prestressed slabs was also under extensive study and two notable tests merit some attention here.

In 1979, Cleland, Franklin and Long (6) conducted tests on eight unbonded post-tensioned flat slabs to examine the behaviour up to ultimate at edge and internal column locations. The models, representing a full panel at 1/4 scale, were subjected to a carefully designed restraining system using series of tee-pieces and struts in order to simulate the behaviour of a panel in a multi-panel structure. This restraining system was essentially that used by Long and Masterson (4) to study the punching behaviour of reinforced concrete slabs. The model was subjected to 16 point loads simulating uniformly distributed load. The major variables in the investigation were the amount and distribution of prestress as well as the profiles of the prestressing tendons. The level of prestress ranged from 1.17 N/mm^2 to 3.52 N/mm^2. Bonded reinforcement supplied in the negative moment regions directly over the column was conformed with the ACI-ASCE Committee 423 (1974) recommendations.

In one of the slabs (EI) 65% of the prestressing tendons were placed in the column strip. In the remainder slabs, the tendons

were fully banded in the direction of moment transfer and uniformly distributed in the other direction. It was found that the level of moment absorbed by the column gave good correlation near the ultimate state using the ACI (318-77) approach while the method of CP110 overestimated the moment at all stages. When moment as well as shear were transferred to the column, the CP110 edge column approach yielded values less conservative than the ACI approach but nevertheless underestimated the test results. A method to calculate the punching capacity of an internal column was proposed. It was based on a shear criterion similar to that suggested in the Concrete Society Technical Report No.17 (29) but differed in the evaluation of the equivalent reinforcement ratio which was changed from $\rho^* = \frac{f_{pu}}{f_y}\rho_{ps} + \rho_s$ to

$$\rho_e = \frac{f_{pb}}{f_y}\frac{d_p}{d}\rho_{ps} + \rho_s \quad \text{--- Eqn. 2.4}$$

where f_{pb} is the tendon stress at ultimate load. This change was deemed logical since unbonded tendons never reach stresses near their ultimate value in a real slab structure. The nominal shear stress at failure was calculated by the following equation

$$v = 2.0\ (\rho_e\ f_{cu})^{1/3} \quad \text{--- Eqn. 2.5}$$

The factor of 2 in the equation was found to be consistent for the test series as well as from results obtained from tests by Burns et al (25,26). For design purposes, the material factor was incorporated and the recommended equation was:

$$v = 1.33\ (\rho_e\ f_{cu})^{1/3} \quad \text{--- Eqn. 2.6}$$

The work of Cleland et al was extended to cover various internal column and slab configurations by Franklin and Long (7). The main variables were the moment/shear ratio of the slab and the boundary conditions. Seven specimens, representing a 1/3 scale model of a prototype structure, were tested; two of which were of unequal span (long/short span ratio about 1.2) and five were of equal span. Four of the specimens had free edges (designated as type B) simulating those tested by Smith and Burns (26) while the remaining three had fixed edges (designated as type M) in order to simulate internal panel behaviour. The restraining system used was basically that of Long and Masterson (4) and Long and Cleland (6). The free edge specimen was 2.54m square and the fixed edge specimen 2.76m square overall. The slight increase of 0.22m in the latter specimen was necessary due to the additional portions required for restraint against rotations. Apart from one specimen (1B) where a 70/30 tendon ratio was used in the column/middle strip distribution, the tendons in each slab were fully banded in one direction and uniformly distributed in the other. The average prestress ranged from 2.29 N/mm^2 to 3.09 N/mm^2 in the unequal span specimens and 2.43 N/mm^2 in the equal span specimens.

A general method of predicting the ultimate punching capacity along the lines originally proposed by Long and Masterson (4) for reinforced slabs was suggested. The method used a flexural criterion in which punching was assumed to occur when the slab moment at the column face caused rupture of the concrete compression zone. However, in order to achieve good correlation

with all relevant test results (15,20,21,25,26), it was necessary to include the enhancing effect due to compressive membrane action. A simplified design equation (30) was proposed to determine the punching capacity of an internal column:

$$V = 10(\omega_e \frac{c}{L})^{0.5} f_{cp}^{0.133} f_{cu} d^2 \quad \text{--- Eqn. 2.7}$$

where ω_e = equivalent reinforcement index $(\omega_e = \rho_e \frac{f_y}{f_{cu}})$

and ρ_e is given by Eqn 2.5

An equation was also developed to check the effect of boundary conditions on the punching capacity of the slab and for the test specimens with free edges, the punching strength was given by

$$V = 20(\omega_e \frac{c}{L})^{0.67} f_{cp}^{0.08} f_{cu} d^2 \quad \text{--- Eqn. 2.8}$$

Equation 2.7 was found to give good correlation with actual failure loads obtained from various tests despite the wide range of variables involved.

2.3 Design Methods

The stresses in prestressed flat slabs are highly indeterminate. Until the advent of simplified design techniques developed in the 1960's, design methods evolved chiefly from experience in the field and intuition rather than from established theory.

The use of classical theory for the elastic analysis of post-

tensioned slabs is difficult if not impossible. Solutions exist for standard cases of square, rectangular and circular slabs (31) for simple loading and boundary conditions. These solutions were generally obtained by representing the loading by means of Fourier series equations. Using this technique, Parme in 1968 (32) made a rigorous study of the distribution of moments and direct forces in flat slabs induced by prestressing and compiled a set of useful design tables for evaluating the prestressing moments in flat slabs of different aspect ratios.

Possibly the largest stride in the practical design of prestressed slabs was the 'load-balancing' concept introduced by T.Y.Lin in 1963 (33), whereby the upward forces arising from the curved profiles of the tendons could be designed to counteract some or all of the vertical downward imposed loads. With this balanced load approach to design, there are no secondary prestressing moments due to continuity that remain unaccounted for, and no attention need be given to whether the tendons are 'concordant' or 'non-concordant', so that a rigorous analysis of the highly redundant stress system is by-passed. The method also provides deflection control.

Koons and Schlegel (34) carried the original load-balancing approach further and presented some practical aids for solving continuity, tendon reversal and reaction loads induced by the tendon profiles.

Numerous studies were then carried out based exclusively on load-balancing approach and led to several design methods for

prestressed slabs.

Saether (35) introduced a structural membrane theory, while an elastic approach for optimum design was proposed by Rozvany and Hampson (36), and Brotchie and Russell (37) respectively. The principal difference of the two methods was that Rozvany and Hampson used load-balancing whereas Brotchie and Russell used the concept of moment-balancing. The structure design by the moment-balancing method and subsequently tested by the latter authors was described in section 2.2.1. A direct design method was also proposed by Wang (38) which was unfortunately complicated and lacked any reference to ultimate strength checks.

2.4 Current Design Practice

2.4.1 Analysis

Currently, there are no guidelines in CP110 on the analysis of prestressed concrete flat slabs, but the Concrete Society Technical Report No.17 (29) suggested that for the analysis at the ultimate limit state, plastic, non-linear or linear elastic theory can be used in conjunction with suitable approximate methods such as the beam method, the equivalent frame method and the load-balancing method.

For building slabs with a regular plan geometry and light, uniform live loading, the load-balancing procedure in conjunction with the equivalent frame model of the structure is a widely used approach and it is specifically recommended by the ACI-ASCE

Committee 423 (1974) for the analysis of post-tensioned flat slabs. In Britain, the Post-tensioned Flat Slab Design Handbook (Concrete Society Technical Report No.25) (39), also gives examples using stiffness factors that take into account the effects of column heads in a manner adopted by the American Code for both reinforced and prestressed slab analysis.

2.4.2 Level of Prestress

In North America in the 1960's, a popular method for designing post-tensioned slabs was to provide a prestressing force and a tendon profile which would balance the slab dead load plus a certain amount of superimposed load, usually taken to be 0.48 kN/m^2 (10 psf). The resulting average prestress generally lies between 1.20-2.50 N/mm^2. The trend nowadays is to allow more tension in the concrete and consequently 70%-100% of the dead load will normally be balanced by the forces in the prestressing wires. However, to minimise cracking, the ACI-ASCE Committee 423 (1974) suggests that an average prestress of 1.4-1.7 N/mm^2 should be maintained. In addition, to prevent excessive elastic and creep deformation, the average prestress is limited to a maximum value of 3.4 N/mm^2. Slabs with an average prestress of less than 0.7, 0.9, and 1.0 N/mm^2 are not recommended in the British (29), American (14,27) and European (40) recommendations respectively.

2.4.3 Serviceability Stress Limitations

When the slabs are designed by approximate methods (e.g. the equivalent frame method), limiting flexural stresses are generally recommended in the American (14), British (29) and European (40) Codes. These limiting stresses are generally less than those normally adopted for prestressed concrete because the maximum moments are usually underestimated by the approximate methods of analysis.

With regards to compressive stress limitation, normal values of $0.45f_c'$ and $0.33f_{cu}$ are specified at positive moment locations under service loads in the respective American and British recommendations, and for the above reason these are reduced to $0.30f_c'$ and $0.24f_{cu}$ respectively in the negative moment regions at the column.

In positive moment regions without bonded reinforcing steel, the American recommendation is a limiting tensile stress value of $2\sqrt{f_c'}$ psi ($0.17\sqrt{f_c'}$ N/mm) and with bonded reinforcement a value of $6\sqrt{f_c'}$ psi ($0.50\sqrt{f_c'}$ N/mm). The corresponding tensile stress limitations according to the British recommendation are $0.15\sqrt{f_{cu}}$ and $0.45\sqrt{f_{cu}}$ and according to the European recommendation $0.16\sqrt{f_c'}$ and $0.48\sqrt{f_c'}$.

In negative moment regions of a slab without bonded reinforcement, all the recommendations are that no tensile stress should be permitted. If additional bonded reinforcement is present, the tensile stress limitations are the same as those for

positive moment regions with bonded reinforcement. All the recommendations, however, concede that the conservative stress limitations can be relaxed for slab design when more rigorous methods of analysis are used or when satisfactory performance under all design conditions (i.e. the serviceability and ultimate limit state design criteria) is checked by tests.

2.4.4 Tendon Arrangements

The distribution of tendons is important since it can affect the flexural behaviour and strength of a flat slab structure. In America, the recommendations of the ACI-ASCE Committee 423 (1974) are generally adopted in practice. The Committee recommends that when the length/width ratio of a panel in a continuous structure does not exceed 1.33, 65% to 75% of the tendons should be placed in the column strip with the remainder in the middle strip. The maximum tendon spacing in the column strip should be 4 times the slab thickness and in the middle strip about 6 times the slab thickness. These recommendations are based primarily on the tests conducted by Lin, Scordelis and Itaya (9) on a slab structure simulating lift slab construction. (section 2.2.1).

In the mid 1970's, several of the prestressed slab constructors in the United States began using the banded tendon arrangement in the construction of prestressed flat slabs. In this type of construction the tendons were placed in a narrow band in the column vicinity in one direction and were uniformly spaced in the other direction. On the basis of field experience and

structural research on this form of construction, the recent ACI 318-83 (27) Code makes specific provisions that permit the use of a banded tendon distribution in one direction. Section 18.12.4 of the Code states that:

"For normal live loads and loads uniformly distributed, the spacing of prestressing tendons or group of tendons in one direction shall not exceed 8 times the slab thickness nor 5 ft (1.52 m)".

In addition, a minimum number of two tendons in each direction is recommended through the critical shear section near the column.

In British (29) and European (40) practice, the tendons are normally distributed with 50% or more of the tendons in the column lines, the others being distributed across the remaining width of the panel. The column lines are defined as the "imaginary beams running over the columns with a width of column size plus slab depth (or effective slab depth in the FIP (1980) (40) Recommendations)". This pattern of tendon arrangement is widely used in construction, notably in European and Far Eastern countries (39).

An entirely different method of tendon arrangement known as "support-strip" prestressing was also advocated by the Bureau BBR (41) in the early 1970's. The tendons are laid to a profile such that the entire downward component of the prestressing force is delivered directly to the column supports through a punching cylinder which is defined as an idealised cylinder concentric with

the column and of diameter equal to the width of the column line. In general the prestressing force is chosen such that its total vertical component induced by tendons crossing the punching cylinder over the column is equal to the dead load plus a portion of the live load in the column (service condition) from the slab under consideration i.e.

$$V_{px} + V_{py} = V_D + nV_L \quad (n < 1) \qquad \text{--- Eqn. 2.9}$$

where V_{px}, V_{py} = vertical component of the prestressing forces in tendons crossing the idealised punching cylinder in X and Y direction respectively

and V_D, V_L = dead and live loads (service condition) on column from slab

The point of inflection of the tendons is assumed to coincide with the circumference of this cylinder. To satisfy the strength requirements, non-prestressed steel is placed over the columns and inside the panel. The slabs prestressed by this tendon arrangement are found to perform satisfactorily under service load conditions even at the low prestress level of 1.0 N/mm^2 (42). By comparison with the previously described tendon arrangements, slab construction using this support-strip method of prestressing is relatively simple as all the tendons can be supplied to the site on a common bobbin and then reeled off and placed simultaneously on common chairs laid on the formwork.

A recent IABSE survey on prestressed concrete flat slabs by Marti, Ritz and Thurlimann (42), shows that in addition to the tendon arrangements described above, there is yet another possible

tendon layout, though it has only been used to a limited extent in construction. In this arrangement the tendons are all banded in the column vicinity in one-direction and the slab is reinforced with bonded non-prestressed steel in the other direction. This, however, tends to induce a cylindrical surface of the slab when stressed and the arrangement would presumably be used in rectangular slabs.

The above different types of tendon arrangement are all considered in the present investigation.

2.4.5 Minimum Area of Non-prestressed Steel

The control of cracking is important in both reinforced and prestressed concrete for reasons of aesthetic appearance and corrosion prevention of reinforcement. With regard to prestressed concrete with unbonded tendons, the cracks tend to be wide and spaced far apart as a result of strain incompatibility of the tendons with the surrounding concrete. In prestressed slabs, the initial cracking is generally localised in the column regions and both analytical and experimental results support the need for a concentration of bonded reinforcement at the peak moment regions at the columns.

The American code ACI 318-83 recommends a minimum area of bonded reinforcement equivalent to 0.075% of the sectional area of a span length of slab in the direction parallel to the reinforcement being determined whereas the ACI-ASCE Committee 423

(1974) suggested an area of 0.15% of the cross sectional area of the column strip in each direction. Both recommendations will result in about similar area of non-prestressed steel.

In Britain, the Concrete Society Technical Report No.17 suggested an area of at least 0.15% of the gross cross section based on a width equal to the width of the column plus twice the slab depth on each side. The requirement in European practice is similar to the American recommendations.

The minimum reinforcement is generally required to be distributed over the column within a width of column size plus 1.5h on each side of the column face, and at least 4 bars should be provided in each direction.

Non-prestressed reinforcement is generally not required in the internal panels of the slab.

2.4.6 Design for Ultimate Limit State

Flexural Strength

In ultimate strength calculations, an assumption has to be made regarding the tendon stress increase at failure. For this estimation, the ACI 318-83 Code recommends two formulae to be used as alternatives according to whether the span/depth ratio is smaller or greater than 35. The British recommendations adopt Table 38 of CP110 for estimating the stress in the tendon while a new approach is introduced in the more recent BS8110 (44).

The FIP recommendations (40) are conservative and suggest that the stress in unbonded tendons at failure be taken as the effective prestress after all losses unless a higher stress can be justified by test results or by a rigorous analysis. The American and British approach will be considered further in Chapter Seven.

Punching Shear Strength

British Recommendations:

Neither CP110 nor its successor BS8110 makes any recommendations for punching shear in prestressed slabs and the designer is referred to specialist literature (section 4.2.2 in BS8110).

The Concrete Society Technical Report No.17 recommends that the shear resistance of a prestressed slab column can be calculated by the equation:

$$V_c = \xi v_c u_{crit} d \qquad \text{--- Eqn. 2.10}$$

where ξ = slab depth factor which varies linearly from 1.0 for h > 300mm and 1.3 for h < 150mm

V_c = ultimate shear stress

U_{crit} = critical perimeter taken at 1.5h from the column

The value of v_c is related to the tensile force available within the critical perimeter and may be calculated from the equation

$$v_c = (\rho^* f_{cu})^{1/3} \quad \text{--- Eqn. 2.11}$$

where $$\rho^* = \frac{pu}{f_y} \rho_{ps} + \rho_s \leq 0.03 \quad \text{--- Eqn. 2.12}$$

The reinforcement ratio ρ_{ps} and ρ_s may be calculated by

$$\rho_{ps} = \frac{A_{ps}}{u_1 d} \qquad \rho_s = \frac{A_s}{u_1 d}$$

where u_1 is the projected length of the critical perimeter normal to the steel under consideration.

In calculating ρ_{ps} and ρ_s, each side of the critical perimeter is considered separately. It is also suggested that the effective enhanced shear forces can be reduced by the vertical components of all the prestressing tendon forces within a perimeter h/2 from the face of the column.

American Recommendations:

The ACI-ASCE Committee 423 (1974) recommends the following equation for the shear strength calculation of two-way prestressed slabs:

$$V_{cw} = (0.29\sqrt{f_c'} + 0.3 f_{cp}) u_{crit} d + V_p \quad \text{--- Eqn. 2.13}$$

The critical section for shear is to be located at d/2 from the column face where d is the greater of 0.8h and the distance from the extreme compression fibre to the centroid of the prestressed reinforcement.

Equation 2.13 was originally proposed for prestressed beams and its use for prestressed slabs is only valid when the average prestress in each direction is not less than 0.86 N/mm^2. Because of limited experimental data, it is also suggested that the values of f_{cp} and f_c' to be substituted in the equation should not be greater than 3.45 N/mm^2 and 34.5 N/mm^2 respectively. With the tendon distribution recommended, V_p is usually small and can be neglected.

In the latest American Code ACI 318-83, the above equation is to be used only at internal columns which have no parts of their cross section closer to a slab edge than four times the slab thickness. The lower and upper limits of f_{cp} and f_c' suggested by Committee 423 are retained. For other columns, the shear strength is to be computed as for reinforced concrete and to be the lesser of

$$V_{cw} = 0.33 \sqrt{f_c'}\ u_{crit} d \qquad \text{--- Eqn. 2.14}$$

$$\text{or} \quad V_{cw} = \left(0.17 + \frac{0.33}{\beta_c}\right) \sqrt{f_c'}\ u_{crit}\, d \qquad \text{--- Eqn. 2.15}$$

where β_c is the ratio of the column's longer side to its shorter side dimension.

PART 2

ANALYSIS OF PRESTRESSING EFFECTS

CHAPTER THREE

Computer Package Used

3.1 Introduction

In this chapter, aspects of the finite element computer package used for analysing the elastic distribution of prestressing moments in an internal panel are presented. The idealisation of tendon profiles together with their associated induced prestressing reactive loads are also discussed.

3.2 PAFEC

PAFEC (Programme for Automatic Finite Element Calculations) is a large programme package designed to enable non-specialist solutions of problems in engineering methods (45,46). It uses extensively FORTRAN IV subroutines for the analysis and the input data modules are formatted in a very straightforward manner. Currently, it is being implemented on the Leeds University AMDAHL 470 V/7 mainframe computer as well as on the PRIME 750 minicomputer. Additional and improved facilities are introduced from time to time.

The PAFEC package is set up to run in 10 sections, known as phases within the package. A given job will not necessarily go through the phases in their numbered order. The main function of each phase is as follows :

Phase 1 : Data modules are read in. Preliminary verification and checking are carried out and the modules are placed onto backing store.

Phase 2 : Automatic mesh generation and element geometry verification.

Phase 3 : The basic structure is drawn and facilities for nodes and elements designation are provided.

Phase 4 : Initial calculation preparation with constraints in the problem considered and numbering system for the degrees of freedom derived in a suitable form for subsequent frontal equation solutions.

Phase 5 : Similar to Phase 3 except with constraints and freedom numbering on the drawing.

Phase 6 : The stiffness matrices of all the elements are found and put onto backing store.

Phase 7 : Main calculation phase (with phase 6) in which the primary unknowns in the problem - such as displacements, temperatures are tackled.

Phase 8 : The primary unknowns are drawn.

Phase 9 : Secondary unknowns (stresses in structural problems) are calculated.

Phase 10 : Stress contours, stress vector plots etc. are drawn for the problem.

The user can control the internal execution of the package by means of a CONTROL module in order to facilitate fast checking and model improvement in the early phases (usually phase 1 to 4) of

the job. Other facilities such as load-factoring and restarting with old or up-to-date data are also available.

3.2.1 Element Used

The PAFEC package offers a large family of elements, ranging from beam to spring elements to triangular and quadrilateral elements for plane stress and bending analysis to three-dimensional cuboid elements for thick plate problems.

The linear analysis of prestressing effect is essentially a plate bending and in-plane stress problem. A 4-noded facet shell element of the type R44200 has been found to be useful for both purposes. It is capable of carrying both bending and membrane loads. Reasonable distortion of the basic square shape is permitted provided the flatness of the element is preserved. There are five degrees of freedom (u_x, u_y, u_z, θ_x, θ_y) at the element level but after transformation to a three dimensional shell, the extra freedom θ_z is introduced. The bending matrices are based on the thin plate theory using an isoparametric transformation.

The output stresses are given in each of the four nodes and also at the centre of the element. They consisted of principal stresses on the top, middle, and bottom surfaces together with their relevant angles. Displacements are given at the four corner nodes only.

Although the element is less accurate than a similar eight-noded element for a similar element mesh, its use has resulted in

a reduced amount of computer time and if a finer mesh layout is used, there is essentially little loss of accuracy. The inclusion of sub-programs for in-plane stress analysis in the element makes the computation of resultant stresses due to bending and in-plane membrane effect at any location in the slab direct and simple.

3.2.2 Choice of Suitable Element Mesh

PAFEC places certain restrictions upon the element geometry and shape. Depending upon the degree of violation, messages of warnings and errors are issued, and in cases where severe distortion of the basic element shape occurs, the programme will fail.

In a quadrilateral element, the following restrictions are borne in mind when deciding upon a suitable element mesh. At the element level

(a) The ratio of length of longest side to the length of shortest side should be less than 5.

(b) The angle at the corner should not be less than 25° or greater than 135°.

Taking advantage of symmetry, only a quarter of the internal slab panel was analysed. The basic dimensions of the experimental model were adopted (Chapter Five section 5.4.1) as the results could be expressed in dimensionless coefficients, if necessary, suitable for general use in models as well as in prototype structures.

The arrangement of a quarter panel relative to its global axes is shown in Fig.3.1. For bending analysis (Fig.3.1a), a ten by ten mesh divides the panel into 100 elements with each mesh length of 75mm. A finer division at the column region marked out a quarter of the 100*100mm square column.

This meshing of the panel had been tested under uniform imposed load and the results in Table 3 show a reasonable good agreement with existing classical solutions (31).

Other reasons for choosing the mesh layout are :

(a) the easy accommodation of variable tendon spacing in either column-line or column-strip distribution (for definitions see Chapter Four section 4.4.2)

(b) the strain measurements on the concrete surfaces corresponded to a number of nodal positions in the mesh and hence comparison between experimental and theoretical results could easily be made.

In-plane stress analysis of the experimental test slabs was carried out using similar meshing in the internal panel with the addition of further meshing at the surrounding edge beams as shown in Fig.3.1b.

3.2.3 Application of Boundary Restraints

The restraints were applied in global directions. The directions of the degree of freedom to be restrained at each

element node is designated in numerical codes of 1 to 6 in the package and refer to u_x , u_y, u_z, θ_x, θ_y , θ_z, respectively. Combination of the numbers is allowed (Fig.3.2).

Referring to Fig.3.2a, in a typical internal panel full moment restraints were applied along the lines of zero shear at the centre of the panel in each of the two directions to simulate the stiffness provided by continuity. At lines of structural symmetry, i.e. at the column centre lines, similar restraints were used. At the centre of the panel, in addition to moment restraints, a zero displacement was also imposed in the vertical plane.

To establish the boundary conditions in the experimental test slabs (Chapter Five), zero vertical displacement as well as zero rotation were imposed along the inner edges of the panel as shown in Fig.3.2b.

Because of symmetry of the loading, the stiffness of the column was of no influence and the column reaction was equal to the total imposed load on the panel. This reaction was applied uniformly over the area of the column in the direction opposite to that of the imposed load, thereby achieving equilibrium with no vertical reaction at the fixed edges.

In in-plane stress analysis, the in-plane displacements in the direction of prestressing were prevented, as shown in Fig.3.2c, along the lines of symmetry in both directions.

3.2.4 Interpretation of Results

The notation compatible with the computer package, shown in Fig.3.2, were used to interpret the output results.

The displacement method used in PAFEC produces displacements at nodes which need no special interpretation. Stresses on the other hand, are function derivatives of the displacements and in many elements do not possess inter-element continuity. Since only one type of element was used in the panel, there were no special difficulties in interpreting the element stresses from the nodal points. Where a number of elements met at an angle, averaging of the nodal values was carried out by a FORTRAN programme by converting initially the principal stresses at each nodal point to longitudinal and transverse stresses and strains and later to obtain the relevant averages.

The longitudinal and transverse moments at each node would then be calculated by multiplying the stresses with a unit width gross section modulus.

3.3 Idealisation of Transverse Prestressing Effect

3.3.1 Tendon Profile

In the original 'load-balancing' method of T.Y.Lin (33), the tendon profile is idealised as a complete parabola in each span. The abrupt change of slope over the support is of course not permissible in practice for continuous tendons. More consistent

with practical layout the tendon profile shown in Appendix 1 is idealised as consisting of two parabolae with opposite curvature at the span and over the support, and a common tangent point at the position of inflection. Three parameters were used to define the parabola, namely e_{OB}, the eccentricity measured from the tendon centroid to the section centroid, λ, the distance ratio of reversed curvature from the centre of support and, β, the ratio of eccentricity at support and at mid-span. The tendon geometry adopted for analysis is shown in Fig.5.10.

3.3.2 Load-Balancing

The basis of the 'load-balancing' method is that a curved tendon when stretched against concrete members, applies transverse load to the concrete due to the curvature of the tensile force. The equivalent uniformly distributed load can be approximated by the equation:

$$W_{bal} \simeq P \frac{d^2e}{dx^2} \qquad \text{--- Eqn. 3.1}$$

With modification due to reversed curvature, the transverse reactive loads from prestressing, shown in Appendix 1, may readily be used in the finite element method in which, depending upon the concentration of tendons, the slab is subjected to areas of uniform downward and upward loads.

For a four-noded element, the total distributed load over each element area was evenly distributed at the corner nodes. When the distributed load extended over more than one element, then the

nodal loads from adjacent elements were added numerically. A computer programme has been written solely for this purpose.

CHAPTER FOUR

Structural Behaviour of Flat Slab Under Prestress

4.1 Introduction

In this chapter, the distribution of elastic prestressing moments in a typical internal square panel is analysed using a finite element computer package as discussed in Chapter Three. Advantages are shown of concentrating the tendons in the column vicinity in a narrow banded pattern as opposed to the wider column strip arrangement as recommended in a number of codes of design.

4.2 Membrane Analogy

In order to illustrate the simultaneous load-relieving forces as well as the active downward loads acting on the slab due to two-dimensional prestressing, a static approach employing 'membrane analogy' proposed by Saether (35) is used. The analogy is strictly a matter of static deductions and does not, therefore, reflect the elastic behaviour of the slab. Only a typical internal panel is considered.

In Fig.4.1, a rectangular panel of span $L_1 * L_2$ is prestressed by tendons placed in both directions. The tendons are parabolically draped with the point of reversed curvature at half the width of the column strip from the centre line of the supports and each is subjected to a constant tensile stressing force. The

induced uniform downward load by the concave curvature of the tendons is assumed to act within the column area of $b_1 * b_2$ and if W_{1cc} and W_{2cc} are denoted for these loads from each orthogonal set of tendons, then the total uniform load acting on the column area is

$$V = (W + W_{1cc} + W_{2cc})\, b_1 b_2 \qquad \text{--- Eqn. 4.1}$$

where W is the external uniform load over the entire panel to be balanced by the tendons

V the total column reaction

Alternatively, V can also be written as

$$V = W L_1 L_2 \qquad \text{--- Eqn. 4.2}$$

It has been shown in Appendix 1 that the total upward reaction is equal to the total downward reaction from the same tendon. Thus within the column strip width in the direction of L_1

$$W_{1cc} b_1 = W_{1cm} (L_1 - b_1) \qquad \text{--- Eqn. 4.3}$$

Similarly in the direction of L_2

$$W_{2cc} b_2 = W_{2cm} (L_2 - b_2) \qquad \text{--- Eqn. 4.4}$$

where W_{1cm}, W_{2cm} are the upward reactive loads produced by the column strip tendon forces of P_{1c} and P_{2c} respectively.

In order to achieve zero load-balancing in the column strip, the downward reactions W_{1mc}, W_{2mc} from the two orthogonal middle strip tendons stressed to a force of P_{1m} and P_{2m} respectively, together with the uniform imposed load W must be made equal to the

upward reactions from the longitudinal column strip tendons. Hence in the L_1 direction

$$W_{1cm} = W_{2mc} + W \qquad \text{--- Eqn. 4.5}$$

and in L_2

$$W_{2cm} = W_{1mc} + W \qquad \text{--- Eqn. 4.6}$$

In the middle area of the panel the two sets of middle strip tendons, consisting of convex parabolae, furnish upward reactions W_{1mm} and W_{2mm} in the directions of L_1 and L_2 respectively. The sum of these reactions is made to balance the load W on the slab within this area and is given by

$$W = W_{1mm} + W_{2mm} \qquad \text{--- Eqn. 4.7}$$

The ratio of W_{1mm} and W_{2mm} is expressed as

$$\frac{W_{1mm}}{W_{2mm}} = n \qquad \text{--- Eqn. 4.8}$$

where n can take the values of 0 to ∞.

For optimum absorption of elastic bending moments in the slab, Saether suggested that n should take the form of

$$n = \frac{L_1^2}{L_2^2} \qquad \text{--- Eqn. 4.9}$$

In each set of the tendons in the middle strip, the total upward and downward reactions along the tendon length are related by:

in L_1 direction $\qquad W_{1mc}\, b_1 = W_{1mm}\, (L_1 - b_1) \qquad$ --- Eqn. 4.10

in L_2 direction $\qquad W_{2mc}\, b_2 = W_{2mm}\, (L_2 - b_2) \qquad$ --- Eqn. 4.11

From the above equations, it can be readily established that as soon as the ratio of n and the column strip widths b_1 and b_2 have been chosen, the ratio of 'prestressing loads' carried by the 'column strip' and 'middle strip' can be determined.

It has been suggested in the original load-balancing concept that a constant balancing load could be furnished by a number of continuous tendons spaced uniformly across the panel. The above arguments clearly show that for uniform load-balancing, the tendons are composed of convex and concave parabolae alternating in the column and middle strip and subjected to a certain degree of distribution in these strips. Saether pointed out that the widths of the column and middle strip should not be the arbitrary division of the panel width as defined in the various codes of practice, but should be related to the column area which is in turn controlled by slab thickness, column size and by the type and arrangement of the reinforcement.

Tendons placed within the column strip (as defined by various codes of practice) are generally considered to provide a better load-carrying capacity than those placed in the middle strip. This is reflected in the ACI-ASCE Committee 423 (1974) recommendations that for panels with an aspect ratio of less than 1.33 by placing 65-75% of the tendons in the column strip with the remainder in the middle strip. In the European (40) and British (29) recommendations, the tendons are more closely spaced over the column with 50% or more tendons banded within the column line which has a width equal to the width of the column plus the

overall slab thickness. These definitions of column strip will clearly result in a different proportions of the tendons being distributed in the various strips. To illustrate this point, the 'membrane analogy' is used in two examples. In the first example, the width of the column strip is assumed to be equal to half the panel width and in the second example, one-tenth of the panel width. In both examples, n is assumed to be 1 for simplicity.

Example 1

$$b_1 = \frac{L_1}{2} \qquad b_2 = \frac{L_2}{2}$$

From eqns.4.7 and 4.8 $\quad W_{1mm} = W_{2mm} = \frac{W}{2}$

Consider the strips in the direction of L_1

Column Strip:

From eqn.4.5 $\quad W_{1cm} = W_{2mc} + W$

From eqn.4.11 $\quad W_{2mc} = W_{2mm} \left(\frac{L_2}{(L_2/2)} - 1\right)$

$$= \frac{W}{2}$$

Hence $\quad W_{1cm} = \frac{W}{2} + W = \frac{3}{2}W$

Total balancing load to be provided by the tendons in the strip (per unit length in direction of span).

$$W_{1cm}\, b_2$$

$$= \frac{3}{2} W \frac{L_2}{2}$$

$$= \frac{3}{4} W L_2$$

Middle Strip

Total load provided by the tendons is

$$W_{1mm} (L_2 - b_2)$$

$$= \frac{W}{2} \left(\frac{L_2}{2}\right)$$

$$= \frac{1}{4} WL_2$$

Ratio of total number of tendons for the column and middle strip:

C.S.	:	M.S.
$0.75WL_2$	:	$0.25WL_2$
75%	:	25%

Example 2

By using $b_1 = 0.1L_1$ and $b_2 = 0.1L_2$, calculations similar to Example 1 show that the ratio of total number of tendons in the column and middle strip is

C.S	:	M.S
$0.55\ WL_2$	:	$0.45\ WL_2$
55%	:	45%

It is interesting to note the similarity of the tendon distribution ratio obtained in the above two examples with that of the American, British and the European recommendations when the width of column strip is approximately equal to that recommended.

According to equations 4.3 and 4.4, the concave curvature of the tendons in Example 1 is extended to 0.25L from the column centre lines. This is inconsistent with the practical value of a catenary tendon profile in which the point of inflection is generally accepted to vary between 0.05L to 0.1L (39). For a correct application of the load-balancing method in which the tendon geometry is a major parameter, it follows that in the 'membrane analogy' above the column area over which the downward reaction of the tendons acts should be at least governed by the practical limits of this point. Based on a similar approach to that of Saether, Candy (48) suggested, after considering the ultimate strength requirements of tendon spacing and the practical limits in which tendons are spaced in the column strip width, a column strip width of L/4 to L/3. From his analysis the point of inflection of the tendon profile is therefore varied from 0.125L

to 0.17L from the column centre lines. However, there is experimental evidence (15,16,17) to indicate that the ultimate load of a slab is dependent solely upon the total prestressing force applied per bay. There is, therefore, no reason why a narrower column strip width should not be used. In fact, in the support-strip method of prestressing (41,42), all the tendons per panel are placed within a column line of width equal to the column size plus overall slab thickness. The slabs prestressed using this pattern of tendon layout are found to perform satisfactorily under serviceability and ultimate load conditions. A summary of the basic design principles in this method is given in Chapter Two in section 2.4.4.

The choice of a narrow column strip with width not greater than the length of curvature reversal of the tendons should therefore result in a more favourable state of stresses in the slab for counteracting the uniform downward load and be preferable to the usual wider column strip width as defined by the various codes of design.

This last point , as indeed the overall effect of any tendon arrangement, must be investigated by a more rigorous analysis. The above extension of load-balancing theory is valuable in giving an appreciation of the overall action of the load and prestressing forces, but an examination of the column region will show that the load cannot be completely balanced over the whole panel and moments will consequently be induced in the slab. This will be considered by means of a finite element analysis using PAFEC

programme.

4.3 Theoretical Distribution of Moments under Uniform Load

The theoretical distribution of moments in a typical panel of a flat slab subjected to uniform vertical loading is schematically illustrated in Fig.4.2, assuming bending in the Y-direction. A similar distribution can be obtained in the other direction. A section of the moment surface parallel to the Y-direction leads to a moment diagram very similar to that obtained for a typical span of a continuous beam. However, the distribution of transverse moments is not uniform, implying that some portions of the slab across its width will be subjected to higher moments than others and the corresponding reinforcement distribution will require to be non-uniform. It is thus obvious that for effective prestressing, the distribution of moments induced by prestressing forces should follow closely the moment surface produced by vertical loading but opposite in sign. It is also obvious that the induced prestressing moments will differ considerably from that of conventional loading due to the fact that vertical reactive loads induced by prestressing are always located along the tendon length and are therefore best considered as local concentrated effects. In a flat slab, as shown in Fig.4.2, the maximum negative and positive moments occur on the column centre lines and it follows logically that a higher percentage of the prestressing tendons should be located in this region.

In the ensuing discussions, the moments resulting from

various tendon arrangements will be compared with the moments produced by a notional uniformly distributed external loading on the slab. This will be defined as the uniformly distributed load that can be balanced by the upward forces of a uniformly spaced catenary tendons in one direction and it will be conveniently called 'balanced service load'.

It is useful, prior to quantitative evaluation, to proceed with a brief qualitative discussion on the structural behaviour of a slab under prestress. A typical internal panel will be examined with tendons draped parabolically in one direction. With tendons draped in both directions, the total effect can be obtained by superposition. For easy reference, the moments parallel to the direction of the tendons are designated as longitudinal and those perpendicular as transverse.

4.4 One-way Prestress

4.4.1 Uniform Tendon Spacing

Consider Fig.4.3a (extracted from ref.32) in which the tendons are uniformly spaced along the Y-direction. All the tendons are similarly draped and subjected to a constant prestressing force. The variation of vertical reactive loads are shown in the X-direction with the change in direction occurring at the points of inflection of the tendons. When the profile is horizontal over the column centre line, the total vertical prestressing load will be equal to the total downward load and

hence there will be no reaction transmitted to the column. Since each strip in the X-direction is loaded identically and no reaction is transmitted to the column, it follows that each strip is subjected to similar deflection as shown in Fig.4.3b. This will result in a uniform moment distribution across the column and mid-panel centre line. The longitudinal moments in the X-direction can be easily obtained by the ordinary beam method. The transverse moments can also be obtained from Poisson's ratio.

4.4.2 Variable Tendon Spacing

If there is a heavier concentration of tendons in the vicinity of the column as shown in Fig.4.4a (from ref. 32), then an increased 'loading' in the column strip will cause the mid-span upward deflection of AB (4.4b) to be greater than the upward deflection of the panel at the centre in the middle strip. This differential deflection will naturally be resisted by the slab with the magnitude of resistance being a function of the transverse to longitudinal span. From the imposed curvature shown in Fig.4.4b, it is apparent that transverse moments will be induced with those in the middle strip of section AB being negative. Since the summation of these moments along the section is zero, it can be deduced that the transverse moments at the column must be positive. Thus eventhough the tendons are longitudinally placed the increase in tendons in the column strip creates beneficial moments in both directions in the column area.

4.4.3 Effect of Increasing Tendons in the Column Vicinity

To show more clearly the effect of increasing the percentage of tendons in the column vicinity, the moments due to prestress were analysed using the PAFEC computer package. The panel chosen has dimensions similar to the test model, i.e. 1.5m square with an overall thickness of 40mm. Tendon geometry is according to Fig.5.10 with the point of inflection at 0.1L from the centre-line of the support. Equal eccentricity is assumed at the support and at mid-span with the overall drape taken to be 0.65h. From the tendon profiles and total prestressing force (taken to be 100 kN across the panel for easy distribution in the column and middle strips) it is calculated that the upward reaction and hence the balanced service load is 7.71 kN/m/m width. To simulate internal panel behaviour, shear and rotation at the edges are assumed to be zero as discussed in Chapter Three.

To ensure a consistent description with regards to tendon distribution, the following definitions of column and middle strips are adopted and used henceforth in the thesis.

Column line : Imaginary beam running over the columns with a width of column size plus slab depth (Concrete Society Technical Report No.17)

Middle width : Imaginary beam whose width is taken as the difference between the width of the panel and that of the column line

Column strip : Imaginary beam running over the columns with a

width equal to one half of the width of the panel (CP110). It should be noted that in a square panel where spans are equal in both directions, the width of column strip as defined above is similar to the width as defined in ACI 318-83 Code.

Middle strip : Imaginary beam whose width is taken as the difference between the width of the panel and that of the column strip.

In the ensuing analysis, two different widths of column strip are used for distributing the tendons. The first has a width equal to half the panel width whereas the second has a width of 0.1L, which in a slab with span/depth ratio of 37.5 and a column size to span length of 0.067 is approximately equal to the width of the column line as defined above (actual width of column line is 0.093L). Henceforth they are referred as 'column-strip' and 'column-line' distribution respectively. A special case of column-line distribution in which all the tendons are concentrated in the column lines, the term 'support-strip' prestressing will be used.

Column-strip Tendon Distribution

Fig.4.5 shows the moment distribution along the transverse section of the panel at the column and mid-panel centre lines. The prestressing moments are expressed as coefficients of the product of balanced service load and the square of the panel span. The moment distribution under uniform balanced service load are also

plotted across the two centre lines and are shown in a similar sense to the prestressing moments for easy comparison.

It can be observed from the figure that a uniform spacing of the tendons in the panel, i.e. 50/50 column/middle distribution ratio, the moment distribution in both column and mid-panel centre lines are uniform as described in section 4.4.1. As the number of tendons increases in the column strip, there is a gradual increase and a similar gradual reduction of moments at the column and at mid-span on the column centre line amounting to about 50% when all tendons in the panel are banded uniformly within the column strip width. Similar trends are observed in the mid-panel centre line moments, though they are rather insensitive to the variation of prestress distribution, with only about 25% increase and reduction at the column supporting-line and mid-span moments respectively for a 100% prestress in the column strip. From a 'moment-balancing' point of view, the distribution of prestressing reinforcement adopting a wide column strip will be very inefficient as far as counteracting the 'balanced load moment' is concerned. Along the column centre line, the resultant prestressing moment distribution is rather 'flat' compared with the rapid varying moment surface of the uniform balanced load. The column region has thus been 'under-prestressed' whereas the mid-span section is 'over-prestressed'. Along the mid-panel centre line, however, the prestress is more appropriate for all ratios of tendon distribution.

Column-line Tendon Distribution

If the column strip width is reduced to 0.1L, better 'moment-balancing' can be obtained as observed in Fig.4.6. Comparing with Fig.4.5, there is a definite improvement in the overall moment surface due to prestress. For example, in the 70/30 column-strip distribution (Fig.4.5), a column sagging moment of $0.070W_{bal}L^2$ is found at the column whereas for the same ratio in the column-line distribution, $0.105W_{bal}L^2$ is obtained indicating an increase of 50%. As more tendons are placed in the column line, increasingly better 'moment-balancing' effect is obtained.

The mid-panel line moments again show a relative insensitivity to the variation of tendon distribution but, similar to column-strip distribution, the prestress is also appropriate for counteracting the imposed load moments for all ratios of tendon distribution.

Induced Transverse Prestressing Moments

Figs.4.7 and 4.8 show the variation of induced transverse moments in sections parallel to the direction of the tendons in a one-way prestress using the column-strip and column-line distribution respectively. It is clearly shown that beneficial moments are created in both directions in the column area by concentrating more tendons in the column vicinity, with significantly higher value (about 45% of the longitudinal moment in a 50/50 distribution ratio) using the column-line distribution

(Fig.4.8). Since the sum of these moments along the section is zero, the effect is such that instead of the prestress relieving the balanced load, the middle strip is being 'loaded' by the prestress. This 'loading' effect on the middle strip is less severe with column-strip distribution (Fig.4.7).

The presence of these aggravating moments in the middle strip can be explained by referring to Fig.4.4. When more tendons are concentrated in the column vicinity, the column strip is subjected to higher prestressing loads which will consequently lead to a higher differential deflection between the centres of the column and the middle strip and impose a negative and positive curvature at the mid-span of the strips respectively. With the same proportion of the total number of tendons in each strip, it is, therefore, expected that higher transverse moments will be induced with column-line distribution.

4.5 Two-way Prestress

The effect of two-way prestress with tendons having the same total force and a similar distribution in each direction is obtained by superposition of the one-way prestressing moments in the two directions.

In the column-strip distribution, in Fig.4.9, the two-way prestress, as expected, shows an overall improvement of moments in the column strip and a reduction in the middle strip when compared with the one-way prestress shown in Fig.4.5. The improvement,

however, is not very significant, being from 13% to 44% at the column when the distribution ratio increases from 50/50 to 100/0. In addition, the maximum moment at the column is not effectively counteracted, for example, in a 70/30 distribution only about 40% of the negative moment due to applied load is cancelled by prestressing. At the mid-span on the column and mid-panel centre lines 'over-prestressing' is found at both the positive and negative moment regions for distribution ratio smaller than 80/20.

When column-line distribution is used, as shown in Fig.4.10, a significant improvement in the column prestressing moment is observed in a two-way prestress, from 50% to about 75% of that in one-way prestress when the distribution increases from a ratio of 50/50 to 100/0 respectively. In a 50/50 distribution, the negative moment at the column due to vertical balanced load is effectively reduced by about 60% and is nearly nullified in a support-strip prestressing where 100% of the tendons are concentrated in the column lines. However the improved support moment is made at the expense of those at the mid-span as there is a gradual decrease in prestressing moment as the distribution ratio increases until in a 70/30 ratio the positive prestressing moment at the mid-span on the column centre line has almost disappeared. At higher distribution ratios this moment changes from a positive to a negative value and subsequently in the support-strip prestressing the original negative moment at mid-span due to balanced load is increased by as much as 125%. However, the resultant concrete stresses are not alarmingly severe. As an example, consider a 10m square panel with a total applied load of say 10 kN/m^2 being

counteracted by the support-strip system of prestress. The negative moment at the mid-span on the column centre line includes 20.0 kNm/m from the imposed load plus 25.0 kNm/m from prestressing. The tensile bending stress at the extreme fibre for a 250mm overall thickness slab is calculated to be 4.32 N/mm^2. When the axial prestress component (about 2.17 N/mm^2) is taken into account, the net concrete tensile stress is reduced to 2.15 N/mm^2 which is well within the permissible value of $0.45\sqrt{f_{cu}}$ in Table 3.3 of Concrete Society Technical Report No.17 for grade 30 concrete.

In Fig.4.10 the resultant prestressing moment distribution from the 55/45 distribution ratio obtained from 'membrane analogy' in Example 2, having similar column line width as in the present finite element analysis, is indicated approximately by a curve lying between those for tendon ratios of 50/50 and 60/40 respectively. Eventhough the point of inflection of the tendon used in Example 2 is taken to be 0.05L from the support whereas 0.1L is adopted in the present analysis, the errors involved are likely to be small. From Fig.4.10 it can be noted that along the mid-panel centre line and in the middle strip section on the column centre line, the moments due to the imposed load are almost cancelled for this tendon distribution ratio. However, in the column region, where it has been assumed in the 'membrane analogy' that the downward prestressing loads over the column area are balanced by the vertical reaction of the column, it is clear that at the centre of the support the prestressing moment only counteracts about 62% of the imposed load moment. Hence a complete load-balancing effect in the 'membrane analogy' cannot be achieved

due to the lack of total static equilibrium in the column area, although the deficiency may be less severe than the analysis suggests owing to the dispersion of the column reaction through the depth of the slab.

The ACI 318-83 Code allows the placement of all the tendons as closely as possible within the column line in one direction, whereas in the other orthogonal direction they are uniformly distributed. The prestressing effects induced in a slab by this pattern of tendon layout are shown in Figs.4.11 and 4.12.

Fig.4.11 shows the variation of prestressing moments transverse to the direction of the banded tendons. When the tendons are uniformly spaced, i.e. in the 10/90 column/middle ratio, the resulting moment distribution is almost identical to that of 50/50 column-line distribution ratio in a two-way prestress in Fig.4.10. The effect of increasing the proportion of prestress in the column line are also similar to Fig.4.10.

At sections parallel to the direction of the banded tendons shown in Fig.4.12, the moment surfaces along the column and mid-panel centre lines due to a variation of tendons in the direction orthogonal to the banded tendons are also practically identical to Fig.4.10 but at slightly higher values because of an increase in induced longitudinal moments in the direction of the banded tendons.

The deflection profiles along the diagonal lines in the panel are shown in Figs.4.13 to 4.15 for the column-strip, column-line

and the banded column-line distribution respectively. They are plotted in the same sense as the balanced load deflections for easy comparison. In Fig.4.13(a) a residual downward deflection is found at the centre of the panel under external balanced service load when the tendons are column-strip distributed. However in Fig.4.14 it is predicted that with a column-line distribution of tendons, a smaller resultant deflection will be obtained under a similar loading condition and an almost perfectly 'deflectionless' slab can be achieved with a 70/30 distribution ratio. With a distribution ratio of 100/0 in the support-strip prestressing the resultant mid-panel deflection at balanced service load is practically zero as shown in Fig.4.14(a). Fig.4.15 shows the deflection profiles produced by banding all the tendons in one direction with those in the other direction uniformly or column-line distributed. There are no significant differences with respect to those in Fig.4.14. Again an almost deflectionless slab can be achieved when a 70/30 distribution ratio is used in distributing the tendons transverse to those being banded.

From the above discussion, it is shown that, weight for weight, tendons placed in the column vicinity and adopting a narrow column line for distribution purposes, create superior and more efficiently distributed counteracting prestressing moments and deflection surfaces than those adopting the wider column strip. In practice concentration of tendons also increases the stiffness of the column area, reduces the maximum crack width and increases the load intensity for initial cracking as will be clearly demonstrated in the following experimental investigations.

PART 3

EXPERIMENTAL INVESTIGATION

CHAPTER FIVE

Experimental Programme

5.1 General

The design and fabrication of slab specimens, together with the testing procedure and method of loading are described in detail in this chapter. The tests consisted of three series of single panel partially prestressed flat slabs with different patterns of tendon distribution and prestressing levels subjected to a limited number of short-term load cycles. The method of test was devised to simulate the flexural behaviour of an internal panel in a multi-panel floor slab by providing fixity to the edges of the panel.

5.2 Prototype Layouts and Design Loads

The prototype on which the test was based was a multi-panel floor slab in a typical medium height apartment or office building with average spans of 10.0m in each direction. The selected levels of live load of 2.0 kN/m^2, superimposed dead load (partitions, ceiling and finishes) of 2.0 kN/m^2 and slab self-weight of 6.0 kN/m^2 (250mm slab thickness) are representative. Preliminary calculations were carried out and a column size of 670mm square was found to be satisfactory for punching shear. The dimensions resulted in a span/depth ratio of 40 and a ratio of column size to span of 0.067 which is again typical in post-tensioned flat slabs

construction. The total service load was readjusted from 10.0 kN/m^2 to 11.0 kN/m^2 in subsequent testing due to an increase in the slab self-weight by scaling as the slabs were constructed to a smaller span to depth ratio than was originally intented.

5.3 Model Scaling

The choice of a suitable model scale and size for the test panel has been limited by

(a) the available working space in the laboratory

(b) the feasibility of providing appropriate scaled-down micro-concrete and reinforcement

(c) the loading requirements and

(d) the required capacity of lifting and loading equipment

From the laws of structural similitude, apart from the equality of strain and Poisson's ratio which are dimensionless, the deflection δ_m and stress σ_m at any point in the model and the modulus of elasticity E_m and density ρ_m of the model material should be in the following relationship with the corresponding prototype values (49):

$$\delta_m = \frac{1}{\lambda_\ell} \delta_p \qquad \text{--- Eqn. 5.1}$$

$$\sigma_m = \frac{1}{\lambda_s} \sigma_p \qquad \text{--- Eqn. 5.2}$$

$$E_m = \frac{1}{\lambda_s} E_p \qquad \text{--- Eqn. 5.3}$$

$$\rho_m = \frac{\lambda_\ell}{\lambda_s} \rho_p \qquad \text{--- Eqn. 5.4}$$

where λ_ℓ, λ_s are the linear scale and stress scale factors respectively.

The relationships for 'applied loads' are as follows :

UDL or pressure loading $\qquad W_m = \frac{1}{\lambda_s} W_p \qquad$ --- Eqn. 5.5

Point loading $\qquad P_m = \frac{1}{\lambda_s \lambda_\ell^2} P_p \qquad$ --- Eqn. 5.6

Bending moment $\qquad M_m = \frac{1}{\lambda_s \lambda_\ell^3} M_p \qquad$ --- Eqn. 5.7

To completely model the behaviour of concrete structures, the stress-strain relationship of the model materials must be geometrically similar to that of concrete. This implies that the stress factor λ_s must be constant at all levels of stress and strain, both compressive and tensile. In direct modelling where similar materials are used in model and prototype construction, the stress factor can be made equal to unity. The properties of the model will then be more simply related to the prototype as follows :

$$\delta_m = \frac{1}{\lambda_\ell} \delta_p \qquad \text{--- Eqn. 5.8}$$

$$\sigma_m = \sigma_p \qquad \text{--- Eqn. 5.9}$$

$$E_m = E_p \qquad \text{--- Eqn. 5.10}$$

$$\rho_m = \lambda_\ell \rho_p \qquad \text{--- Eqn. 5.11}$$

and

$$W_m = W_p \qquad \text{--- Eqn. 5.12}$$

$$P_m = \frac{1}{\lambda_\ell^2} P_p \qquad \text{--- Eqn. 5.13}$$

$$M_m = \frac{1}{\lambda_\ell^3} M_p \qquad \text{--- Eqn. 5.14}$$

5.4 Test Slabs

5.4.1 Shape and Dimensions

Within the constraints imposed, a 1/6.67 scale model was deemed to be satisfactory for the present investigation. The choice of this model scale had largely been dictated by the availability of a rubber bag which could conveniently provide pressure to simulate uniformly distributed loading over an area of 1.5m square. By direct geometrical scaling all test slabs were therefore made 1.5m square with 300mm wide edge beam added to the sides in order to provide a sufficient degree of fixity to the slab during testing. The overall dimensions are shown in Fig.5.1. The thickness of all test slabs was 70mm at the surrounding edge beams and 40mm in the internal 1.5m square test panel. The span/depth ratio of 37.5 was slightly smaller than 40 in the prototype but was accepted in view of the difficulties of fixing the reinforcement frames in the test slab. A monolithic column stub 100mm square and 30mm high was cast at the centre of the panel which gave a ratio of column size to span of 0.067.

5.4.2 Range of Variables

Level of Prestress

In these tests, since the slabs were designed to crack under full service load, it was felt that a suitable basis for investigation was to partially prestressed them with medium to low levels of prestress. Accordingly, three levels of prestress were chosen, namely 1.50, 0.90 and 0.70 N/mm^2.

Calculations based on a unit width of slab with an internal test span of 1.5m and slab thickness of 40mm, with the tendon profiles shown in Fig.5.10, indicated that the average prestress obtained from twelve 2.98mm diameter wire (section 5.5.2), each stressed to 70% of its characteristic ultimate strength with 10% allowance for losses was 1.54 N/mm^2. The balanced load in the slab would be 7.11 kN/m/m width. Slabs prestressed with seven and six wires with the above tendon profiles would result in prestress levels of 0.89 and 0.77 N/mm^2 respectively. The corresponding balanced loads would be 4.15 and 3.55 kN/m/m width.

The resultant flexural stresses in the column and middle strips of the actual internal square panels, calculated from the moments caused by the total service load taking due accounts of the secondary effects and levels of prestress and expressed as a dimensionless ratio of 'Degree of Prestress' (50,51) are shown in Table 5.1.

Tendon Distribution and Arrangement

The test slabs were divided into three main series based on the average concrete prestress levels with four slabs in series A and B and two in series C. Slabs in series A were moderately prestressed and those in B and C were at low prestress levels.

The distribution of tendons in the various slabs, illustrated in Figs.5.2 to 5.6, were as follows :

Series A and B

Slabs A1 and B1 : In each direction, 50% or more of the tendons (six in A1, three in B1) were banded along the column line and the remainder evenly distributed in the middle width. This arrangement is consistent with the recommendations from Concrete Society and FIP(1980). (Fig.5.2)

Slabs A2 and B2 : The ACI-ASCE Committee 423 (1974) recommendations were adopted in which 67% (eight) and 71% (five) of the tendons in A2 and B2 respectively were distributed within the column strip (L/2) and the remainder in the middle strip in each direction. (Fig.5.3)

Slabs A3 and B3 : All the tendons (twelve in A3, seven in B3) were banded and placed as closely as possible within the column line in one direction and uniformly distributed in the other direction. This banded tendon arrangement is currently very popular in flat slabs construction due to the relative ease of the

tendon placing operations and less likelihood of crossing tendons interferring with one another during placing. The arrangement is explicitly provided in the recent ACI 318-83 Code (Clause 18.12.4). (Fig.5.4)

Slabs A4 and B4 : All tendons (twelve in A4 and seven in B4) were evenly distributed in each of the two directions. This distribution is rarely used in practice for reasons of economy; in this programme it is used as an index of comparison for the other arrangements. (Fig.5.5)

Series C

Slab C1 : All tendons (six) in each direction were banded within the column line. This support-strip method of prestressing was originally advocated by the Bureau BBR (41) in the early 1970's and had been used successfully in construction. (Fig.5.6)

Slab C2 : The prestressing tendons (twelve) were banded and placed as closely as possible within the column line in one direction whereas none was deployed in the other. This could represent the extreme use of one-way prestressing in a two-way square slab and was used to study the induced prestressing effects orthogonal to the direction of the tendons. (Fig.5.6)

Negative and Positive Non-prestressed Reinforcement

The details of non-prestressed reinforcement and its arrangement are shown in Figs.5.7 to 5.9.

From Table 5.1, a maximum tensile stress of 4.32 N/mm^2 was found to exist at the negative moment region in the column strip in series A slabs. This value was slightly greater than the allowable value of $0.45\sqrt{f_{cu}}$ recommended by the Concrete Society, hence a small amount of bonded reinforcement was required in these areas. In the positive moment region, the maximum concrete tensile stress was 0.93 N/mm^2 and non-prestressed reinforcement was therefore not needed.

Present British practice, as reflected in the Concrete Society Report required a minimum area of supplementary bonded steel over the column region equal to 0.15% of the cross-sectional area which is based on a width equal to the width of the column plus twice the slab depth on each side of the column. This is useful to control cracking and improves the overall behaviour and ductility of the slab-column connection. Thus a mat of four 3.14mm diamater mild steel wires were provided in each direction in series A slabs. (Fig.5.7) These were positioned at 35mm centres and had a total length of 500mm each.

In series B and C, the amount of non-prestressed steel in the slabs was calculated from yield-line analysis of series A slabs. A similar yield pattern was assumed regardless of the different patterns of tendon distribution, and all test slabs were designed to fail at about the same ultimate load.

Accordingly, in series B slabs (Fig.5.8), seven 3.14mm diameter wires of 500mm length each were placed at 40mm centres at

the column within the critical width as defined in Concrete Society Report (clause R 3.4.1.2). Eight 2.68mm diameter wires of 500mm length were placed as negative reinforcement across the column lines. In addition, the same diameter wires were used as positive reinforcement and were positioned at 75mm centres at the edges. Their length varied from 550 mm to 660mm and were arranged to the requirements of CP110.

Similar quantities and arrangement of non-pretressed reinforcement were used in slab C1.

In slab C2 (Fig.5.9), four 3.14mm diameter wires at 35mm centres were positioned within the column width in the direction of prestress. In the other orthogonal direction in which the prestress level was zero, ten 3.14mm diameter wires at 25mm centres were placed within the critical column width. Negative reinforcement in the column lines consisted of 2.68mm diameter wires at 75mm centres. Similar wires were spaced at 35mm centres at the N and S edges of the slab as positive reinforcement.

5.4.3 Tendon Profile

The tendon profile in a typical internal panel, shown in Fig.5.10, with maximum eccentricities at the support and at mid-span was adopted. Parabolic equations of the profile are given in Appendix 1. The point of inflection was located at a distance of 0.1L from the column centre line.

5.5 Materials

5.5.1 Concrete Mix

The mix was designed to give a grade 50 concrete according to CP110 with a compressive to tensile strength ratio of about 12. In the design of the concrete mix, it was considered essential to comply with the geometrical similitude requirements for meaningful experimental results to be obtained. The maximum aggregate size usually specified for the prototype mix is 19mm, so that with a scale factor of 6.67 the largest size aggregates would be 2.8mm. This was achieved by using coarse fraction retained by the BS1881 (1983) (52) 2.36mm sieve from zone 3 sand. The fine aggregates would consist of the fraction of zone 3 sand retained by the 2.36mm sieve. Several trial mixes were carried out and an A/C ratio of 4.5 and a W/C ratio of 0.56 were chosen. The quantities of each component for 250 kg fresh concrete are listed in Table 5.2.

All the slabs were cast in the laboratory and the actual strength obtained for each slab is given in Table 5.4.

For each mix, the concrete was proportioned by weight. The materials in the required proportions were fed into the mixer and turned over for about one minute before the required quantity of water was added. The concrete was then mixed for two minutes and then taken to the casting bed. Three different mix batches were required using the 250 kg capacity mixer for each slab. The compacting factor varied between 0.87 and 0.91.

5.5.2 Prestressing Wires

Single high strength cold drawn wires with a nominal diameter of 2.98mm were used in all test slabs. Samples of the prestressing wire were subjected to tensile tests and a typical stress-strain curve is plotted in Fig.5.11. The wires have an average modulus of elasticity of 186.0 kN/mm^2 and a minimum breaking load of 12.50 kN.

5.5.3 Non-prestressed Reinforcement

The non-prestressed reinforcement consisted of smooth mild steel wires. At the column region, 3.14mm nominal diameter wires were used whereas 2.68mm nominal diameter wires were used at the edges and across the column lines. Typical stress-strain curves obtained from tensile tests are plotted in Figs.5.12 and 5.13, in which the average 0.2% proof stress, ultimate tensile stress and modulus of elasticity are also given. The use of a larger diameter wire at the column made the task of fixing strain gauges easier and the results more reliable.

5.6 Fabrication of Slab Specimens

5.6.1 Formwork

The mould for casting consisted of a 2.5m square and 19mm thick wooden base board fixed rigidly to a trestle-type metal

base. 30mm thick 'Darvic' industrial plastic, carefully dimensioned to 1.5m square was firmly attached to the wooden base with 10mm screws. The sides of the mould were formed by 70mm steel angles, bolted to the wooden base. To form the holes through which the slab was to be fastened to the test rig, 25mm diameter metal cylinders were secured to the base in the appropriate places. The whole table was raised by concrete blocks at each corner to a height of about 600mm above the floor in order to provide access to the underside. To prevent excessive deformation during casting, the table was supported at the centre by a screw-jack. Prior to the placing of reinforcement, the table was thoroughly coated with oil.

5.6.2 Fixing of Prestressing Wires

Each wire was cut to a length of 3.5m to provide for wedging and stressing. The wires were generously greased before being inserted into a 3mm internal diameter plastic tube. This was to prevent bonding of the wire to the surrounding concrete and to reduce friction during post-tensioning. To ease the insertion of wires, the plastic tubes were cut into half lengths of 1.75m and warmed gently prior to insertion. At the centre of the wire where the two parts of the tube met, thorough degreasing and joining by rubber tape provided a continuous unbroken covering to the prestressing wire.

The vertical forms of the slab (70mm angles) were drilled with 7mm locating holes into which the post-tensioning wires were

inserted. Wires in the N-S direction were inserted first; wires in the E-W direction were inserted thereafter. All wires were arranged so that lengths of approximately 700mm were left at the stressing ends.

At this point, 2mm wedge-type grip CCL anchorages were placed at both ends of the wires and separated from the side forms by 19mm wooden cubes in order to facilitate the striking of side forms after the curing period. The wires were then held taut by applying a slight tension to prevent any possible rotation or translation.

The parabolic profile of each wire was accurately maintained by fixing the tubes at a number of points along their length. For this purpose, accurately cut wooden cubes of different heights were placed under the wires at the points of inflection (150mm from the column centre line) and at the low points 600mm from the column centre line. Fine tying wires, after looping round the tube and threading through a 2mm hole drilled through the base board at these points, were used to anchor the tube in position by twisting round a short 3mm diameter steel bar at the underside of the board. Prior to casting, 30mm concrete cubes were placed directly under the wires at the column centre lines in order to achieve the proper parabolic profile. For tendons passing directly over the column stub, 60mm cubes were used.

At the edge beams, full length 10mm diameter plastic tubes were placed concentrically to provide ducts for the 7mm pre$_{A}^{S}$tressing wires. These wires were later stressed to the force

necessary to minimise the reduction of prestress in the test panel by the stiffer frame formed by the edge beams. Completed non-prestressed reinforcement frames are shown in Plates 1,2 and 3.

5.6.3 Fixing of Non-prestressed Reinforcement

The column reinforcement was firmly attached to the plastic tubes by means of spring clips. Negative reinforcement along the column lines was fixed to a number of orthogonal wires which were in turn supported by propping stools. To prevent lateral movement, each stool was tied to the nearest prestressing wire. (see Plates 4 and 5)

Positive reinforcement at the panel edges were arranged in rectangular mats and each wire was allowed an anchorage length of 100mm into the edge beam. In slab C2, the positive reinforcement was arranged predominantly in the N-S direction. (see Plates 6 and 7)

To secure the reinforcement mats to the base board, fine tying wires were used at appropriate places by a process similar to the fixing of prestressing wires. All reinforcement had a design concrete cover of 5mm.

Four full length mild steel bars of 6mm diameter were provided at the four edge beams. In addition to these bars, a steel cage fabricated from nine 6mm diameter steel links were placed at the corners of the edge beams to control spalling, chipping or cracking at the time of stressing.

5.7 Casting Procedure

For each test slab, three separate batches of concrete were required. Concrete from each batch was carefully placed in the mould in two separate stages after each of which stage full compaction was ensured by vigorous vibration. The vibrator was mounted on a metal trestle and was moved slowly across the top of the mould. After the final batch of concrete had been placed and compacted, the slab surface was tamped and trowelled to give a smooth finish. Five hours later, it was covered with damp hessian and polythene sheets for curing.

From each batch of concrete, four 100mm cubes, two 150mm * 300mm cylinders and three 100 * 100 * 500mm prisms were cast. In addition, four 50mm cubes, two 75mm * 150mm cylinders and two 50 * 50 * 250mm prisms were also cast in order to assess the scaling effect. All control specimens, excepting the larger prisms and cylinders, were put on top of the slab and exposed to similar curing conditions. The larger cylinders and prisms were placed on the floor adjacent to the slab and covered with damp hessian and polythene sheets and checks were made daily to ensure that the hessian remained damp. Each slab was cured for ten days.

5.8 Testing Apparatus

5.8.1 Test Rig

The rig used to test the slab was a specially built steel grillage structure shown in Fig.5.14. It consisted of two I-

section steel joists in each direction and was assembled by continuous welding along the lines of contact.

Holes were drilled and tapped along the outer and inner rims of the rig in order to receive the 20mm diameter high-tensile fastening bolts. Due to the nature of the testing, it was necessary to provide a 250mm deep concrete block, cast-in-situ, inside the test rig to use as supporting face for the rubber pressure bag. The concrete used was grade 30 and ready mixed.

5.8.2 Method of Loading

A complete uniformly distributed load was achieved by using a 1.5m square rubber pressure bag attached to the departmental compressed air system. The amount of air delivered was regulated by using step-down valves (Fig.5.16) and measured using a 100mm Schaffer Diaphragm pressure gauge which has a ±1% sensitivity over a range of 0-400 mbar (0-40 kN/m^2). The gauge was connected to a system of three needle valves to enable combinations of inlet, outlet and isolated air pressure to be read to the nearest 1.0 kN/m^2.

In consequence of using the above system of distributed loading, the slab had to be tested in an inverted position and only one surface was visible. As the invisible bottom surface was of primary importance in the observation of cracks formation, this was felt to be a disadvantage.

The equivalent column reaction was applied by using a hand-

operated 10-ton capacity hydraulic jack. An accurate determination of this column reaction could be obtained from a 100-kN steel proving ring placed between the hydraulic jack and the column stub. Fig.5.17 shows the calibration graph for the proving ring. Using a system of two needle valves (Fig.5.16), the hydraulic pressure inside the jack could be easily reduced or maintained to a high degree of accuracy. A complete test setup is shown in Plate 8.

5.9 Lifting and Positioning of Test Slabs

The slab was lifted after 14 days from the casting mould. For lifting purposes, four 25mm diameter solid metal cylinders with a central threaded hole were cast into the corners of the slab. Prior to lifting, all side forms were struck and the fine wires used to keep the prestressing steel in position were cut. Any sharp protrusions on the top surface of the slab were ground off in order to protect the pressure bag. By means of lifitng hooks bolted to the metal cylinders, the slab was lifted from the mould by the overhead electric crane and rested on the floor at its four corners on temporary improvised supports. By gradual lifting at two corners, the slab was slowly overturned.

Before placing the slab on the rig, a layer of cement grout, sandwiched between two plastic sheets, was uniformly applied over the edges of the rig to act as bedding material.

5.10 Instrumentation

5.10.1 Dynamometer

To monitor stress changes, a number of dynamometers, one at each end of the prestressing wire, was used. The dynamometers, each 100mm long, were fabricated from 28mm outside diameter extruded duralamin tubes with an average wall thickness of 1.5mm. To eliminate the necessity of allowing for accidental eccentricity, centralizing mild steel collars were used.

The middle portion of each dynamometer was smoothed using fine grain emery paper and cleaned using Butanone. Two TML PC10 electrical resistance strain gauges were fixed, one on opposite sides, to the prepared surfaces using M-Bond AE-10 adhesive resin. The gauges were left to cure under a uniform pressure applied by a specially machined split barrel and clamp. After the initial curing period, the gauge leads were soldered to plastic-coated wires to form a full self compensating bridge circuit. The gauges were then protected by using M-Coat D (air drying Acrylic coating) and two-part M-Coat G.

Each dynamometer was connected via a Plessy 7-pin plug to the Intercole Compulog IV data logging system and was calibrated before every test. A typical calibration graph is plotted in Fig.5.18. The separate components and overall dimensions of the dynamometer are also shown in the figure.

5.10.2 Non-prestressed Reinforcement

Prior to mounting the electrical resistance strain gauges, a position 50mm from the centre of the 500mm long mild steel wire was smoothed by emery paper. The surface was cleaned using Butanone and a 2mm gauge length TML PL-2 strain gauge was fixed by using super-glue. The strain gauge leads were soldered to the connecting PTFE wires and then waterproofed using the M-Coat D and two-part M-Coat G. The finished product was left to cure and prior to placing in the slab, a thin coating of rubber bituminous paint was applied over the waterproofing to ensure further protection against moisture penetration.

5.10.3 Strain Measurement on Concrete Surface

Strain measurements were made on the slab surface by means of electrical resistance gauges and a demountable mechanical (Demec) extensometer. The results obtained from the latter were not satisfactory, however, because of the large gauge length/slab depth ratio and the relatively low sensitivity. They have, therefore, been disregarded.

The surface of the slab in contact with the pressure bag was instrumented by a number of two-directional 20mm TML PL20 and unidirectional 60mm PL60 strain gauges. Due to symmetry, only a quarter of the slab surface was monitored. Efforts were concentrated along the column centre lines with additional gauges placed at the edges and centre of the quarter panel as shown in

Fig.5.19 and 5.20.

To observe and detect initial cracking load, 4 TML PL60 gauges were arranged and fixed in directions perpendicular to the column perimeter and in such a manner any negative cracking at the column would take place within the 60mm gauge length, an arrangement which proved successful in testing. (see Fig.5.19)

In series B and C slabs, strain gauges were also used on the visible side of the slab and were fixed in both position and direction corresponding to a number of gauges at the bottom surface. The layouts of these gauges are shown in Figs.5.21 and 5.22.

Before mounting the gauges, the slab surfaces were allowed to air-dry for at least two days. Grid lines were marked and areas in which the gauges were to be placed were rubbed down with emery papers and air-vaccumed to remove any loose aggregates and dust. A thin coat of two-part quick setting Araldite epoxy resin was applied and after a day of curing, was rubbed down to a smooth surface. The gauges were fixed by super-glue adhesive.

All gauges were connected to the Intercole Compulog IV data logging system by Plessy plugs.

Both surfaces of the slab were whitened with paint to ease the detection and tracing of cracks during and after testing.

5.10.4 Deflection

The deflected profiles of the slab were measured along one of the column centre lines and also along a quarter panel line using 'Baty' dial gauges with a resolution of 0.025mm. At the edges, finer resolution gauges of 0.0025mm were used. All dial gauges were mounted by magnetic stands on to a rectangular steel section bridge which spanned the slab at a distance of approximately 250mm from the centre line of the panel. Each end of the bridge was fixed to a set of two restraining high tensile bolts by means of a steel plate and a G-clamp device. A complete setup is shown in Plate 8 and the positions of dial gauges are shown in Fig.5.23.

5.10.5 Crack Detection and Measurement

During testing, the formation of cracks was observed by a hand-lamp and their widths measured by an 'Ultra-LOMARA 250b' microscope with magnification of 40 and resolution of 0.02mm.

After testing, the slab was turned over and cracking patterns on the bottom surface were traced and photographed.

5.11 Slab Post-tensioning

Before post-tensioning, the slab was thoroughly checked for possible hair cracks. Only in C1 was a fine-hair crack observed on the top surface of the slab. This was caused by a slipping accident at the moment of transferring the test slab to the rig.

The crack did not close up and neither did it propagate during post-tensioning.

Edge channels (Fig.5.15) were placed and holding bolts were inserted and slightly hand-tightened to allow for in-plane contraction of the slab to take place during stressing. Dial gauges were placed at predetermined positions. The column hydraulic jack was adjusted and locked in position so that any upward movement of the column during stressing could immediately be registered by the proving ring and by dial gauges placed next to the column stub. Adjustment was then necessary to bring back the slab to its initial position. By these means, possible cracking was prevented on the top surface of the slab.

All prestressing wires were stressed from the West and South ends of the slab. The stressing started from the centre wires and proceeded outwards and only two wires were stressed at one time in each direction.

The anchorages used were of the wedge-type grip and supplied by CCL for stressing 2mm diameter wires. The wedges did slip on several occasions but were very effective considering the number of reuses (about four times) to which each was subjected. Stressing device was the CCL mono-wire hydraulic jack.

First, 6mm thick steel bearing plates and anchorages (together with dynamometers at monitored wires) were positioned at the dead ends of stressing and wedges were pushed home by tapping. At stressing ends, similar bearing plates and anchorages were

inserted. The prestressing wire was then taken through the stressing jack and anchored at the end of the ram by a second anchorage. Concrete surface strains and deflections were taken before stressing and readings from the dynamometers were taken prior to stressing individual monitored wires. Each wire was stressed to 80% of its characteristic strength in order to off-set the frictional losses over the wire length and slip losses of the wedges. At the required stressing force, the hydraulic gauge reading and wire elongation were checked and noted. For wires monitored by dynamometers, the force was further checked by using the dynamometer calibration graphs. When the correct force was achieved, the first anchorage wedge was pushed home against the slab and the jack retracted and the whole assembly moved to the next stressing point. Occasionally, restressing was required to correct unacceptable losses due to wedge slipping. The post-tensioning operation took between three to five hours to complete.

The stabilised initial prestressing force in the wires obtained by dynamometers varied from 7.12 kN to 8.36 kN with frictional losses varied from 5.5% to 8.4%. The total losses due to time-dependent effects over the test period was minimal and within 1.5%. Table 5.5 summarises the prestressing operations and the average concrete prestress obtained in all test slabs.

5.12 Clamping of Test Slabs

The clamping operation was carried out immediately after post-tensioning by tightening the 20mm diameter high tensile bolts

using a torque wrench. The operation was divided into three stages and at each stage, bolts at the outer rim were tightened first followed by those in the inner rim. A consistent centre-to-outwards tightening procedure was adopted.

By adjusting the column hydraulic jack after every stage of clamping, a zero relative movement of the column was maintained thereby preventing any accidental cracking on the top part of the slab. In addition, concrete surface strains were also constantly checked at critical sections to ensure the resulting stresses at these regions remained below the concrete tensile strength.

After clamping, the final residual column load obtained for 'zero' displacement of the column was kept constant at the column stub prior to any testing. The residual column loads are shown in Table 5.5.

5.13 Testing Procedure

All test slabs were loaded to the service load of 11.0 kN/m^2 under which all were cracked. The load was then reduced to zero. In series A slabs, the loading was continued in the second cycle from zero up to failure; whereas in series B and C slabs, a further cycle of loading to service load was carried out before loading to failure in the final third cycle. Each test took 5 to 6 hours to complete and two days were needed to complete the whole sequence of testing. All tests were carried out a day after post-tensioning.

Before commencing the test, strains and deflection readings were taken at the residual column load level. The slab was then loaded to twice its residual column load and a further set of readings were noted. It was then returned to its initial position before actual testing commenced. This procedure was necessary in order to

(a) extrapolate from the readings the initial prestrains

(b) cancel the 'drifting' effect of resistance strain gauges during subsequent test cycles

The errors due to residual strains from this preliminary loading were negligible since the maximum residual column load was about 3.39 kN which was insufficient to cause flexural cracking at the maximum moment regions. The slab could be expected to behave elastically.

Air pressure load was then applied in steps of 1.0 kN/m^2 and a stabilizing column reaction for each pressure load increment, calculated to be 2.25 kN over the total slab surface area, was subsequently applied by the hydraulic jack. The procedure was repeated thereafter. During unloading, the column load was gradually removed while bleeding of the air from the pressure bag was carried out simultaneously. Deflection and strain readings were taken at regular intervals. The load-deflection relationship was continuously plotted throughout the test. The cracking load was recorded and widths of cracks, if any, were measured at selected service loads.

All slabs, with the exception of C1 and C2 were tested until punching of the centre column occurred. Since after punching the cracking pattern could not be fully traced, the slabs C1 and C2 were loaded to a little less than their ultimate flexural loads.

Detailed observations and results are presented in Chapter Eight.

5.14 Testing of Control Specimens

The testing of control specimens was carried out the day after completion of testing of each slab. The properties for the test series are shown in Table 5.4.

For the smaller specimens, a scaled down loading rates were used, shown in Table 5.3, as it is generally recognised that an increase in the rate of loading will result in higher strength. All tests were carried out in accordance with BS 1881 (1983).

CHAPTER SIX

Limitations of Experimental Test Slabs

6.1 Basic Assumptions

As mentioned in Chapter Three as well as in Chapter Five, the loading arrangement used in this investigation of a typical internal panel under uniform load is to apply a simultaneous opposite column reaction equal to the total load on the panel surface.

The assumptions are based on the overall requirements of equilibrium. Neglecting the finite widths of supports, for any uniformly loaded span with a width defined by lines of zero shear, as shown in Fig.6.1, then

$$\int_{-b/2}^{+b/2} M_y \, d_x + \tfrac{1}{2}\left(\int_{-b/2}^{+b/2} M_{1y}' \, dx + \int_{-b/2}^{+b/2} M_{2y}' \, dx \right) = \tfrac{1}{8} W b L^2 \qquad \text{--- Eqn. 6.1}$$

where M_y is the positive moment per unit width at mid-span in the Y-direction

M_{1y}' and M_{2y}' are the negative moments per unit width at support lines 1 and 2 and

W is the uniform load on the panel

The integrals are for the full width. A similar equation can be written for X-direction moments. The total positive and negative moments across the panel width in any one direction can be simply obtained from an encastered beam subjected to

simultaneous uniform downward load over the whole span and at the centre, an upward reaction whose magnitude is equal to the total load on the span as shown in Fig.6.2a. These moments can be calculated using the well-known equations of

$$+ve \qquad M = \frac{WL^2}{24} \qquad \text{--- Eqn. 6.2}$$

$$-ve \qquad M = \frac{WL^2}{12} \qquad \text{--- Eqn. 6.3}$$

For prestressed slabs a similar argument can be applied; the uniform load being replaced by upward and downward reactive loads from the convex and concave part of the tendon profile respectively as shown in Fig.6.2b. Where tendons are symmetrically draped about the mid-span and are horizontal at the column centre lines, the total upward reaction is equal to the total downward reaction and hence no resultant column reaction is induced. The induced positive and negative moments at the support and at mid-span are give by

$$+ve \quad M_p = \frac{2}{3} P\, e_{OB}\, (1 - \beta)(1 - \lambda) \qquad \text{--- Eqn. 6.4}$$

$$-ve \quad M_p = \frac{1}{3} P\, e_{OB}\, (1 - \beta)(1 + \lambda) \qquad \text{--- Eqn. 6.5}$$

where P is the total prestressing force or force per unit width across the panel width in question. e_{OB}, λ and β are defined in Chapter Three section 3.3.1.

The basic equilibrium requirements expressed by equations 6.1 to 6.5 are respected in each direction and the total moments in both orthogonal directions are independent of one another.

6.2 Deformation Characteristics of Internal Panel and Experimental Test Slab

Eventhough overall equilibrium requirements can be easily obtained in a single-panel test slab, it will be difficult to represent precisely the behaviour of an internal panel. In the experimental work, the condition of zero rotation along the lines of zero shear of the internal panel is achieved by rigidly attaching the broad edge beams to the test-rig. It can be appreciated that such a testing arrangement will directly impose in the slab an extra degree of rigidity or stiffness. The moment fields in the slab will therefore be somewhat different to that of an actual internal panel, though the major characteristics of behaviour are represented.

To illustrate this point it is useful to consider briefly the deformed surface of an internal panel under uniform and prestress loading.

6.2.1 Uniform Loading

Fig.6.3 is a schematic sketch of the deformed surface of an internal panel supported by point or finite size columns. Under uniform load, the mid-span point of the column centre line will deflect vertically downwards by a small amount a_c. In the centre of the panel in addition to a_c, there will be a further deflection

of a'_m due to the flexibility of the surrounding column lines in both directions. Along the column centre lines and lines of zero shear, the slope will be zero.

In the test slab, the clamping of the edges to give a zero slope can only be achieved at the expense of preventing free deformation from occurring in the direction of the edges. Consequently, the total deflection a_m at the centre of the panel is reduced to a_c. A degree of stiffness is therefore introduced into the test slab, the effect of which is related to the difference between a_m and a_c. The ratio of this difference with the original deflection a_m will indicate the overall accuracy of the test slab in reflecting the behaviour of the internal panel. However, it should be emphasised that at the mid-span point on the column centre line, the deflection a_c relative to the column remains unaffected in the slab and hence the longitudinal moment surface at a section through this line will be identical to that in the internal panel. It is, therefore, justifiable to employ the proposed experimental model in studying the flexural behaviour of a square panel as the positions of maximum positive and negative moment occur on the column lines in both directions are accurately reflected in the test slab.

Fig.6.4 shows the comparison of deflection contours between the test model and an internal panel under similar uniform load. It can be observed that within a circle centred on the column with a radius of L/2, the deflection profiles in the test slab satisfactorily reflect those in the internal panel.

6.2.2 Prestress Loading

As mentioned earlier in Chapter Four section 4.4.2, the amount of deformation produced in an internal panel under prestressing loads is dependent upon the distribution of prestressing tendons in the column and middle strips. For a given number of tendons, due to the intrinsically 'heavier' prestress loads on the column strips as a result of higher concentration of tendons, the differential deflection at the centre of the panel and the mid-span point on the column centre lines will be lower in slabs with column-strip tendon distribution and higher in those with uniform distribution. The effect of the restraints of the testing arrangement on the deformation due to prestress will, therefore, depend upon the manner in which the tendons are distributed, and will be smaller in slabs with a higher proportion of tendons in the column vicinity.

Table 6.1 summarises the actual elastic deflections a_c and a_m in an internal panel due to prestress loading; the designation corresponds to each test slab with identical prestressing intensities and tendon distribution. Table 6.1a only includes those slabs with a symmetrical tendon arrangement in both directions and Table 6.1b, those with an unsymmetrical arrangement. It can be observed that the ratio of the difference between a_m, a_c and a_m ranges from 0.26-0.32 in slabs A1, B1, A3, B3, in which column-line distribution of tendons is used. Higher ratios of 0.39 and 0.36 are found in slabs A2 and B2 respectively

and in slabs A4 and B4 with uniform tendon spacing the ratio is 0.5 each. There is an uneven distortion in slab C2 and consequently the distribution of moments will be considerably different from the corresponding internal panel. In slabs where column-strip and uniform distribution of tendons are used, the extent of the discrepancy in the test slabs with respect to their actual internal panels will be higher than in those prestressed with column-line distribution; the discrepancy being related to the ratio. Ratio of unity indicates complete conformity with an actual internal panel.

6.3 Elastic Moment Distribution in Internal Panel and Experimental Test Slab

Numerical integration has been carried out across each strip in the internal panel, as defined by CP110, using Simpson's rule and the total panel moment calculated. The individual strip moments have been expressed as a percentage of the total panel moment for the direction considered; their derived moment coefficients are given in Table 6.2. The panel results under uniform load, as shown, agree closely with CP110.

The strips and total panel moment in the experimental slab, expressed as a percentage of their internal panel values, are shown in Table 6.3. In the column strip, in general, there is a reduction of positive strip moment in the negative moment region in each test slab, amounting to about 8% to 10% in slabs A1, A3, B1, B3, C1 and 14% to 19% in slabs A2, A4, B2, B4, and an increase

of negative strip moment of 16% to 18% in slabs A1, A3, B1, B3, C1 and 19% to 22% in A2, A4, B2 respectively in the positive moment region.

In the middle strip, a high reduction of strip moment is obtained in both negative and positive moment regions. These results are expected as the strip is near to the restrained edge.

The total moment in the experimental slabs shows an overall reduction compared with their respective internal panels. The proportion of reduction in each slab is very similar to the ratio given in Table 6.1. This difference in total moment represents the moment that has been absorbed by the restrained edges of the test slab.

It may be misleading to determine the accuracy of the test models only by comparing the strip moments with their internal counterparts as no indication is given of their actual distribution. In order to do this, the theoretical elastic moment fields in both longitudinal and transverse direction in the experimental test slabs and in their corresponding internal panels are shown in Figs.6.5 to 6.11. Fig.6.5 shows the moment fields under conventional uniform load. For slabs A1, A2, A3, A4, C1, C2 the prestressing moment fields are shown in Figs.6.6 to 6.11 respectively. The moment fields in series B slabs bear similar resemblance to those in series A and are omitted for clarity. The actual moment distribution under experimental conditions are seen to compare well with their respective internal panels, although slight variations are found in slabs A2, A4, and C2 as shown in

Figs.6.7, 6.9 and 6.11 respectively. The longitudinal and transverse moment surface in the two orthogonal directions for all the slabs are also plotted in Figs.6.12 to 6.17. The analysis using a line load representation of the transverse prestressing effects along each tendon length is included to compare with the normal method based on uniformly loaded areas. The former is referred to as finite plate analysis 2 and the latter finite plate analysis 1. There is very little difference between results obtained with these two methods of representation.

In graphs (a1) and (b1) in all the above figures, where longitudinal moments along the column centre line in both directions are shown, with the exception of slab C2 (Fig.6.17), there is an almost perfect duplication of those produced in the internal panel. The maximum positive and negative prestressing moments are thus preserved in the test slab under laboratory conditions. In graphs (a2), (b2) in all the figures where the transverse moment distribtuion is shown, again across the column centre line in both directions, reasonable agreement with those in the internal panel is obtained within the column strip width (L/2).

6.4 In-plane Prestress Distribution in Experimental Test Slabs

Possibly the greatest difficulties in using a single panel test slab to simulate internal panel behaviour is its inability to allow full distribution of in-plane prestress from the anchorage ends. This could well exaggerate the prestressing effects under

flexure especially in slabs with column-line prestressing. In a post-tensioned slab, the average prestress in a multi-span structure is governed by the total prestressing force per bay and due to the very large stiffness of the slab in its own plane, the in-plane prestress in an internal panel is not seriously affected by the concentration of tendons in the vicinity of a column and may be assumed to be uniformly distributed and therefore equal to the average value.

The actual distribution of in-plane prestress for each test slab is shown in Figs.6.18 to 6.23 for slabs A1, A2, A3, A4, C1 and C2 respectively. Again the distribution in series B slabs is omitted. The experimentally obtained average prestressing force is used in the finite element analyses and applied as a single in-plane point load at the far end of the edge beams at the appropriate tendon anchorage positions. The in-plane prestress contours in each direction are shown in graphs (a) and (b) in the figures. The distribution across the middle section of the panel and across the edges in each of the two directions are plotted in graphs (a1), (a2) and (b1), (b2) in all the figures respectively. The average value of prestress based on gross sectional area is also included for comparison purposes.

It can be observed from Fig.6.18(a1) and (b1) that despite the concentration of tendons in the column lines in slab A1, the in-plane prestress is practically constant within the column strip width. In slab A3, in Fig.6.20(a1), an increase of about 37% of average prestress is noted in the middle section transverse to the

direction of banded tendons. A similar increase is also observed in Fig.6.23(a1) for slab C2. For the rest of the slabs, the in-plane prestress is very nearly uniform in the middle section within the column strip width. At the edges, there is predictable increase in in-plane stresses around the region of banded tendons as shown in graphs (b1) and (b2) in all the figures.

In slab C2, in the middle section parallel to the direction of banded tendons, positive tensile stresses are induced as shown in Fig.6.23(b1). However, the magnitude is small being about 0.3 N/mm^2 at the column region and 0.8 N/mm^2 towards the edges.

CHAPTER SEVEN

Yield Line Analysis of Test Slabs

7.1 General

The yield line analysis of concrete slabs developed by Johansen is a method of determining the limit state of collapse by considering the yield lines or hinges which occur in the slab as a mechanism forms. All deformations are assumed to be concentrated at the yield lines and elastic displacements are neglected. The slab is assumed to remain rigid in regions between yield lines which act as axes of rotation for the movements of the various segments in the mechanism. Full moment redistribution is assumed and the yield lines are assumed to be capable of undergoing large rotation under progressive loading without increasing the moment. The idealized moment-curvature relationship may be plotted as shown in Fig.7.1.

For the purpose of analysis, a collapse mechanism is assumed. The direction and position of the yield lines forming the mechanism will depend primarily on the loading and boundary conditions of the slab and in general are defined by certain parameters whose values can be found by a differentiation process in which either the bending moments acting along the yield lines are maximised or the collapse load is minimised.

7.2 Ultimate Moments of Resistance

Once a yield line mode for a valid mechanism has been postulated, it remains to determine the values attributed to the ultimate moments of resistance about the various yield lines.

It is assumed that all of the reinforcement crossing a yield line is yielding and the yield moment in one direction is quite independent of the yield moment given by the reinforcement at right angles. The effect of compression reinforcement is generally neglected, since for an under-reinforced section, it has little influence on the section strength. Where the yield line is not normal to the direction of the reinforcement, it is further assumed that the reinforcement crossing that yield line must remain straight, i.e. no kinking. The ultimate moment of resistance about the yield line is assumed to be given by the components, normal to the yield line, of the ultimate resisting moment in the direction of the reinforcement.

Thus if m_x and m_y are the ultimate moments of resistance per unit length in the reinforcement directions, see Fig.7.2, then the ultimate moment of resistance of yield line AB is given by

$$m_n AB = m_x BO \cos\alpha + m_y AO \sin\alpha$$

$$m_n = m_x \cos^2\alpha + m_y \sin^2\alpha \qquad \text{--- Eqn. 7.1}$$

7.3 Virtual Work Method

The yield line approach permits two methods for calculating

the collapse load, the energy or virtual work method and the equilibrium method. The latter involves the setting up of equilibrium equations of the rigid regions between yield lines using nodal forces. Special procedures are needed in certain circumstances (53), and in general, the straightforward nature of the work method is preferable for calculating the collapse load.

In the virtual work method, it is assumed that there is no loss of energy and displacements are small. The initial step in the analysis is to determine a valid mechanism by which the slab is to collapse under ultimate load. A suitable yield line pattern is postulated and knowing the reinforcement in the structure, the ultimate moments of resistance along the yield lines can be calculated using ordinary reinforced concrete theory. Correspond to this yield line pattern, the collapse load is determined by equating the work done by external load on the slab to the internal energy dissipation in all the yield lines acting together.

In general, the external loss of work is caused by the slab deflecting through a virtual displacement. A point, normally on a yield line is given an arbitrary unit displacement δ and displacements and rotations of the other parts of the slab can then be expressed in terms of this unit displacement. The loss of work due to the displacement of the load is then given by

$(W\,\delta)$ = (Total load) * (Vertical distance the load has moved through) --- Eqn. 7.2

The work absorded by the yield lines can be expressed by

$(M_n\theta_n)$ = (Total moment acting along the yield line) *

(Rotation of the yield line) --- Eqn. 7.3

For an orthogonal arrangement of reinforcement in the X and Y axes, equation 7.3 can be further written as follows: (referring to Fig.7.2)

$$\sum_{1}^{i} (M_n\theta_n) = \sum_{1}^{i} (M_x\theta_x) + \sum_{1}^{i} (M_y\theta_y)$$

$$= \sum_{1}^{i} (m_x L_x\theta_y) + \sum_{1}^{i} (m_y L_y\theta_y) \quad \text{--- Eqn. 7.4}$$

where L_x, L_y are the projected lengths of L_n on to X and Y axes respectively

θ_x , θ_y are the components of θ_n about the X and Y axes

By taking a series of yield line patterns, different values of the ultimate load can be obtained, the lowest being the correct solution.

7.4 Application of Yield Line Theory to Post-tensioned Slabs with Unbonded Tendons

As mentioned earlier, one of the prerequisites for the perfectly plastic behaviour at the yield lines is that the reinforcement must have a definite yield point, capable of sustaining the yield stress up to several times the elastic strain at first yield. The stress-strain curve of prestressing tendons, however, does not usually show such characteristics. At ultimate

load, unlike the ordinary non-prestressed reinforcement, yielding of post-tensioned unbonded tendons may not happen; the flexural failure of the slab being precipitated by the crushing of the concrete at the compression face following large deformation with little increase in load.

Provided punching shear resistance is adequately provided for, under-reinforced post-tensioned slabs generally exhibit a large degree of ductility at failure as indicated by experiments (8,9,10,13,15,16,17,54). This ductile behaviour has encouraged many reseachers in the field of prestressed concrete to use yield line theory to predict the ultimate load of the prestressed slab. Some of the previous works are summarised as follows :

Scordelis et al (8,9) reported satisfactory use of yield line theory in determining ultimate load in two-way prestressed slab with unbonded tendons.

Gamble (10) supported the use of yield line theory in a report of a slab tested in Australia, although the slab did not actually fail in flexure such as to permit comparison with test results.

Nawy and Chakrabarti (13) similarly used yield line theory to predict the failure load of their model prestressed slabs and obtained satisfactory results.

Burns et al (15,16,17) computed the ultimate failure load from the observed failure mechanisms for three two-way multi-panel post-tensioned prestressed slabs and obtained good correlation

with observed test values when the actual amount of column non-prestressed reinforcement was taken into account.

More recently, Okafar and Perry (54) concluded, after considering the post-yield behaviour of bonded prestressed slabs, that yield line theory gives better results for under-reinforced prestressed slabs than ordinary reinforced concrete slabs. The reason for this was that the slab elements of prestressed slabs bounded by yield lines approximated more closely to the rigid-plastic behaviour assumed in the yield line theory than those of ordinary reinforced concrete slabs.

7.4.1 Tendon Stress Increase at Ultimate Load

For the analysis of unbonded post-tensioned slabs CP110 has certain recommendations regarding the stress increase in the prestressing tendons at ultimate load. Table 38 in the code provides data for unbonded tendons which gives the stress in the tendons at ultimate as a proportion of the effective prestress, and the depth of compressive block as functions of $(f_{pe}A_p)/(f_{cu}bd)$ and (L/d), where L is the effective span. The tabulated values assume that the effective prestress after all losses have occurred does not exceed $0.6f_{pu}$. In the tabulated values, the maximum value of L/d quoted is 30 and a 23% to 11% increase in tendon stress at ultimate is estimated for a prestressing index of 0.025 to 0.02 respectively.

For unbonded tendons, the ACI (318-77) code provides the formula

$$f_{pb} = f_{pe} + 68.9 + \frac{f_c'}{100\rho_{ps}} \text{ N/mm}^2 \quad \text{--- Eqn. 7.5}$$

with f_{pb} being restricted to be not greater than f_{py}, nor (f_{pe}+ 414) N/mm^2. f_{py} is the specified yield strength of the tendons. The above equation is based on beam tests for specimens with a maximum span to depth ratio of 28. Increase of about 38% to 10% in tendon stress are indicated for the prestressing index of 0.025 to 0.02 respectively.

Some of the recent tests on thin slabs with unbonded tendons (6,7,15,16,17), however, indicated that the values given by the above ACI formula as well as from CP110 Table 38 overestimate the amount of stress increase in tendons at ultimate load. In their multi-panel one-third scale model slabs, Burns and Hemakom (15,16) reported an increase in tendon stress at failure of between 2%-13%. In separate single panel tests with carefully simulated internal panel boundary conditions, Long and Franklin (7) obtained a maximum tendon stress increase of the order of 10%. It thus appears that the use of the present CP110 Table 38 values and the ACI 318-77 formula for predicting the tendon stress increase at failure would be unsafe as span to depth ratio greater than 30 are usually adopted for relatively thin slab construction.

In the light of this experimental evidence, the recent ACI 318-83 code has restricted equation 7.5 to members with span to depth ratio of 35 or less and for members with greater span to

depth ratio, the formula is modified to

$$f_{pb} = f_{pe} + 68.9 + \frac{f_c'}{300\rho_{ps}} \text{ N/mm}^2 \quad \text{--- Eqn. 7.6}$$

and f_{pb} is restricted to be not greater than f_{py}, nor $(f_{pe} + 207)$ N/mm^2.

BS8110, the successor of CP110, however, adopts a general equation for estimating the unbonded tendon stress at ultimate. Unlike the American approach, this method is assumed to be valid for all values of L/d.

$$f_{pb} = f_{pe} + \frac{7000}{L/d}\left(1 - 1.7\,\frac{f_{pu}A_p}{f_{cu}bd}\right) \quad \text{--- Eqn. 7.7}$$

and f_{pb} is restricted to be not greater than $0.7f_{pu}$.

Fig.7.3 shows a comparison of the different approaches. It is apparent that the methods diverge considerably at low effective prestress indices $\frac{f_{pe}\rho_{ps}}{f_{cu}}$.

In view of the lack of a general equation for predicting the stress in the prestressing tendons at ultimate load with sufficient accuracy, an estimate based on values recorded in various tests is used in the flexural strength analysis of the slabs. Detailed discussion of the tendon stress at ultimate will be covered in Chapter Eight.

7.5 Flexural Strength of Test Slab

7.5.1 Modes of Failure

Fig.7.4a shows the general collapse mechanism of a fixed test

slab subjected to uniform loading over the slab surface together with a simultaneous equivalent column reaction applied opposite to the direction of the uniform load. The effect of post-tensioning is assumed to be evenly spread in both directions at the ultimate stage. The square slab is assumed to fail by an overall flexural mechanism arising from the yield lines which radiate from the column perimeter and extend to the edges of the slab, ending with straight cut-off fans at the corners. The yield lines are assumed to be symmetrically disposed and hence only one quarter of the test slab needs to be analysed.

The moments of resistance of yield lines (Fig.7.4a) AG, CG and CE are designated as $p_1 m$, $p_2 m$ and $p_3 m$ respectively where m is the moment of resistance of the positive yield line BC at the edges of the slab.

To calculate the collapse load, the work method is used. The edges of the slab are assumed to undergo a virtual unit displacement relative to the centre column. The rotations and displacements of the various segments bounded by the yield lines are shown in Fig.7.5.

From equation 7.2, the work done by loads for a small unit displacement of the slab is given by

$$\Sigma(W\delta) = \frac{W_u}{12} [3c(L-c) + 2(L-c)(L-c-2x) + 4x(L-c-x) + 6x^2]$$

--- Eqn. 7.8

where W_u is the ultimate collapse load.

The energy dissipated in bending in the yield lines is

determined from equation 7.4 and is given by

$$\Sigma(M_n\theta_n) = m(L-2x)\theta + p_1mc\theta + p_2m(L-c-2x)\theta + p_2m\sqrt{2}x\phi + p_3m\sqrt{2}x\phi$$

where $\theta = \frac{2}{L-c}$

$$\phi = \frac{\sqrt{2}}{L-c-x}$$

$$\Sigma(M_n\theta_n) = 2m\,\frac{L-2x}{L-c} + 2m\,\frac{p_1c}{L-c} + 2m\,\frac{p_2(L-c-2x)}{L-c} + 2m\,\frac{p_2x}{L-c-x} + 2m\,\frac{p_3x}{L-c-x}$$

$$= 2m\left[\frac{(L-2x)(1+p_2) + (p_1-p_2)c}{L-c} + \frac{(p_2+p_3)x}{L-c-x}\right]$$

--- Eqn. 7.9

From equations 7.8 and 7.9, the expression

$$W_u = f(x) \qquad \text{--- Eqn. 7.10}$$

can be obtained.

To obtain the minimum value of the collapse load, equation 7.10 will normally be differentiated with respect to x and equated to zero. However, a clearer minimisation process could be achieved by plotting the values of W_u with various values of x.

From the cracking patterns observed in the test slabs at failure (Figs.8.50 to 8.59), an alternative mode of failure involving partial circular corner fans can also be distinguished, notably in slabs using the wider column strip (0.5L) width for tendon distribution purposes. This mode will now be considered.

The yield line pattern in this mode is idealised and shown in Fig.7.6a. with the moments of resistance at various yield lines in Fig.7.6b. The same notation are adopted as for the cut-off corner mode. Referring to Fig.7.7 where the displacements and rotations of the slab are shown and together with Fig.7.6, it can be readily established that the work done by load displaced a unit displacement in the slab is given by

$$\Sigma(W\delta) = W_u \left[\frac{c}{4}(L-c) + \frac{1}{3}(L-c)^2 \tan\rho + \frac{(L-c)^2}{12}\left(\frac{\pi}{2} - 2\rho\right)\sec^2\rho + A'\right]$$

where

$$A' = \frac{1}{4}\left\{L^2 - \left[c^2 + 2c(L-c) + (L-c)^2\tan\rho + \frac{(L-c)^2}{2}\sec^2\rho\left(\frac{\pi}{2} - 2\rho\right)\right]\right\}$$

--- Eqn. 7.11

The energy dissipated at the yield lines by bending is given by:

$$\Sigma(M_n\theta_n) = 2mR_1\theta + 2p_1mc\theta + (p_2+p_3)m\alpha + 2p_2mR_2\theta$$

where $R_1 = \frac{1}{2}(L-c)\tan\rho + \frac{c}{2}$

$$R_2 = \frac{1}{2}(L-c)\tan\rho$$

$$\theta = \frac{2}{L-c}$$

$$\alpha = \frac{\pi}{2} - 2\rho$$

$$\Sigma(M_n\theta_n) = 2m\left(\tan\rho + \frac{c}{L-c}\right) + 2m\frac{p_1c}{L-c} + m(p_2+p_3)\left(\frac{\pi}{2} - 2\rho\right) + 2p_2m\tan\rho$$

$$= 2m\left[(1+p_2)\tan\rho + \frac{1+p_1}{L-c}c + \frac{(p_2+p_3)}{2}\left(\frac{\pi}{2} - 2\rho\right)\right]$$

--- Eqn. 7.12

A similar minimisation process is carried out by plotting W_u for various values of ρ.

When x is equal to zero and ρ is equal to 45°, it can be shown that the work equations of both failure modes will give the same value of collapse load.

7.5.2 Calculation of Ultimate Moments of Resistance

The moments of resistance across the yield lines can be calculated using various assumptions for the concrete compressive stress block. The one used in this analysis is based on the British code CP110 recommendation using the experimental mean strengths of concrete and steel. The ultimate moment of resistance was calculated without the material safety factors of 1.15 and 1.5 for steel and for concrete respectively.

For the test slabs, the post-tensioning tendons vary continuously along the span and hence for diagonal yield lines, the moments of resistance also vary along the line. To resolve these changing moment values, for any particular diagonal yield line an average value of moment of resistance is used. For an isotropically reinforced slab, Equation 7.1 is reduced to

$$m_n = m_x = m_y \qquad \text{--- Eqn. 7.13}$$

and hence for yield line CG in Fig.7.4b, for example, the average moment of resistance is given by

$$(m_{CG})_x = \frac{m_{x_C} + m_{x_G}}{2} \qquad \text{--- Eqn. 7.14}$$

where m_{x_C} and m_{x_G} are the moments of resistance about the X-axis at

C and G respectively

A more 'exact' evaluation of the average moment value can be determined by integrating the variable moment along CG and divided by the length. This procedure is not used in the analysis as it is likely to result in no significant difference from the above 'straight' averaging values.

7.6 Membrane Enhancement

Membrane action, which could be either tensile or compressive, has a considerable effect on the ultimate load of a slab. A classic example is provided by Ockleston who in 1952, tested a real structure and recorded collapse loads that were more than twice the values predicted by yield line theory. He identified the cause as compressive membrane action. Despite considerable research effort over the recent years, the analytical solutions developed to include this effect into the ultimate load behaviour of reinforced concrete slabs are far to complicated for used in design and depend on parameters that are difficult to quantify in actual slab systems.

In the test slab, it is anticipated that membrane action could be induced due to the restriction of the horizontal movement by the edge fixing system. The effect may occur at loads in excess of the design ultimate load when deflections become excessive. This action will subsequently increase the ultimate load of the slab and is ignored in the analysis and is simply regarded as an enhancement factor for the ultimate load. It is to

be expected therefore that in general the actual collapse loads of the experimental slabs will be higher that the design ultimate loads. This aspect will be further noted in Chapter Eight.

CHAPTER EIGHT

Experimental Results and Discussion

8.1 Introduction

In this chapter the observations made during the tests and the results of the investigation are discussed.

Ten post-tensioned square panels simulating internal panel behaviour were tested. The main variable was the tendon arrangement. The other variables were the amount of non-prestressed steel in the critical moment regions and the level of prestress. A summary of the main features of the slabs is given in Table 8.1 and a diagram showing the patterns of tendon layout is presented in Fig.8.1 in order to assist discussion of the test results.

Where appropriate, the experimental results are compared with the recommendations of the major codes of design. The replacement of the current CP110 code by BS8110 took place when the present thesis wds already at an advanced stage and since, as in the previous code, only meagre recommendations are made for the design of prestressed slabs, and there are no major alterations except for the introduction of a new approach for the calculation of the tendon stress increase at ultimate, the discussion is mainly referred to CP110. However, the new approach for tendon stress calculation in BS8110 will be reviewed.

8.2 State of Stresses Before Testing

One of the objectives of the present investigation was to devise an experimental model with imposed boundary conditions in order to reflect as realistically as possible the state of stresses in an internal panel of a multi-bay slab under the influence of prestress. The out-of-plane (bending) prestressing effect is essentially a localised action along the individual tendon lengths. In Chapter Six, it has been shown that the major characteristics of this bending effect are satisfactorily reproduced in the test model especially along the column centre lines. It has also been pointed out that there will be an unrealistic stress distribution in the test model with a higher than average in-plane prestress in some parts of the model, particularly where there is a closely banded tendon arrangement in the column region. In multi-panel slabs, the dispersion of stresses over three or more spans would be considerably greater and could be assumed to be approximately uniform. The models were therefore tested to determine the validity of representing the prestressing forces as a combination of axial stress and uniformly distributed equivalent transverse prestressing loading on the structure as discussed in Chapters Three and Four.

Unfortunately, it was not experimentally practicable to isolate the effects of the in-plane and bending components and it is therefore not always immediately obvious whether the discrepancies that arise are in the in-plane or out-of-plane

analysis. Consequently, the comparisons will be made by comparing the experimental values with the combined axial and bending effects.

In the absence of dead load, the resultant flexural stresses due to prestress in series A and C slabs are sufficient to cause cracking at the central portion of the panel. To minimise this risk, a careful programme of controlled loading on the column was carried out during and after the post-tensioning operation, as discussed in Chapter Five section 5.11. As a result direct measurement of the prestressing effect (i.e.prestrain) was not possible, and the situation was further complicated by a certain amount of drifting in the electrical gauge readings during subsequent testing. In order to overcome these problems, a simple procedure of preliminary loading prior to testing (Chapter Five section 5.13) was carried out in each slab so as to extrapolate from the results the required prestrain values.

The average prestressing force per tendon and the resultant uniform axial concrete prestress for all the slabs prior to the application of loads are tabulated in Table 5.5. The prestressing force was determined from the average value obtained by dynamometers fitted to a limited number of tendons in each of the two orthogonal directions. The concrete prestress has been calculated with the gross sectional area across the whole panel width. The average slab thickness was obtained by measuring samples of concrete at a number of locations in the panel after breaking up each slab after test. The axial prestress should

strictly have been computed using the transformed concrete section properties but the results would not have differed significantly from those based on the gross sectional area.

In all the following comparisons, tensile concrete strains are taken to be positive and the actual values of Poisson's ratio and the modulus of elasticity have been used to convert the theoretical stresses to strains.

The comparisons are made for prestrain in the longitudinal and transverse direction along one of the column centre lines, as it has been shown that the stresses here are a good representation of those in an internal panel. The prestrain distribution in an internal panel having a similar tendon arrangement is also included in the comparisons in each slab to reveal the additional discrepancies of the model. The prestrains in this case are computed by superposition of the bending and uniform axial compressive effects. Top and bottom prestrains are obtained theoretically for both the internal panel and test model using a simple computer programme. The prestrain distribution is plotted in the X-direction and bending in this direction is referred in the figures as longitudinal.

Figs.8.2 to 8.5 show the soffit prestrain in series A slabs whereas Figs.8.6 to 8.9 show the top prestrain distribution in series B slabs. Soffit prestrains in the series B slabs resembled those in series A with the values reduced by a factor of about 0.6 and are omitted. It can be seen from the above figures that, comparatively higher compressive stresses are obtained in the

column region of slabs having banded tendon arrangements, for example slabs A1 (Fig.8.2) and A3 (Fig.8.4). The resultant tensile strains (top surface) are also higher in these cases as shown in Figs.8.6 (B1) and 8.8 (B3). In all the figures, the difference between model and internal panel represents the extent to which the modelling conditions have modified the prestrain distribution. However, the general shape of the distribution is very similar. The experimental results are generally scattered about the two theoretical lines, but they tend to be closer to the test model analytical results. The trend is particularly obvious in the transverse distribution in slabs with a uniform tendon arrangement, for example slabs A4 (Fig.8.5) and B4 (Fig.8.9).

A fairly symmetrical distribution of prestress is shown from the symmetrical plot of the prestrain distribution for slabs with an identical tendon arrangement in both directions as shown in Figs.8.2, 8.3, 8.5, 8.6, 8.7, 8.9.

Figs.8.10 and 8.11 show the top and soffit prestrains in slab C1 where the tendons are concentrated within a narrow band width (150.0mm) at the column. Slight variations in the transverse prestrain (experimental) in Fig.8.10 could be attributed to the existence of a top flexural crack at the middle area of the panel in the X-direction (see Fig.8.58) which was caused by an accidental slipping in the process of transferring the slab to the test rig. It is interesting to note that the induced compressive stresses at the column are comparable to those in A1 eventhough the prestressing force is about 50% of that of A1.

Fig.8.12 shows the soffit strain distribution in slab C2 where all the tendons are placed in the X-direction with none deployed in the other direction. The influence of the model on the axial component of prestress can be clearly observed at the edges and has been faithfully duplicated by the experimental results. About 40% of the longitudinal prestress is induced in the transverse direction in the column region (Fig.8.12(b)).

From the above figures, it can be observed that in the A series slabs and to some extent in slab C2, the stresses along the edges in the model are completely unrealistic with respect to an internal panel eventhough the central portion of the model shows a fairly reasonable representation. This confirms the results discussed in Chapter Six. In the B series slabs and slab C1, the resultant stresses are comparatively small. The results obtained from these slabs under loading could be expected to give a reasonable representation of an actual panel. It can further be inferred from the experimental results that had a simpler model extending only to the line of contraflexure been used in the present test series, the probability of an exaggerated prestressing effect would have been greater.

From the preceeding discussion, it is apparent that banding of the tendons close to column region induces a comparatively high prestressing moment and hence resultant stresses which are advantageous in counteracting the bending stresses due to uniform loading. By comparison, their pre and post-cracking behaviour would be expected to be better. On the other hand compression

failures or crushing of the concrete could be an inherent danger at an edge column with a heavily banded tendon arrangement, especially when a high average concrete prestress is specified. Consequently careful attention would have to be given to the detailing of tendons and rebars at the anchorages.

8.3 Deflection at Service Load

8.3.1 General Behaviour

First Cycle Loading

Load-deflection curves up to the service load level (11.00 kN/m^2) for each of the ten slabs are shown in Figs.8.13 to 8.22. The deflection plotted is the average of the two gauge readings GC01 and GC02 (refer Fig.5.23 for gauge positions), with reference to the supporting frame. This represents the relative deflection of the centre of the column line with respect to the column in an internal panel of a multi-panel slab.

In general, the deflections of the slabs are influenced by the flexural rigidity and hence the slab thickness, the quality of concrete, the level of prestress and non-prestressed reinforcement, the extent of cracking and the pattern of tendon layout.

Two phases of behaviour can be observed. The first phase is indicated by an approximately straight line showing linear elastic behaviour usually associated with the uncracked section. The

extent of the linear portion is influenced by the compressive stresses induced at the bottom surface of the slab in the column region by the prestressing forces (i.e. the top surface over the support in normal slab construction) as well as by the limiting tensile strength of the concrete. The second phase of behaviour is characterised by an increasing rate of deflection and a deviation from the previously linear path of the curve. This indicates the development of localised flexural cracking at the slab/column connection. There are, however, also indications of more extensive cracking in slabs having a lower prestress level and more widely spaced tendon distribution. There is a short transition length over which micro-cracking develops.

After cracking, the rate of increase of deflection under progressive loading which corresponds to the rate of reduction of the slab stiffness, depends primarily upon the rate of penetration of the cracks through the depth of the slab and the distribution of cracking over the surface. It is largely a function of the total area of steel crossing the cracks. The rate of increase of deflection can be observed from the figures to be greatest in series A and B slabs where the tendons were uniformly distributed (Figs.8.16 and 8.20). With a banded arrangement of tendons (A1, A3, B1, B3, C2), the increase in deflection after cracking is less marked and the distinction between the cracked and uncracked phase is not clearly defined as shown from their load-deflection curves (Figs.8.13, 8.15, 8.17, 8.19, 8.22). In slab C1 (Fig.8.21), part of the deflection increments after cracking could be due to the existence of a top flexural crack in the centre panel prior to

testing as mentioned in section 5.11. Due to the lack of reinforcement, the depth of the crack was probably considerable.

In slab A2 (Fig.8.14), which was the first slab to be tested in the present investigation, an error in the calculation of the service load led to an overloading of the slab to 14.00 kN/m^2. The deflection in the uncracked phase of this slab was found to be higher than that obtained from elastic plate analysis. This was partly due to a certain amount of settlement as a result of using hard-board as bedding material at the supported edges and partly to the application of insufficient torque to the restraining bolts. These errors were corrected in later tests by replacing the hard-board with a firmer bedding of cement grout and adopting a careful procedure for tightening (section 5.12).

Upon unloading, the load-deflection curve does not retrace its loading path, but forms a hysteresis loop. The area of the loop is widest in slabs with a low level of prestress and with tendons distributed uniformly or in wide bands, e.g. B2 (Fig.8.18) and B4 (Fig.8.20). Their residual deflections were also found to be the largest in the series.

The residual deflection on unloading is probably influenced by the level of prestress in the concrete, the extent of cracking at service load and the non-elastic time-dependent effects of the concrete. Part of the residual deflection was recovered in the course of time, particularly in slabs having a closely banded tendon arrangement in the column region.

Second and Subsequent Cycle Loading

The load-deflection curves from the service load level to failure in the second cycle in series A slabs (Figs.8.13 to 8.16) and the third cycle in series B and C slabs (Figs.8.17 to 8.22) have been omitted for clarity. In general, upon reloading, the load-deflection curves exhibit approximately linear behaviour in all the slabs. The familiar increase in the rate of deflection after the decompression load, usually observed in prestressed beams, can hardly be discerned from the figures. The total deflection at service load was slightly greater than that in the previous loading cycles.

The unloading path of the curves follows closely the previous unloading path. The hysteresis loop area is considerably smaller than in the first cycle in the lower prestress level of series B (B2, B4) and slab C1. The measured deflections of all the slabs are shown in Table 8.2.

Longitudinal Deflection Profiles

Figs.8.23 to Fig.8.25 show typical longitudinal deflection profiles along the column centre line in the E-W direction at selected load levels in the first loading cycle. For comparison, the deflection profiles from the elastic plate analysis are superimposed on to the experimental profiles in Figs.8.23 and 8.24. It can be observed from the profiles of slab A2, shown in

Fig.8.23, that there is evidence of settlement at the edges at progressive loading and in the elastic plate analysis, the line of support has therefore been moved back 50mm (considered to be the maximum possible in the test) from the edges of the support. The resultant elastic deflection profiles were, however, still slightly below the experimental profiles in the uncracked elastic phase (estimated cracking load was 7.00 kN/m^2). These, and indeed the majority of the discrepancies in deflection were results of 'softness' of the hard-board bedding material aggravated by the slab rotating at the edges due to an unsatisfactory tightening of the restraining bolts. The degree of these errors cannot be determined precisely.

Fig.8.24 shows typical profiles in a test slab where corrections were made to the restraining system. The figure shows the deflection profiles of slab A3 and good correlation can be observed with the elastic plate analysis prior to cracking. Points of contraflexure can be identified at the ends of the span. After the formation of flexural cracks at the slab/column connection, the reduced stiffness allows large rotations of the slab to take place adjacent to the column, resulting in an increasing rate of deflection in the slab at higher loads. The resultant profiles then gradually deviate from the elastic solutions. The deflection profiles of the same slab in the second cycle of loading up to failure load is shown in Fig.8.25. At loads greater than about 15 kN/m^2, the increase in rotation at both ends of the span was not primarily due to any slip or slackness in the restraint system, but to the transverse cracking of the tension face (top surface)

of the slab at the edges. This is a factor always present in a real structure when sudden punching shear failure of the column is prevented prior to the general flexural failure of the slab.

Symmetrical Behaviour of Test Slabs

To assess the influence of tendon layout on the behaviour of test slabs and the symmetry of loading, the deflections on the column centre lines 375mm from the centre of the panel in the North, East and West directions (see Fig.5.23) have been plotted. However, only one deflection gauge in the North direction could be placed because at the other positions access was required for Demec gauge measurements. In the East and West directions, gauges were placed at 300mm (GE1, GW1) and 450mm (GE2, GW2) from the centre of the panel and the deflections at 375mm in each of these two directions were taken as the average of the two adjacent gauges.

Some typical load-deflection curves in the final loading cycle to failure are shown in Figs.8.26 to 8.29.

Fig.8.26 shows the load-deflection curve of slab C1 which had a symmetrical distribution of tendons banded closely within the column width in both directions. Despite the defect in this test specimen (see section 5.11), there is consistency in the symmetrical performance of the slab throughout the loading range.

Where a symmetrical arrangement of tendons is used in both directions, it is thus established, as anticipated, that there is

little variation in the deformation of the slab at the three points. However, this may not be true when the tendon arrangement is unsymmetrical, for example in slabs A3, B3 and particularly C2 where it is prestressed in one direction only with the other direction reinforced with ordinary non-prestressed bars. Figs.8.27 and 8.28 show the load-deflection curves of slab A3 and B3 respectively. In both slabs, the tendons are closely banded in the column area in one direction (E-W in the figure) and uniformly distributed in the other orthogonal direction. The figures show that tendon layout has little influence on the symmetrical behaviour of the slabs even at loads approaching failure. The maximum deviation is found in slab A3 (Fig.8.27) near failure where the deflection at GW1/GW2 exceeds that at the other two points by about 6%.

In the whole test series, the greatest deviation from symmetrical behaviour is found in slab C2 (Fig.8.29) with a maximum difference of about 12% between gauges. From Fig.8.29, it appears that the slab is slightly stiffer in the N-S direction than in the prestressed E-W direction. This could probably be attributed to better crack control in this direction due to the presence of a larger amount of non-prestressed steel in both the negative and positive moment regions. In the E-W direction, the non-prestressed reinforcement consisted of only four 3.14mm diameter bars at the column. This nominal amount of non-prestressed steel, together with the strain incompatibility between the unbonded tendons and the adjacent concrete, would probably lead to a few wide cracks at the slab/column connection

resulting in larger slab rotations at the column in this direction. The modification of the prestressing effects due to the testing arrangement (namely about 30% increase in the induced column transverse prestressing moment compared with the internal panel of an actual multi-panel structure with identical prestress), could also have had some stiffening effect on the test slab in the N-S direction.

8.3.2 Computation of Slab Instantaneous Deflection using Equivalent Frame Method

Computation Procedures

The present use of ultimate strength design concepts and high strength materials resulting in shallow flexural elements can lead to deflection problems. Generally for Class 1 and Class 2 prestressed members, the serviceability requirement of deflection need not be checked as long as the concrete remains uncracked but should deflection or camber calculation be necessary, the use of elastic uncracked section analysis usually produces highly accurate results. In contrast, partially prestressed concrete (Class 3) and ordinary reinforced concrete members can and generally do crack under working load and the computation of deflections may be rather complicated. This is particularly true in flat slabs when most of the cracking at service load is limited to the region of the slab/column connection with slight or no cracking in the positive moment regions in the span. The calculation of deflections can be further complicated by the large

number of significant parameters, such as the aspect ratio of the panels, the vertical and torsional stiffness of any supporting beams, the stiffening effect of drop panels and column capitals as well as by the extent of cracking and the time-dependent nature of the material response.

For short-term elastic deflection, the code CP110 permits the use of elastic plate theory and numerical analysis by, for example, the finite difference and finite element methods. Although there are techniques which may be introduced into these methods to account for the effects of progressive cracking, they are probably too complex and expensive to apply in design practice. Certain approximate methods of calculation are, however, available and usually yield reasonable results within the limits of their applicability. A method at present widely adopted in design practice for computing the deflection (pre or post-cracking) of ordinary reinforced concrete floor systems was originally proposed by Nilson and Walters (55). The procedure, described in Appendix 2, is based on the equivalent frame method and applies equally to the direct design methods of the ACI or CP110 codes, in which moment coefficients are used in lieu of a moment analysis.

Simplification of Computation Procedures in Test Slabs

The fixity of the edges of the test slabs prevented mid-span deformation of the region representing the middle strip. In addition to which the symmetrical loading condition also prevented

transfer of moment from the slab to the centre column. The contribution of column rotation to the mid-panel deflection was therefore zero. The resultant deflection of the test panel a_c under uniform load was simply given by equation A2.2 in Appendix 2 with the 'reference' deflection $a_{f,ref}$ obtained from equation A2.9 in conjunction with A2.10. Hence (see Fig.8.30)

$$a_c = a_{cx} = a_{cy} \qquad \text{--- Eqn. 8.1}$$

The total column strip moment (negative plus positive strip moments) under experimental conditions was found theoretically to be 0.998 of the actual column strip moment in an internal panel under uniform loading. Little error can be introduced if the lateral distribution factor (LDF) i.e. M_{strip}/M_{frame} used in equation A2.2 in Appendix 2 for the column strip in the test panel is evaluated using actual internal column strip and total panel moments. From the PAFEC elastic plate analysis, the apportionment of the column strip negative and positive moment in an internal square panel (Table 6.2) is 50.9% and 20.7% respectively of the total statical panel moment. Hence the lateral distribution factor for the column strip is 0.72. [CP110 empirical design moment coefficients would give a value of (LDF)=0.68 in internal panel whereas from the moment apportionment coefficients in Table 17 of the Code for equivalent frame moment analysis of slab,

$$(LDF) = \frac{75\%(-ve) + 55\%(+ve)}{2 \times 100\%} = 0.65$$

The computed deflections of the test slabs will be discussed in later section.

Cracked Section Analysis

The original proposal of Branson for calculating the cracked moment of inertia, I_{cr}, (equation A2.8) of partially prestressed members, is based on the 'fully cracked' transformed concrete section, accounting for the tendon and reinforcement areas as in a reinforced concrete section but disregarding the effect of the prestressing force in modifying the neutral axis location (57). The neutral axis of bending is therefore the same as the centroid of the cracked transformed section and the position of zero stress (i.e. the neutral axis) in the section coincides with its centroid. However, under service load, a cracked partially prestressed concrete member is recognised to be stiffer because of the presence of an additional compressive force and the neutral axis position can vary in the section depending on the magnitude of the applied moment and the axial prestressing force. In the case of the unbonded tendon, the situation is further complicated by the strain incompatibility between tendon and surrounding concrete. Any strain changes in the unbonded tendon will be distributed throughout its length (assuming 'free slipping') and related to the extension of the concrete at the level of the tendon.

It is commonly accepted that in prestressed concrete, once cracks are present, the transition from the uncracked or closed cracks phase to the cracked phase takes place at the load at which

the stress in the concrete ceases to be compressive at the cracked face. The reason is the loss of tensile capacity of the concrete at the first occurrence of cracking. Although cracking may be considered to begin when decompression of the concrete occurs at the tensile face, the Concrete Society Report on Partial Prestressing (60), has given a more convenient method in relating the stresses in the cracked section to a reference load in which the stress in the concrete, on average, is zero in the total reinforcement present (tendons and non-prestressed reinforcement). The corresponding reference load can be calculated making due allowance for the maximum losses of prestress and the effect of non-prestressed reinforcement on these losses. In a determinate structure, the position of the reference force coincides with that of the prestressing tendons or the average position of prestressed and non-prestressed reinforcement acting together. In indeterminate structure, the position of the reference force is shifted due to the non-concordancy of the tendons which introduces secondary prestressing moments into the structure. This problem can be overcome easily if the secondary prestressing moments can be considered to exert effects similar to those of externally imposed loads. Hence referring to Fig.8.31, the reference force in a rectangular section of unit width b, subjected to both primary and secondary prestressing moment M_{sec} in addition to a reference load moment M_o, can be obtained from the equation:

$$P_o = P_e + \alpha_e \left[\frac{P_e}{A_c} + \frac{M_p}{I_g}\left(d - \frac{h}{2}\right)\right]\left[\phi_{SF} A_p + A_s\right] \text{ --- Eqn. 8.2}$$

where P_e = Effective prestressing force

A_c, I_g = Gross concrete sectional area and moment of inertia

A_p, A_s = Area of unbonded tendons and non-prestressed reinforcement

d = average effective depth given by

$$d = \frac{A_p d_p + A_s d_s}{A_p + A_s} \qquad \text{--- Eqn. 8.3}$$

α_e = modular ratio (E_s/E_c)

and ϕ_{SF} = strain factor at the level of tendon

Fig.8.32 shows the stress and strain distribution of a partially prestressed section in the cracked phase. The force in the total reinforcement has increased from the reference force P_0 to $P_0+\delta P$ due to the increase of the stresses in both prestressing and normal reinforcing steel. Notice that the level of the prestressing force has been assumed to be located at the average level of the total reinforcement. The moment due to external load is M and the maximum compressive stress in the concrete is f_c.

In order to calculate the moment of inertia I_{cr} of the cracked section for use in equation A2.8 (Appendix 2), taking account of the changes in the neutral axis depth due to the combined effect of the compressive force and moment, it is necessary to determine the value of x by eliminating the f_c and f_s (Fig.8.32) from the two equilibrium equations of force and moment and the equation derived from strain distribution, assuming plane section to remain plane.

For a rectangular section, the resulting cubic equation can be written as:

$$\left(\frac{x}{d}\right)^3 + 3\left(\frac{M}{P_o d} - 1\right)\left(\frac{x}{d}\right)^2 + 6\alpha_e \frac{M}{P_o d}\left(\frac{\phi_{sF} A_p + A_s}{bd}\right)\left(\frac{x}{d}\right) -$$

$$6\alpha_e \left(\frac{M}{P_o d}\right)\left(\frac{\phi_{sF} A_p + A_s}{bd}\right) = 0$$

--- Eqn. 8.4

The cracked moment of inertia is hence given by:

$$I_{cr} = \frac{bx^3}{12} + bx(\bar{y} - \frac{x}{2})^2 + \alpha_e A_s (d_s - \bar{y})^2 + \alpha_e A_p (d_p - \bar{y})^2$$

--- Eqn. 8.5

where $\bar{y}$ = centroid of the transformed cracked section

In determining I_{cr} from equation 8.5, the total area of non-prestressed and prestressed reinforcement placed within the column strip width (L/2) of the test slab is used and assumed to be uniformly distributed across the width. The axial prestress is also assumed to be uniformly distributed in the transverse direction eventhough this is not strictly true.

A complication in evaluating the value of the depth of the neutral axis x from equation 8.4 is the unknown value of strain factor ϕ_{SF} which is used to relate the strain in the tendon to that in the adjacent concrete. It is a function of several variables and is equal to unity when the steel is perfectly bonded to the concrete. The factor was originally proposed by Baker (61) for the theoretical calculation of the ultimate load of beams reinforced by ordinary reinforcement or by prestressing tendons with different degrees of bond and a value of 0.1 was suggested for the design of unbonded prestressed beams. Pannell (62) and Janney et al (63) subsequently carried out experimental investigations on unbonded prestressed beams to determine the limiting value of the

strain factor at the ultimate limit state but their results were not applicable to service load behaviour.

The strain factor at a section may be defined as the average change in tendon strain throughout the tendon length for a unit change of concrete strain at tendon level. A rigorous evaluation of the strain factor at service load may be carried out using a flexural formula with due consideration of the effect of increase in tendon force due to deformation of the slab under load.

In the case of straight tendons, the average change of tendon strain can be evaluated by summation of the total extension of the concrete at the level of the tendon divided by the tendon length. In the case of tendons with varying eccentricity, the calculations become tedious since the moment of inertia after cracking and the depth of neutral axis change along the span. The situation could be further complicated if the moment surface also varies along the span. Iteration procedures would need to be used to obtain the strain factor at any load lavel.

In the present investigation, the strain factor is assumed to be zero throughout the loading range. This was justified by the fact that the observed increase in tendon stress at service load was insignificant, e.g. only about 0.7% of the effective prestress in tendon passing directly over the column in the most severely cracked slab of B4, possibly because of the limited length in the region of the column within which the large moments were concentrated. However, it may be conceded that some variations in tendon stress could arise due to friction between the wire and the

polythene tube.

Comparison of Computed with Measured Deflection

The deflection computed using the weighted moment of inertia or I-Effective equation of A2.8 (Appendix 2) is particularly sensitive to the value of the cracking moment and hence the cracking load. The computed cracking load in the column strip (negative moment region) using the tensile concrete strength obtained by the split cylinder test in conjunction with the average column strip prestressing moments (shown in Table 6.2) and average prestress distribution was not realistic as it was usually about 2 kN/m^2 higher than that obtained using the combined axial and bending stresses at the column face from the plate analysis. The cracking load was therefore calculated by the latter method and the results for all the test slabs are shown in Table 8.5.

In computing the deflection under uniform loading, the positive moment regions in the column strip as well as in the middle strip are assumed to be uncracked eventhough minute hair cracks were observed in series B and C slabs at the edges of the panel at loads ranging from 10.00 kN/m^2 to 11.00 kN/m^2 (Table 8.5). This will not have significantly altered the results as the cracking only took place when the load was almost equal to the service load.

Table 8.3 shows the measured and computed deflection at service load calculating the latter by the equivalent frame

method. The computed deflection using gross section moments of inertia I_g with $\alpha = 1.0$ (slab wholely uncracked) are included in line 3 for comparison with the elastic plate solutions in line 2. It can be observed that the equivalent frame method is fairly accurate and only underestimates the plate solution by about 6% (shown in line 8). The reduced accuracy for slab A2 (line 3/line 2 = 0.87) is due to the correction adjustment of the elastic calculation for the reason explained in section 8.3.1. Slab A2 will not, therefore, be considered in the following discussion.

The computed deflections, taken account of cracking in the column area are shown for various values of α. In addition to $\alpha = 0.7$ (line 4) and $\alpha = 0.5$ (line 6) discussed in Appendix 2, values of $\alpha = 0.6$ and $\alpha = 0.4$ are also tabulated.

In general, when $\alpha = 0.7$, the computed deflection underestimates the measured value with a maximum deviation of 27% and 37% (line 9) in slabs B2 and B4 respectively. The reason for these deviations in the two slabs is the considerable loss of slab stiffness as a result of radial diagonal cracks extending from the corners of the column towards the corners of the edges.

Better correlation with measured deflection is achieved as the value of α is reduced to 0.5 or 0.4 as shown from lines 6 and 7 in the table. With a so-called simple average (27) of the effective moment of inertia of the negative and positive moment regions, i.e. $\alpha = 0.5$, the correlation is particularly good for the series A slabs as well as for slab C1 with a mean of 1.02 (line 11). In slabs B1 and B3, the computed deflection

overestimates the measured value by 23% and 22% (line 11) respectively. The reason is due to a better control of crack propagation in these slabs by the larger area of non-prestressed reinforcement (7 bars) at the columns compared with only 4 bars in the A series slabs. In the latter series, the non-prestressed reinforcement was situated within the column width (100 mm), whereas in B series slabs, it covered a larger critical width (220 mm). It thus appears that for a low level of prestress, special attention needs to be given to the distribution of the reinforcement at the supports.

In the one-way prestressed slab C2, the deflection is computed from the average value obtained from separate bending analysis. In the direction of prestress, the modified concrete section analysis, taking account of the compressive prestressing force, is used whereas ordinary reinforced concrete section analysis is applied in the non-prestressed direction. It is interesting to note that a good correlation with the measured deflection could be obtained using either $\alpha = 0.7$ or $\alpha = 0.6$. With $\alpha = 0.5$, an overestimate of about 12% is indicated.

To account for the more severe state of cracking in slabs B2 and B4, $\alpha = 0.4$ seems to produce a closer correlation with measured values (lines 7 and 12).

Figs.8.33 to 8.35 show typical comparisons of measured and computed load-deflection curves for slabs A4 ($\alpha = 0.5$), B4 ($\alpha = 0.4$), and C2 ($\alpha = 0.6$) respectively for the complete range of loading up to service load. It can be observed that the elastic

solution using PAFEC will predictably underestimate the deflection after cracking but the computed load-deflection curve from the equivalent frame method is generally reasonably close to the measured load-deflection curve.

In general, it can be concluded that the use of a weighted average of the effective moment of inertia of the negative and positive moment regions (i.e. α = 0.7 in eqn A2.10), gives reasonable correlation (within 13%) for all the slabs with a higher prestress level (A series) and for some lower stressed slabs particularly those having tendons banded close to the column area (B1 and B3). However, the method generally underestimates the deflection of those slabs with uniformly or widely spaced tendons. The use of the average moment of inertia (α = 0.5) seems to provide a fair overall correlation for the test series. Kripanarayanan and Branson (56) arrived at similar conclusions when the equivalent frame method was used to compute the deflections of numerous multi-panel column-supported and beam-supported ordinary reinforced concrete slabs. They stated that, α = 0.7 generally resulted in deflections within $\pm$25% and with α = 0.5, within $\pm$20% of the measured values.

8.3.3 Estimating the Internal Panel Deflections

The resultant deflection of a prestressed slab, either short-term or long-term, is of particular importance when the serviceability requirements for deflection is to be satisfied. Slabs on average to high level of prestress generally meet these

requirements. There are however, practically no experimental data on the behaviour of slabs with the variously recommended minimum prestress levels e.g. 0.9 N/mm^2 in the ACI Code, and 0.7 N/mm^2 in the Concrete Society Report. In this section, the estimation of internal panel deflections under various tendon arrangements will be made by direct proportioning from the test results.

Let a_m be the total elastic mid-panel deflection under uniform loading and a_c the deflection of the mid-span point of the column centre line, both relative to the supporting columns, so that the ratio of a_m and a_c can be expressed in dimensionless form of a_m / a_c.

It has been demonstrated (section 6.2) that the testing arrangement gives an accurate representation of a_c but, owing to the boundary conditions does not model a_m correctly. It is assumed that under uniform loading, the ratio is the same in the post-cracking as well as in the pre-cracking phase. From the PAFEC analysis the ratio a_m / a_c in an internal panel is 1.34. Therefore, if a_e is the measured deflection of the column with respect to the supported edges (i.e. the experimental value of a_c), then by direct proportion, the deflection of the centre of an internal panel will be given by

$$a = 1.34\ a_e$$

The net deflection after deducting the camber a_p due to prestressing which can be conveniently obtained from the PAFEC analysis, is then

$$a = 1.34\, a_e - a_p \qquad \text{--- Eqn. 8.6}$$

For long-term deflection, a simple approach is usually employed in practice whereby the additional time-dependent deflection is obtained by multiplying the short-term deflection by a prescribed factor. In the ACI Code (1983), the general value of this factor is 2 and it is reduced to take account of the stiffening effect of compressive reinforcement using the expression, $2-1.2\ (A_s'/A_s)$ where A_s' and A_s are the compressive and tensile non-prestressed steel areas respectively. The Code permits the use of the above factor for predicting the long-term deflection of two-way slab systems. Since compression steel is seldom provided in slabs, the simple multiplier of 2 is often used.

An alternative method suggested in the CP110 Code (section 4.3.7.1) is to use an effective (long-term) modulus of elasticity E_{ce} to calculate the total deflection. This is given by

$$E_{ce} = \frac{E_c}{(1 + \phi_c)}$$

where E_c is the initial modulus and ϕ_c the creep coefficient. In the present investigation, due to the lack of experimental data for long-term creep of the concrete, a creep value of 36 * 10 N/mm^2 per unit length is used as recommended in CP110 for post-tensioned members.

The results of the successive steps in estimating the deflections of an internal panel from the test results are tabulated in Table 8.4. The measured deflection a_e at service load

(11.00 kN/m^2) is shown in line 1e in the top sub-table whereas the elastic prestressing camber a_p and the total elastic deflection in the mid-panel of the internal panel a_m are shown in lines 1i and 2i respectively in the centre sub-table. The estimated short-term internal panel deflection is shown in the same sub-table and the long-term deflection in the lower sub-table. The estimates for slabs A2 and C1 are not conclusive because of the defects in these specimens prior to testing already mentioned, and will not, therefore, be included in the following discussion.

It can be observed from the centre table that the short-term deflections of the slabs (in line 3i) are all within the specified serviceability deflection limit (span/350 = 4.29 mm) of the Code CP110.

The estimated long-term deflections of the slabs using the effective modulus of elasticity (CP110) and those predicted by the ACI approach using a multiplier factor of 2 are shown in lines 4i and 5i respectively. The deflections determined by the ACI method are generally slightly higher than those using the CP110 approach.

From line 6i in which the ratios between the computed deflection and the allowable limit using the CP110 method are shown, it can be seen that the deflections of all the slabs except B2 and B4 are within the criterion for service load.

The estimated long-term deflection can be considered as an upper bound value because the long-term load is taken to be the full service load (DL + LL) although in practice, this will seldom

apply. A more reasonable estimate of the long-term effect is obtained by calculating the deflection due to the sustained dead load plus an instantaneous short-term deflection due to the service live load. The resultant deflection under these loading conditions will obviously be less severe than that presented. The results have not been included in the table but it may be stated that all the slabs would satisfy the serviceability requirement.

It should be emphasised that the experimental span to depth ratio (shown in Table 8.2) is less than the nominal value of 40 used in the design for the prototype slab. This is mainly due to the difficulties in working to a close tolerance in the construction of the test slabs. From the PAFEC analysis, it has been found that an approximate increase of elastic deflection (for both internal panel and experimental slab) by factors ranging from 1.50 to 1.10 will need to be made if a constant span to depth ratio of 40 is to be used in each slab. The adjusting factors are shown in line 7i in Table 8.4 for all the slabs. Assuming other factors to be constant, the adjusted long-term deflections are shown in line 8i. It can be observed that slabs B1, B3 and C2 are all close to the allowable deflection limit whereas slabs B2 and B4 will be totally unserviceable for long-term loading. It appears that when the slabs are stressed to an average level of prestress such as those in the A series, there is little difficulty in meeting the deflection criterion at the serviceability limit state. These results appear to confirm the findings of Brotchie and Beresford from a long-term test of a multi-panel slab structure (11) eventhough in their case the slab had a span to

depth ratio of 48.

A survey of Table 8.4 indicates that the influence of tendon arrangement on deflections is significant when a low level of prestress is used. Hence in B1 and B3 where the tendon are banded in the column vicinity and there is a relatively larger amount of non-prestressed steel over the column (0.5% as opposed to the minimum of 0.15% recommended in Concrete Society), the resultant deflections are almost only slightly greater than those of the corresponding slabs with a greater number of tendons i.e. A1 and A3. It is interesting to note that in C2 where all the tendons are concentrated in a narrow band in the column region in one direction, with none in the other orthogonal direction, both short-term and long-term deflections compared favourably with those of slabs with a similar tendon layout in each direction. This investigation has shown that a partially prestressed slab designed to either the Concrete Society or the ACI larger prestress limits will behave satisfactorily provided attention is given to the detailing of the tendon layout and non-prestressed reinforcement. More research needs to be carried out to confirm this finding.

8.3.4 The Influence of Tendon Arrangements on Load-Deflection Behaviour

A direct comparison of the load-deflection relationship of the slabs has not been possible due to the influence of numerous variables, in particular the average thickness, on the slab

flexural stiffness. It was calculated that a difference of only 1mm in the slab thickness would produce 8% difference in deflection. Working to such a close tolerance was not possible in casting, as constant topping-up and trowelling were necessary before the slab was left to be cured. In addition, the slab properties could also be affected by the degree of compaction and the amount of fines in the concrete.

To eliminate these anomalies and to facilitate a direct comparison of the deformation characteristics, the measured deflection at the mid-panel of the slabs is expressed as a dimensionless ratio of the corresponding elastic value at the same load. The elastic deflection from the PAFEC analysis was deemed unsatisfactory because of the above mentioned uncertainties in the slab. Instead it was obtained from the experimental load-deflection curves i.e. from Figs.8.13 to 8.22 for the test series. It was assumed that up to the first occurrence of cracking, the slabs exhibited perfect linear-elastic behaviour. The linear elastic load-deflection curve was thus obtained by joining the origin to the point of cracking and projecting this line to estimate the deflection at service load. The ratio of the experimental to the above theoretical elastic deflection for loads above the cracking load could then be used to determine the influence of the tendon arrangement on the deformation of the slabs.

Fig.8.36 shows the comparison of the above ratios for all the test slabs. The applied load is plotted against the ratio a_e/a_t

where a_e, a_t are the measured and theoretical elastic deflections respectively. The uncracked condition of the slab is indicated when this ratio is equal to unity and the cracked phase when it is greater than unity.

From Fig.8.36 it can be observed that when the tendons are closely banded in the column vicinity for example in A1, A3, B1, B3 and C2, there is a comparatively higher cracking load (see Table 8.5) and stiffer post-cracking load-deflection behaviour. This is analogous to the behaviour of a partially prestressed beam with a higher level of prestressing force. Since the flexural behaviour of the slabs is affected by the degree of cracking in the column region, the slow rate of increase of deflection after cracking indicates that the deterioration of flexural stiffness is effectively controlled by the banding arrangement of the tendons.

Fig.8.36 also indicates that where a medium level of prestress is used, there is no significant difference in service load-deflection in the slabs whether the tendon layout is designed according to the British (Slab A1), or American (Slab A2,A3) recommendations. However, when the prestress level is near to the limiting values, the influence of tendon arrangement on the load-deflection behaviour becomes obvious. With tendons widely spaced in the column and middle strips (L/2) (Slab B2), or uniformly distributed in the span (Slab B4), minimal prestressing moments are expected within the critical moment regions. As a result, these slabs generally exhibit early cracking behaviour and rapid deterioration of flexural stiffness at progressive loading. In

contrast, when the tendons are closely banded in the column area as in B1 and B3, the performance at the serviceability limit state is significantly improved. Also if enough non-prestressed steel is used to restrain and control the propagation of flexural cracking, the post-cracking behaviour of these slabs can be seen to be as good if not better than those slabs prestressed with greater prestressing force (A series). Non-prestressed steel placed over the column as observed in these tests, has a great influence on the flexural stiffness of the slabs after cracking and should therefore always be used at the critical sections in the slabs with a low prestress level.

The advantages (41,42) claimed for the support-strip method of prestressing i.e. slab C1 have not been fully investigated in the present study eventhough this method of tendon layout does seem to produce a favourable behaviour of the slab.

The results obtained from slab C2 show that despite an unsymmetrical tendon layout, considerable prestressing moments (about 40% of the longitudinal column moments) can be induced in the column region in the direction transverse to that of the tendons and these have been found to be beneficial for counteracting the load moments in this direction.

There are, however, no particular advantages in this type of tendon arrangement in a multi-panel square slab structure. The tendon layout could be employed more appropriately in rectangular panels where the tendons could be placed predominantly in the longer span in the column region in order to provide high

counteracting prestressing moments in the long direction and yet induce sufficient transverse moments in the less critical short span.

8.4 Cracking

8.4.1 Bottom Surface

Circumferential Cracking

The application of increasing load to the test slabs always resulted in an initiation of flexural cracking at the column connection at the bottom surface and generally at service load level, a complete circumferential crack pattern had formed around the column periphery. Although it was impossible to observe the development of this cracking visually, a simple method was devised to detect the onset of cracking in this region. This consisted of placing four electrical strain gauges (PL-60) each 60mm in gauge length on the surface of the slab opposite the column faces. The first cracking invariably occurred within these gauges.

Typical curves of load against concrete tensile strain are shown in Figs.8.37 and 8.38 for slabs A1 and A4 respectively. The direction and location of the strain gauges are indicated in the figures. The discontinuity in the curves signifies the onset of cracking at the column periphery.

Although the prestrains in slab A4 in Fig.8.38 are reasonably close to one another at the zero load level, which is to be

expected if the tendon layout is identical in both directions, considerable scatter of the results is generally found as indicated in the prestrain profiles in Figs.8.2 to 8.5. These anomalies are probably due to the sequence of stressing in the slabs, the local variations in concrete properties, the application of unequal torques to the restraining bolts and the extrapolation from preliminary test results (section 5.13) to obtain the prestrains. In view of these uncertainties, only representative curves due to uniform applied loads are shown in Figs.8.39 to 8.41 for series A, B and C slabs respectively. In slab A2, because PL-60 strain gauges were not placed over the column periphery, the load-strain curves shown in Fig.8.39 are those of slabs A1, A3 and A4 only.

A study of these figures indicates that series A slabs generally exhibit a higher flexural cracking capacity than that of series B and C slabs. Within series A and B (Figs.8.39 and 8.40), the cracking load is about the same for all the slabs having closely banded tendons in the column area and is slightly higher than for slabs having other tendon patterns. Although the slabs in series B have only about 60% of the prestressing force of series A slabs, the initial cracking load for B1 is about equal to that of A4. This indicates a relatively high local compressive prestress as a result of the closer spacing of the tendons in the column area. The flexural cracking capacity of slabs C1 and C2 shown in Fig.8.41, is about the same. Both values are, however, comparable to that of slab A4 inspite of having a lower prestress level.

Table 8.5 shows the flexural cracking loads of the slabs at the column faces and along the edges together with their corresponding computed results obtained from the PAFEC analysis taking the split cylinder strength as equivalent to the tensile strength of the concrete. The computed results are shown for the slab with (a) internal panel and (b) test slab boundary conditions in order to assess the influence of axial stress distribution on the cracking capacity of the model. The observed cracking load as noted in Table 8.5 is not, however, sufficiently accurate (it could only be estimated to within ± 1.0 kN/m^2) to allow a comparison with the PAFEC solutions but it appears that the influence of axial prestress in a closely banded tendon arrangement is not very great when the level of prestress in the slab is low.

Upon reloading in the second and subsequent cycles, the stage at which the surface strain changes from compressive to tensile, accompanied by reopening of the cracks, and the decompression load at which this occurs can be distinguished by the discontinuity in the load versus strain curves of the slabs as shown in Figs.8.42 to 8.44. The decompression load as observed from Fig.8.42 is about 4.00 kN/m^2 for slabs A1 and A3 and about 3.00 kN/m^2 for slab A4. In series B and C slabs in Figs.8.43 and 8.44 respectively, the decompression loads are not particularly well defined. This is a possible indication of the cracks reopenning at an early loading or of incomplete closure of these cracks because of insufficient local compressive force to reverse the slipping of the non-prestressed steel.

Cracking Along the Column Centre Lines

In addition to the above mentioned PL-60 strain gauges two-directional PC-20 gauges were also fixed to the concrete surface at 100mm, 225mm and 375mm (i.e. 50mm, 175mm and 325mm from the column faces) from the panel centre lines in the East, West and South directions (see Figs.5.19 to 5.22). With increasing load, tensile cracks which originated at the column faces gradually propagated towards the edges along the column centre lines. Some of these cracks were found to penetrate the gauges located 50mm and 175mm from the column face. Typical examples may be seen from Figs.8.45 and 8.46 for slab A4 in which it can be observed that a N-S crack (gauge 34 in Fig.8.45) extended from the South column face to a distance of 50mm at an applied load of 9.00 kN/m^2 and covered a further distance of about 150mm at 10 kN/m^2 (gauge 36 in Fig.8.46).

The cracking was usually found to occur at a load level slightly above the initial flexural cracking load of the column periphery and it was also found to be less extensive in the series A slabs. However, in slabs B2 and B4, all the gauges 50mm from the column faces in the East, West and South directions were affected by cracking at an early stage when the applied load was only about 6.00 kN/m^2 in B2 and 5.00 kN/m^2 in B4. Limited cracking was generally found in the rest of the slabs in the B series as well as in C1 and C2; in the slab C2, the cracks were predominantly

transverse to the direction of prestress.

This type of cracking was probably limited to the column region at service load level as most of the gauges 225mm and 325mm from the column faces were not affected.

Radial Cracking

No specific gauges were placed to detect radial tensile cracks which propagated from the corners of the column towards the slab edges with which they made an angle of between 45° to 60°. However, in a number of slabs, the radial cracks were found to have crossed the PC-20 gauge placed in the centre of the quarter panel as shown in Figs.8.47 and 8.48 (gauges 46,47 in both figures) for slabs B1 and B3 respectively. In the test series, only slab B4 showed any sign of extensive radial cracking at the fairly early loading stage of about 11.0 kN/m^2 as can be observed in Fig.8.49 (gauges 46,47).

The failure crack patterns shown in Figs.8.50 to 8.59 for all the slabs consisted mainly of circumferential cracking on the top surface at the edges and radial cracking on the bottom surface. The bottom cracks were fine and the pattern was traced after failure using an illuminated hand microscope. Those cracks visible to the naked eye have been indicated in the diagrams by bold lines; they were comparatively few in number and some of them can be observed to have fanned out to the side faces of the slab forming a failure mechanism which shows corner effects as

described in Chapter Seven. These dominant cracks formed hinges which divided the panel into separate segments and allowed each to rotate as flexural failure became imminent. Short lengths of radial crack could also be seen interspersed between the major cracks. In slabs having a lower prestress level and a larger quantity of non-prestressed reinforcement, the number of radial cracks increased.

Following punching of the column, the crack patterns in the column area were obliterated by extensive damage to the concrete surface. All the slabs except C1 and C2 were tested until this mode of failure occurred. In slabs C1 and C2 where testing was terminated at about 90% of the failure load, the crack patterns, shown in Figs.8.58 and 8.59, present a clearer picture of the extent of the negative cracking. The cracking of slab C1 in Fig.8.58 is predominantly aligned in the E-W direction. The locations of these cracks in the column region correspond approximately to that of the non-prestressed steel wires. In slab C1, the E-W steel was placed nearest to the surface and it appears that these wires acted as crack initiators. This phenomenon is obvious in slab C2 (Fig.8.59) in which the N-S steel wires (of which there were ten in the critical width) were positioned nearest to the surface and consequently the number of cracks was greatest in this direction.

8.4.2 Top Surface

The initial cracking on the top surface invariably occurred

along the slab edges. In series A slabs, hair-line cracks were not generally observed along the edges until at about 60-70% of the failure load and none was found at service load level. In series B and C slabs, most of the cracking took place at about 11.0 kN/m^2. The cracking associated with this load was, however, slight when compared with the negative cracking in the column region. These cracks usually terminated at a distance of about 150mm to 200mm from the corners of the slab.

Following cracking at the edges cracks would eventually formed across the corners of the slab after about five to six load increments. The bold lines on the top surface crack pattern in Figs.8.50 to 8.59 indicate the direction and position as well as the load at which the corner cracks commenced. The hair-line cracks on either side of these corner cracks, which occurred after further load increments, can be seen to be more numerous and closely spaced in series B and C slabs. This is due to the presence of non-prestressed steel at the corners of the panel which effectively controlled the cracking behaviour.

On removing the column load after failure, the slab recovered almost to its original shape. During this process, the prestressing tendon forces tended to put the concrete into tension with the result that radial yield lines penetrated to the top surface of the slab. The dotted lines in Figs.8.50 to 8.59 mark the approximate extent of this cracking and typical top and bottom surface crack patterns are also shown in Plate 9.

8.4.3 Crack Widths

The crack widths on the top surface do not provide any significant insight into the behaviour of the slab. In series B and C slabs, the crack widths at service load level at the edges of the slabs were difficult to measure and no attempts were made to do so. Of more importance were the crack widths on the bottom surface in the column region which was impossible to measure optically or mechanically. The concrete tensile strains obtained from the PL-60 electrical strain gauges, however, may provide an alternative means of estimation eventhough it is conceded to be a highly arbitrary process. The increase in concrete strain after cracking can be obtained by deducting the prestrain from the total strain up to service load and the associated crack width can thus be estimated by multiplying this average incremental strain by the gauge length. It is a conservative estimate because the limiting tensile strain of the concrete is included in the net result to account for the amount of strain increase due to micro-cracking of the concrete surface. To check the performance of the gauges after cracking, the total concrete strain up to service load in the initial cycle of loading may be compared with that in any subsequent loading cycle and the two values should correspond within the experimental limits if the surface cracks inside the gauge length have stabilised. The results obtained using the above method are presented in Table 8.6.

From Table 8.6, it can be seen that the total concrete strain is almost the same in the initial and subsequent loading cycle

with a maximum variation of about -153.0 μm/m in slabs B4. The estimated average crack widths are consistent with the deflections with severest cracking in slabs B2 and B4 (crack widths 0.081 and 0.15mm respectively). It is interesting to note that all the crack widths are within the CP110 limits (0.2 mm) eventhough the 'hypothetical tensile stress' calculated as for an uncracked section at the column face exceeds the limits in Table 32 of the code in all the slabs.

Linear scaling from these results to estimate the crack widths in full size multi-panel slab could lead to spurious conclusions. Although the ultimate behaviour of a structure can be predicted from a model with reasonable accuracy (64), there is no clear relationship between the cracking behaviour of a model and its prototype. The information on crack width correlation is sparce. Hatcher et al (65) carried out a duplication test of a 45-foot square multi-panel slab structure previously tested by Guralnick and LaFraugh (66) using a 1/4 scale model and obtained good correlation of ultimate strength but stated that "the crack widths are reported only as a measure of the degree of yielding and should not be scaled". Clark carried out 41 tests on 1/10 scale model of slabs spanning in one direction and the results (67) when compared with previous tests of 1/3.7 scale model of the same prototype (68) indicated that for the same load, the model strains differed from the prototype strains and even at the same strain level, the crack widths were not in scale. From these tests, it was shown that the crack width in a model was a function of the material properties and of the absolute size rather than

the scale of the model and it was further stated that the prototype strain and crack width could only be predicted from a model test if the material properties of both the model and prototype were known accurately (68).

More tests would, therefore, be needed to confirm the present test data on cracking and crack widths in partially prestressed slabs.

8.5 Concrete Strains

The majority of the strain gauges (PC-20) were concentrated along the column centre lines as it had been shown that the stresses here were most representative of those in an actual internal panel.

The prestrains obtained from these gauges have been discussed in section 8.2, while others where cracking had been detected as the cracks crossed the gauges are shown in section 8.4.1. In view of the large quantity of strain results and their similarity with one another at identical positions in the different slabs, only a typical set of results for slab B1 will be presented.

Fig.8.60 shows the longitudinal strain profiles (from the bottom surface gauges) along the column centre line in the E-W direction whereas Fig.8.61 shows the transverse strain profiles along the same centre line. The strain profiles plotted are those due to applied loads (excluding the prestressing effects) prior to the formation of cracking in the slab. The agreement with the

elastic strain profiles from the PAFEC analysis is good, with typical peak tensile strains over the support and high compressive strains near the edges. Fig.8.60 should give a realistic representation of the actual strains (and hence stresses) in a square internal panel whereas in Fig.8.61, the transverse strain distribution is modified as a result of the experimental boundary conditions in the model and will not, therefore, be a good representation of the actual transverse strain distribution. The point of contraflexure indicated by the experimental profiles shown in Fig.8.60 is practically the same as the theoretical point. It in fact remains fairly constant in the slab even at high loading as can be observed from Fig.8.62 in which the variations of concrete strain with load are shown at a point 225mm from the panel centre lines which is close to the theoretical position of contraflexure (about 275mm). The figure shows that the longitudinal strains (gauges 24, 50 and 63) remain small and essentially constant at low applied loads.

A reversal of stresses from compressive to tensile (gauge 24) in the top surface at failure loads indicates that a shift of the position of contraflexure has taken place as a result of redistribution of stresses from the negative to the positive moment region.

In slab C2, the location of contraflexure does not seem to be affected by the highly unsymmetrical reinforcement layout as can be observed from Fig.8.63 (gauges 30, 45 and 74). This observation is found to be true in all the slabs irrespective of their tendon

distribution patterns.

The development of in-plane radial compressive stresses can be observed in Fig.8.64 where the load against compressive strain in the top surface at positions 100mm from the panel centre lines are plotted in the East, West and South directions. The figure shows that there is a gradual increase in radial compressive stresses (gauges 26, 29 and 34) with increasing loads. In conjunction with the observations made in Fig.8.62 (gauge 24), it can be deduced that a ring of compression exists immediately outside the column area and extends approximately to the position of contraflexure. Masterson (4) and Franklin (30) had shown that this compressive effect can significantly enhance the punching capacity of either ordinarily reinforced or unbonded post-tensioned slabs. Working along the lines of Masterson, Franklin assumed that the punching of the column in an internal panel was imminent when the slab moment at the column face caused rupture of the concrete compression zone. The compressive membrane action was analogous to a problem of a thick hollow cylinder concentric about the column and subjected to a uniform internal pressure. When the pressure inside this compression zone became large enough to cause radial cracking of an outside tension ring, the enhancement due to compressive membrane action was considered to have reached its maximum and punching failure ensued. Masterson originally assumed that the compression zone extended to the position of contraflexure but from a parametric study of limited test results in which various radii of the compression zone were considered, Franklin arrived at a radius equal to 0.125L which was deemed to

give the most consistent prediction of the punching capacity of numerous post-tensioned slabs. The observations made in Figs.8.62 and 8.64 appear to have confirmed his findings. Although an actual measurement of the concrete strains adjacent to the compressive column face was not possible in these tests, nevertheless, rupture of the concrete was observed by concrete spalling around the column perimeter on the top surface of the slab prior to punching failure and it is very likely that the limiting compressive concrete strain (generally taken to be between 0.0035-0.0038) was reached at the ultimate load. The membrane effect on punching capacity of the test slabs will be further considered in section 8.8.

Indications of a flexural failure mode of the slab are given in the figures already discussed as well as by the load versus compressive concrete strain at 675mm from the centre lines as shown in Fig.8.65. A near flat plateau of the curves (gauges 40, 60 and 67) signifies the imminence of flexural collapse. The discontinuity of the transverse strains (gauges 41, 61 and 66) at loads of about 16.0 kN/m^2 is probably due to stress redistribution following extensive radial cracking across the slab panel (see Fig.8.47). This figure, in conjunction with others presented earlier in this section, again demonstrated the symmetrical behaviour of the slab.

8.6 Tendon Stress

Load cells were placed at the ends of a number of tendons in

each slab to monitor the stress changes over the complete range of loading. In general, there was an insignificant stress increase of not exceeding 0.7% of the effective prestress at service load. For this reason, only the percentage increase in tendon stress in the final loading cycle is shown in Figs.8.66 to 8.75 for all the slabs. Selected anchorage and jacking end percentages are used including values both for tendons passing directly over the column and for some near the edges of the slab. The use of these end values is deemed satisfactory since the small slab span and the relatively flat tendon profile create less friction on the tendons than for those placed in longer, deeper members. The slab deformation also tends to produce an approximately uniform tendon stress increase throughout the length of the unbonded tendon.

From Figs.8.66 to 8.75 it can be seen that there is a relatively insignificant stress increase in the tendons until severe cracking has taken place in the slab. The maximum final stress increase is between 3% and 16% of the effective prestress. Similar results were also observed in the multi-panel slabs tested by Burns et al (15,16,17) as well as in tests using single panel models bounded by the mid-panel lines for example those tested by Burns et al (25,26) and Long et al (6,7).

The average tendon stress increase over the effective prestress in the slabs is compared with the calculated values according to CP110, ACI (318-83) and to equation 52 in the BS8110. The results are tabulated in Table 8.7. CP110 predicts much higher tendon stresses than both the other codes and the test results at

failure, possibly partly because the recommendations were based on tests on beams and do not, therefore, provide for the high L/d ratios obtained in slabs. The use of the ACI (318-83) equation 18-5 for L/d greater than 35 yields a closer agreement with the experimental results. However, when the effective prestress index is smaller than about 0.020 (series B and C1 slab) the calculated values do not differ very much from those of CP110. By comparison, equation 52 in BS8110 generally gives an improved agreement with the test results for all the slabs with their different effective prestress indices. The various approaches, however, have all predicted a higher tendon stress increase than those obtained experimentally.

8.7 Ultimate Behaviour

8.7.1 Flexural Strength

In flat slab design two types of failure mechanism are usually considered, either the straight line mechanism or the conical fan mechanism. In the multi-panel tests of Burns et al (15,16), the slabs failed basically by a folding type of collapse in which positive yield lines formed along lines joining the centres of the column lines and negative lines along the lines joining the columns. With the present test arrangement the straight line type of failure will not develop owing to the imposed boundary conditions of the slabs. Consequently two possible yield line patterns with corner effects have been considered in Chapter Seven. The equations and process for finding

the minimum ultimate load and the associated yield line pattern have also been explained in detail (see section 7.5).

For a yield line pattern with straight cut-off corner (Figs.7.4 and 7.5), the minimum ultimate load is obtained when the variable distance x is about 0.530m from the edges of the slabs. A minimum 'stationary' ultimate load is, however, obtained for the failure pattern with partial circular fan mode (Figs.7.6 and 7.7) when the radius of the corner fan is equal to 0.675m exactly.

The observed ultimate loads and the computed results with various failure patterns are shown in Table 8.8. The observed failure load is seen to agree closely with the computed results when corner effects are neglected (mode 1). By comparison, the ultimate loads for failure patterns with straight cut-off corner (mode 2) and circular corner fan (mode 3) are conservative. The ultimate load computed for mode 3 in the table is generally about 5% higher than for mode 2. Although mode 1 type of failure in Table 8.8 seems to be consistent with the observed failure load, a survey of the top and bottom crack patterns af the slabs (shown in Figs.8.50 to 8.59) indicates that corner effects simplified as either mode 2 or mode 3 pattern are involved. Nevertheless, it is not easy to differentiate between the crack patterns of either modes. From these observations, it may be concluded that the minimum flexural strength of the slabs should be computed according to either mode 2 or mode 3 yield pattern, although the use of either modes will produce a very similar result. It may thus be easier to use the simpler yield pattern with straight cut-

off corners and regard the results as the theoretical flexural strength of the slabs. Any loads in excess of this ultimate load may be attributed to the enhancement due to compressive membrane action. The onset of this effect cannot be ascertained with any degree of accuracy but it is believed that the effect is induced when the lateral displacements of the slab are prevented by the stiffness of the supporting frame. Similar situations also occur in the internal panels of a continuous floor slab.

8.7.2 Punching Shear Strength

The present investigation is not specifically designed to study the punching shear behaviour of the column connection, but the results have been presented as they may provide additional information in this area.

Series A and B slabs were tested until the slabs failed initially in a general flexural mode followed shortly by a secondary punching shear failure. The punching shear load was thus equal to the flexural failure load. The shear failure was induced by large deflection and accompanying large curvature at the negative moment yield lines of the column connection and was violent with considerable damage to the concrete surface typified by the column punching out a plug of concrete in the shape of a truncated pyramid with the base at the top of the slab. All tendons remained intact after failure. Spalling of the concrete was observed at the top surface column connection prior to failure. The bottom surface of slabs C1 and C2 was examined after

failure and no visible inclined shear cracking was detected near the column area.

The failure surfaces were not uniform in the slabs. The angle between the side of the pyramid and the top surface of the slab varied from 15°-17° in slabs A1 and B1 and between 25°-30° in slabs A2,A4,B2,and B4. In slabs A3 and B3 where the reinforcement was highly unsymmetrical, being closely banded around the column area in one direction (E-W) and uniformly distributed in the other direction (N-S), the inclined angle varied from a minimum of about 18° at the East and West faces of the column to a maximum of approximately 34° at the South and North column faces. This unequal failure surface was mainly the effect of the close banding of the tendons in the E-W direction. Plate 10 shows the typical failure surfaces of slabs with symmetrical and unsymmetrical layout of tendons whereas Figs.8.50 to 8.59 are the plotted failure surfaces for all the slabs.

The ultimate shear capacity of the test series is shown in Table 8.9 and is compared with the predictions of the ACI 318-83 and Concrete Society methods. Thevertical component, V_p, of the effective prestress forces from the tendons located within a distance of h/2 from the column faces is included.

For a prestress level less than 0.86 N/mm^2, the ACI code recommends that the punching shear of prestressed slabs should be computed as for reinforced concrete and thus for the B series and C1 slabs, the shear capacity is taken to be $V = 0.33\sqrt{f'_c}\, u_{crit} d$. The shear capacity of each slab is taken to be the average determined

for each direction.

From Table 8.9 it is apparent that both methods predict capacities that are very conservative even when the contribution of the prestress over the column is taken into consideration. The ACI method, however, shows slightly higher value than that of Concrete Society's. This poor agreement can be largely attributed to the nominal shear stress approach used by both codes of design. The shear capacity is calculated by multiplying a nominal shear stress at the critical section by the length and depth of that section. The use of this nominal shear stress was originally recommended in the ACI code in a simplified approximate formula to calculate the web cracking shear of prestressed beams, assumed to occur when the principal tensile stress became equal to $0.33\sqrt{f'_c}$ at the centroidal axis of the section. British practice, on the other hand, has adopted the same method as for a reinforced concrete slab with minor modifications to the method of evaluation of the permissible nominal shear stress. The shear capacity of each side of the critical section is calculated separately for its appropriate centric prestress and the average value is obtained to give the resultant shear capacity of the slab (3). The nominal stress used in these methods does not represent the actual stress nor its distribution because it is particularly sensitive to the location of the critical section. Since it decreases rapidly with increasing distance from the column as the length of the section increases and the shear force decreases. Added to this complication, the nominal stress that can develop in a slab in an area where both principal moments are significant is also larger

than in a beam. This difference can generally be attributed to three factors (70): (i) the location of the inclined shear cracks, (ii) the triaxial stress conditions in the concrete at the apex of the crack and (iii) the proportionally greater dowel forces in the slabs where non-prestressed bars or bonded tendons are present.

Other factors considered to be of some influence on the punching strength of the slabs are scale effects and the enhancement due to compressive membrane action.

From the few comparative tests of models and prototypes, it appears that scale effect is not significant on shear strength provided the reinforcement and concrete mixes are appropriately scaled. Roll et al (71) built 1/2 scale models of the specimens of Moe (22) and Hognestad and Elsner (23) and obtained excellent correlation between the shear strength of the models and prototypes. Guedelhoefer and Janney (72) conducted similar tests with the same results. Batchelor and Tissington (73) tested models with scales ranging from 1/6 to 1/15 of a hypothetical prototype bridge and observed no significant effect of scale on the local punching strength of partially restrained slabs. From the punching tests of 1/6 and 1/4 scale models of an internal panel, Long confirmed Batchelor's findings and concluded that scale effects do not exist when realistic amounts of slab reinforcement are used (74) but he emphasised that to minimise the problems associated with scaling, the model should be made as large as possible.

Perhaps the single major factor which contributes to the

observed high shear strength capacity of the slabs is the enhancement due to self-generated in-plane forces or membrane action in the slabs. In-plane outward displacements occur with yielding in the slab surrounding a column. Since, however, the outer boundary of the yield portion is elastic these displacements are restrained and axial forces are generated. In the present test arrangement compressive in-plane forces, which can be inferred from Fig.8.64 are induced in the central yielding region due to restraint of the slab by the rigid external frame.

In the area of ordinary reinforced concrete, much reseach has been directed to the effect of membrane forces in increasing the punching capacity of a slab. With regards to post-tensioned unbonded slabs, Franklin et al (30) have similarly incorporated these effects into a design formula for predicting the punching capacity of the column in an internal panel. Their works have been summarised in Chapter Two.

Table 8.10 shows the computed punching strength of present test series using Franklin's simplified design formula (equation 2.7). Using the local reinforcement ratio within the column critical width, the equivalent reinforcement ratio ρ_e was calculated according to equation 2.4, originally proposed by Cleland. The punching capacity is also computed by the method proposed by Cleland (equations 2.4 and 2.5).

It can be observed that both predictions agree fairly well with the observed punching strength of the slabs. Although Cleland's used a similar shear criterion as in Concrete Society,

the modifications he proposed were found to give results better than those of the latter. By comparison, the flexural criterion for punching assumed in Franklin's method yields a slightly better agreement with the observed strength. It is interesting to note that the predicted higher punching capacity for slabs with closely banded tendons over the column is confirmed by the tests. The portion of the load balanced by prestress is not included in the predictions using either methods, if it were the values would be slightly improved.

It seems, therefore, justifiable to use a flexural criterion like that of Franklin for investigating the punching shear behaviour of a post-tensioned unbonded slab having average prestress between 1 N/mm^2 and 3 N/mm^2 and with reinforcement index between 0.075 and 0.25 (30). The present test results have also demonstrated that Franklin's simplified design formula and Cleland's method can be applied to slabs with average prestress lower than 1 N/mm^2. However, for design purposes Cleland's approach is easier to use although it is more conservative.

Further study is needed to determine the influence of banded tendon arrangements on the shear strength of post-tensioned slab, particularly the shear strength of a column with moment transfer which has been demonstrated by Long et al (5,6,7) to be more critical than that of a vertically loaded column.

CHAPTER NINE

Conclusions and Suggestions for Further Research

9.1 Conclusions

9.1.1 Analysis of Prestressing Effects

The representation of the effect of curved prestressing tendons by a transverse load was found to be ideal for use in thin-plate bending analysis using finite element methods.

In the so-called membrane analogy, the proportioning of the total transverse prestressing load over the arbitrarily subdivided slab did not produce complete load-balancing because of the unbalanced load in the column region which introduced stresses into the slab.

It was found to be advantageous for a proportion of the tendons to be banded in fairly narrow column lines e.g. as defined in the Concrete Society Technical Report No.17 (29) rather than in wider column strips as is sometimes recommended.

The support-strip method of prestressing (with all the tendons concentrated in the column lines) effectively counteracted the imposed load moments at the supports but introduced undesirably large moments of the same sense as the imposed load moments in the middle strips between the columns.

The commonly adopted arrangement of banding all the tendons

in the column vicinity in one direction while uniformly distributing those in the other direction (ACI 318-83) has an almost identical prestressing effect to that of a 50/50 two-way column-line distribution (Concrete Society).

Under balanced service load, column-line distribution with a tendon ratio of 70/30 resulted in negligible deflection at mid-panel.

9.1.2 Experimental Investigation

Limitations of Test Slabs

The restrained edges of the test slab were an imperfect model of the deflected profile along the centre lines of an internal panel in a multi-panel slab although the zero slope of the surface in the direction normal to the centre lines was correctly reproduced.

The longitudinal moment distribution along the column centre lines (which included the maximum positive and negative moment) was a good representation of the moment distribution in the actual slab.

The degree of accuracy of the test slab in representing the effect of prestressing was greatest with column-line banding of the tendons and less with column-strip or uniform distribution.

The increase of in-plane stiffness provided by the edge beams of the test slab helped to disperse the in-plane component of the

prestress and an approximately correct uniform distribution of prestress resulted across the middle section of the slab within the column strip width. Unrepresentative high stresses were induced at the edges of the slab.

The total prestress (i.e. in-plane and bending) in the test slab appropriately reflected that in an actual internal panel with a similar tendon distribution within a circle of diameter L/2 centred on the column.

The effect of a uniformly distributed imposed load could be satisfactorily represented in the test slab within a similarly centred circle of diameter L.

Testing Arrangement

The method of loading using an air pressure bag and hand operated hydraulic jack proved to be satisfactory and permitted easy application of uniformly distributed load over the whole concrete surface while maintaining the equilibrating column load.

The test set-up, however, prevented visual observation of cracking and measurement of crack widths in the critical column region. In addition, the operation of turning over the slabs after casting was inconvenient and introduced a risk of premature cracking.

The use of small scale reinforcement and the CCL 2mm wedge-type grip anchorages was satisfactory but the non-prestressed

steel could be improved by some form of deformation to give a more realistic bond with the surrounding concrete.

Within the above experimental limitations, the models with restrained edges satisfactorily reflected the behaviour of a real internal slab structure and allowed redistribution of stresses to take place.

State of Stresses Before Testing

It was not possible to isolate the individual prestress components, i.e. bending and in-plane, experimentally but the overall effects observed in the tests were in fair agreement with the results of the finite element analyses.

High compressive stresses occurred, as predicted, in the column region (bottom surface) of slabs with closely banded tendons. This phenomenon was clearly shown with the support-strip method of tendon arrangement in Cl in which the stresses were comparable with those in other slabs with 50% higher prestress.

Banding of the tendons in the column area induced favourable stresses in the column in the direction transverse to prestress where there was as mush as 40% of the longitudinal prestress.

Serviceability Performance of Test Slabs

Prior to cracking, the load-deflection curves were approximately linear and showed good correlation with elastic

plate solutions.

When the tendons were closely banded in the column vicinity e.g. as recommended by the ACI 318-83 and Concrete Society, the slabs exhibited higher cracking capacity and stiffer post-cracking load-deflection behaviour. This was because the deterioration of flexural stiffness was effectively controlled by the high concentration of steel (both tendons and non-prestressed reinforcement) in the region of the cracks.

In series A and B, slabs with tendons widely spaced in the column and middle strips or uniformly distributed in the span exhibited early cracking and rapid deterioration of flexural stiffness under further loading. This was because the prestressing moments were inefficiently distributed, with the high load moments at the column not adequately counteracted and with the prestress unnecessarily large in the mid-panel region. The residual deflections and crack widths in these slabs were also found to be the greatest in each series.

Tendon layout had little influence on the symmetrical behaviour of the slabs even at loads approaching failure.

Computed Deflections

The short-term deflection of the test slabs was computed by the equivalent frame method as recommended by the ACI Code. An empirical constant α originally suggested by Kripanarayanan and Branson (56) was adopted to signify the reduction of effective

slab stiffness due to differential cracking of the positive and negative moment regions in the span. α has a value less than unity.

When α=1.0 (i.e. slab uncracked) the computed service load deflection was fairly accurate and only underestimated the plate solution by about 6%.

After cracking, the computed load-deflection curves were generally reasonably close to the measured load-deflection curves provided the experimental cracking loads and the appropriate value of α were used.

With α=0.7 (evaluated from recommendations of ACI Committee 435 (58)), fair agreement with test results was obtained (within 13%) for all the slabs in the A series and for some in the B series especially those with tendons closely banded in the column region. The method generally underestimated the deflections of slabs with a low prestress level in which the tendons were also widely spaced (B2,B4).

With a simple average of α=0.5 (as recommended in the ACI 318-83 Code), good correlation was obtained for most of the test slabs. Kripanarayanan and Branson (56) arrived at a similar conclusion regarding the deflection of ordinary reinforced concrete slabs.

Internal Panel Deflections

No direct conclusions can be drawn from this investigation about the short-term and long-term behaviour of an actual internal square panel under various tendon arrangements. However, a simple procedure of multiplying the experimental deflection by the ratio of the theoretical elastic deflection of an internal panel to that of the test slab indicated that the deflection of the internal panels of the corresponding multi-panel slab structures should satisfy the serviceability requirement.

The long-term deflections calculated by the ACI and CP110 methods seemed to suggest that slabs with a medium prestress level (series A) would behave satisfactory since the resultant deflections were within the limit required (L/350). However, in slabs with the minimum prestress level recommended in various codes and with tendons widely spaced in the span it is possible that the slabs would not be serviceable under long-term loading.

Tendon Stress

The CP110 and ACI methods for estimating the tendon stress at ultimate load were unconservative for the test series which was normally less than 14% above the effective prestress. By comparison the BS8110 method resulted in a slightly better correlation with the observed values but it was still unconservative. A more extensive investigation of the validity of the BS8110 method should be carried out.

Ultimate Flexural Strength

All test specimens showed excellent ductility at failure and there was no observable difference in ductility between the slabs in each series.

Although all the slabs were considered to have failed in flexure at about the same ultimate load, the predicted result using yield line theory underestimated the actual failure load by 37% to 63%. This was assumed to be because the ultimate strength was enhanced by membrane action caused by the restraints imposed along the edges which prevented in-plane movement of the slabs.

Punching Shear Strength

Punching shear failure was secondary and was induced by large deflection accompanying large curvature at the negative moment yield lines at the column connection.

The Concrete Society approach and the ACI method significantly underestimated the failure loads of all slabs providing safety factors from 2 to 2.7 and 1.7 to 2 respectively.

The equivalent reinforcement percentage proposed by Cleland et al (6) gave a better correlation with the test results than the method of the Concrete Society although the approach was basically similar. The flexural method of Franklin et al (30) for punching shear which took account of the enhancement due to membrane action

seemed to yield the closest agreement with the results of present test series.

9.2 Suggestions for Further Research

(1) A detailed study of prestressing effects e.g. using the finite element method needs be carried out with particular reference to internal, edge and corner panels of slabs with a wide range of aspect ratio in order to determine the most appropriate tendon layout pattern.

(2) On the basis of the present investigation and those of other researchers, it was shown that the application of correct boundary conditions is an important factor in the study of slab behaviour and more tests should be carried out with models reflecting the actual structural behaviour as realistically as possible.

(3) The combined use of the ACI equivalent frame and I-effective methods give a satisfactory prediction of the deflection of partially prestressed unbonded slabs, provided the correct value of α is used. This may require further verification by tests to ascertain the most appropriate α value for computing the deflection of partially prestressed slabs.

(4) The support-strip method of prestressing highlights the problems of punching shear and two-dimensional load-balancing in the slab and has not been fully

investigated in the present study. More research should be carried out especially since it has been demonstrated in field construction to be a more efficient and better method of prestressing a flat slab.

(5) The behaviour of edge panels with particular reference to slabs subjected to moment-transfer as well as punching shear has not been included in the present investigation. A detailed study is needed as it has been shown by various reseachers that the problem of shear is more critical in the combined loading condition than in that of the vertically loaded column.

(6) The effects of membrane action greatly enhanced the ultimate strength of a slab. Although this problem has been approached by several investigators, the full extent of membrane action has not yet been evaluated, particularly in prestressed slabs.

(7) Because of time restrictions, most investigations into slab behaviour are of a short-term nature and information is lacking on the long-term behaviour of partially prestressed unbonded slabs with particular reference to the effects of creep, tendon arrangement and prestress level on deflection as well as on ultimate strength.

REFERENCES

REFERENCES

1. BRITISH STANDARDS INSTITUTION, "Code of Practice for the Structural Use of Concrete. Part 1 : Design, Materials and Workmanship", London, pp.156, CP110 : Part 1, 1972

2. COMITE EURO-INTERNATIONAL DU BETON and FEDERATION INTERNATIONALE DE LA PRECONTRAINTE, "International Recommendations for the Design and Construction of Concrete Structures", FIP Sixth Congress, Prague. (English edition published by Cement and Concrete Association), June 1970

3. CLARK, B.E., "The Shear Strength of Post-tensioned Flat Slab Floors", ICE Proc., Part 2, Vol.65, March 1978, pp.175-187

4. LONG. A.E. and MASTERSON D.M., "Improved Experimental Procedure for Determining the Punching Strength of Reinforced Concrete Flat Slab Structures", Shear Symposium, Volumn SP-42, ACI, Detroit, 1974, pp.921-935

5. GILBERT, S.G. and LONG, A.E., "Behaviour of Flat Slab/Edge Column Joints", Advances in Concrete Slabs Technology, Proc. of the International Conference on Concrete Slabs at Dundee University, 3-6th April, 1976, pp.185-196

6. CLELAND, D.J., FRANKLIN, Y. and LONG, A.E., "The Punching Strength of Post-tensioned Slabs at the Column", Advances in Concrete Slab Technology, Proc. of the International Conference on Concrete Slab at Dundee University, 3-6th,

1976, pp.197-207

7. FRANKLIN, S.O. and LONG, A.E., "The Punching Behaviour of Unbonded Post-tensioned Flat Plates", Proc. ICE, Part 2, Vol.73, Sept.1982, pp.602-631

8. SCORDELIS, A.C., PISTER, K.C. and LIN, T.Y., "Strength of a Concrete Slab Prestressed in Two Directions", ACI Journal, Vol.28, No.3, Sept. 1956, pp.241-256

9. SCORDELIS, A.C., LIN, T.Y., and ITAYA, "Behaviour of a Continuous Slab Prestrssed in Two Directions", ACI Journal, Vol.56, No.6, Dec. 1959, pp.441-459

10. GAMBLE, W.L., "An Experimental Investigation of the Strength and Behaviour of a Prestressed Concrete Flat Plate", Report T 80-9, Division of Building Research, Commonwealth (of Australia) Scientific and Industrial Research Organisation, Melbourne, 1964

11. BROTCHIE, J.F. and BERESFORD, F.D., " Experimental Study of a Prestressed Concrete Flat Plate Structure", Civil Engineering Transactions, Institution of Engineers, Sydney, Australia, Oct. 1967, pp.276-282

12. ACI STANDARD, 318-71, "Building Code Requirements for Reinforced Concrete (318-71)", American Concrete Institute, Detroit, 1971.

13. NAWY, E.G. and CHAKRABARTI, P., " Deflection of Prestressed Concrete Flat Plates", PCI Journal, March/April 1976,

pp.86-102

14. ACI-ASCE COMMITTEE 423, "Tentative Recommendations for Prestressed Concrete Flat Plates", ACI Journal, Vol.71, No.2, Feb. 1974, pp.61-71

15. BURNS, N.H. and HEMAKOM, R., "Tests of Scale Model Post-tensioned Flat Plates", Journal of Struct. Div., ASCE, Vol.103, No.ST6, June 1977, pp.1237-1255

16. BURNS, N.H. and HEMAKOM, R., "Test of Post-tensioned Flat Plate with Banded Tendons", Journal of the Struct. Div., ASCE, Vol.111, No.9, Sept. 1985, pp.1899-1915

17. KOSUT, G.M., BURNS, N.H. and WINTER, C.Y., "Test of Four-panel Post-tensioned Flat PLate", Journal of Struct. Div., ASCE, Vol.111, No.8, Sept. 1985, pp.1916-1929

18. ACI STANDARD 318-77, "Building Code Requirements for Reinforced Concrete (ACI 318-77)", ACI, Detroit, 1977

19. HAWKINS, N.W. and MITCHELL, D., " Progressive Collapse of Flat Plate Structures", ACI Journal, Vol.77, No.1, July 1979, pp.775-809

20. SCORDELIS, A.C., LIN, T.Y. and MAY, H.R., "Shearing Strength of Prestressed Lift Slabs", ACI Journal, Vol.55, No.4, Oct. 1958, pp.485-506

21. GROW, J.B. and VANDERBILT, M.D., "Shear Strength of Prestressed Light-weight Aggregate Concrete Flat Plates",

PCI Journal, Vol.12, No.4, Aug. 1967, pp.18-28

22. MOE, J., "Shearing Strength of Reinforced Concrete Slabs and Footings Under Concentrated Loads", Development Department Bulletin D47, Portland Cement Assosiation Research and Development Laboratories, April 1961, 135 pp.

23. HOGNESTAD, E., ELSNER, R.C. and HANSON, J.A., "Shearing Strength of Reinforced Structural Light-weight Aggregate Concrete Slabs", ACI Journal, Vol.61, No.6, June 1964, pp.643-656

24. YITZAKI, D., "Punching Strength of Reinforced Concrete Slabs", ACI Journal, Vol.63, No.5, May 1966, pp.527-540

25. GERBER, L.L. and BURNS, N.H., "Ultimate Strength Tests of Post-tensioned Flat Plates", PCI Journal, Vol.16, No.6, Nov/Dec 1971, pp.40-58

26. SMITH, S.W. and BURNS, N.H., "Post-tensioned Flat Plate to Column Connection Behaviour", PCI Journal, Vol.19, No.3, May/June 1974, pp.74-91

27. ACI STANDARD 318-83, "Building Code Requirements for Reinforced Concrete (318-83)", American Concrete Institute, Detroit, 1983

28. HAWKINS, N.M., "Lateral Load Resistance of Unbonded Post-tensioned Flat Plate Construction", PCI Journal Jan/Feb 1981 pp.94-113

29. CONCRETE SOCIETY, "Flat Slabs in Post-tensioned Concrete with Particular Regard to the use of Unbonded Tendon - Design Recommendations", Concrete Society Technical Report No.17, 1979

30. FRANKLIN, S.O., CLELAND, D.J. and LONG, A.E., "A Flexural Method for the Prediction of the Punching Capacity of Unbonded Post-tensioned Flat Slabs at Internal Columns", Proc. ICE, Part 2, Vol.73, June 1982, pp.227-298

31. TIMOSHENKO, S.J., "Plates and Shells", Mc.Graw-Hill Book Co., New York, Internal Student Edition, 1981

32. PARME, A.L., "Prestressing Flat Plates", PCI Journal, Vol.73, No.6, Dec. 1968, pp.14-32

33. LIN, T.Y., "Load-balancing Method for Design and Analysis of Prestressed Concrete Structures", ACI Journal, Vol.60, No.6, June 1963, pp.719-742

34. KOONS R.J. and SCHLEGEL, G.L., "A Practical Approach to the Design of Continuous Structures in Prestressed Concrete", PCI Journal, Vol.8, No.4, Aug. 1963, pp.35-56

35. SAETHER, K., "The Structural Membrane Theory Applied to the Design of Prestressed Flat Slabs", PCI Journal, Vol.8, No.5, Oct. 1963, pp.68-79

36. ROZVANY, G.I.N. and HAMPSON, A.J.K., "Optimum Design of Prestressed Flat Plates", ACI Journal, Vol.60, No.8, Aug. 1968, pp.1065-1082

37. BROTCHER, J.F. and RUSSELL, J.J., "Flat Slab Structures", ACI Journal, Vol.61, No.8, Aug. 1964, pp.959-996

38. WANG, C.H., "Direction Method for Prestressed Concrete Slabs", PCI Journal, Vol.13, No.3, June 1968, pp.62-72

39. CONCRETE SOCIETY, "Post-tensioned Flat-Slab Design Handbook", Concrete Society Technical Report No.25, Jan. 1984

40. FEDERATION INTERNATIONALE DE LA PRECONTRAINTE (FIP), "Recommendations for the Design of Flat Slabs in Post-tensioned Concrete (using Unbonded and Bonded Tendons)", Cement and Concrete Association, Slough, June 1980

41. BUREAU BBR, "Support-Strip Prestressing for Flat Slabs", Bureau BBR Publication, 6th. Dec. 1973

42. WUTHRICH, W., "Post-tensioned Concrete Flat Slabs in Building Design and Construction - The Support-Strip Method", A paper presented at the 9th International Congress of FIP, Stockholm, 6-10th. June 1982

43. MARTI, P., RITZ, P. and THURLIMANN, B., "Prestressed Concrete Flat Slabs", IABSE Surveys S-1/77, 1977, 17 pp.

44. BRITISH STANDARD INSTITUTION, "Structural Use of Concrete. Part 1 : Code of Practice for Design and Construction", London, BS8110, Part 1, 1985

45. PAFEC 75, "Theory, Results", PAFEC Ltd, Nottingham, Dec. 1975

46. PAFEC 75, "Data Preparation", PAFEC Ltd, Nottingham, Nov. 1978

47. POWER, C.A., "Prestressed Flat Slabs", New Zealand Engineering (Wellington), Vol.21, No.8, Aug. 1966, pp.321-327

48. CANDY, C.F., "Prestressed Flat Slabs", New Zealand Engineering (Wellington), Vol.19, No.7, July 1964, pp.258-261

49. HOSSDORF, H., "Model Analysis of Structures", Published by Van Nostrand Reinhold Company Ltd., 1974

50. BACHMANN, H., "Partial Prestressing of Concrete Structures, IABSE Survey", S-11/79, International Association for Bridge and Structural Engineering, Nov. 1979

51. BACHMANN, H., "10 Thesis on Partial Prestressing", FIP proc. of a symposium on partial prestressing, Bucharest, Vol.1, Sept. 1980, pp.92-103

52. BRITISH STANDARDS INSTITUTION, "BS1881, Part 4 and 5 : Method of Testing Concrete", London, 1983

53. WOOD, R.H., "Plastic and Elastic Design of Slabs and Plates", Thames and Hudson, 1961

54. OKAFAR, H.O. and PERRY, S.H., "Post-yield Behaviour of

Bonded Prestressed Concrete Square Slabs subjected to Concentrated Loading", The Struct. Engineer, Vol-60B, No.2, June 1982, pp.21-33

55. NILSON, A.H. and WALTERS, D.B., "Deflection of Two-way Floor Systems by the Equivalent Frame Method", ACI Journal, Proc. Vol.72, No.5, May 1975, pp.210-218

56. KRIPANARAYANAN, K.M. and BRANSON, D.E., "Short-time Deflection of Flat Plates, Flat Slabs and Two-way Slabs", ACI Journal, Proc., Vol.73, No.57, Dec. 1976, pp.686-690

57. BRANSON, D.E., "Application of the I-Effective Method in Calculating Deflections of Partially Prestressed Members", PCI Journal, Vol.27, No.5, Sept/Oct 1982, pp.62-77

58. ACI COMMITTEE 435, "Deflections of Continuous Beams", ACI Journal, Proc. Vol.70, No.12, Dec. 1973, pp.781-787

59. ACI COMMITTEE 435, "State-of-Art Report : Deflection of Two-way Reinforced Concrete Floor Systems", Deflections of Concrete Structures, SP-43, ACI, Detroit, 1974, pp.55-81

60. THE CONCRETE SOCIETY, "Partial Prestressing - Report of a Concrete Society Working Party", Technical Report No.23, May 1983

61. BAKER, A.L.L., "A Plastic Theory for Ordinary Reinforced and Prestressed Concrete including Moment Redistribution in Continuous Members", Magazine of Concrete Research, Vol.1, No.2, June 1949, pp.57-66

62. PANNELL, F.N., "The Ultimate Moment of Resistance of Unbonded Prestressed Concrete Beams", Magazine of Concrete Research, Vol.21, No.66, March 1969, pp.43-53

63. JANNEY, J.R., HOGNESTAD, E. and MC.HENRY, D., "Ultimate Flexural Strength of Prestressed and Conventionally Reinforced Concrete Beams", ACI Journal, Proc., Vol.52, No.6, Feb. 1956, pp.601-620

64. ACI Publication, SP-24, "Models for Concrete Structures", ACI, Detroit, 1970, 495 pp.

65. HATCHER, D.S., SOZEN, M.A. and SIESS, C.P., "Tests on a Reinforced Concrete Flat Plate", Journal of the Structural Division, ASCE Proc., Vol.91, Oct. 1965, pp.205-231

66. GUARALNICK, S.A. and LA FRAUGH, R.W., "Laboratory Study of a 45-Foot Square Flat Plate Structure", ACI Proc., Vol.60, Sept. 1963, pp.1107-1185

67. CLARK, L.A., "Flexural Cracks Similitude in Slabs Spanning One-way", Technical Report 42.496, C & CA, London, 1974, 25pp.

68. CLARK, L.A., "Cracks Similitude in 1:3.7 Scale Models of Slabs Spanning One-way", Technical Report 42.455, C & CA, London, March 1971, 24pp.

69. FREYERMUTH, C.L., "Practice of Partial Prestressing for Continuous Post-tensioned Structures in North America", PCI

Journal, Jan/Feb, 1985, pp.155-182

70. CRISWELL, M.E. and HAWKINS, N.W., "Shear Strength of slabs : Basic Principles and Their Relation to Current Method of Analysis", Shear Symposium, Vol. SP-42, ACI, Detroit, 1974, pp.641-675

71. ROLL, F., ZAIDI, S.T.H., SABNIS, G.M. and CHUANG, K., "Shear Resistance of Perforated Reinforced Concrete Slabs", SP-30, Cracking, Deflection and Ultimate Load : Concrete Slab System, ACI, Detroit, 1971, pp.77-102

72. GUEDELHOEFER, O.C. and JANNEY, J.R., "Correlation of Models and Prototype Results", Symposium on Models of Concrete Structures, ACI Convention, Dallas, Texas, April, 1972

73. BATCHELOR, B de V and TISSINGTON, J.R., "A Study of Partially Restrained Two-way Bridge Slab subjected to Concentrated Loads", Report on Project Q-47 of the Ontario, Joint Highway Research Programme, Queen's University, March, 1972

74. LONG, A.E., "A Review of Recent Developments in Concrete Modelling", Reinforced and Prestressed Micro-concrete Models, The Construction Press, 1980

TABLES

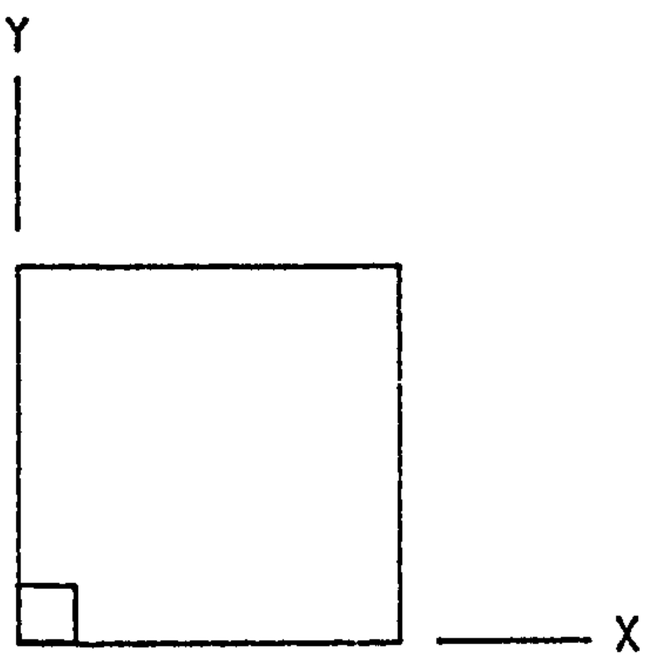

(c/L = 0.1)

	M (0,0)	M_x (L/2,0)	M_y (L/2,0)	M (L/2,L/2)	a (L/2,L/2)
Finite element (1)	-0.4387	0.115	-0.0399	0.0736	0.2015
Classical soln. (2)	-0.4410	0.114	-0.0410	0.0740	0.2016
(1) / (2) * 100%	99.48	101.05	97.32	99.46	99.95

Moment in kNm/m

Deflection in mm

Table 3 Accuracy of element mesh for bending analysis

Slab	Ave. Conc. Prestr. N/mm^2	Column Strip				Middle Strip			
		Negative Moment Region		Positive Moment Region		Negative Moment Region		Positive Moment Region	
		N/mm^2	DEG	N/mm^2	DEG	N/mm^2	DEG	N/mm^2	DEG
A1	1.54	+3.50	0.64	+0.90	0.81	+0.53	0.84	+0.07	0.98
A2	1.54	+4.04	0.58	+0.81	0.83	-0.70	1.21	-0.34	1.10
A3 (x)	1.54	+2.98	0.69	+0.46	0.90	+0.14	0.96	-0.13	1.04
A3 (y)	1.54	+3.03	0.69	+0.50	0.89	+0.21	0.94	-0.09	1.03
A4	1.54	+4.32	0.55	+0.93	0.80	-1.52	1.45	-0.85	1.25
B1	0.89	+6.13	0.37	+2.40	0.49	+1.36	0.60	+1.31	0.60
B2	0.89	+6.33	0.35	+2.34	0.50	+1.05	0.69	+1.29	0.62
B3 (x)	0.89	+5.50	0.43	+2.22	0.52	+1.84	0.46	+1.39	0.60
B3 (y)	0.89	+5.74	0.41	+2.17	0.53	+1.53	0.55	+1.36	0.60
B4	0.89	+6.71	0.33	+2.57	0.45	+0.65	0.81	+1.01	0.70
C1	0.77	+5.69	0.42	+2.35	0.49	+2.63	0.22	+1.99	0.41
C2 (x)	1.54	+3.39	0.65	+0.32	0.93	+0.03	0.99	+0.24	0.93
C2 (y)	0.00	+7.98	0.00	+4.32	0.00	+5.13	0.00	+3.74	0.00

+ve : Tensile
-ve : Compressive

DEG : Degree of Prestress

Table 5.1 Resultant stresses in column and middle strips in internal prestressed panels at full service load

Water	25.45 kg.
Cement (OPC)	45.45 kg.
Coarse sand	81.82 kg.
Fine sand	122.73 kg.

Table 5.2 Proportions of 250 kg. of concrete (*)

* Approximate quantity for each mix

Specimens	Loading rates* (kN/min)
100 mm cubes	180
50 mm cubes	45
150 mm cylinder	318
75 mm cylinder	80

* Correspond to 0.3 N/sq.mm/sec.

Table 5.3 Loading rates for control specimens

Slab	Compressive (N/mm^2)		Tensile (N/mm^2)		Modulus of Elasticity (kN/mm^2)	Poisson's Ratio	Time of Testing (Days)
	Cube	Cylinder	Split Cylinder	Flexural			
A1	51.60	40.81	3.18	4.12	26.34	0.16	30
A2	47.43	33.37	2.61	3.89	24.89	0.15	28
A3	50.31	39.78	3.16	4.32	27.12	0.16	28
A4	51.44	40.54	3.20	4.92	27.36	0.15	28
B1	50.93	40.63	2.89	4.44	27.09	0.16	30
B2	52.87	33.64	2.95	3.94	29.09	0.14	44
B3	48.52	36.24	2.94	4.40	23.88	0.15	30
B4	45.39	38.63	2.91	3.16	26.89	0.15	28
C1	49.21	40.20	2.96	4.46	26.70	0.14	28
C2	49.50	38.57	2.81	4.16	26.35	0.15	28

Table 5.4 Properties of concrete in test slabs

Slab	Average Slab Thickness (mm)	E-W Direction (x)			N-S Direction (y)			Residual Column Load after Clamping (kN)
		Ave. Prestressing Force per Tendon (kN)		Average (*) Concrete Prestress (N/mm^2)	Ave. Prestressing Force per Tendon (kN)		Average (*) Concrete Prestress (N/mm^2)	
		P_e	$\frac{P_e}{P_{pu}}$		P_e	$\frac{P_e}{P_{pu}}$		
A1	42.5	7.64	0.61	1.49	7.56	0.60	1.48	3.39
A2	39.6	7.64	0.61	1.59	7.48	0.60	1.55	2.94
A3	38.7	7.59	0.60	1.55	7.73	0.62	1.57	3.13
A4	38.7	7.90	0.63	1.63	7.73	0.62	1.60	1.47
B1	41.6	7.53	0.60	0.85	7.54	0.60	0.85	1.53
B2	42.9	7.58	0.60	0.87	7.72	0.62	0.85	0.96
B3	40.9	7.86	0.63	0.87	7.73	0.62	0.89	2.24
B4	39.3	7.59	0.60	0.90	7.58	0.60	0.90	1.15
C1	40.5	7.51	0.60	0.74	7.69	0.61	0.73	2.89
C2	42.5	7.59	0.60	1.45	--	--	--	3.13

* Taking accounts of edge beam prestressing forces

Table 5.5 Average prestressing force in test slabs

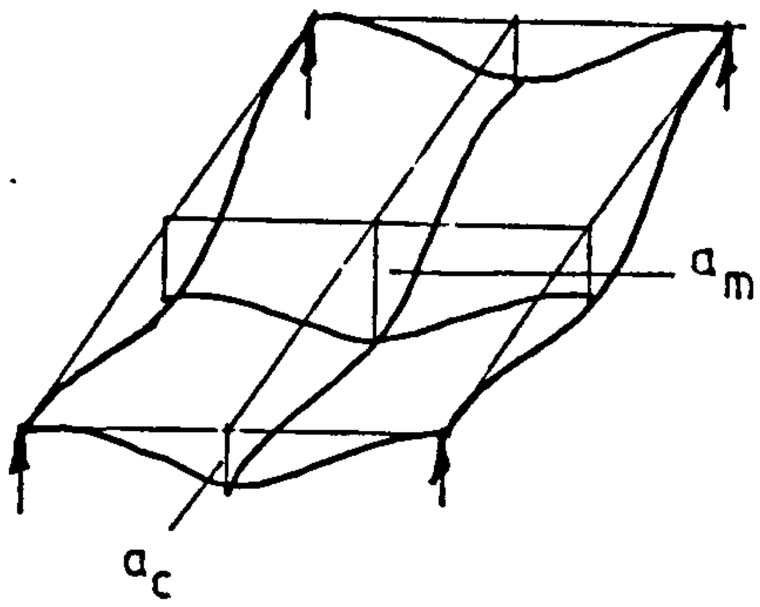

Uniform Loading

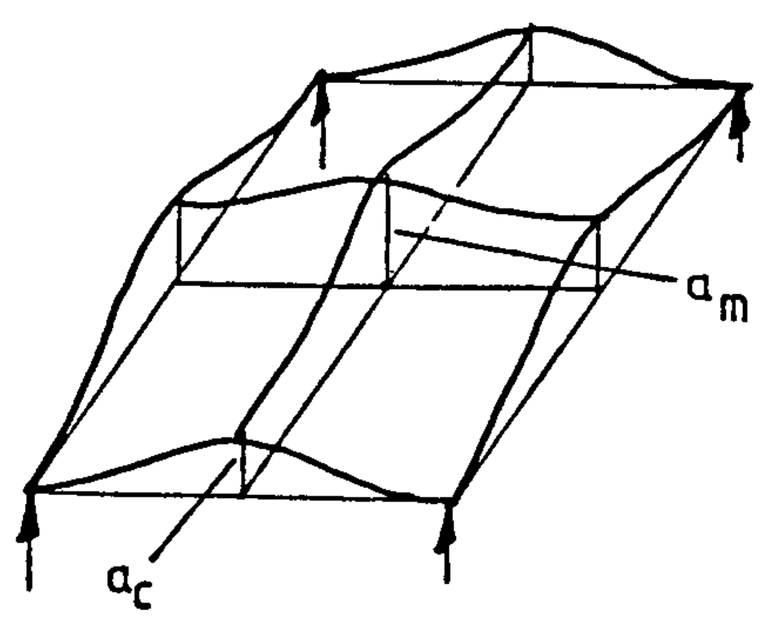

Prestress Loading

	a_m (mm)	a_c (mm)	$\frac{a_m - a_c}{a_m}$
UDL	-1.96	-1.49	0.25
A1	1.25	0.90	0.28
A2	1.19	0.72	0.39
A4	1.17	0.58	0.50
B1	0.72	0.49	0.32
B2	0.69	0.44	0.36
B4	0.68	0.34	0.50
C1	0.68	0.65	0.04

UDL : Uniformly Distributed Load

(a) : Symmetrical tendon arrangement

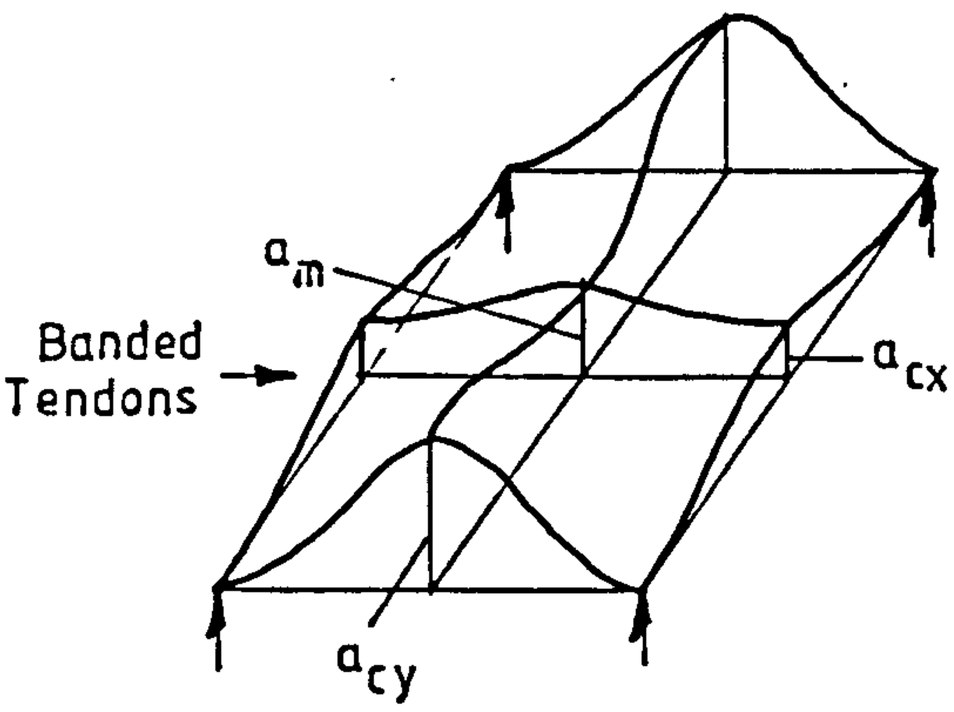

Prestress Loading

	a_m (mm)	a_{cx} (mm)	a_{cy} (mm)	$\frac{a_m - a_{cx}}{a_m}$	$\frac{a_m - a_{cy}}{a_m}$
A3	1.25	0.91	0.91	0.27	0.27
B3	0.74	0.55	0.55	0.26	0.26
C2	0.66	0.91	0.32	-0.38	0.52

(b) : Unsymmetrical tendon arrangement

Table 6.1 Theoretical elastic deflections in internal prestressed panels

	Column Strip		Middle Strip		Total Moment / $W_{bal} L^3$	Balanced Service Load W_{bal} kN/m/m width
	- ve	+ ve	- ve	+ ve		
UDL CP110	50.9 (46.0)	20.7 (22.0)	13.2 (16.0)	15.2 (16.0)	0.1170 (0.1140)	
A1	46.0	22.7	14.0	17.3	0.0995	
A2	36.9	20.7	23.1	19.3	0.0998	
A3 (x)	45.3	23.2	14.7	16.8	0.0996	7.11
A3 (y)	45.3	23.2	14.7	16.8	0.0996	
A4	32.2	17.9	27.8	22.2	0.0998	
B1	43.4	21.8	16.6	18.3	0.0999	
B2	38.2	21.5	21.7	18.6	0.0999	
B3 (x)	45.5	23.4	14.2	16.8	0.1001	4.15
B3 (y)	49.5	23.2	10.4	16.9	0.0999	
B4	32.2	17.9	27.8	22.1	0.0995	
C1	63.2	28.8	-3.3	11.4	0.0996	3.55
C2 (x)	43.0	25.4	16.9	14.7	0.0996	7.11

UDL : Uniformly Distributed Load

Table 6.2 Moment distribution coefficients in internal prestressed panels

	Column Strip				Middle Strip				Total Moment / $W_{bal} L^3$		(1) − (2) / (1)
	− ve		+ ve		− ve		+ ve				
	I.P	T.S (% I.P)	I.P	T.S (% I.P)	I.P	T.S (% I.P)	I.P	T.S (% I.P)	I.P (1)	T.S (2)	
UDL	0.0595	93.9	0.0242	114.4	0.0154	26.8	0.0178	13.4	0.117	0.0904	0.23
A1	0.0458	92.0	0.0226	116.1	0.0139	20.8	0.0172	11.0	0.0995	0.0731	0.27
A2	0.0368	86.2	0.0206	122.2	0.0230	25.5	0.0193	6.5	0.0998	0.0630	0.37
A3 (x)	0.0451	92.2	0.0231	114.6	0.0146	26.4	0.0167	12.9	0.0996	0.0741	0.26
A3 (y)	0.0451	92.2	0.0231	114.6	0.0146	26.4	0.0167	12.9	0.0996	0.0741	0.26
A4	0.0321	80.4	0.0179	131.7	0.0277	22.1	0.0222	-7.9	0.0998	0.0537	0.46
B1	0.0434	90.4	0.0218	118.3	0.0166	21.1	0.0183	6.1	0.0999	0.0695	0.30
B2	0.0382	87.8	0.0215	119.2	0.0217	27.5	0.0186	3.5	0.0999	0.0657	0.34
B3 (x)	0.0455	92.5	0.0234	113.7	0.0142	25.6	0.0168	14.7	0.1001	0.0749	0.25
B3 (y)	0.0493	93.1	0.0234	113.7	0.0104	12.9	0.0169	14.2	0.0999	0.0761	0.25
B4	0.0320	80.4	0.0178	131.6	0.0277	22.0	0.0220	-7.8	0.0995	0.0535	0.46
C1	0.0629	99.2	0.0287	102.4	-0.0033	34.0	0.0113	5.8	0.0996	0.0974	0.02
C2 (x)	0.0428	80.9	0.0253	27.5	0.0168	20.2	0.0146	18.8	0.0996	0.0472	0.53
C2 (y)	0.0151	153.3	0.0033	740.7	-0.0151	11.8	-0.0033	-106.7	---	0.0473	---

I.P : Internal Panel T.S : Test Slab UDL : Uniformly Distributed Load

Table 6.3 Comparison of prestressing moments in test slabs and in actual internal panels

Slab	E - W Direction			N - S Direction			No. of 3.14 mm n.p.s. wires within Column Area	% of n.p.s. wires	
	No. of Tendons	Distr. of Tendons in Column Strip	Ave. Prestress f_{cp} N/mm^2	No. of Tendons	Distr. of Tendons in Column Strip	Ave. Prestress f_{cp} N/mm^2		Negative Moment Region	Positive Moment Region
A1	12	50% - 6 (1)	1.54	12	50% - 6 (1)	1.54	4	0	0
A2	12	67% - 8	1.54	12	67% - 8	1.54	4	0	0
A3	12	100% - 12 (2)	1.54	12	50% - 6	1.54	4	0	0
A4	12	50% - 6	1.54	12	50% - 6	1.54	4	0	0
B1	7	43% - 3 (3)	0.89	7	43% - 3 (3)	0.89	7	0.13	0.19
B2	7	71% - 5	0.89	7	71% - 5	0.89	7	0.13	0.19
B3	7	100% - 7 (4)	0.89	7	50% - 3.5	0.89	7	0.13	0.19
B4	7	50% - 3.5	0.89	7	50% - 3.5	0.89	7	0.13	0.19
C1	6	100% - 6 (1)	0.77	6	100% - 6 (1)	0.77	7	0.13	0.19
C2	12	100% - 12 (2)	1.54	0	----	0.00	4 (E-W) 10 (N-S)	0 (E-W) 0.15 (N-S)	0 (E-W) 0.36 (N-S)

Column Strip Width = 750.0 mm (0.5L)

(1) Band Width = 150.0 mm
(2) Band Width = 330.0 mm
(3) Band Width = 100.0 mm
(4) Band Width = 180.0 mm

% of non-prestressed wires in the negative and positive moment regions is similar in both directions

Table 8.1 Details of test series

Line No. \ Slab		A1	A2	A3	A4	B1	B2	B3	B4	C1	C2
(1)	Span/Depth Ratio	35.3	37.9	38.8	38.8	36.1	35.2	36.7	38.2	37.0	35.3
(2)	Defln. at 11 kN/m^2 (1st. Cycle)	1.50	3.12	2.05	2.20	1.60	1.93	1.81	3.16	2.28	1.55
(3)	Defln. at 11 kN/m^2 (2nd. Cycle)	1.55	3.21	2.12	2.30	1.66	2.09	1.91	3.34	2.41	1.63
(4)	Defln. at 11 kN/m^2 (3rd. Cycle)	--	--	--	--	1.69	2.15	1.95	3.46	2.42	1.69
(5)	Residual Deflection (after 1 cycle)	0.12	0.30	0.10	0.22	0.14	0.24	0.17	0.59	0.27	0.12
(6)	Defln. at Ultimate Load	16.34	17.31	16.25	14.75	22.49	14.90	16.25	15.53	15.15	14.66
(7)	Ultimate Load (kN/m^2)	34.0	27.0	30.0	28.0	32.0	29.0	28.0	26.0	29.0	30.0

Deflection in mm

Table 8.2 Summary of deflections

Line No. \ Slab	A1	A2	A3	A4	B1	B2	B3	B4	C1	C2	
(1) Measured	1.50	3.12	2.05	2.20	1.60	1.93	1.81	3.16	2.28	1.55	
(2) Elastic	1.30	1.85	1.68	1.66	1.34	1.13	1.61	1.61	1.48	1.30	
(3) α = 1.0	1.23	1.61	1.58	1.56	1.26	1.08	1.52	1.52	1.40	1.23	
(4) α = 0.7	1.38	1.96	1.80	1.91	1.61	1.41	1.87	1.98	1.77	1.48	
(5) α = 0.6	1.45	2.11	1.89	2.06	1.77	1.56	2.03	2.21	1.94	1.60	
(6) α = 0.5	1.52	2.29	1.98	2.24	1.97	1.77	2.22	2.49	2.14	1.73	
(7) α = 0.4	1.59	2.50	2.09	2.44	2.19	2.02	2.44	2.85	2.40	1.88	
(8) (3) / (2)	0.94	0.87	0.94	0.94	0.94	0.95	0.94	0.94	0.95	0.95	
(9) (4) / (1)	0.92	0.63	0.88	0.87	1.01	0.73	1.03	0.63	0.78	0.96	Mean = 0.87
(10) (5) / (1)	0.97	0.68	0.92	0.94	1.11	0.81	1.12	0.70	0.85	1.03	Mean = 0.94
(11) (6) / (1)	1.01	0.73	0.97	1.02	1.23	0.91	1.22	0.79	0.94	1.12	Mean = 1.02
(12) (7) / (1)	1.06	0.81	1.02	1.11	1.37	1.05	1.35	0.90	1.05	1.21	Mean = 1.12

Equivalent Frame Method

Deflections in slab A2 are not considered in the mean values

Table 8.3 Experimental and computed deflections

Line No. \ Slab	A1	A2	A3	A4	B1	B2	B3	B4	C1	C2
(1e) Measured (a_e)	1.50	3.12	2.05	2.20	1.60	1.93	1.81	3.16	2.28	1.55
(11) Prestressing Camber from PAFEC (a_p)	0.90	1.19	1.25	1.19	0.54	0.47	0.73	0.66	0.54	0.54
(21) Elastic Deflection from PAFEC (a_m)	1.73	2.48	2.25	2.22	1.79	1.51	2.16	2.16	1.98	1.74
(31) Short-term Deflection (1e) *1.34- (11)	1.11	2.99	1.50	1.76	1.60	2.12	1.69	3.57	2.52	1.54
(41) Long-term Deflection (CP110)	2.16	5.67	2.96	3.49	3.16	4.34	3.14	7.03	4.94	3.00
(51) Long-term Deflection (ACI)	2.22	5.98	3.00	3.52	3.20	4.24	3.38	7.14	5.04	3.08
(61) (41) / Allowable (CP110)	0.50	1.32	0.69	0.81	0.74	1.01	0.73	1.64	1.15	0.70
(71) Adjusting Factor for Span/Depth ratio = 40	1.45	1.18	1.10	1.10	1.37	1.50	1.30	1.15	1.26	1.45
(81) Adjusted Long-term Defln. (41) * (71)	3.13	6.69	3.26	3.84	4.33	6.51	4.08	8.08	6.22	4.35

Deflection in mm

Allowable Deflection (CP110) : Span / 350.0 = 4.29 mm

For long-term deflection calculation $k_c = 36 * 10^{-6}$ N/mm^2 per unit length

Service Load = 11 kN/m^2

i = Internal panel of a multi-panel slab

e = Single slab with experimental boundary conditions

Table 8.4 Estimation of short and long-term deflections in internal panels

Slab	Column Periphery				Slab Edges					
	N - S Span		E - W Span		N - S Span		E - W Span			
	N	S	E	W	N	S	E	W		
A1	--	8	--	8	18	15	15	17	Observed	
	8.4				15.0				I.P	Computed
	9.9				21.6				E.P	
A2	--	--	--	--	14	--	18	18	Observed	
	6.3				12.3				I.P	Computed
	7.2				21.1				E.P	
A3	--	8	--	7	--	15	22	22	Observed	
	8.2				13.9				I.P	Computed
	8.9				21.7				E.P	
A4	7	7	6	6	16	16	18	--	Observed	
	6.2				11.8				I.P	Computed
,	7.1				17.3				E.P	
B1	7	7	7	7	15	15	15	15	Observed	
	5.6				10.5				I.P	Computed
	6.2				14.1				E.P	
B2	5	6	5	5	11	--	11	--	Observed	
	5.4				11.4				I.P	Computed
	6.0				14.8				E.P	
B3	9	9	9	9	11	11	11	11	Observed	
	6.2				11.1				I.P	Computed
	6.9				16.3				E.P	
B4	5	5	4	4	11	--	--	11	Observed	
	4.4				9.1				I.P	Computed
	4.9				12.0				E.P	
C1	8	5	6	6	11	--	11	11	Observed	
	6.4				10.7				I.P	Computed
	7.2				14.6				E.P	
C2	6	7	9	8	11	11	15	15	Observed	
	5.0		8.2		7.4		16.3		I.P	Computed
	5.3		9.2		11.7		19.8		E.P	

I.P : Internal Panel of a Multi-panel Slab

E.P : Experimental Panel

Load in kN/m^2

Table 8.5 Observed and computed cracking loads .

Slab	Ave. Total Concrete Strain			Ave. Cracking Strain (2)	$\frac{f_t'}{E_o}$ (3)	Total Tensile Strain (1) - (2) + (3)	Ave. Crack Width (mm)	Hypothetical Tensile Stress at Column Face (N/mm^2)
	1st. Cycle (1)	2nd. Cycle	3rd. Cycle					
A1	1093	1151	--	400	121	814	0.049	+6.87
A2	--	--	--	--	--	--	--	+10.57
A3	894	925	--	515	117	496	0.030	+8.07
A4	1150	1187	--	342	117	880	0.053	+11.95
B1	965	--	1012	274	107	798	0.048	+10.68
B2	1389	--	1361	160	101	1330	0.081	+12.65
B3	960	--	1064	391	123	692	0.042	+9.90
B4	2572	--	2419	175	108	2506	0.150	+13.68
C1	1296	--	1376	248	111	1159	0.070	+9.76
C2	1269	--	1298	507	107	869	0.052	+7.14 (P) +10.56 (N)

Strain = $1.0 * 10^{-6}$

Service Load = 11 kN/m^2

P = Prestressed Direction

N = Non-prestressed Direction

Table 8.6 Approximate crack widths at service load

Slab	$\frac{\rho_{ps} f_{ps}}{f_{cu}}$	% Increase in Effective Tendon Stress			Test (%)	$\frac{\text{Test}}{\text{CP110}}$	$\frac{\text{Test}}{\text{BS8110}}$	$\frac{\text{Test}}{\text{ACI}}$
		CP110 (Table 38)	BS8110 (Eqn. 52)	ACI 318-83 (Eqn. 18-5)				
A1	0.028	23.0	13.2	15.8	8.8	0.38	0.67	0.56
A2	0.032	22.7	13.1	14.7	7.4	0.33	0.56	0.50
A3	0.031	22.8	13.0	14.9	6.0	0.26	0.46	0.40
A4	0.031	22.8	12.8	14.8	5.1	0.22	0.40	0.34
B1	0.016	23.9	13.8	23.0	14.3	0.60	1.03	0.62
B2	0.016	23.9	13.7	22.9	7.3	0.31	0.53	0.32
B3	0.018	23.8	13.3	21.0	9.8	0.41	0.74	0.47
B4	0.020	23.6	13.7	19.7	7.5	0.32	0.55	0.38
C1	0.015	23.9	13.8	24.1	10.2	0.43	0.74	0.42
C2	0.029	23.0	13.1	15.5	9.8	0.43	0.75	0.63

Table 8.7 Observed and computed tendon stress increase at ultimate load

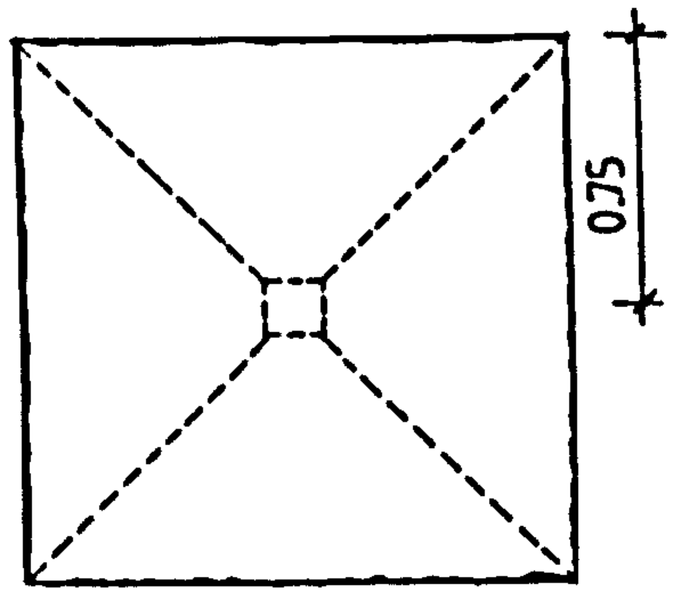

Mode 1

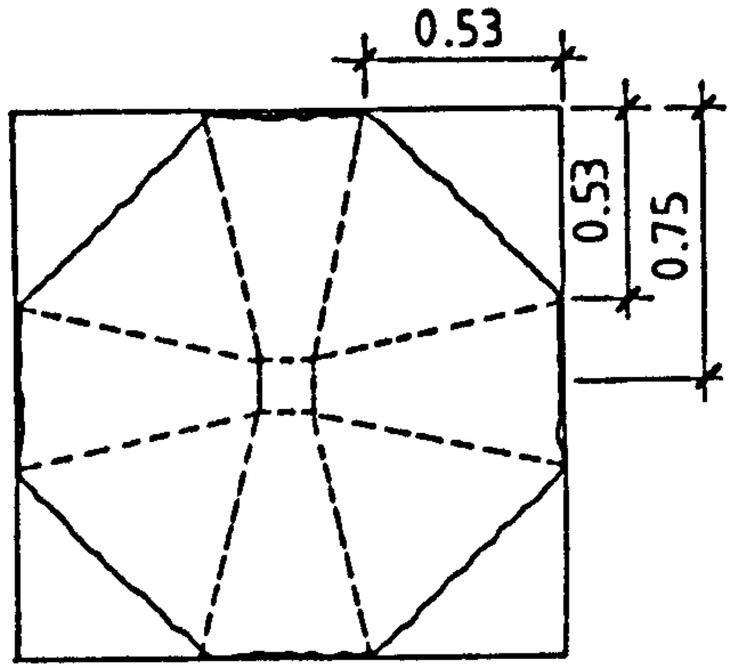

Mode 2

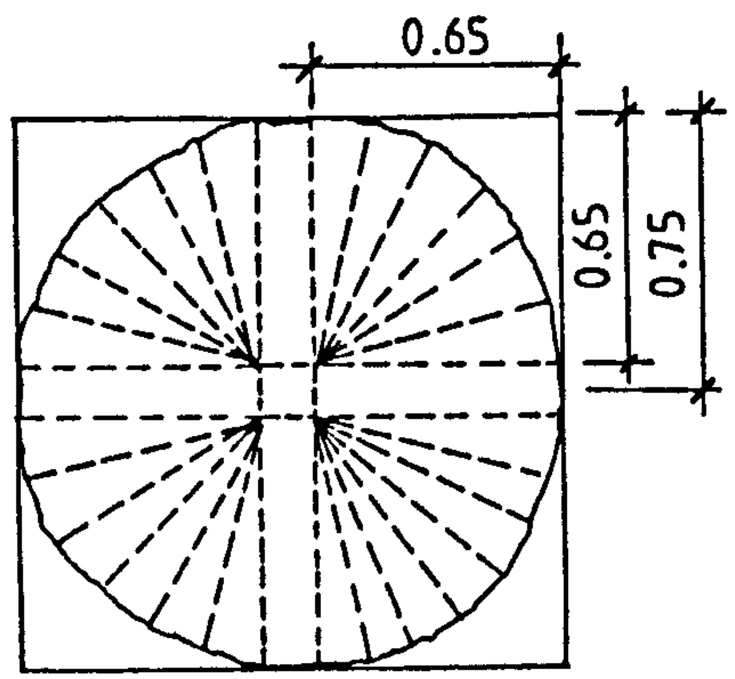

Mode 3

Slab	Observed Failure Load (1)	Calculated Failure Load			(1)/(2)	(1)/(3)	(1)/(4)
		Mode 1 (2)	Mode 2 (3)	Mode 3 (4)			
A1	34.0	27.0	20.8	20.0	1.26	1.63	1.70
A2	27.0	24.9	19.0	18.3	1.08	1.42	1.48
A3	30.0	24.9	19.3	18.6	1.20	1.55	1.61
A4	28.0	25.3	19.6	18.9	1.11	1.43	1.48
B1	32.0	27.2	21.0	20.2	1.18	1.52	1.58
B2	29.0	27.4	21.2	20.3	1.06	1.37	1.43
B3	28.0	26.5	20.5	19.7	1.06	1.37	1.42
B4	26.0	24.6	19.0	18.3	1.06	1.37	1.42
C1	29.0	24.3	18.8	18.1	1.19	1.54	1.60
C2	30.0	24.8	19.1	18.4	1.21	1.57	1.63

Load in kN/m^2

Table 8.8 Observed and computed flexural strength

Slab	Concrete Society (C.S)				ACI 318-83				V_p	C.S V_o	ACI V_{ow}	V_{Test}	$\frac{V_{Test}}{V_o}$	$\frac{V_{Test}}{V_{ow}}$
	f_{cu}	ρ^*	v_o	V (1)	f_o	f_{cp}	v_{ow}	V (2)	(3)	(1) + (3)	(2) + (3)			
A1	51.60	0.024	1.08	30.7	40.81	1.49	2.30	36.8	5.6	36.3	42.4	76.5	2.11	1.80
A2	47.43	0.011	0.81	22.0	33.37	1.57	2.17	34.8	1.9	23.9	36.7	60.8	2.54	1.66
A3	50.31	0.017	0.95	25.6	39.78	1.56	2.30	36.8	4.0	29.6	40.8	67.5	2.28	1.65
A4	51.44	0.011	0.83	22.3	40.54	1.62	2.33	37.3	1.9	24.2	39.2	63.0	2.60	1.61
B1	50.93	0.018	0.97	27.0	40.63	0.85	2.10	33.6	2.8	29.8	36.4	72.0	2.42	1.98
B2	52.87	0.010	0.81	22.9	33.64	0.86	1.94	31.1	0.9	23.8	32.0	65.3	2.74	2.04
B3	48.52	0.018	0.96	26.5	36.24	0.88	2.01	32.2	3.7	30.2	35.9	63.0	2.09	1.75
B4	45.39	0.010	0.77	20.9	38.63	0.90	2.07	33.2	0.9	21.8	34.1	58.2	2.68	1.72
C1	49.21	0.028	1.11	30.5	40.20	0.74	2.10	33.6	5.6	36.1	39.2	--	--	--
C2	49.50	0.016	0.92	25.9	38.54	1.45 (x)	2.14	34.3	3.2	29.1	37.5	--	--	--

Punching Shear in kN

Stress in N/mm^2

Table 8.9 Comparison of observed and computed punching shear capacity (Concrete Society and ACI)

Slab	d (mm)	f_{cp} (N/mm^2)	f_{pb} (N/mm^2)	f_{cu} (N/mm^2)	ρ_{pe} ($*10^{-3}$)	ρ_e ($*10^{-3}$)	ρ_e ($*10^{-2}$)	ω_e	V_{CL} (kN)	V_{FR} (kN)	V_{Test} (kN)	$\frac{V_{Test}}{V_{CL}}$	$\frac{V_{Test}}{V_{FR}}$
A1	33.7	1.49	1186	51.60	6.404	4.088	1.674	0.183	48.6	68.6	76.5	1.57	1.16
A2	33.2	1.57	1165	47.43	2.134	4.088	0.806	0.096	37.3	44.5	60.8	1.63	1.36
A3	33.8	1.56	1165	50.31	4.054	4.088	1.173	0.131	42.0	57.1	67.5	1.61	1.18
A4	33.2	1.62	1178	51.44	2.134	4.088	0.811	0.089	37.9	46.7	63.0	1.66	1.35
B1	33.7	0.85	1236	50.93	3.201	7.156	1.340	0.149	47.0	56.6	72.0	1.53	1.27
B2	34.0	0.86	1177	52.87	1.067	7.156	0.912	0.097	42.9	48.4	65.3	1.52	1.35
B3	33.5	0.88	1228	48.52	3.467	7.156	1.391	0.162	46.2	55.7	63.0	1.37	1.13
B4	34.0	0.90	1170	45.39	1.067	7.156	0.911	0.113	39.0	45.0	58.5	1.50	1.30
C1	33.5	0.74	1202	49.21	6.616	7.156	2.013	0.231	50.6	65.8	--	--	--
C2	33.0	1.45	1195	49.50	5.764	7.305	1.872	0.213	50.1	63.8	--	--	--

CL : Cleland

FR : Franklin

Table 8.10 Comparison of observed and computed punching shear capacity
(Cleland and Franklin)

FIGURES

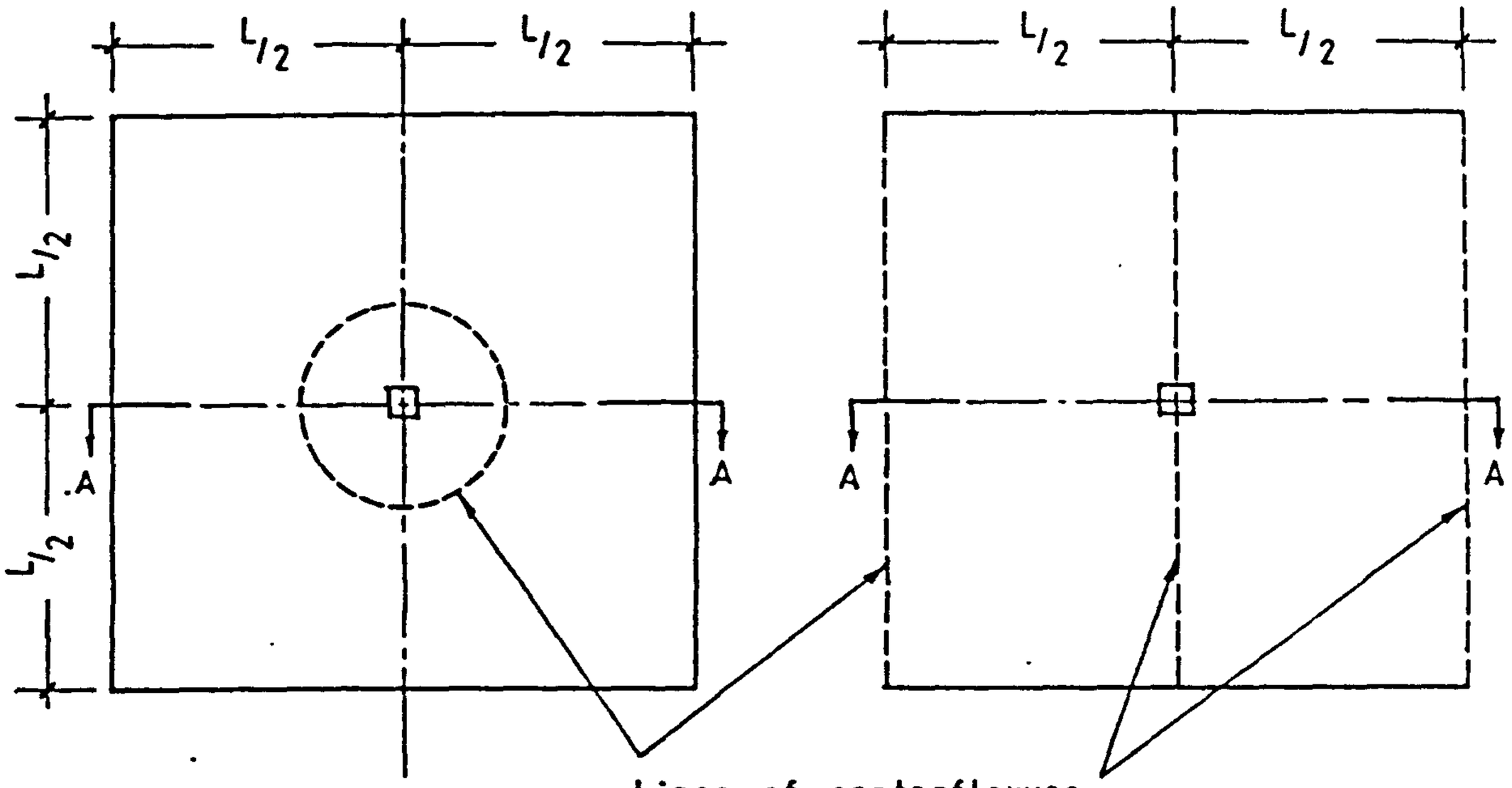

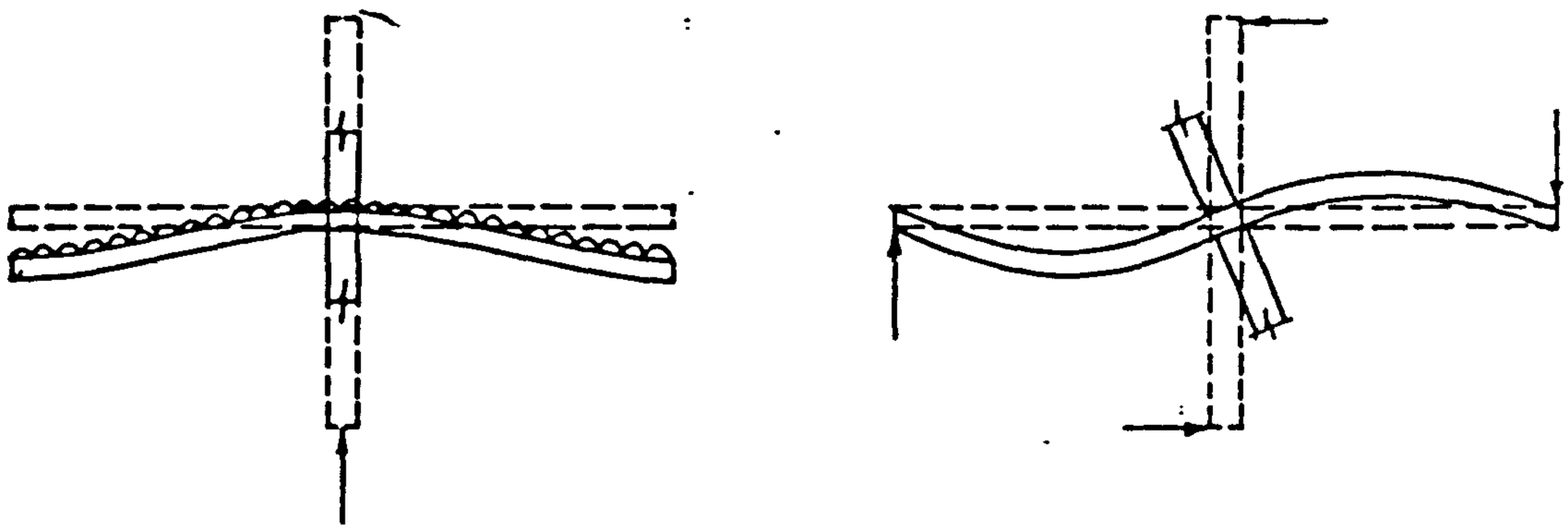

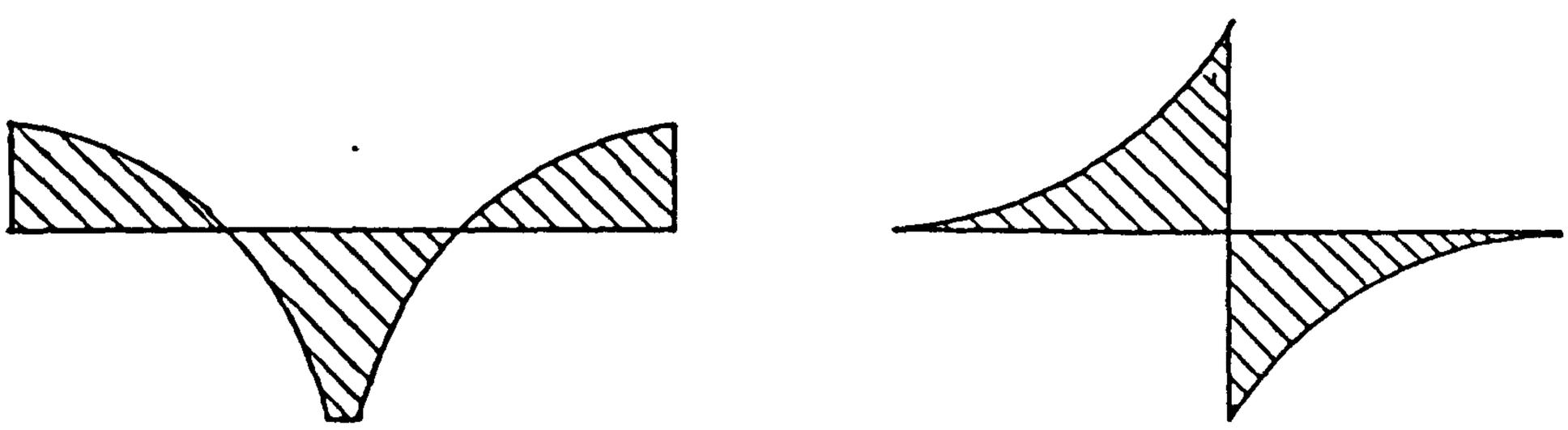

Fig. 1.1 Typical internal panel of a flat slab structure

(From ref. 4)

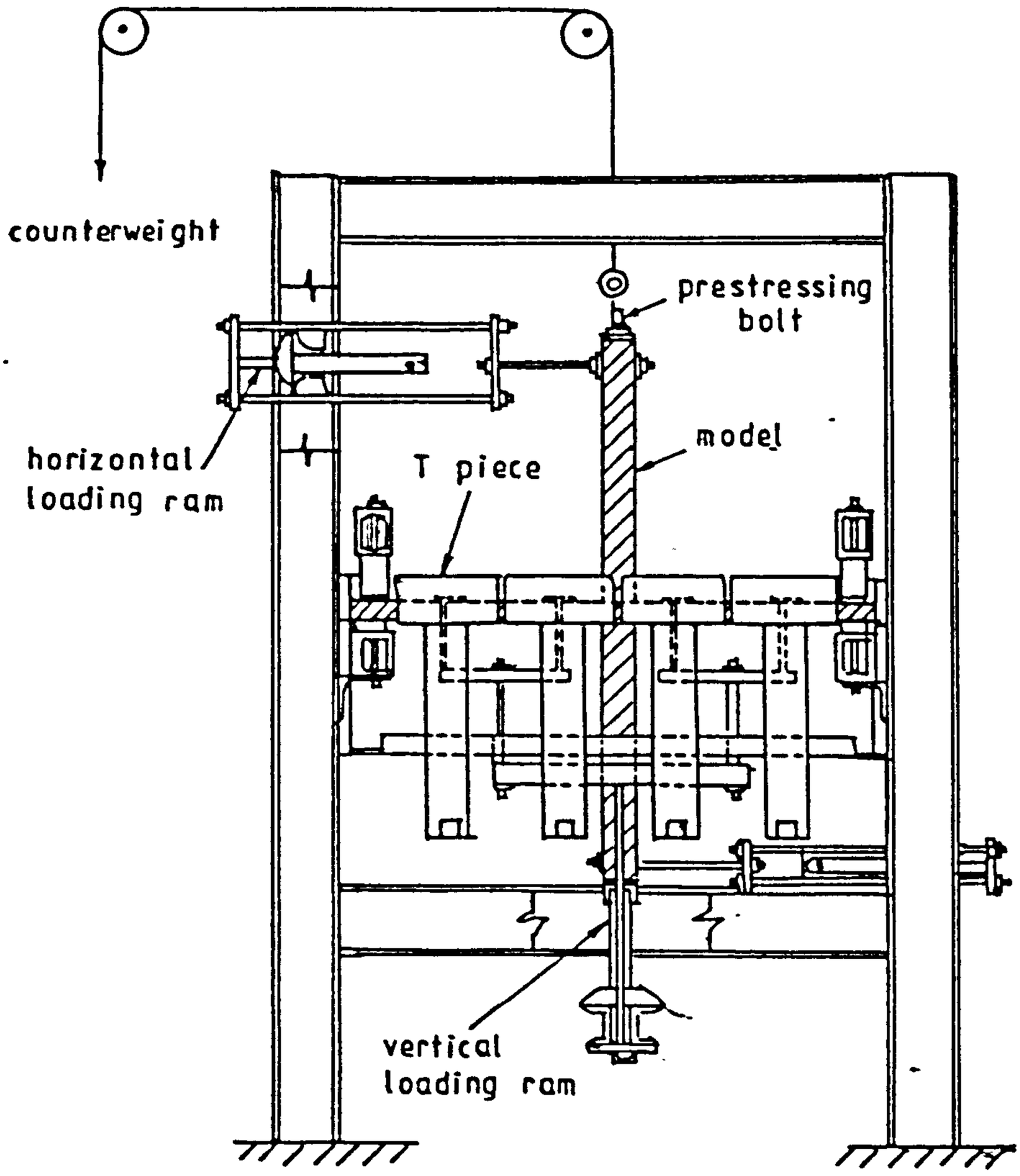

Fig. 1.2 Loading setup (ref. 4)

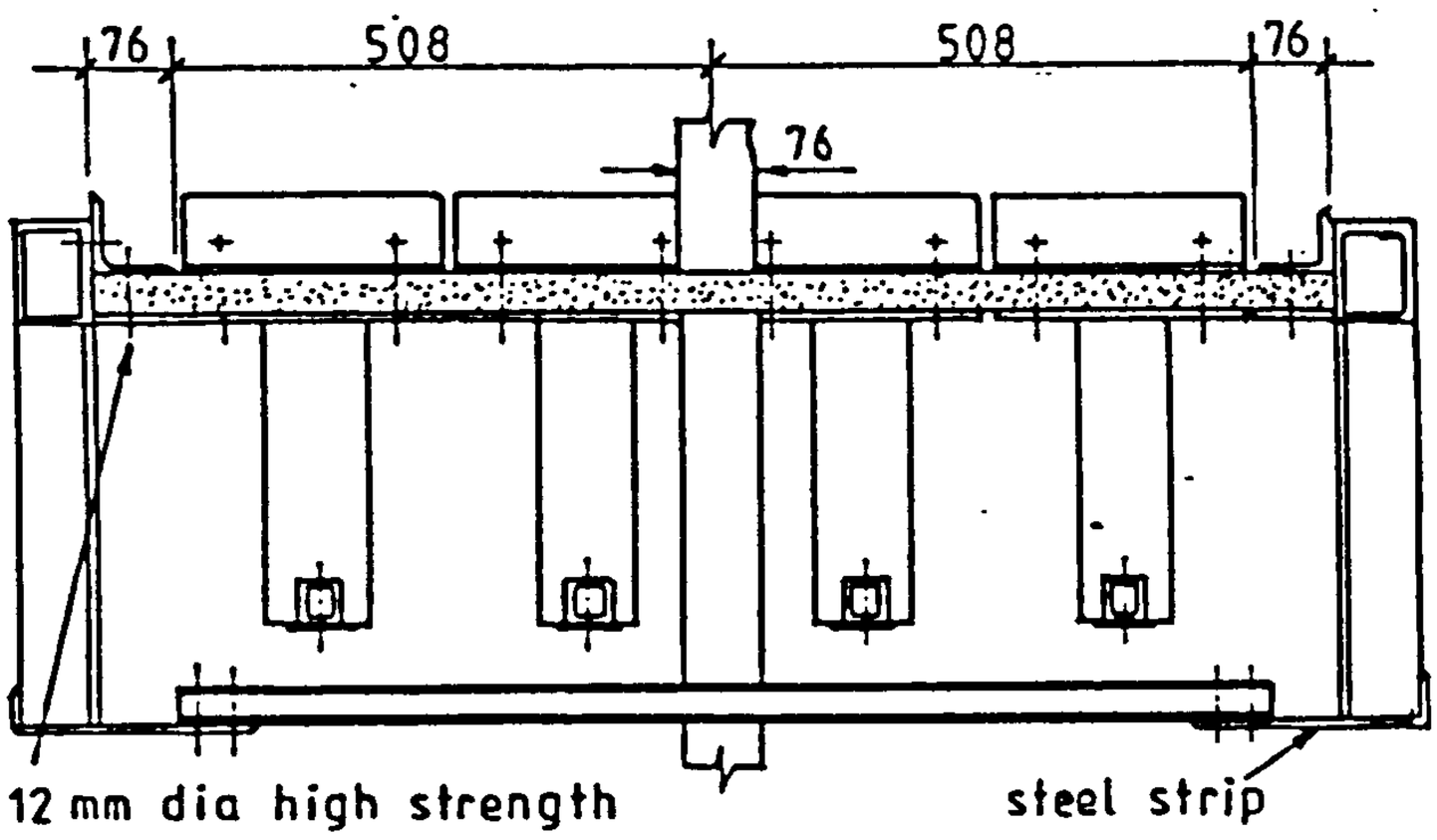

(a) Details of edge restraining system

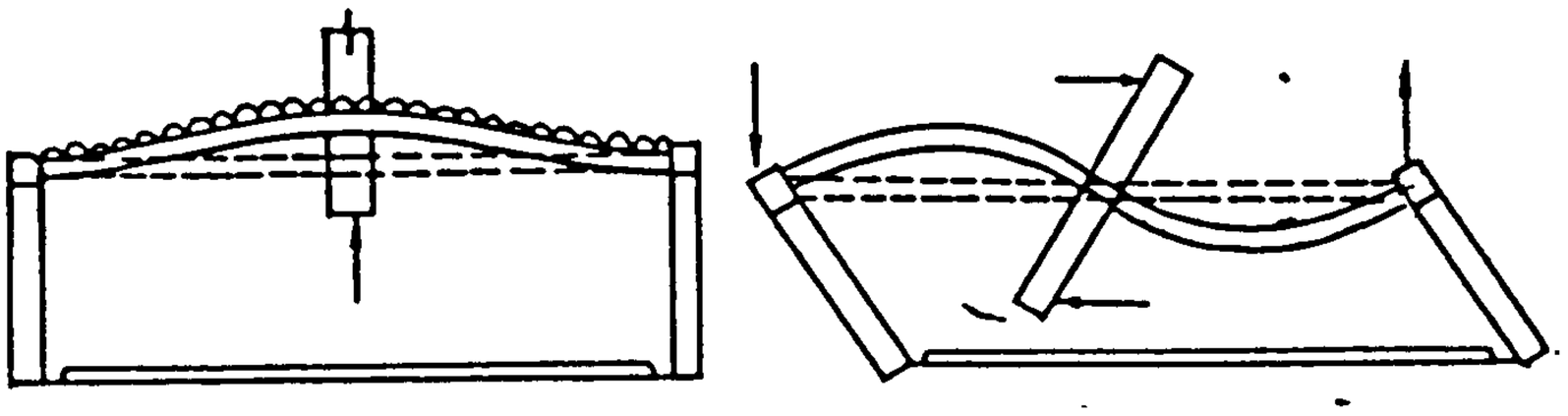

(b) Idealized function of edge restraints

Fig. 1.3 System of edge restraints
(ref. 4)

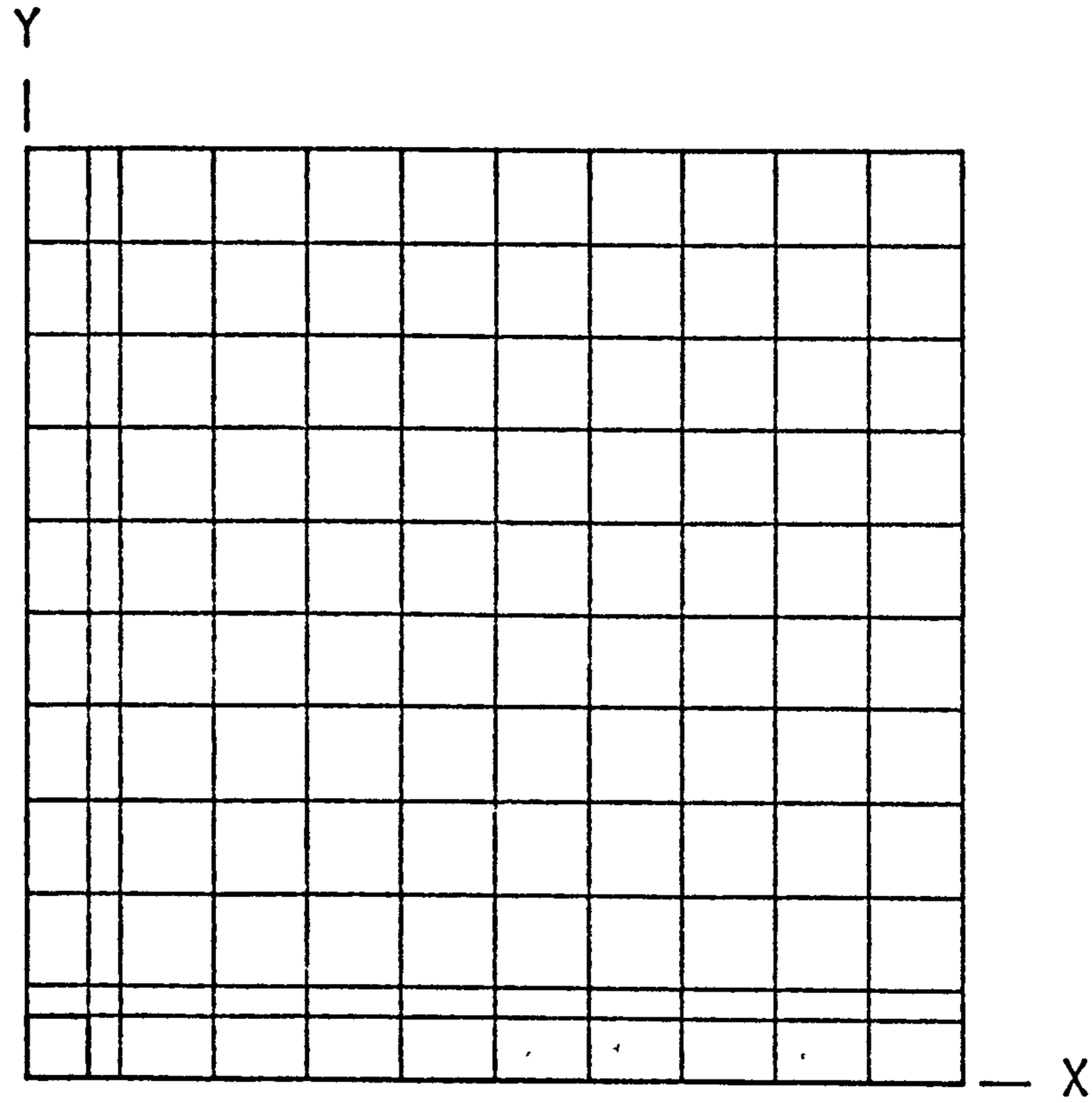

(a) Bending analysis

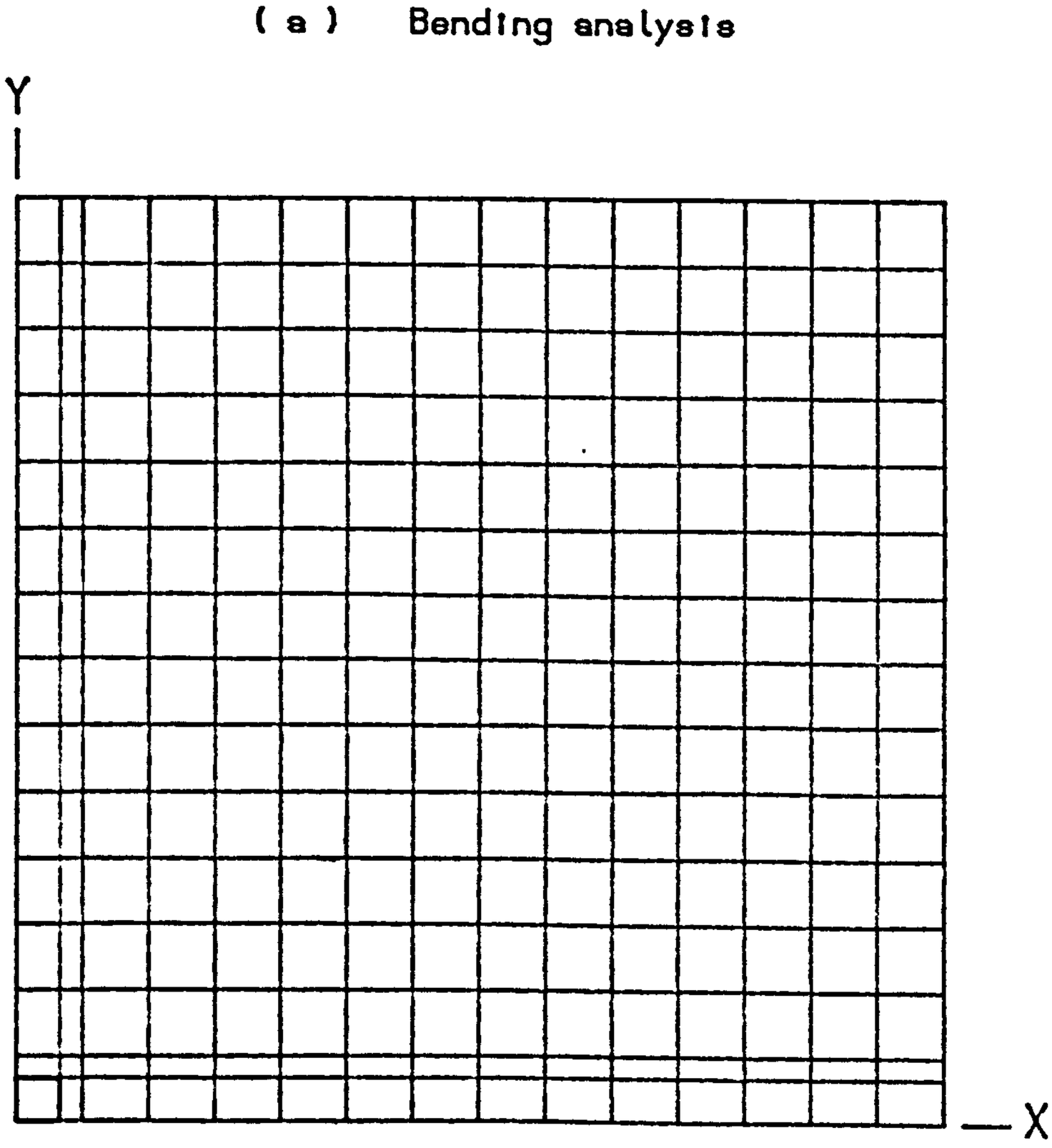

(b) In-plane prestress analysis

Fig. 3.1 Meshing of quarter panel for finite element analysis

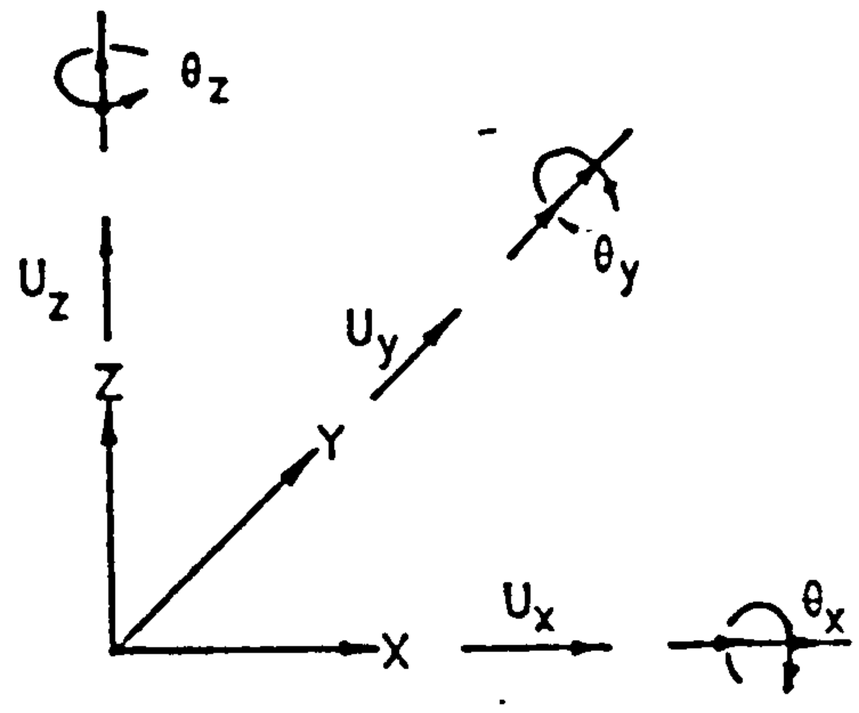

	Translations			Rotations		
Degree of freedom	U_x	U_y	U_z	θ_x	θ_y	θ_z
Numerical code in PAFEC	1	2	3	4	5	6

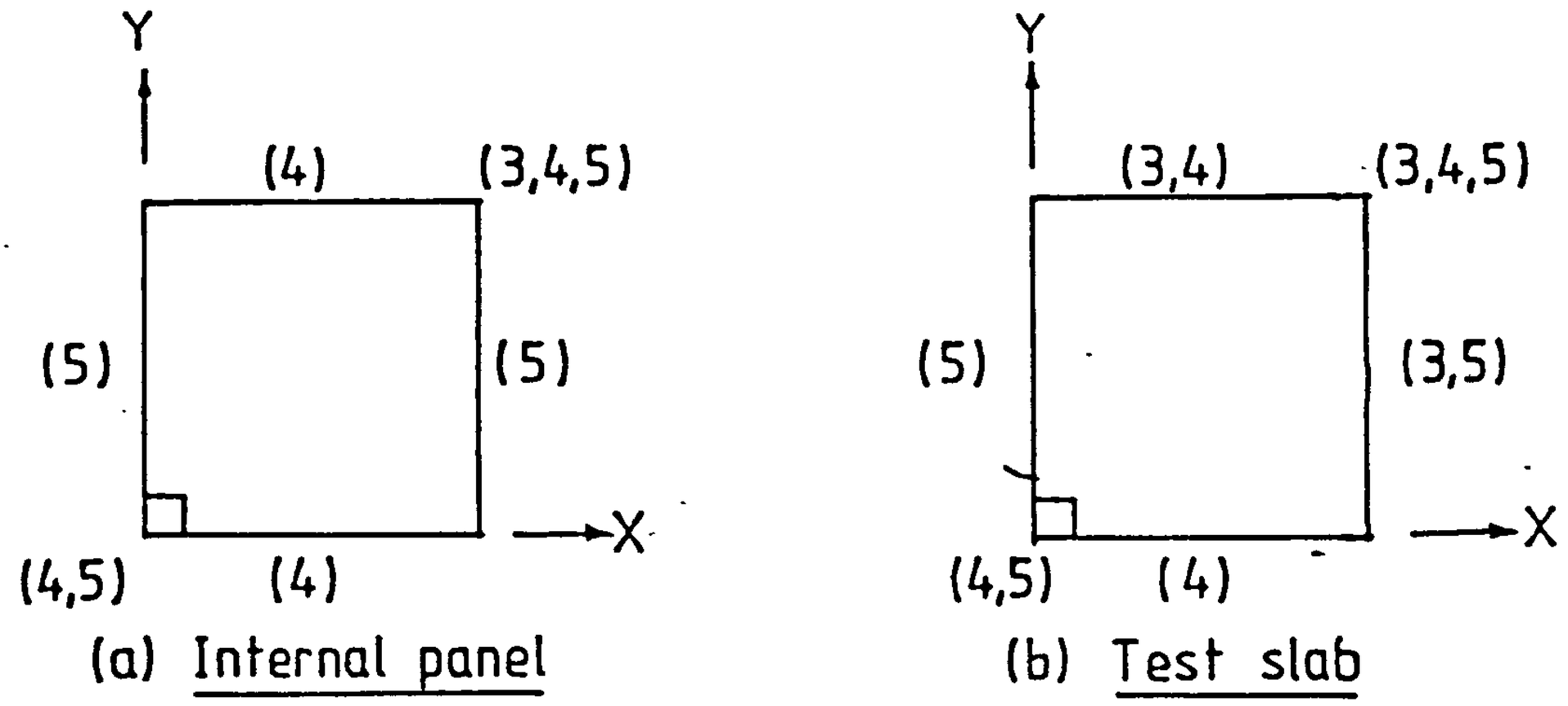

Bending Analysis

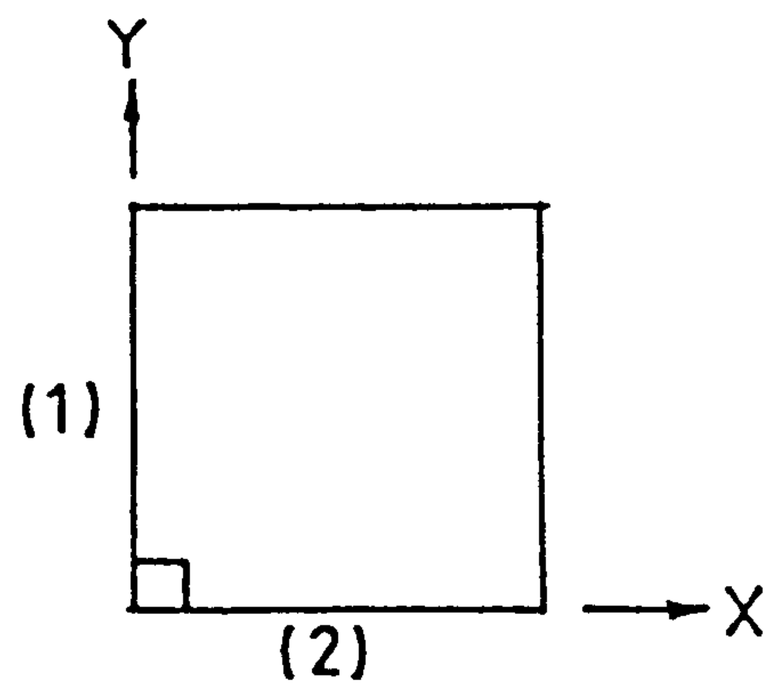

Fig. 3.2 Notation and Boundary Constraints in PAFEC Analysis

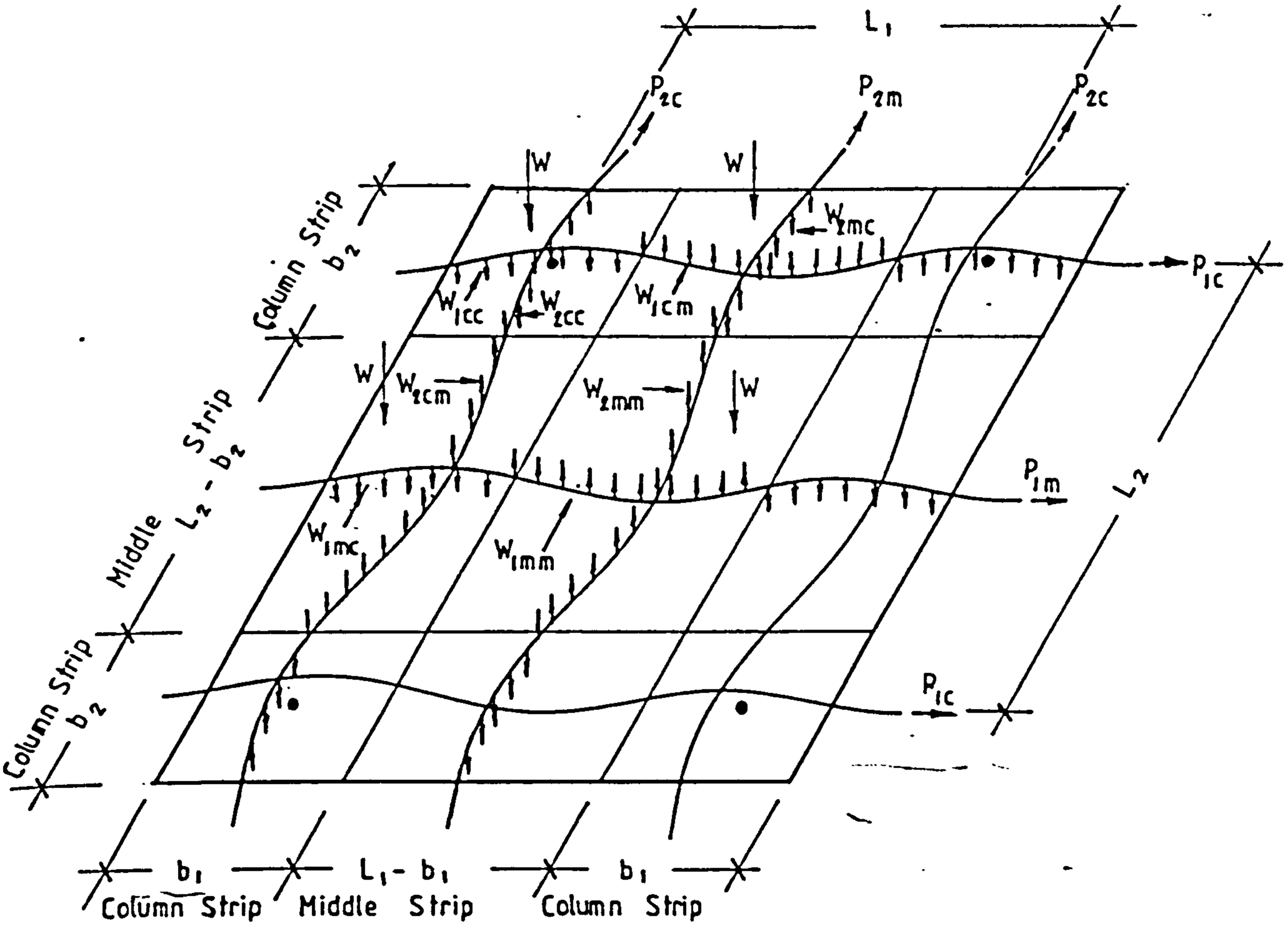

Fig. 4.1 Membrane Analogy (Reference 35)

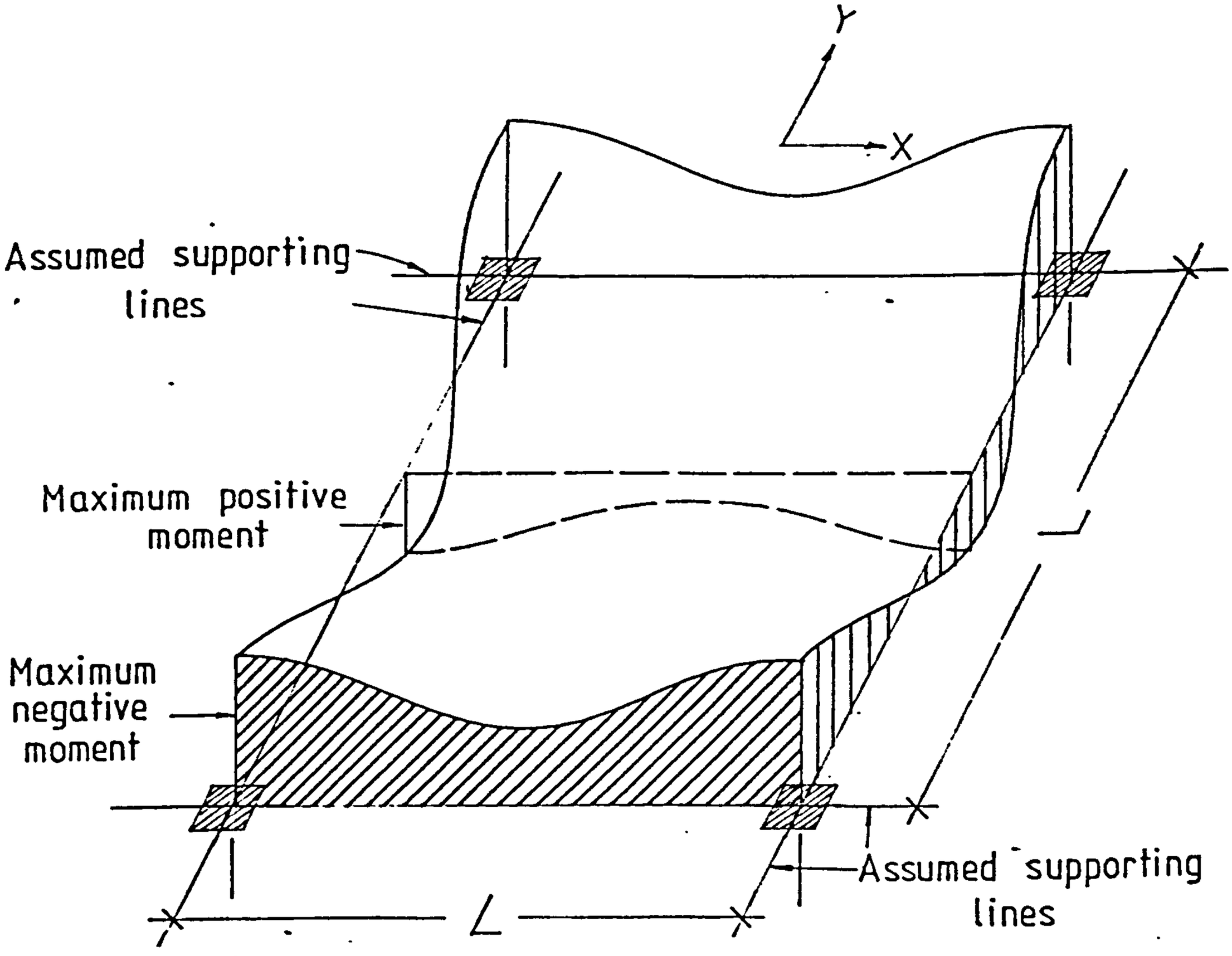

Moment distribution transverse to Y-direction

Fig.4.2 Theoretical moment distribution in a square flat slab analysed in one-direction

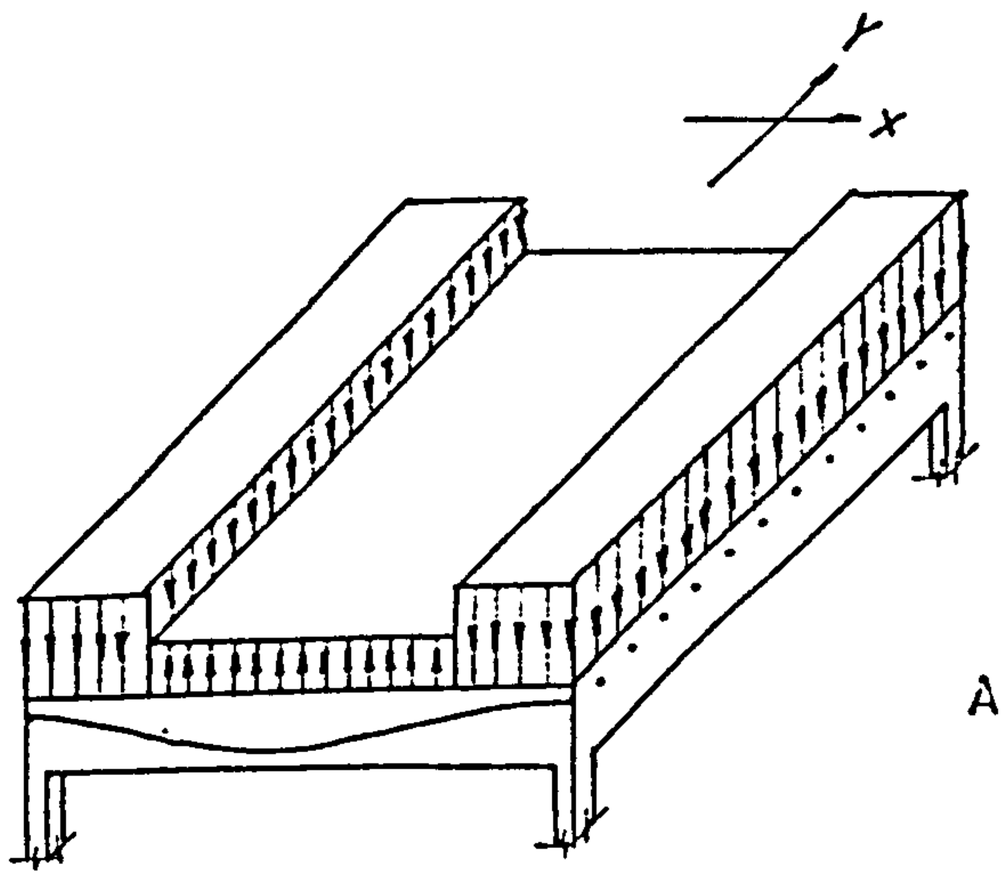

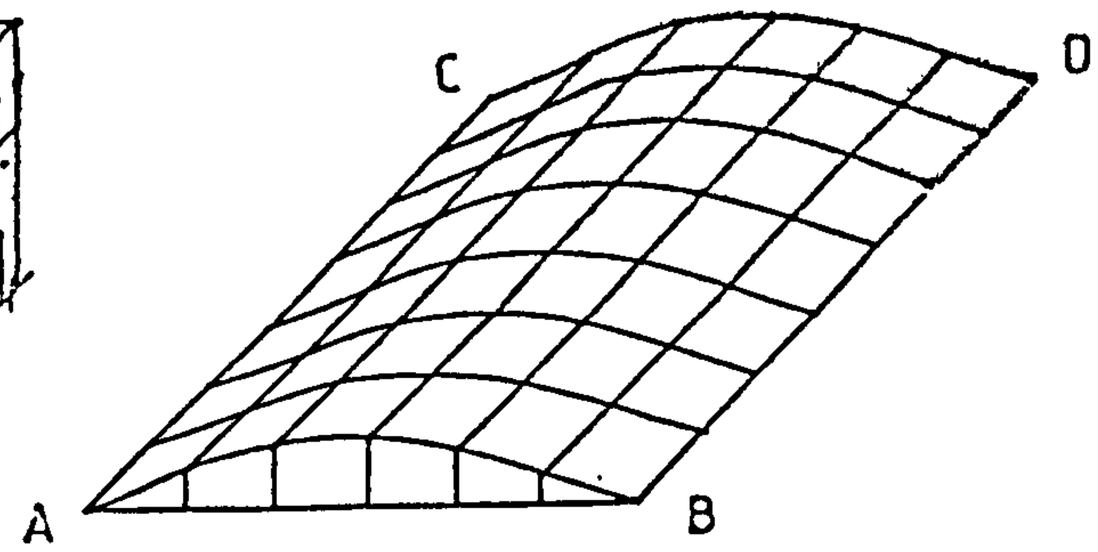

(a) Transverse prestress loads

(b) Deformed surface

Fig. 4.3 Uniform tendon spacing

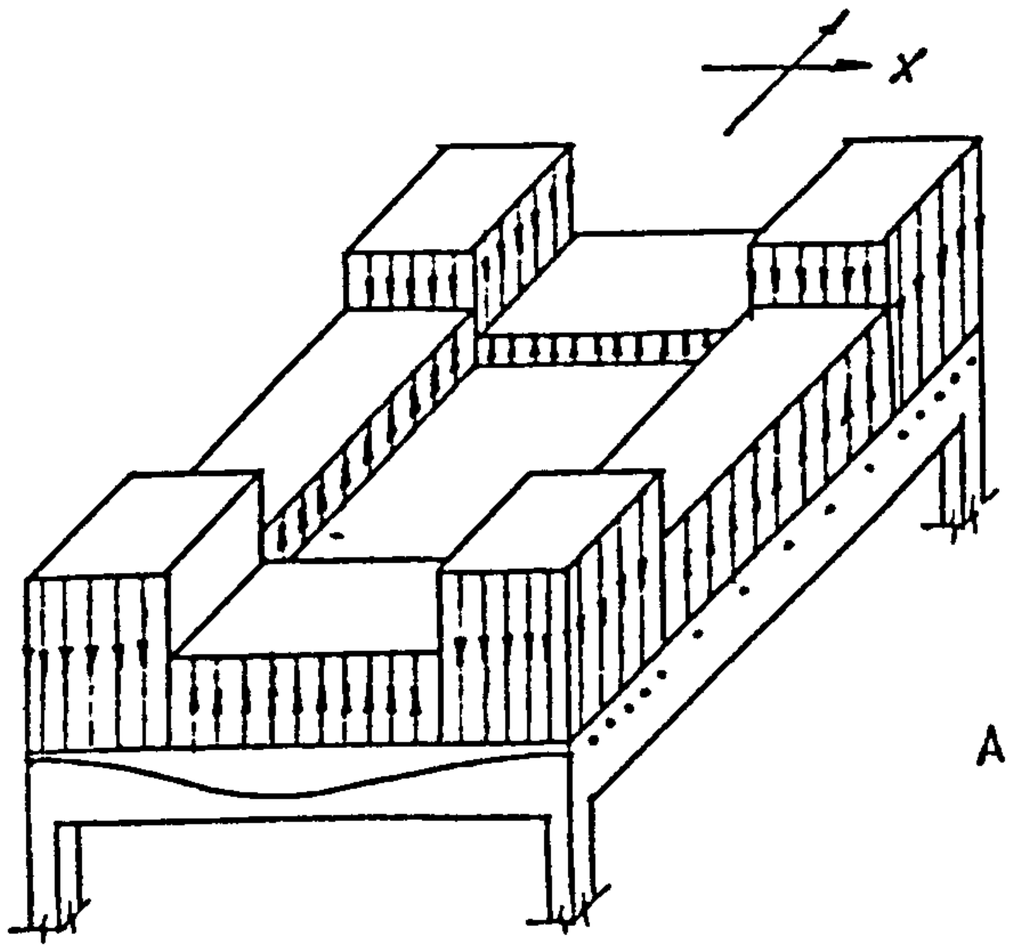

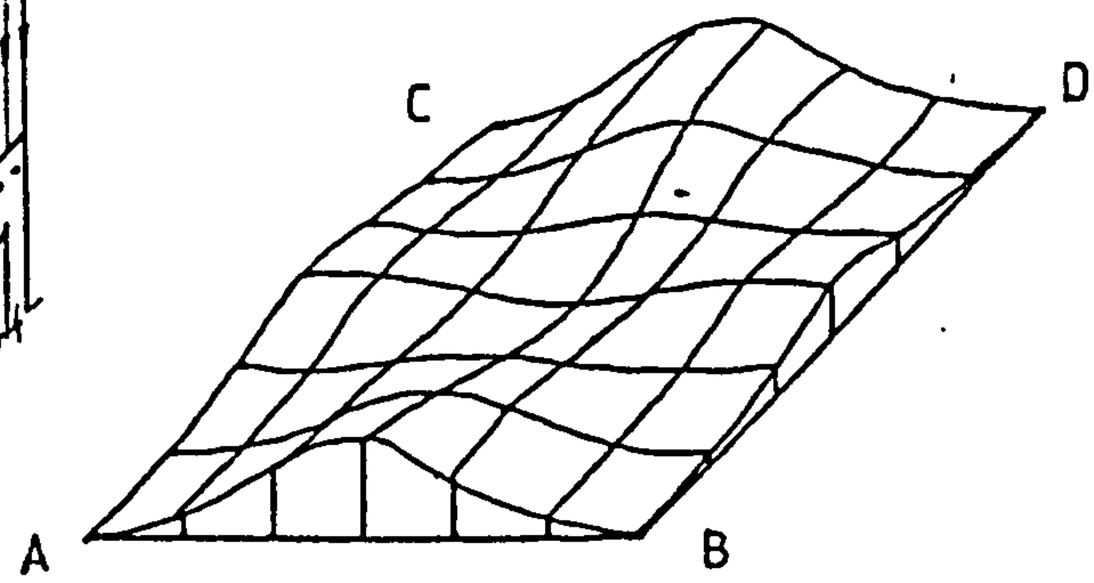

(b) Transverse prestress loads

(b) Deformed surface

Fig. 4.4 Variable tendon spacing
(From ref. 32)

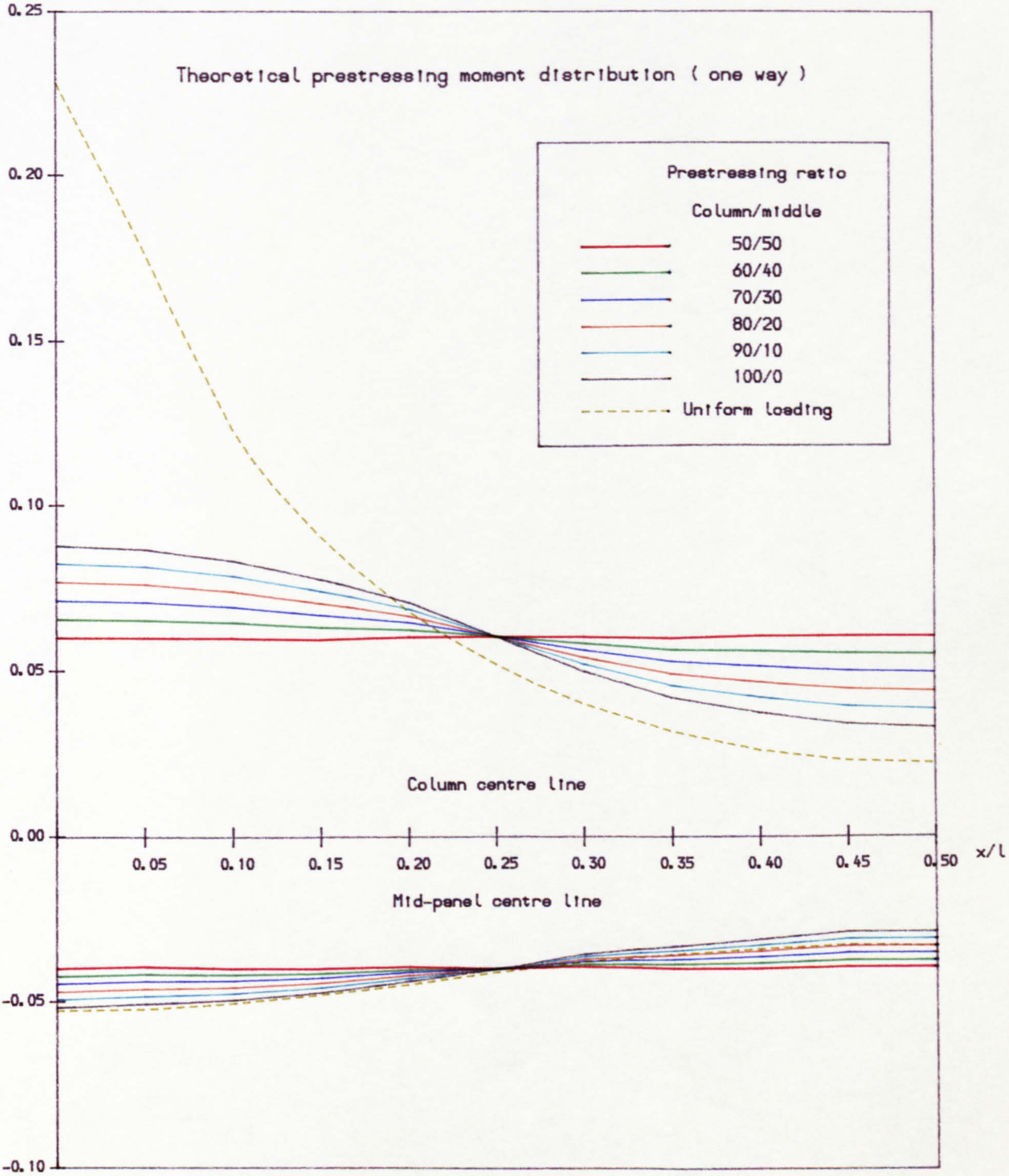

Fig. 4.5 Effect of variation of column-strip/middle-strip prestressing intensities
(Column-strip width/span ratio : 0.5)

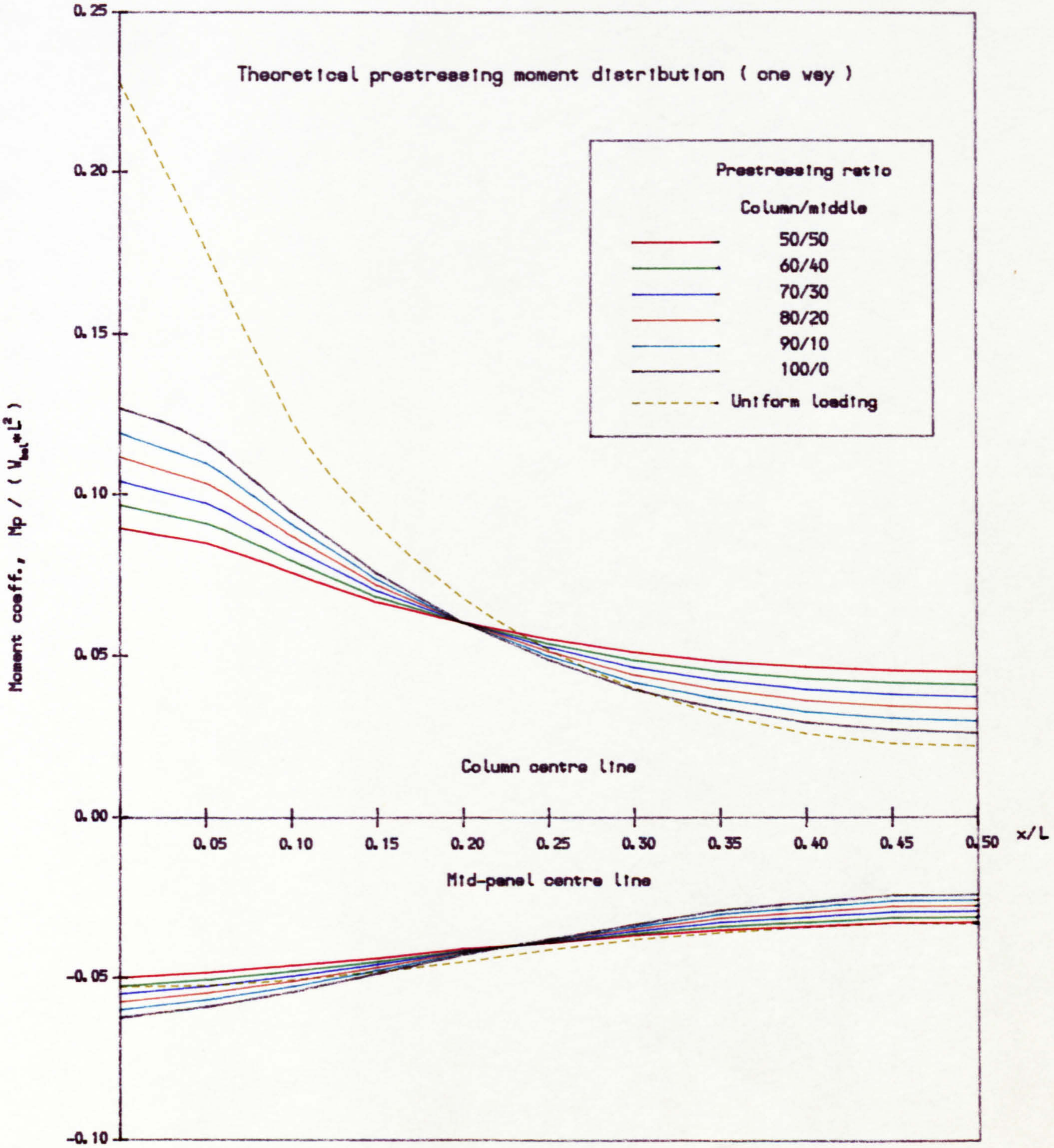

Fig. 4.6 Effect of variation of column-line/middle-width prestressing intensities
(Column-line width/span ratio : 0.1)

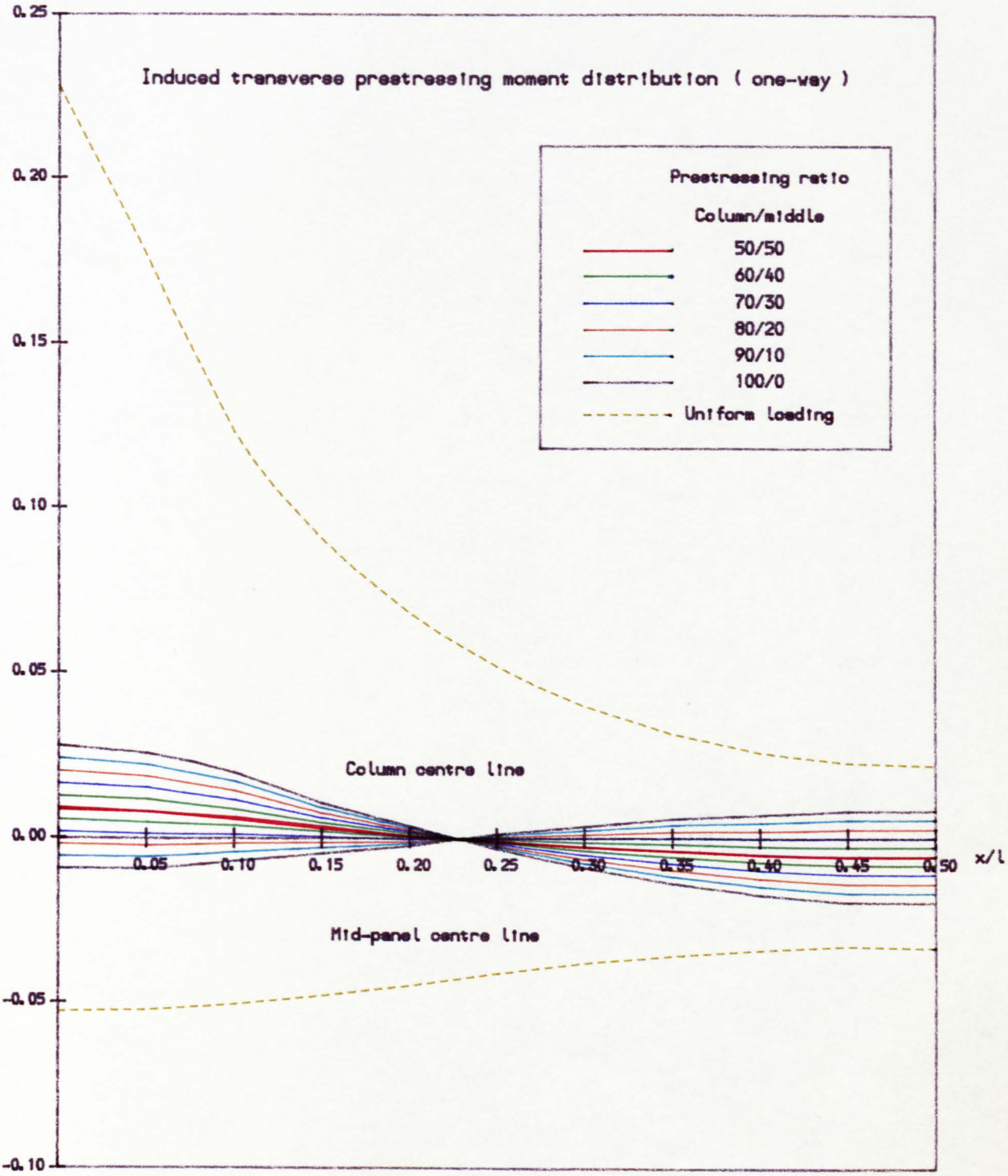

Fig. 4.7 Effect of variation of column-strip/middle-strip prestressing intensities
(Column-strip width/span ratio : 0.5)

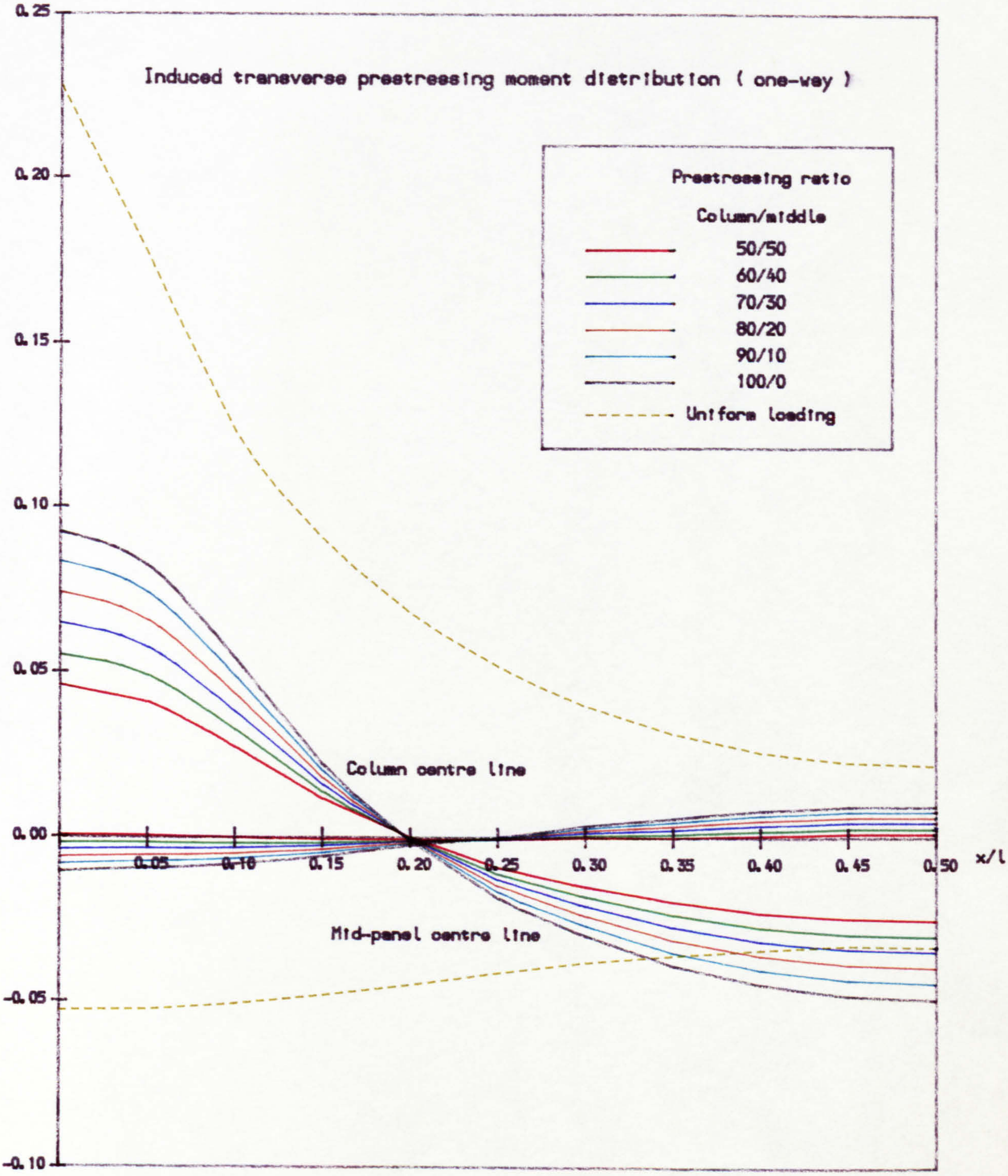

Fig. 4.8 Effect of variation of column-line/middle-width prestressing intensities
(Column-line width/span ratio : 0.1)

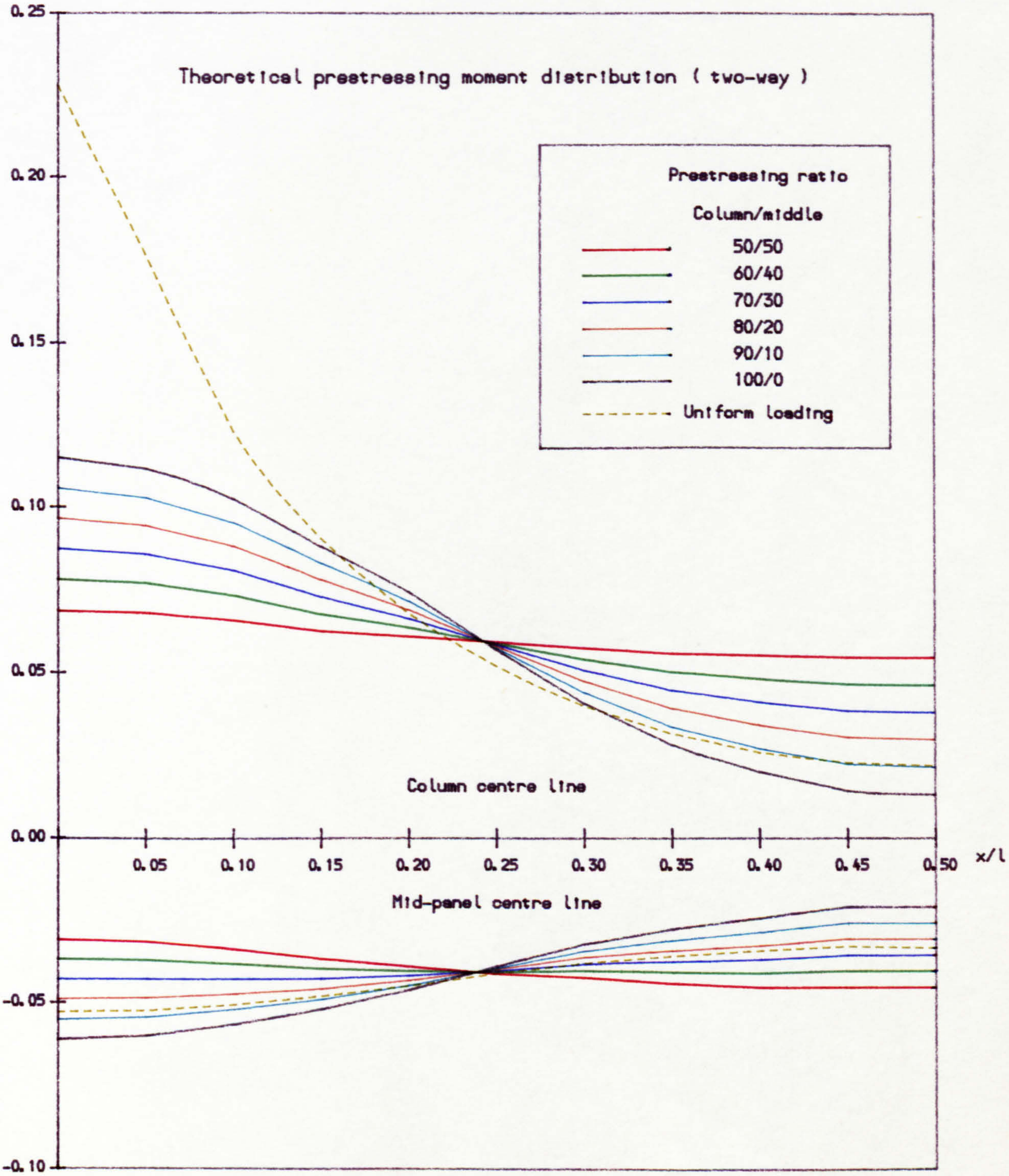

Fig. 4.9 Effect of variation of column-strip/middle-strip prestressing intensities
(Column-strip width/span ratio : 0.5)

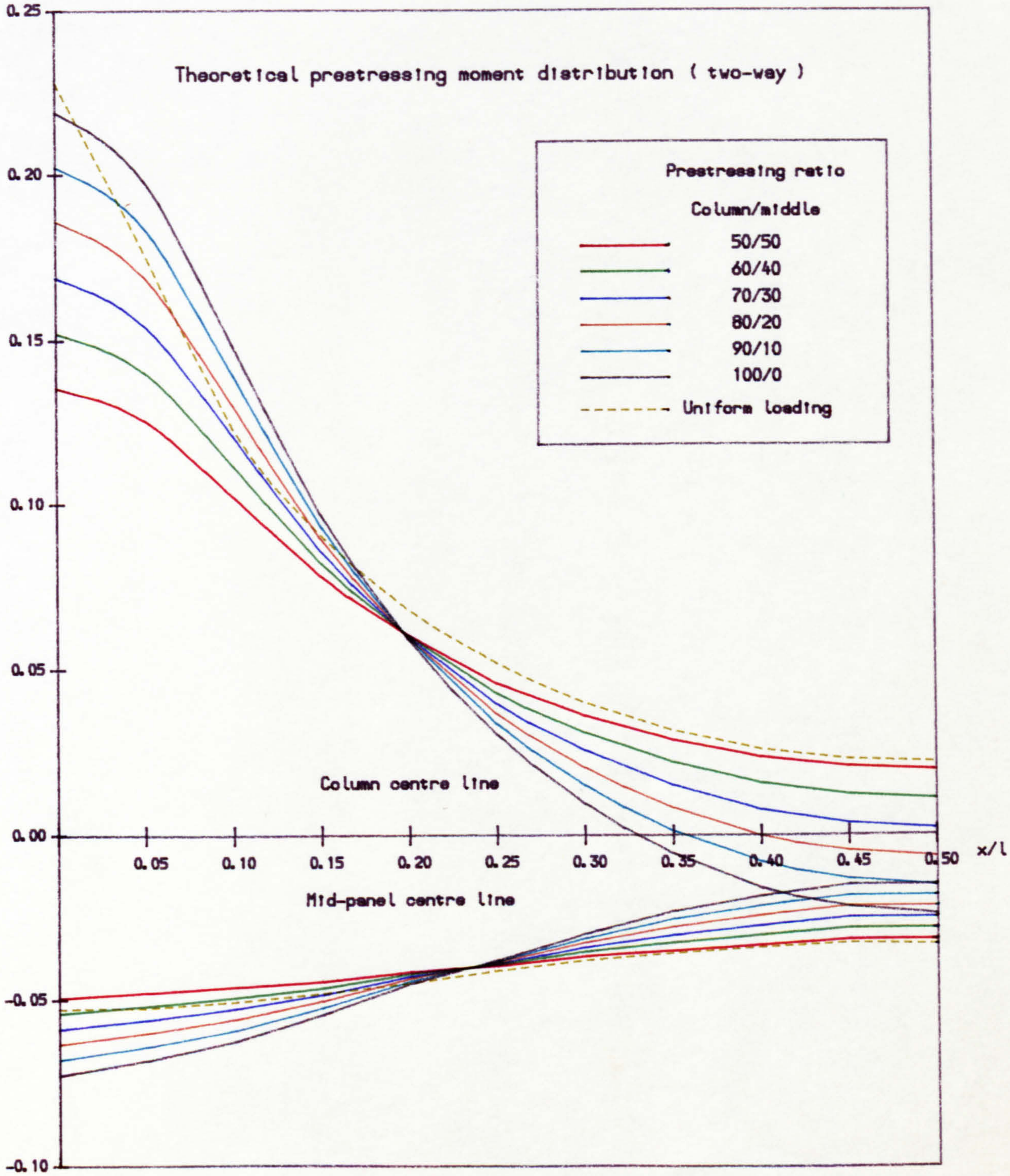

Fig. 4.10 Effect of variation of column-line/middle-width prestressing intensities
(Column-line width/span ratio : 0.1)

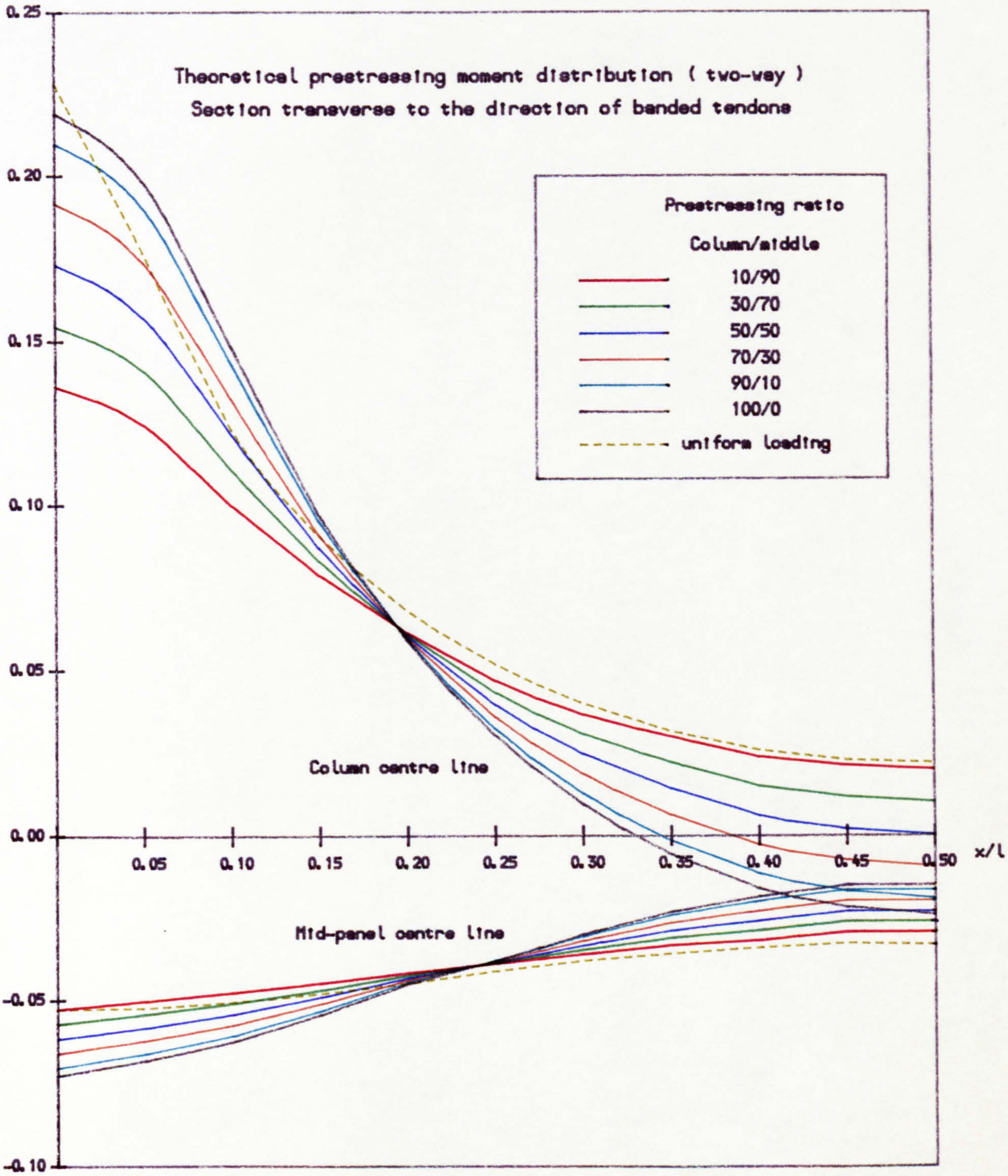

Fig. 4.11 Effect of variation of column-line/middle-width prestressing intensities (Column-line width/span ratio : 0.1)

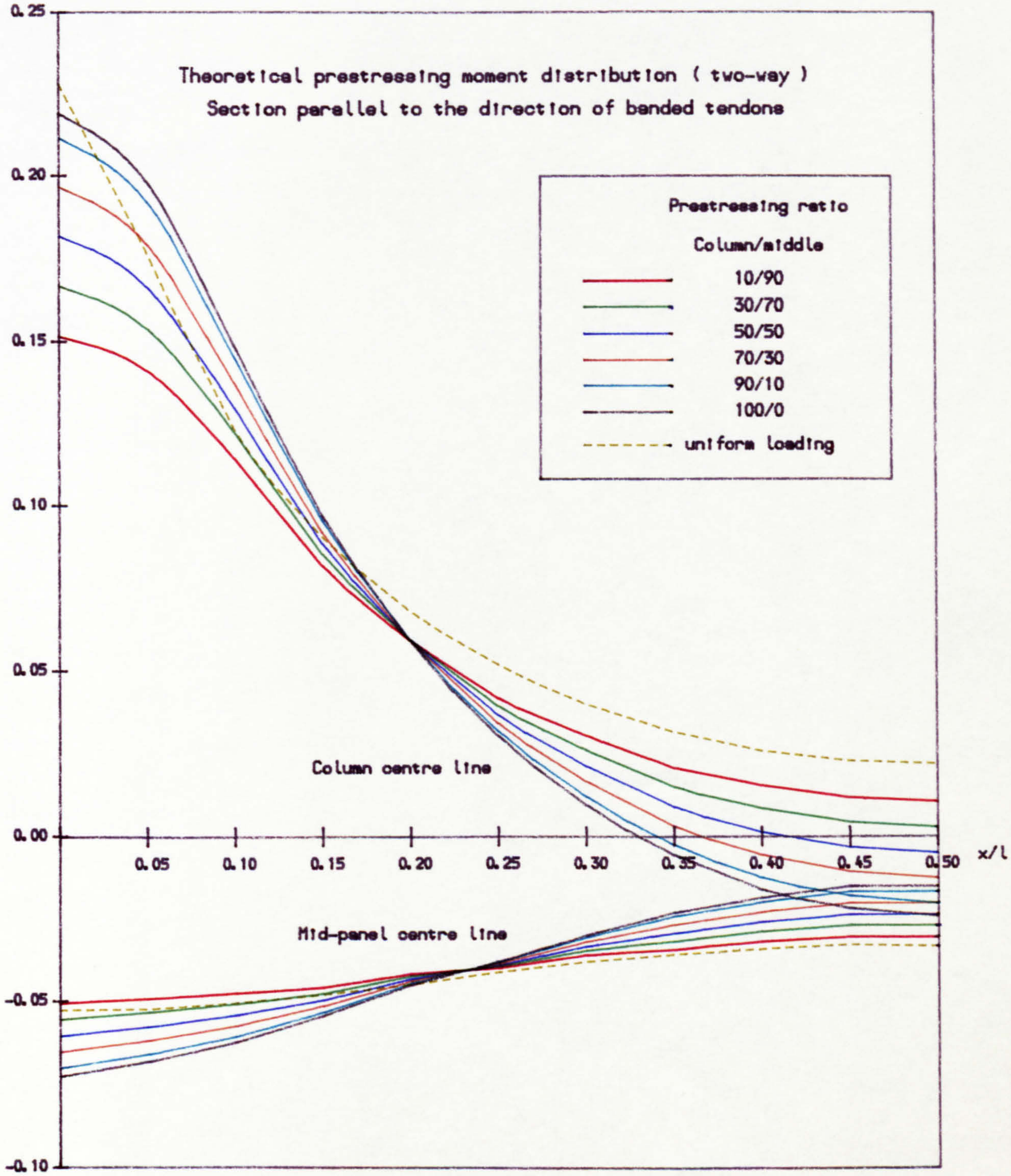

Fig. 4.12 Effect of variation of column line/middle width prestressing intensities
(Column-line width/span ratio : 0.1)

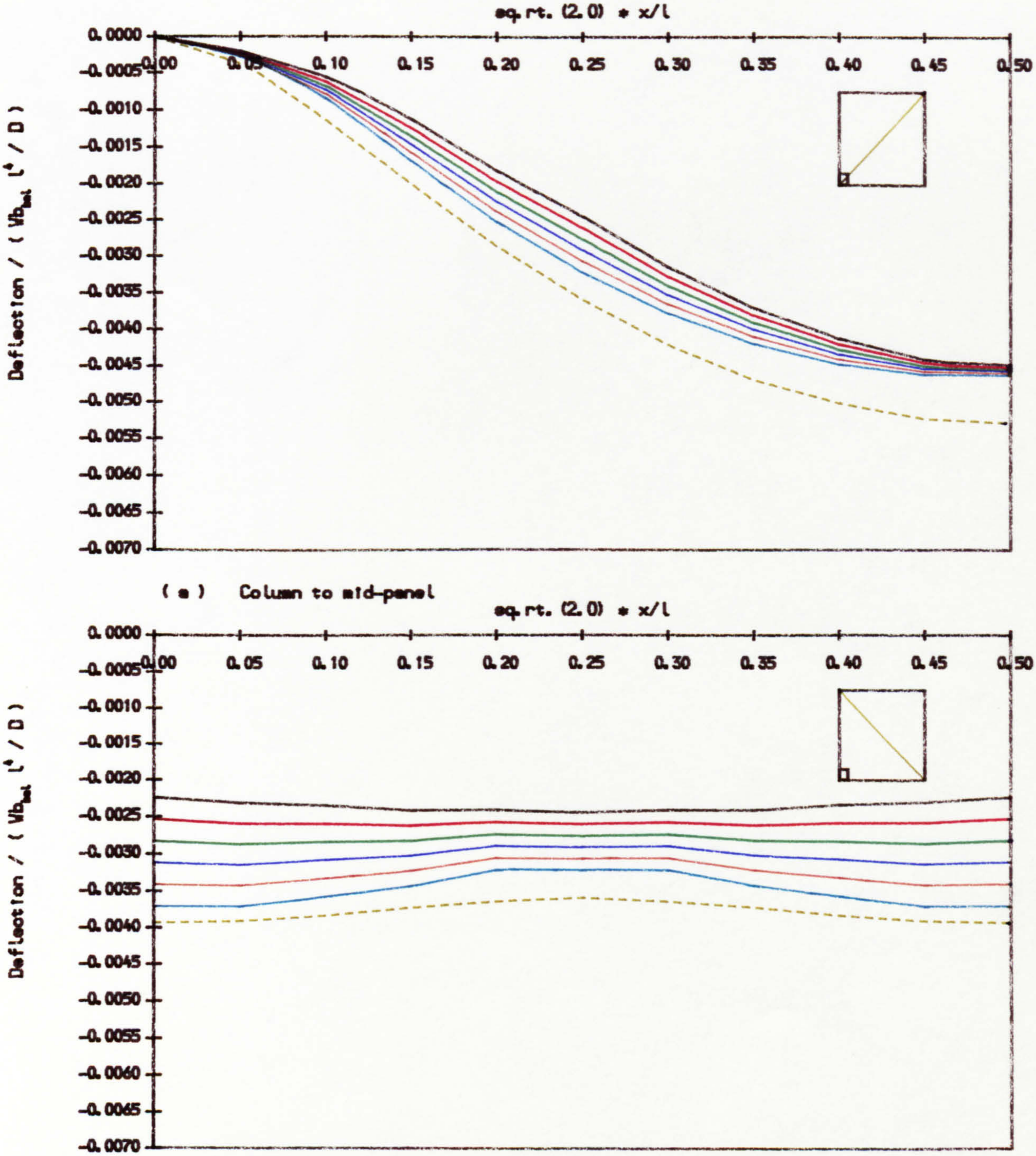

(a) Column to mid-panel

(b) Mid-span to mid-span (on column centre lines)

Prestressing ratio Column/middle
50/50
60/40
70/30
80/20
90/10
100/0
uniform loading

Fig. 4.13 Diagonal deflection profiles for variable column-strip/middle-strip prestressing
(Column-strip width/span ratio : 0.5)

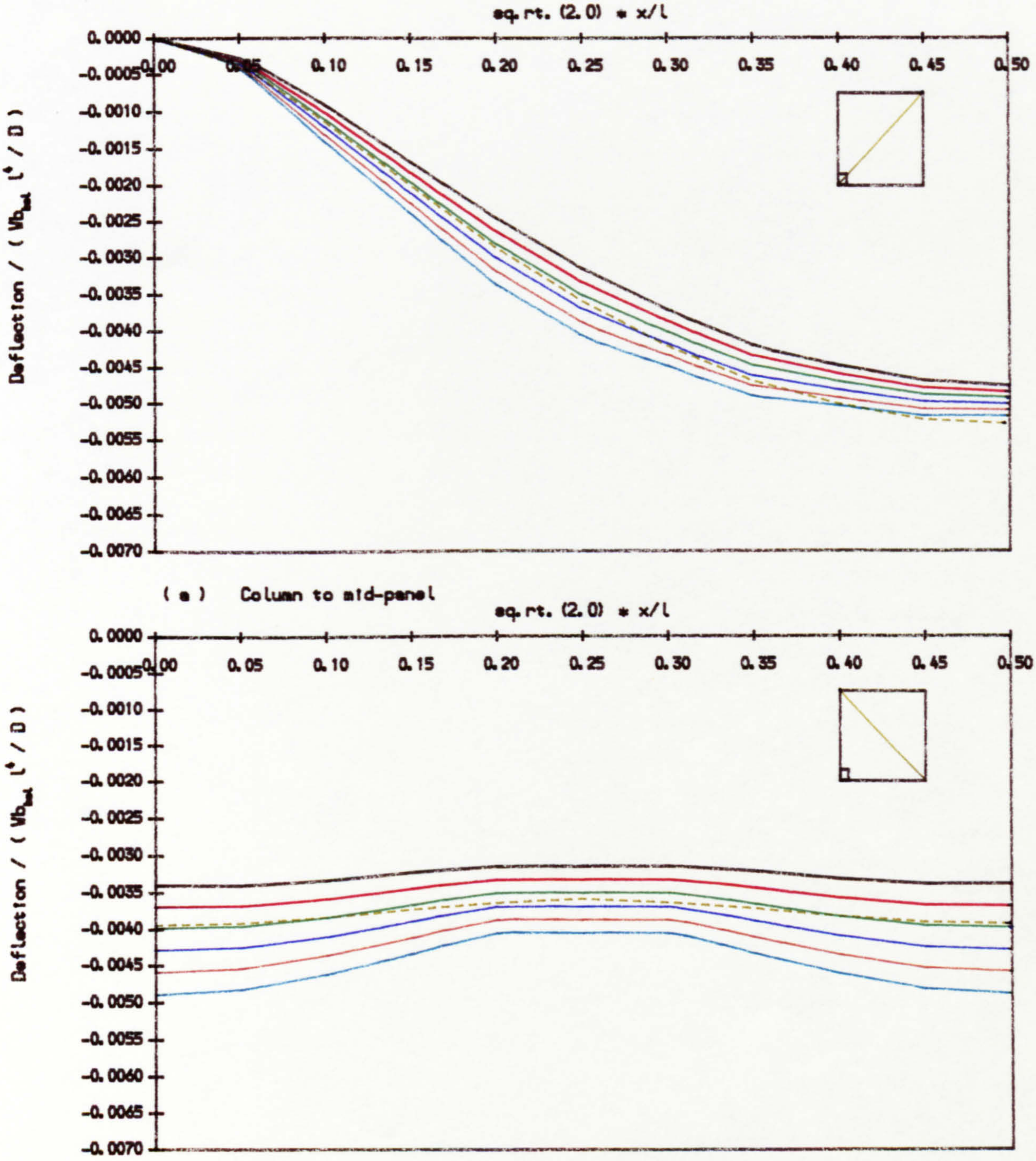

(a) Column to mid-panel

(b) Mid-span to mid-span (on column centre lines)

Prestressing ratio Column/middle
50/50
60/40
70/30
80/20
90/10
100/0
uniform loading

Fig. 4.14 Diagonal deflection profiles for variable column-line/middle-width prestressing
(Column-line width/span ratio : 0.1)

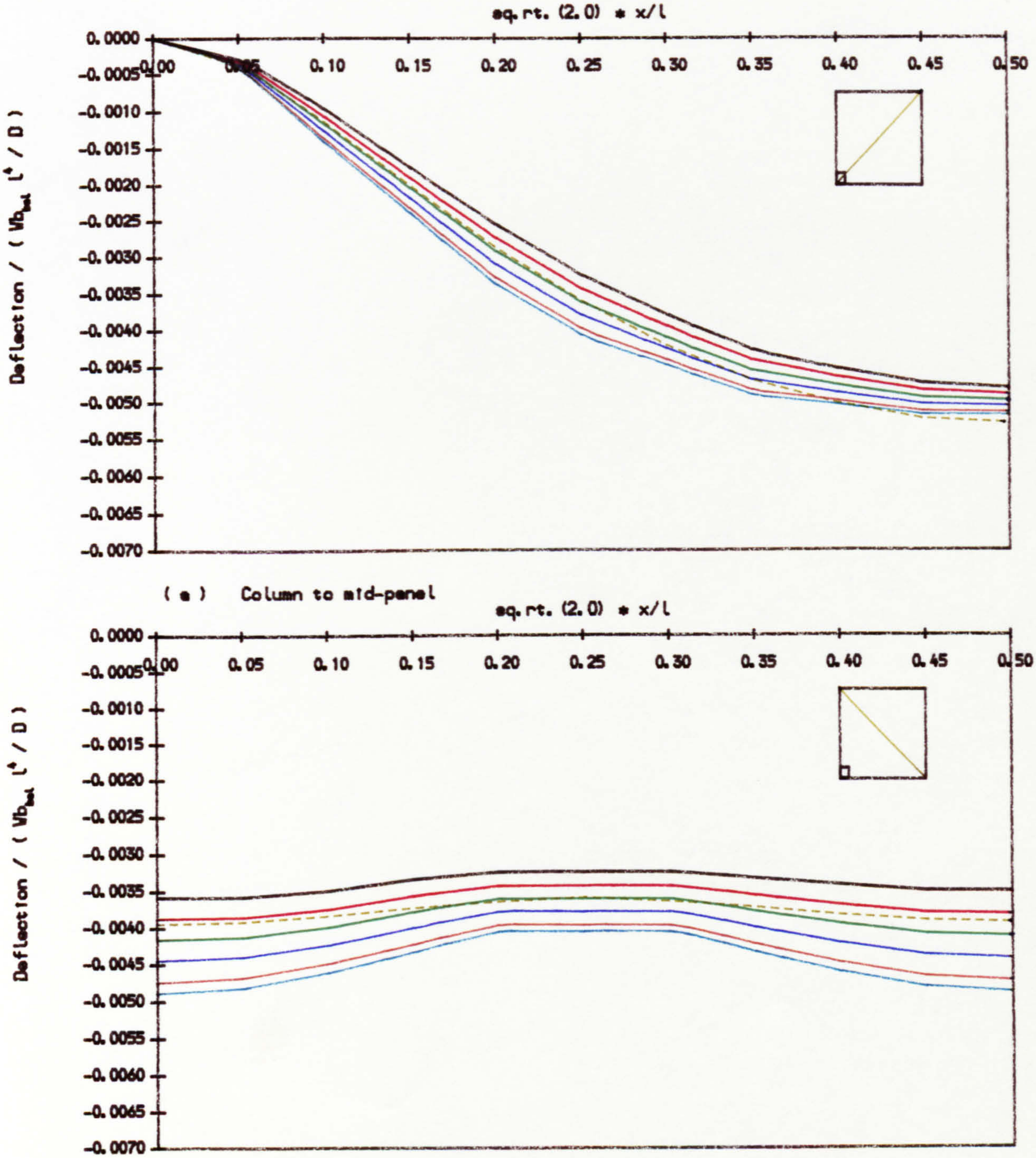

(a) Column to mid-panel

(b) Mid-span to mid-span (on column centre lines)

Prestressing ratio Column/middle
10/90
30/70
50/50
70/30
90/10
100/0
uniform loading

Fig. 4.15 Diagonal deflection profiles for variable column-line/middle-width prestressing (with banded tendons in column line in one direction)

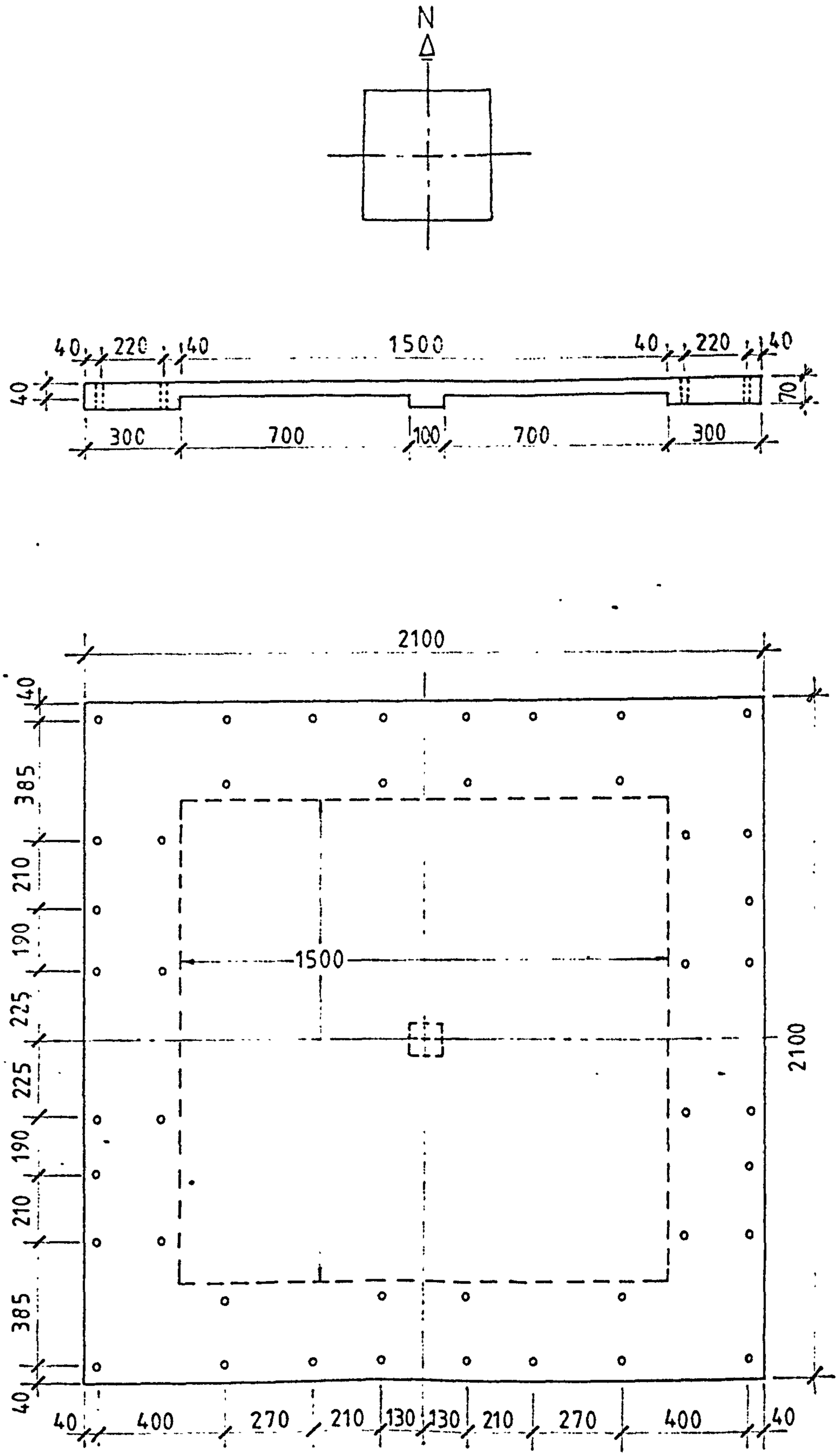

Fig. 5.1 Test slab dimensions

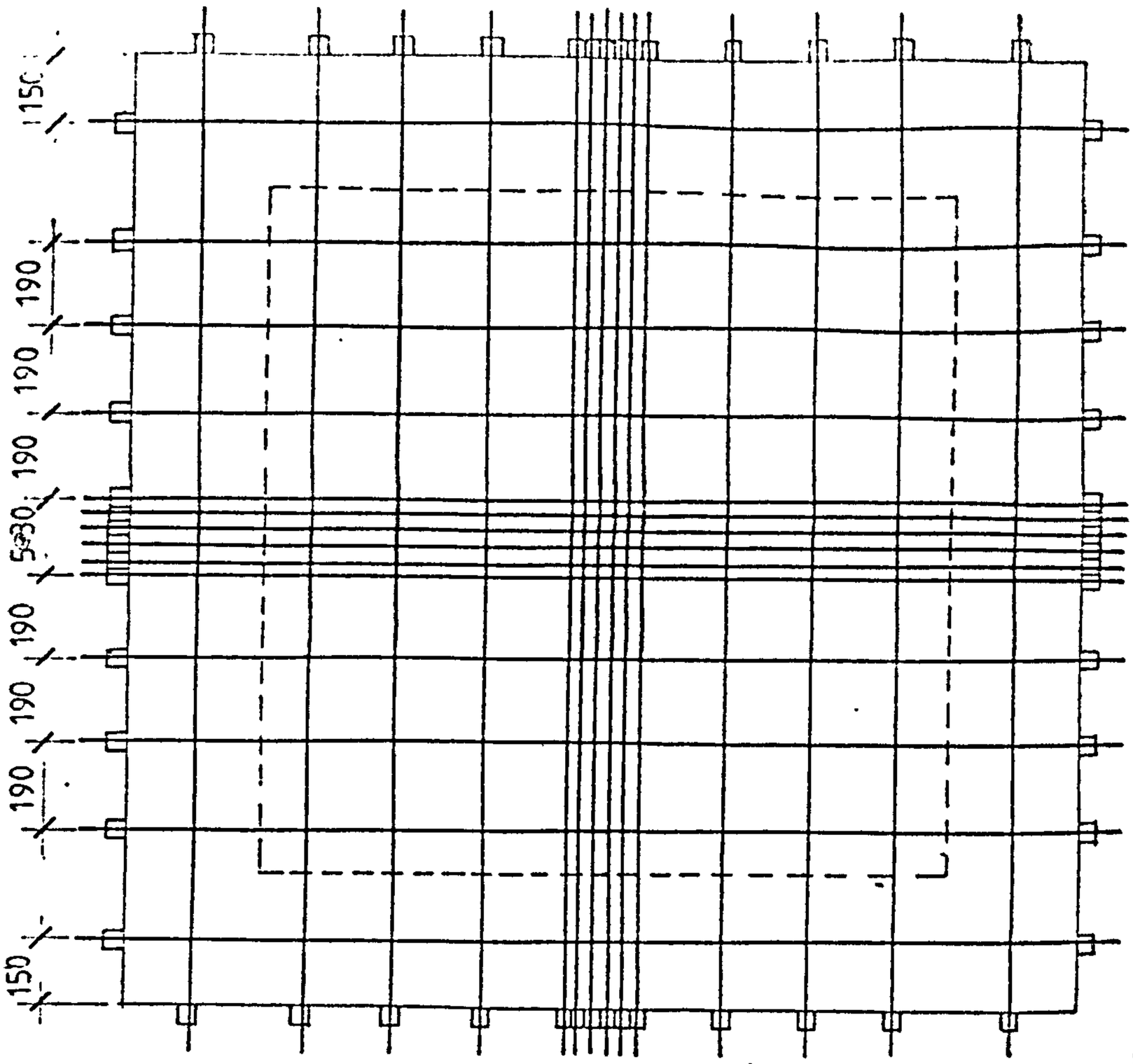

SLAB A1

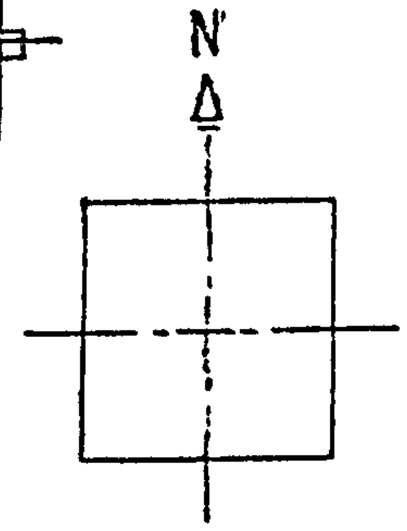

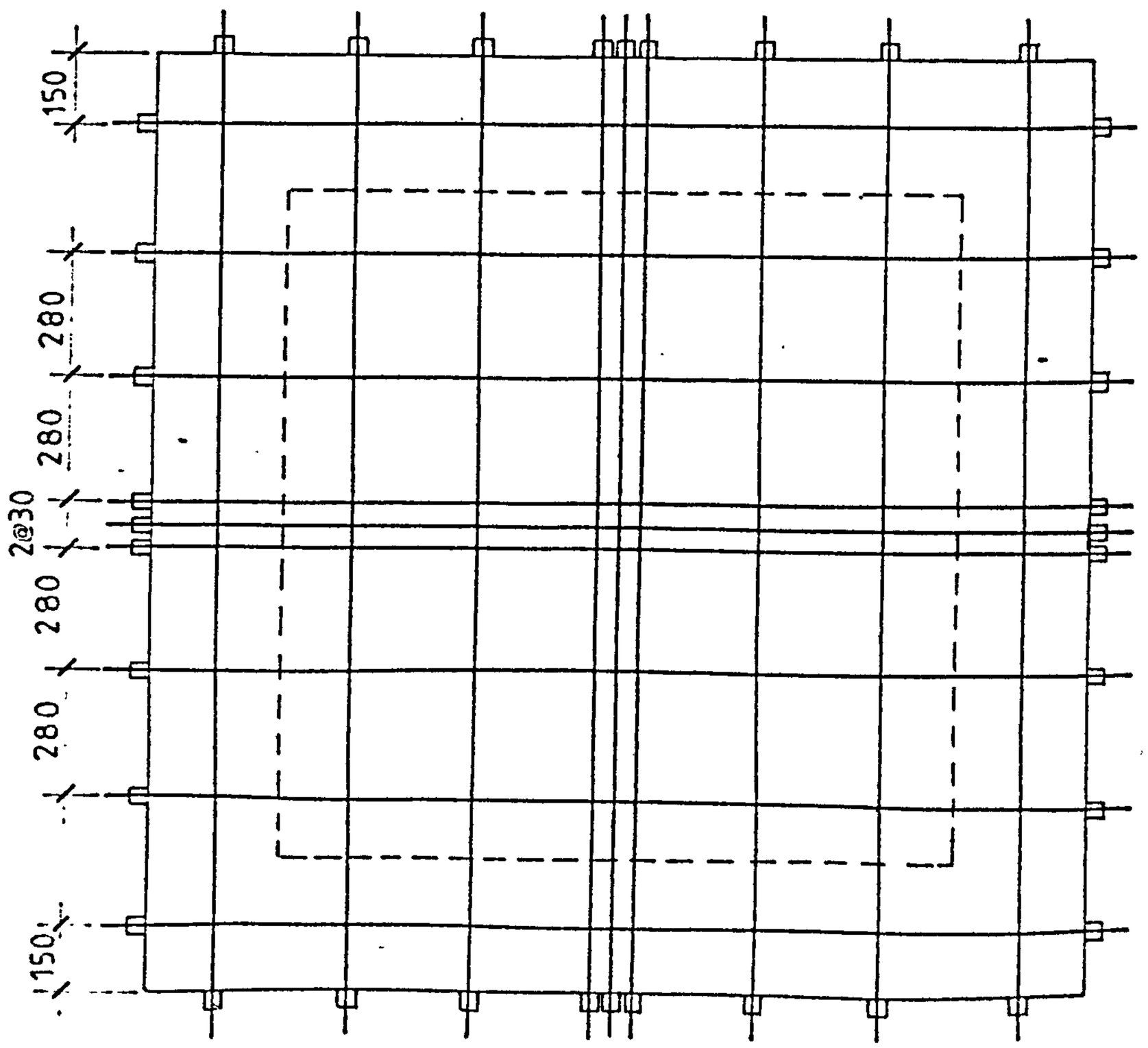

SLAB B1

Fig. 5.2 Tendon arrangement of slabs A1 & B1

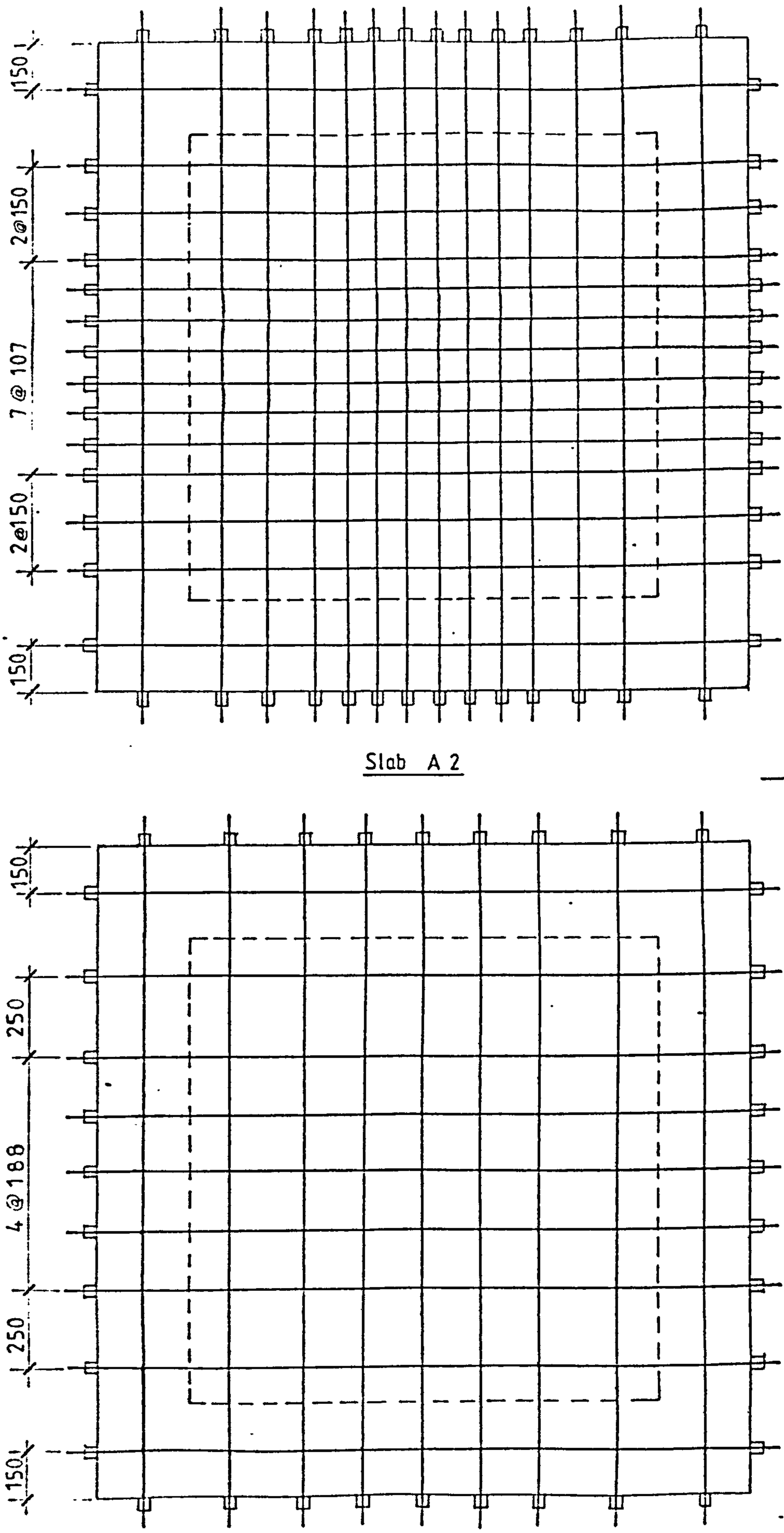

Fig. 5.3 Tendon arrangement of slabs A2 & B2

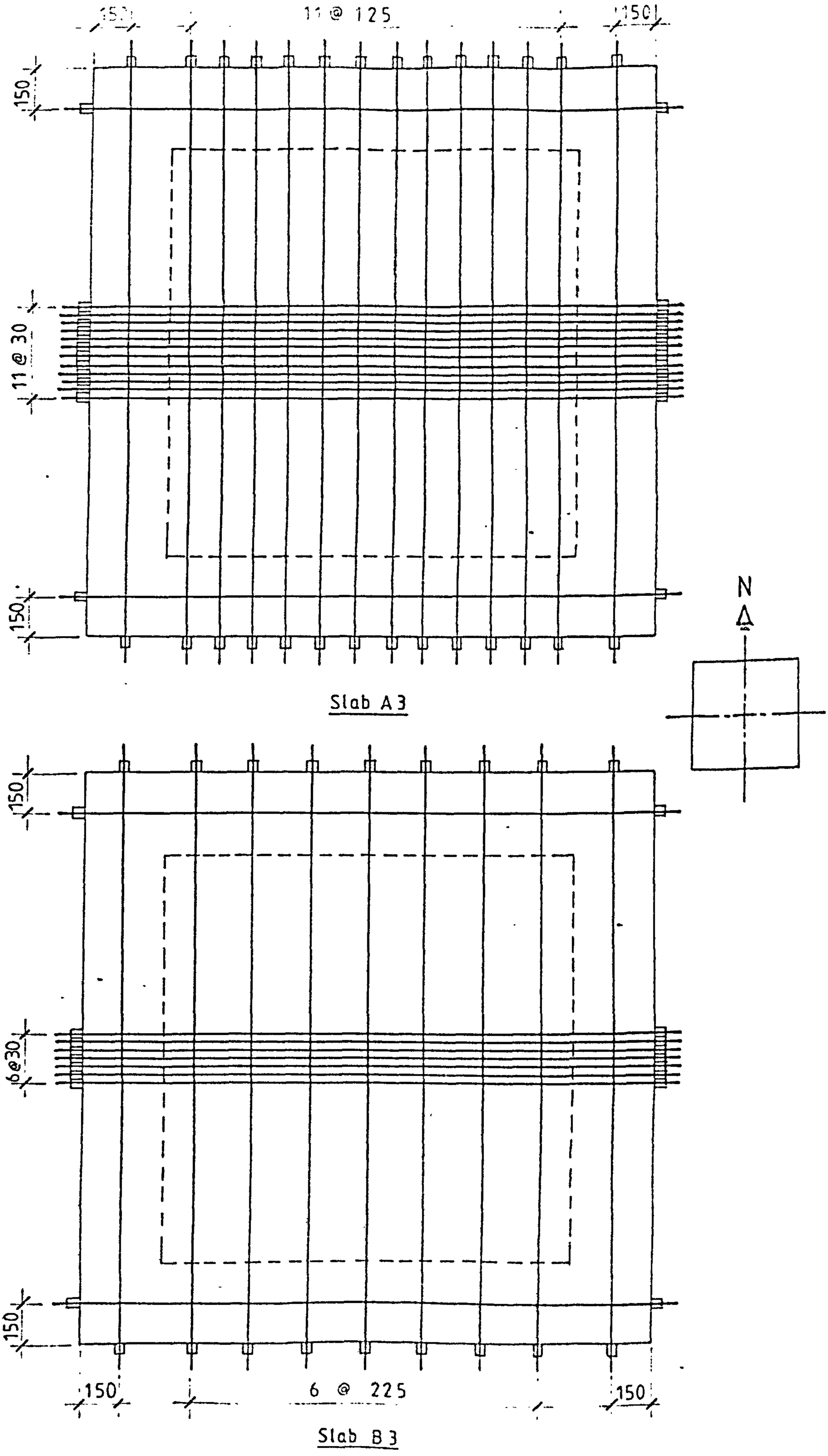

Fig. 5.4 Tendon arrangement of slabs A3 & B3

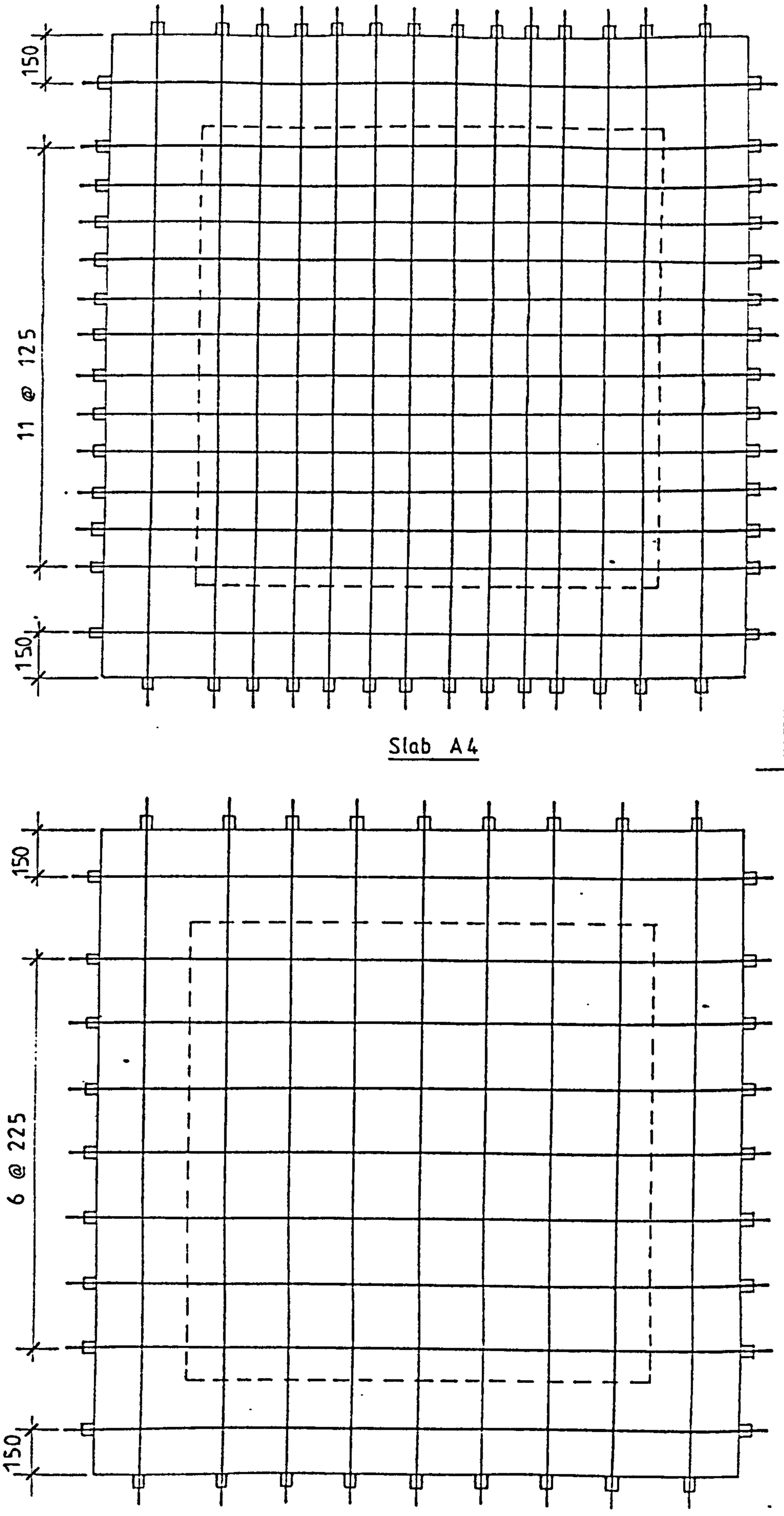

Fig. 5.5 Tendon arrangement of slabs A4 & B4

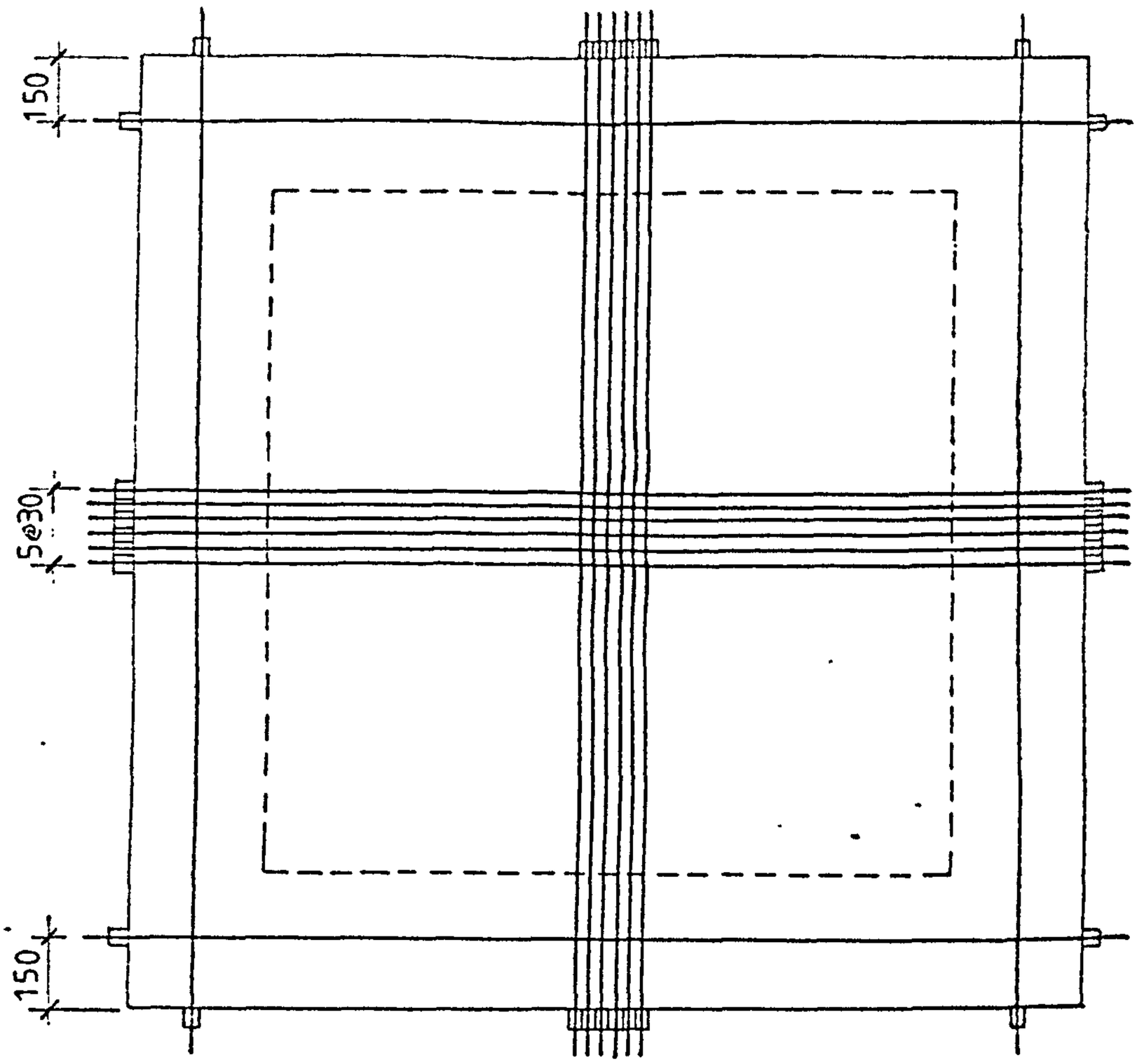

Slab C1

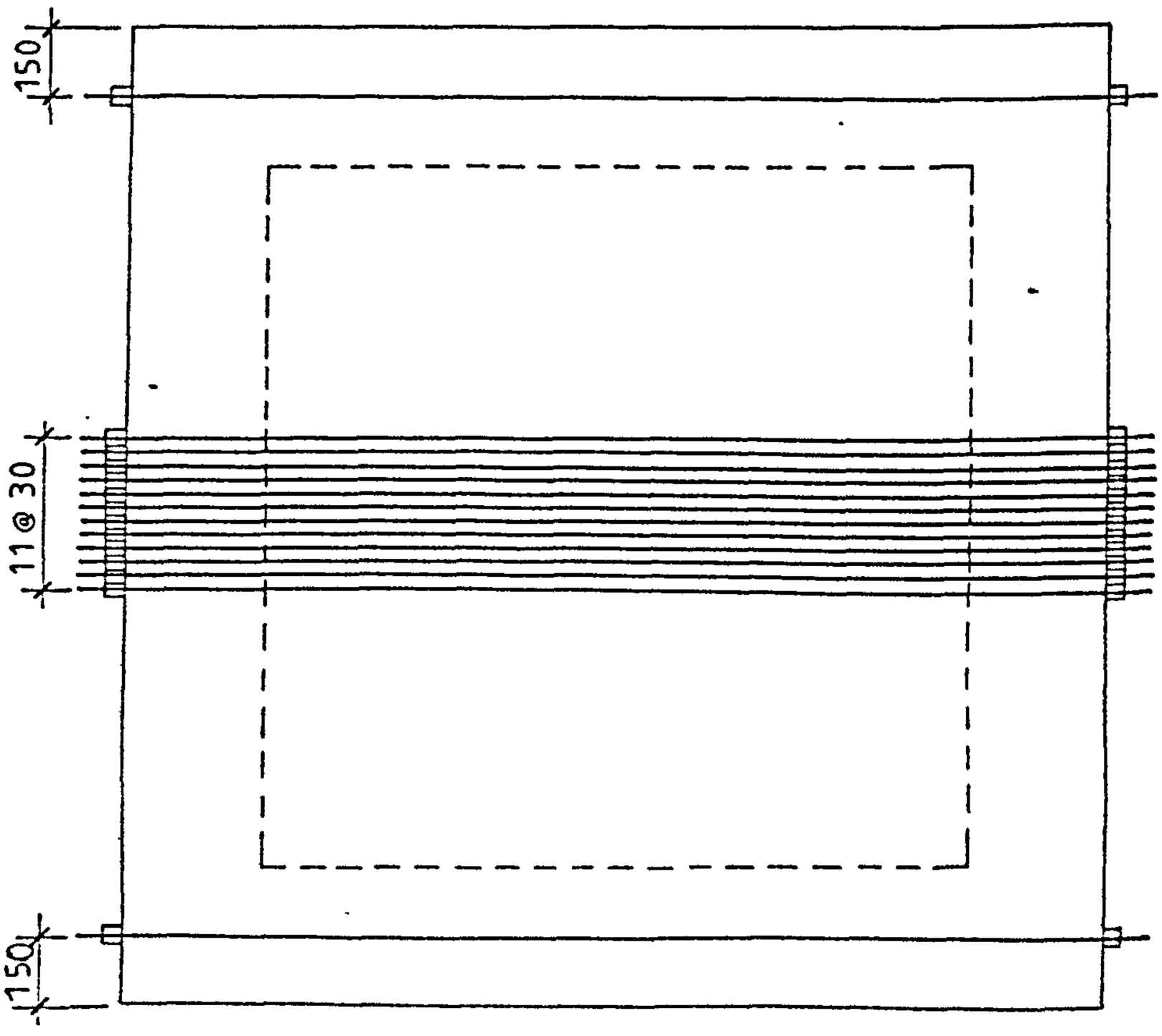

Slab C2

Fig. 5.6 Tendon arrangement of slabs C1 & C2

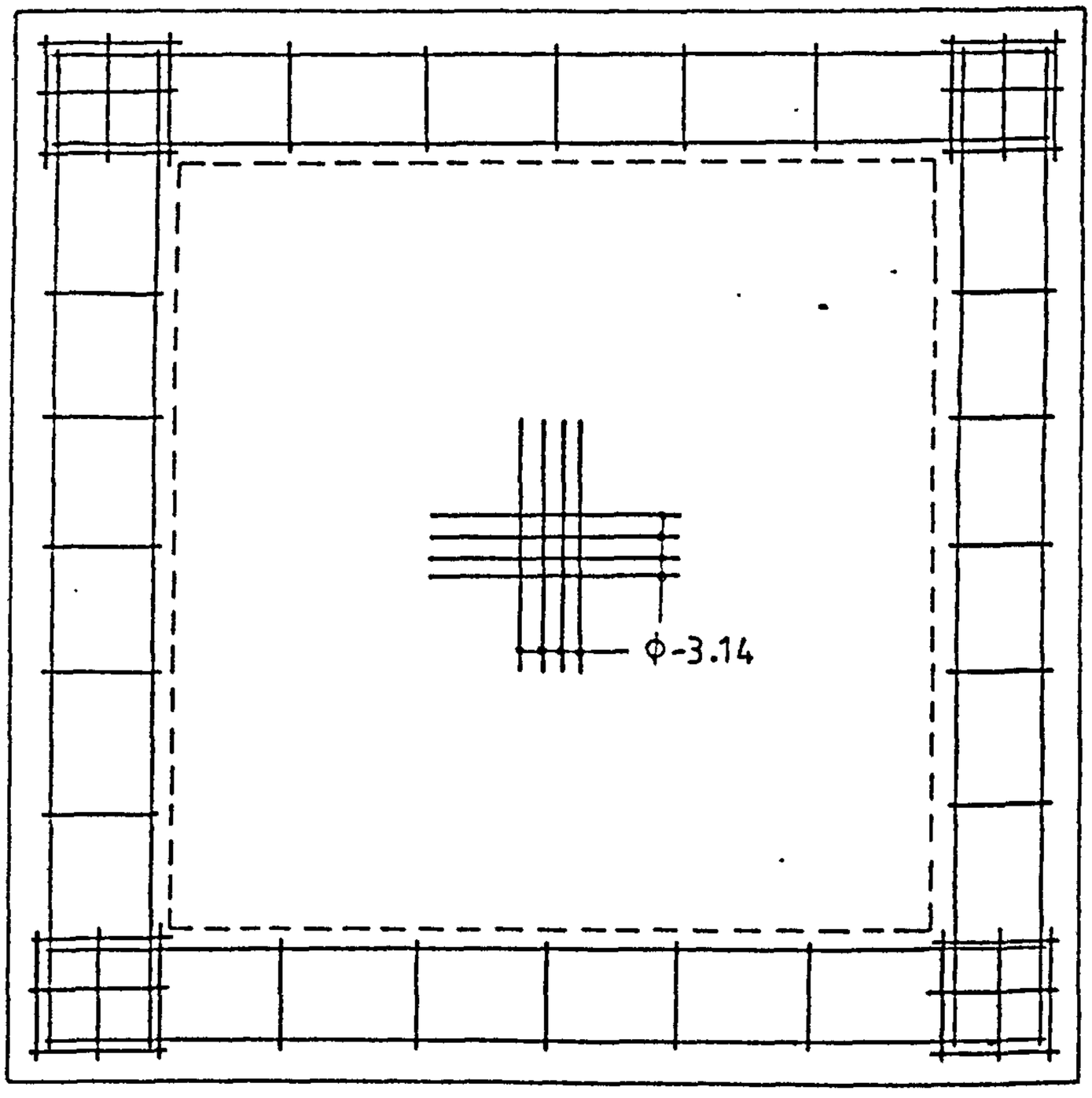

Fig. 5.7 Top reinforcement in series A slabs

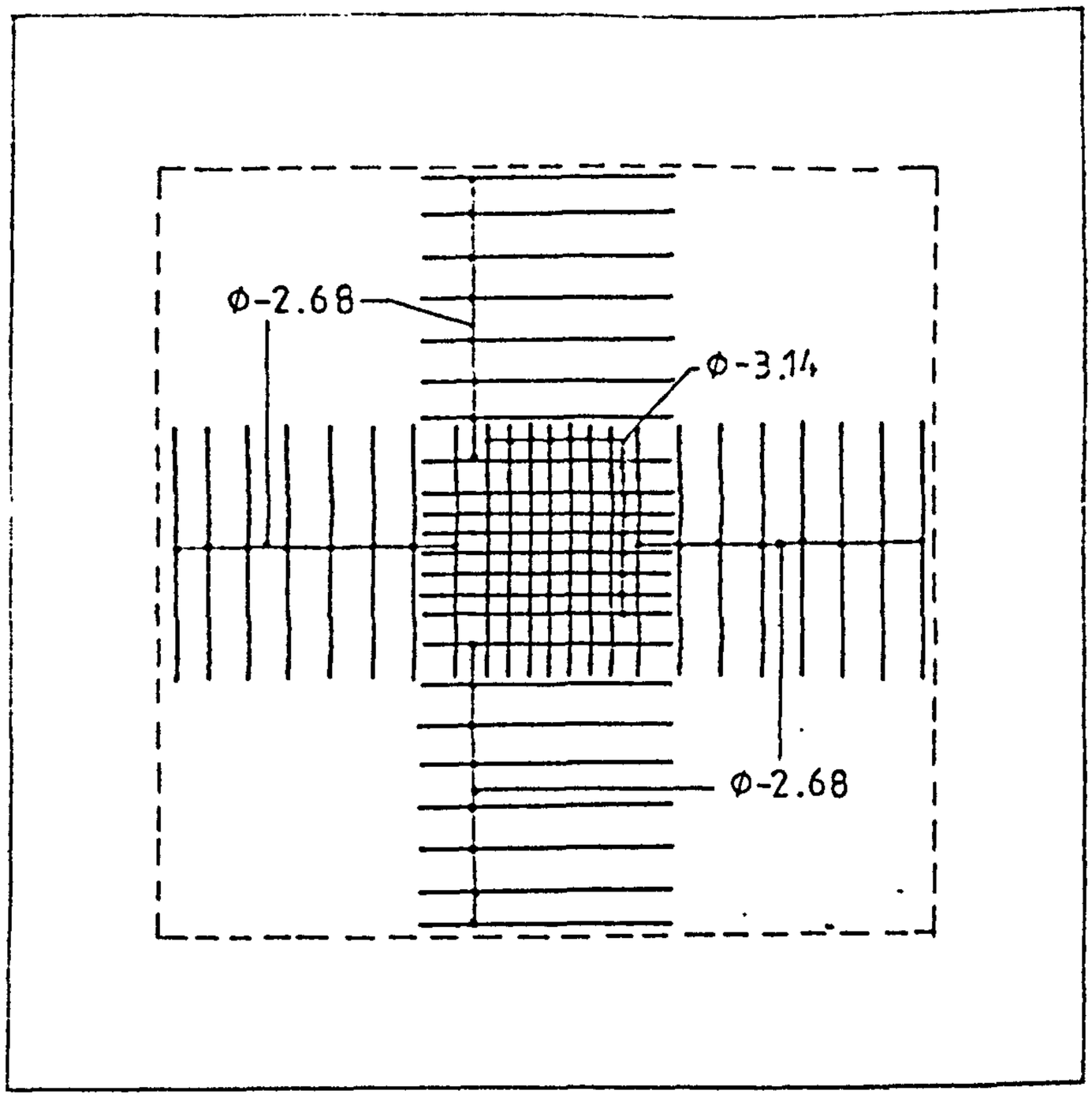

Negative reinforcement

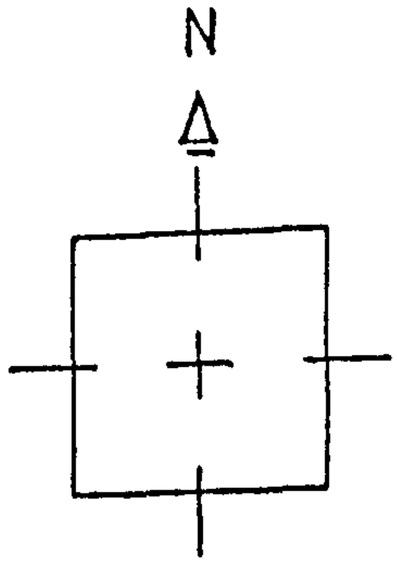

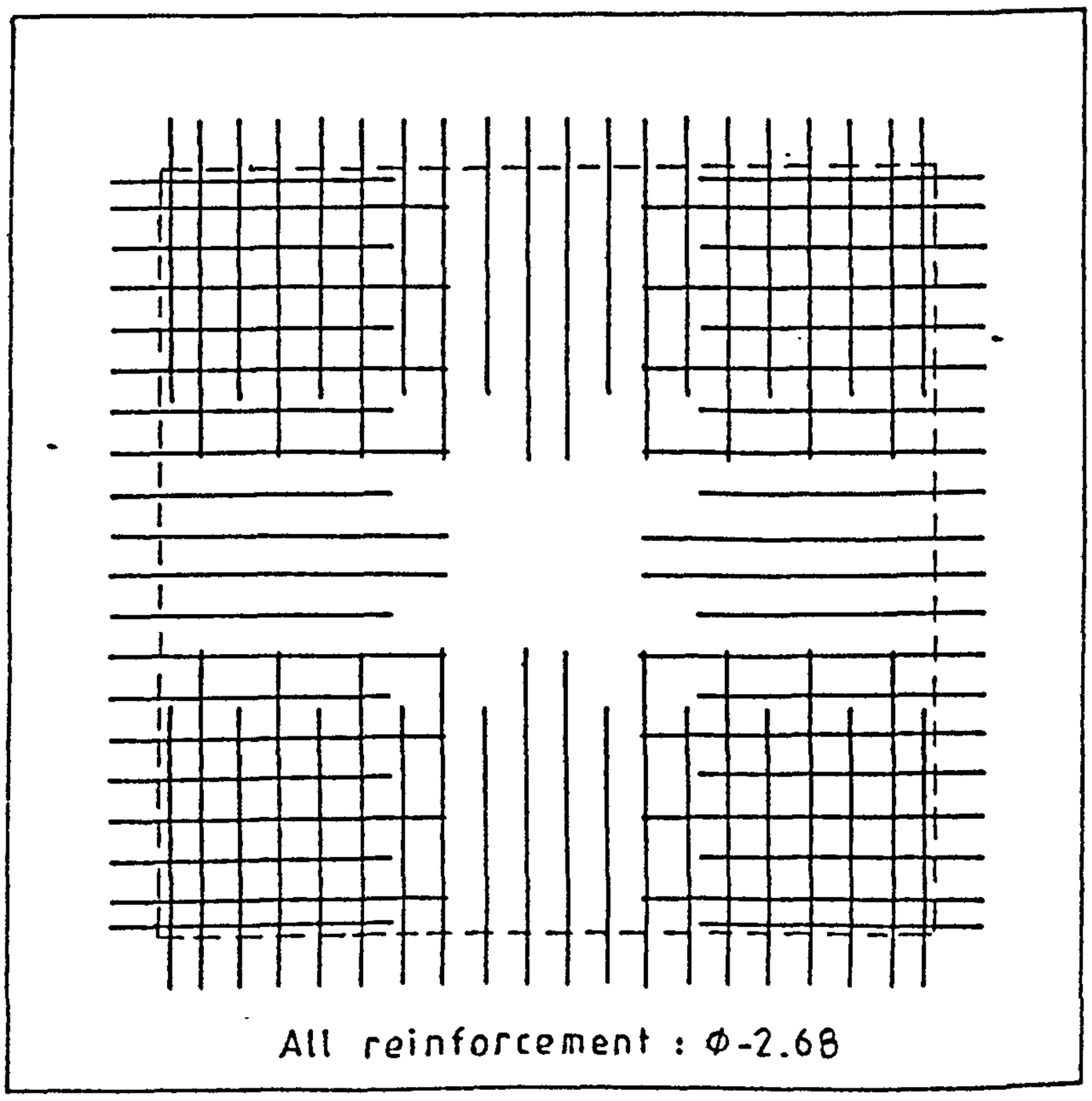

Positive reinforcement

Fig. 5.8 Non-prestressed reinforcement in series B and C 1 slabs (Edge beam reinforcement similar to Fig. 5.7)

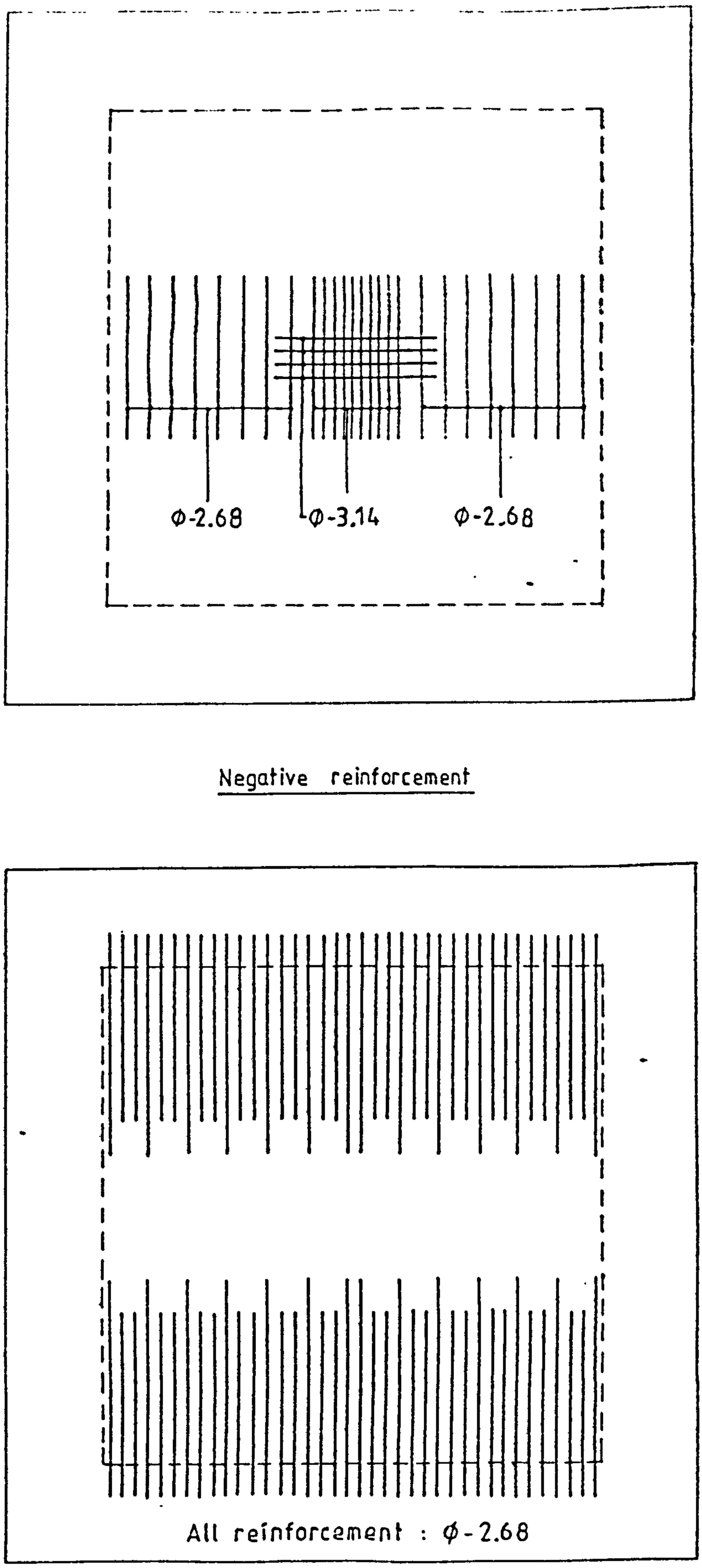

Fig. 5.9 Non-prestressed reinforcement in slab C 2
(edge beams reinforcement similar to Fig. 5.7)

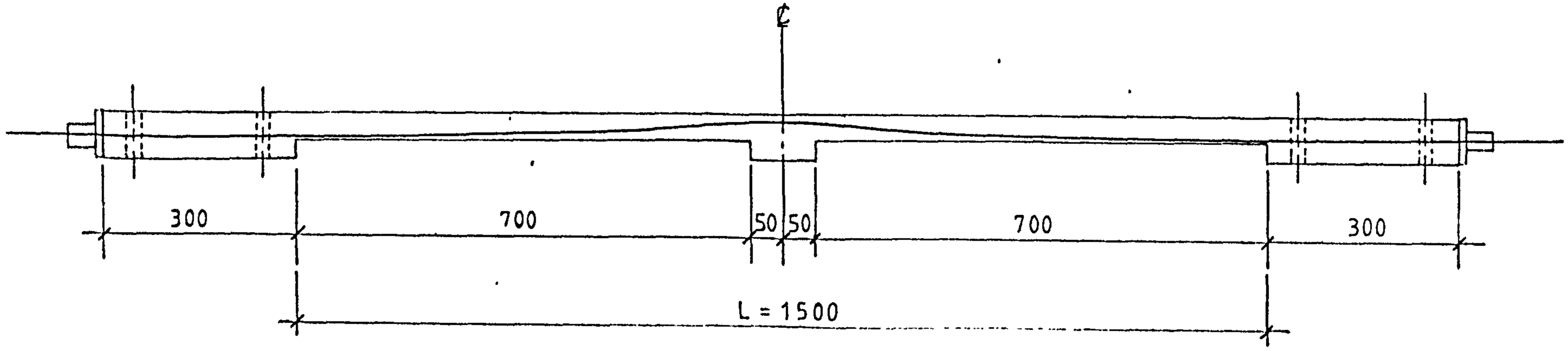

	Column Centre Line ℄	Point of Inflection 0.1L	Panel Edge 0.5L
Tendon Eccentricities (mm)	+13.0	$^{+}_{-}$11,7	-13.0

Fig. 5.10 Effective tendon profile of prestressing wire

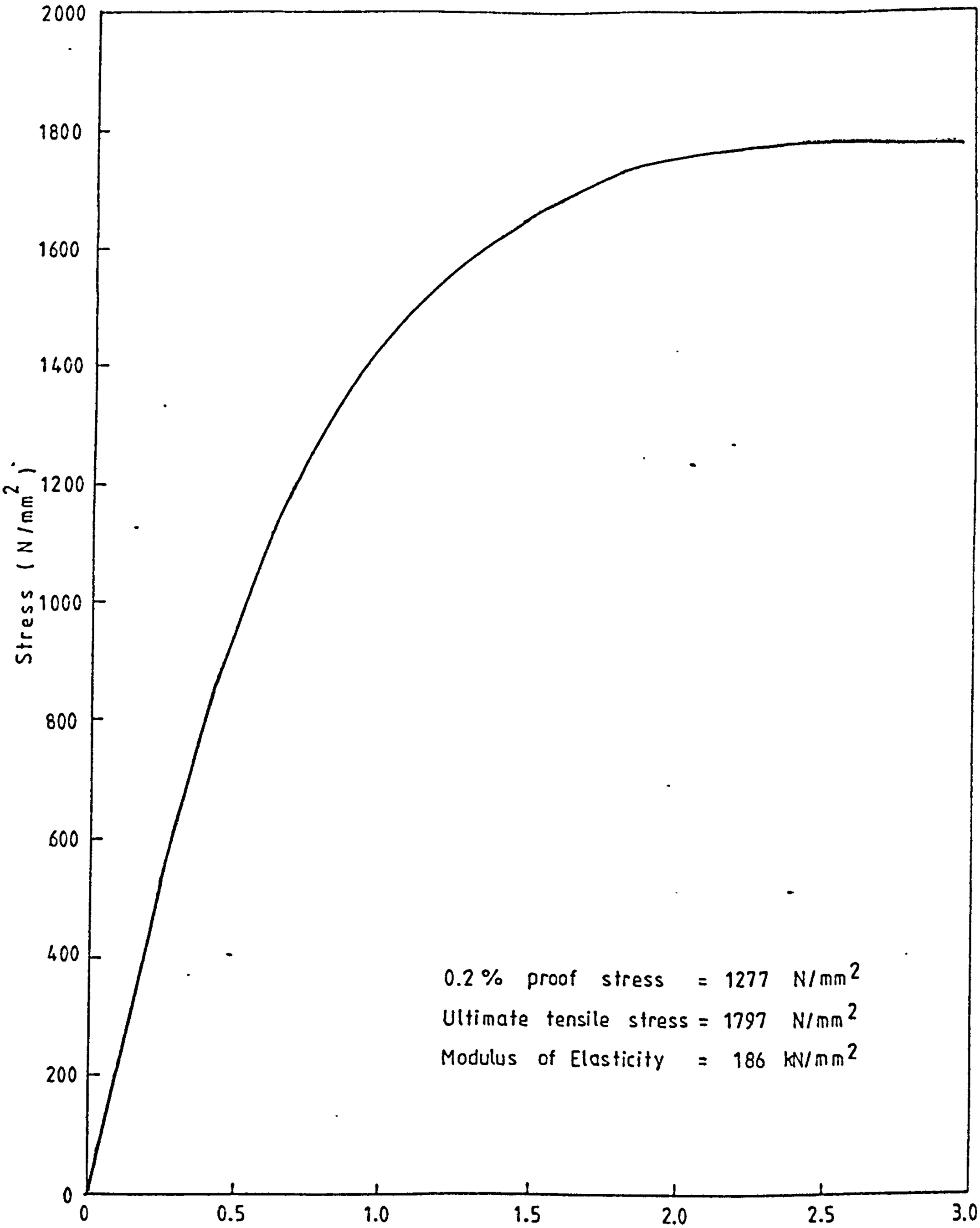

Fig. 5.11 Stress-strain characteristic curve of 2.98 mm diameter prestressing wire

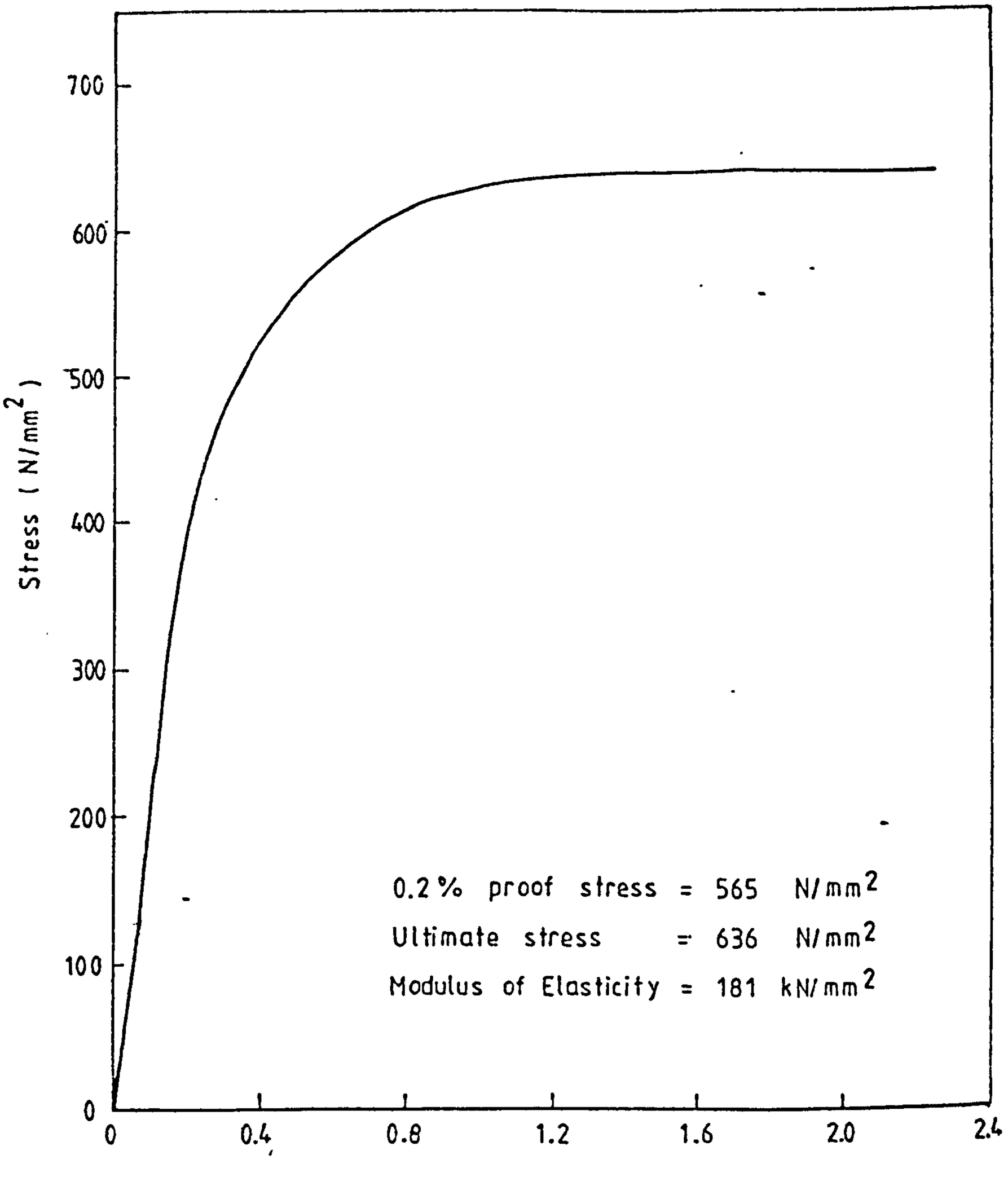

Fig.5.12 Stress-strain characteristic curve of 3.14 mm diameter non-prestressed wire

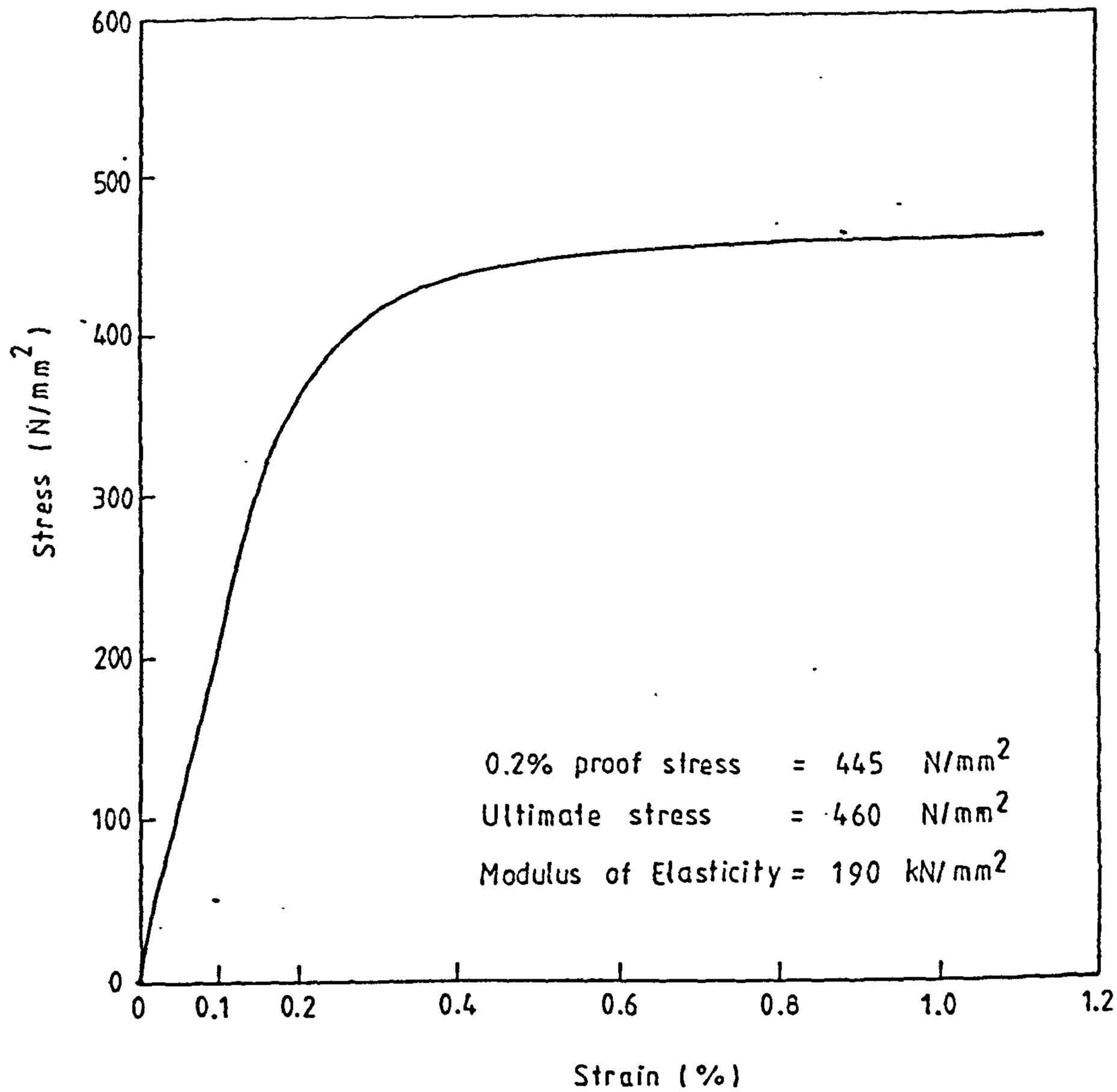

Fig.5.13 Stress-strain characteristic curve of 2.68 mm diameter non-prestressed steel

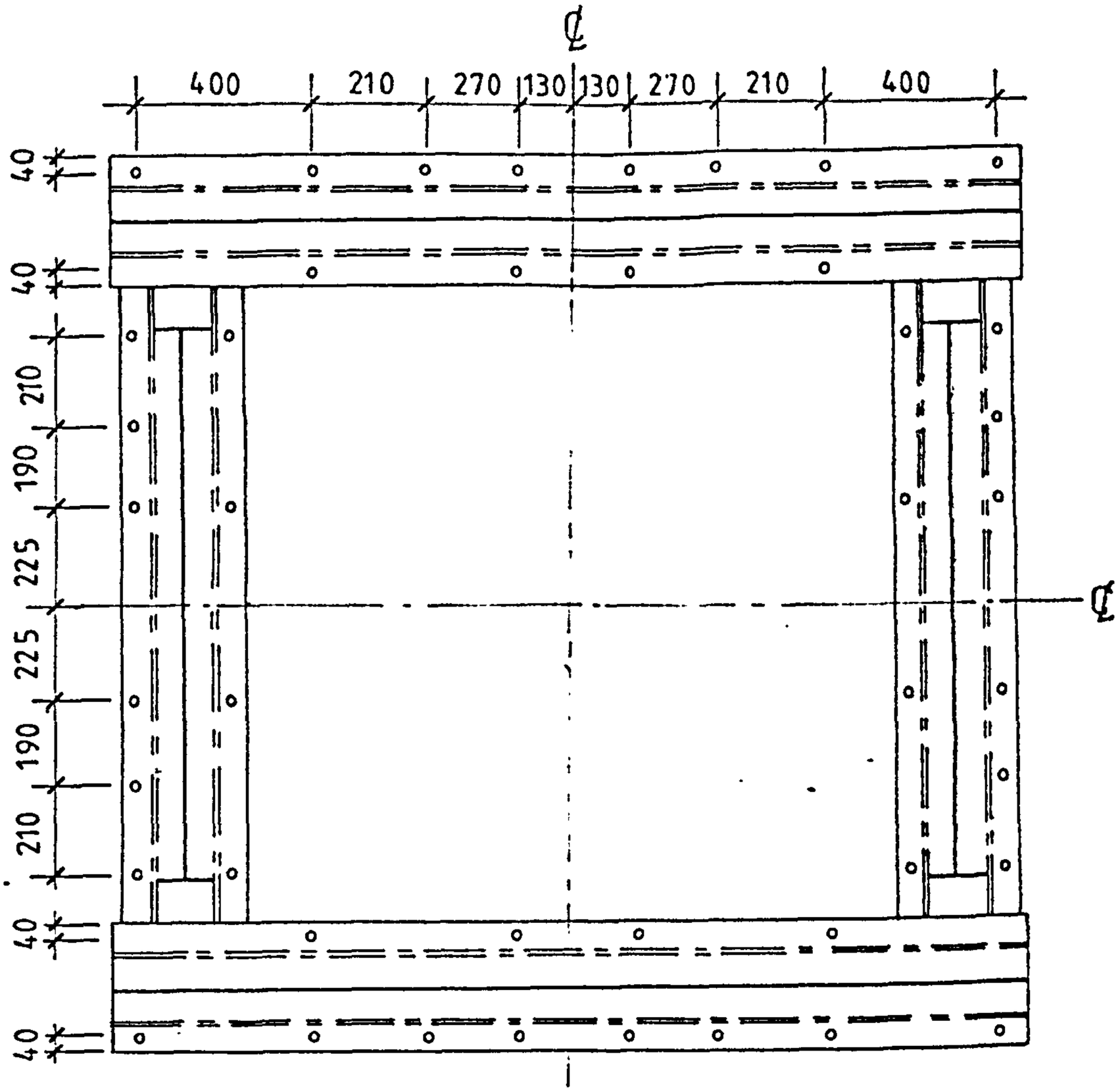

Fig. 5.14 Test rig

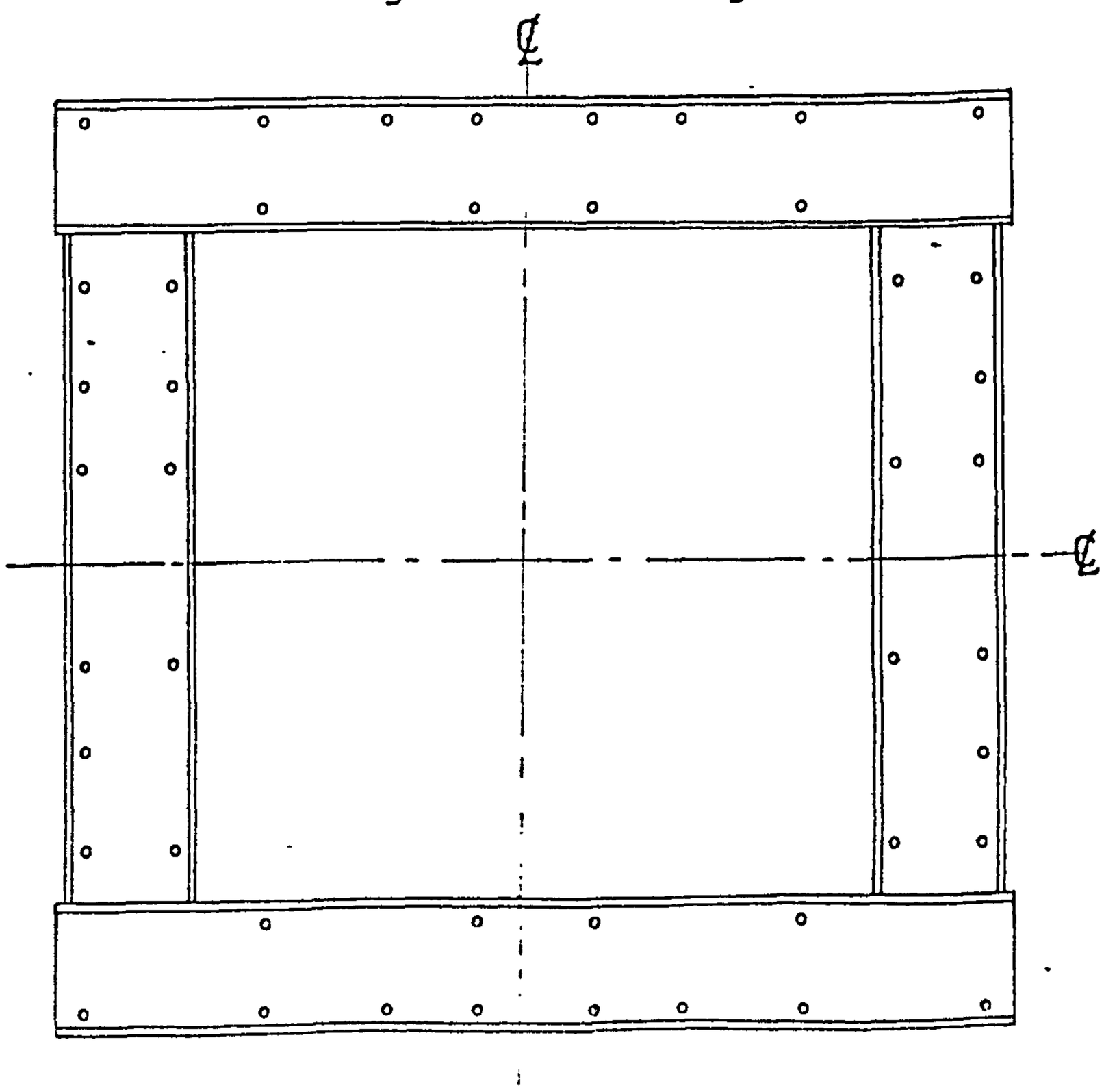

Fig. 5.15 Top channels for clamping

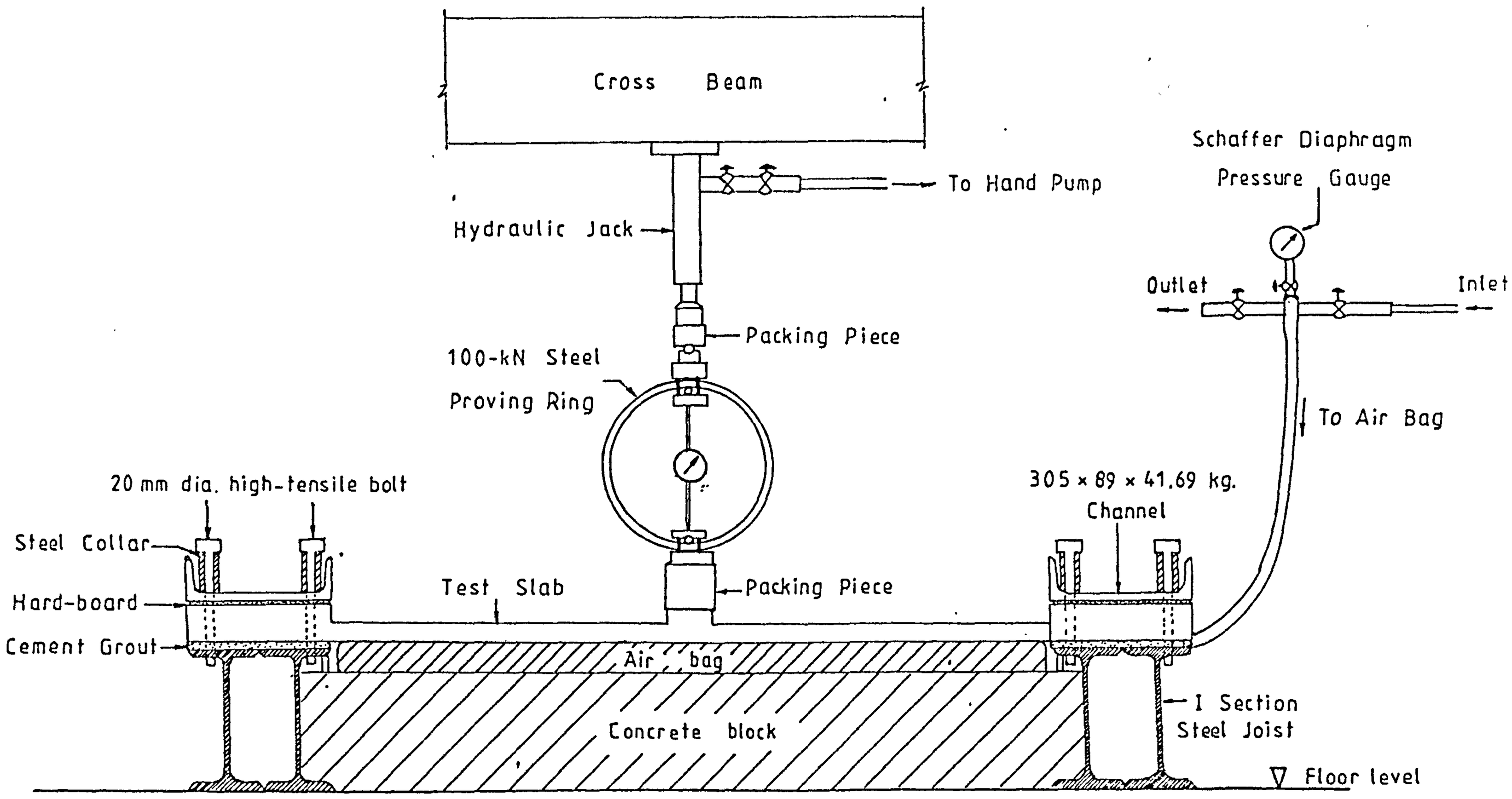

Fig. 5.16 Loading arrangement

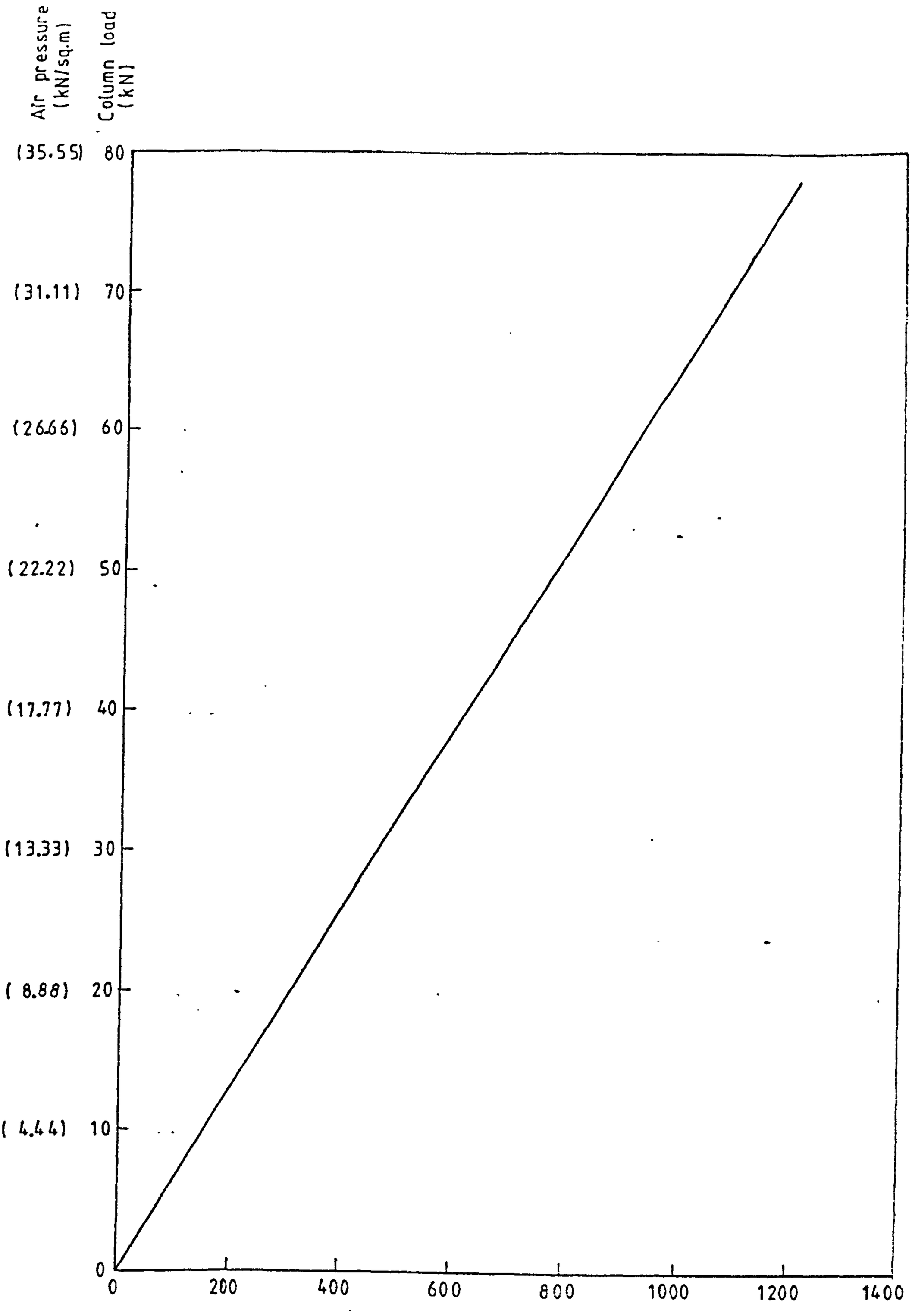

Fig. 5.17 Calibration graph for 100-kN steel proving ring

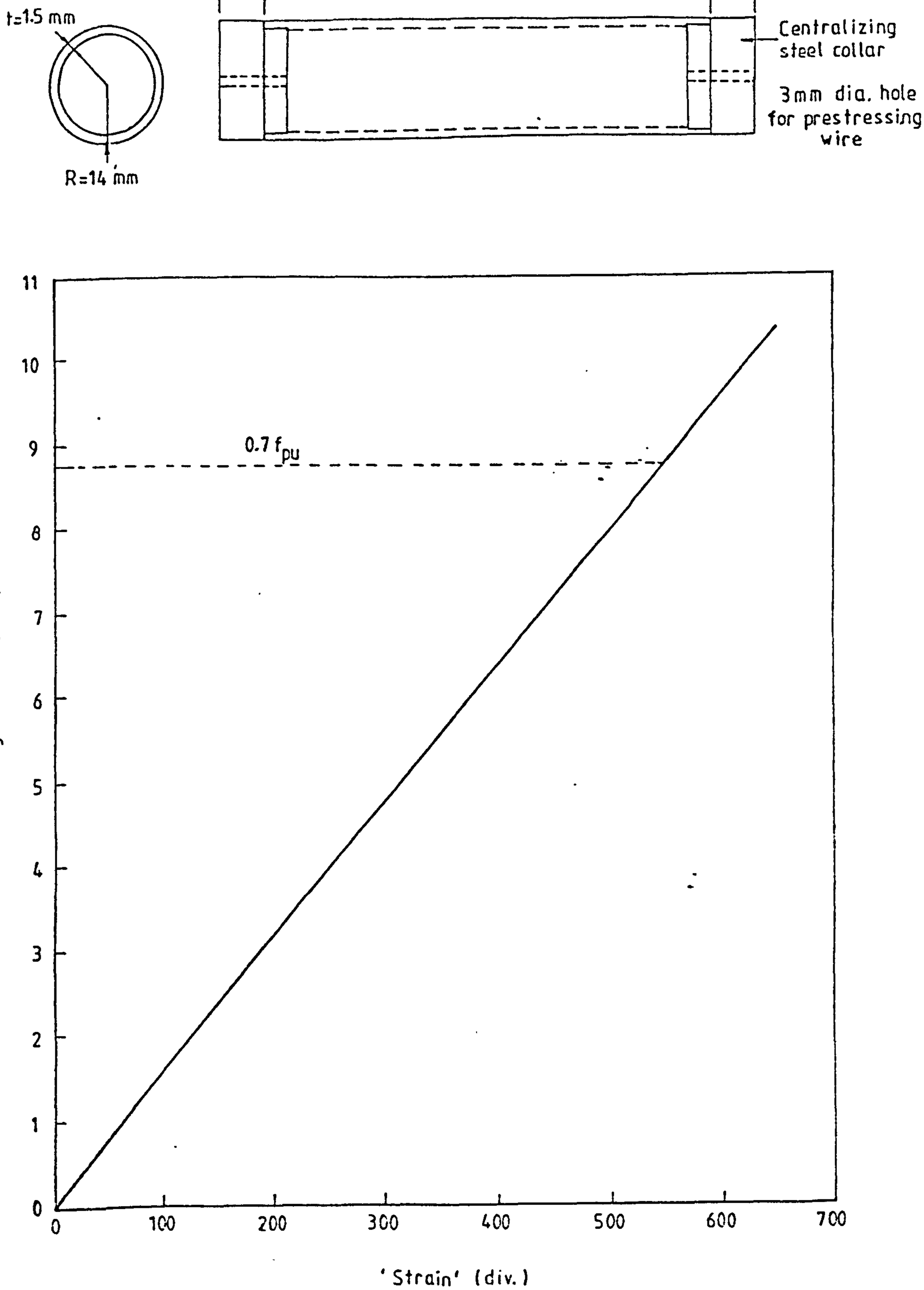

Fig. 5.18 Calibration graph of dynamometer (typical)

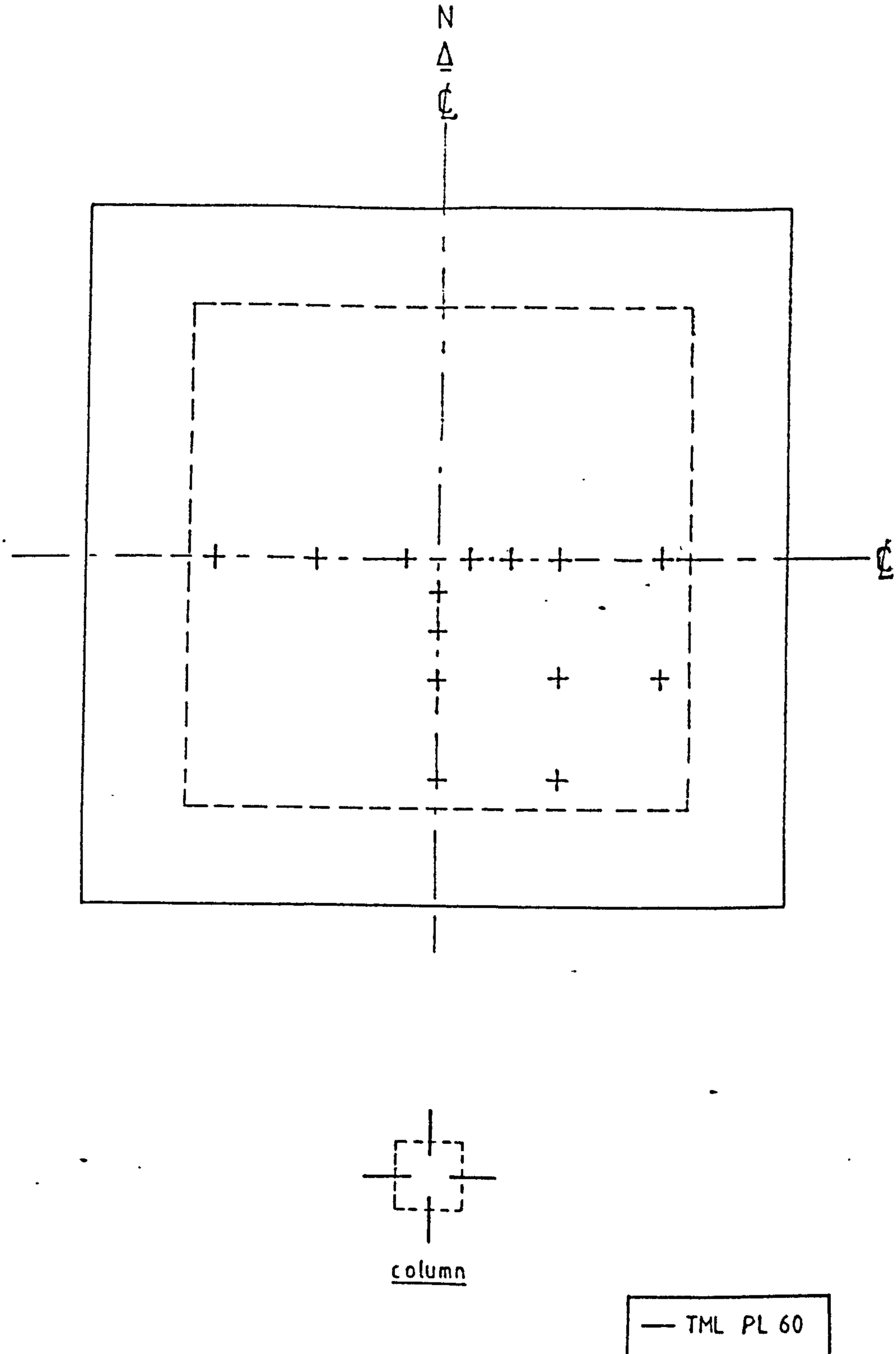

Fig. 5.19 Positions of electrical strain gauges on bottom surface of test slab (A1, A3, A4, B1, B2, B3, B4, C1)

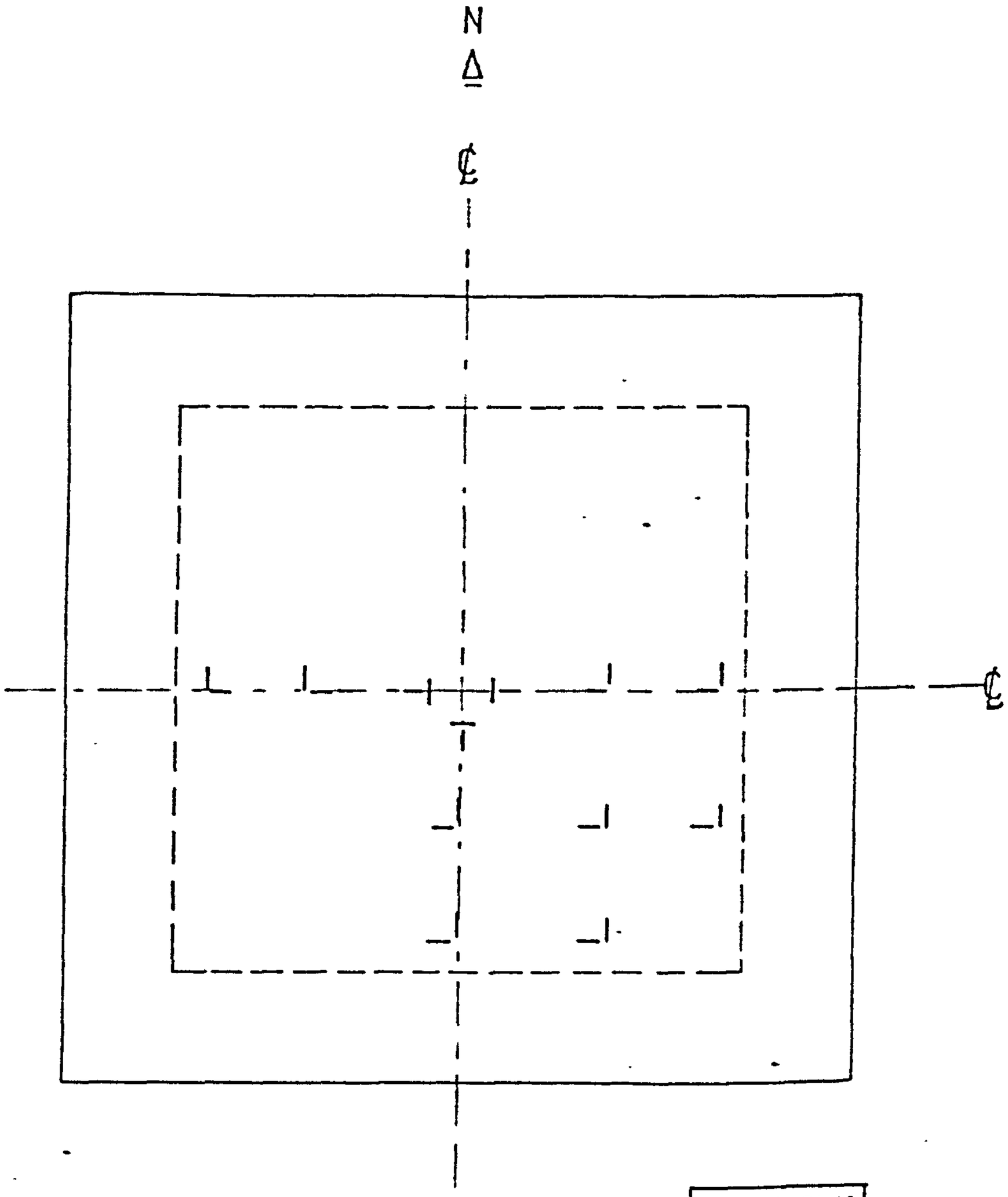

Fig.5.20 Positions of electrical strain gauges on bottom surface of slab A2

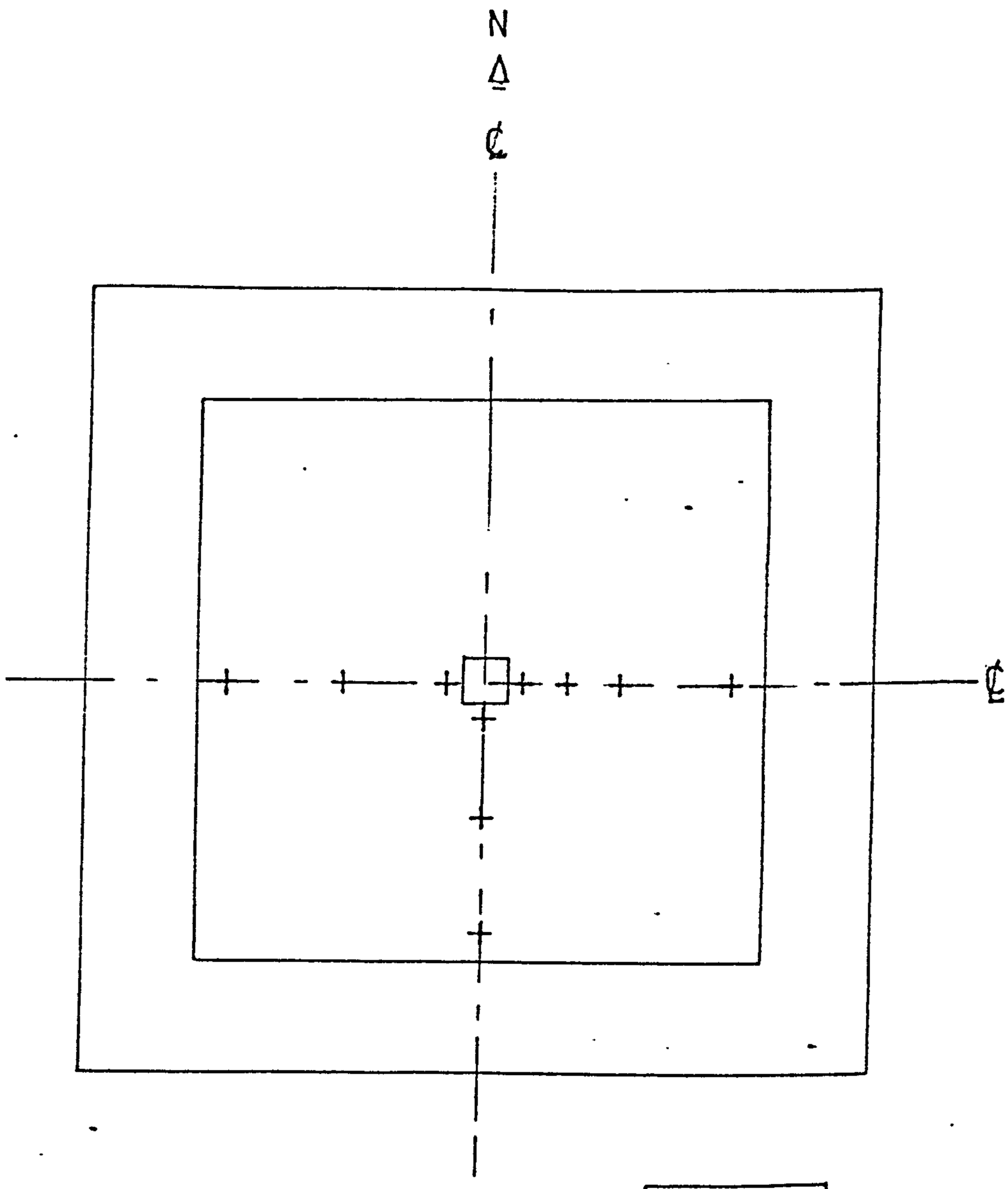

Fig.5.21 Positions of electrical strain gauges on top surface of test slab (B1, B2, B3, B4, C1)

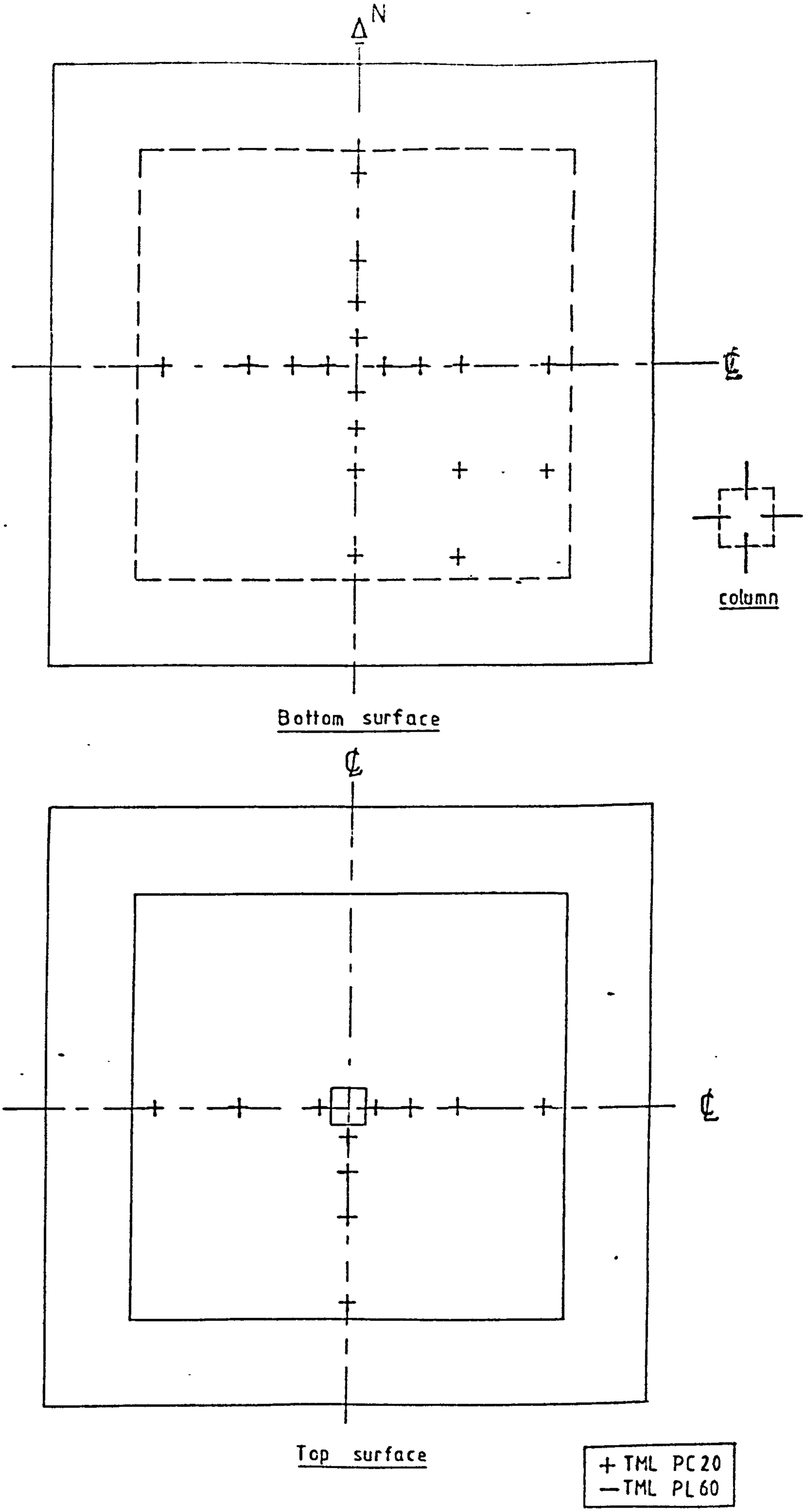

Fig. 5.22 Positions of electrical strain gauges on concrete surfaces of slab C 2

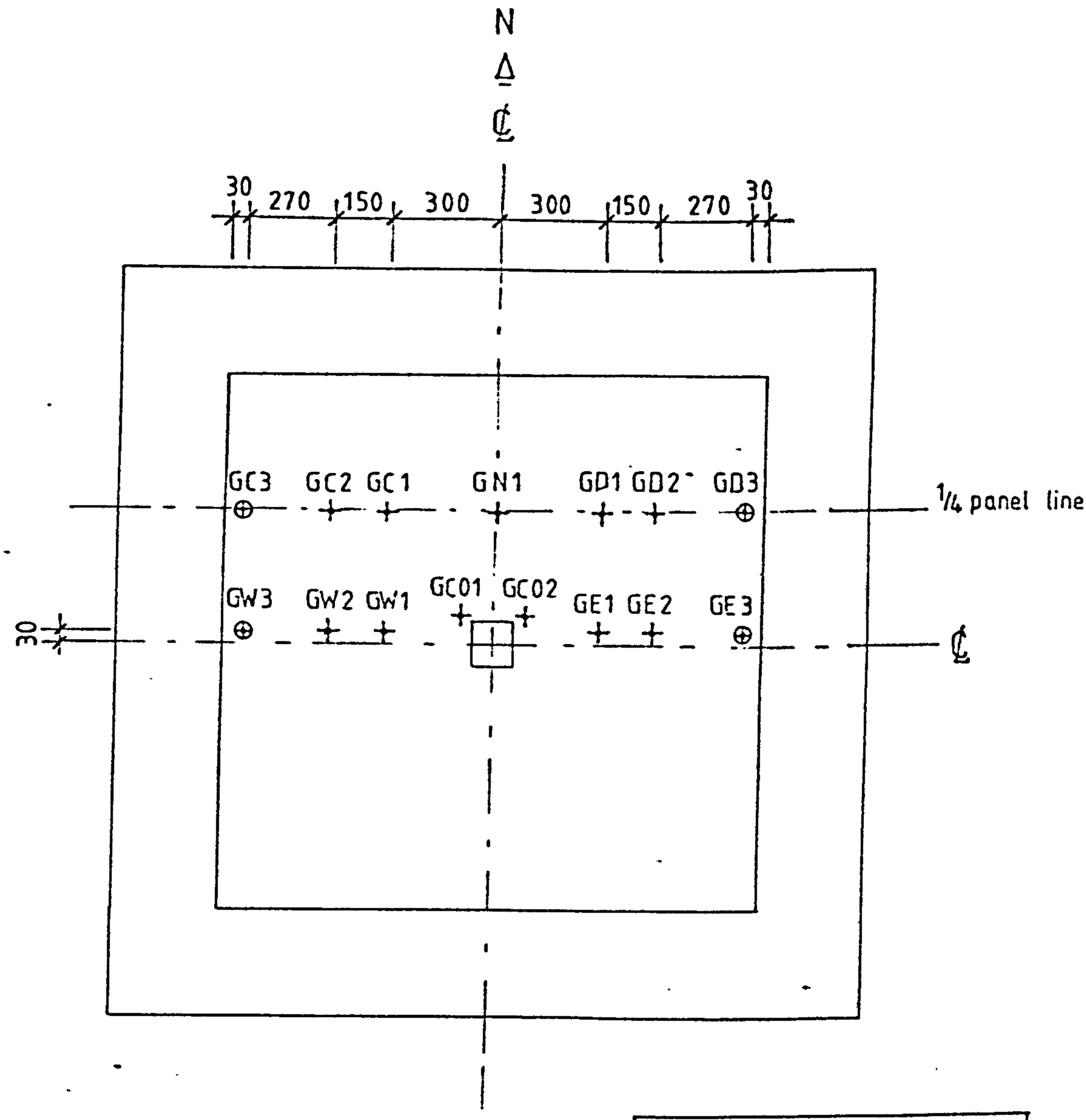

Fig. 5.23 Positions of dial gauges

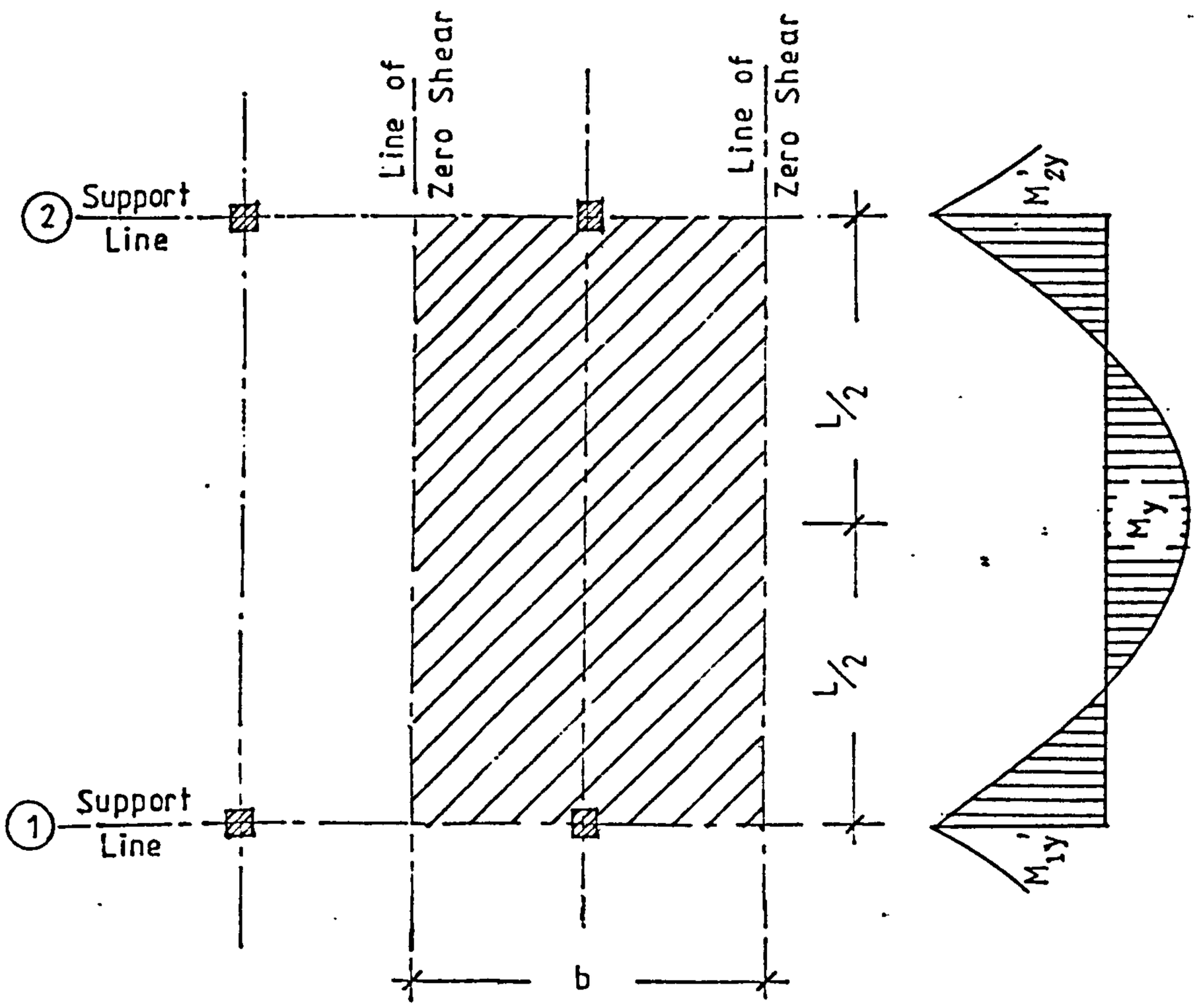

$$\int_{-b/2}^{+b/2} M_y \, dx \pm \frac{1}{2}\left(\int_{-b/2}^{+b/2} M_{1y}' \, dx + \int_{-b/2}^{+b/2} M_{2y}' \, dx \right) = \frac{w}{8} b L^2$$

Fig. 6.1 Moment diagram in slab under uniform loading

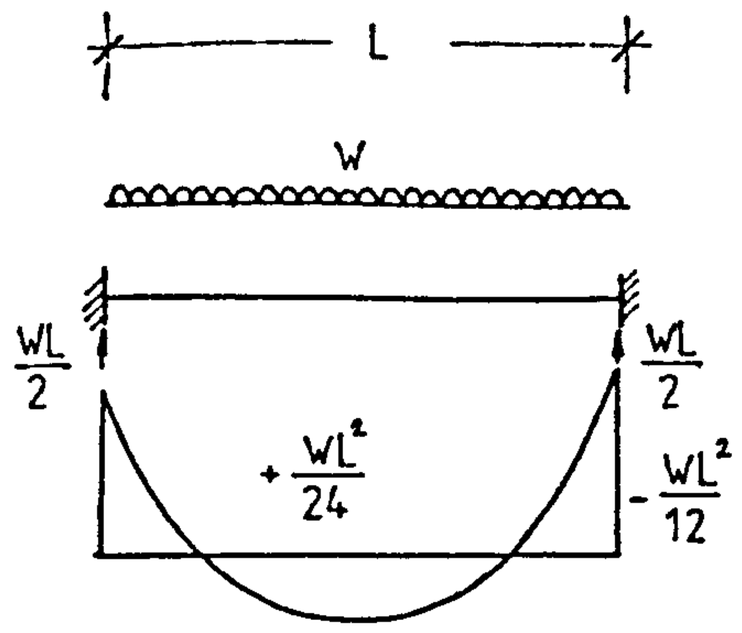

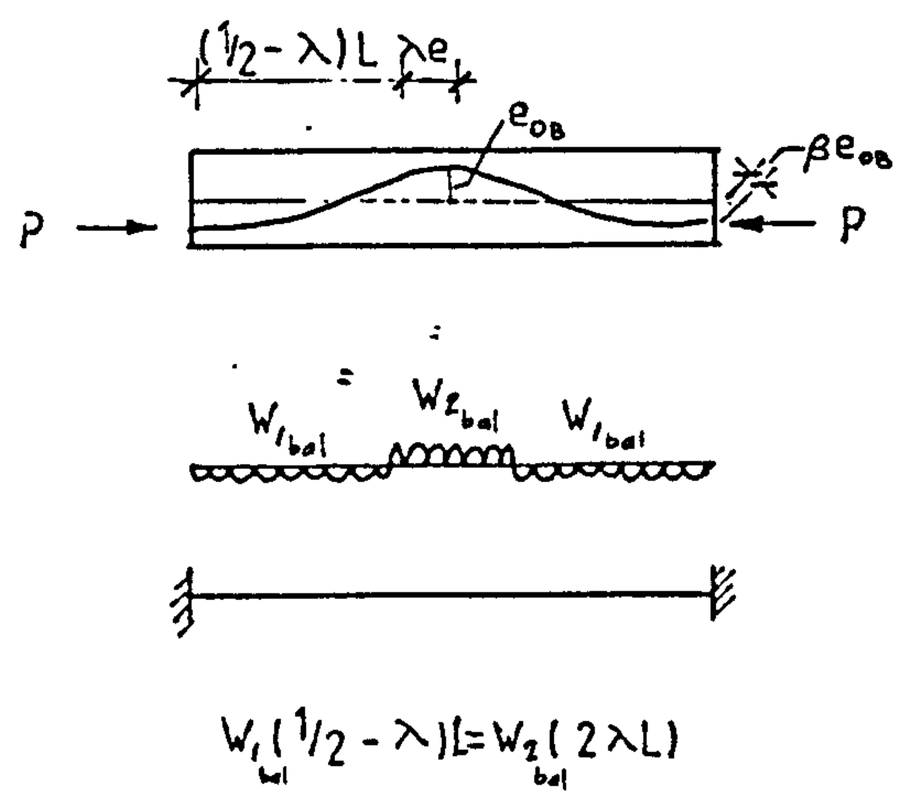

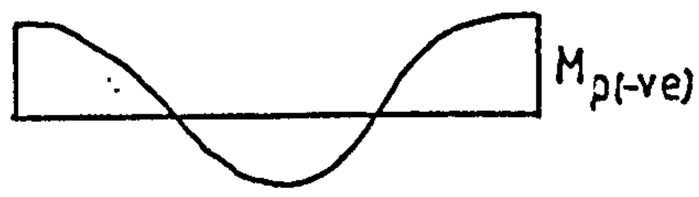

$$M_{p(+ve)} = \frac{2}{3} P e_{ob}(1-\beta)(1-\lambda)$$

$$M_{p(-ve)} = \frac{1}{3} P e_{ob}(1-\beta)(1+\lambda)$$

(b) Prestress Loading

(a) Uniform Loading

Fig. 6.2 Bending moment diagram for internal span in one direction

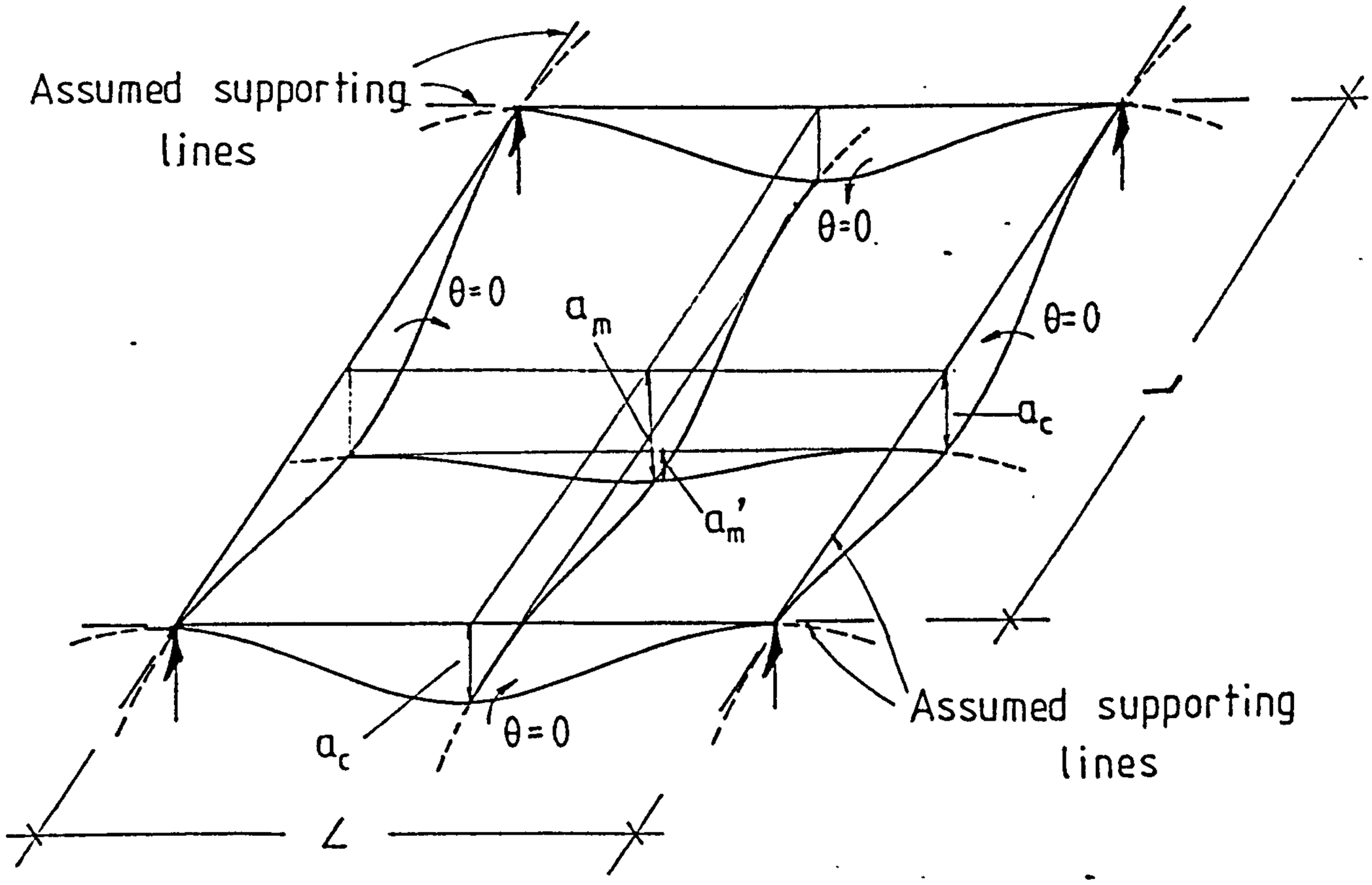

Fig. 6.3 Deformed surface of a typical internal square panel under uniform load

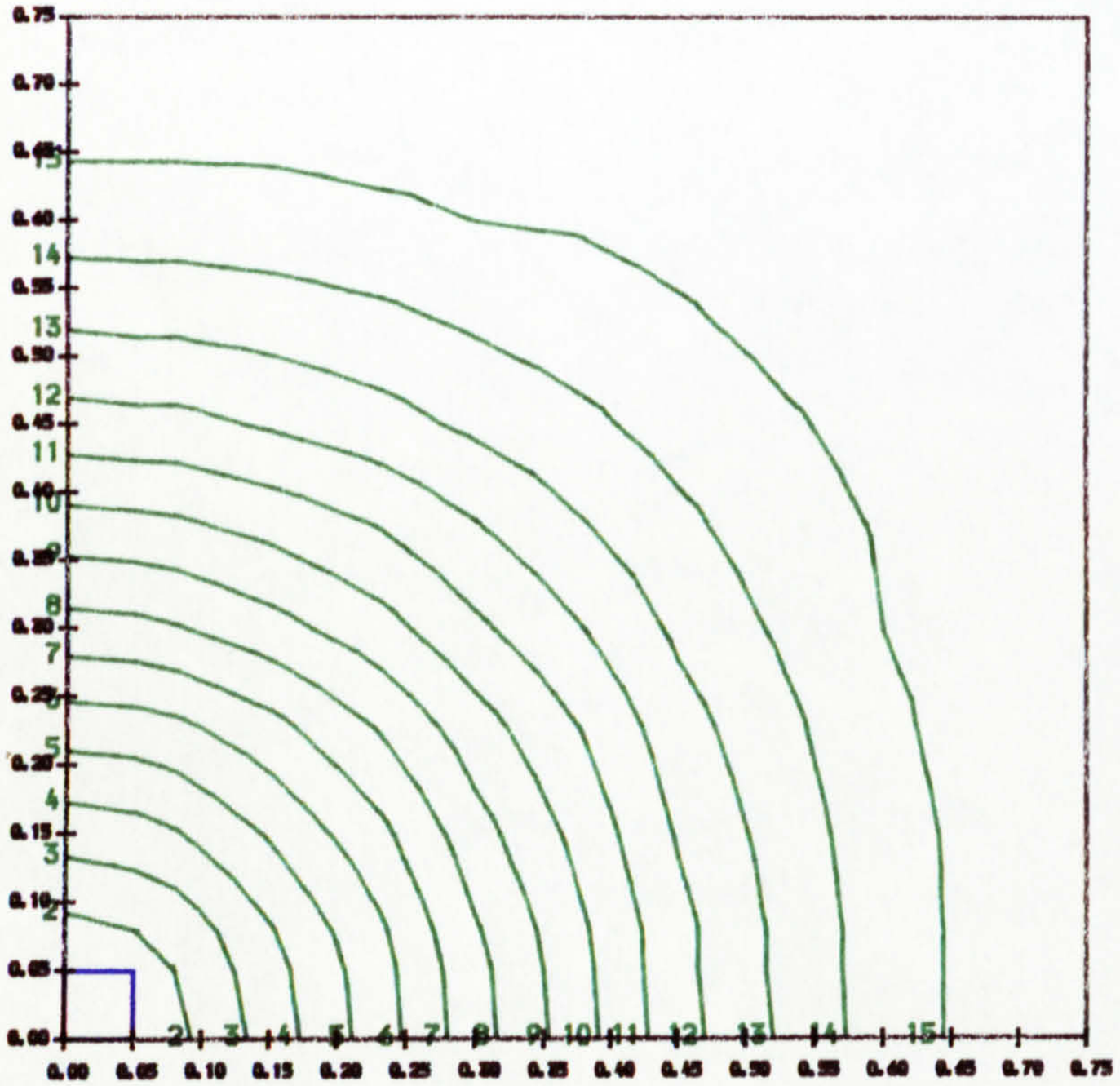

Laboratory test slab

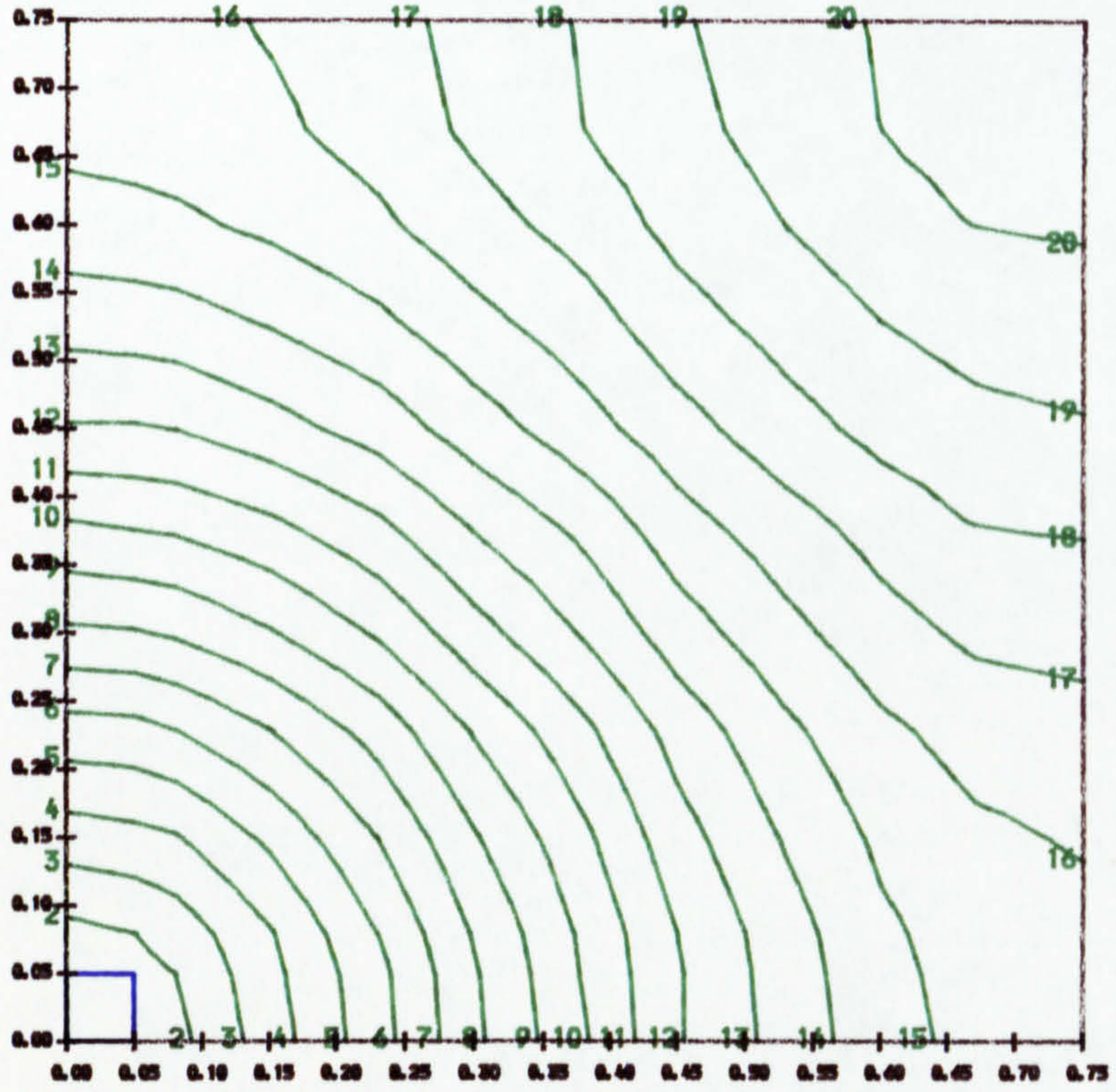

Interior flat slab floor panel

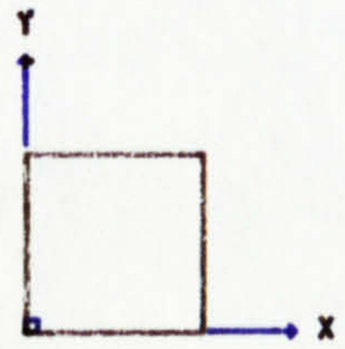

(1)	0.00	mm	(11)	1.00	"
(2)	0.10	"	(12)	1.10	"
(3)	0.20	"	(13)	1.20	"
(4)	0.30	"	(14)	1.30	"
(5)	0.40	"	(15)	1.40	"
(6)	0.50	"	(16)	1.50	"
(7)	0.60	"	(17)	1.60	"
(8)	0.70	"	(18)	1.70	"
(9)	0.80	"	(19)	1.80	"
(10)	0.90	"	(20)	1.90	"

Fig. 6.4 Comparison of uniform load deflections in experimental and interior flat slab floor panel

Laboratory test slab

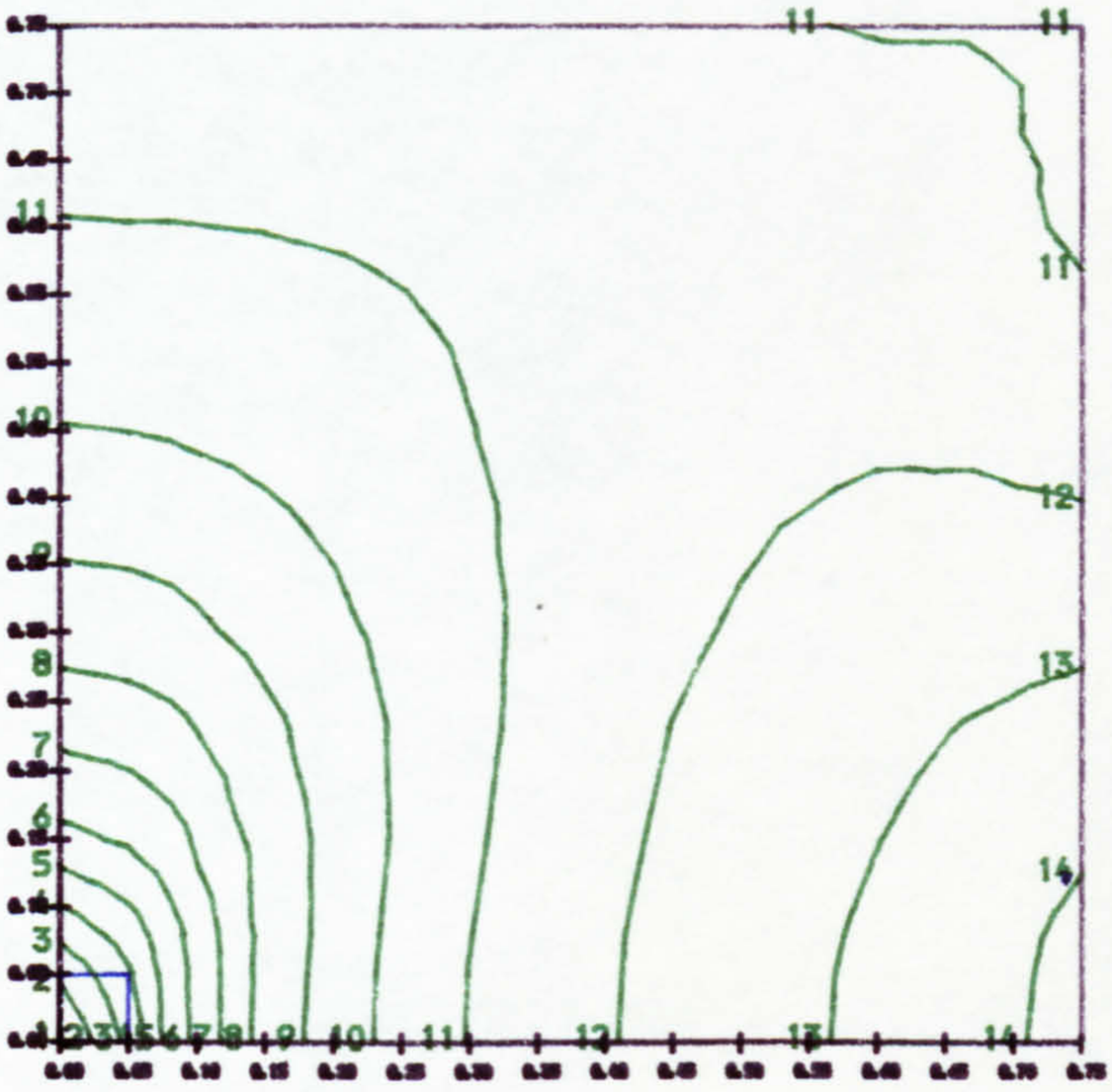

(a1) Bending moment Mx

Interior flat slab floor panel

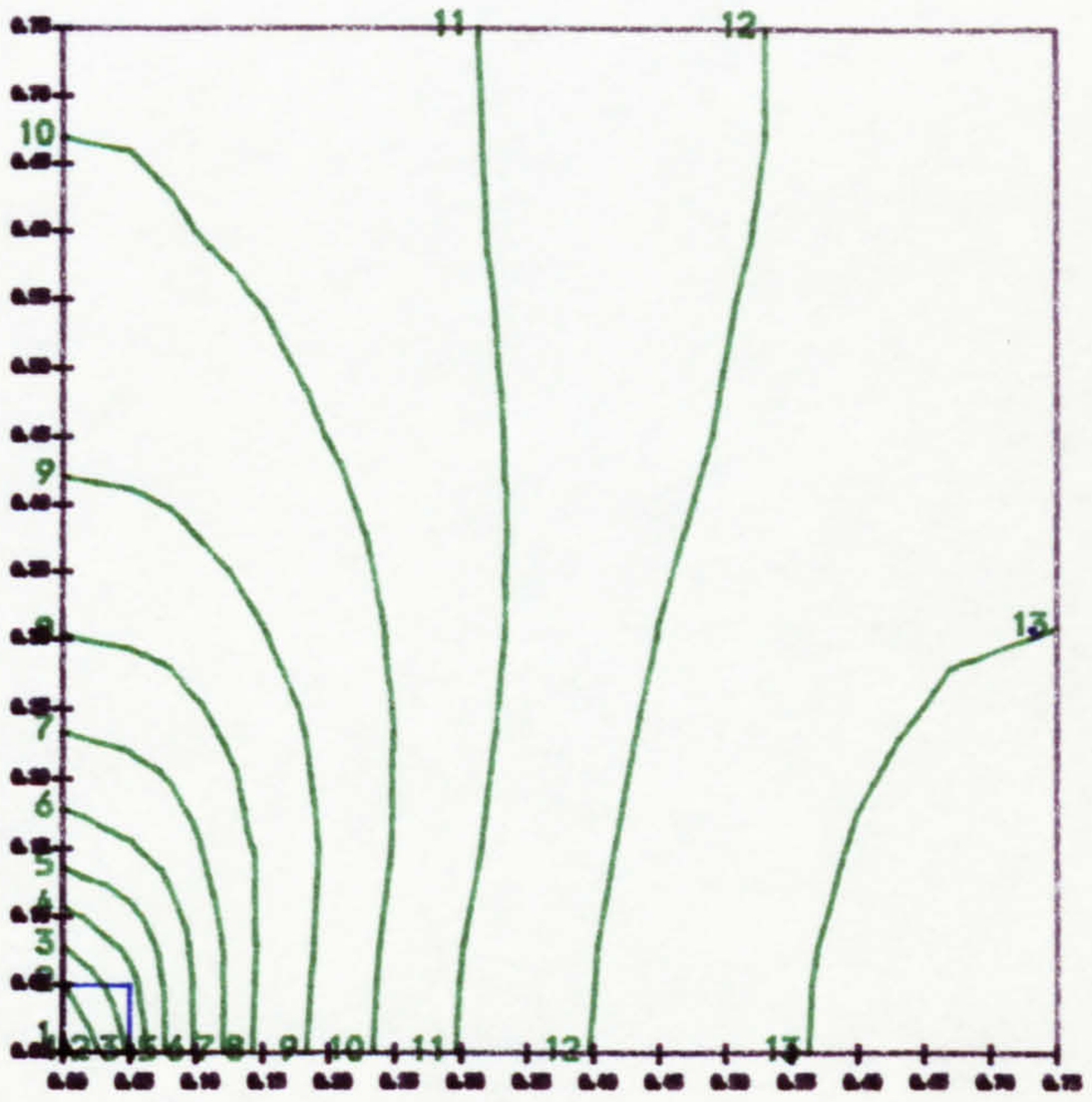

(b1) Bending moment Mx

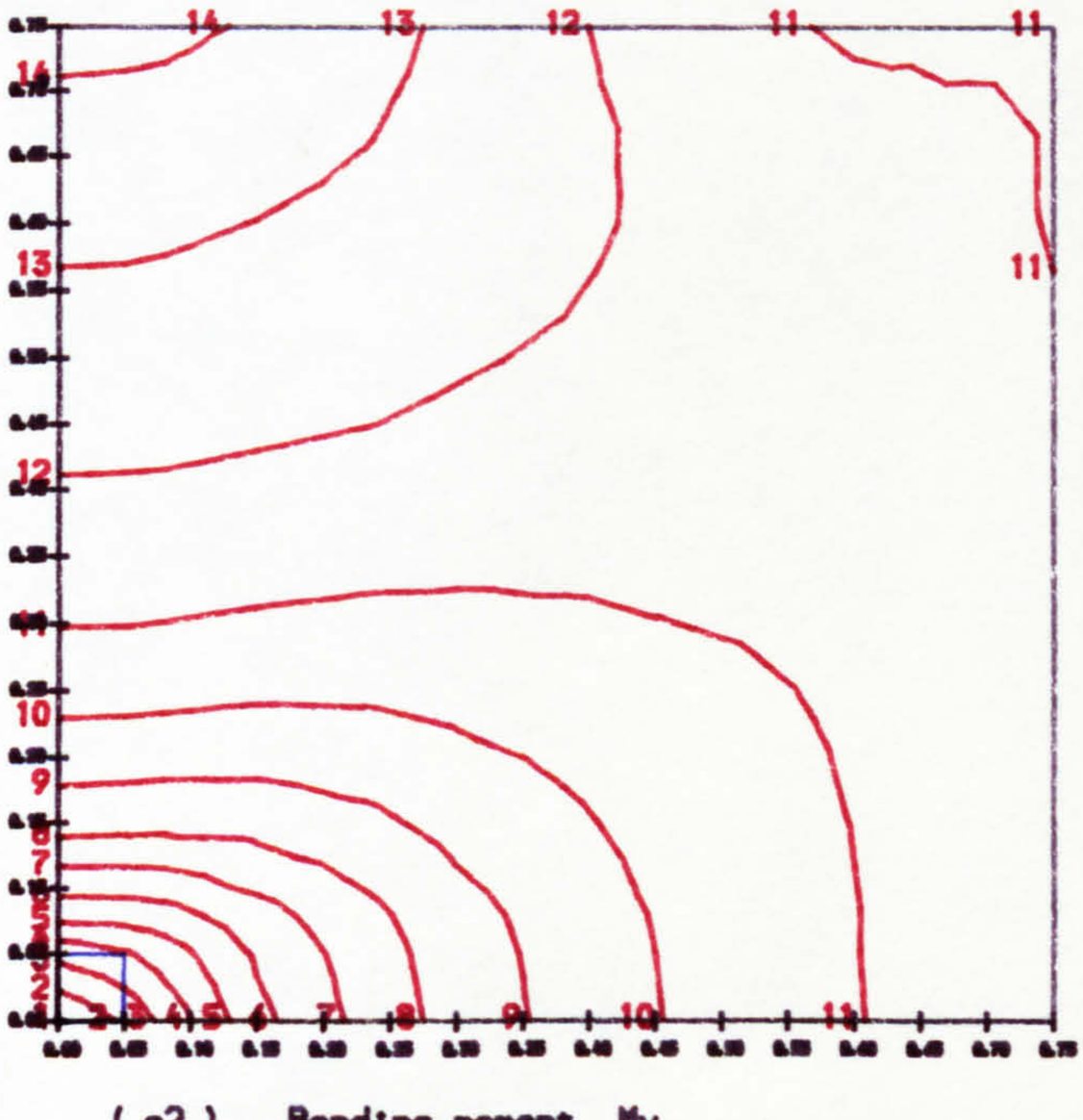

(a2) Bending moment My

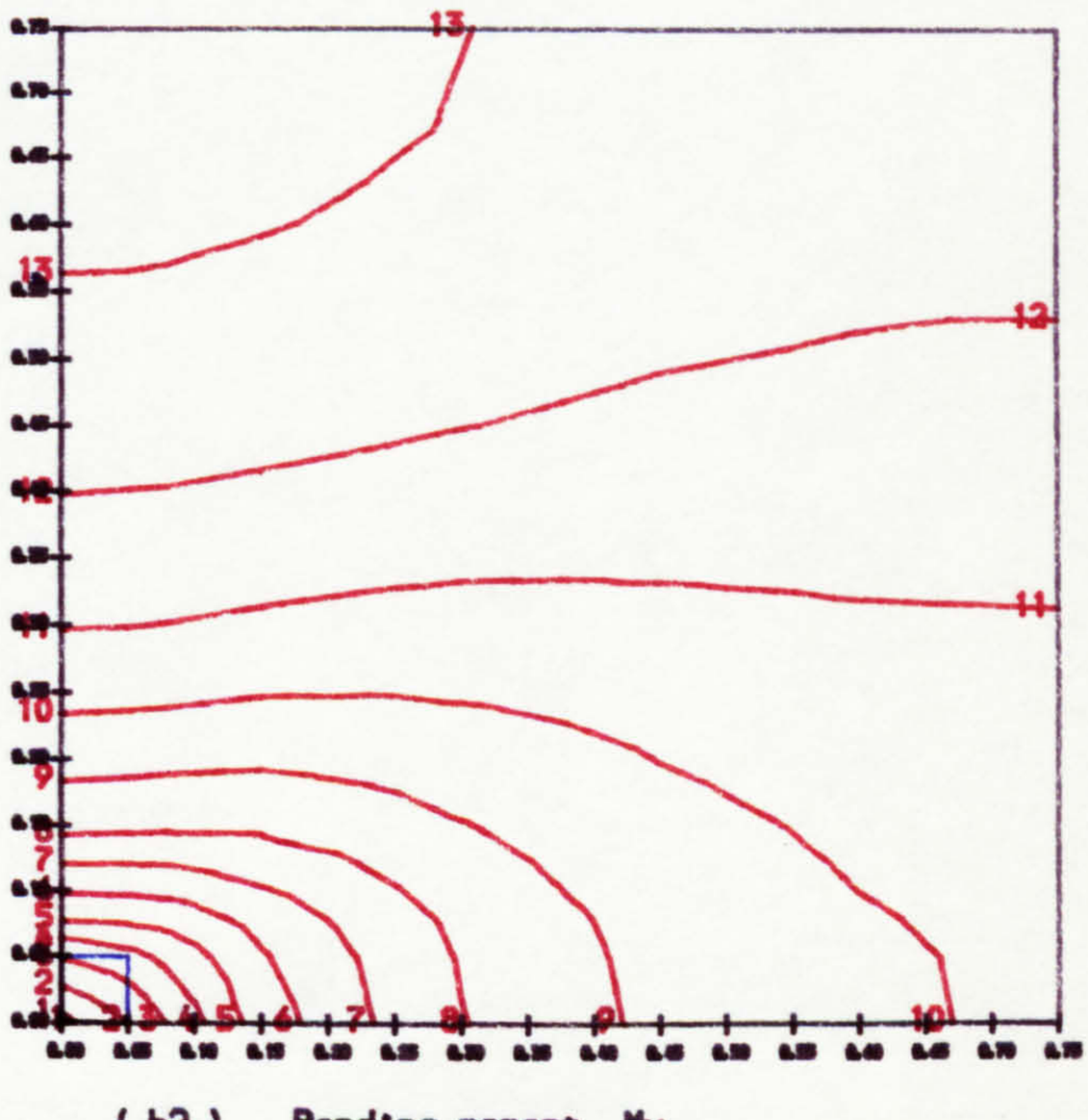

(b2) Bending moment My

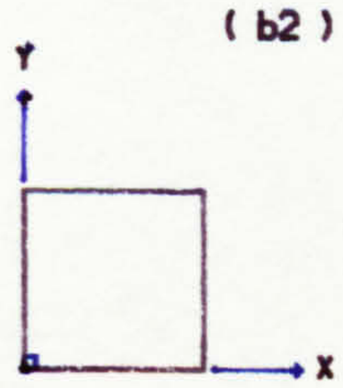

(1)	-5.00 kNm/m	(8)	-1.50 kNm/m
(2)	-4.50 "	(9)	-1.00 "
(3)	-4.00 "	(10)	-0.50 "
(4)	-3.50 "	(11)	0.00 "
(5)	-3.00 "	(12)	0.50 "
(6)	-2.50 "	(13)	1.00 "
(7)	-2.00 "	(14)	1.50 "

Fig. 6.5 Comparison of uniform load moment distribution in experimental and interior flat slab floor panel

Laboratory test slab

Interior flat slab floor panel

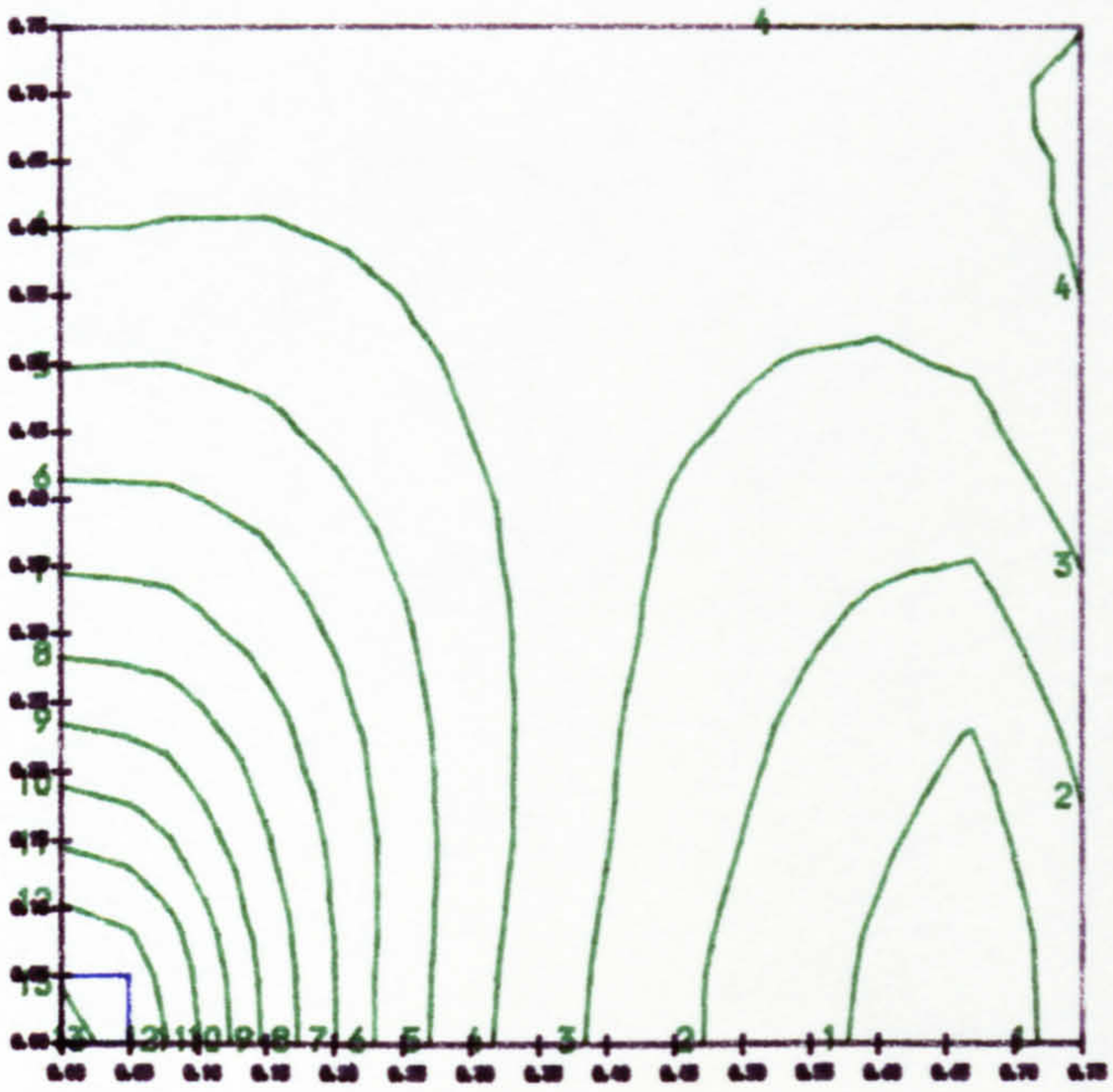

(a1) Prestressing moment Mpx

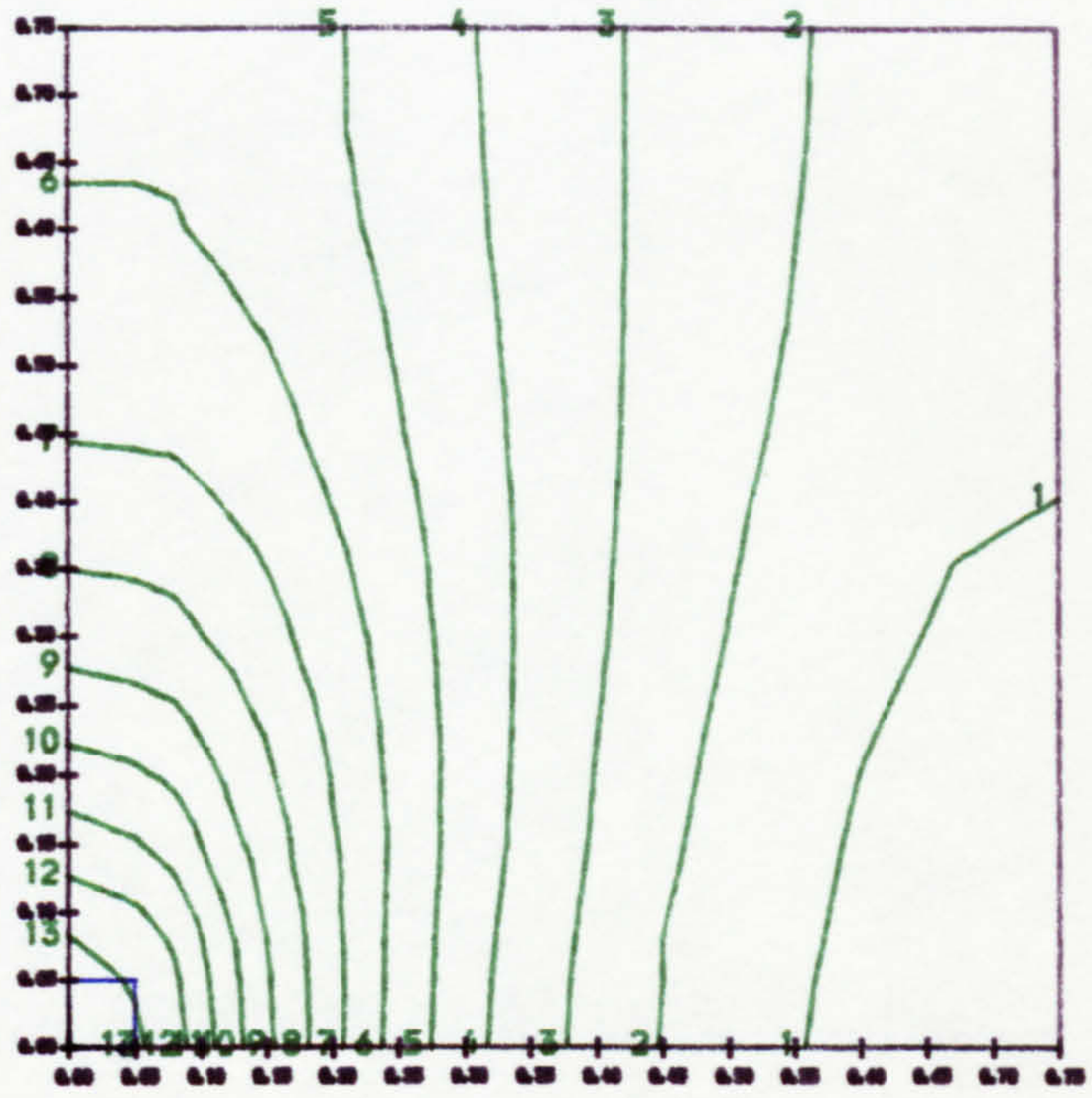

(b1) Prestressing moment Mpx

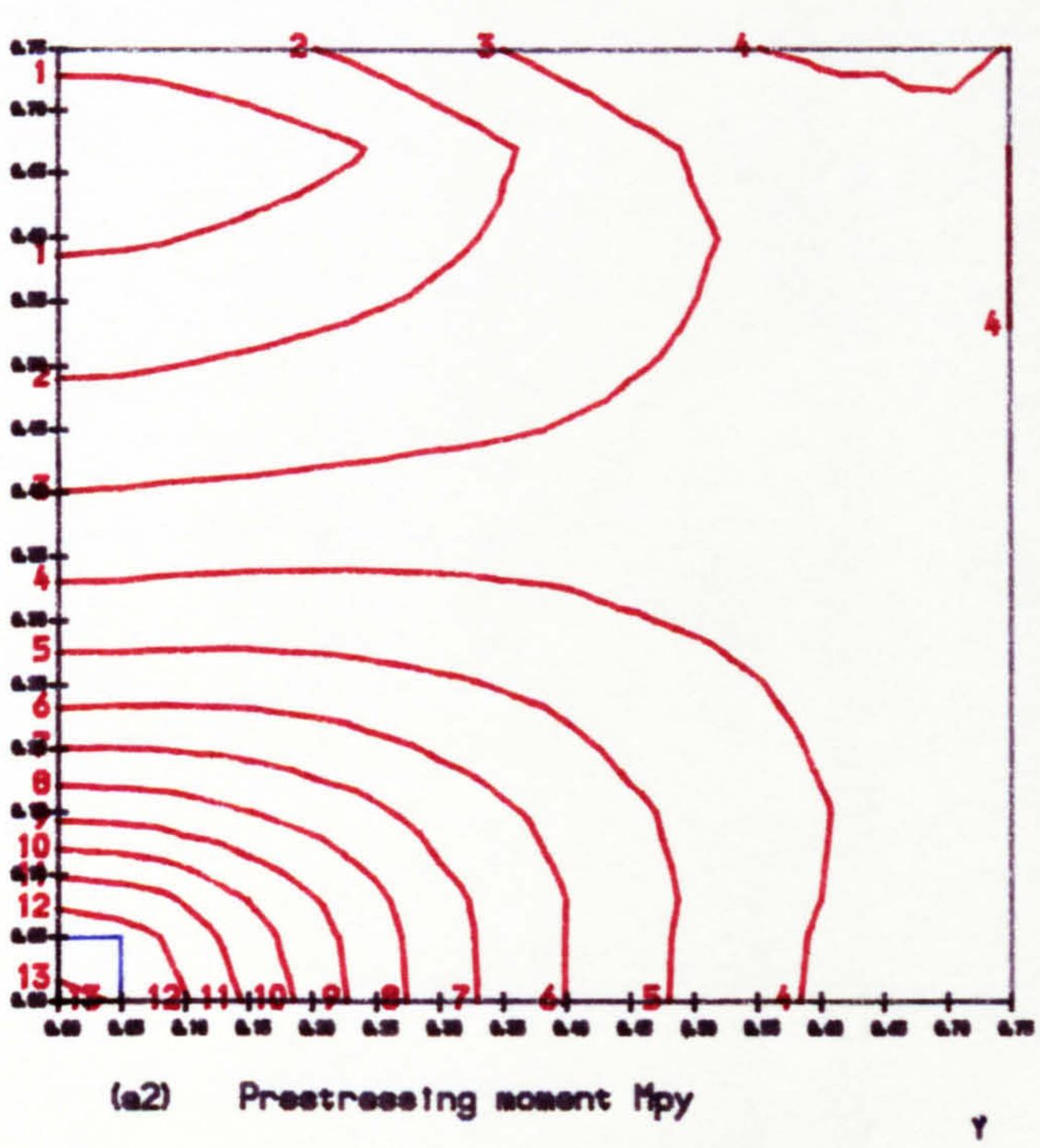

(a2) Prestressing moment Mpy

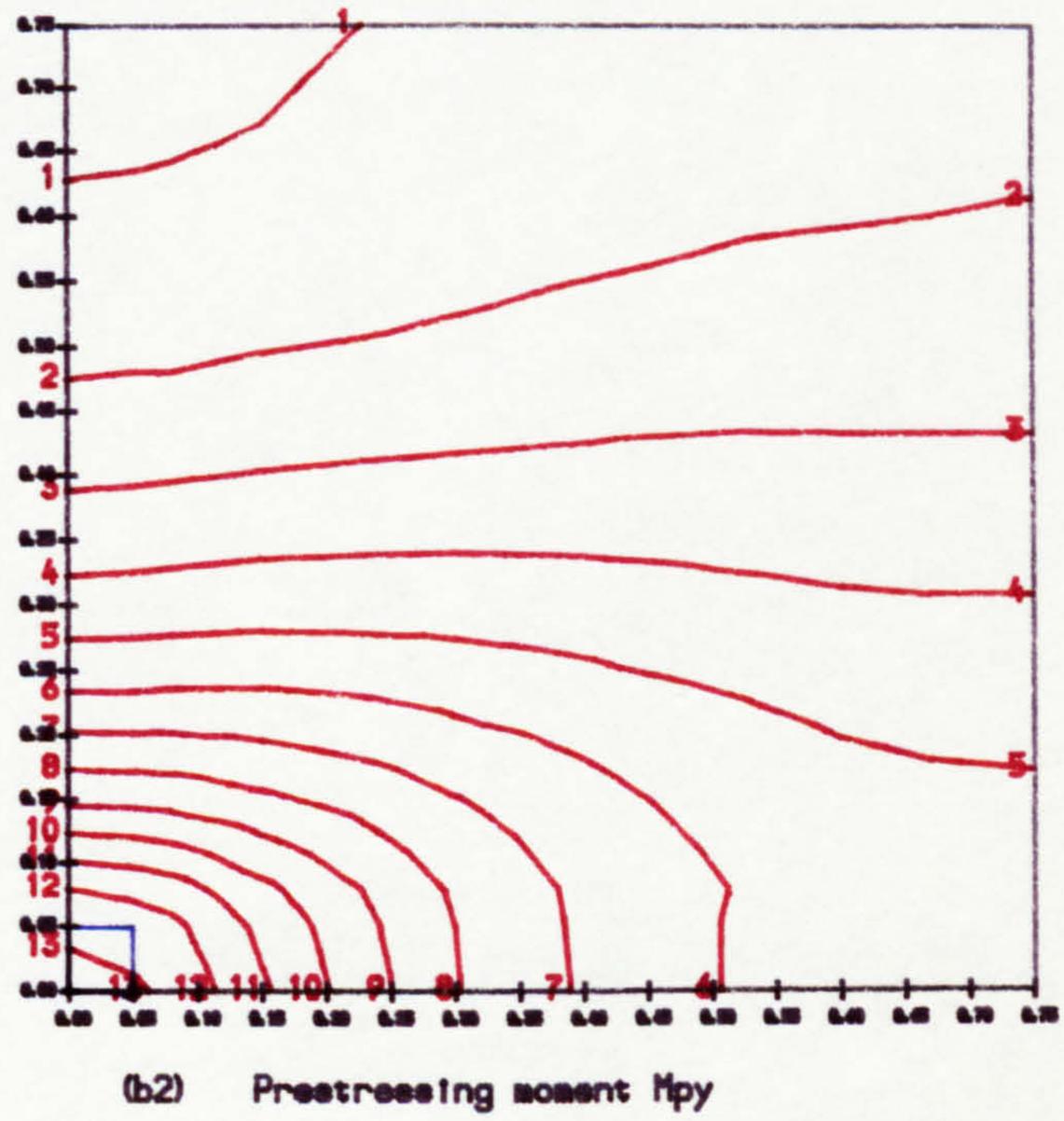

(b2) Prestressing moment Mpy

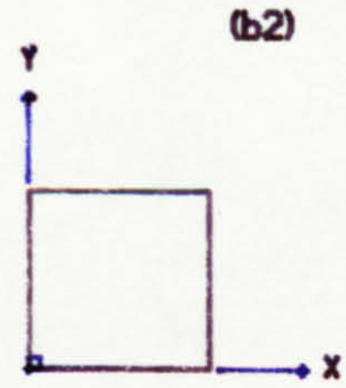

(1)	-0.60	kNm/m	(8)	0.80	kNm/m
(2)	-0.40	"	(9)	1.00	"
(3)	-0.20	"	(10)	1.20	"
(4)	0.00	"	(11)	1.40	"
(5)	0.20	"	(12)	1.60	"
(6)	0.40	"	(13)	1.80	"
(7)	0.60	"			

Fig. 6.6 Comparison of prestressing moment distribution in experimental and interior flat slab floor panel, Slab A1

Laboratory test slab

Interior flat slab floor panel

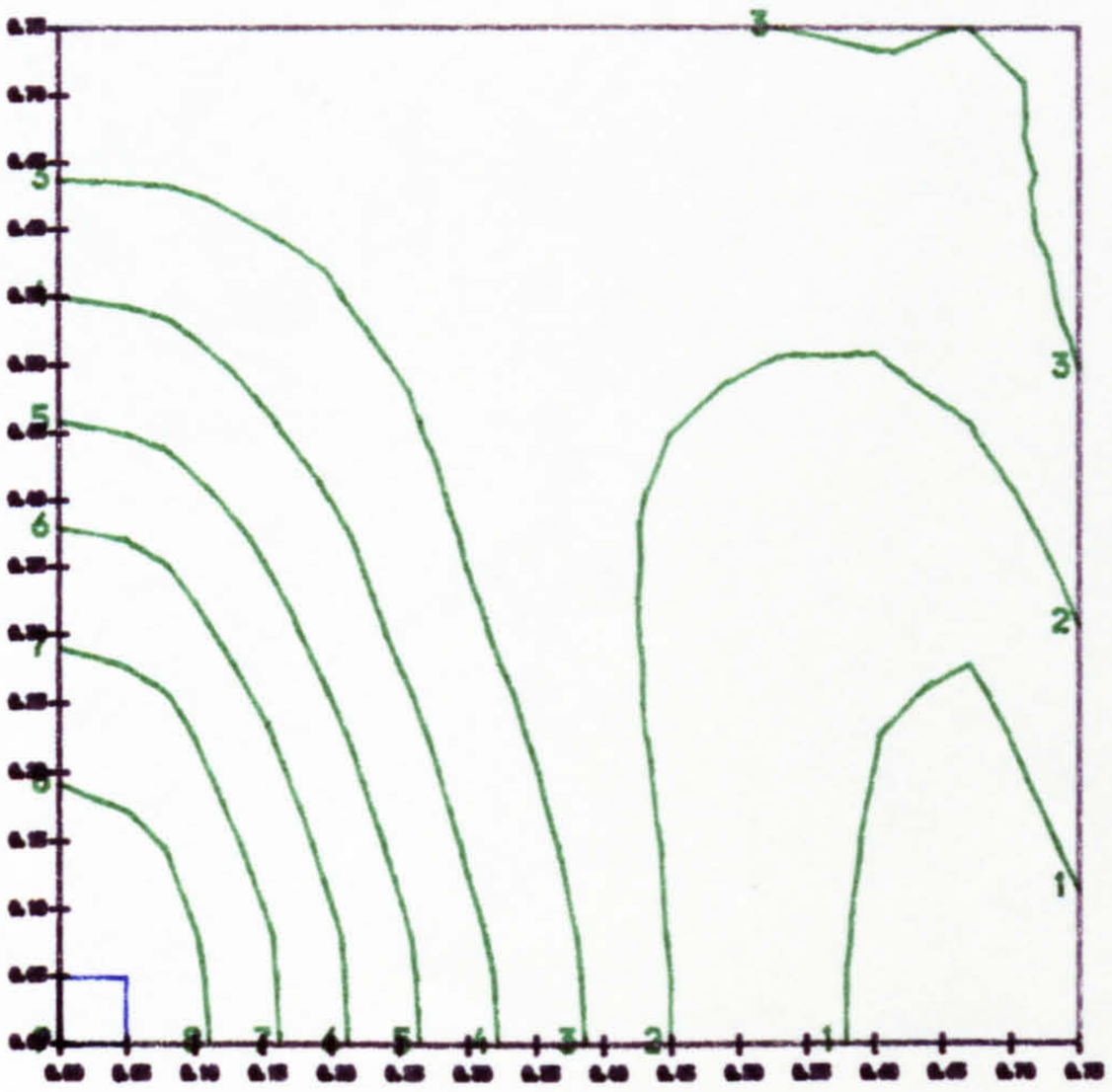

(a1) Prestressing moment Mpx

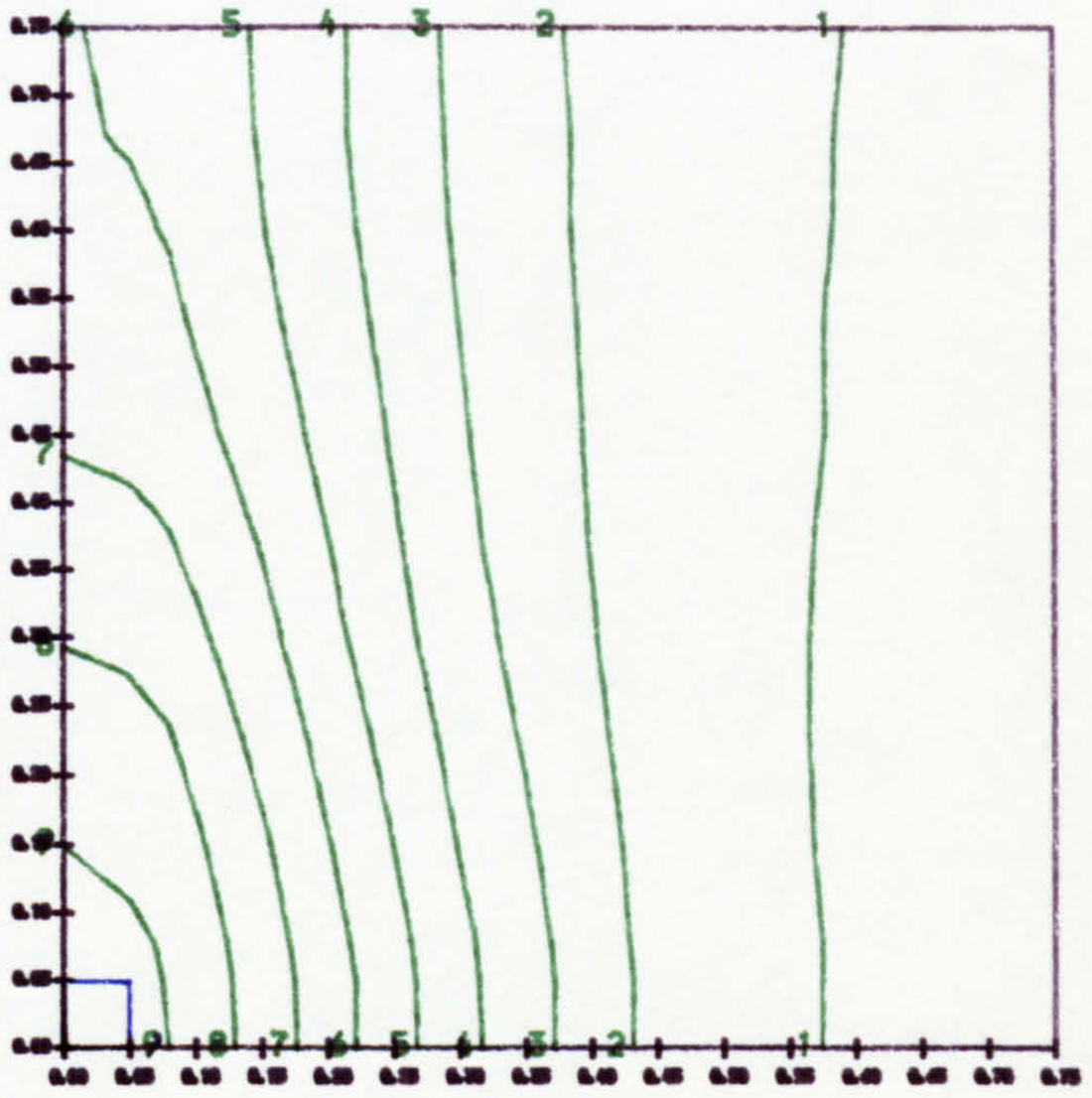

(b1) Prestressing moment Mpx

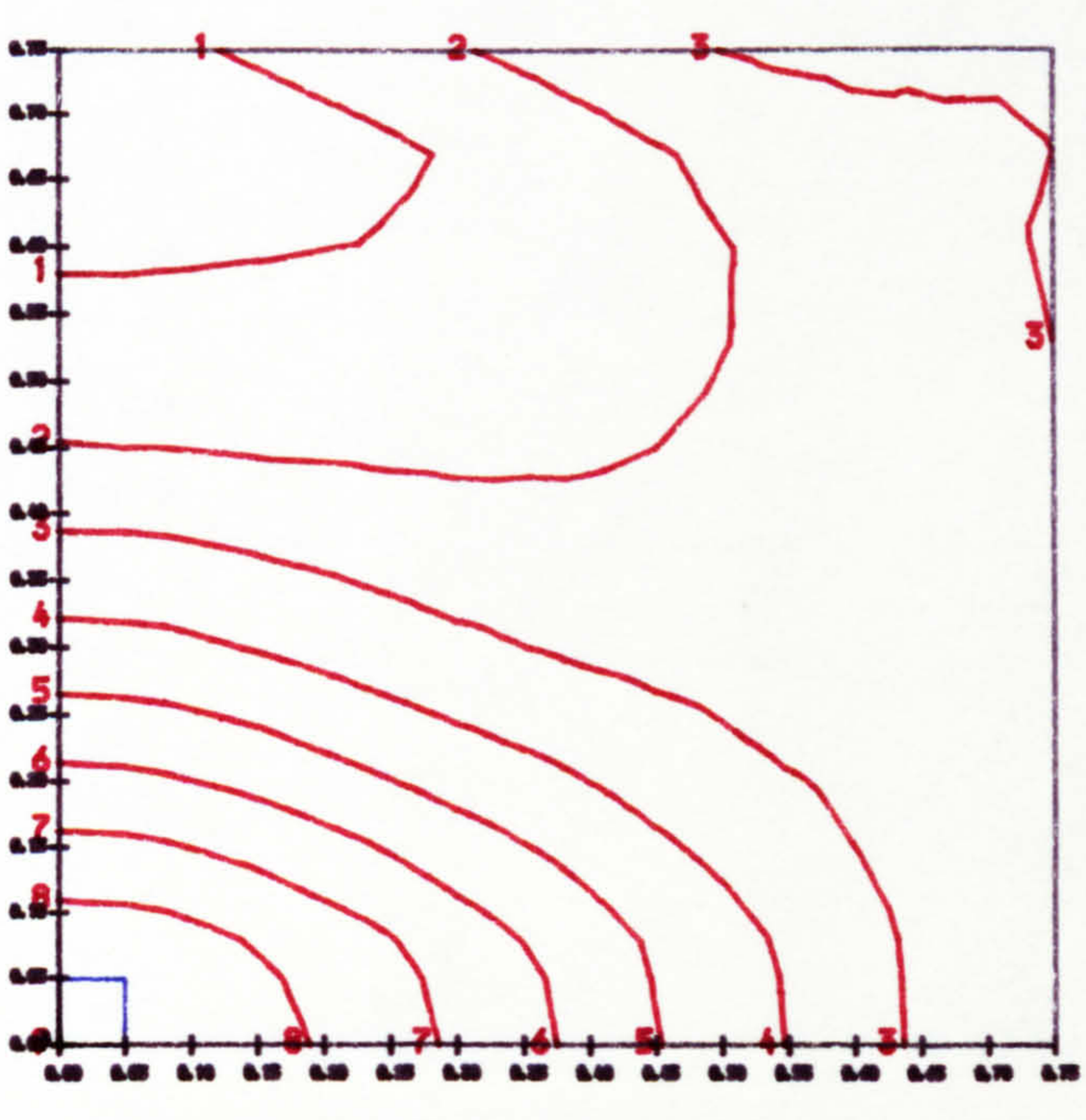

(a2) Prestressing moment Mpy

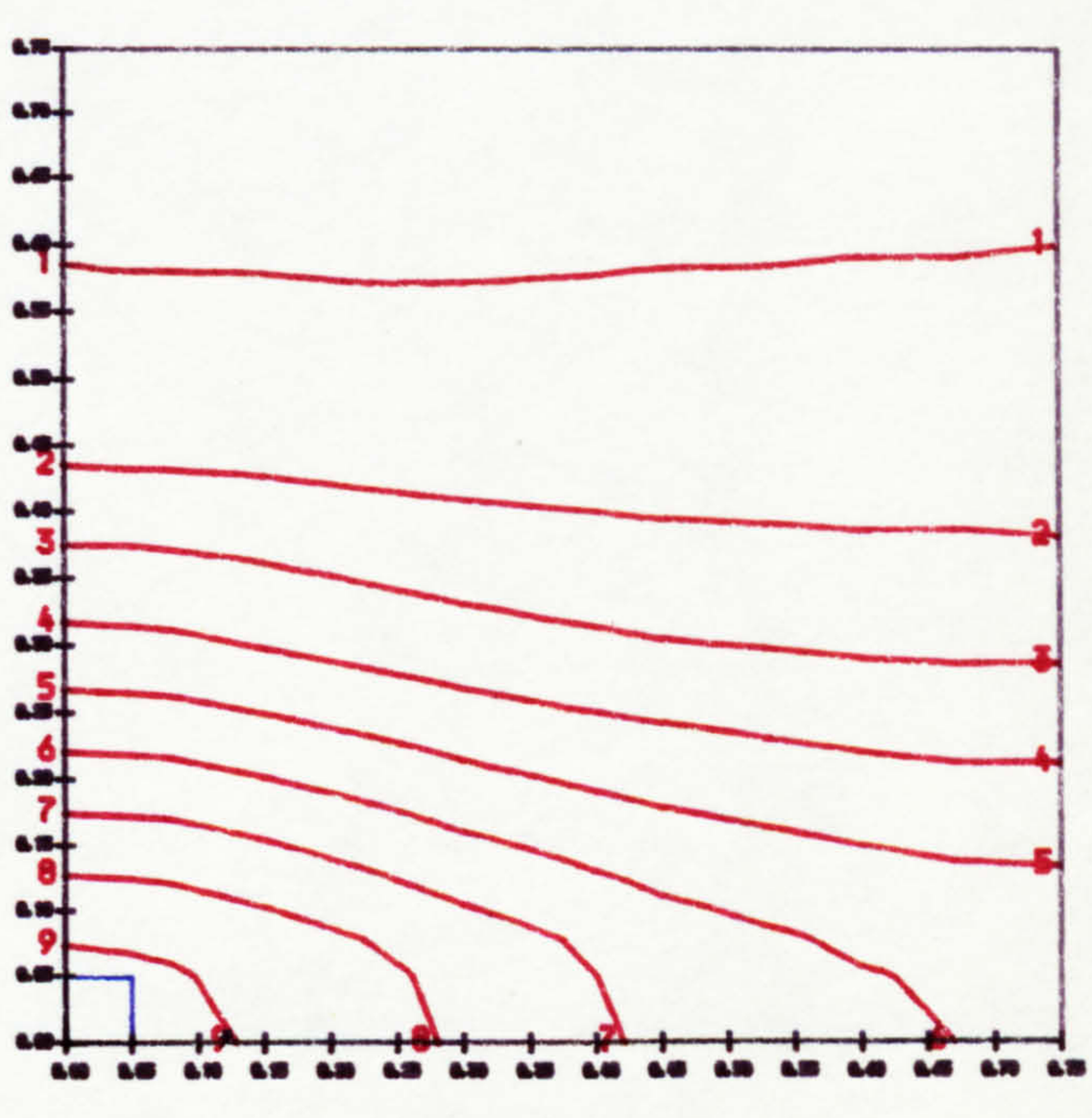

(b2) Prestressing moment Mpy

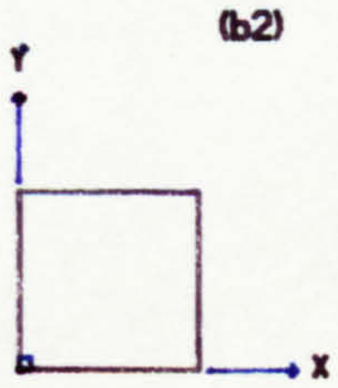

(1) -0.50 kNm/m
(2) -0.20 "
(3) 0.00 "
(4) 0.20 "
(5) 0.40 "
(6) 0.60 kNm/m
(7) 0.80 "
(8) 1.00 "
(9) 1.20 "

Fig. 6.7 Comparison of prestressing moment distribution in experimental and interior flat slab floor panel, Slab A2

Laboratory test slab

Interior flat slab floor panel

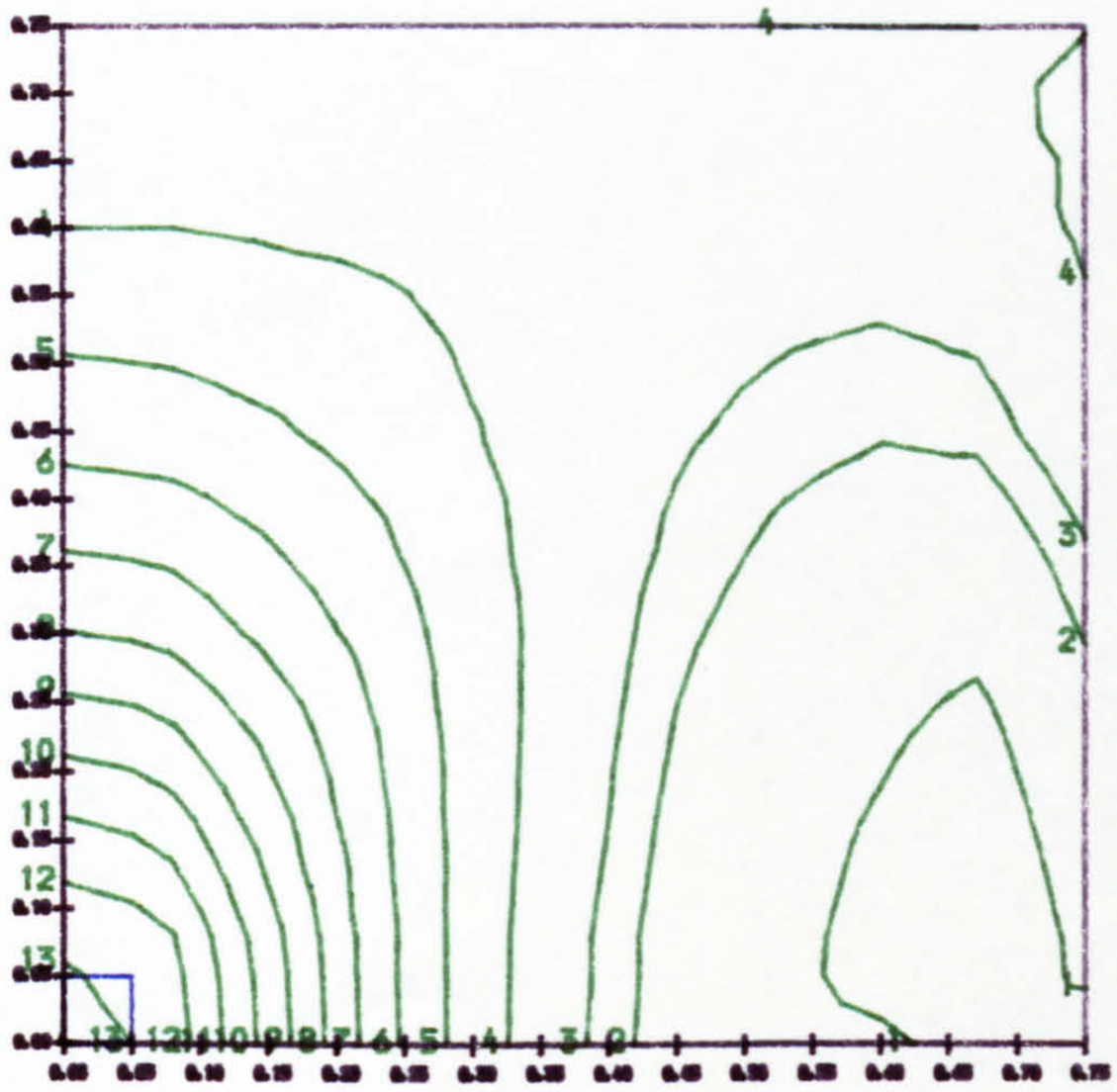

(a1) Prestressing moment Mpx

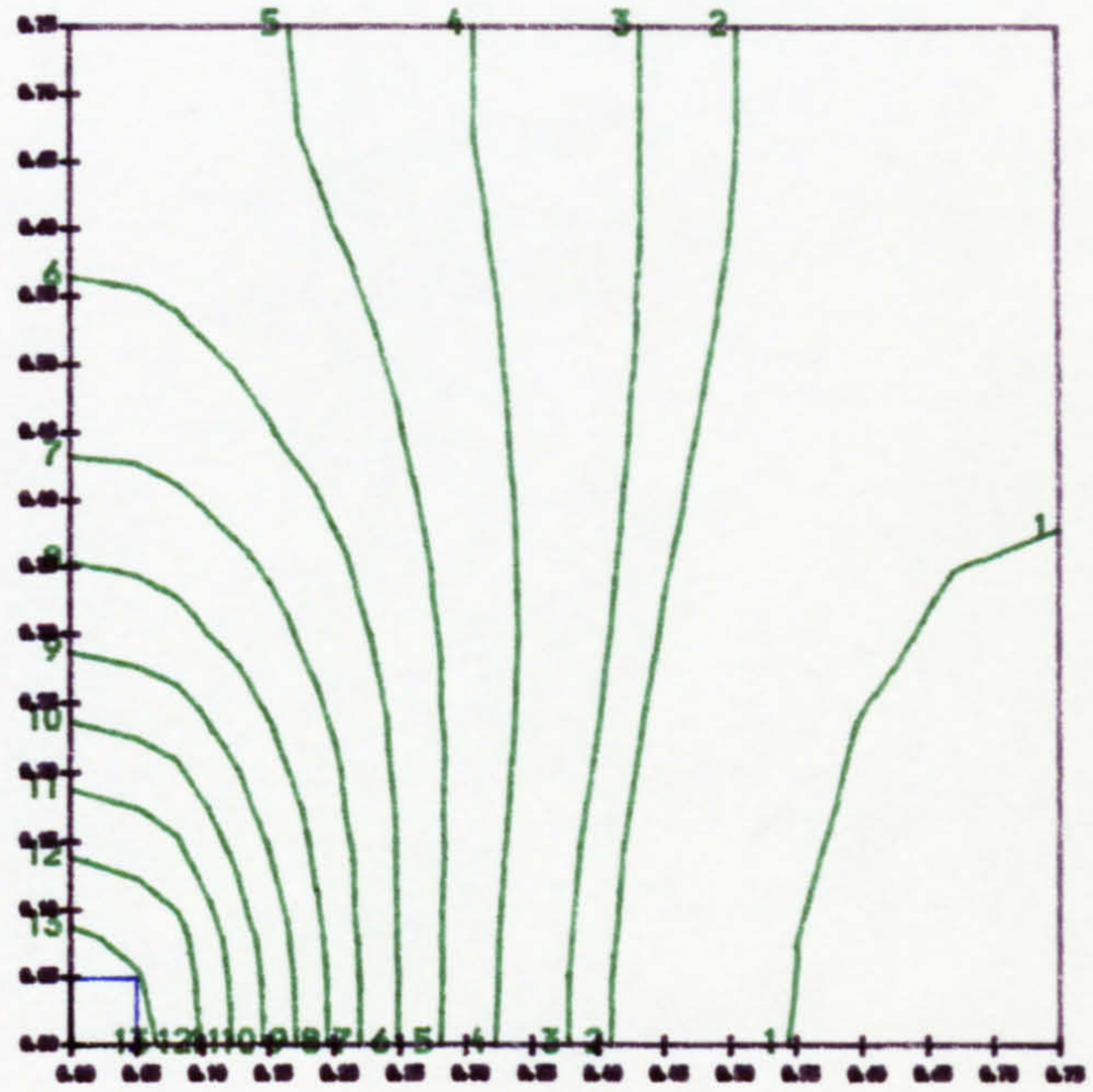

(b1) Prestressing moment Mpx

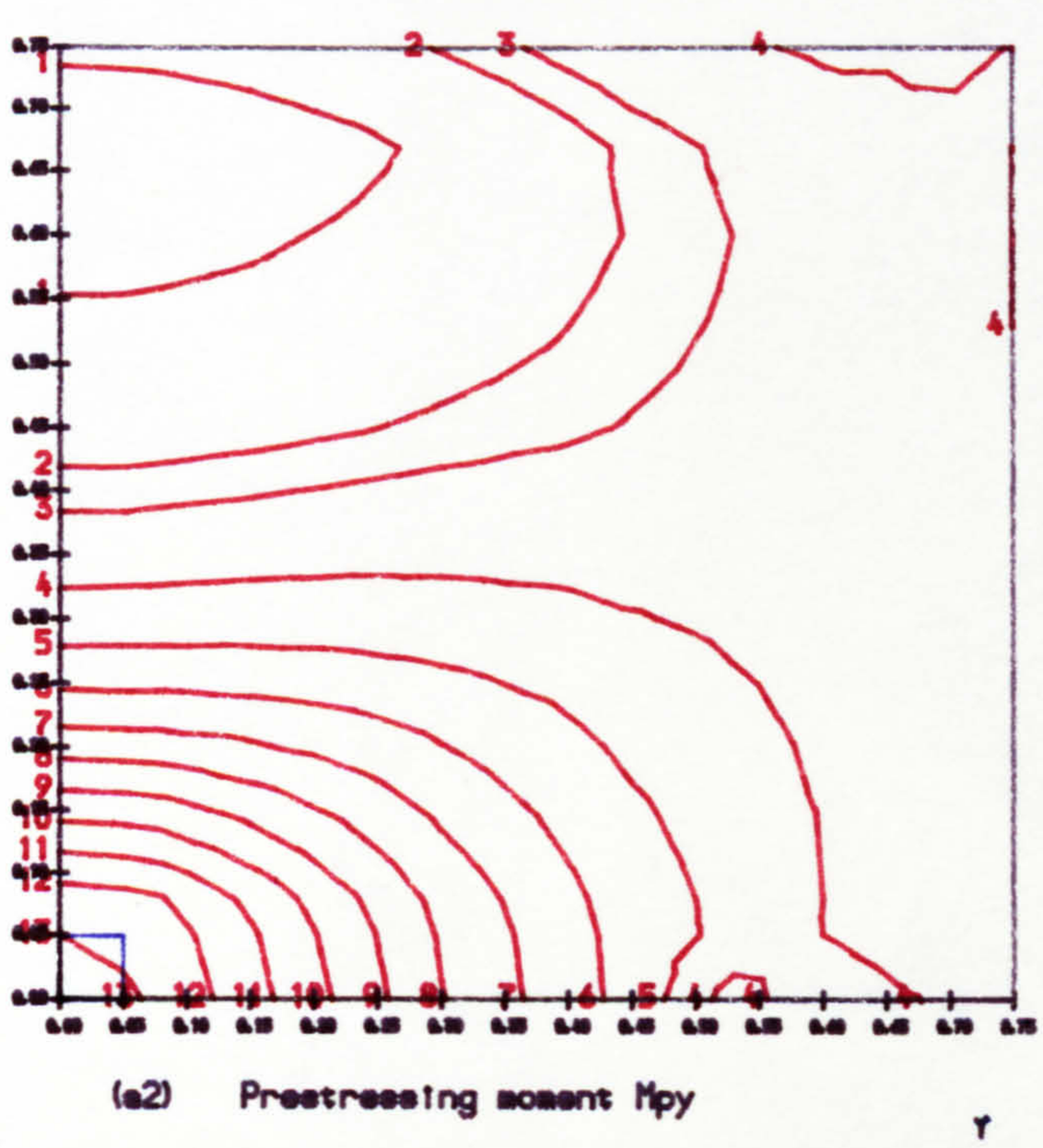

(a2) Prestressing moment Mpy

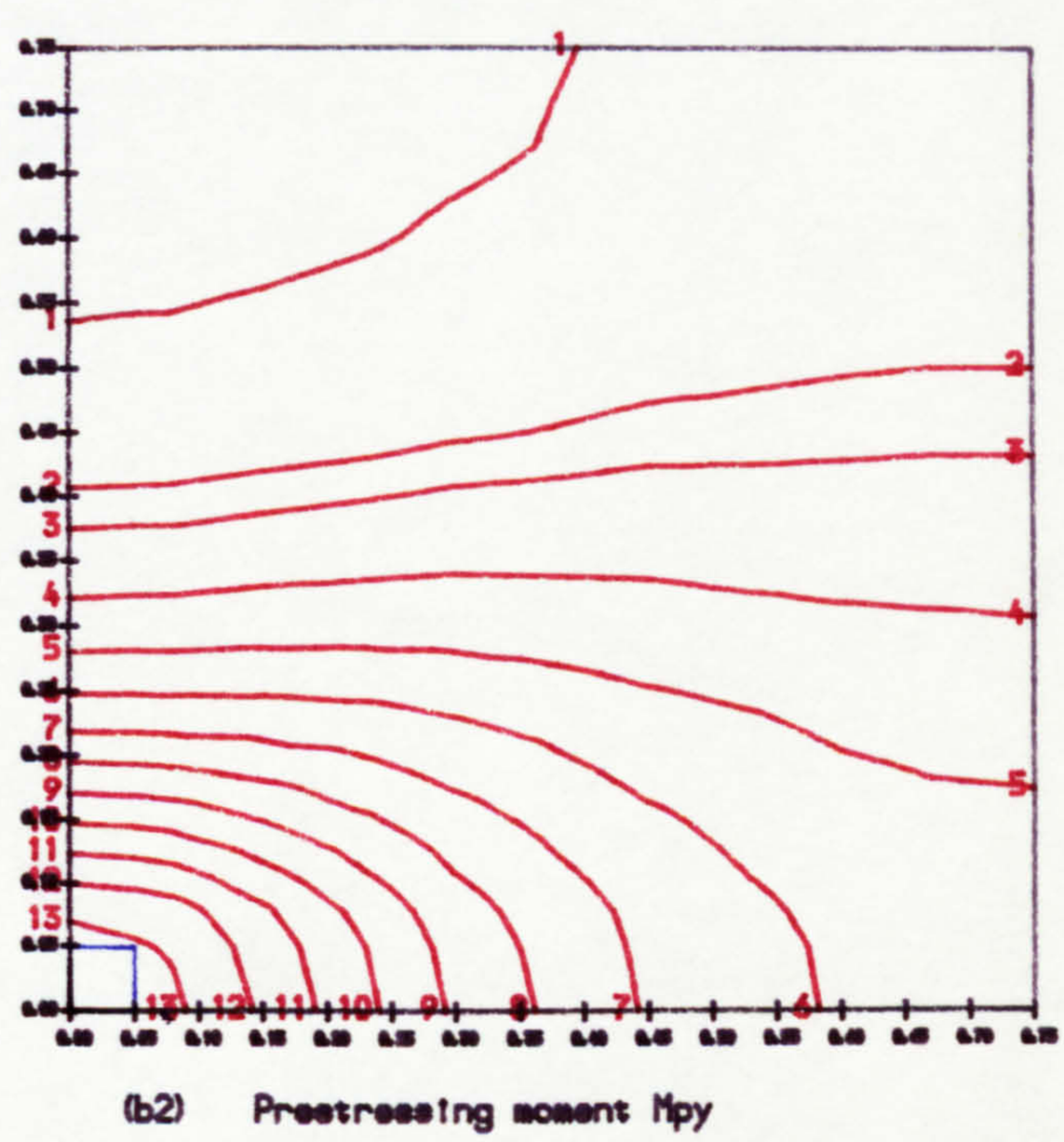

(b2) Prestressing moment Mpy

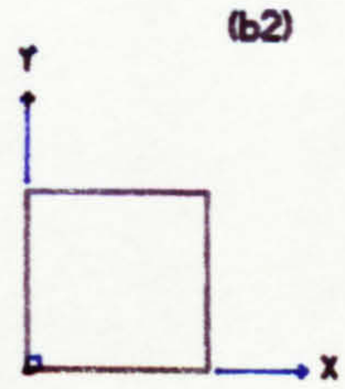

(1)	-0.60	kNm/m	(8)	0.80	kNm/m
(2)	-0.30	"	(9)	1.00	"
(3)	-0.20	"	(10)	1.20	"
(4)	0.00	"	(11)	1.40	"
(5)	0.20	"	(12)	1.60	"
(6)	0.40	"	(13)	1.80	"
(7)	0.60	"			

Fig. 6.8 Comparison of prestressing moment distribution in experimental and interior flat slab floor panel, Slab A3

Laboratory test slab

Interior flat slab floor panel

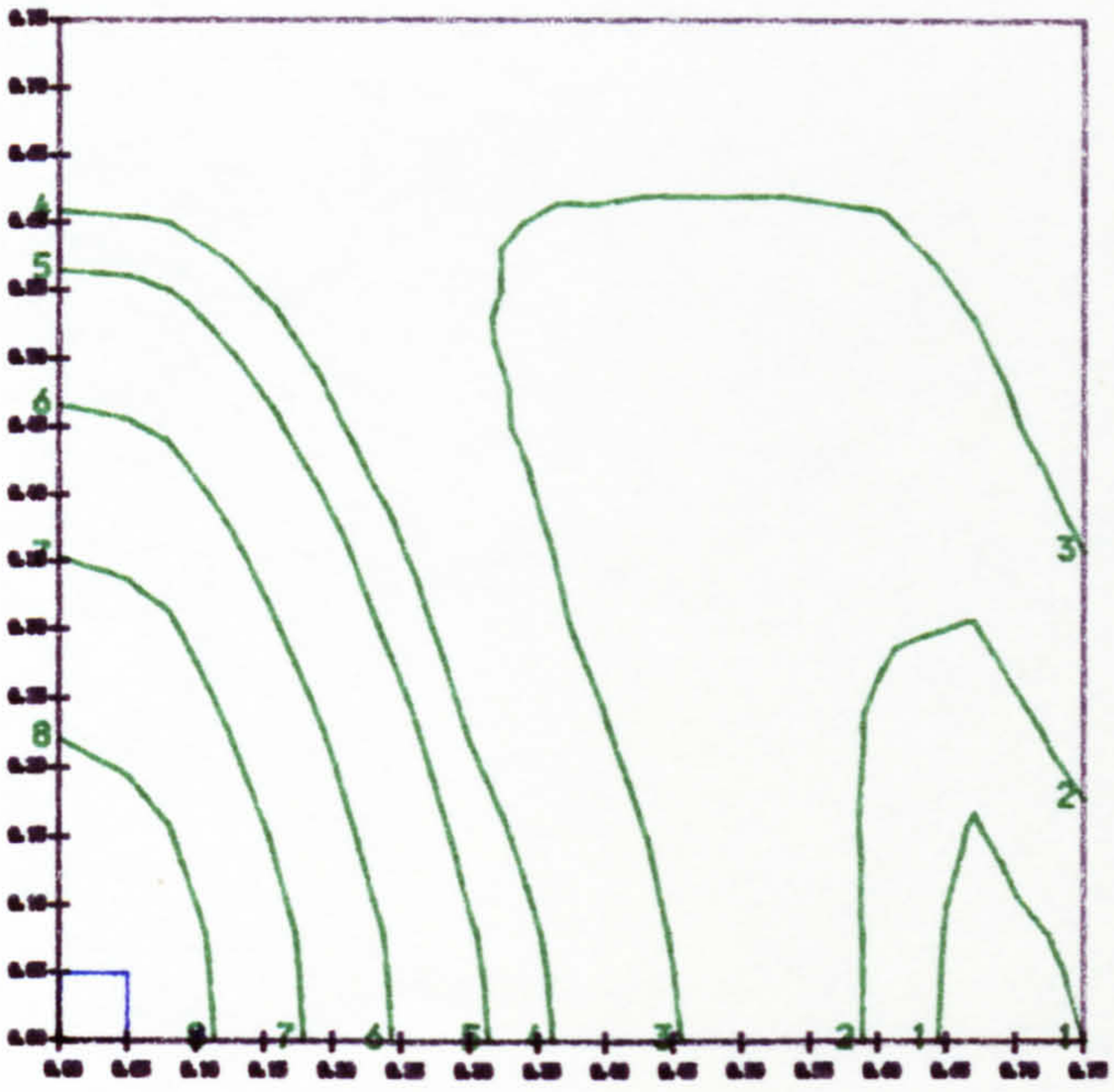

(a1) Prestressing moment Mpx

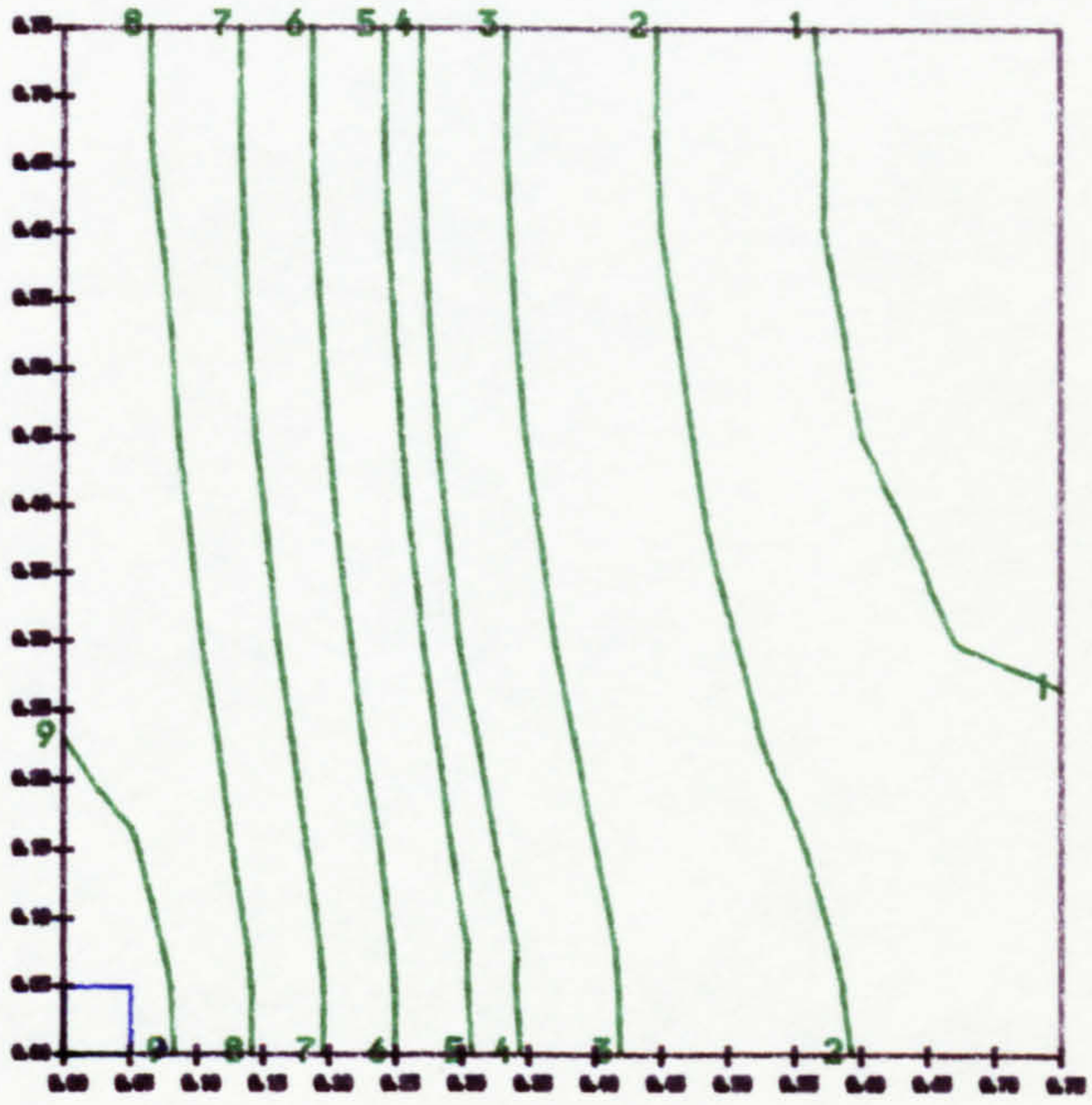

(b1) Prestressing moment Mpx

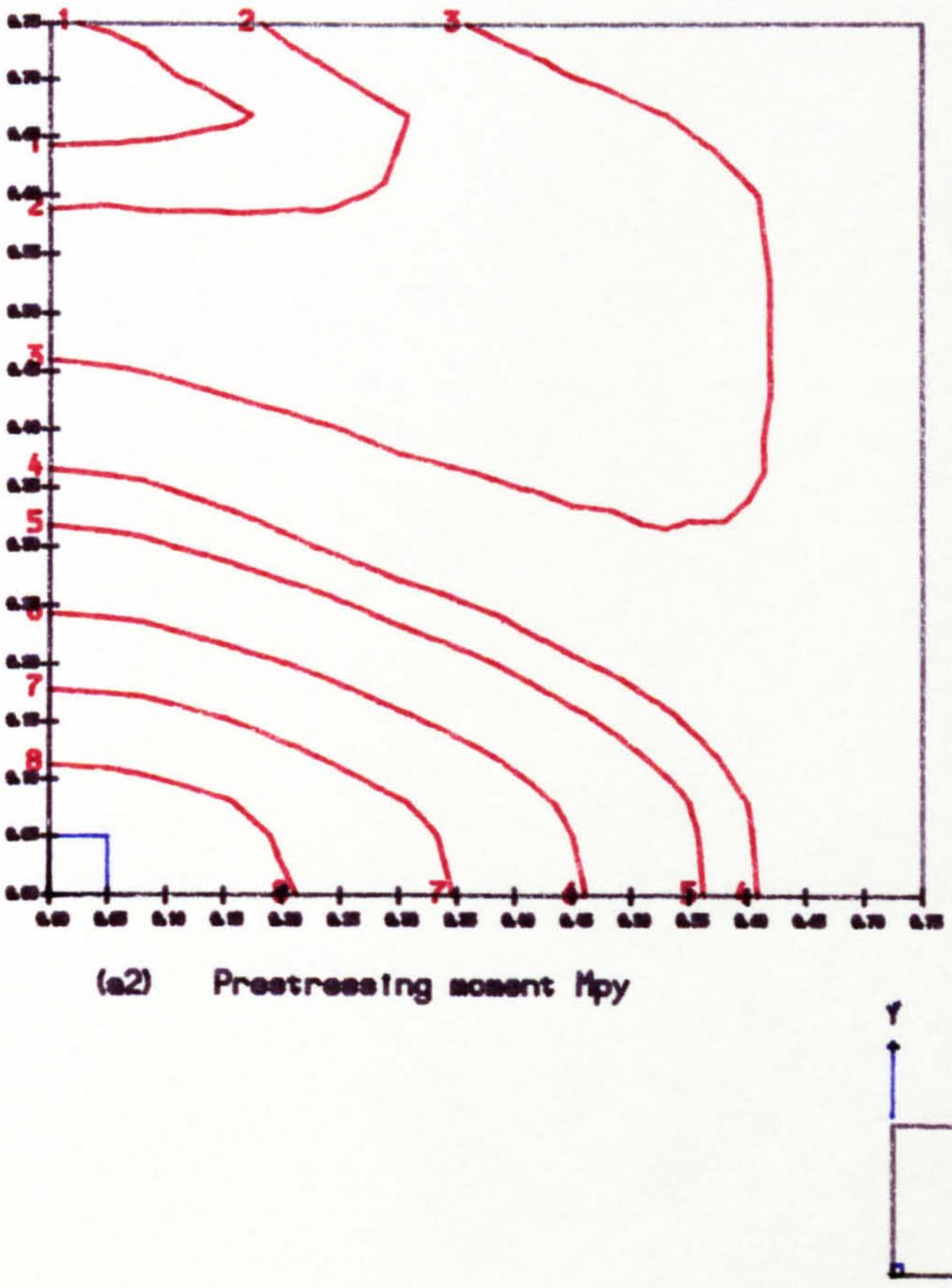

(a2) Prestressing moment Mpy

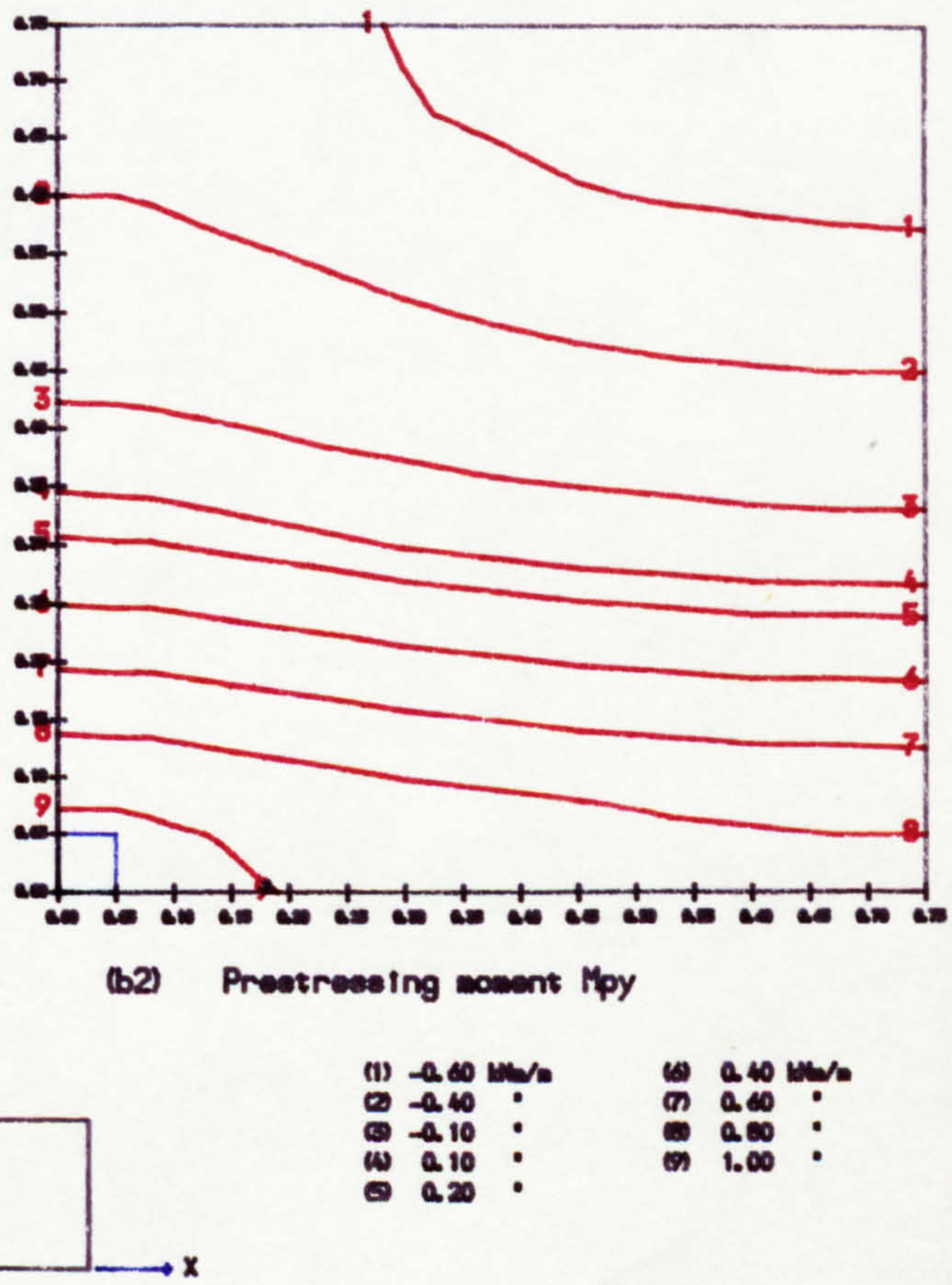

(b2) Prestressing moment Mpy

(1)	-0.60 kNm/m	(6)	0.40 kNm/m
(2)	-0.40 "	(7)	0.60 "
(3)	-0.10 "	(8)	0.80 "
(4)	0.10 "	(9)	1.00 "
(5)	0.20 "		

Fig. 6.9 Comparison of prestressing moment distribution in experimental and interior flat slab floor panel, Slab A4

Laboratory test slab

Interior flat slab floor panel

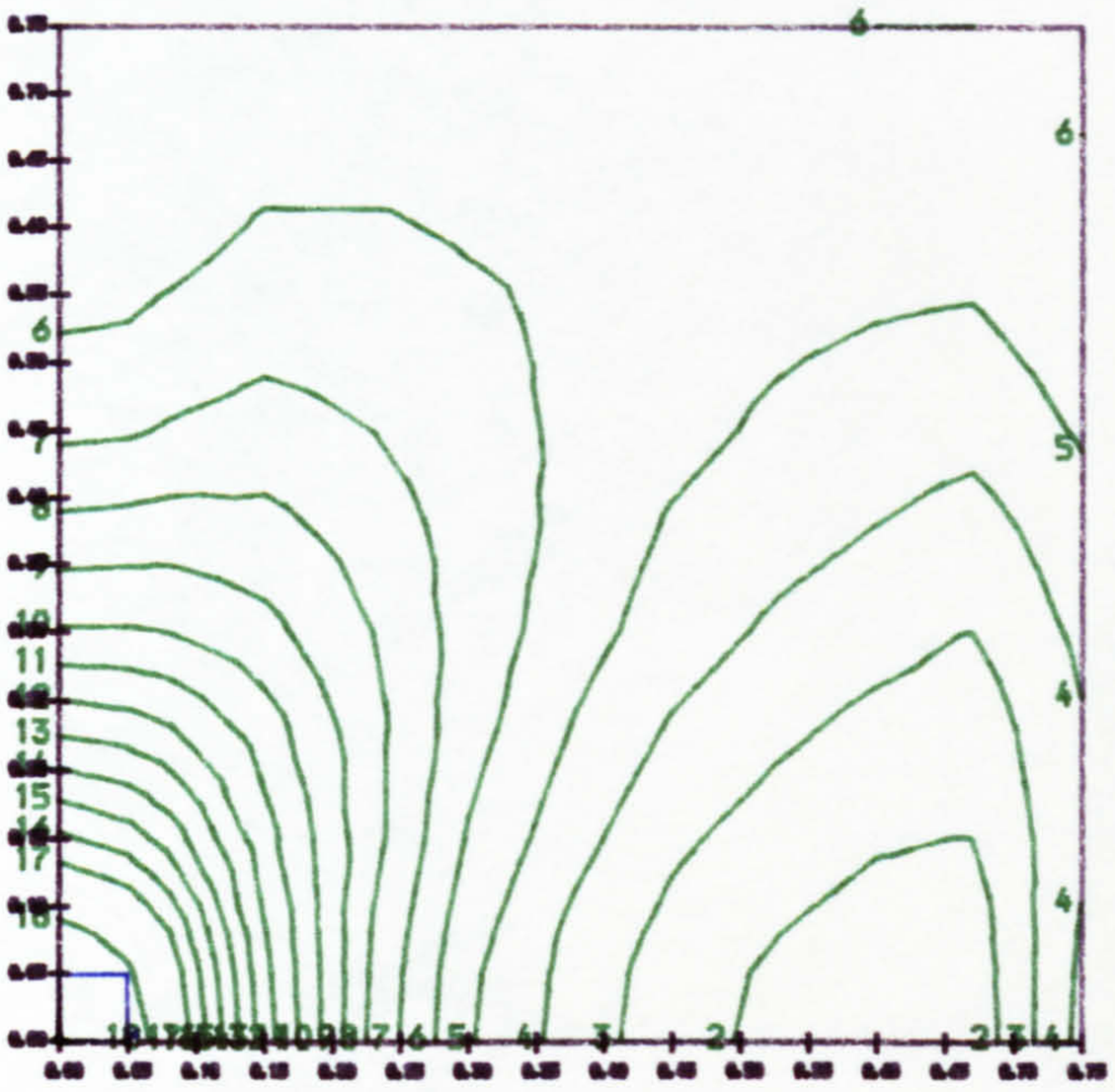

(a1) Prestressing moment Mpx

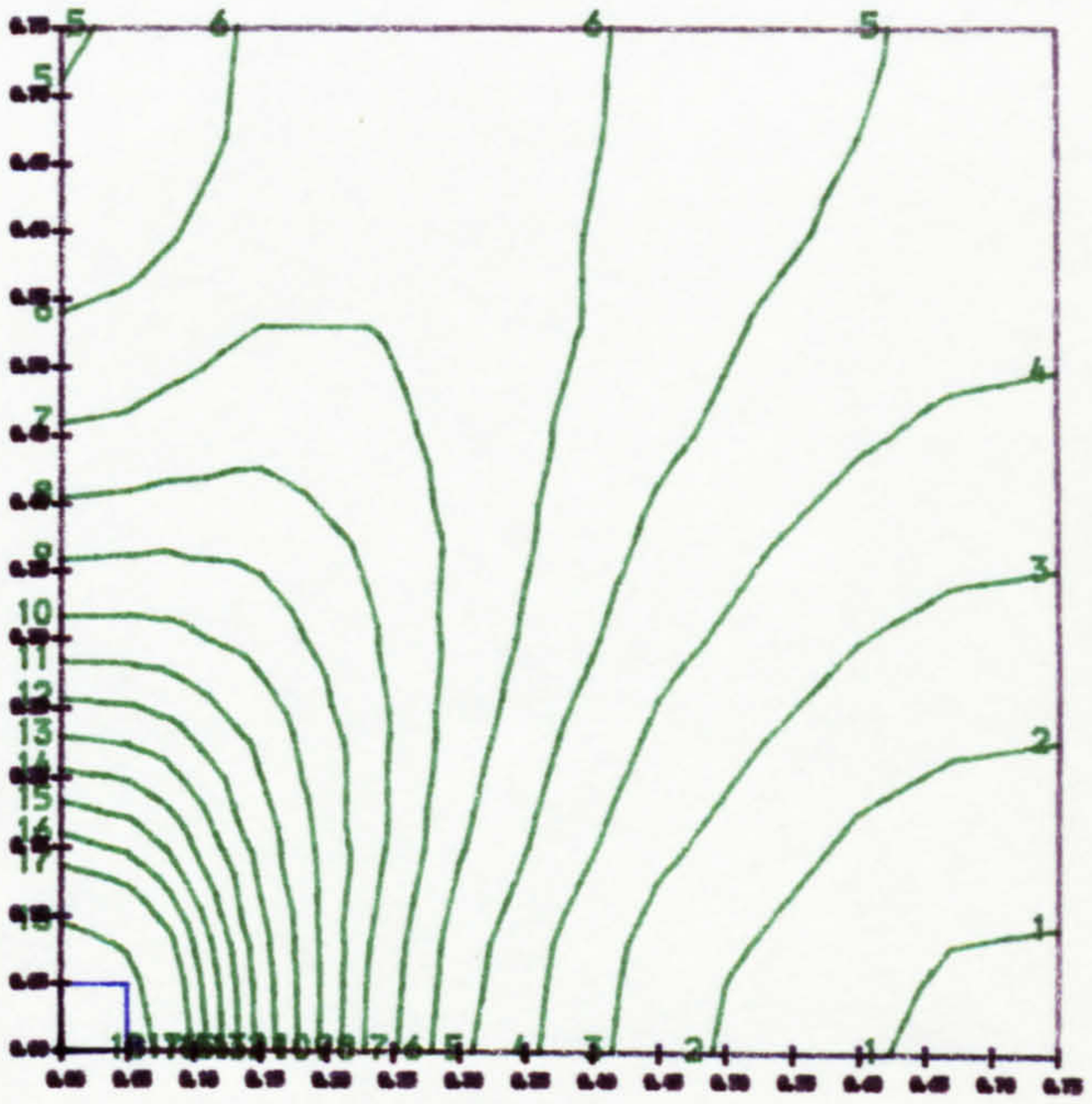

(b1) Prestressing moment Mpx

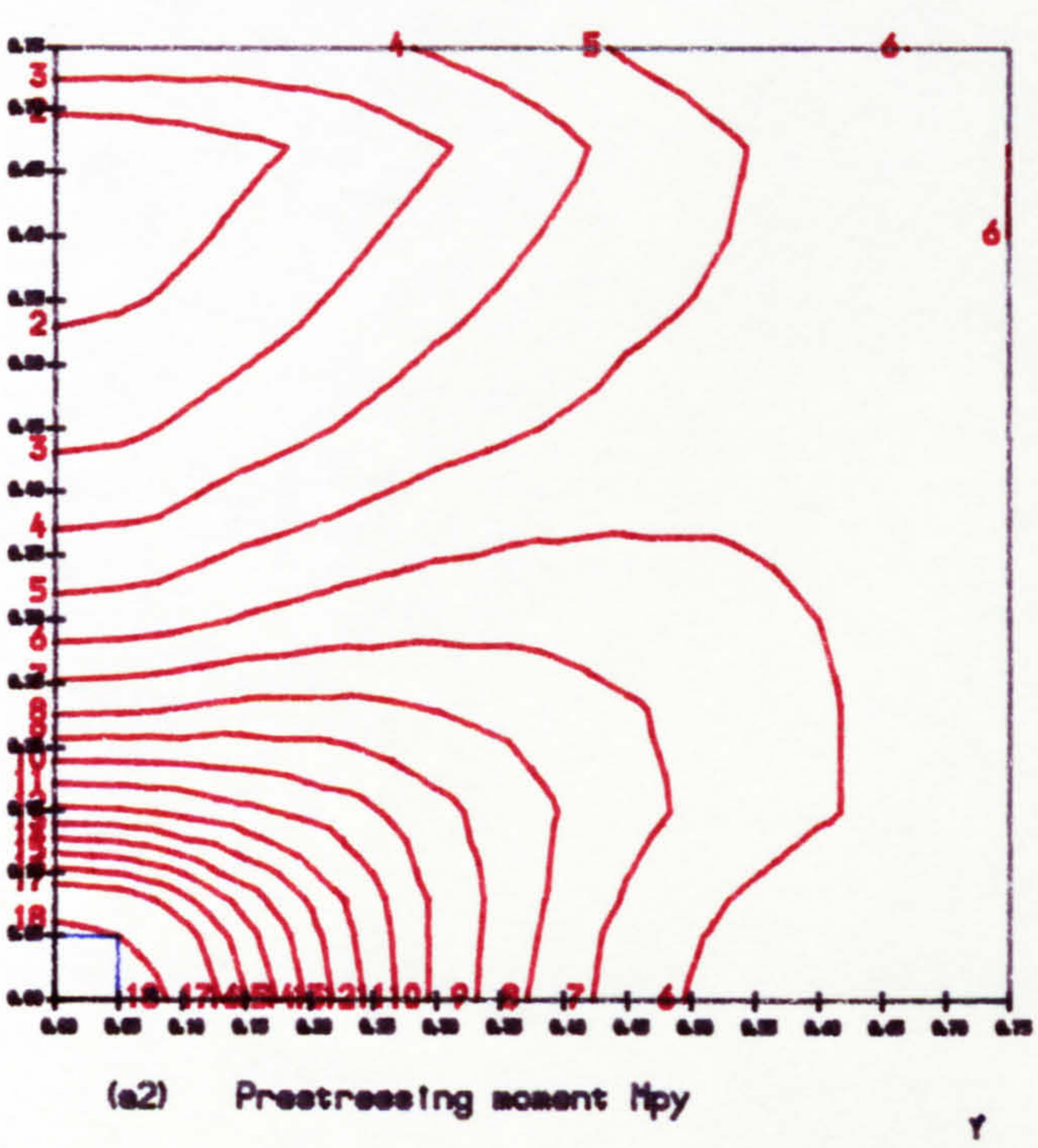

(a2) Prestressing moment Mpy

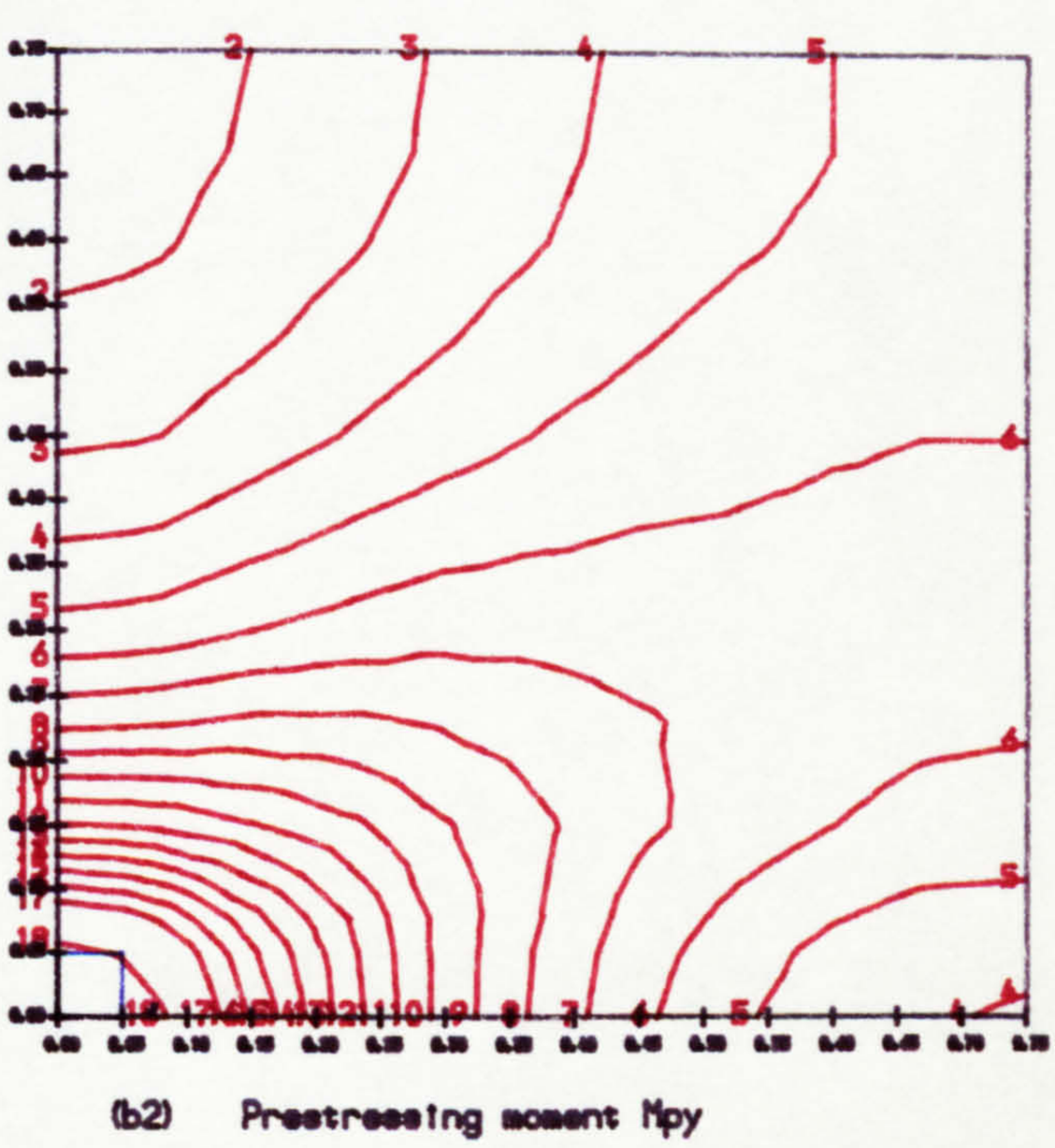

(b2) Prestressing moment Mpy

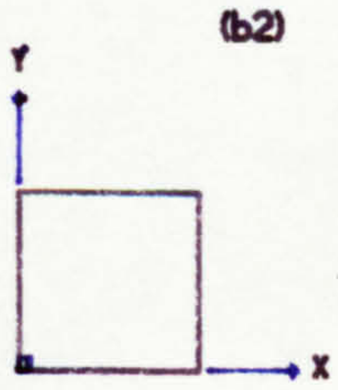

(1)	-0.50	kNm/m	(10)	0.40	kNm/m
(2)	-0.40	"	(11)	0.50	"
(3)	-0.30	"	(12)	0.60	"
(4)	-0.20	"	(13)	0.70	"
(5)	-0.10	"	(14)	0.80	"
(6)	0.00	"	(15)	0.90	"
(7)	0.10	"	(16)	1.00	"
(8)	0.20	"	(17)	1.10	"
(9)	0.30	"	(18)	1.30	"

Fig. 6.10 Comparison of prestressing moment distribution in experimental and interior flat slab floor panel, Slab C1

Laboratory test slab

Interior flat slab floor panel

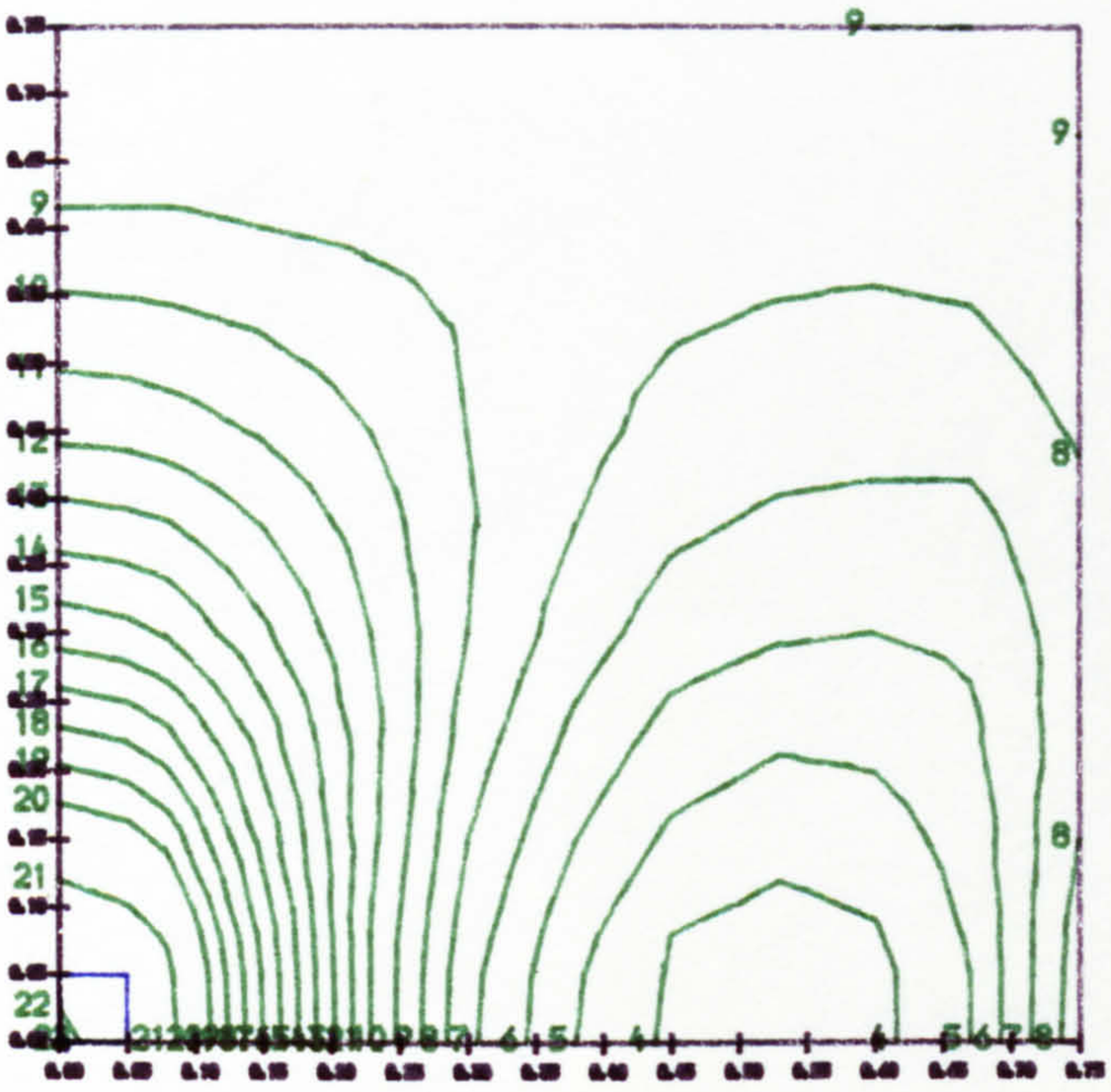

(a1) Prestressing moment Mpx

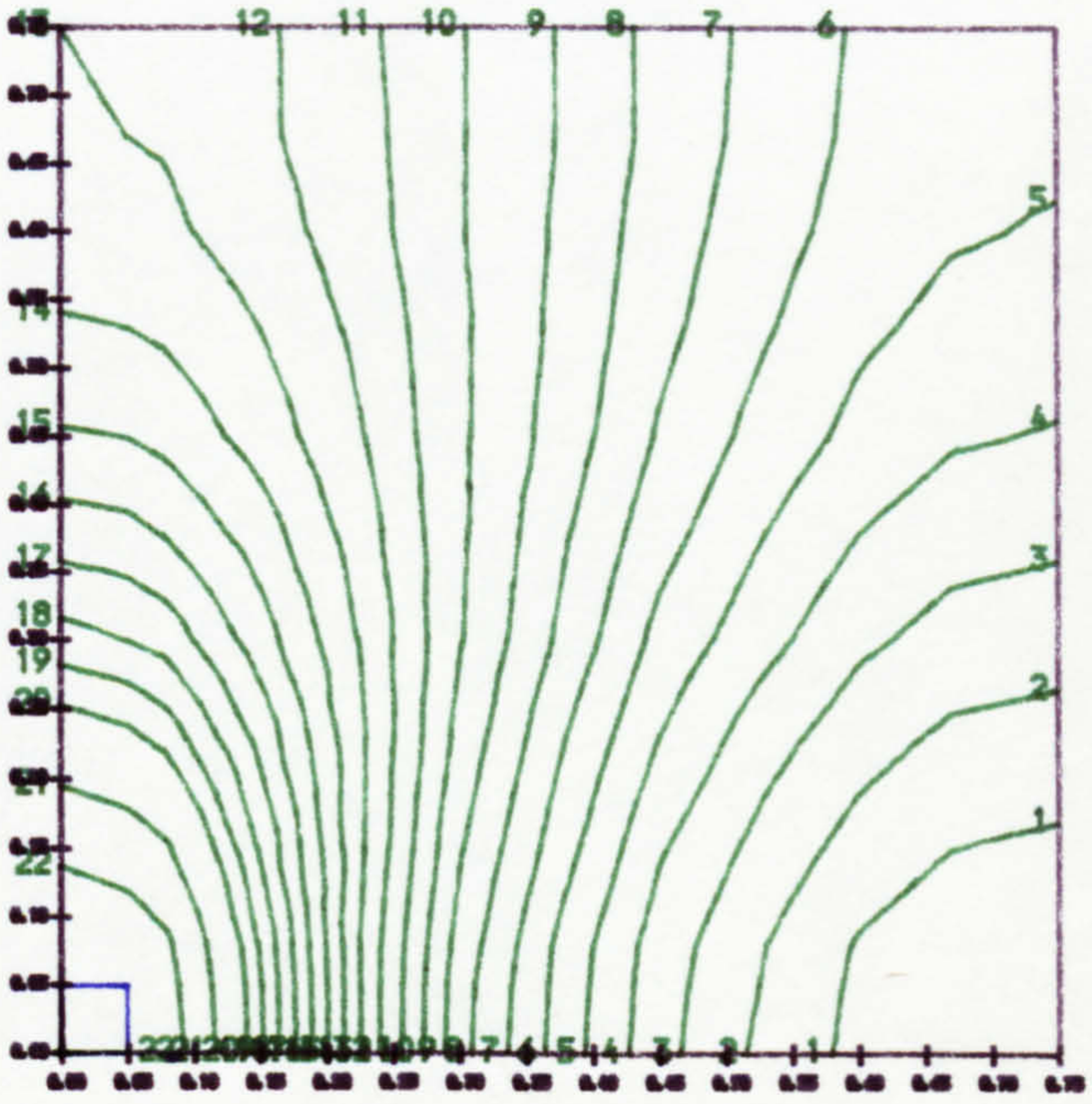

(b1) Prestressing moment Mpx

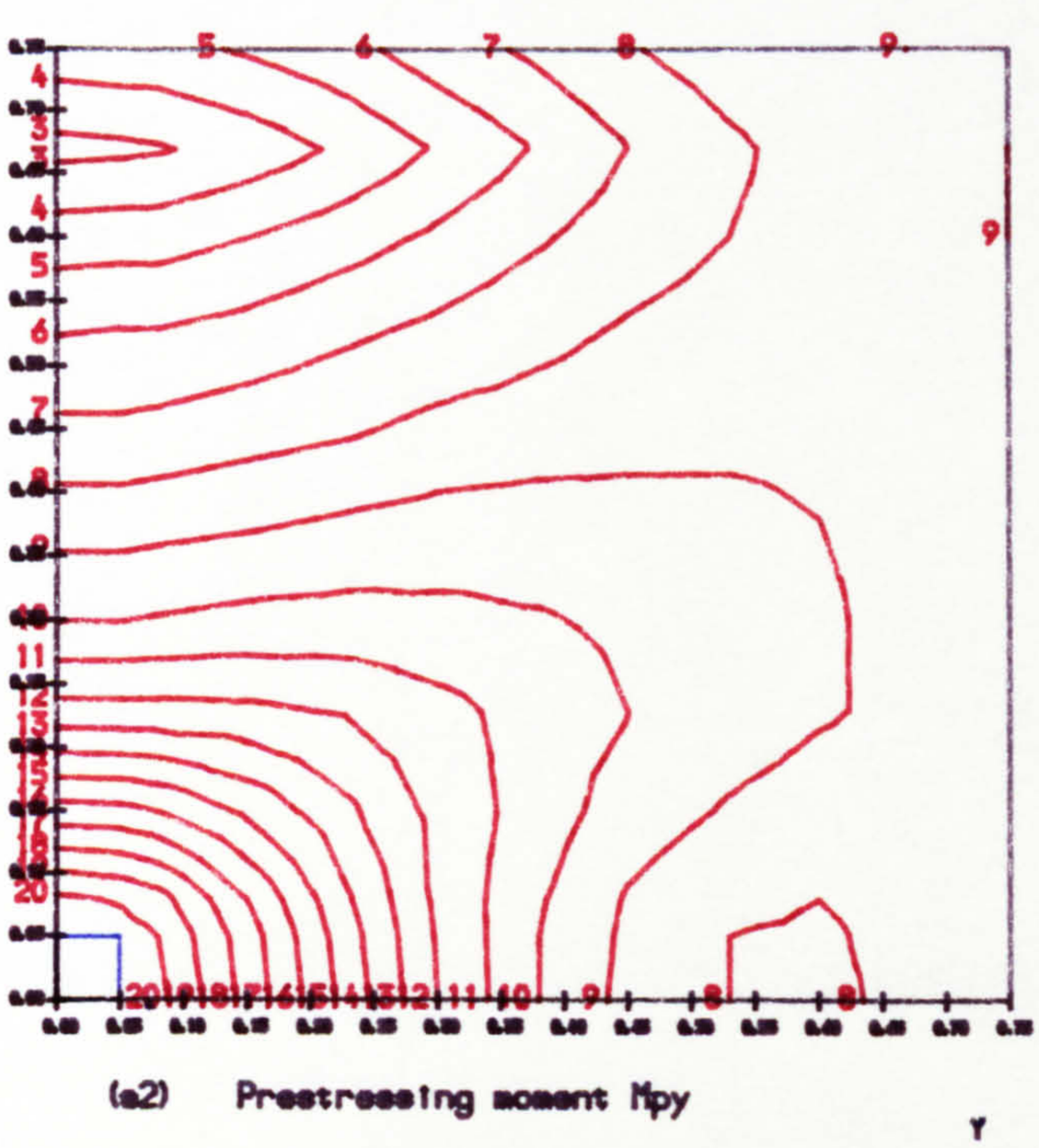

(a2) Prestressing moment Mpy

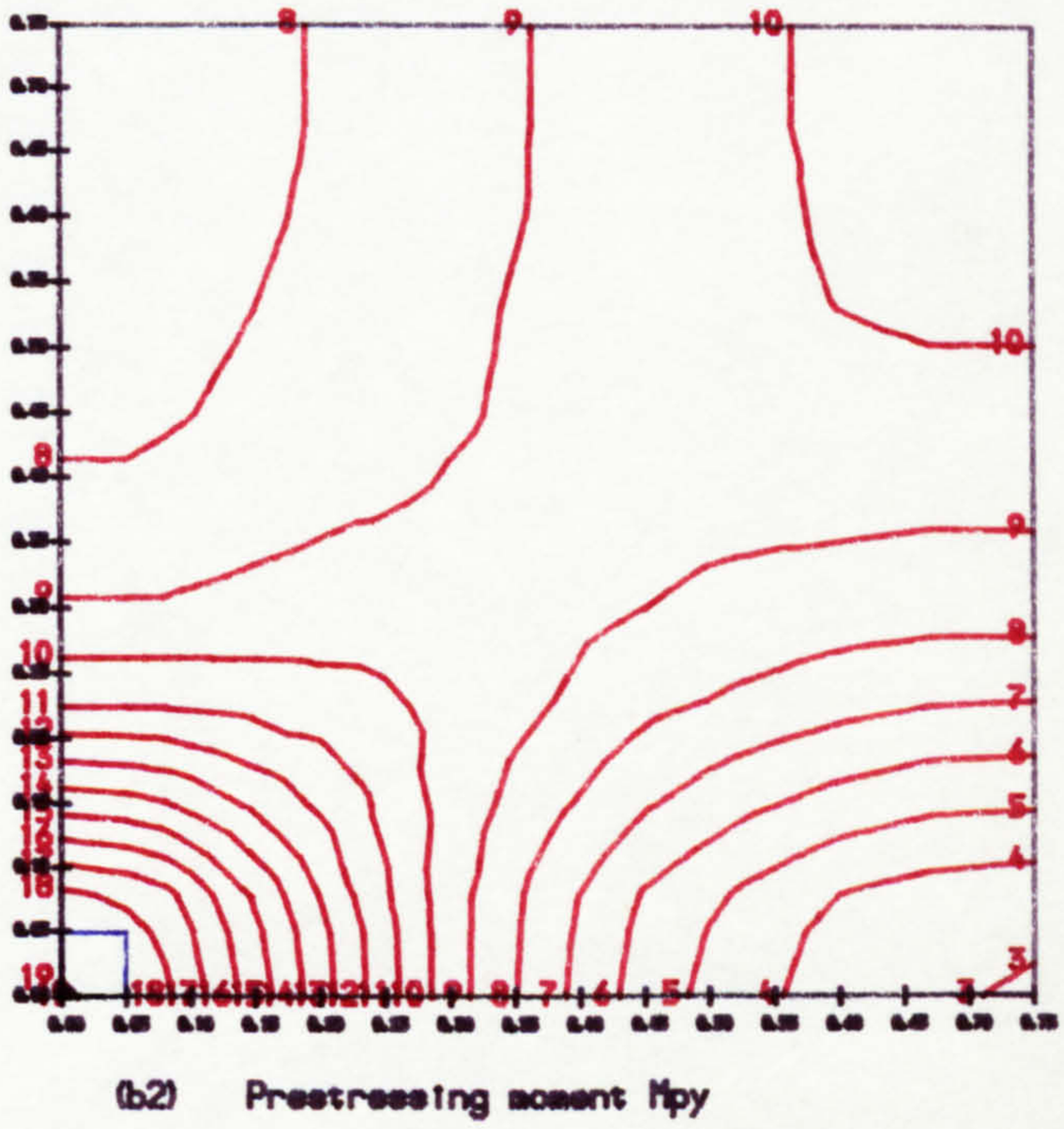

(b2) Prestressing moment Mpy

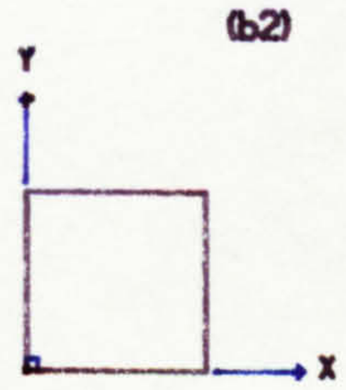

(1)	-0.80	kNm/m	(12)	0.30	kNm/m
(2)	-0.70	"	(13)	0.40	"
(3)	-0.60	"	(14)	0.50	"
(4)	-0.50	"	(15)	0.60	"
(5)	-0.40	"	(16)	0.70	"
(6)	-0.30	"	(17)	0.80	"
(7)	-0.20	"	(18)	0.90	"
(8)	-0.10	"	(19)	1.00	"
(9)	0.00	"	(20)	1.10	"
(10)	0.10	"	(21)	1.30	"
(11)	0.20	"	(22)	1.50	"

Fig. 6.11 Comparison of prestressing moment distribution in experimental and interior flat slab floor panel, Slab C2

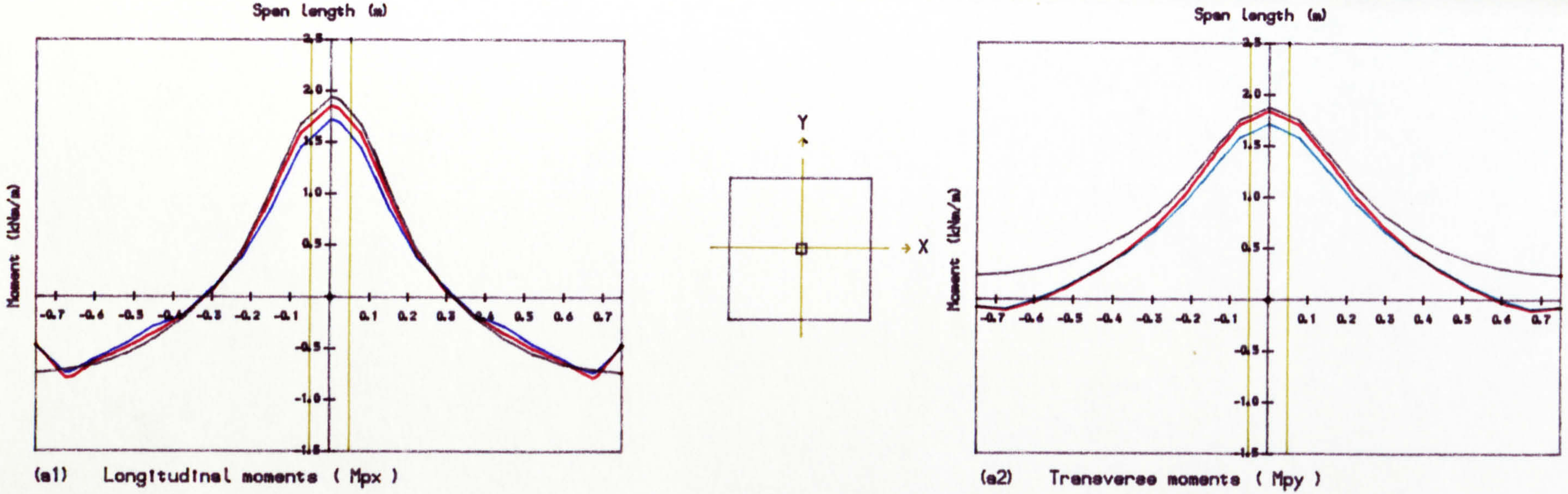

(a1) Longitudinal moments (Mpx)

(a2) Transverse moments (Mpy)

(a) Prestressing moment profile along slab centre line at Y=0.00 m

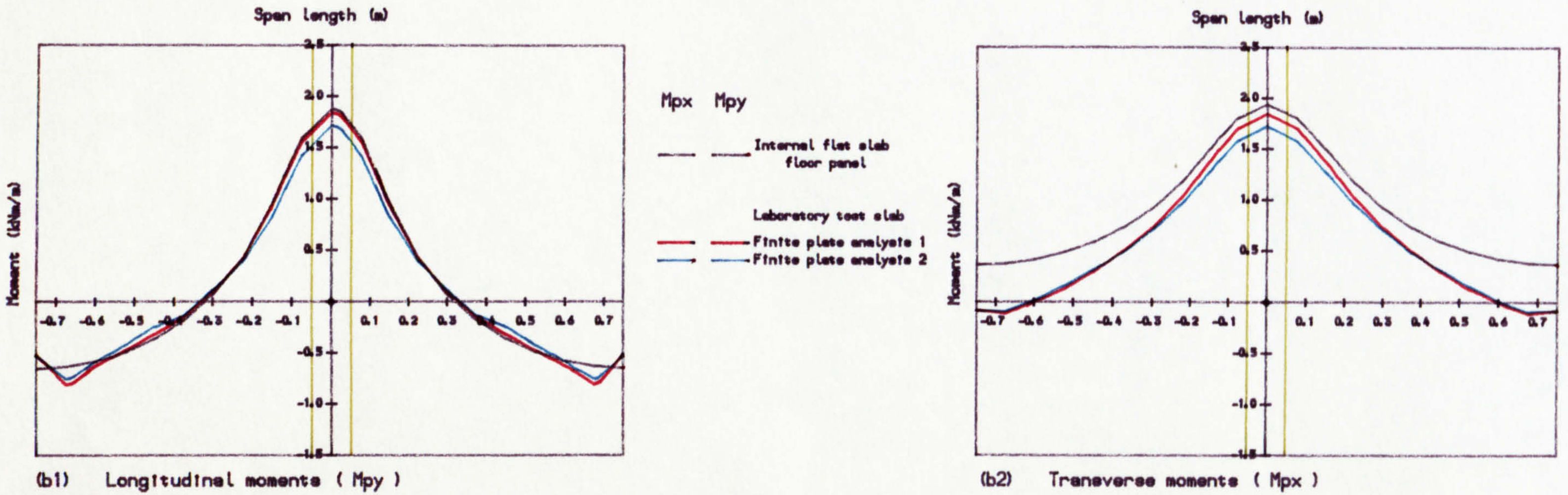

(b1) Longitudinal moments (Mpy)

(b2) Transverse moments (Mpx)

(b) Prestressing moment profile along slab centre line at X=0.00 m

Fig. 6.12 Theoretical prestressing moment profiles along slab centre lines, Slab A1

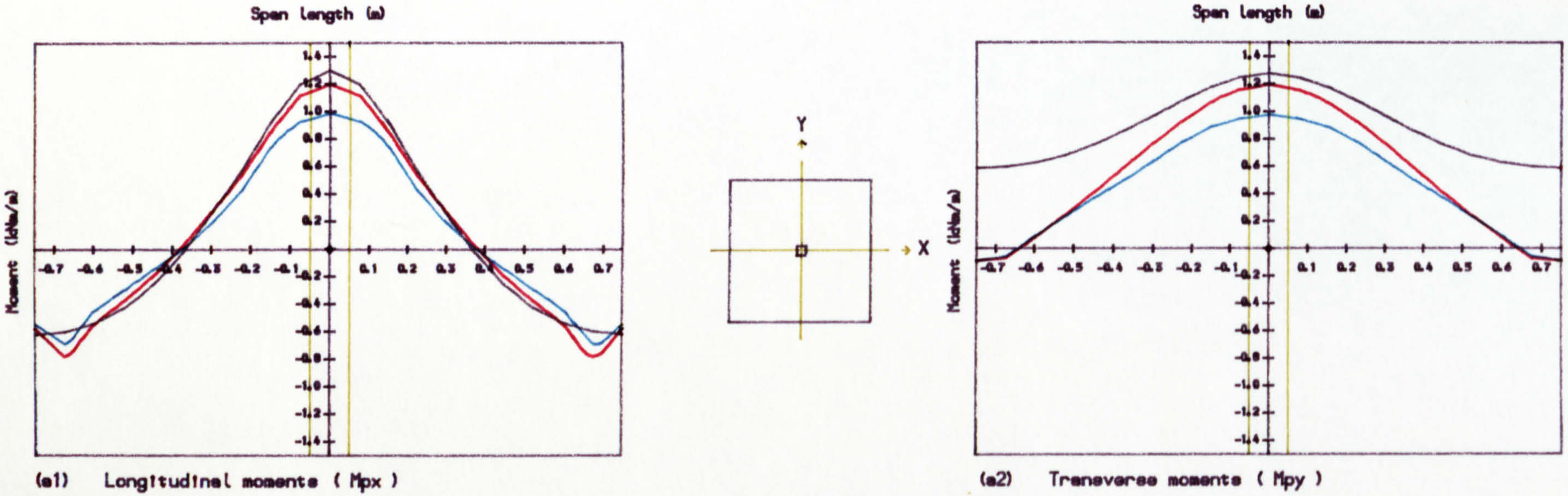

(a1) Longitudinal moments (Mpx)

(a2) Transverse moments (Mpy)

(a) Prestressing moment profile along slab centre line at Y=0.00 m

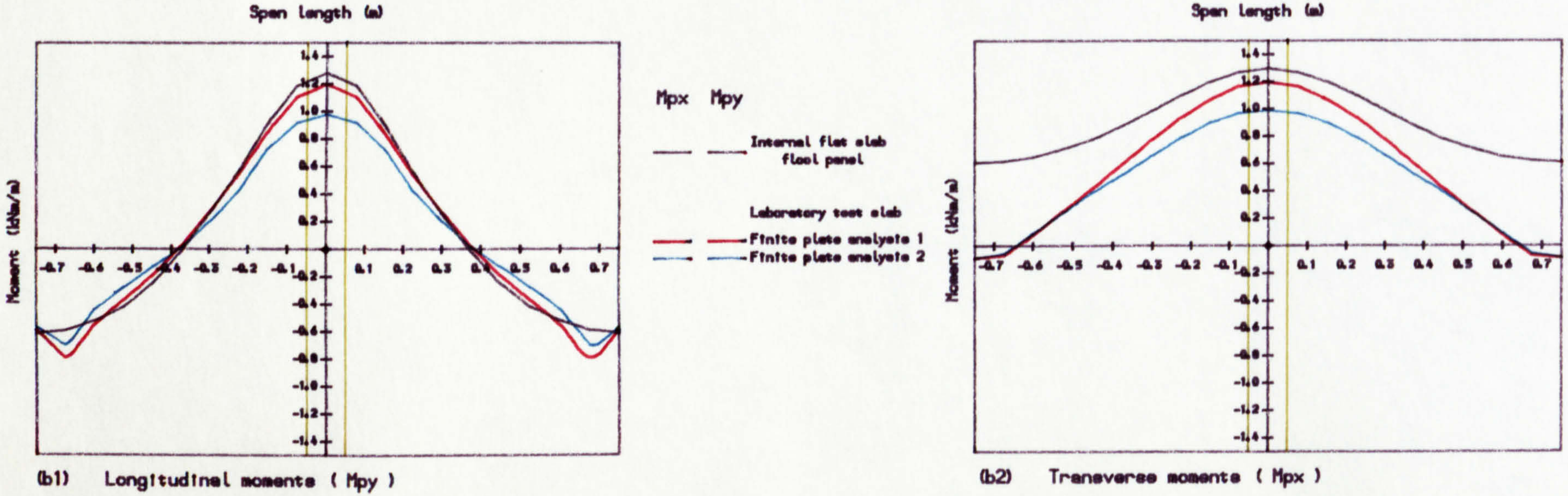

(b1) Longitudinal moments (Mpy)

(b2) Transverse moments (Mpx)

(b) Prestressing moment profile along slab centre line at X=0.00 m

Fig. 6.13 Theoretical prestressing moment profiles along slab centre lines, Slab A2

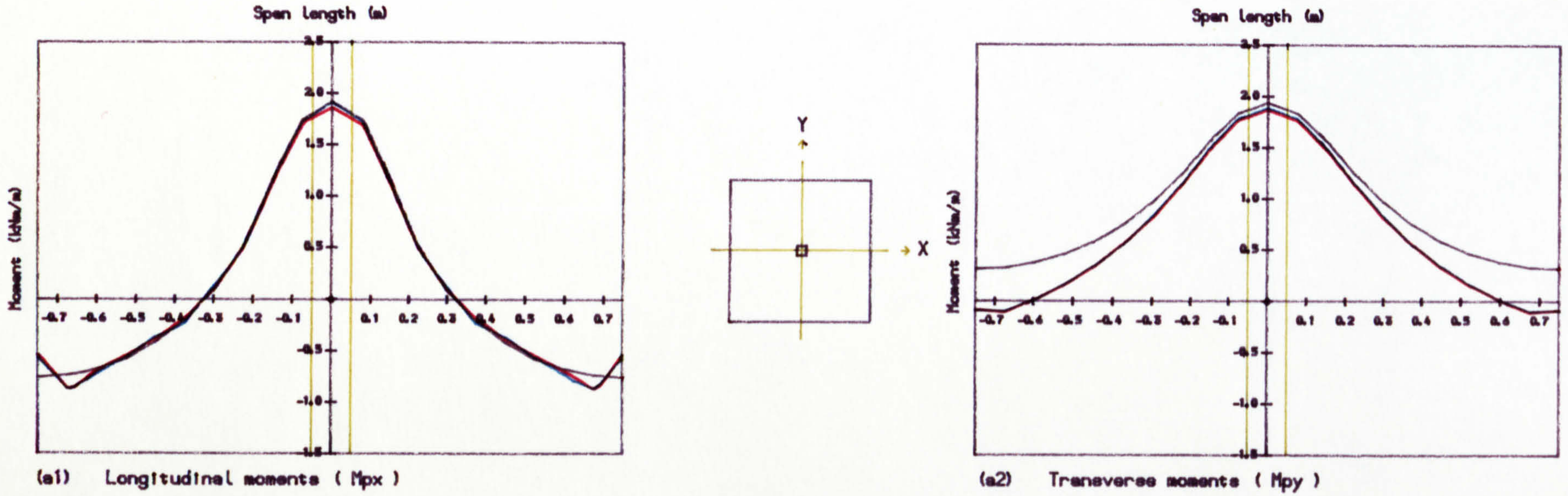

Fig. 6.14 Theoretical prestressing moment profile along slab centre lines, Slab A3

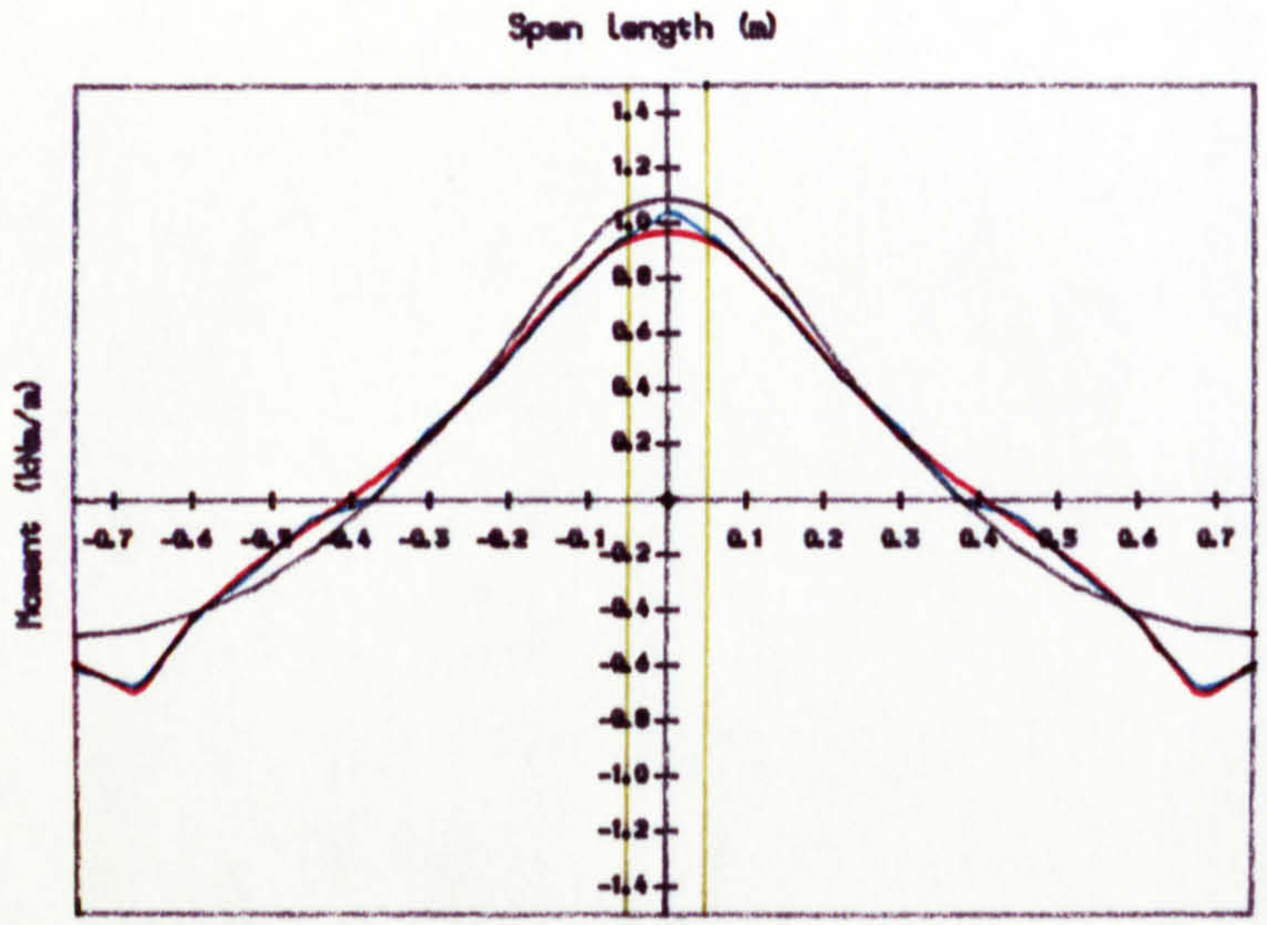

(a1) Longitudinal moments (Mpx)

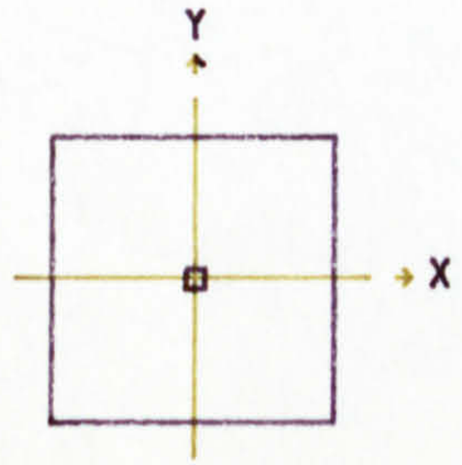

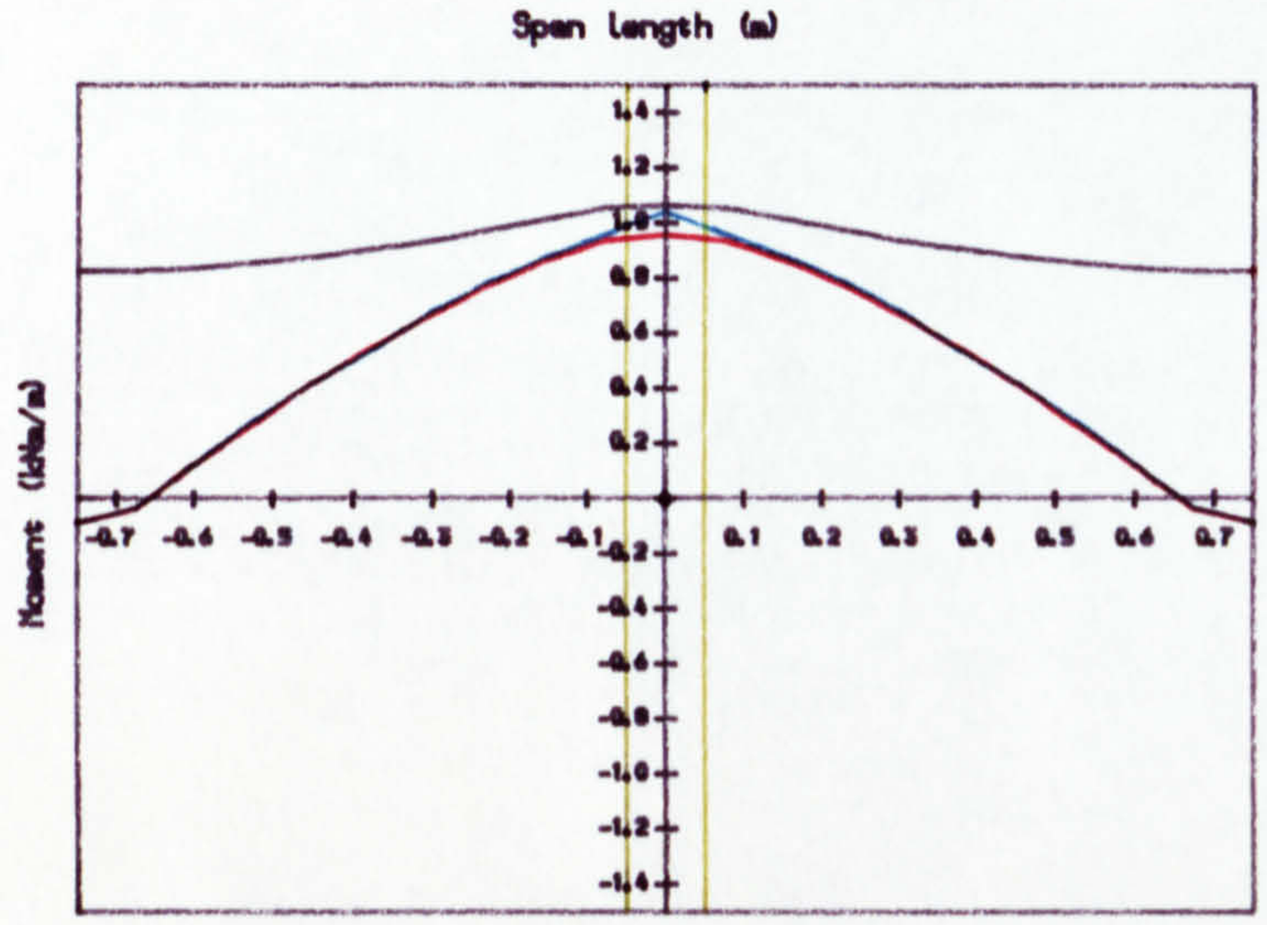

(a2) Transverse moments (Mpy)

(a) Prestressing moment profile along slab centre line at Y=0.00 m

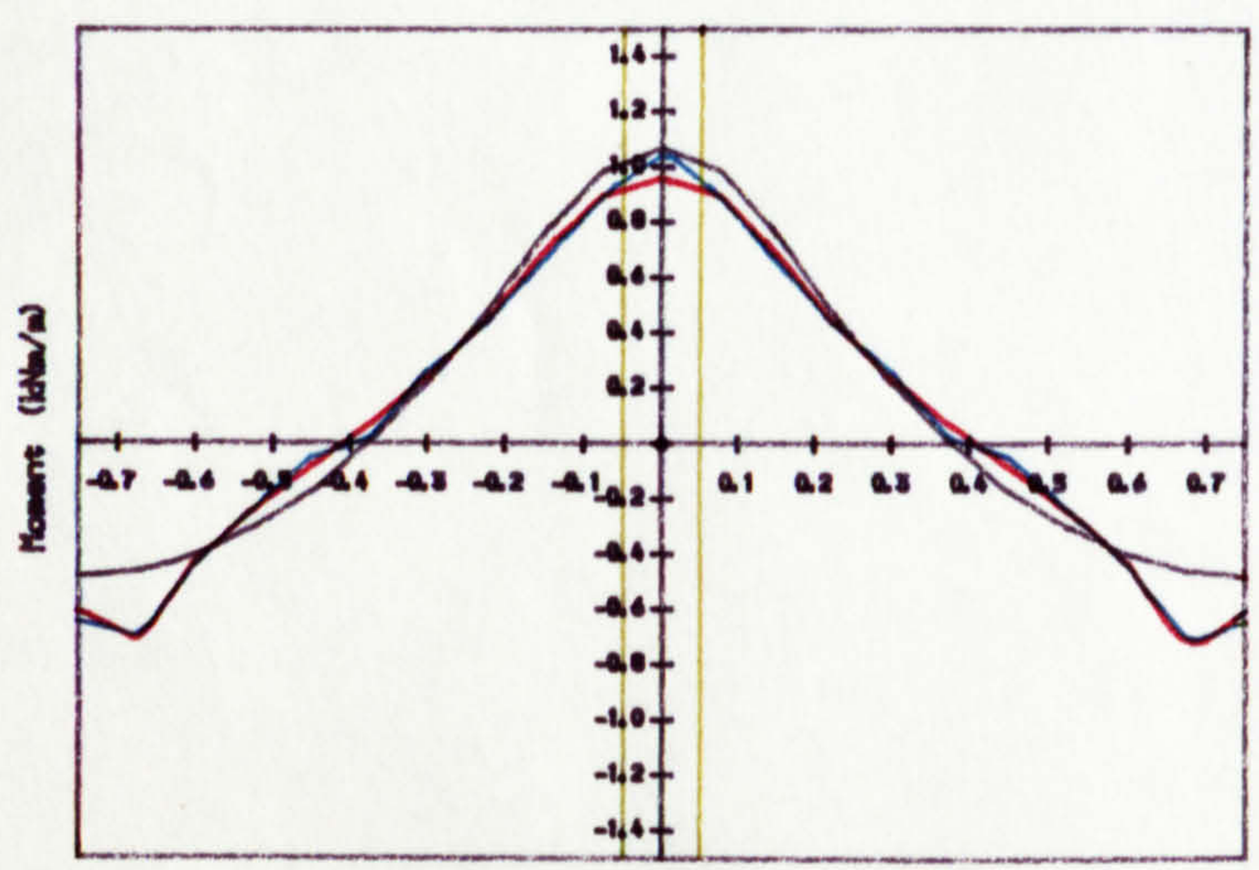

(b1) Longitudinal moments (Mpy)

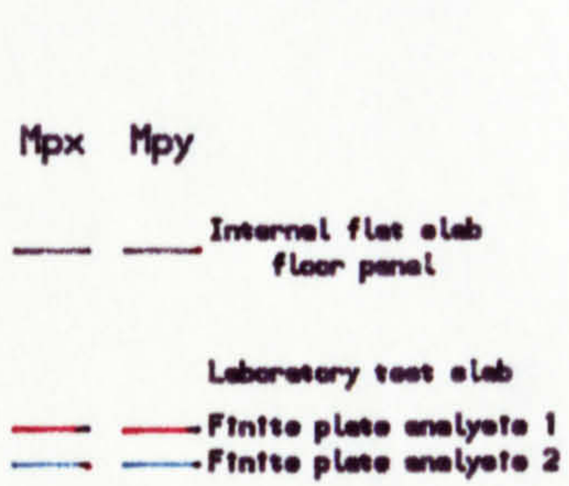

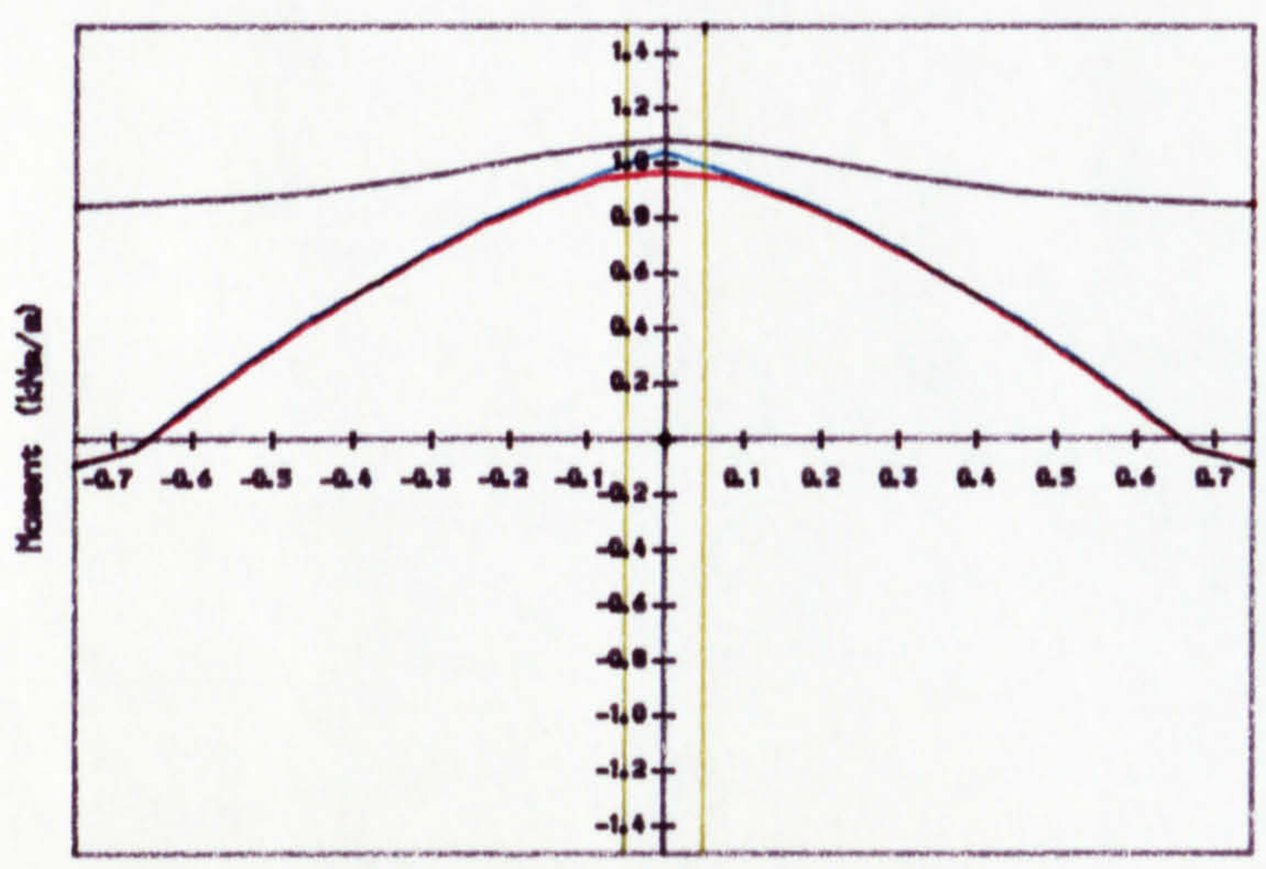

(b2) Transverse moments (Mpx)

(b) Prestressing moment profile along slab centre line at X=0.00 m

Fig. 6.15 Theoretical prestressing moment profiles along slab centre lines, Slab A4

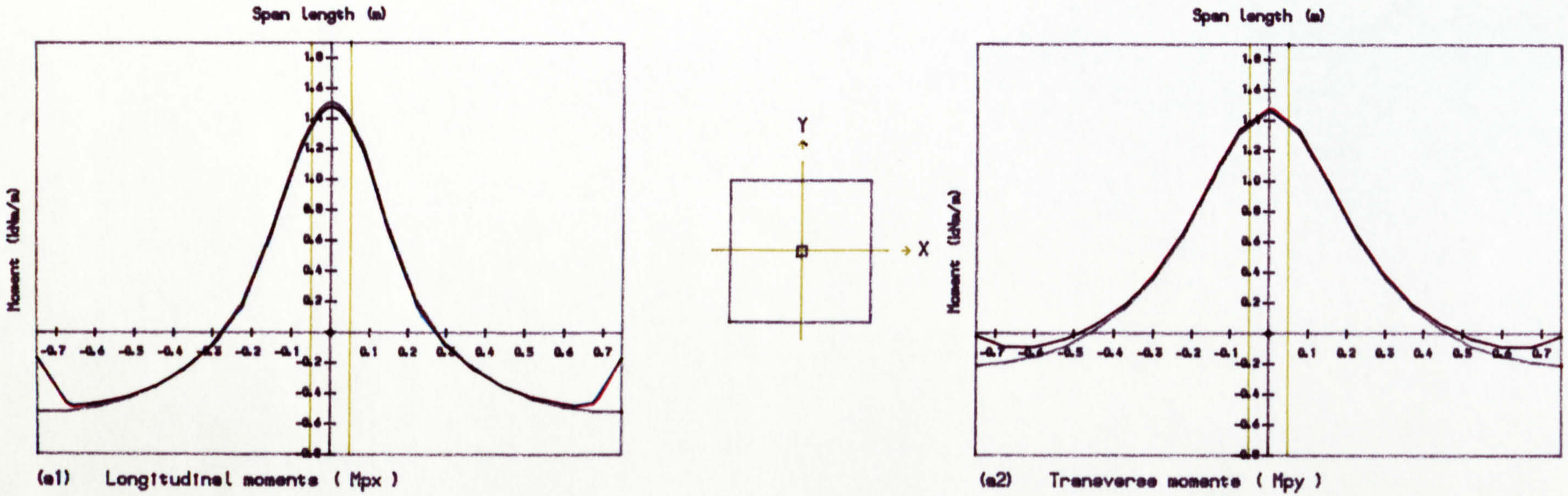

(a) Prestressing moment profile along slab centre line at Y=0.00 m

(b) Prestressing moment profile along slab centre line at X=0.00 m

Fig. 6.16 Theoretical prestressing moment profiles along slab centre lines, Slab C1

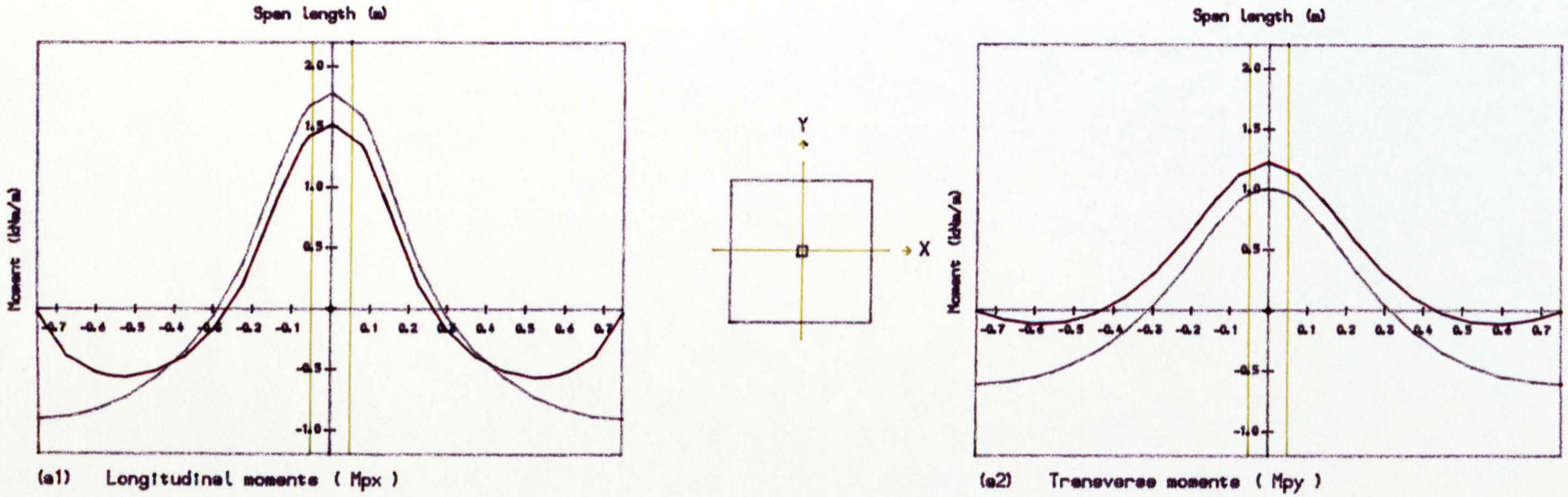

(a) Prestressing moment profile along slab centre line at Y=0.00 m

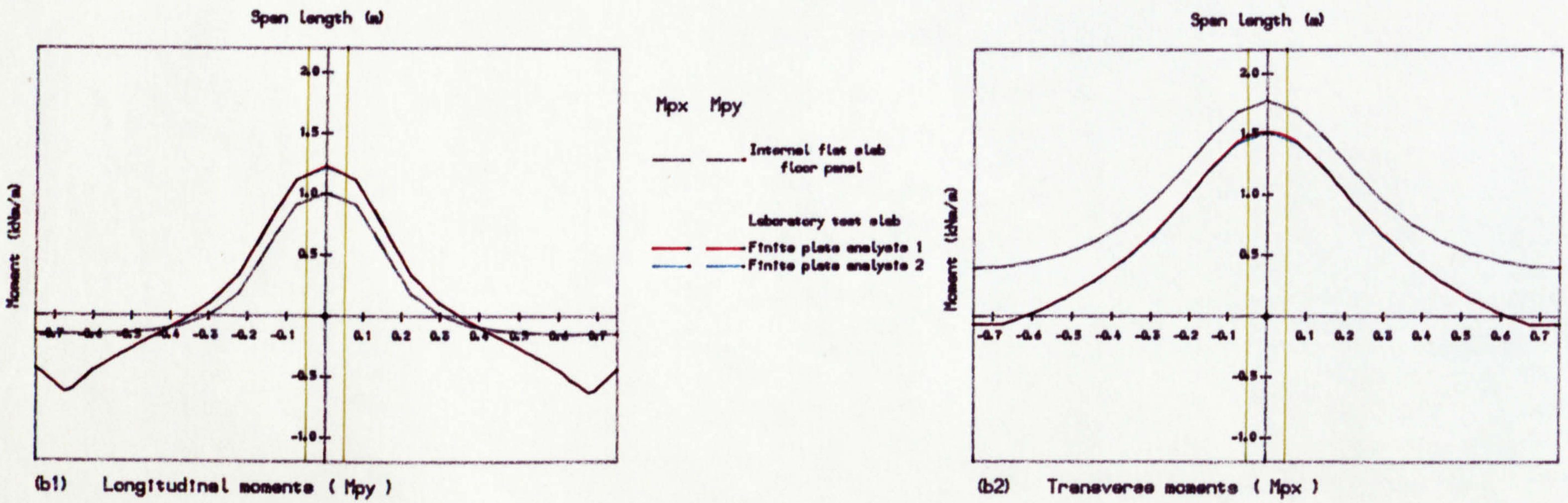

(b) Prestressing moment profile along slab centre line at X=0.00 m

Fig. 6.17 Theoretical prestressing moment profiles along slab centre lines, Slab C2

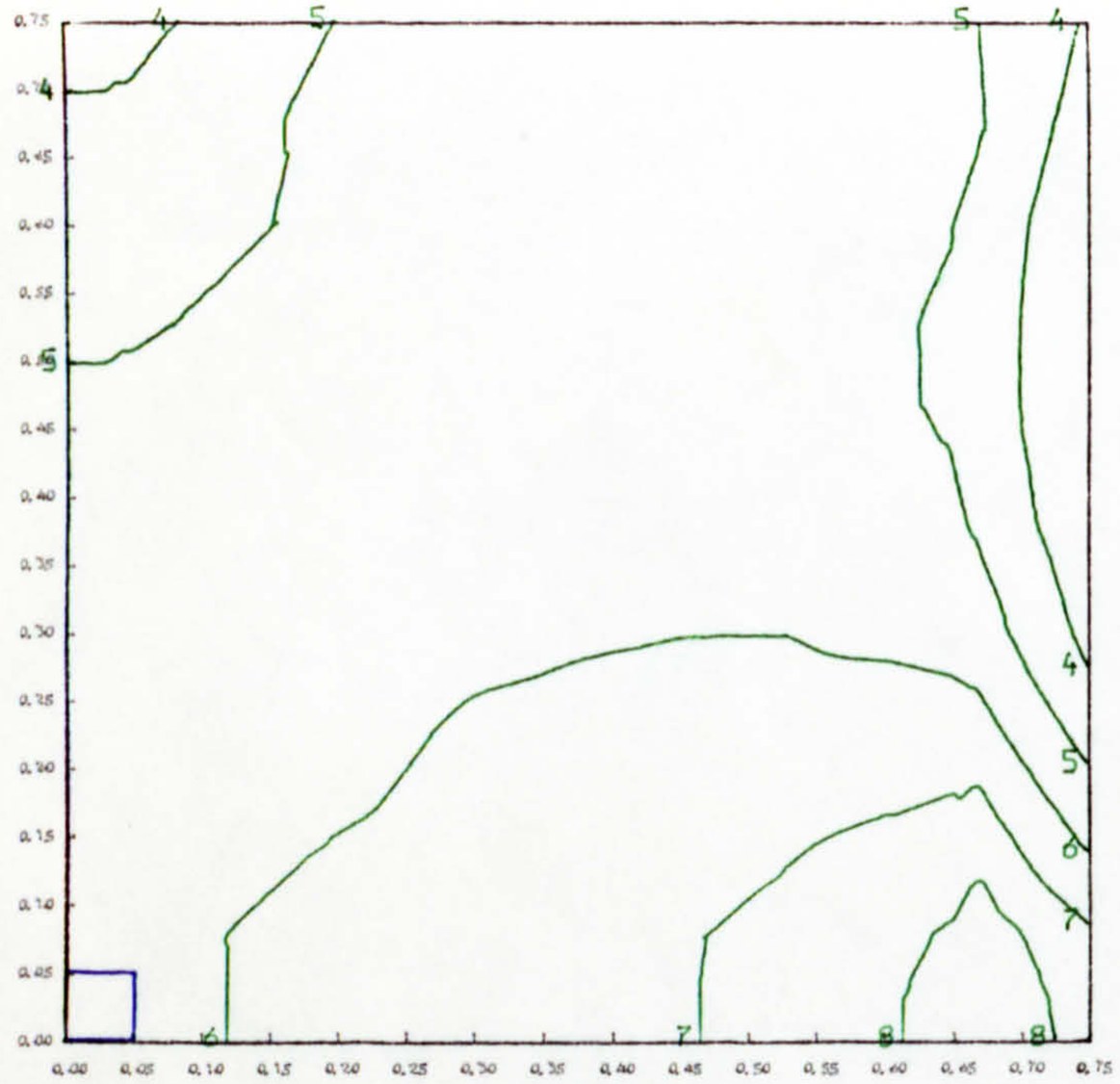

(a) Axial prestress normal to x-axis

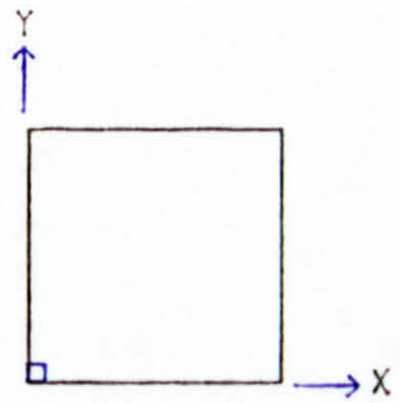

(1) -0.60 N/mm2
(2) -0.80 "
(3) -1.00 "
(4) -1.20 "
(5) -1.40 "
(6) -1.60 "
(7) -1.80 "
(8) -2.00 "

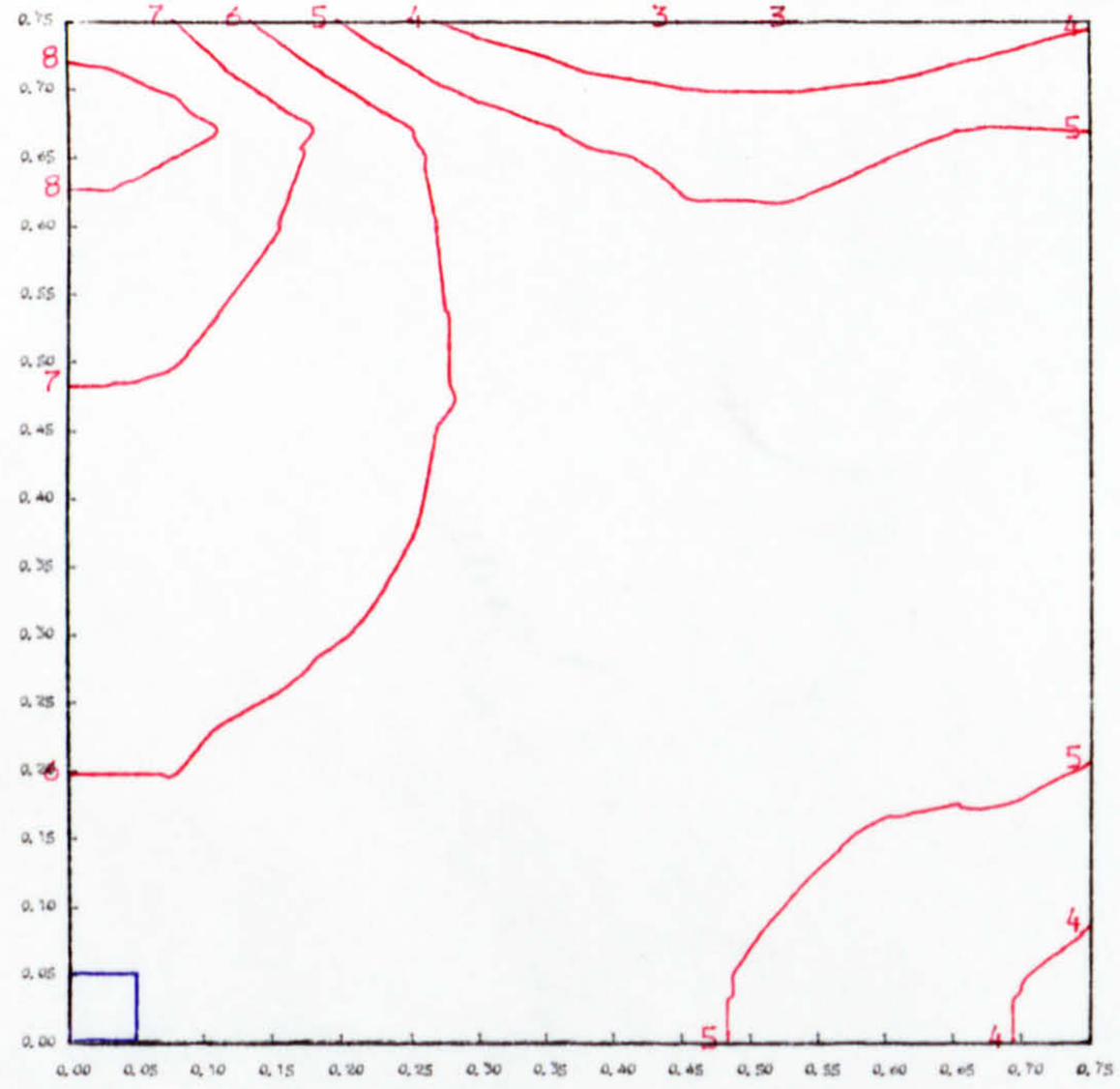

(b) Axial prestress normal to y-axis

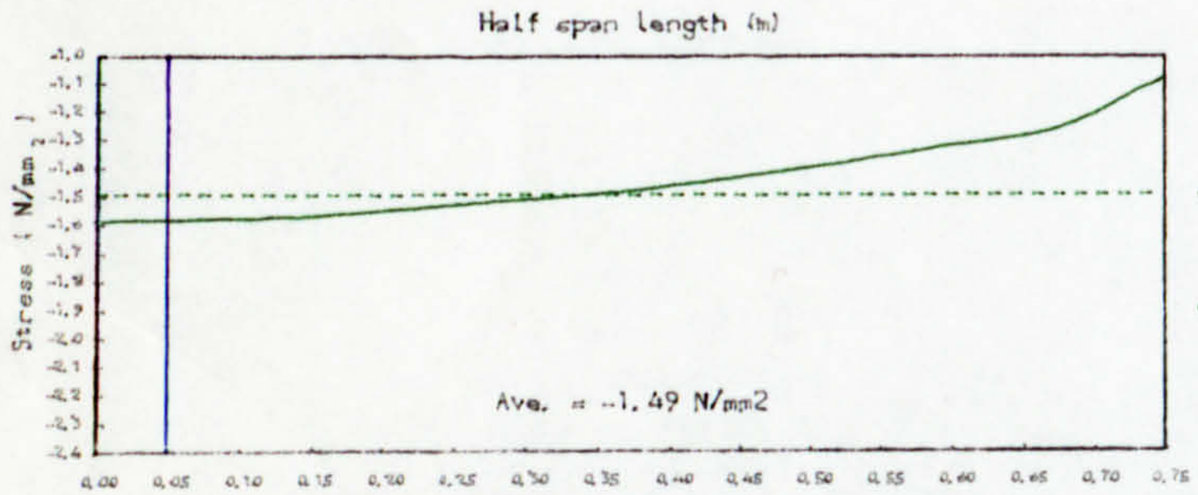

(a1) Axial prestress profile along X=0.00 m

Finite plate analysis

Assumed uniform prestress

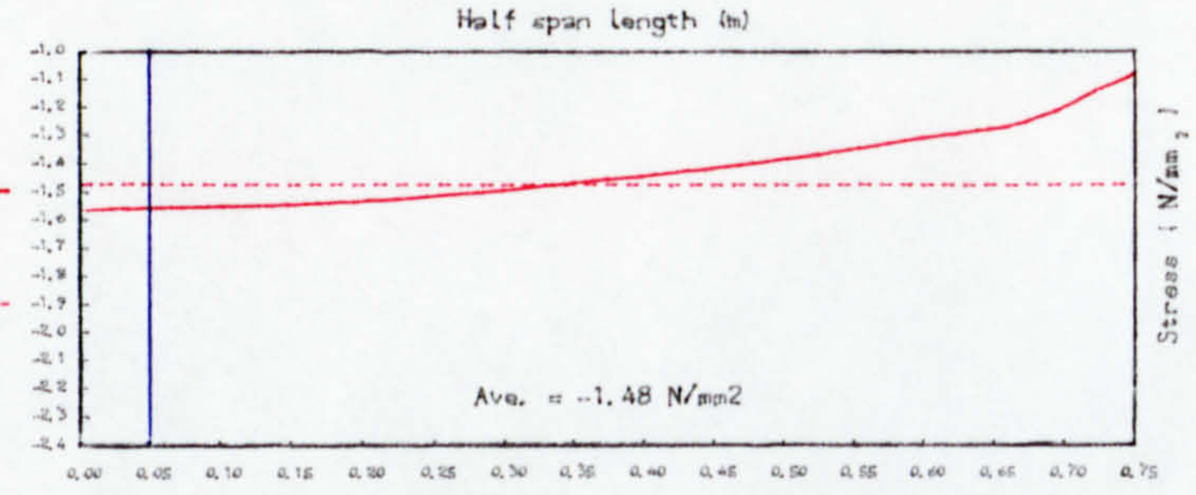

(b1) Axial prestress profile along Y=0.00 m

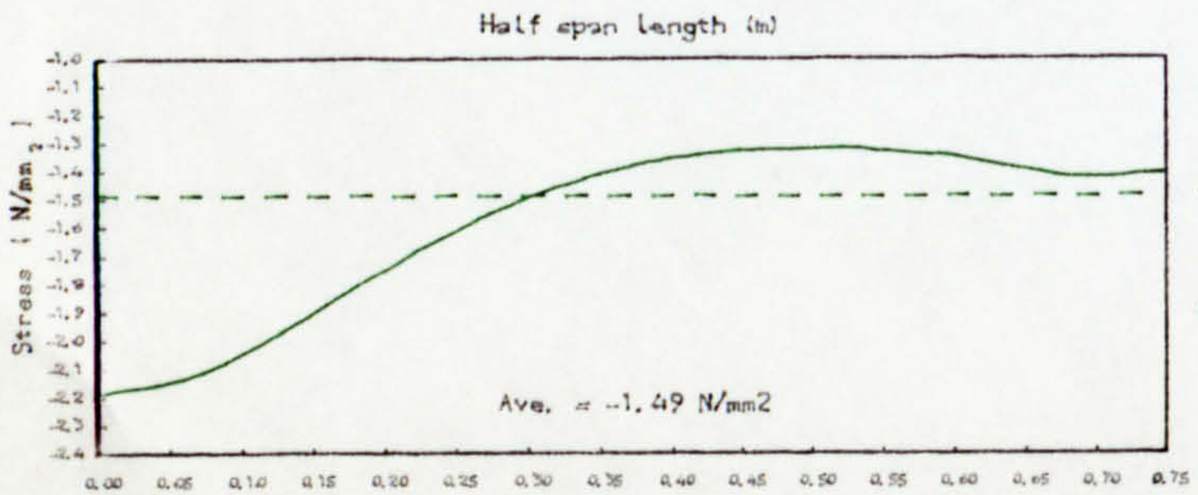

(a2) Axial prestress profile along X=0.675m

Finite plate analysis 2

Assumed uniform prestress

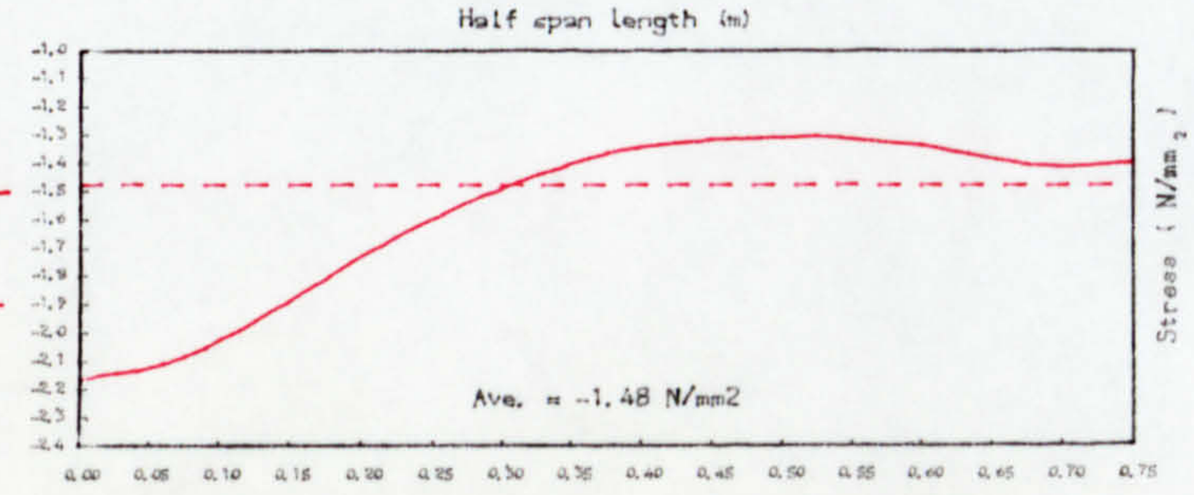

(b2) Axial prestress profile along Y=0.675m

Fig. 6.18 In-plane prestress distribution, Slab A1

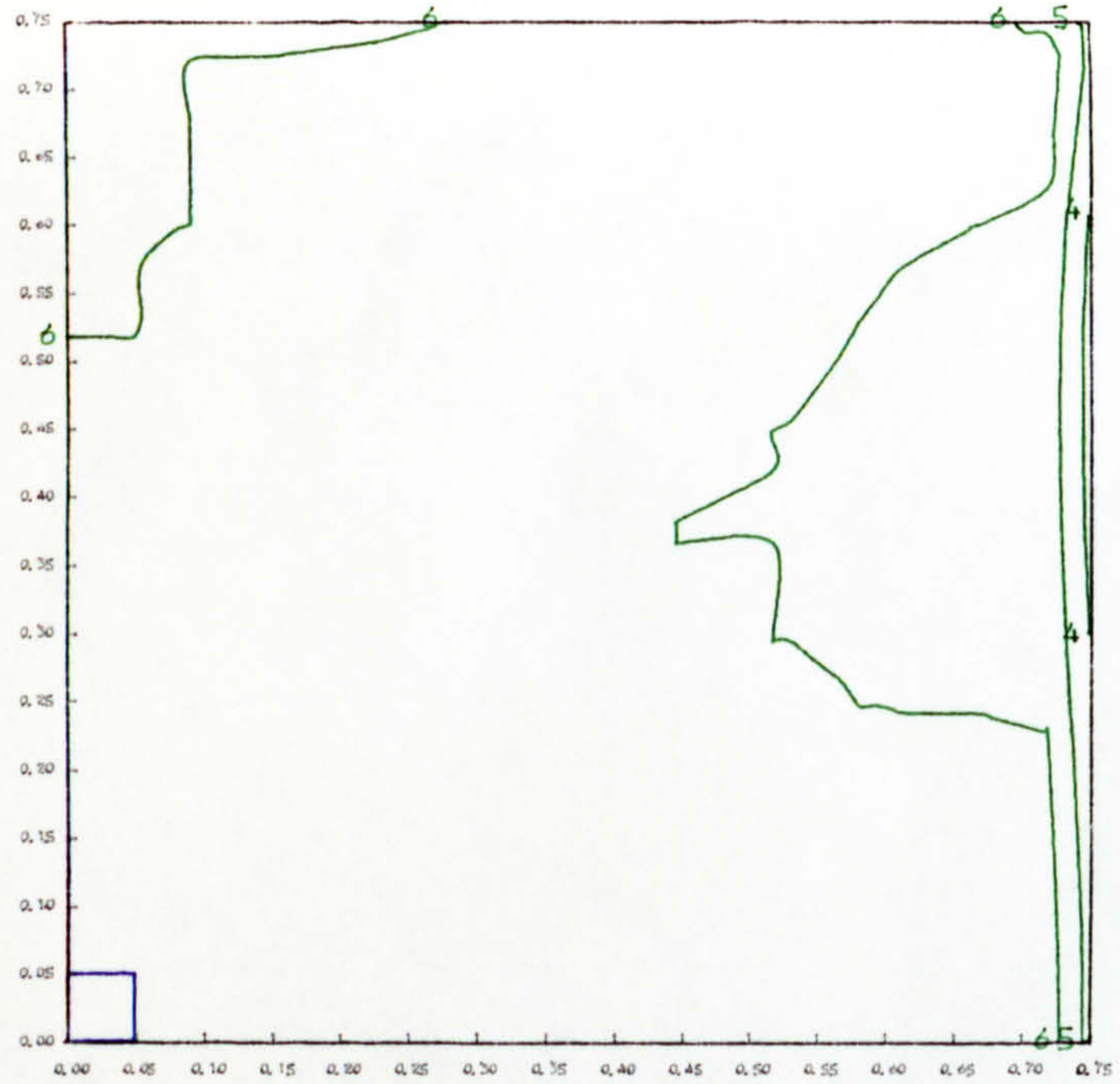

(a) Axial prestress normal to x-axis

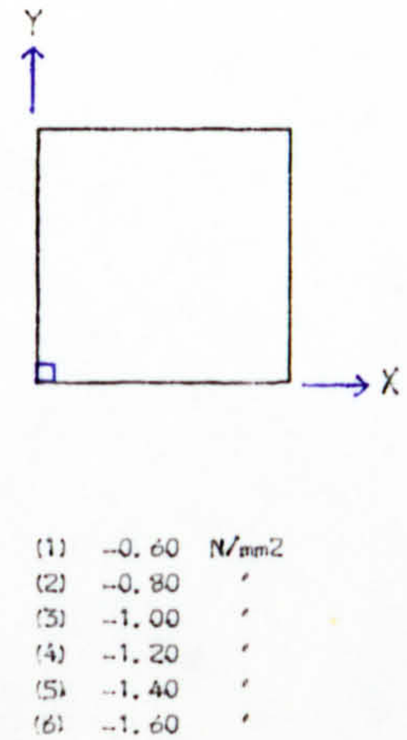

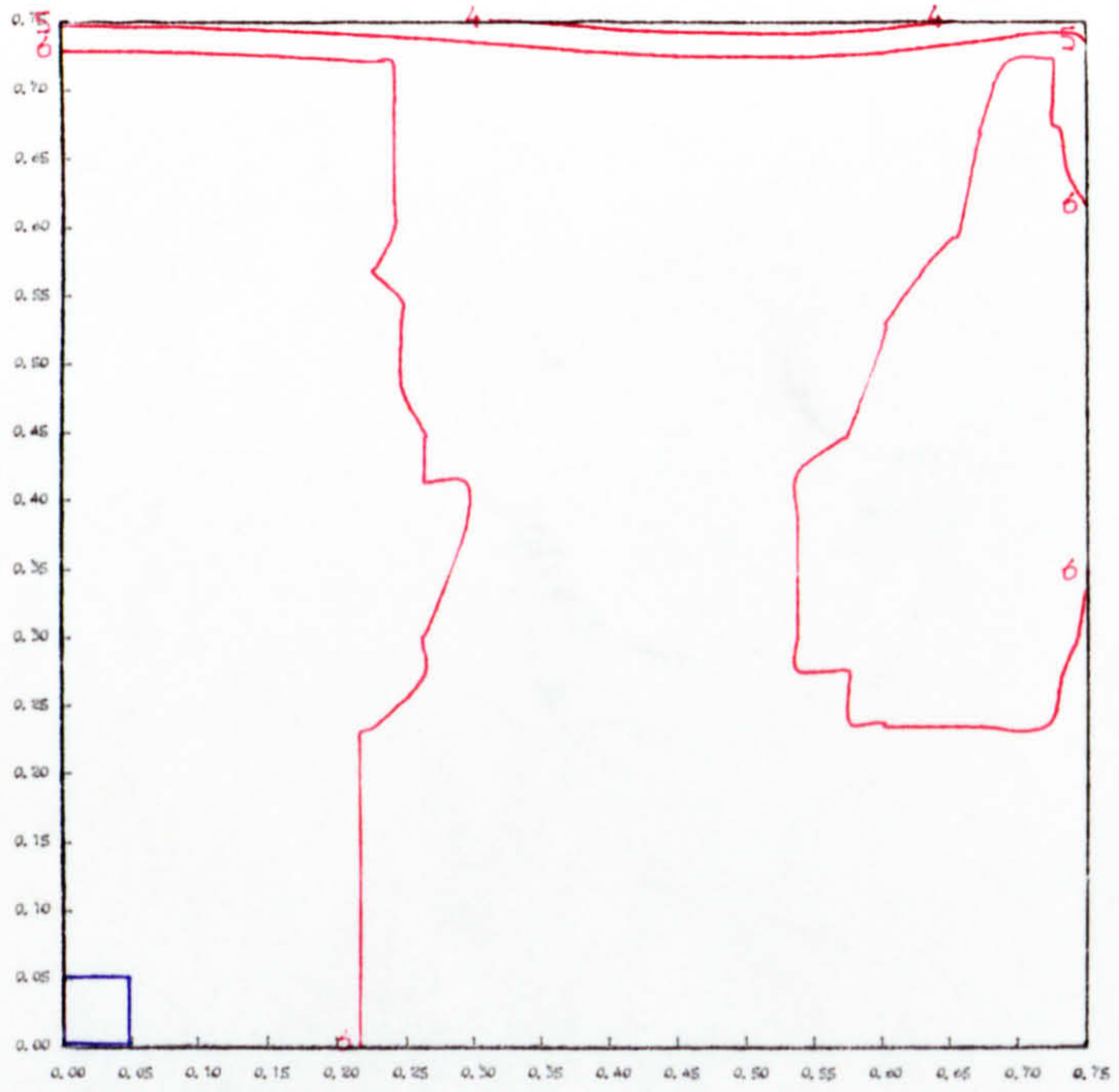

(b) Axial prestress normal to y-axis

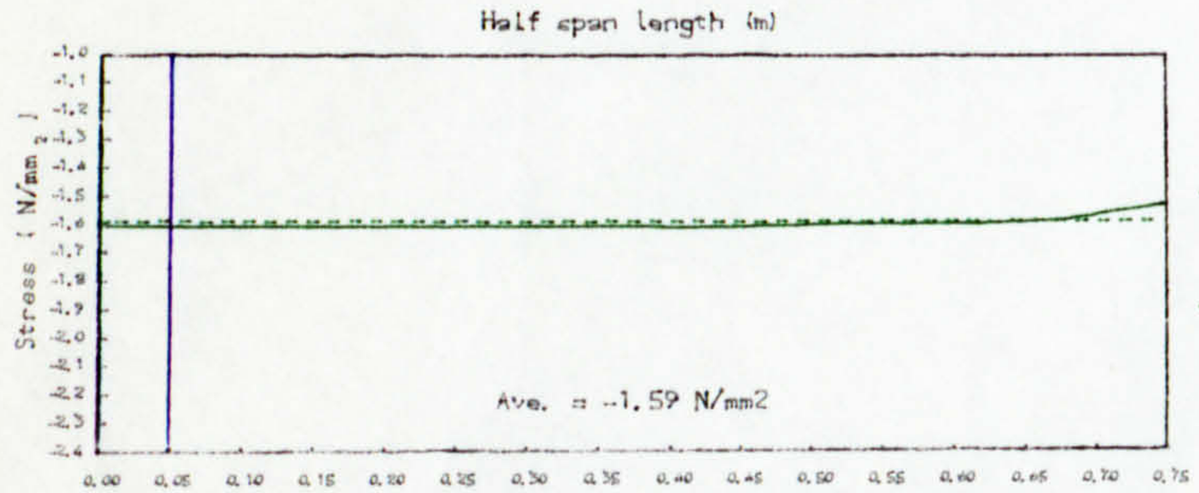

(a1) Axial prestress profile along X=0.00 m

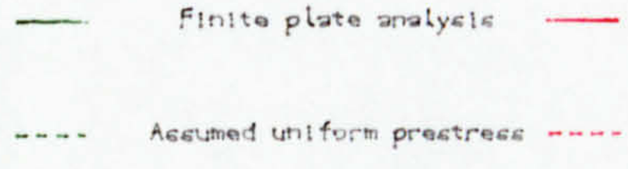

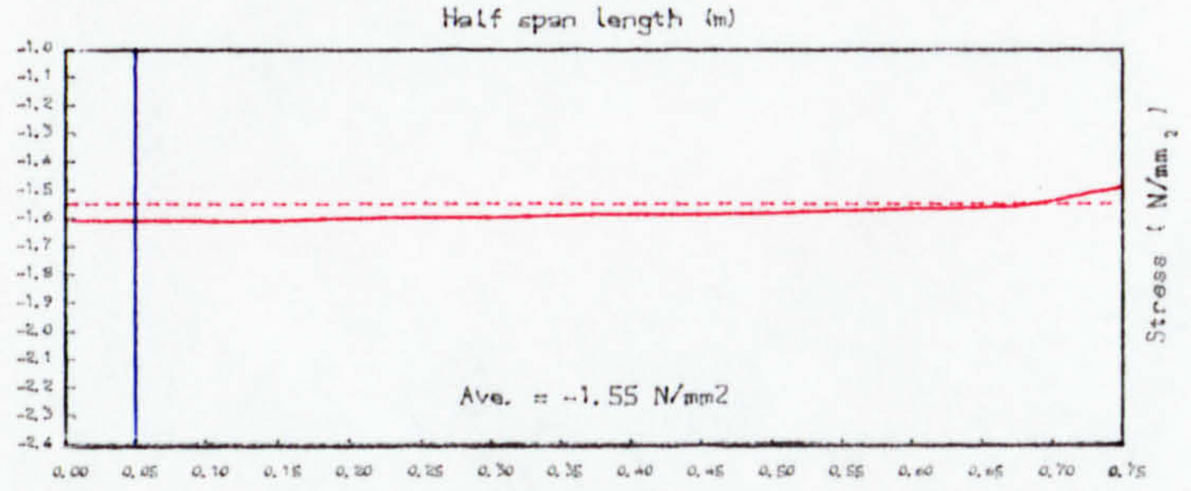

(b1) Axial prestress profile along Y=0.00 m

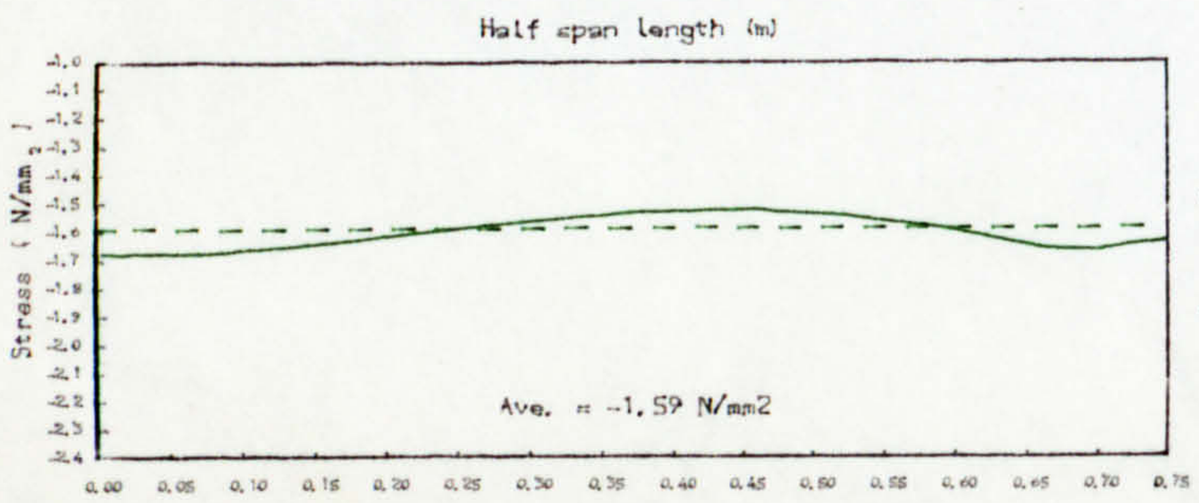

(a2) Axial prestress profile along X=0.675m

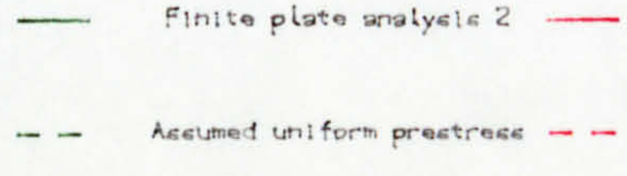

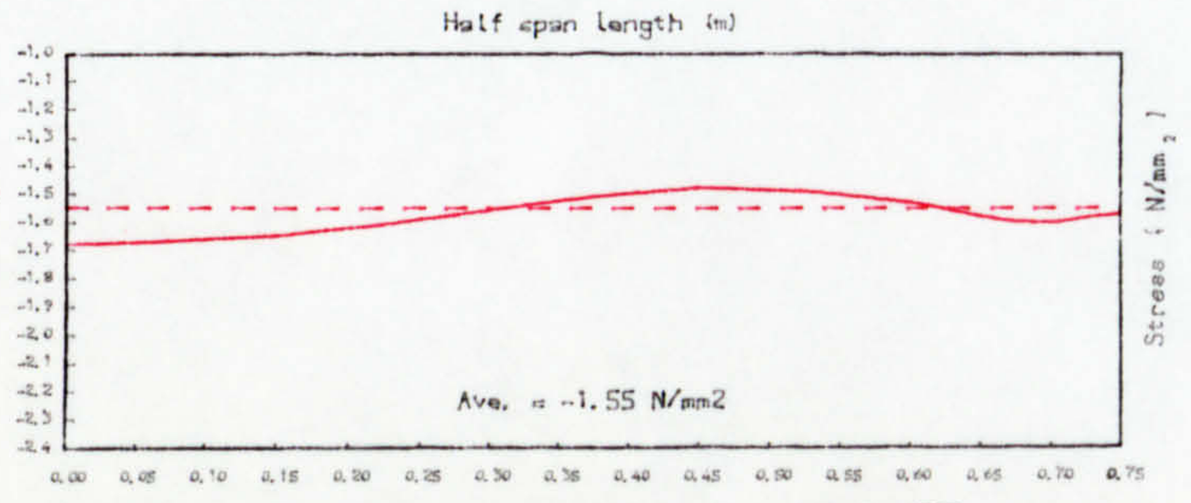

(b2) Axial prestress profile along Y=0.675m

Fig. 6.19 In-plane prestress distribution, Slab A2

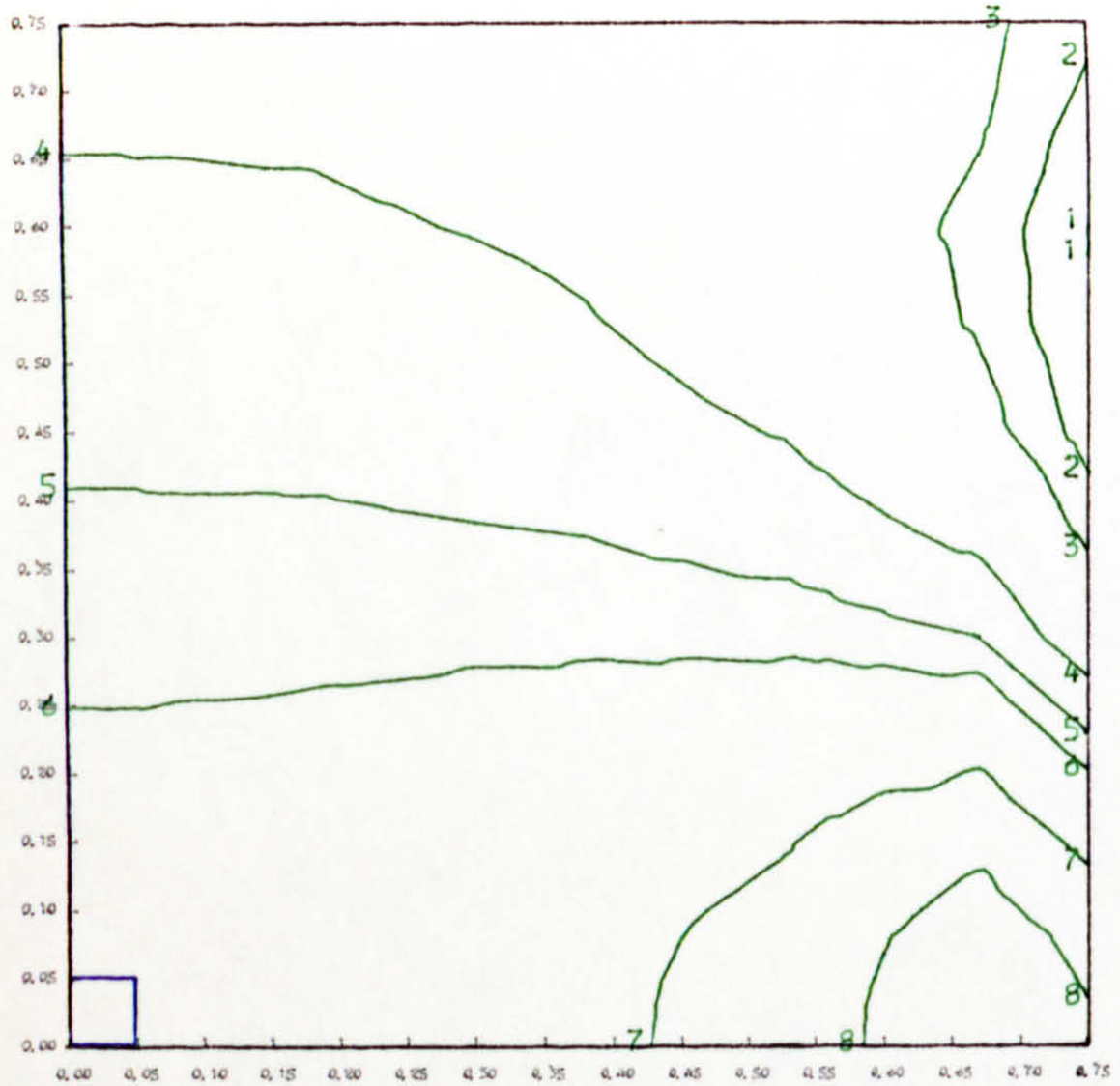

(a) Axial prestress normal to x-axis

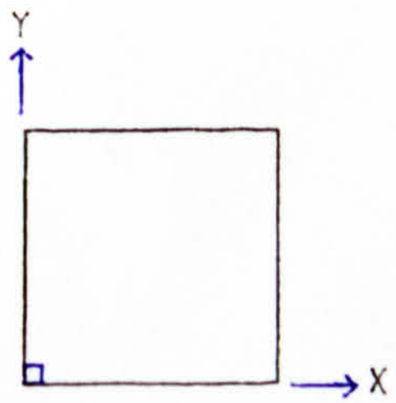

(1)	-0.60	N/mm2
(2)	-0.80	"
(3)	-1.00	"
(4)	-1.50	"
(5)	-1.80	"
(6)	-2.00	"
(7)	-2.50	"
(8)	-3.00	"

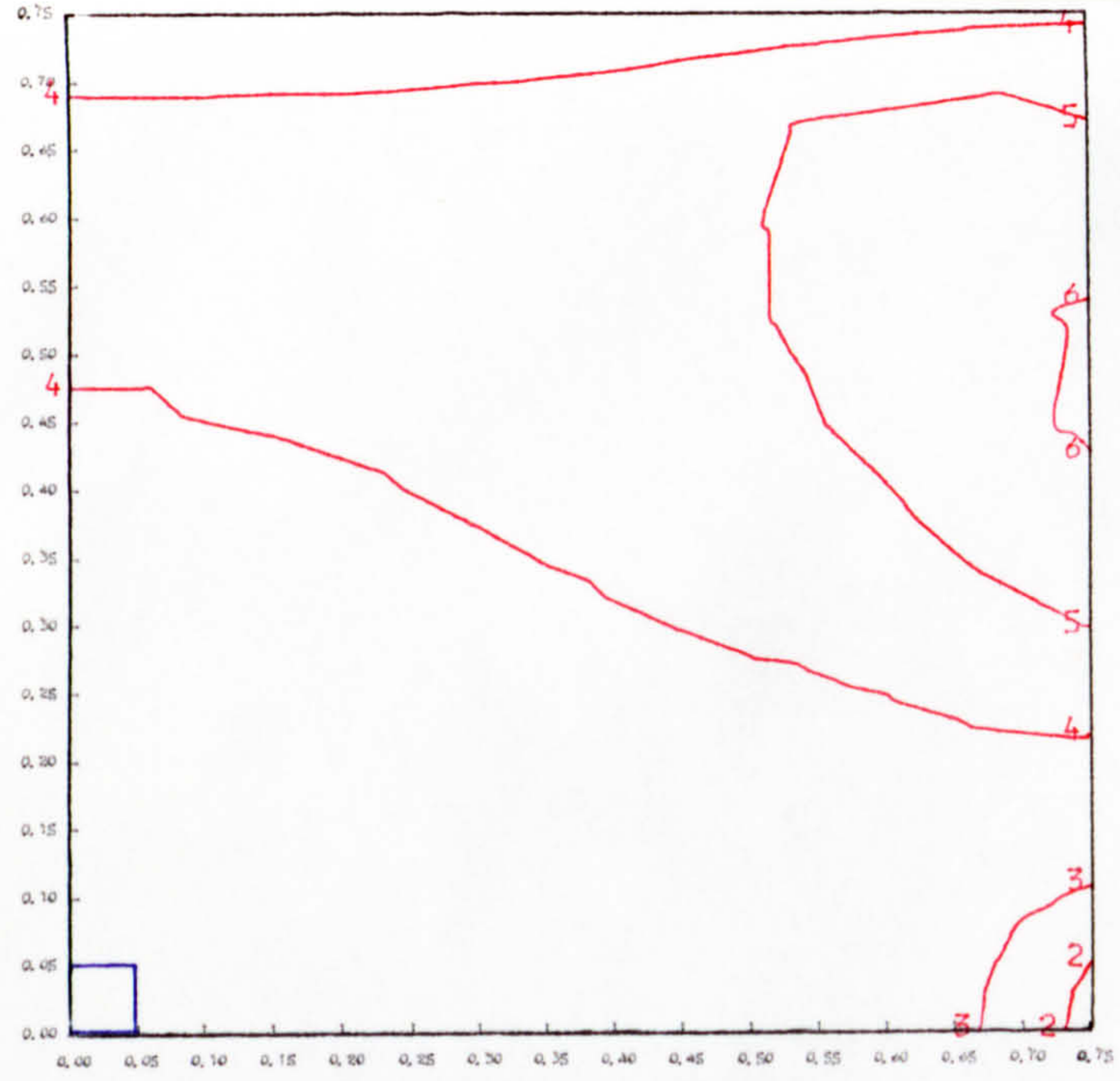

(b) Axial prestress normal to y-axis

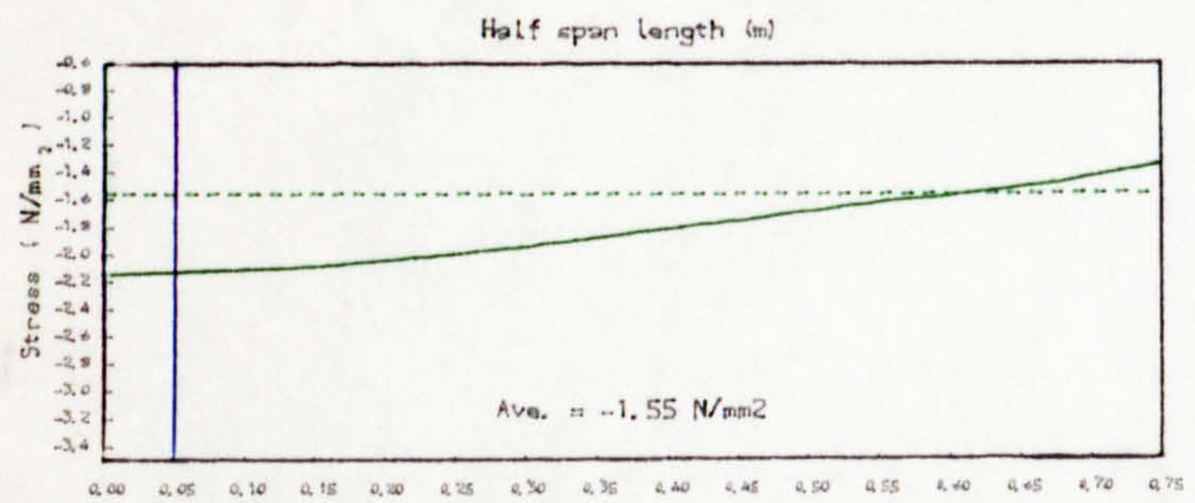

(a1) Axial prestress profile along X=0.00 m

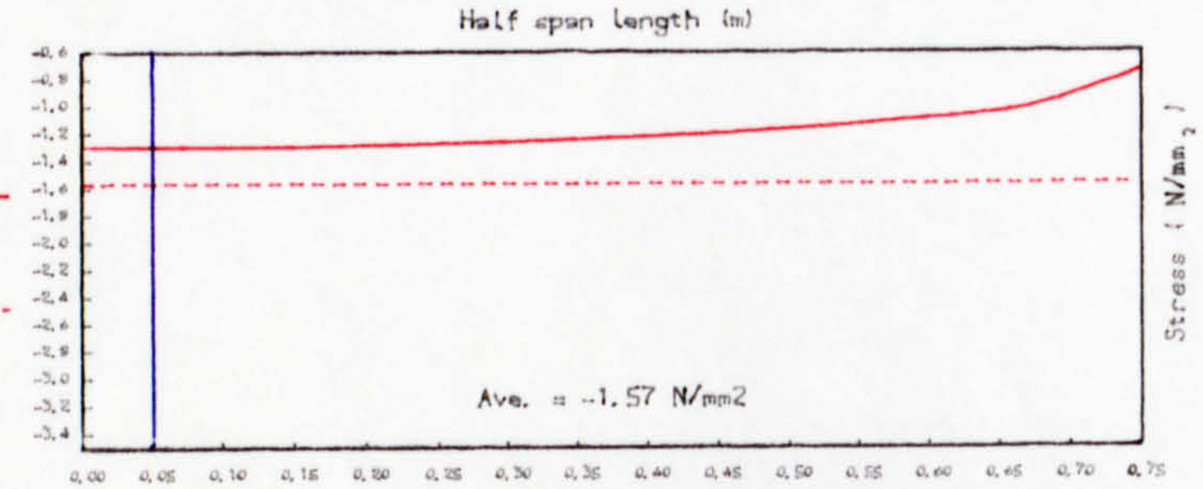

(b1) Axial prestress profile along Y=0.00 m

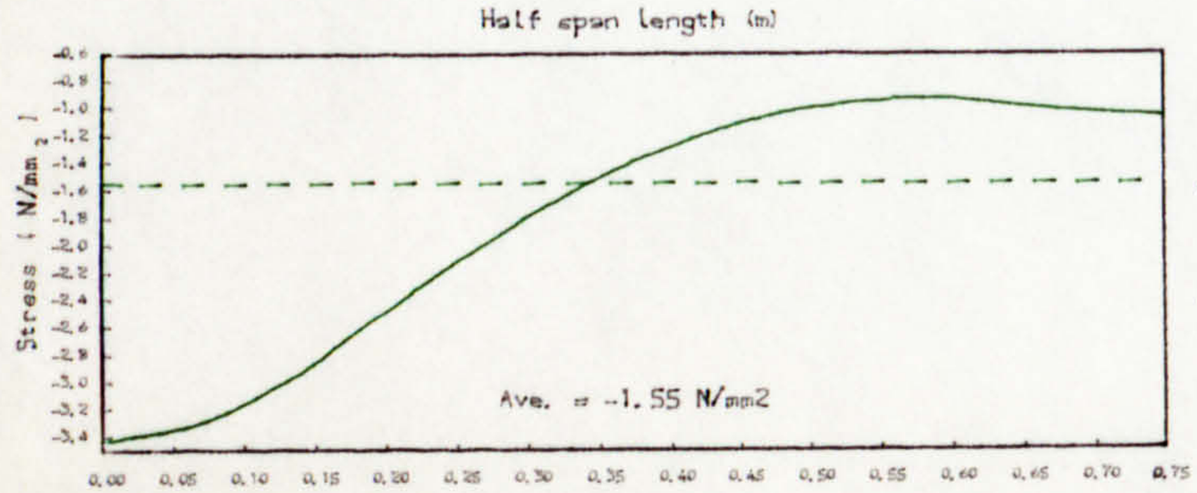

(a2) Axial prestress profile along X=0.675m

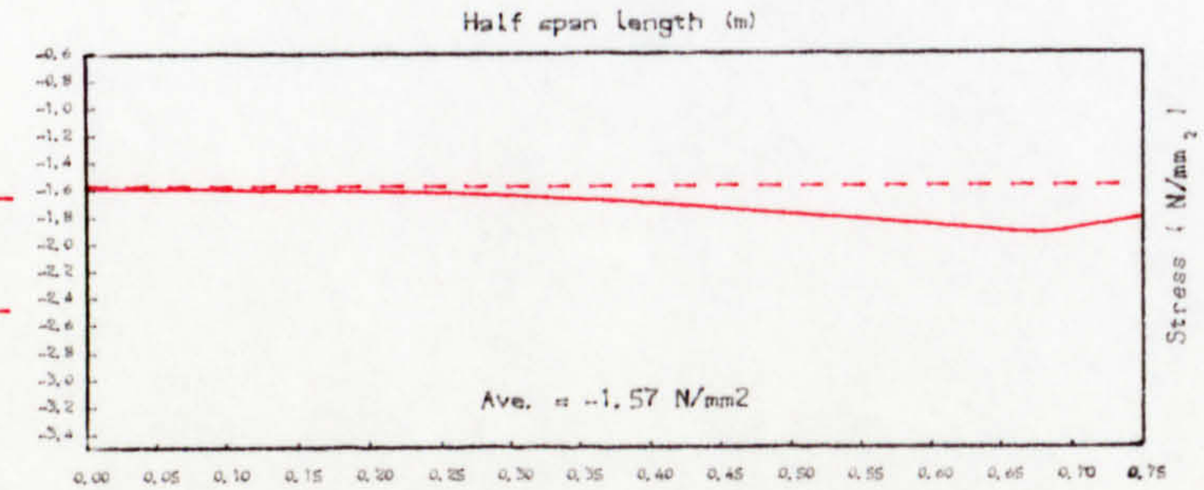

(b2) Axial prestress profile along Y=0.675m

Finite plate analysis

Assumed uniform prestress

Finite plate analysis 2

Assumed uniform prestress

Fig. 6.20 In-plane prestress distribution, Slab A3

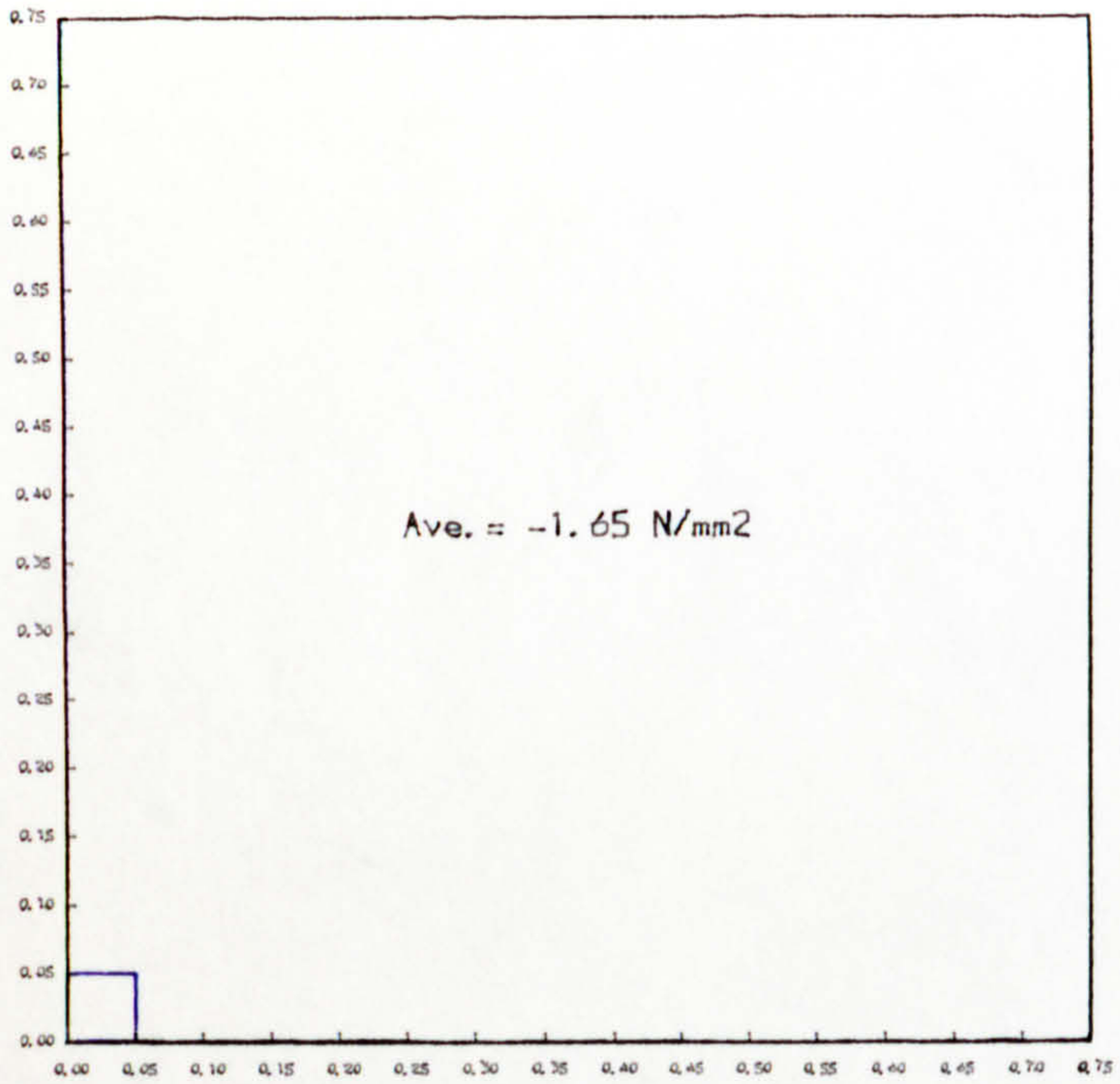

(a) Axial prestress normal to x-axis

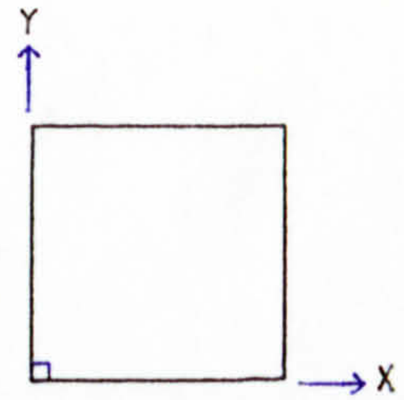

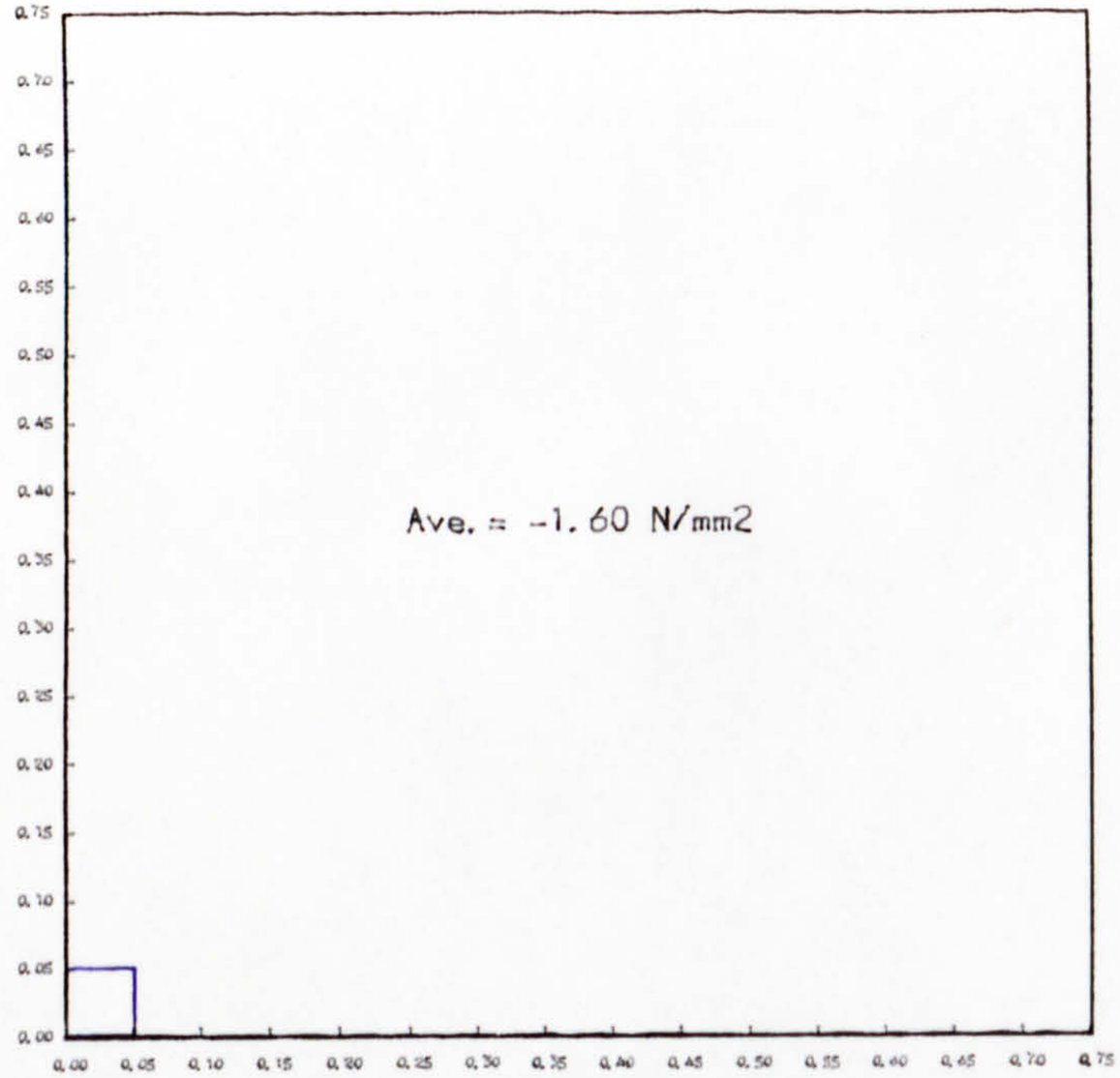

(b) Axial prestress normal to y-axisY

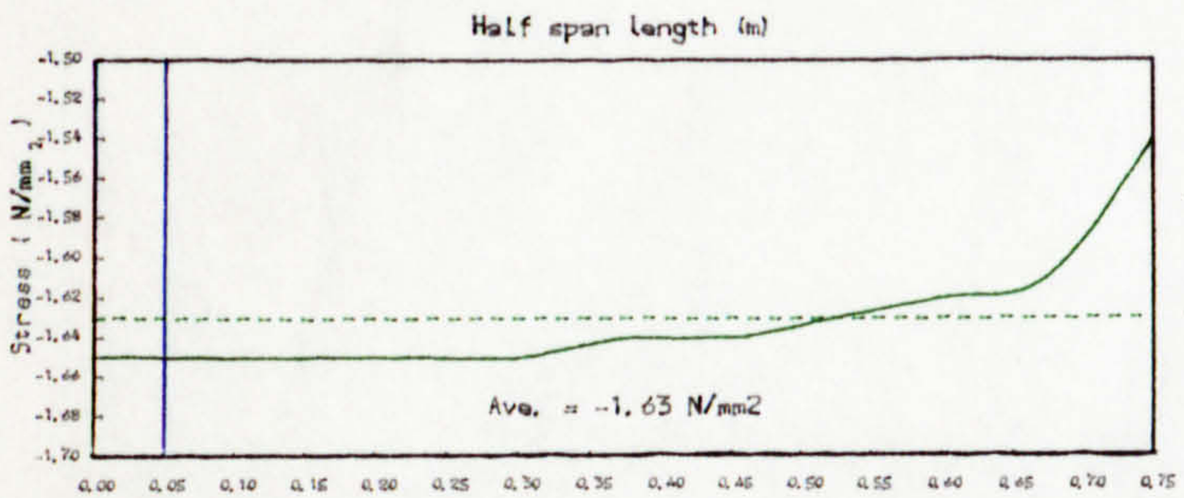

(a1) Axial prestress profile along X=0.00 m

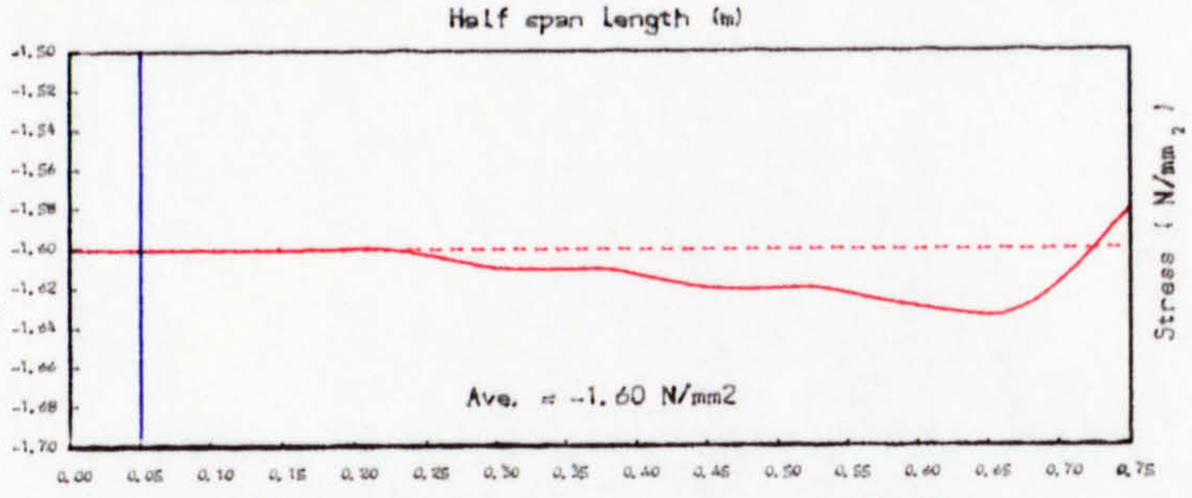

(b1) Axial prestress profile along Y=0.00 m

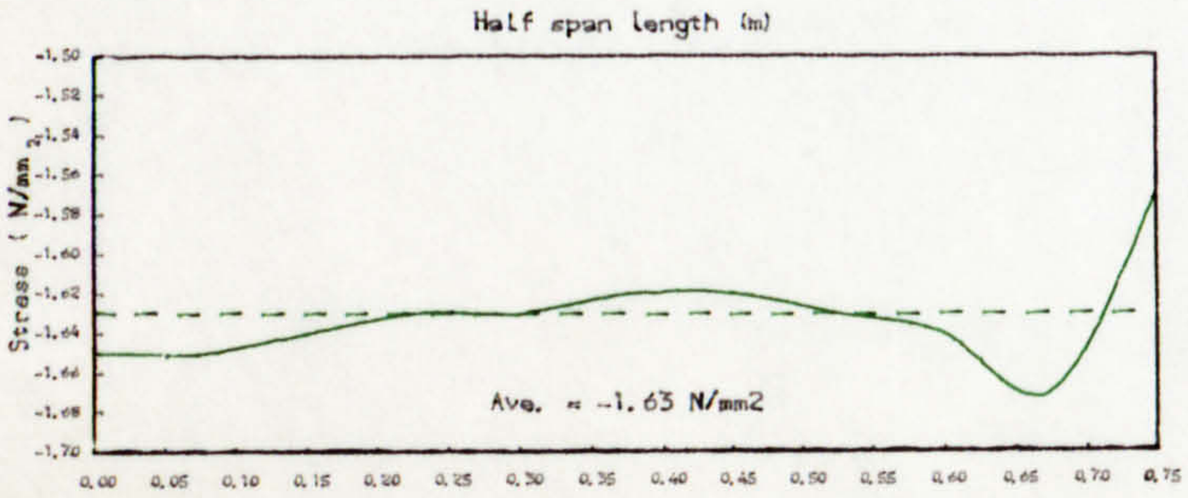

(a2) Axial prestress profile along X=0.675m

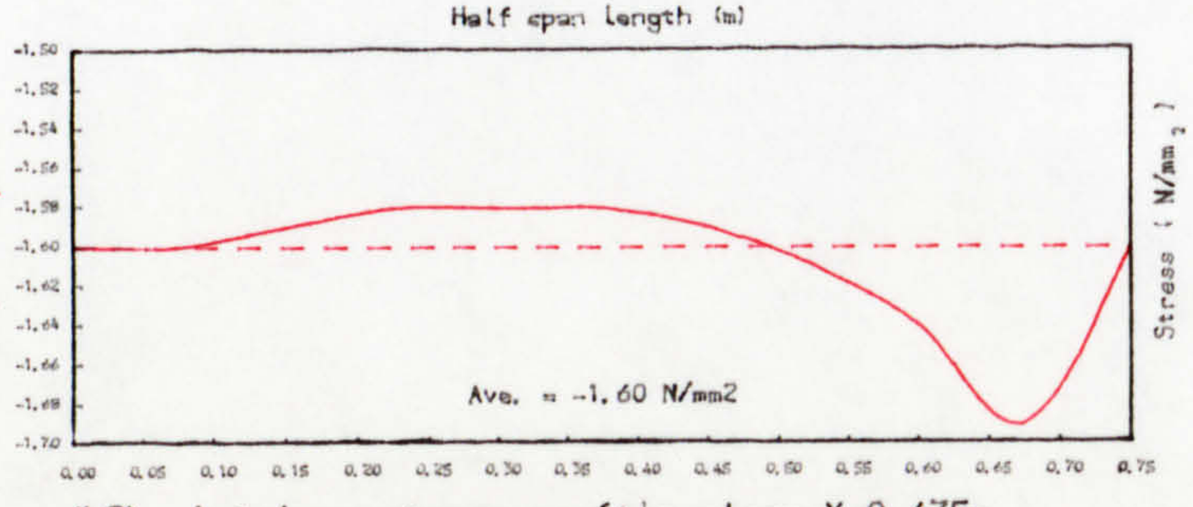

(b2) Axial prestress profile along Y=0.675m

Fig. 6.21 In-plane prestress distribution, Slab A4

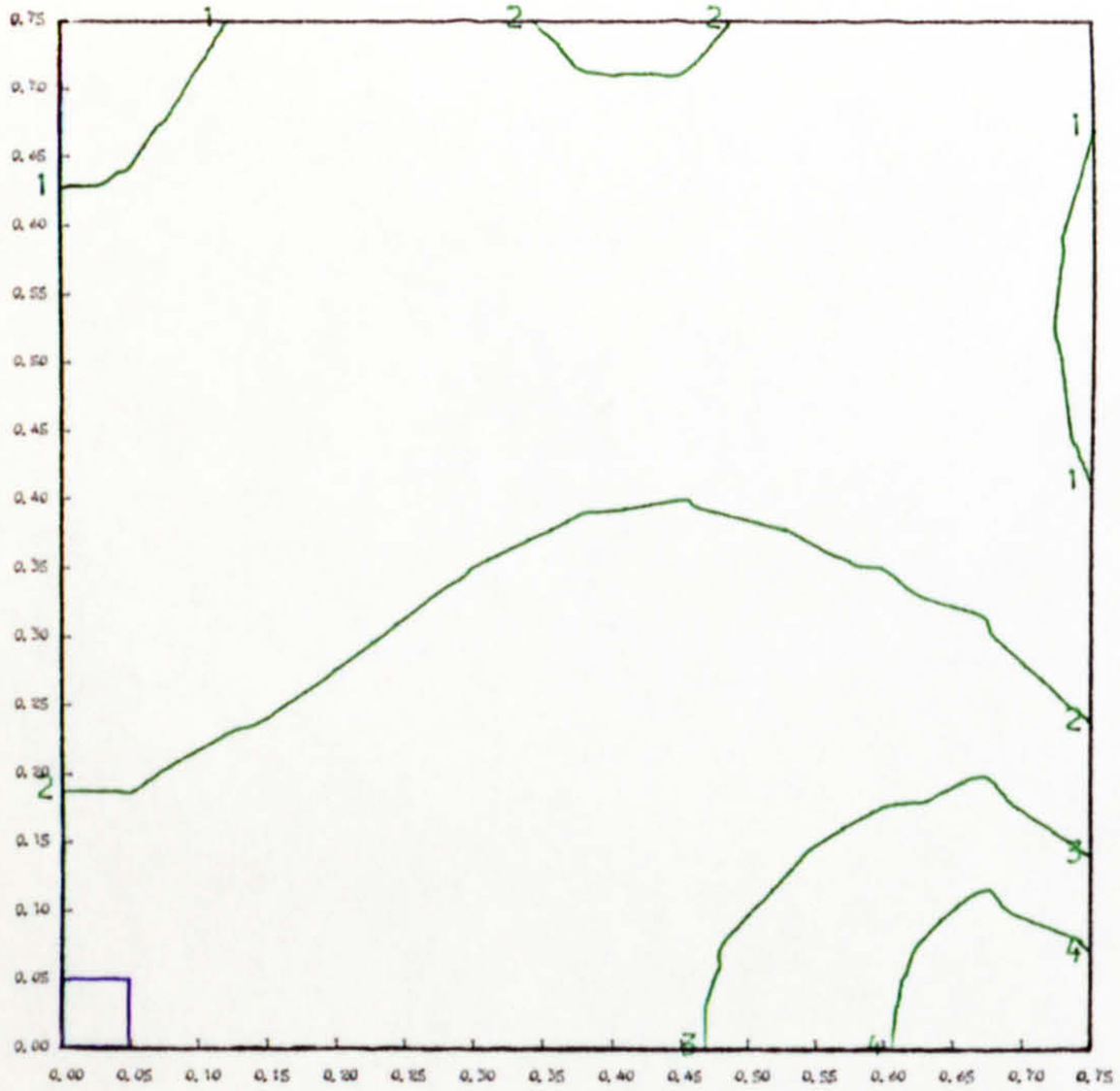

(a) Axial prestress normal to x-axis

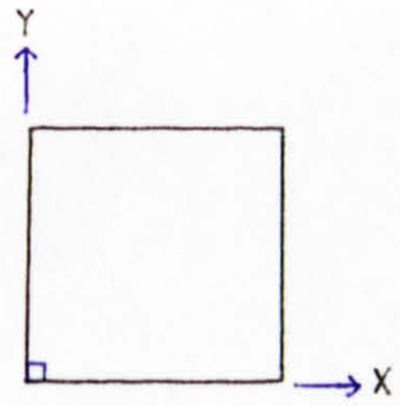

(1) -0.40 N/mm2
(2) -0.80 "
(3) -1.20 "
(4) -1.50 "

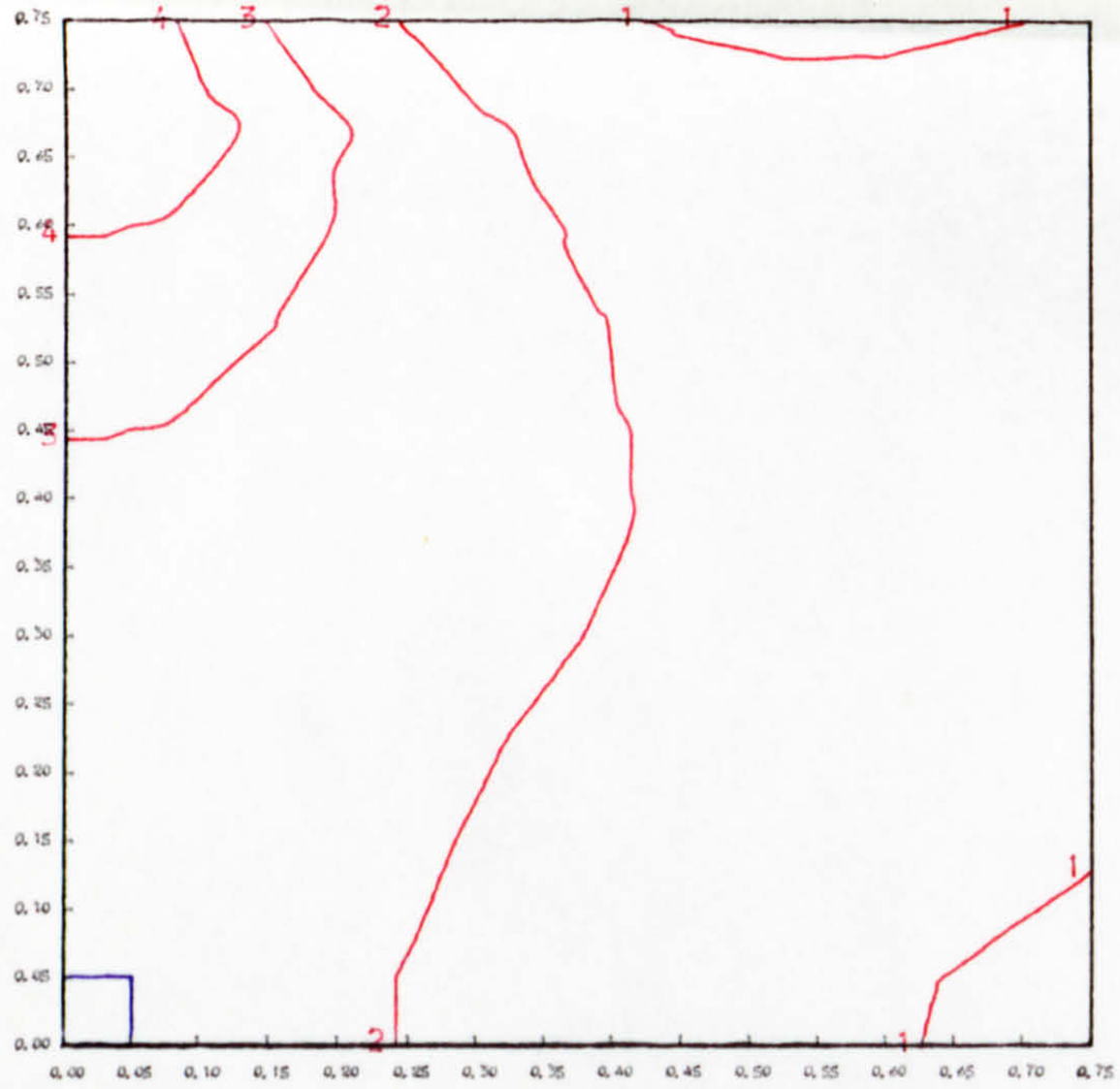

(b) Axial prestress normal to y-axis

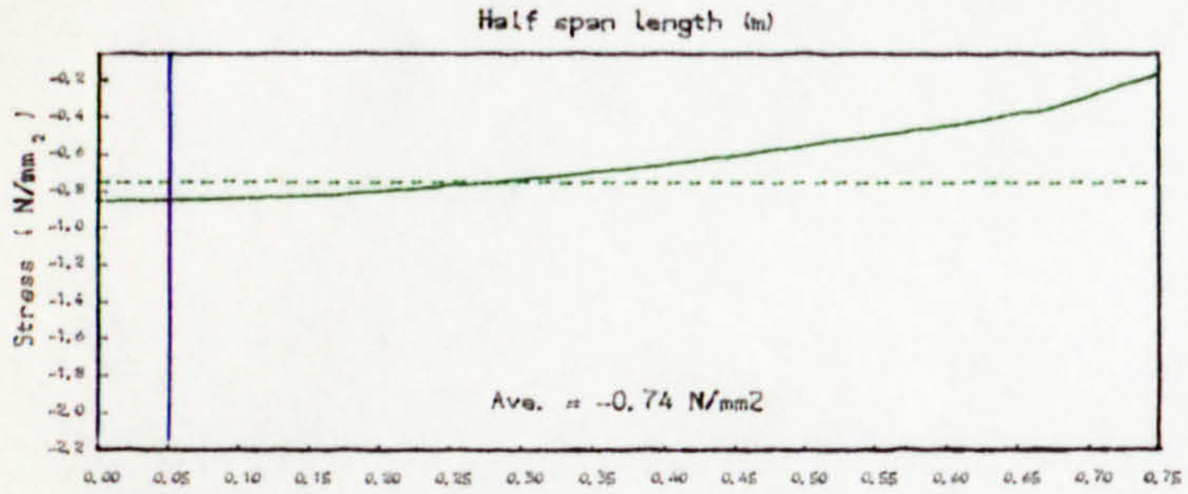

(a1) Axial prestress profile along X=0.00 m

Finite plate analysis

Assumed uniform prestress

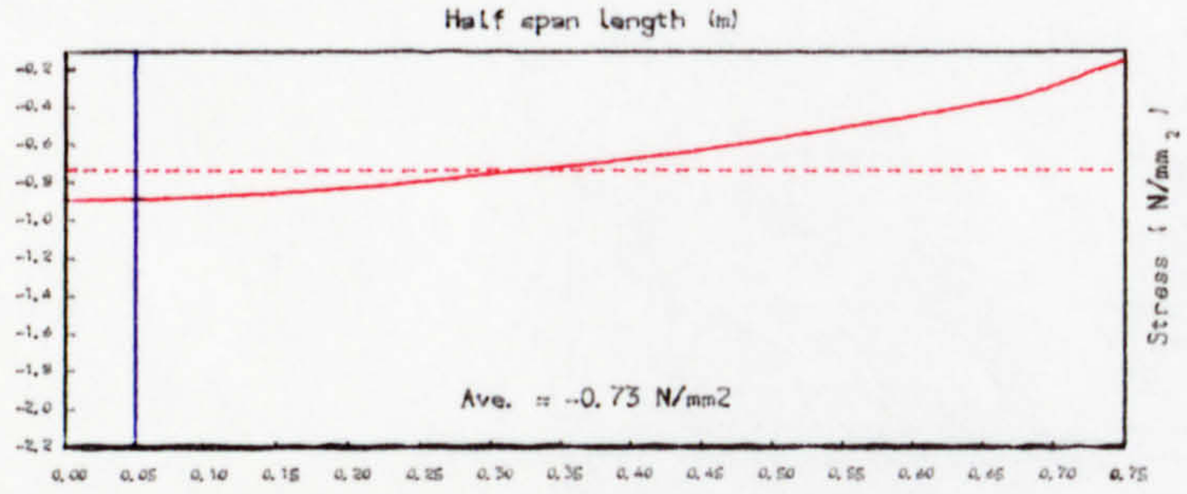

(b1) Axial prestress profile along Y=0.00 m

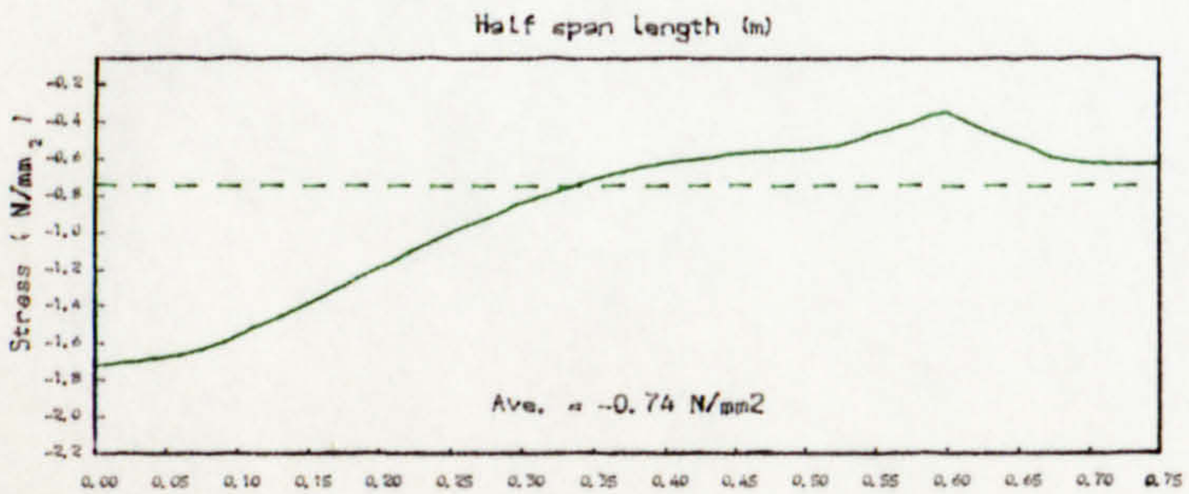

(a2) Axial prestress profile along X=0.675m

Finite plate analysis 2

Assumed uniform prestress

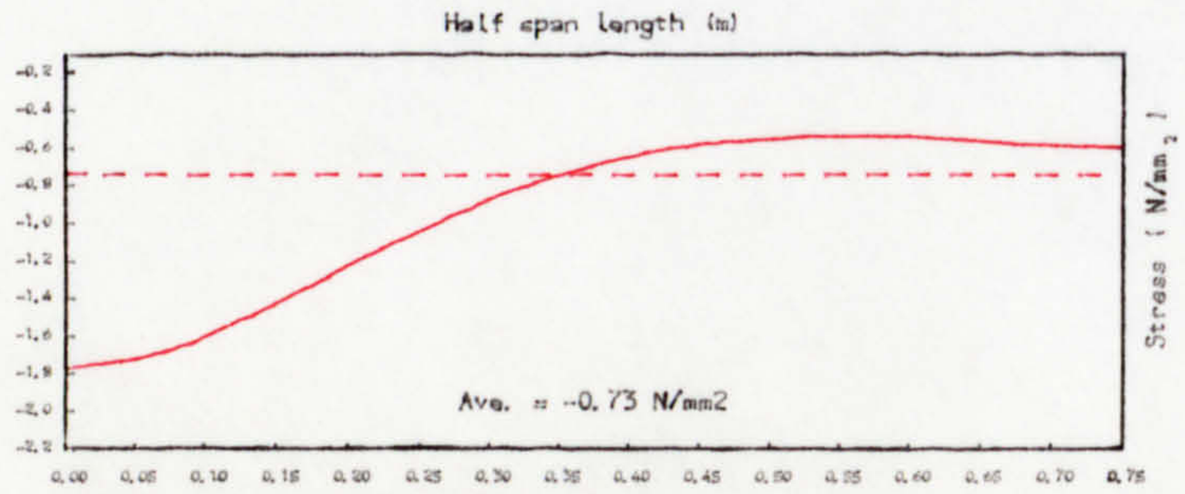

(b2) Axial prestress profile along Y=0.675m

Fig. 6.22 In-plane prestress distribution, Slab C1

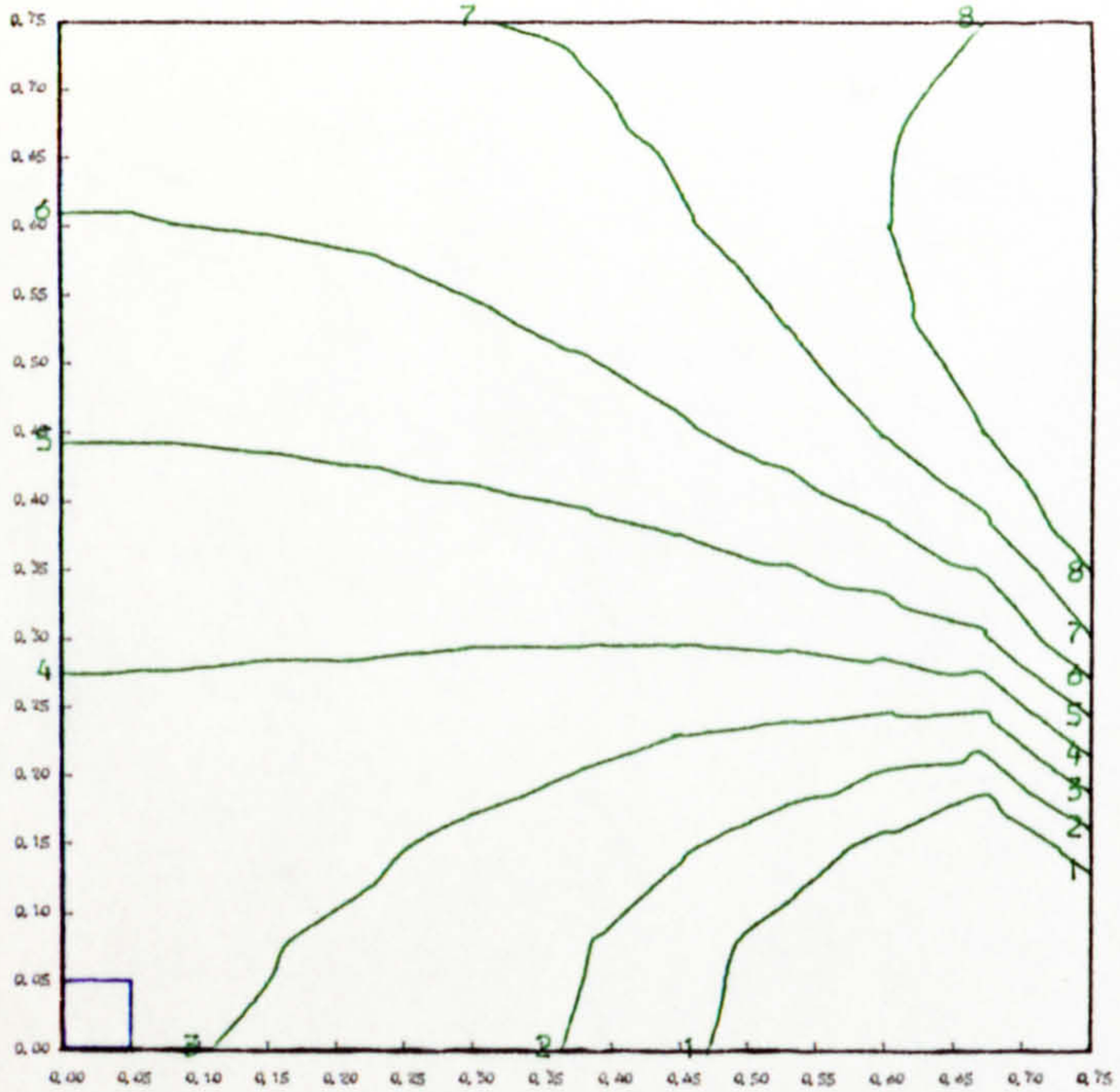

(a) Axial prestress normal to x-axis

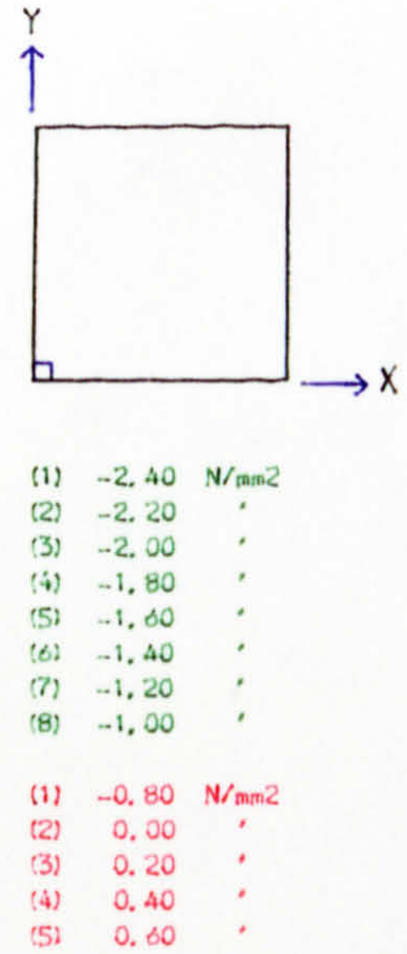

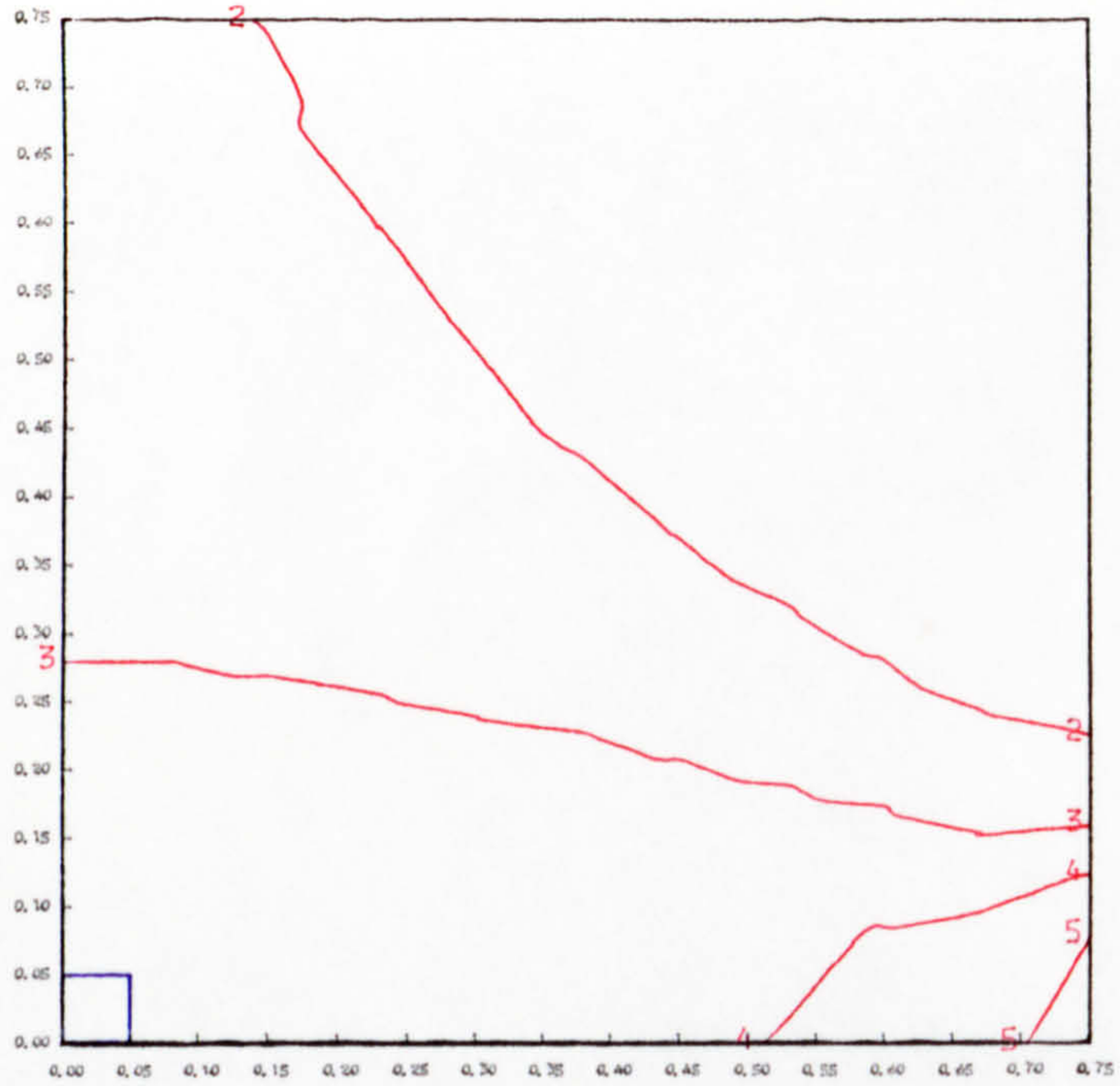

(b) Axial prestress normal to y-axis

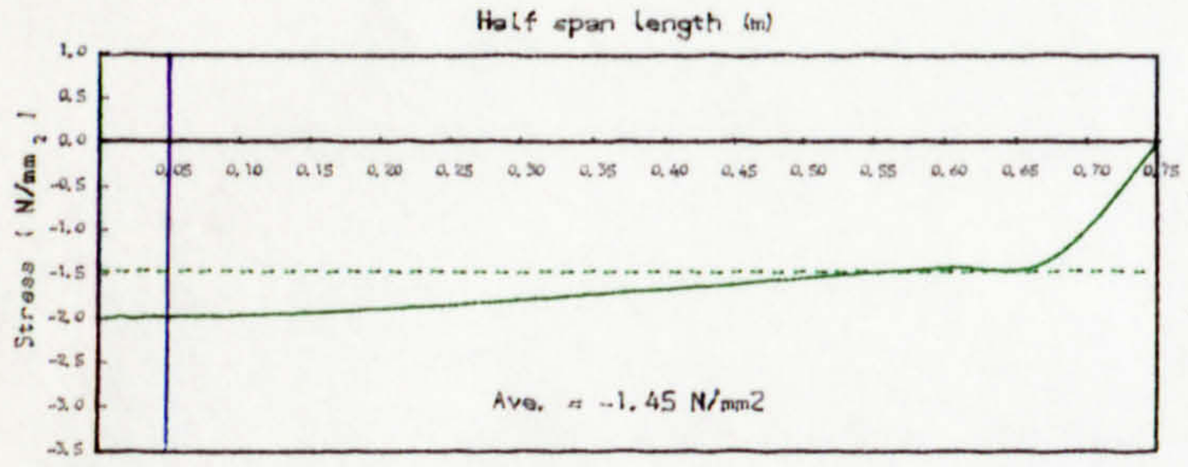

(a1) Axial prestress profile along X=0.00 m

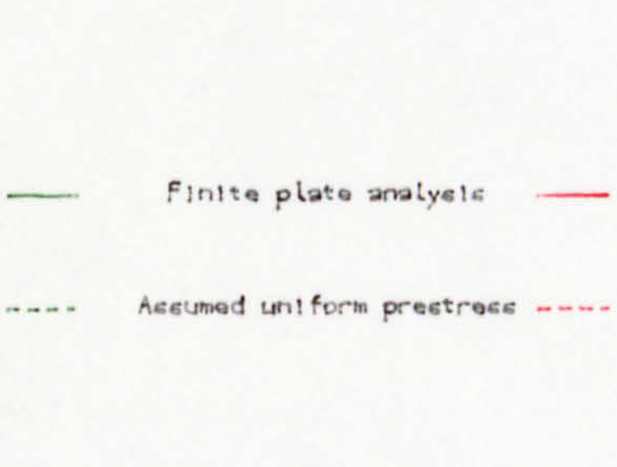

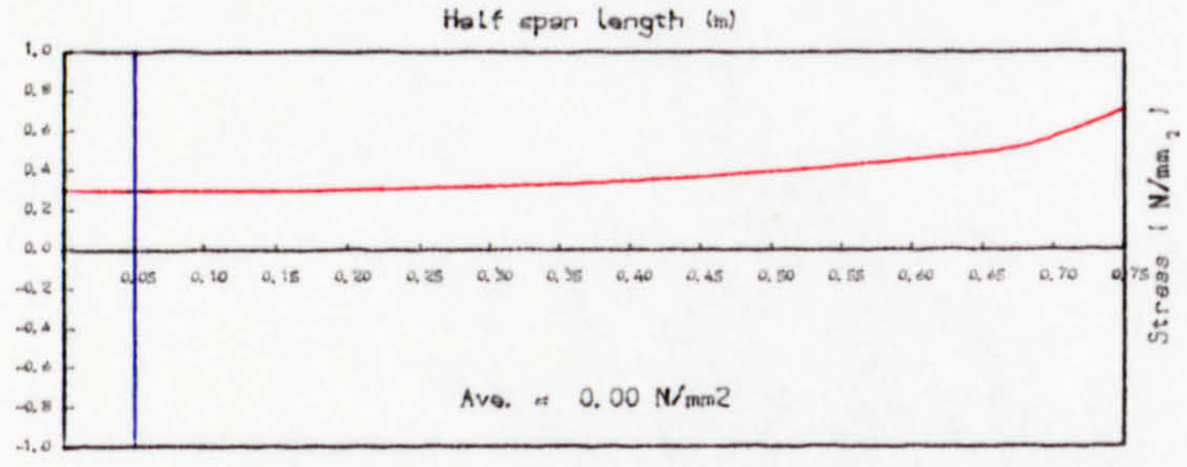

(b1) Axial prestress profile along Y=0.00 m

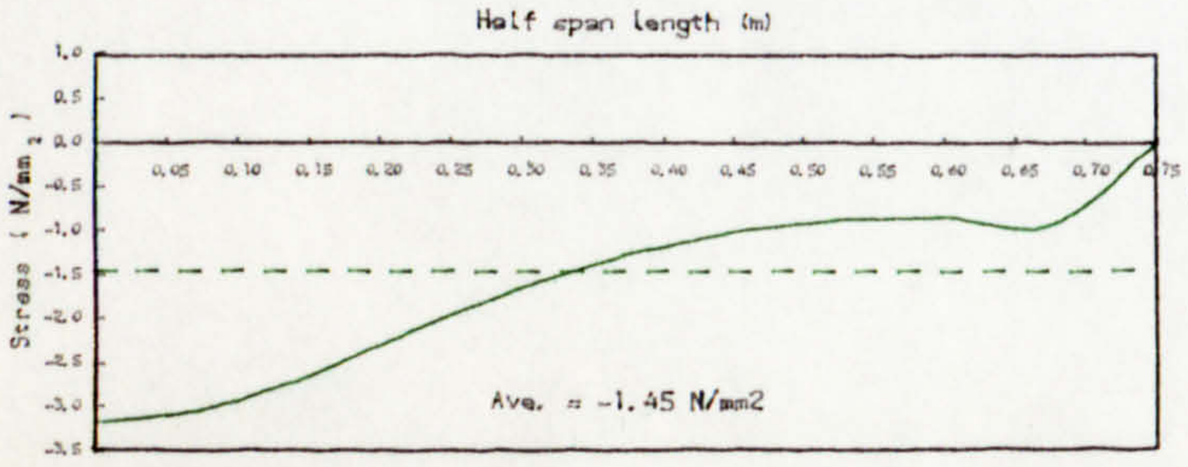

(a2) Axial prestress profile along X=0.675m

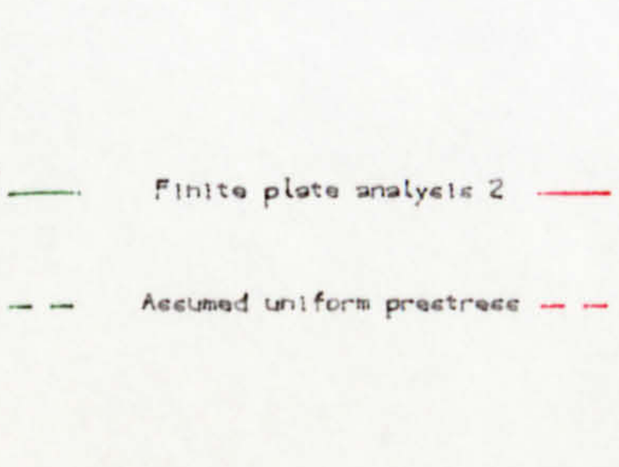

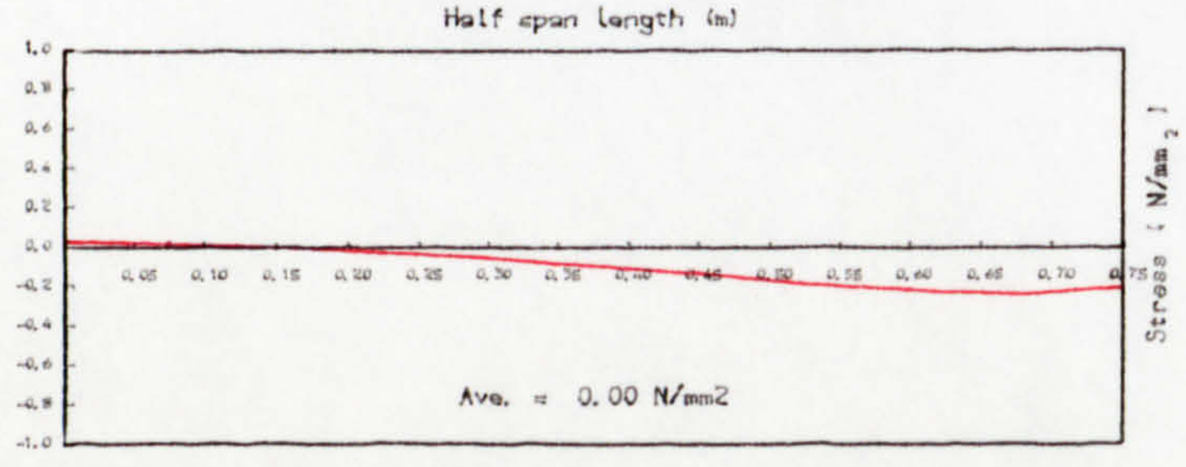

(b2) Axial prestress profile along Y=0.675m

Fig. 6.23 In-plane prestress distribution, Slab C2

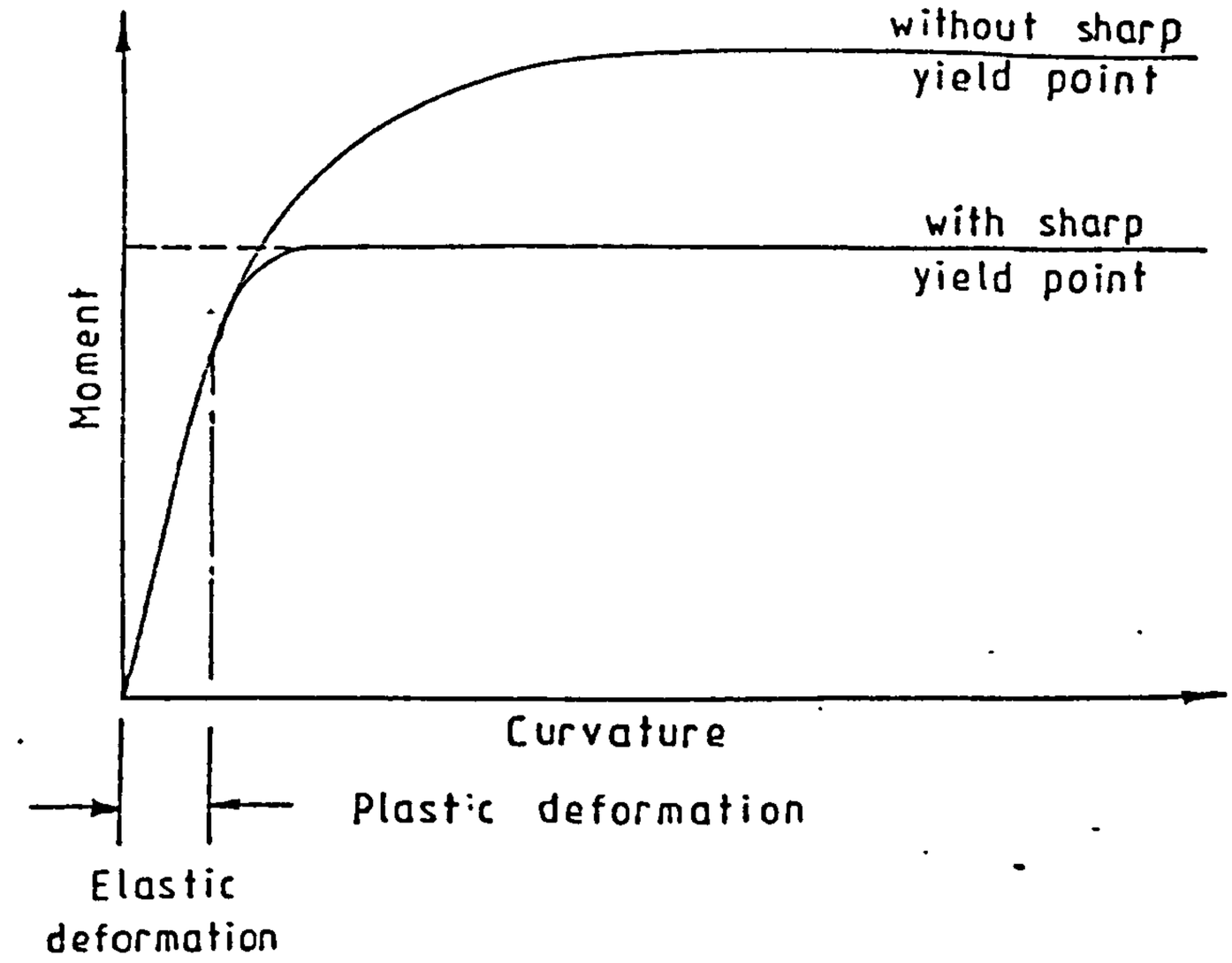

Fig. 7.1 Idealized moment-curvature relationship

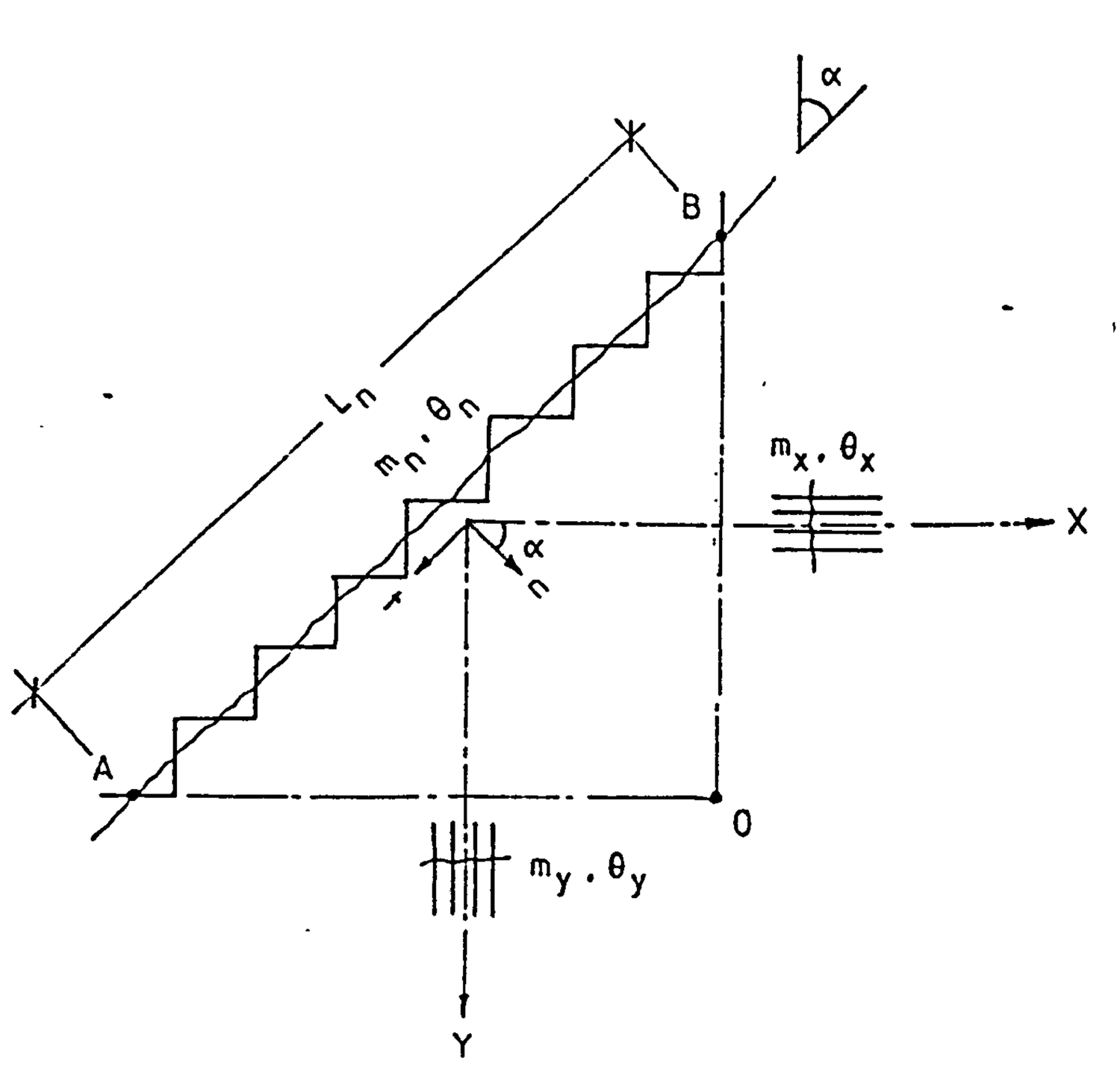

Fig. 7.2 Yield line and moment components

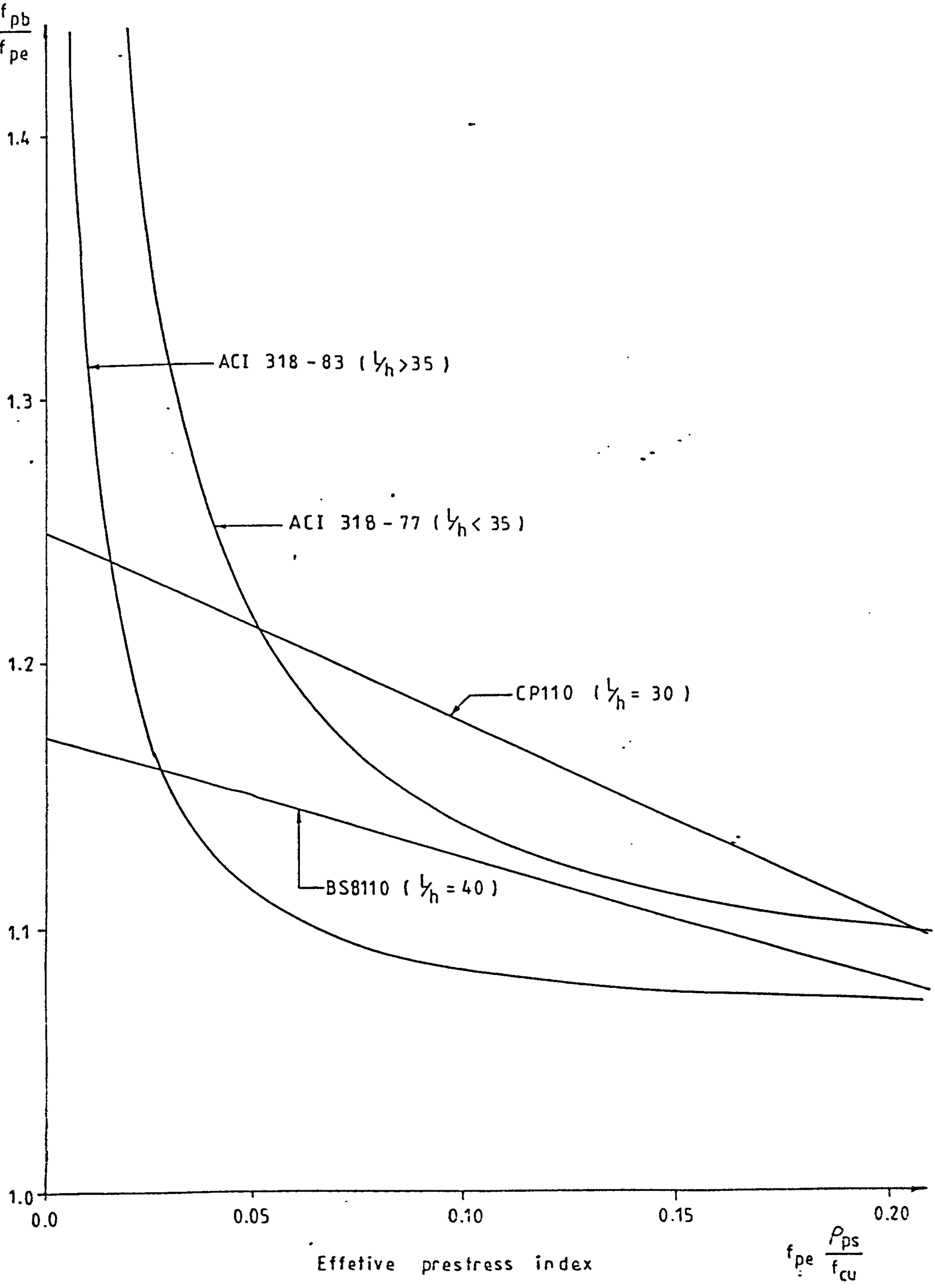

Fig. 7.3 Comparison of CP110, BS8110 and ACI methods for estimating tendon stress at failure

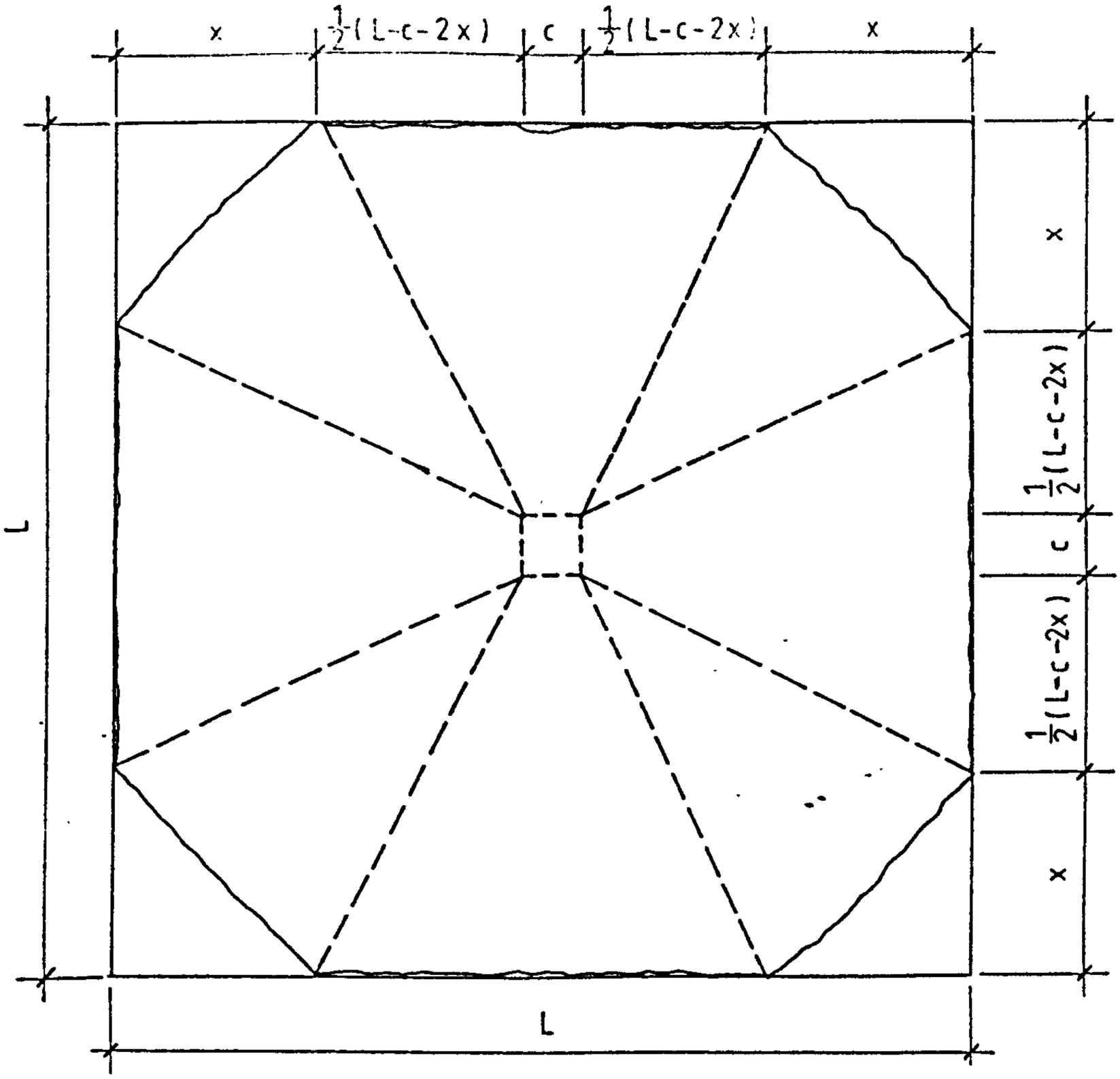

(a) Yield line pattern

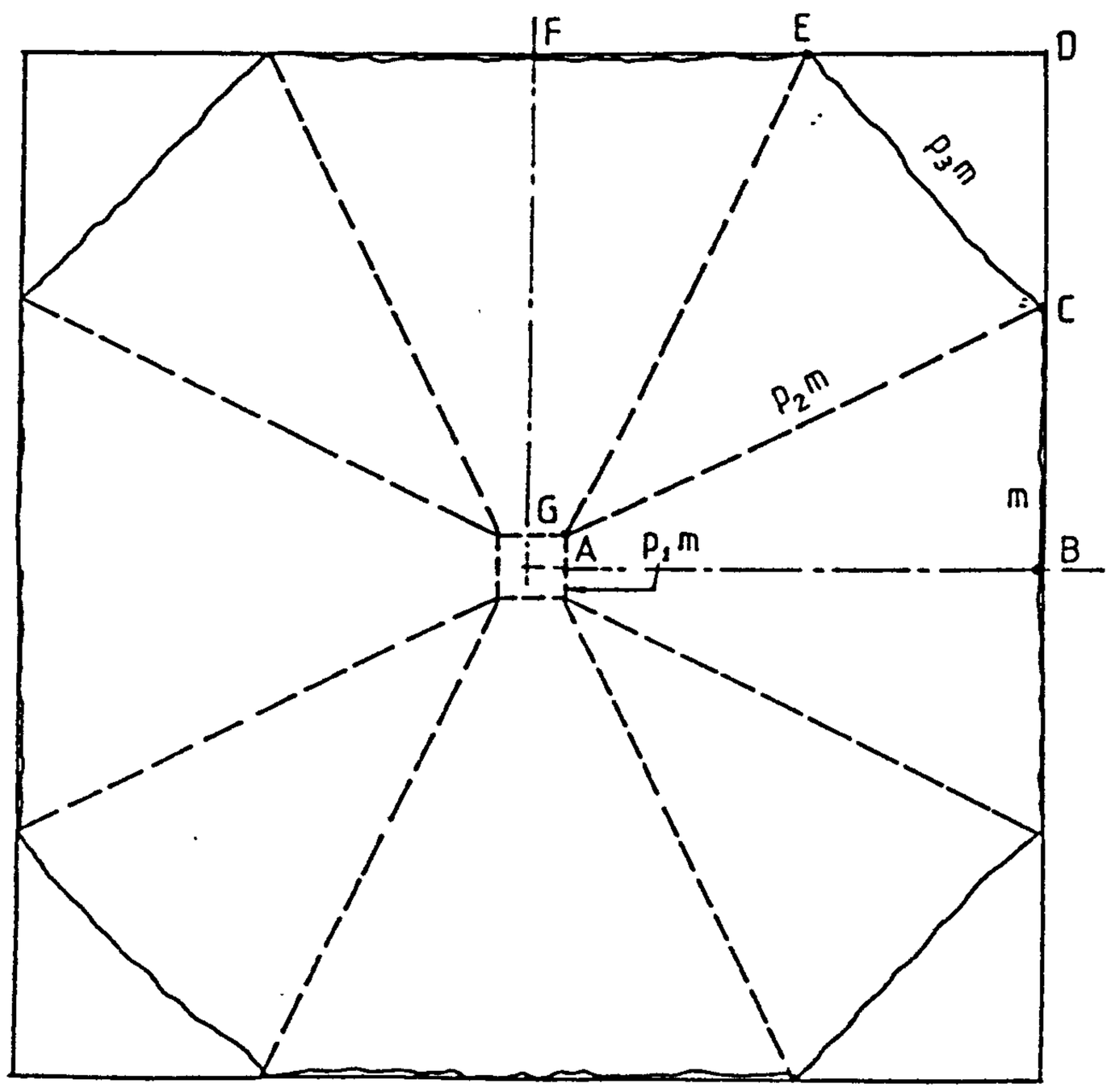

(b) Moments of resistance

Fig. 7.4 Mode of failure with cut-off corner

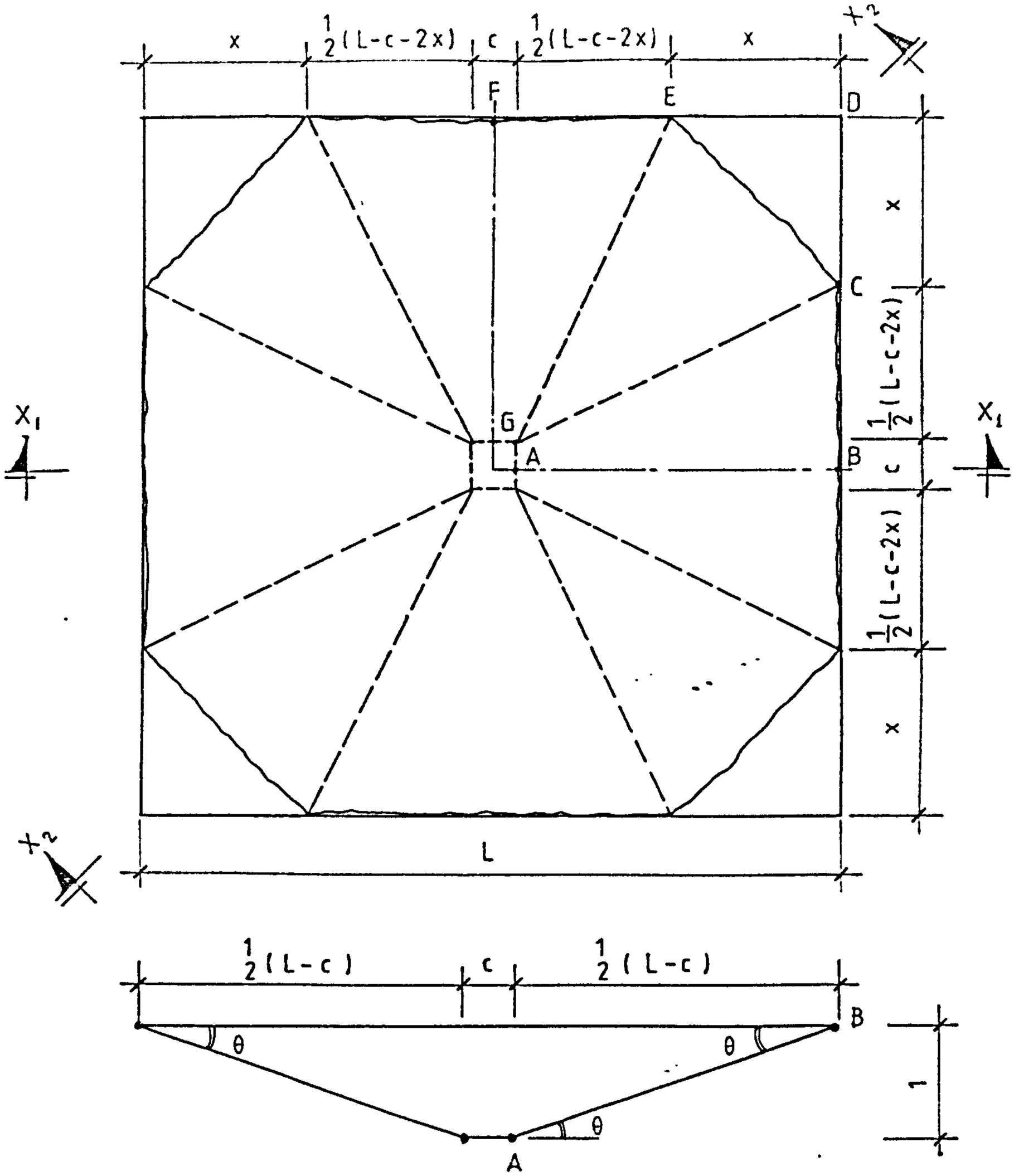

Section $X_1 - X_1$

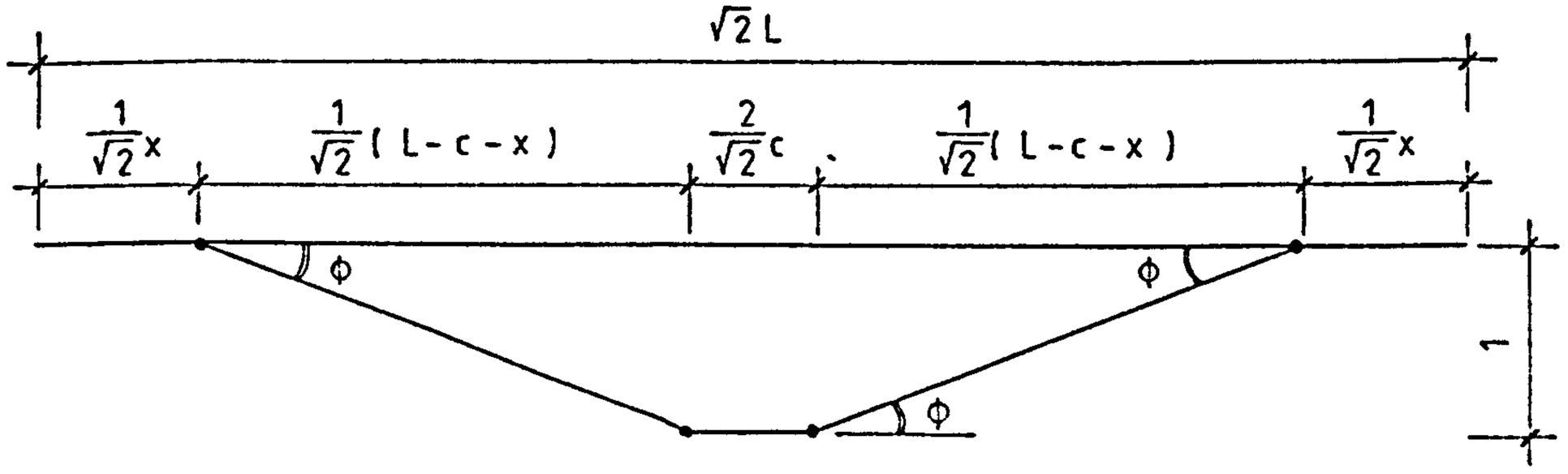

Section $X_2 - X_2$

Fig. 7.5 Displacements and rotations (cut-off corner)

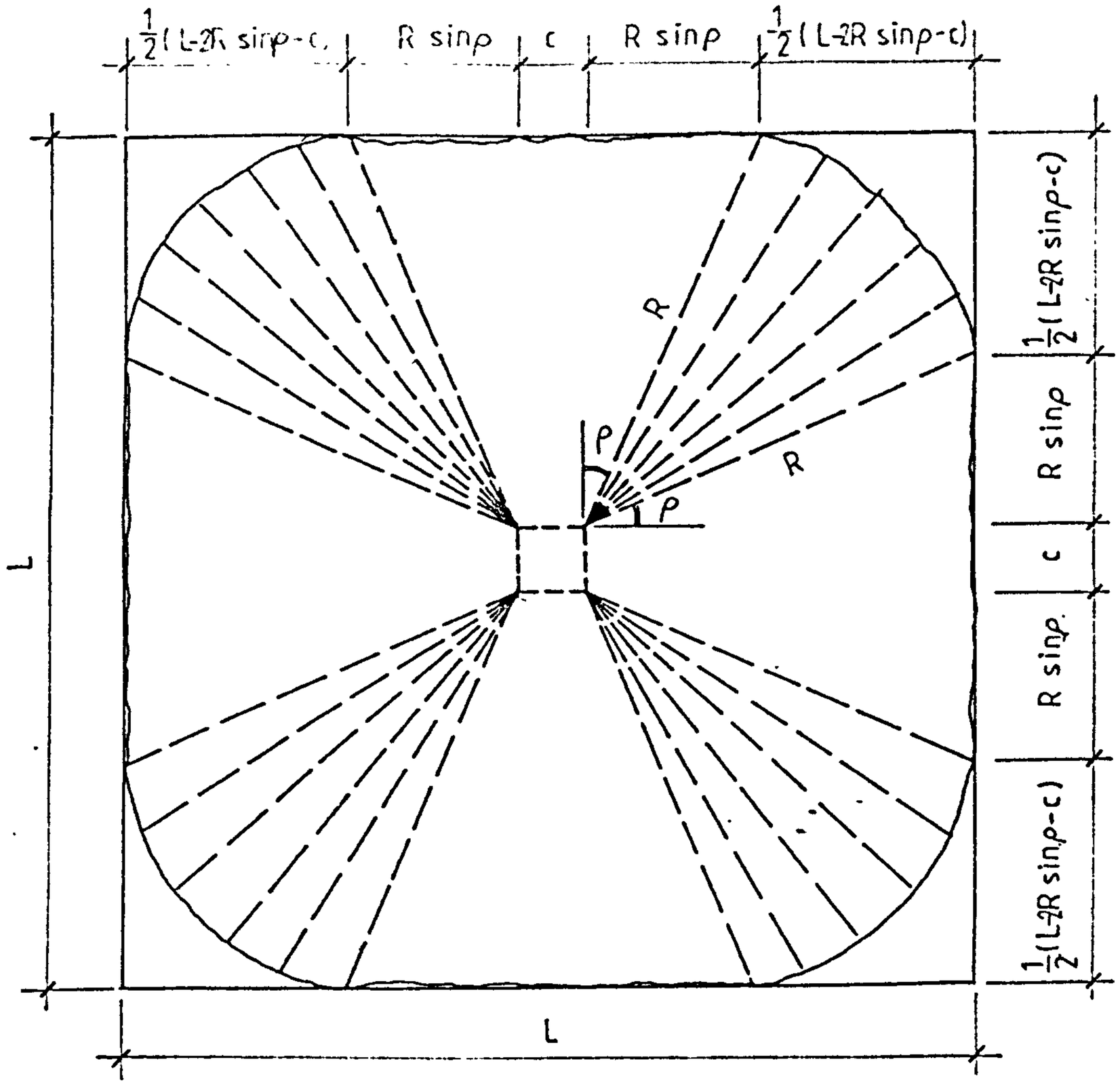

(a) Yield line pattern

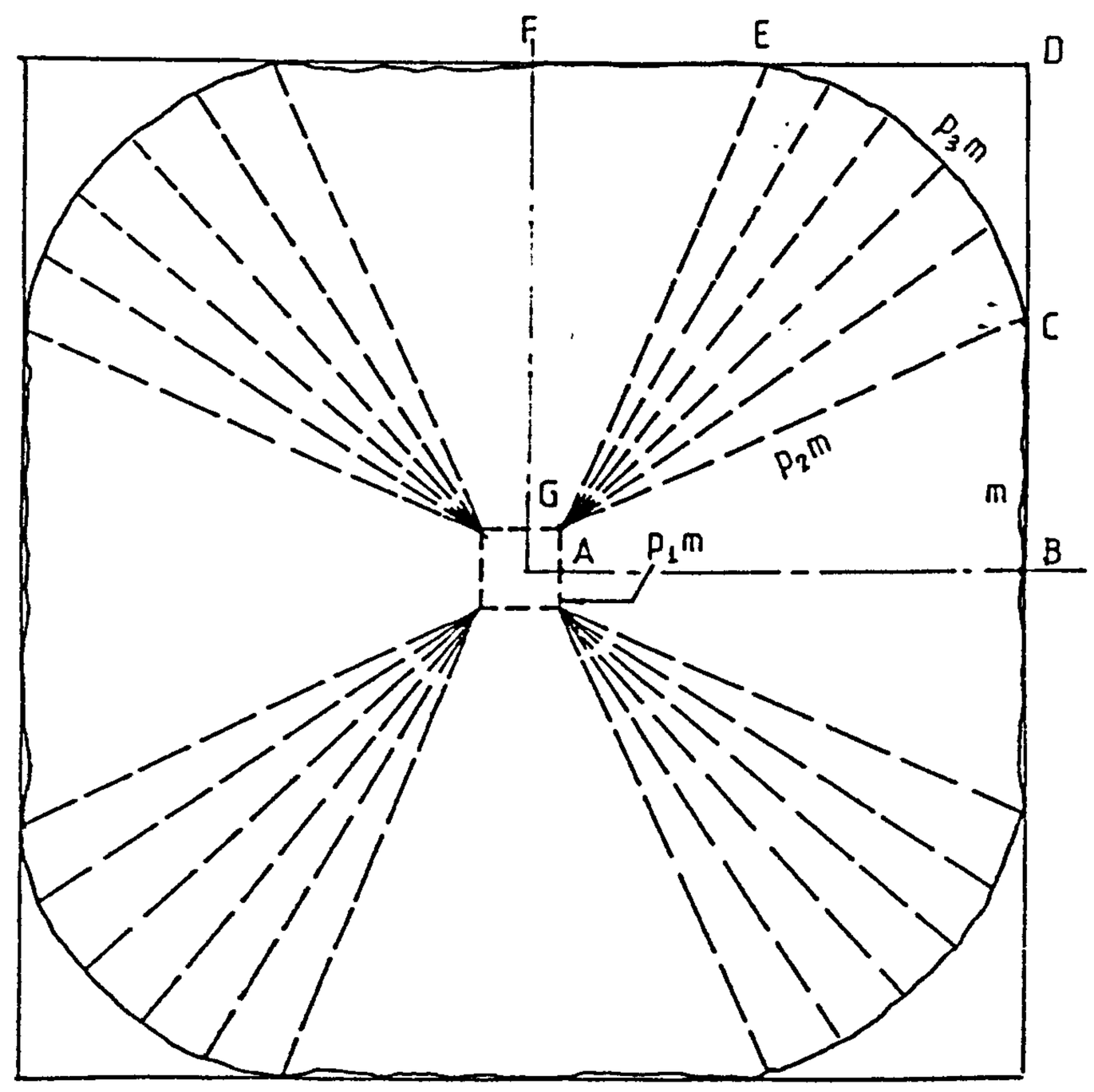

(b) Moments of resistance

Fig. 7.6 Mode of failure with partial circular corner fan

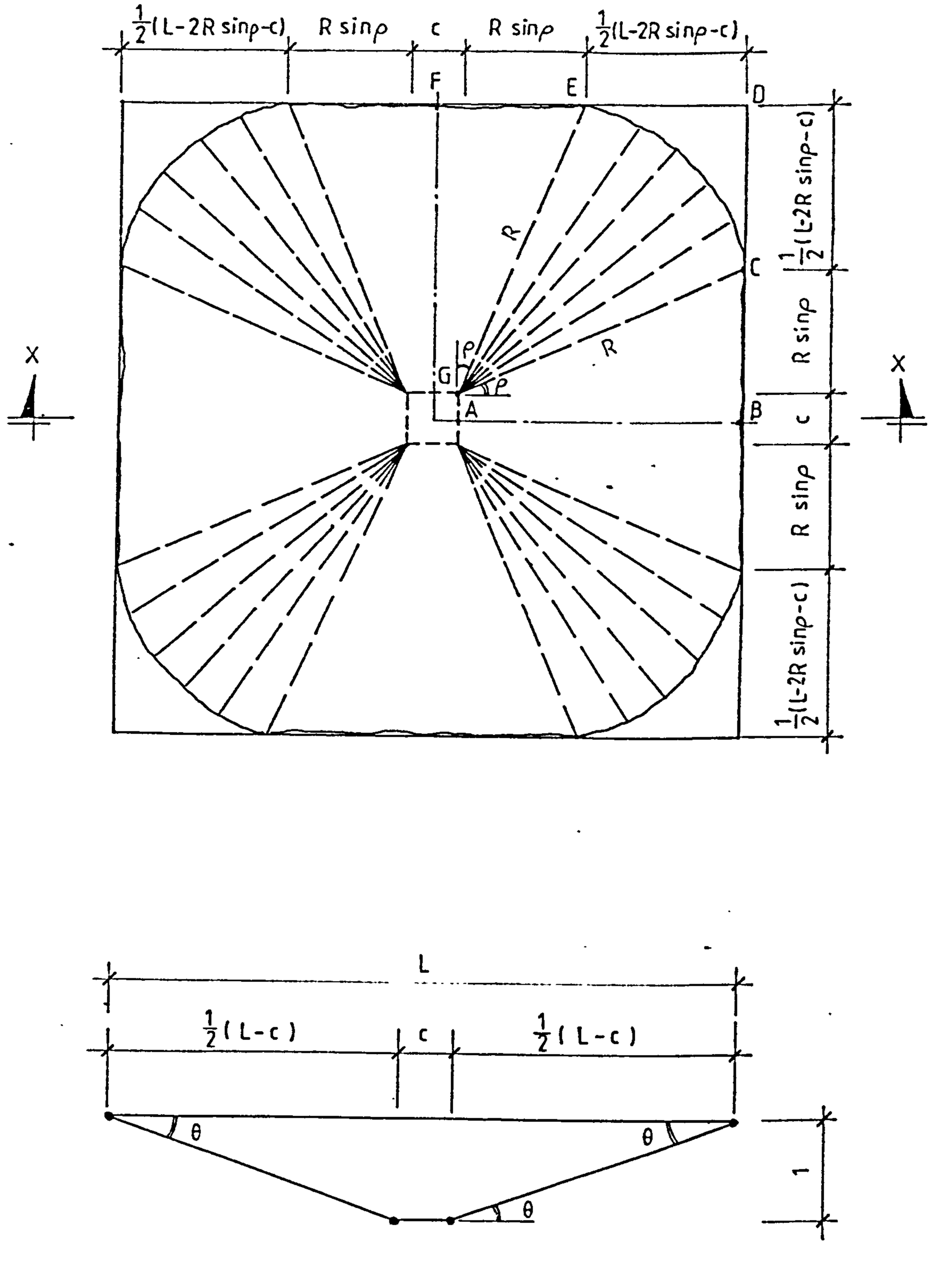

Section X-X

Fig. 7.7 Displacements and rotations
(partial circular corner fan)

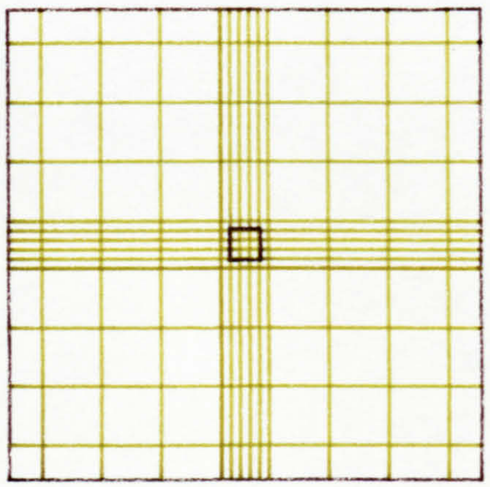

Slab A1

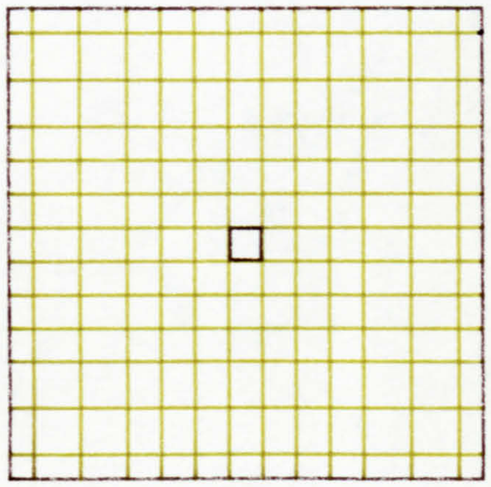

Slab A2

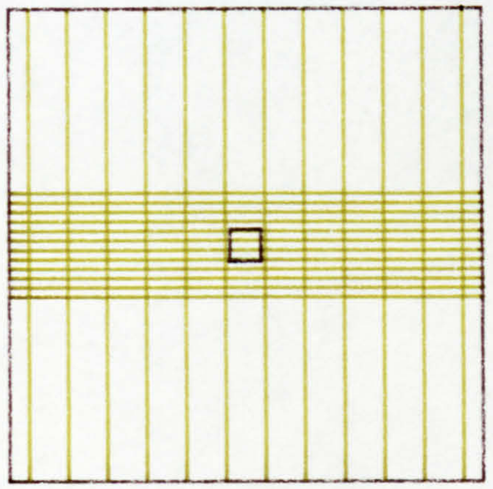

Slab A3

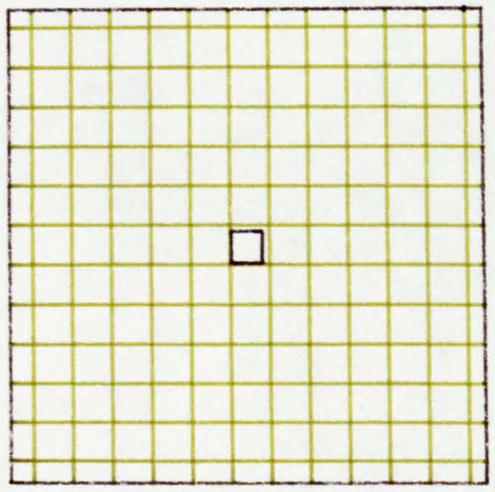

Slab A4

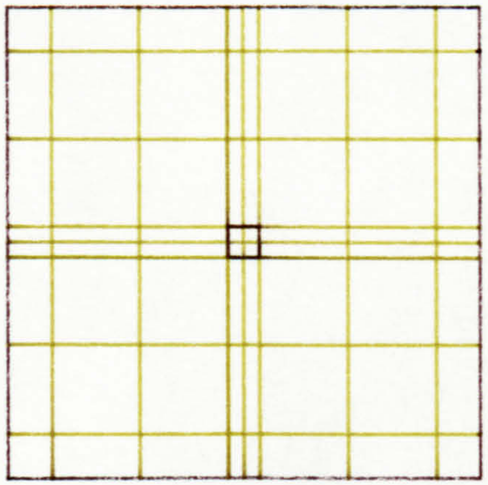

Slab B1

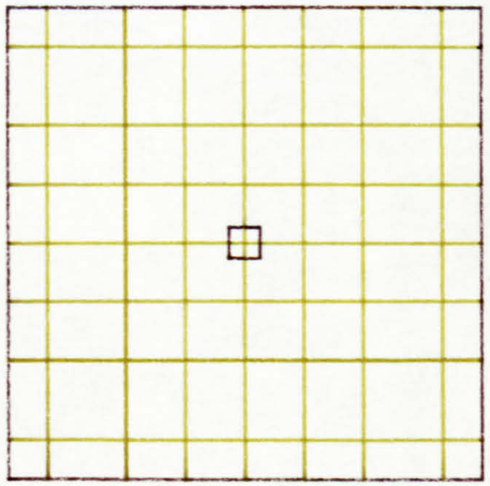

Slab B2

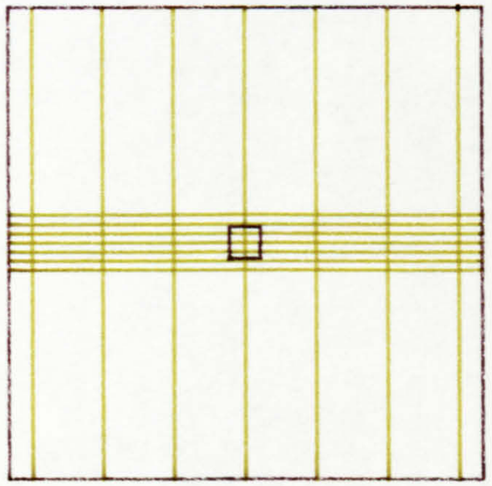

Slab B3

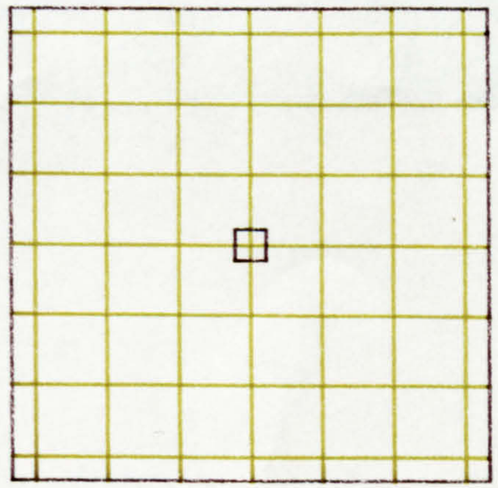

Slab B4

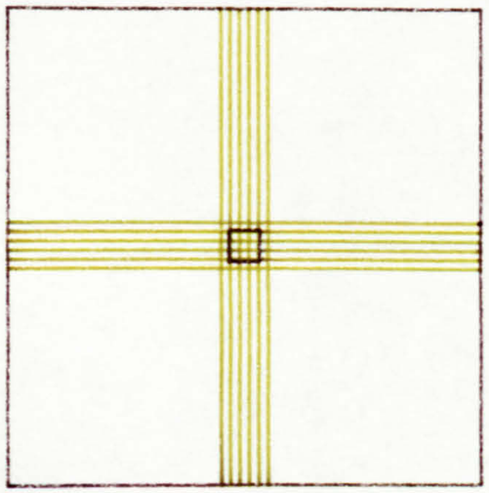

Slab C1

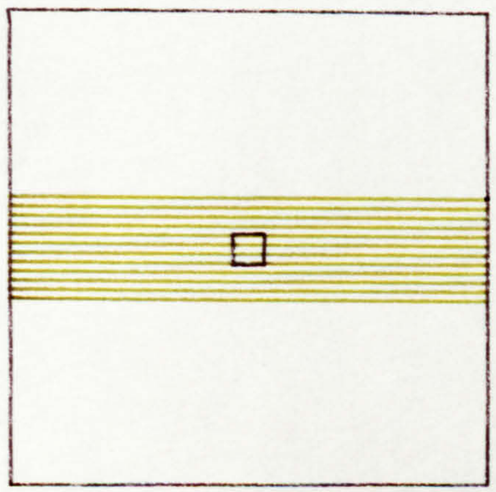

Slab C2

Fig. 8.1 Summary of tendon arrangements in test series

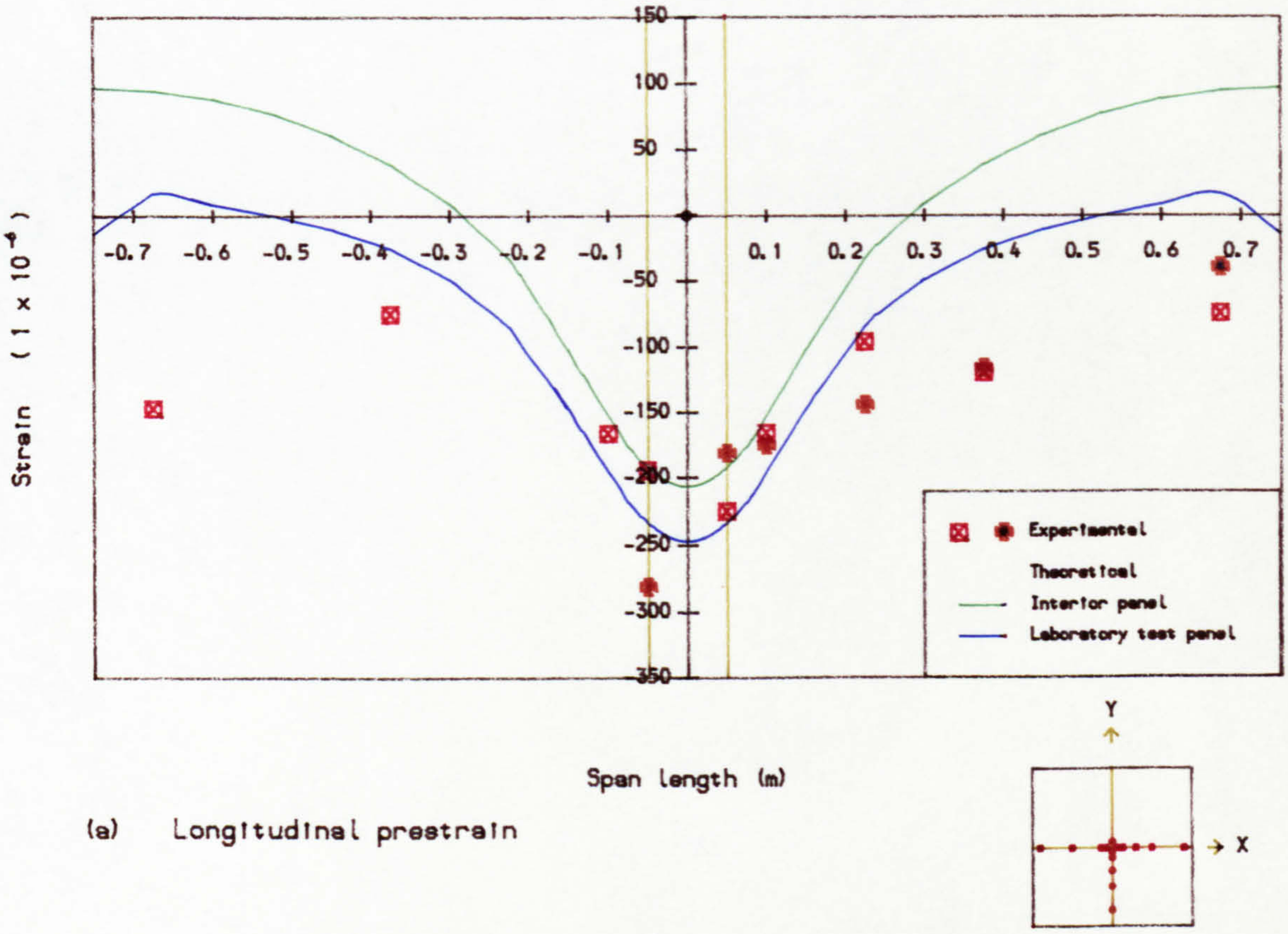

(a) Longitudinal prestrain

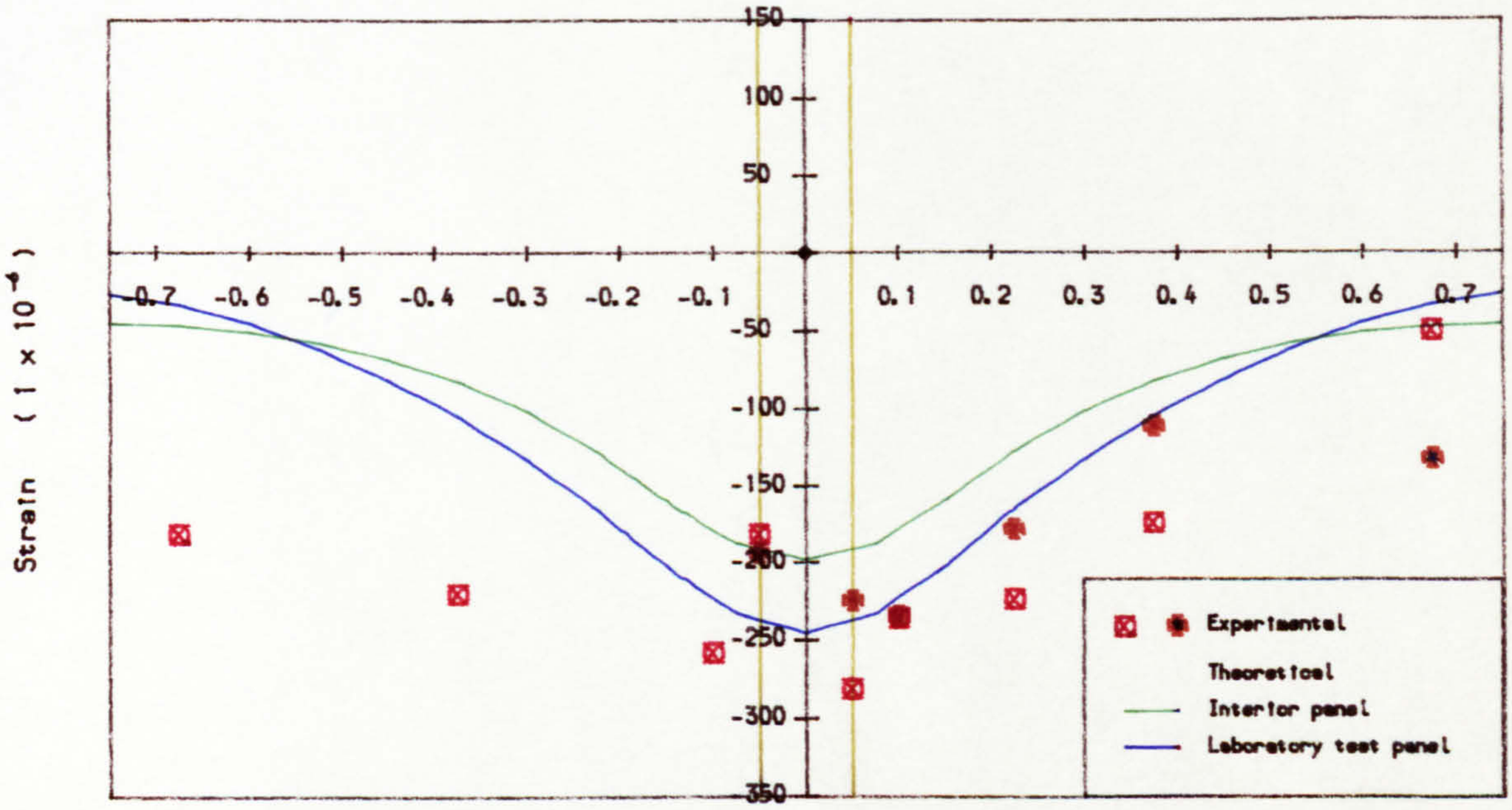

(b) Transverse prestrain

Fig. 8.2 Soffit strain across slab centre line due to full prestress, Slab A1

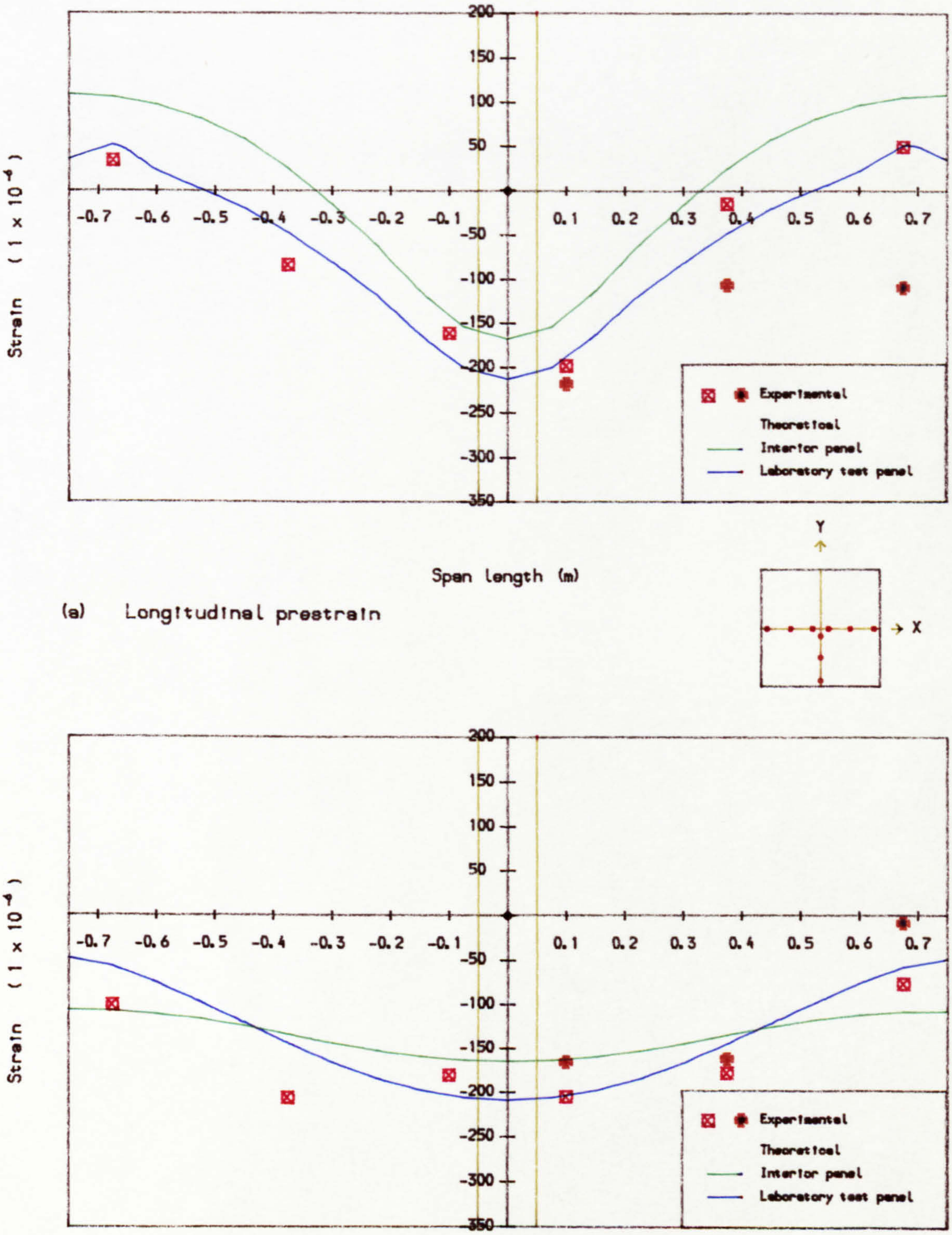

(a) Longitudinal prestrain

(b) Transverse prestrain

Fig. 8.3 Soffit strain across slab centre line due to full prestress, Slab A2

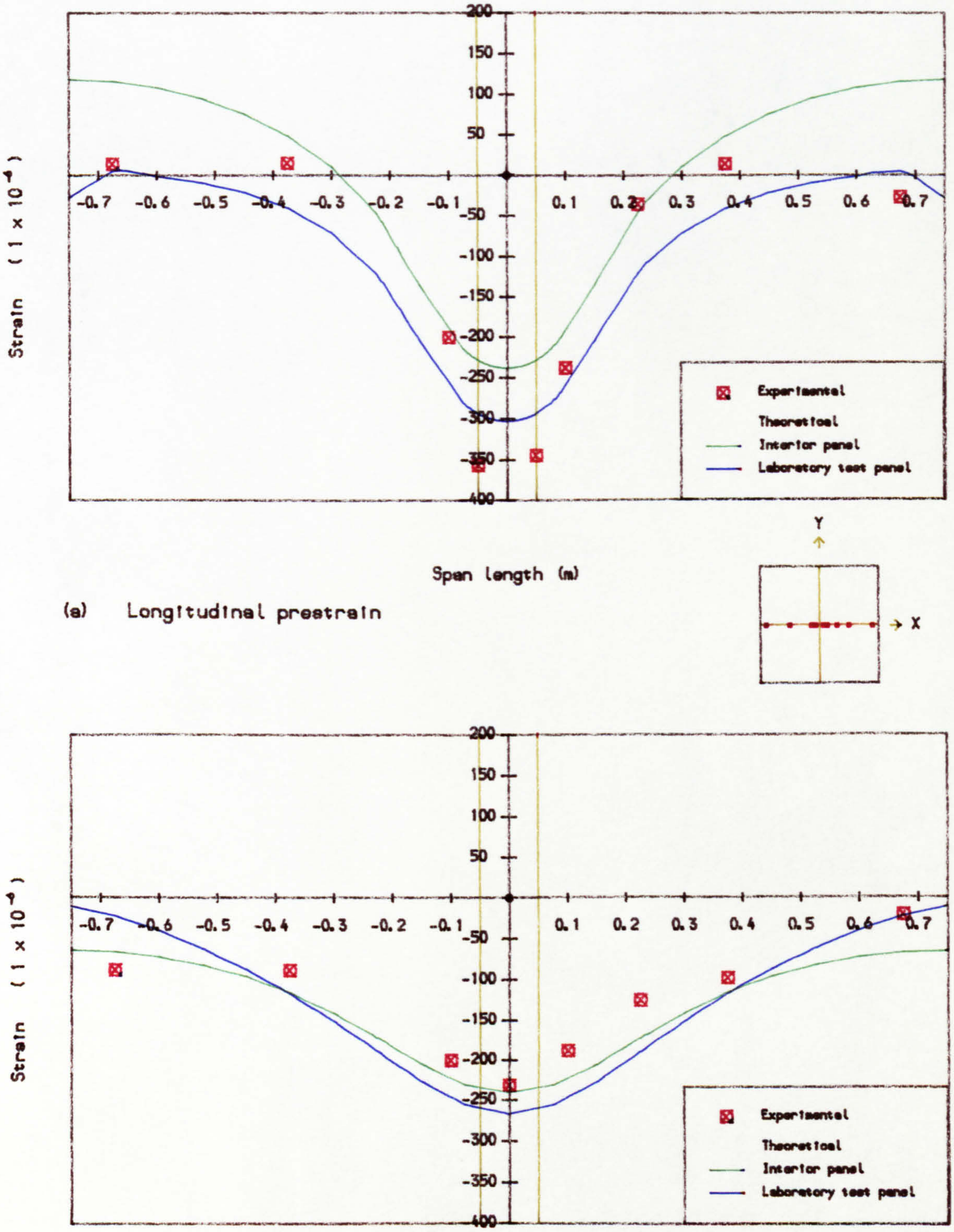

(a) Longitudinal prestrain

(b) Transverse prestrain

Fig. 8.4 Soffit strain across slab centre line due to full prestress, Slab A3

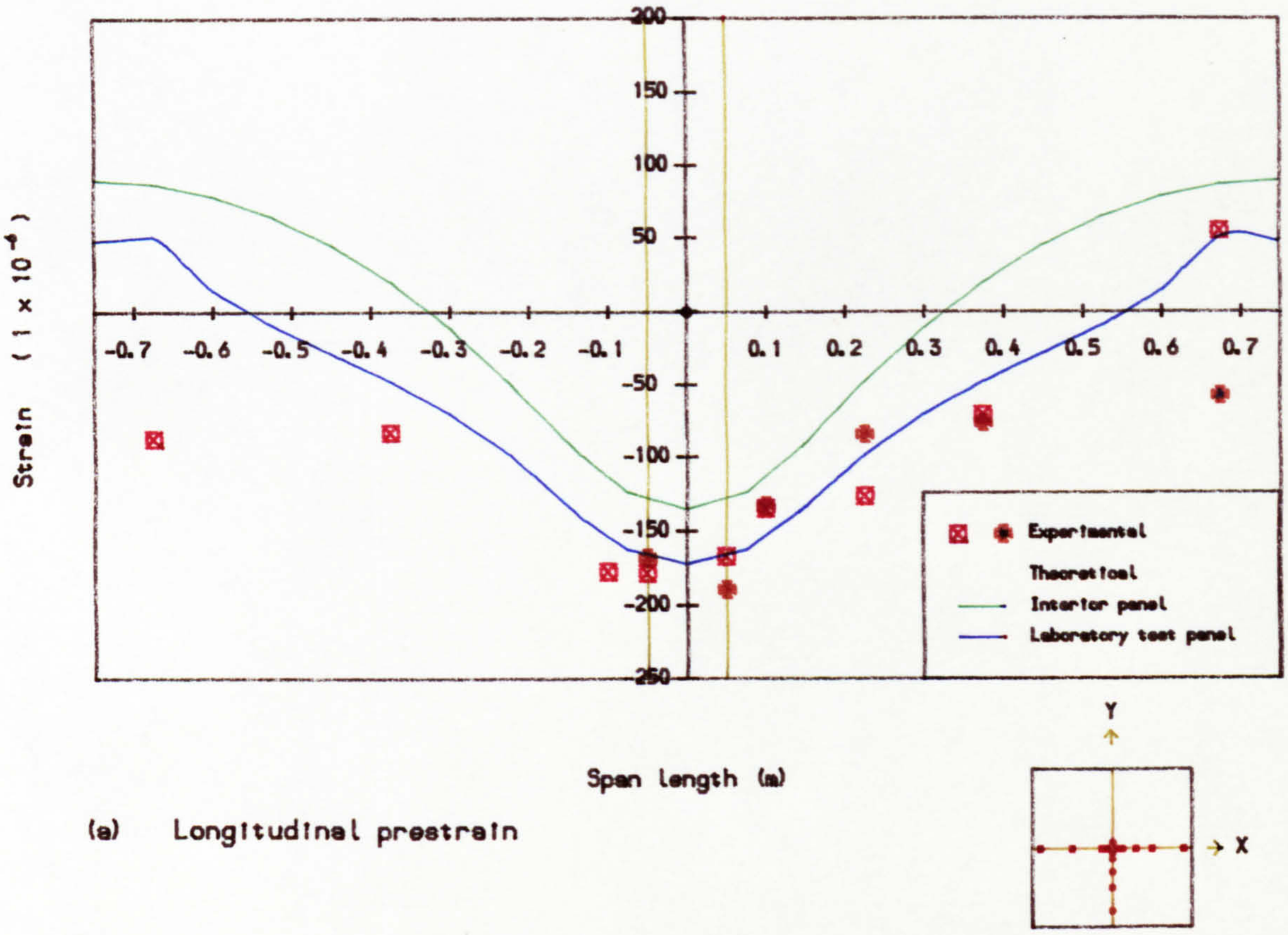

(a) Longitudinal prestrain

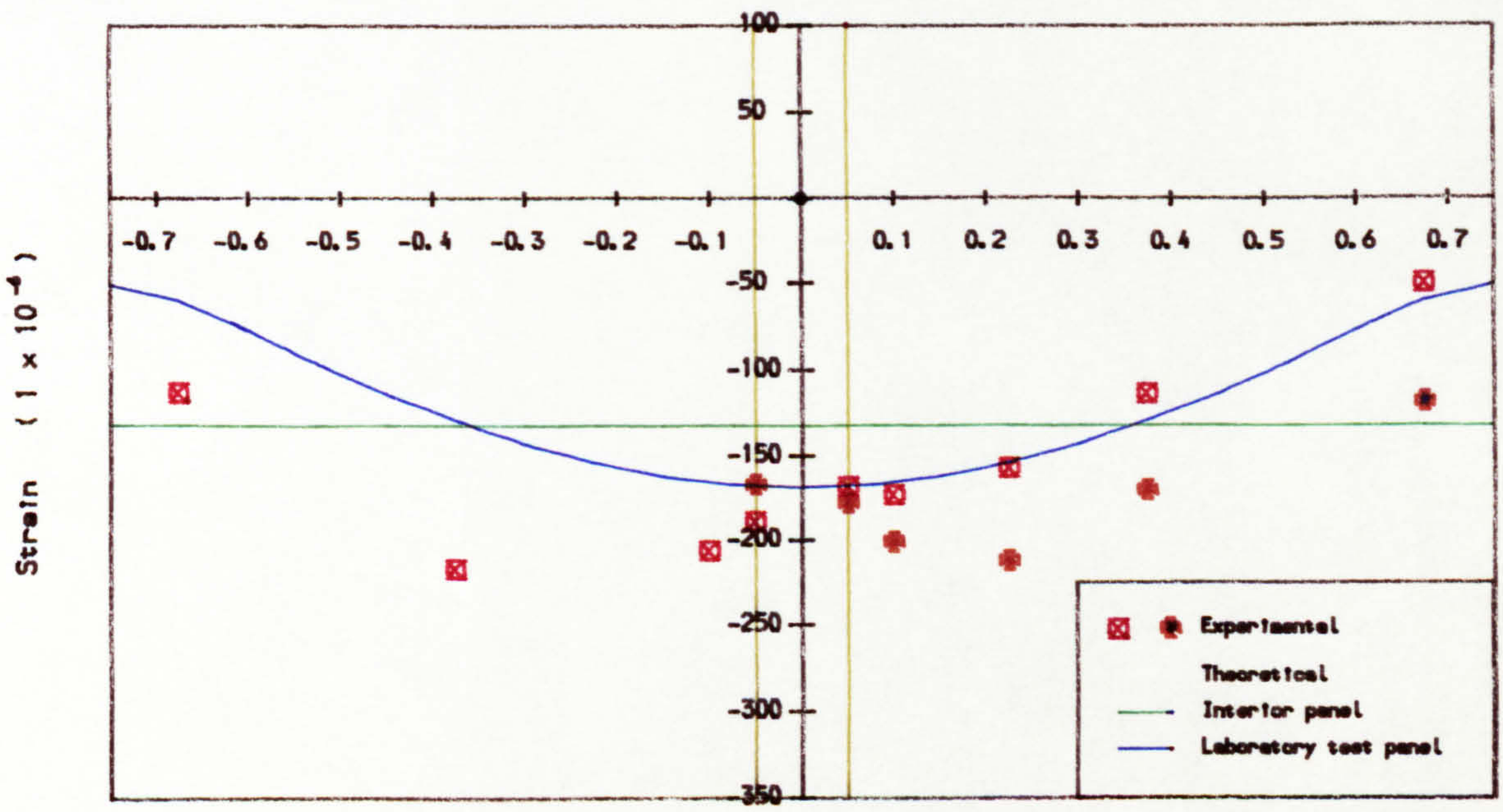

(b) Transverse prestrain

Fig. 8.5 Soffit strain across slab centre line due to full prestress, Slab A4

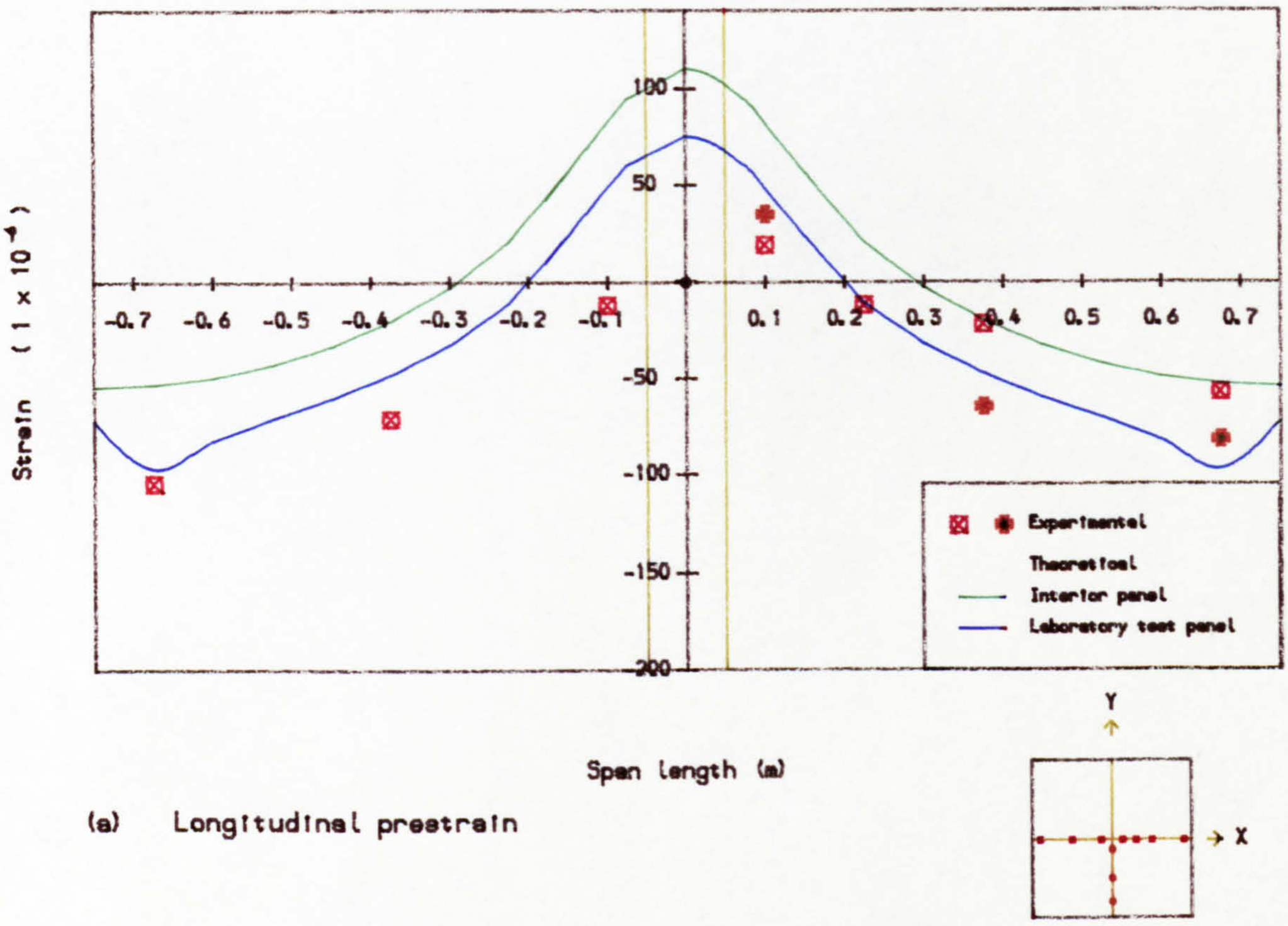

(a) Longitudinal prestrain

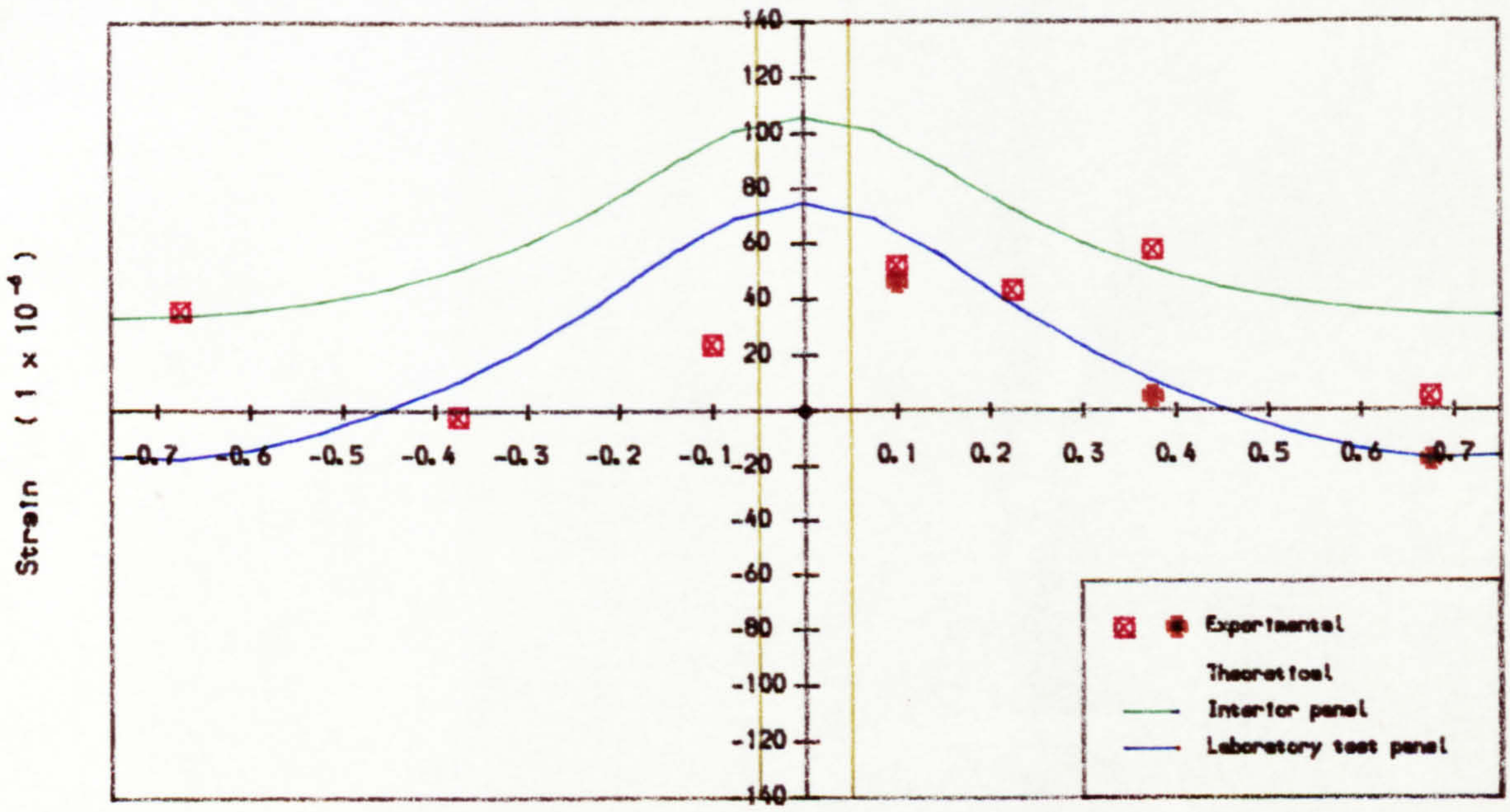

(b) Transverse prestrain

Fig. 8.6 Top surface strain across slab centre line due to full prestress, Slab B1

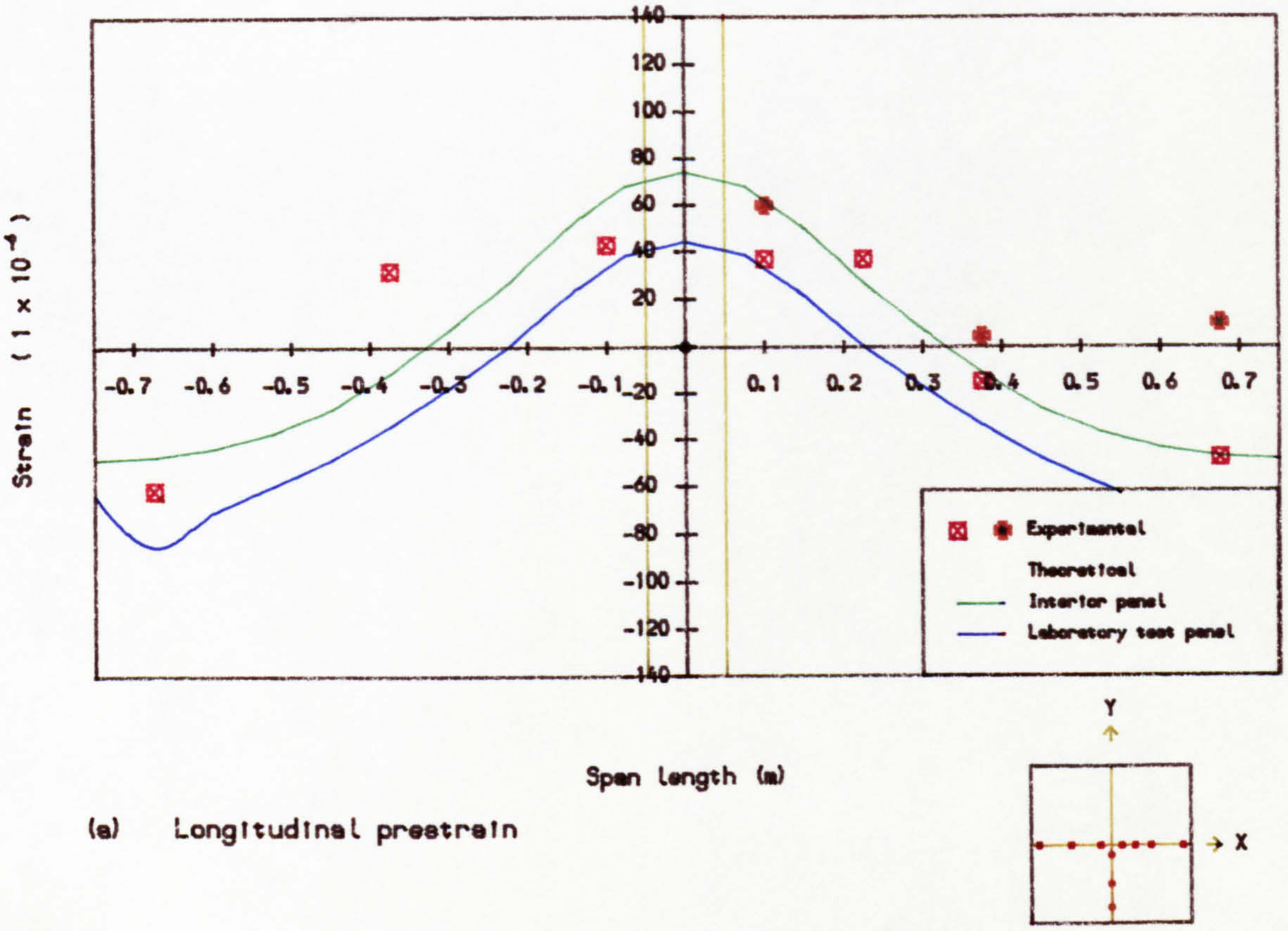

(a) Longitudinal prestrain

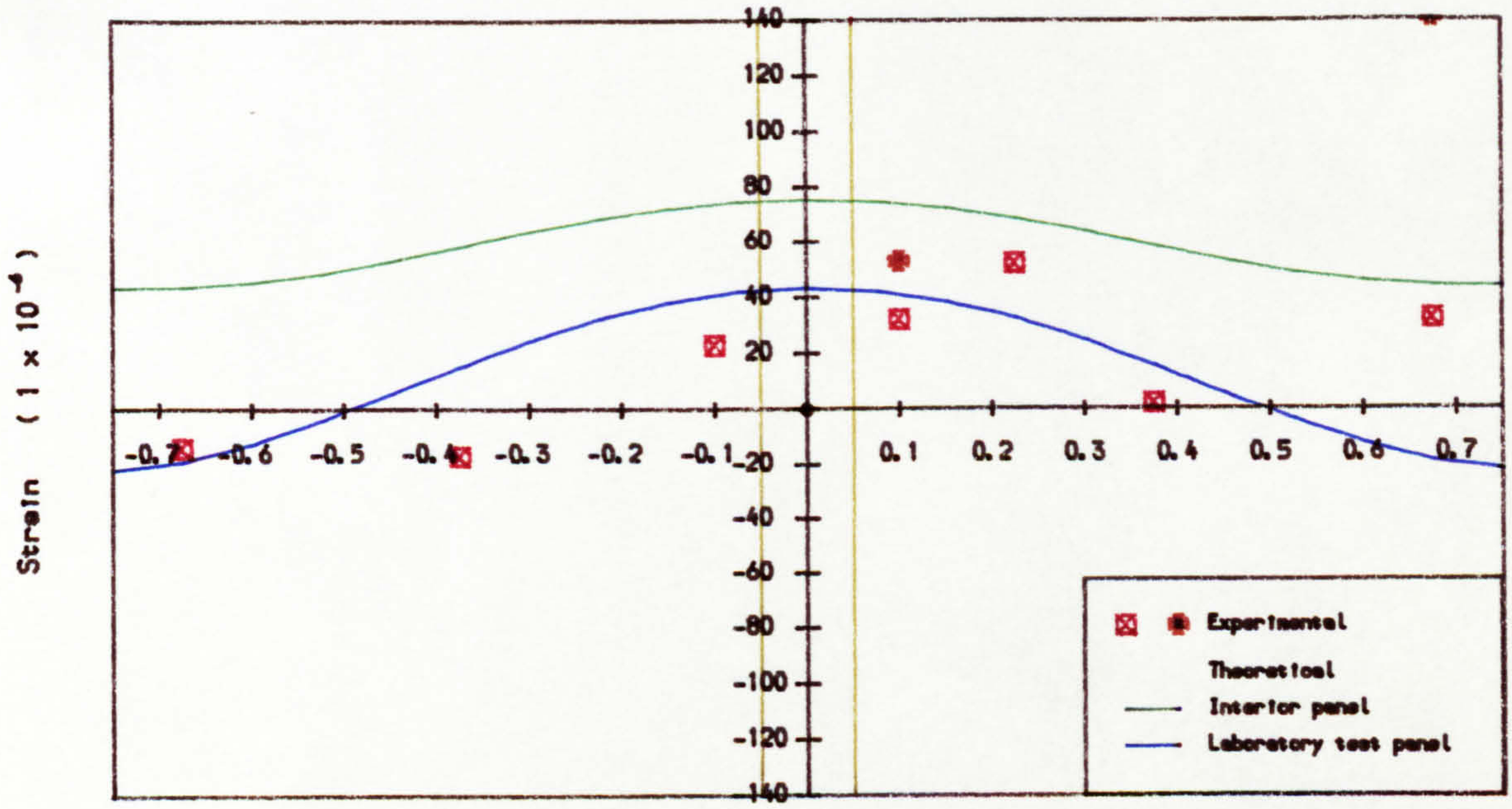

(b) Transverse prestrain

Fig. 8.7 Top surface strain across slab centre line due to full prestress, Slab B2

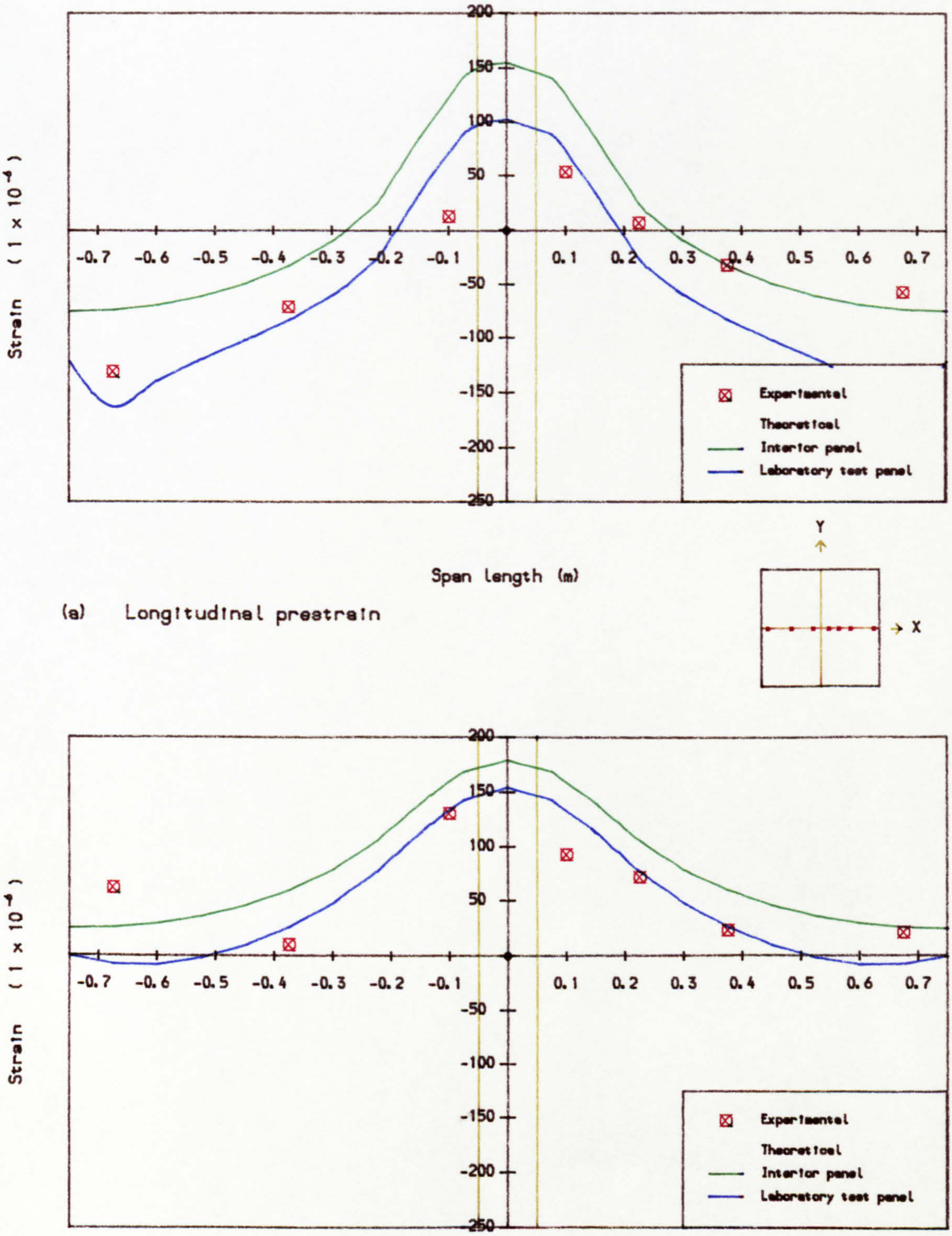

(a) Longitudinal prestrain

(b) Transverse prestrain

Fig. 8.8 Top surface strain across slab centre line due to full prestress, Slab B3

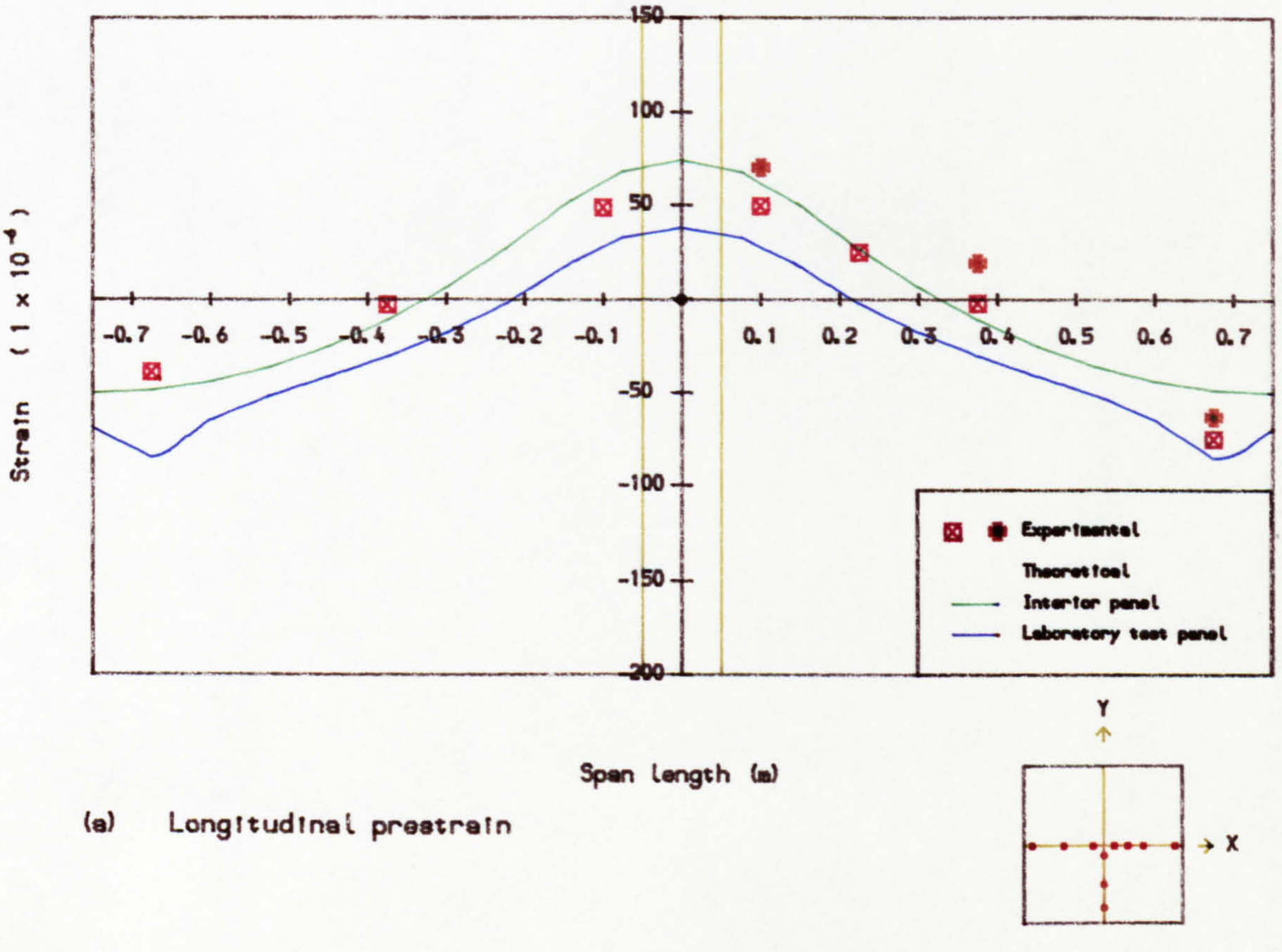

(a) Longitudinal prestrain

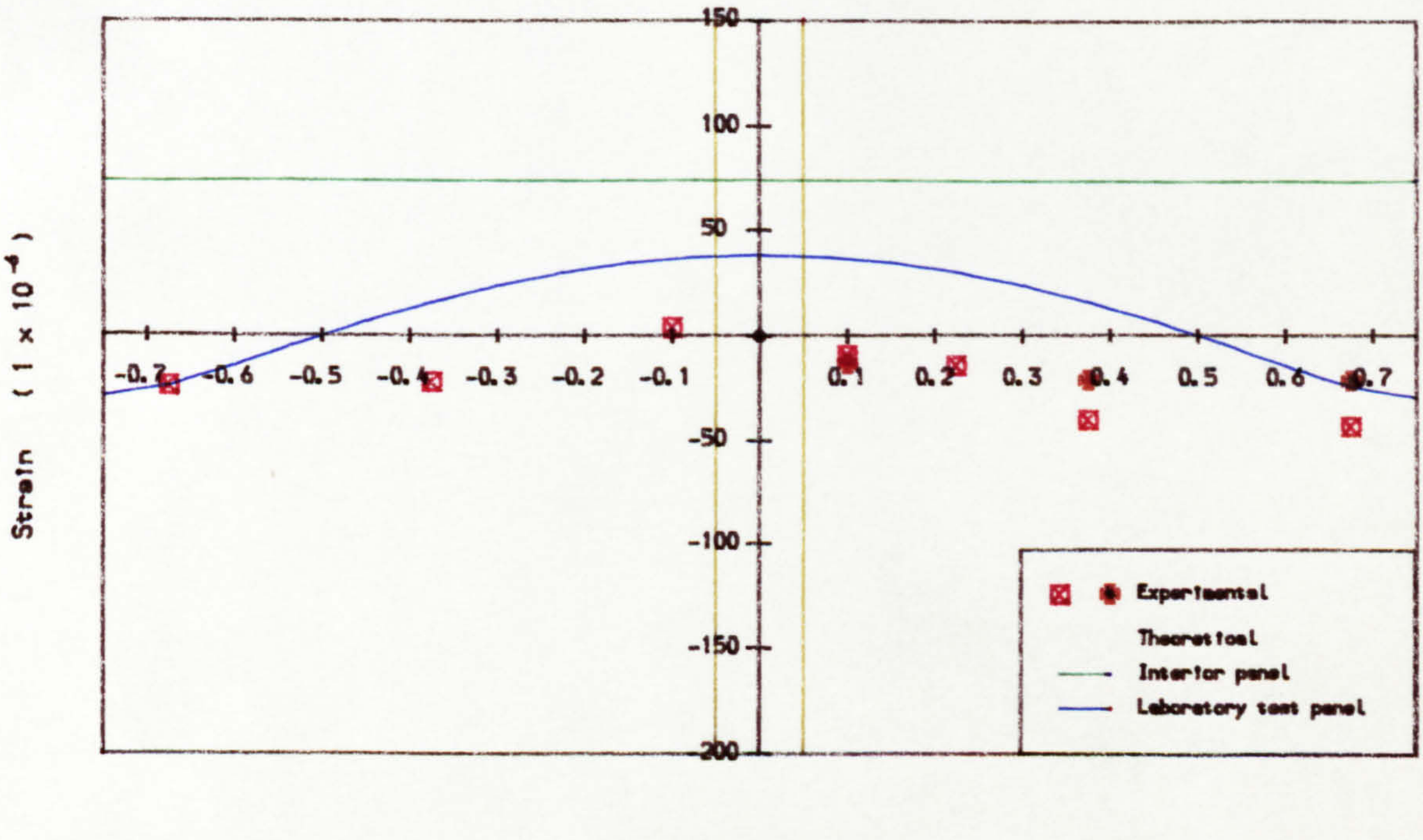

(b) Transverse prestrain

Fig. 8.9 Top surface strain across slab centre line due to full prestress, Slab B4

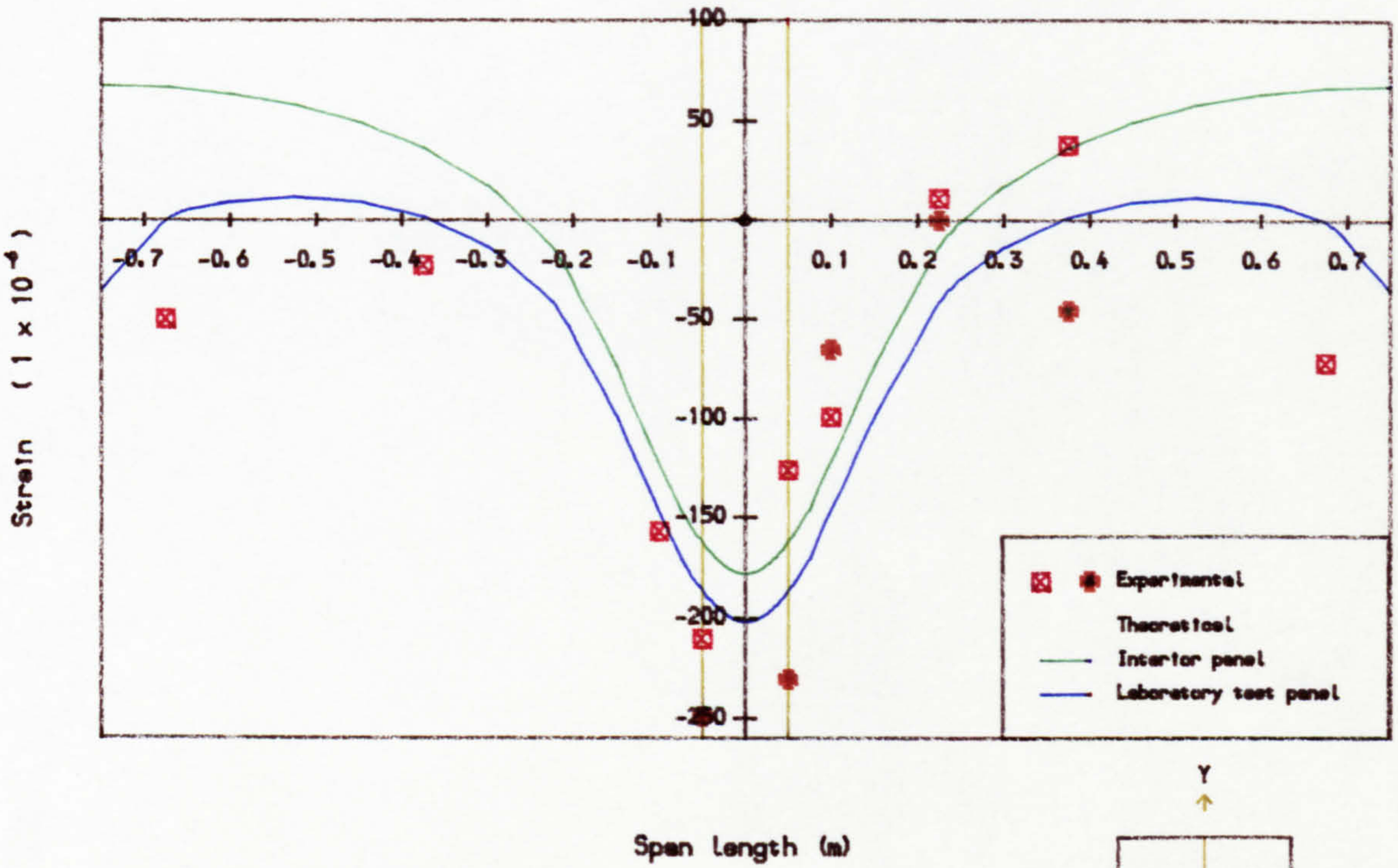

(a) Longitudinal prestrain

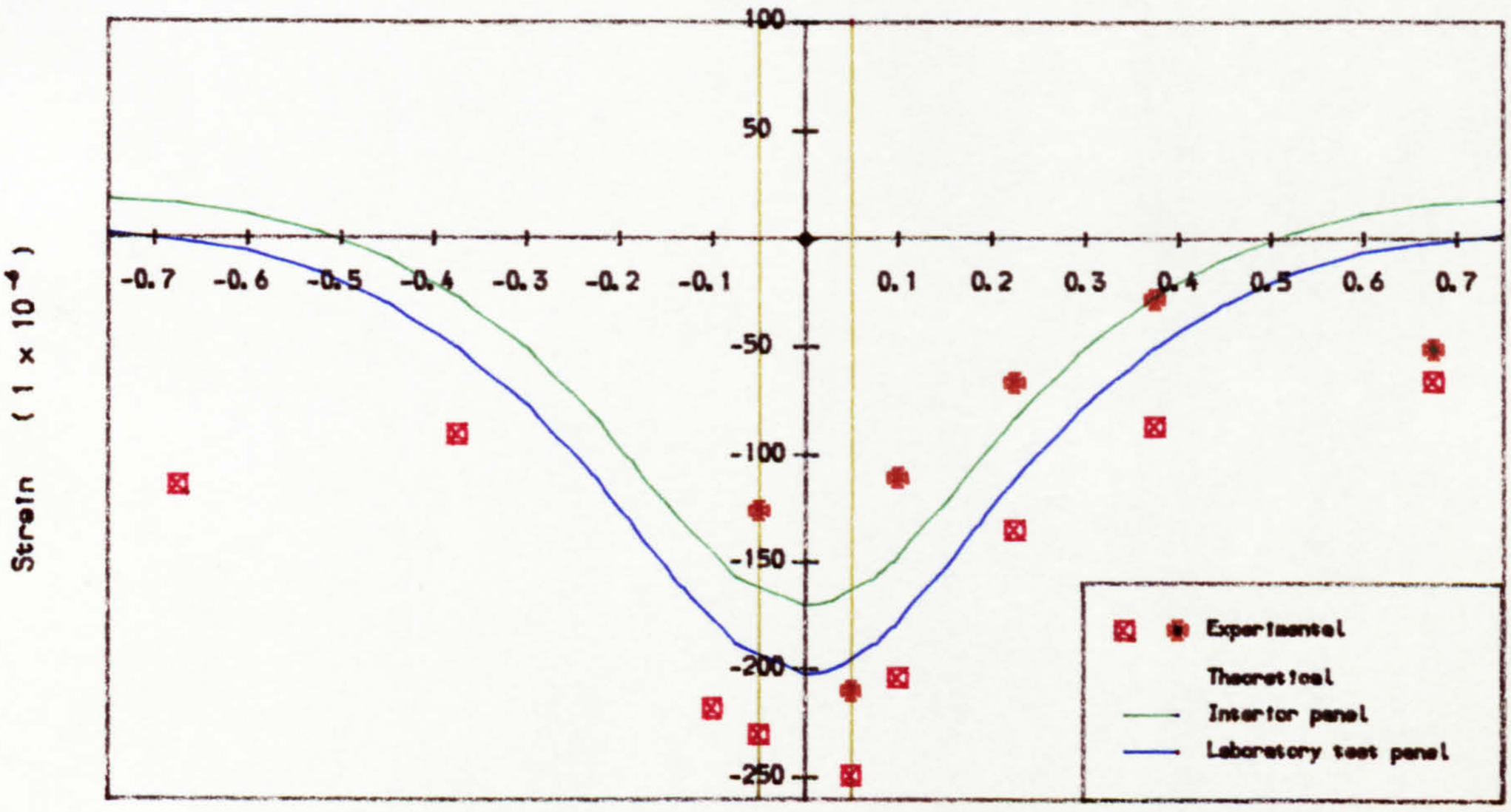

(b) Transverse prestrain

Fig. 8.10 Soffit strain across slab centre line due to full prestress, Slab C1

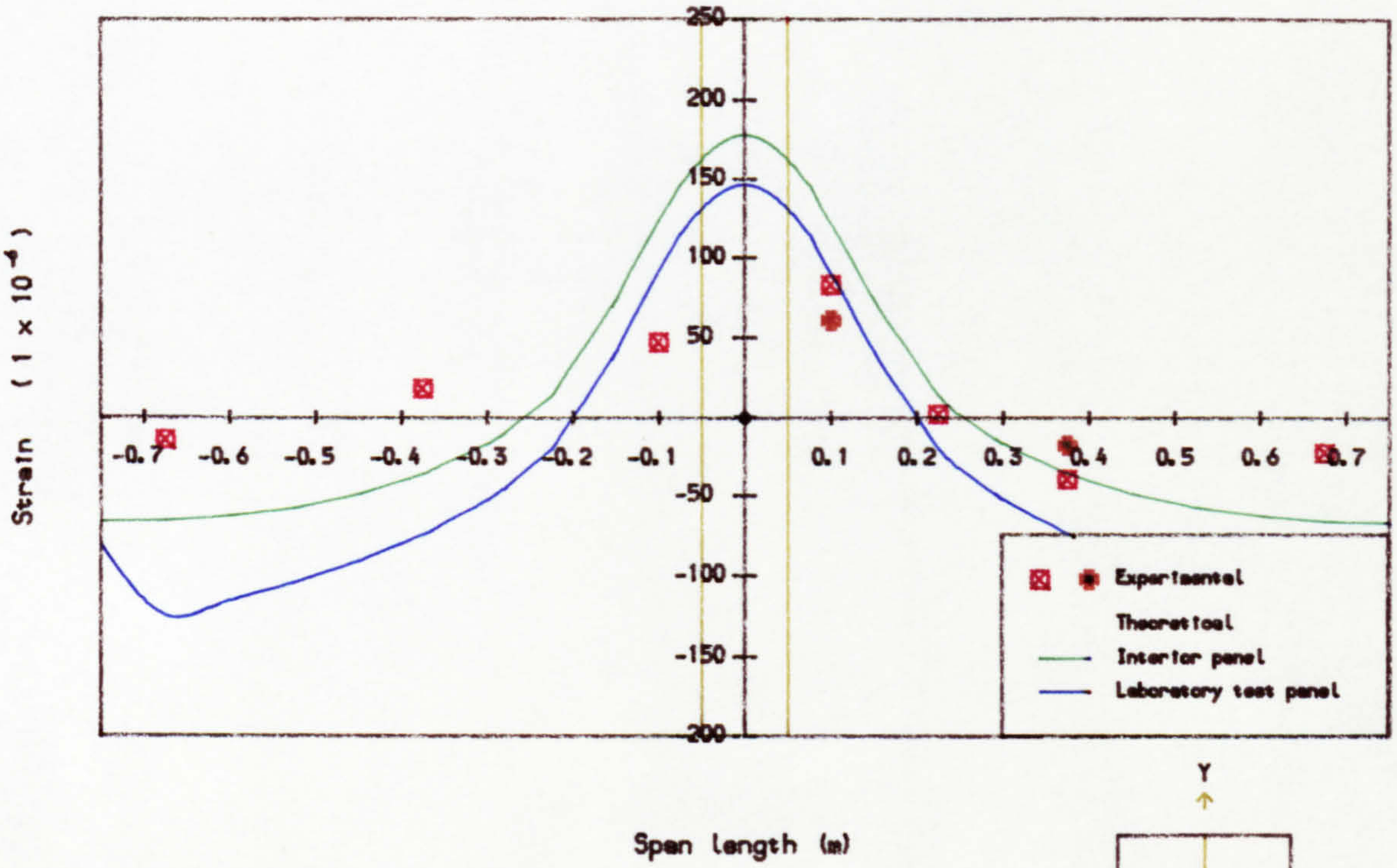

(a) Longitudinal prestrain

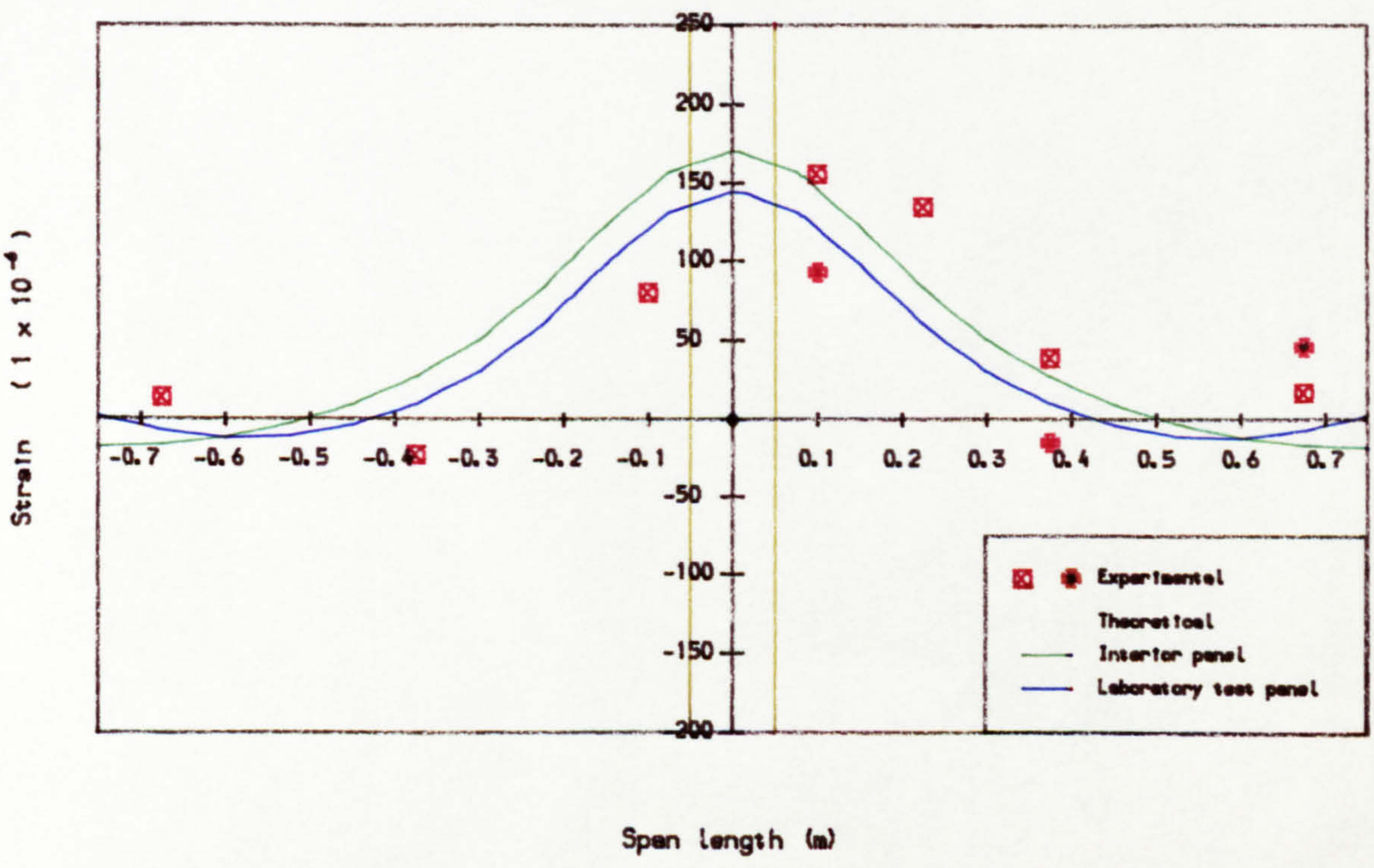

(b) Transverse prestrain

Fig. 8.11 Top surface strain across slab centre line due to full prestress, Slab C1

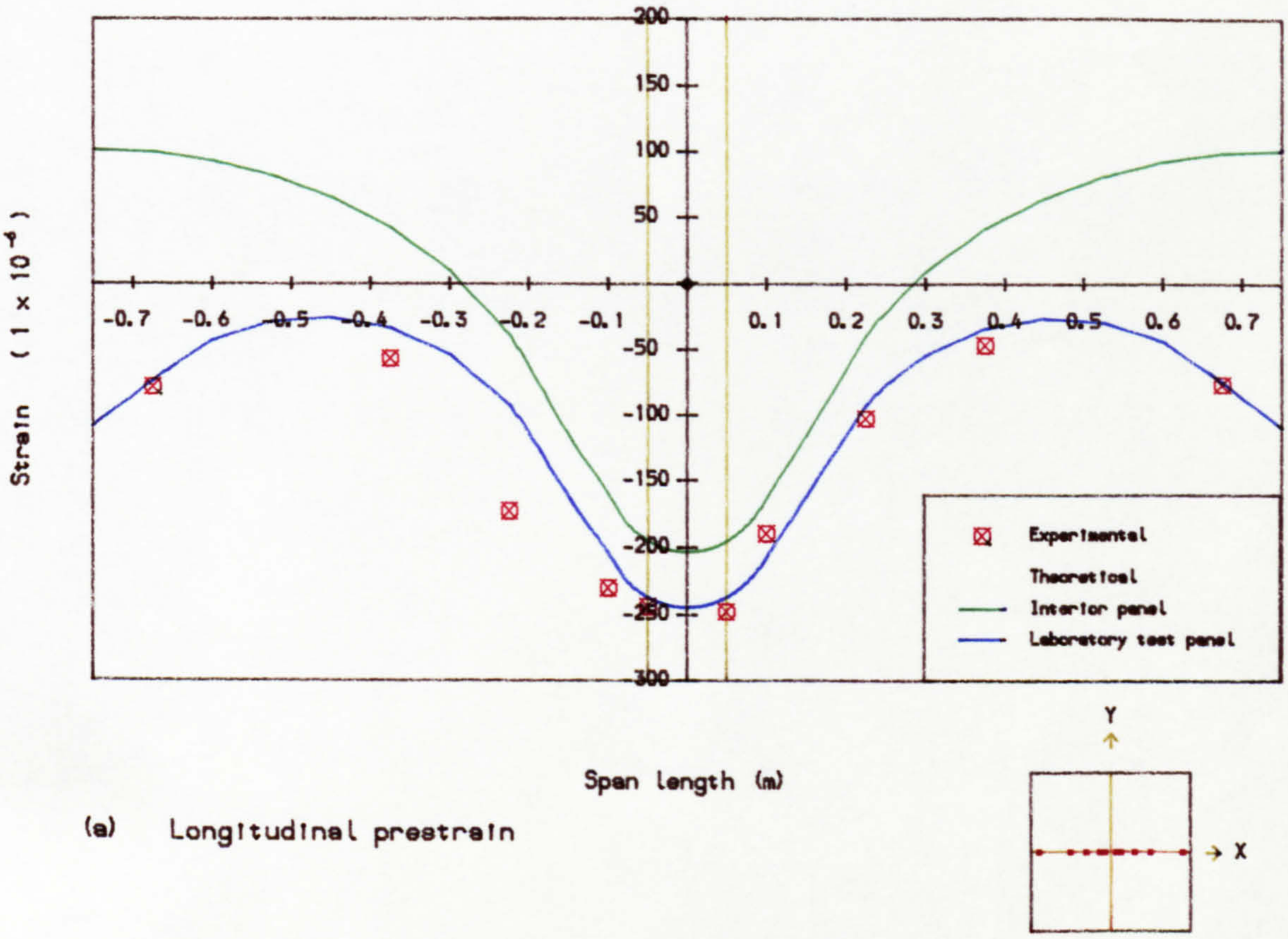

(a) Longitudinal prestrain

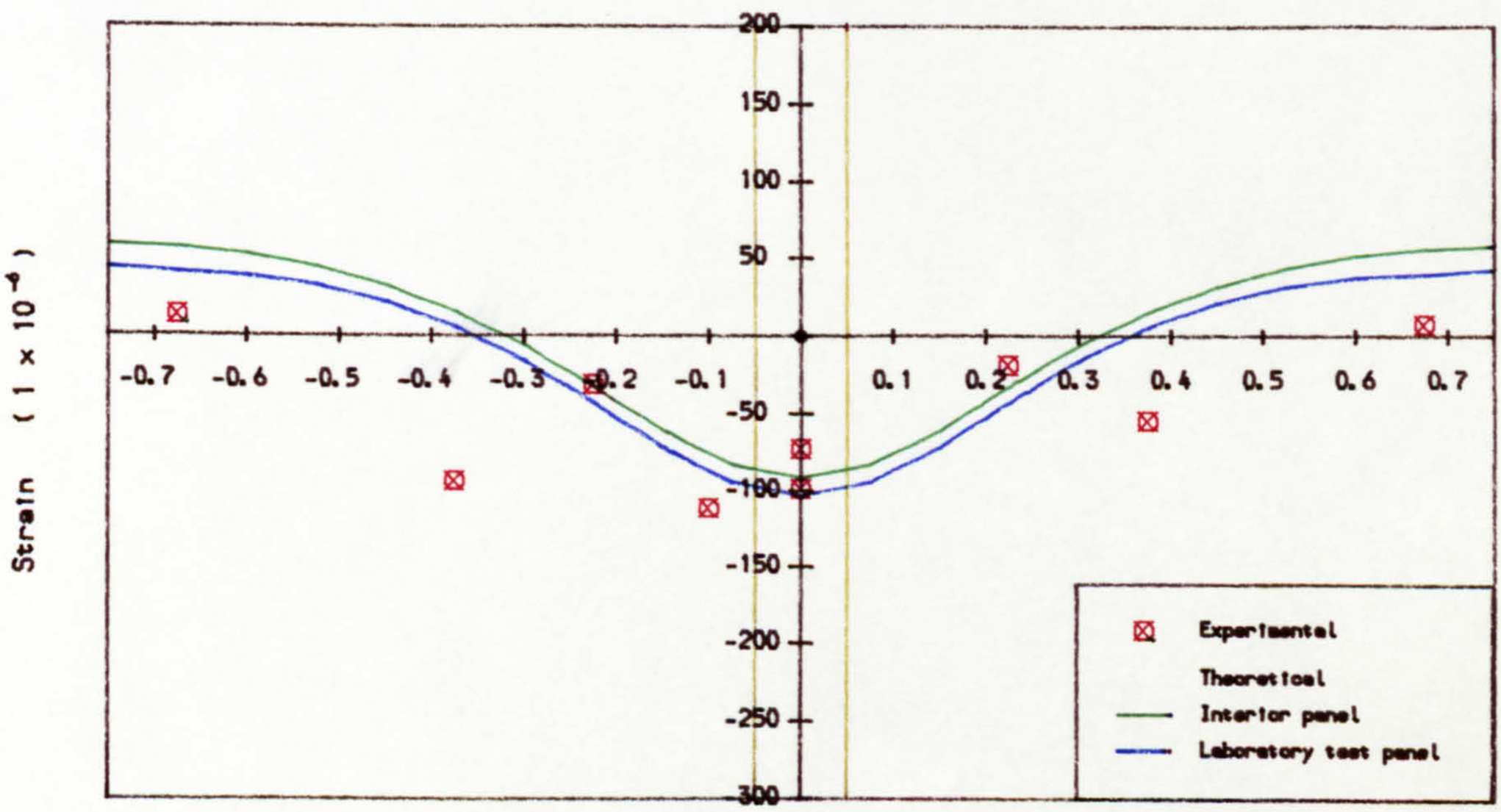

(b) Transverse prestrain

Fig. 8.12 Soffit strain across slab centre line due to full prestress, Slab C2

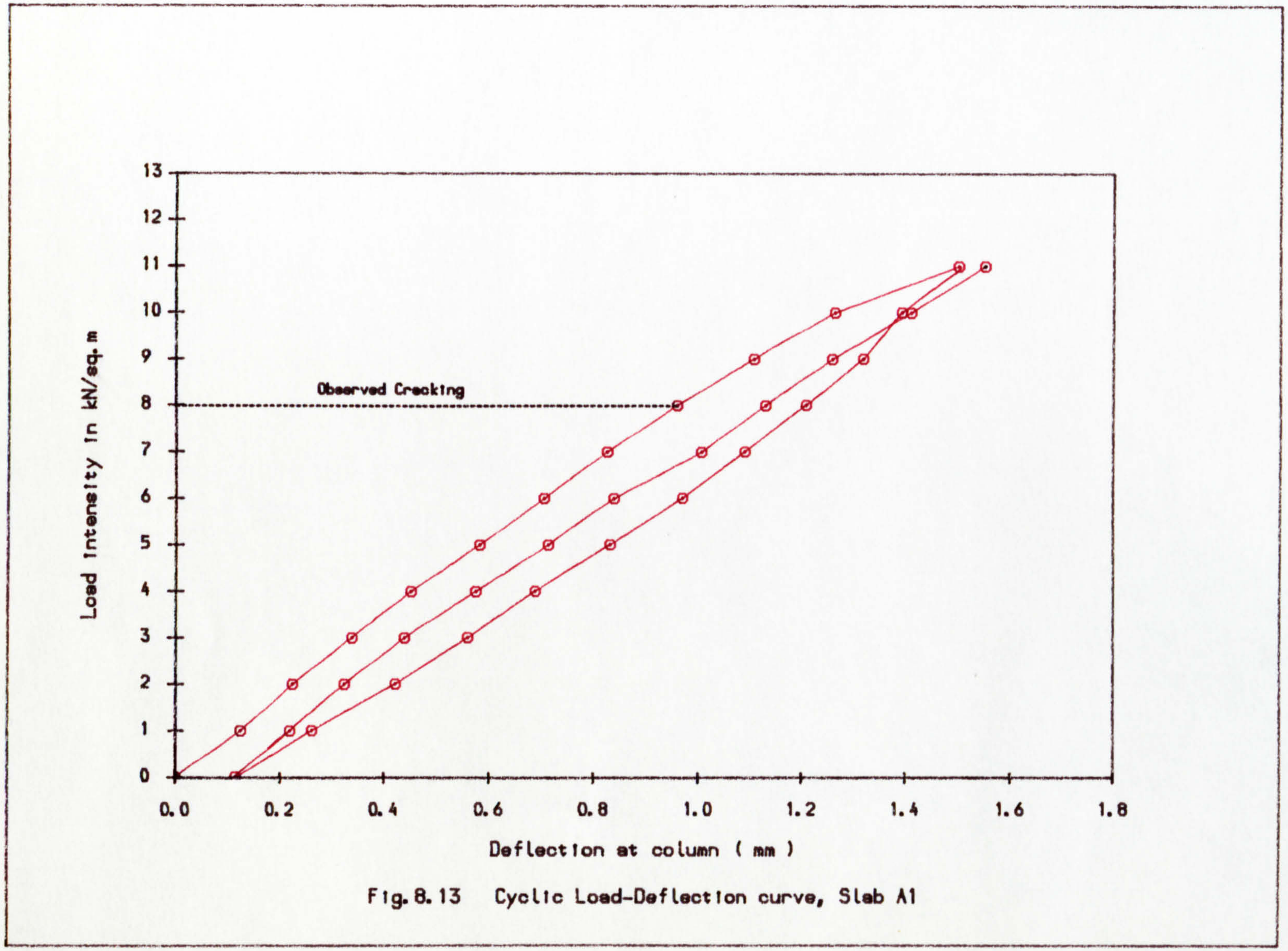

Fig. 8.13 Cyclic Load-Deflection curve, Slab A1

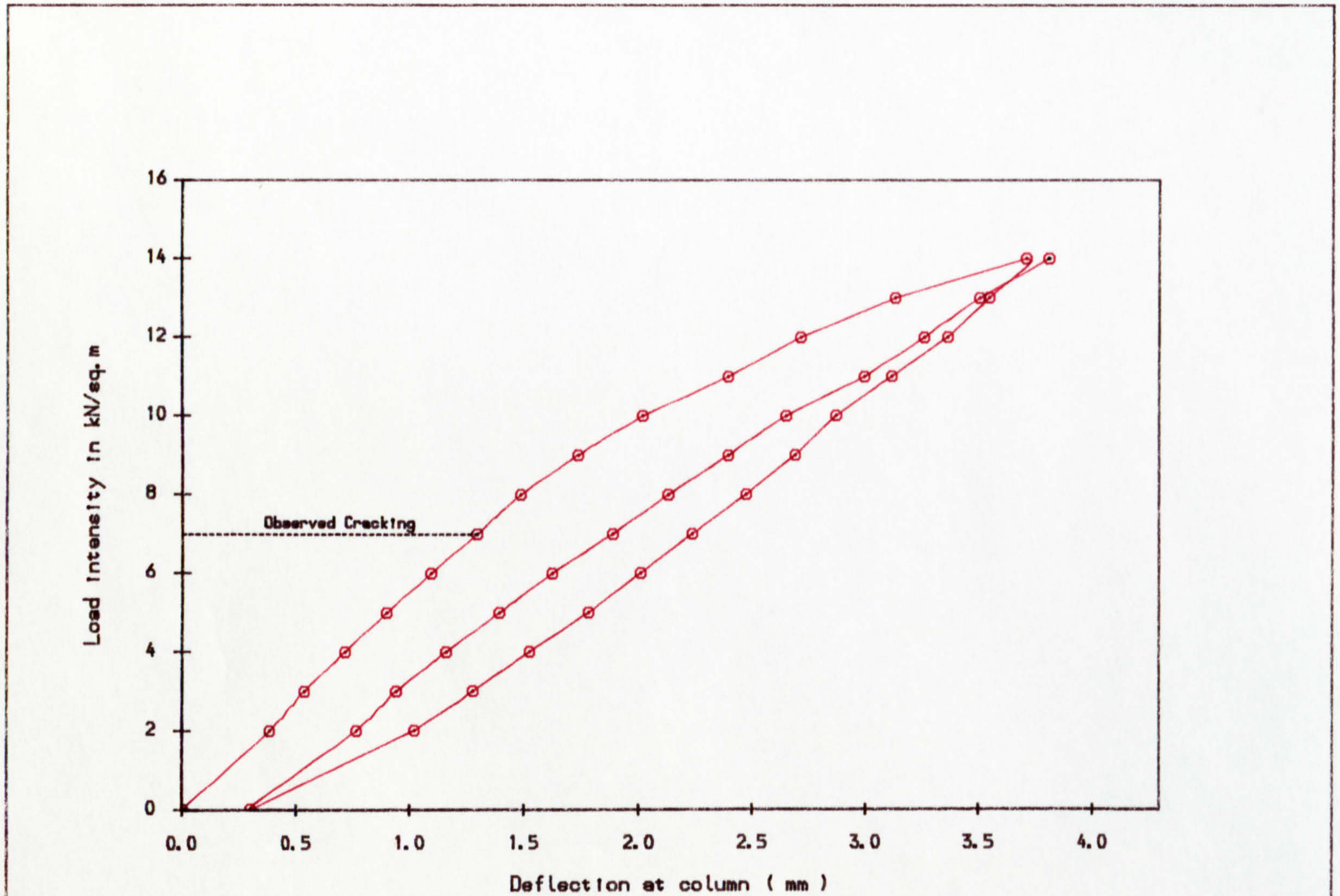

Fig. 8.14 Cyclic Load-Deflection curve, Slab A2

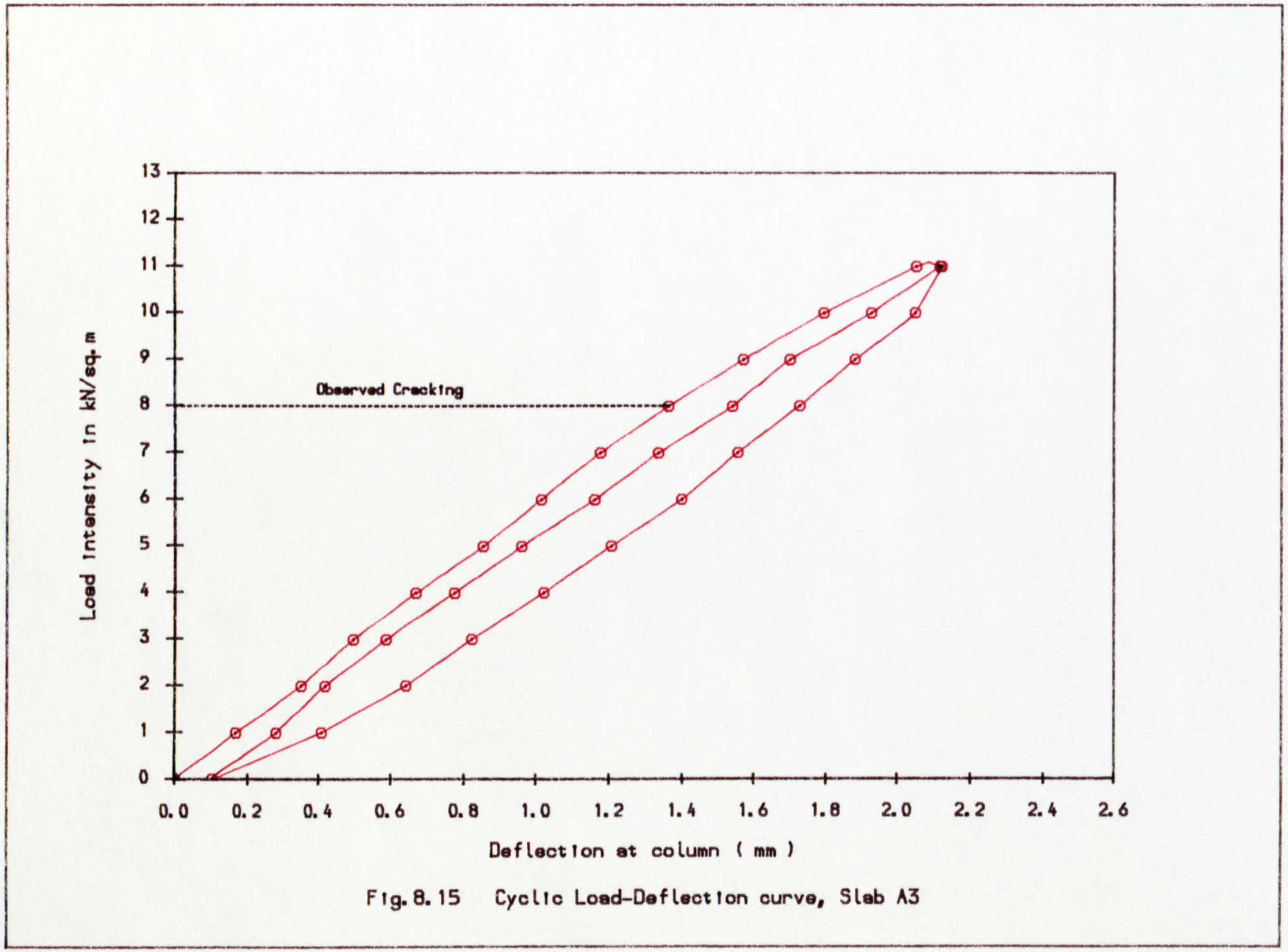

Fig. 8.15 Cyclic Load-Deflection curve, Slab A3

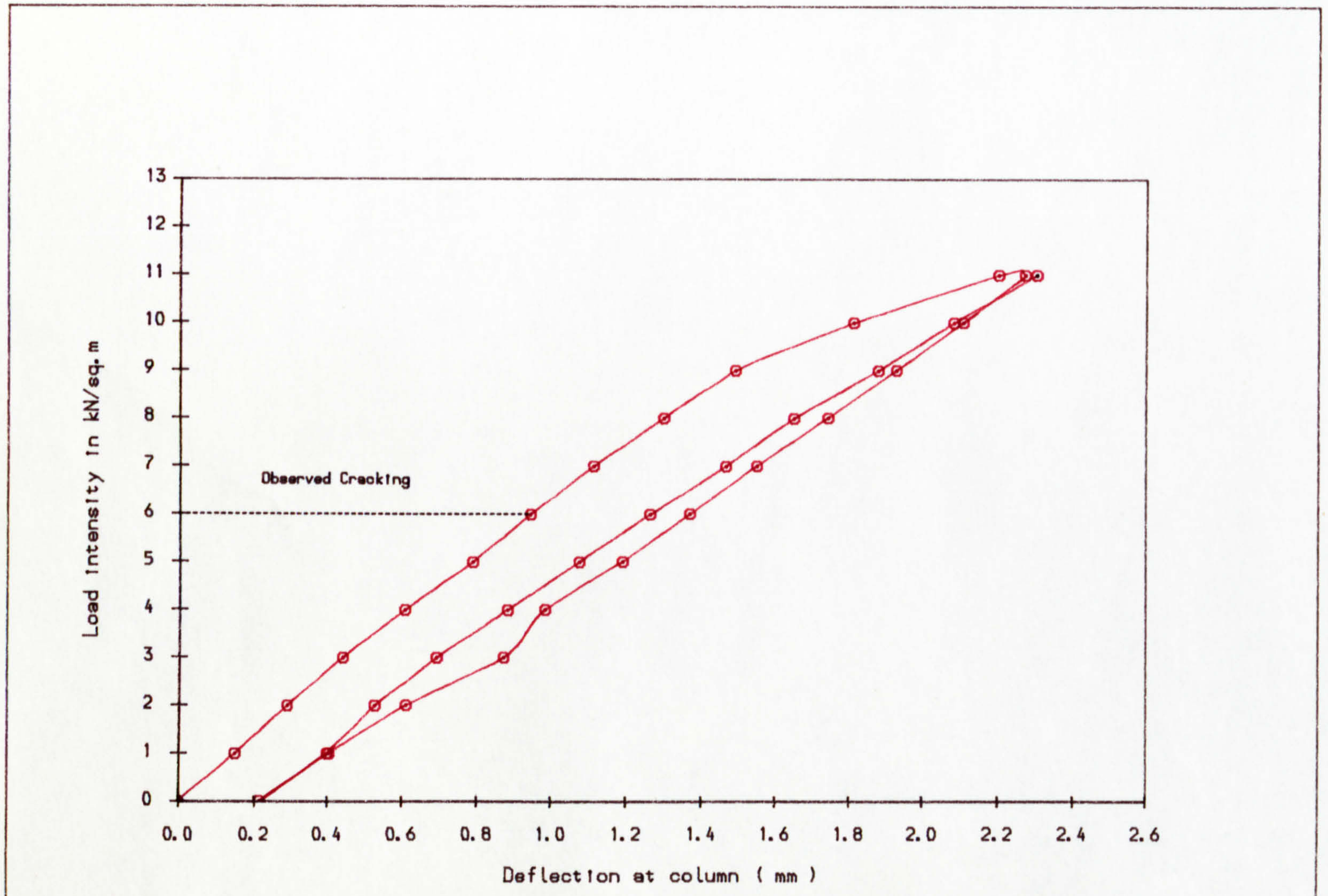

Fig. 8.16 Cyclic Load-Deflection curve, Slab A4

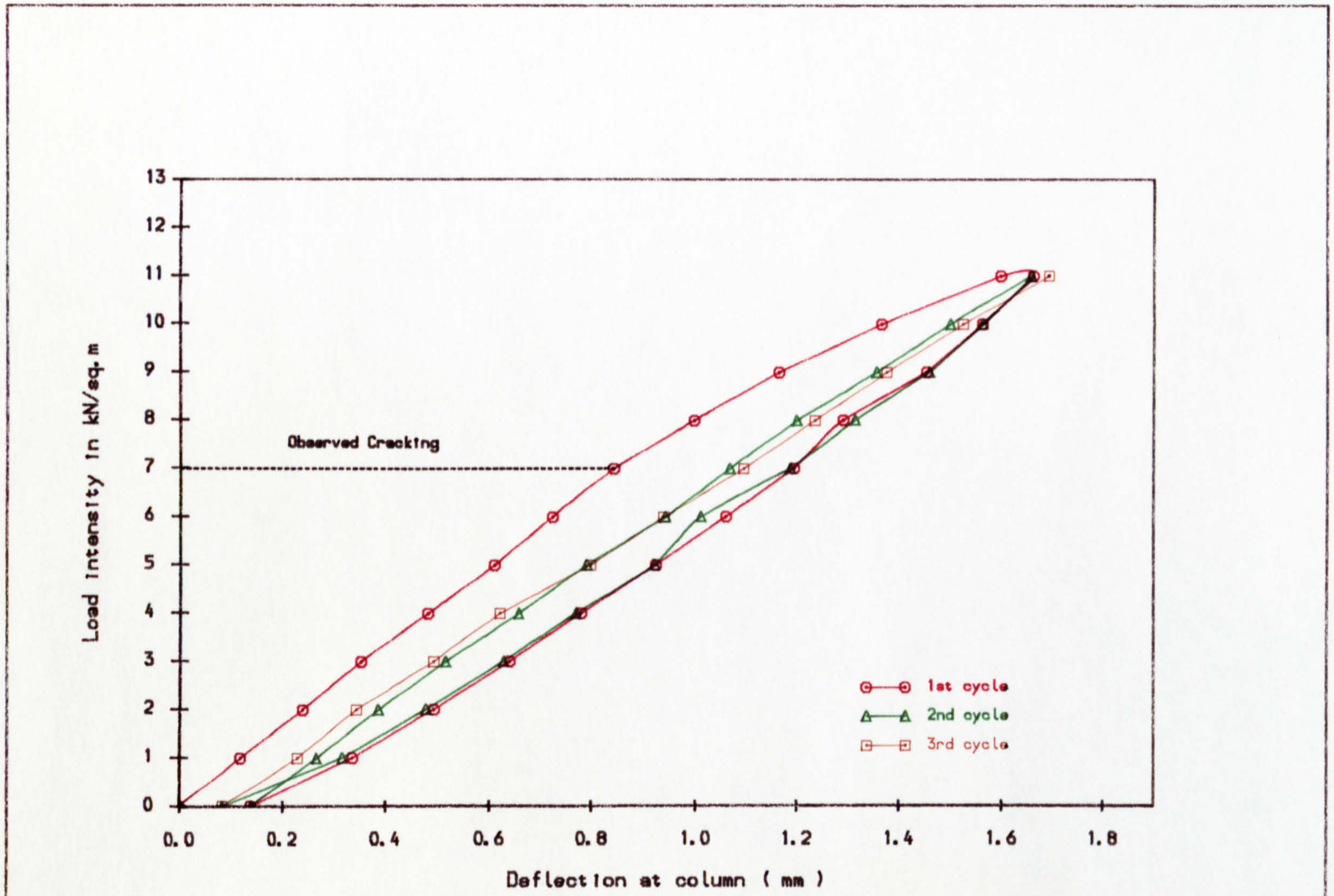

Fig. 8.17 Cyclic Load-Deflection curve, Slab B1

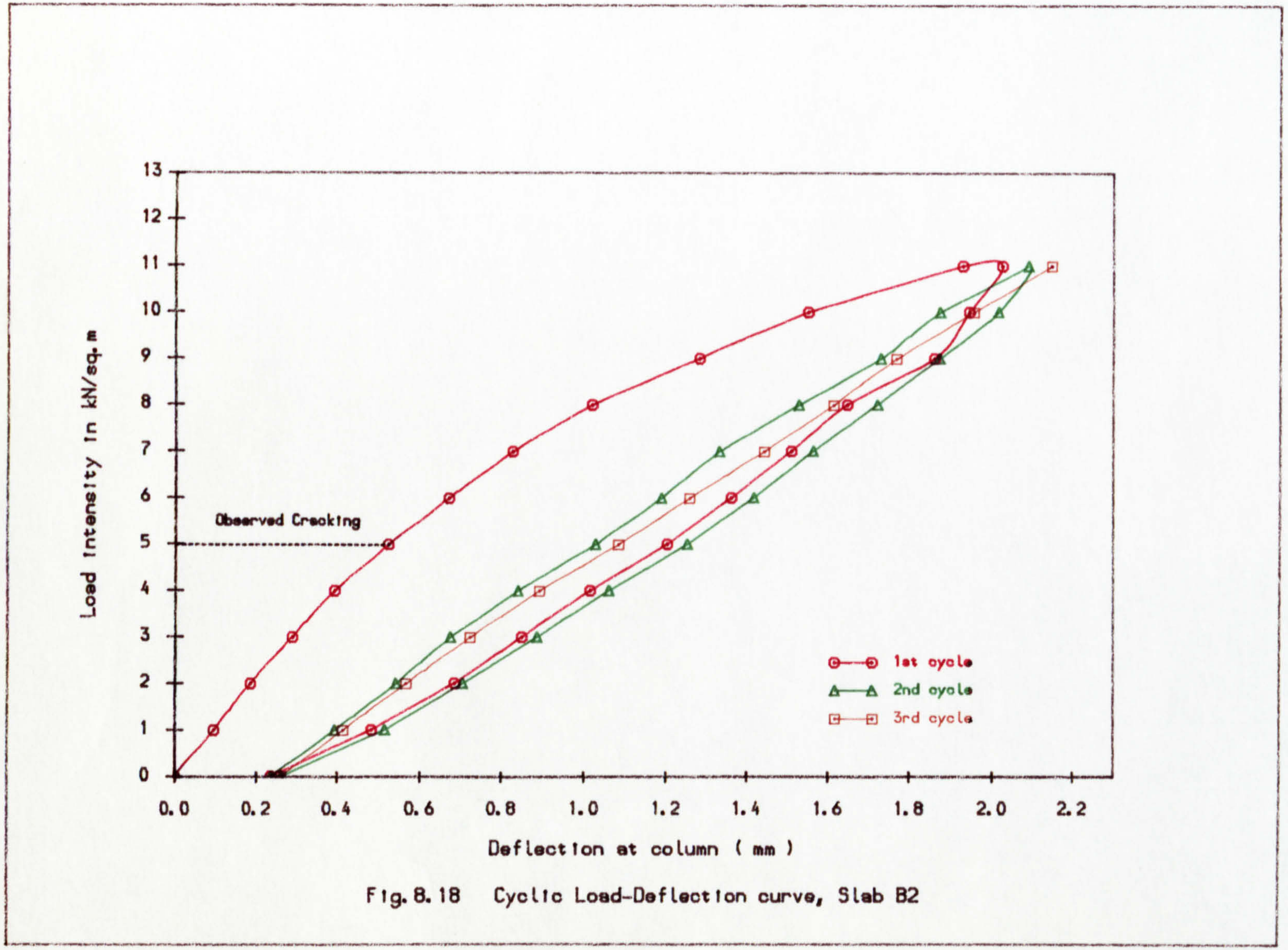

Fig. 8.18 Cyclic Load-Deflection curve, Slab B2

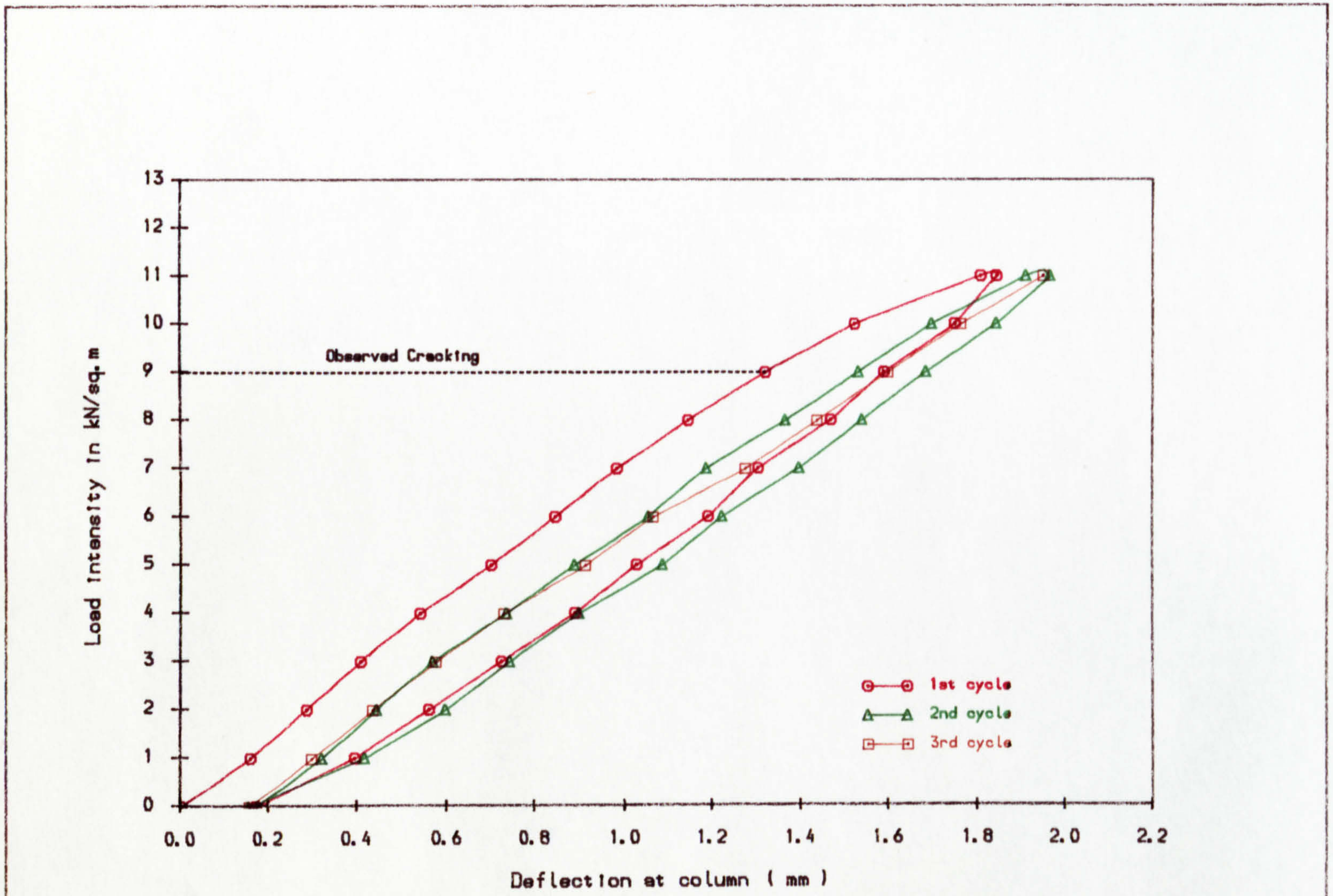

Fig. 8.19 Cyclic Load-Deflection curve, Slab B3

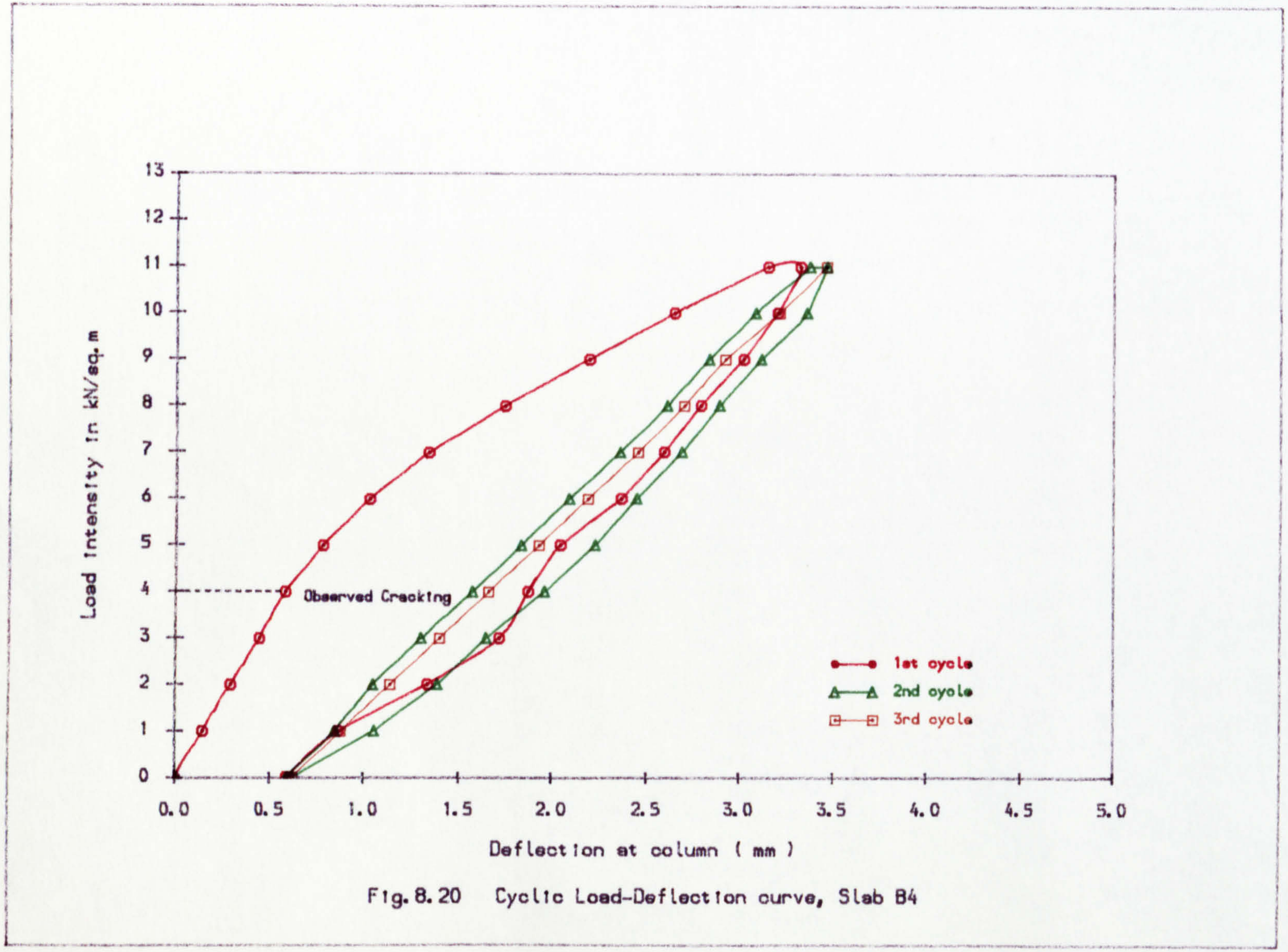

Fig. 8.20 Cyclic Load-Deflection curve, Slab B4

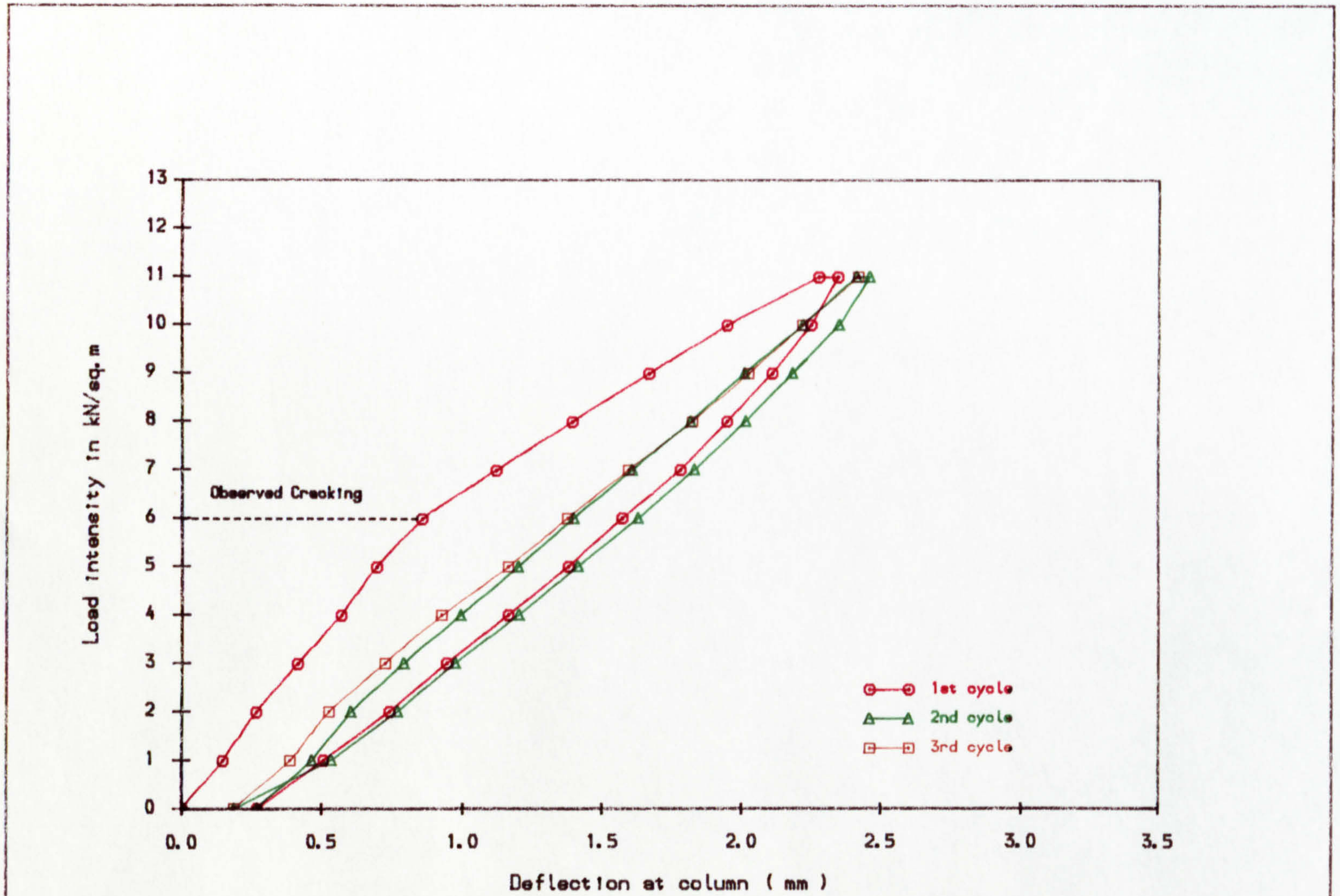

Fig. 8.21 Cyclic Load-Deflection curve, Slab C1

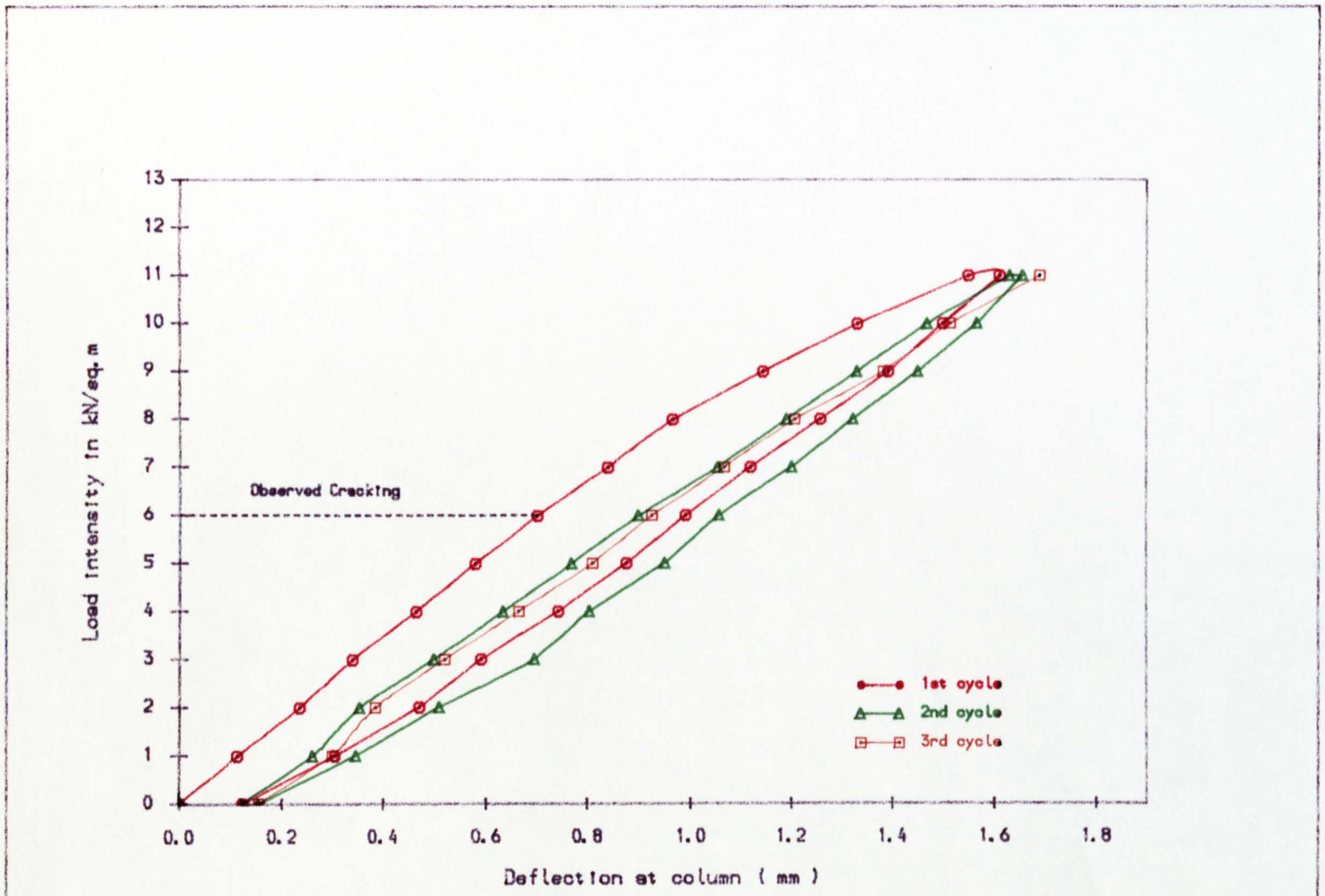

Fig. 8.22 Cyclic Load-Deflection curve, Slab C2

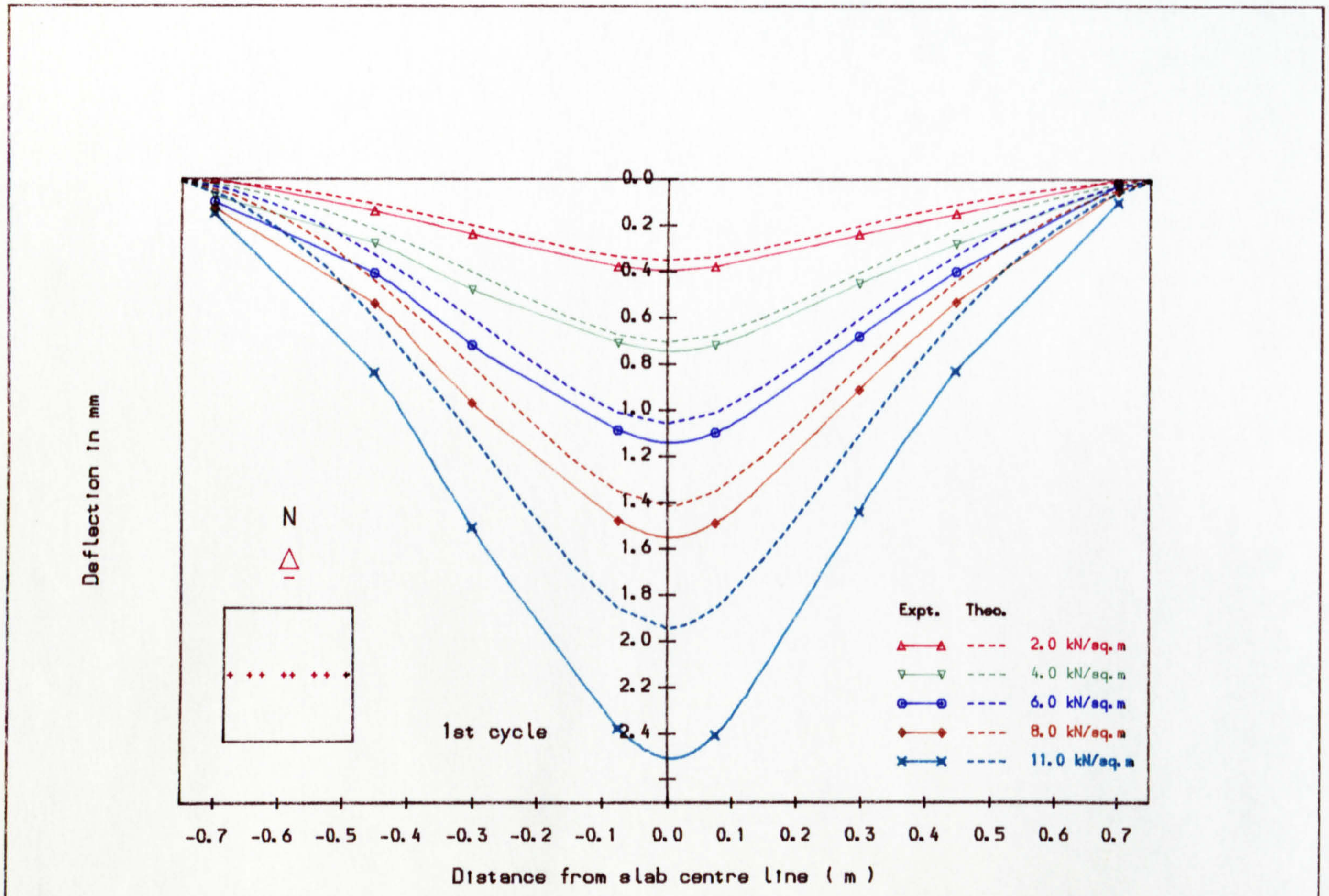

Fig. 8.23 Experimental and Theoretical deflected profiles along slab centre line, Slab A2

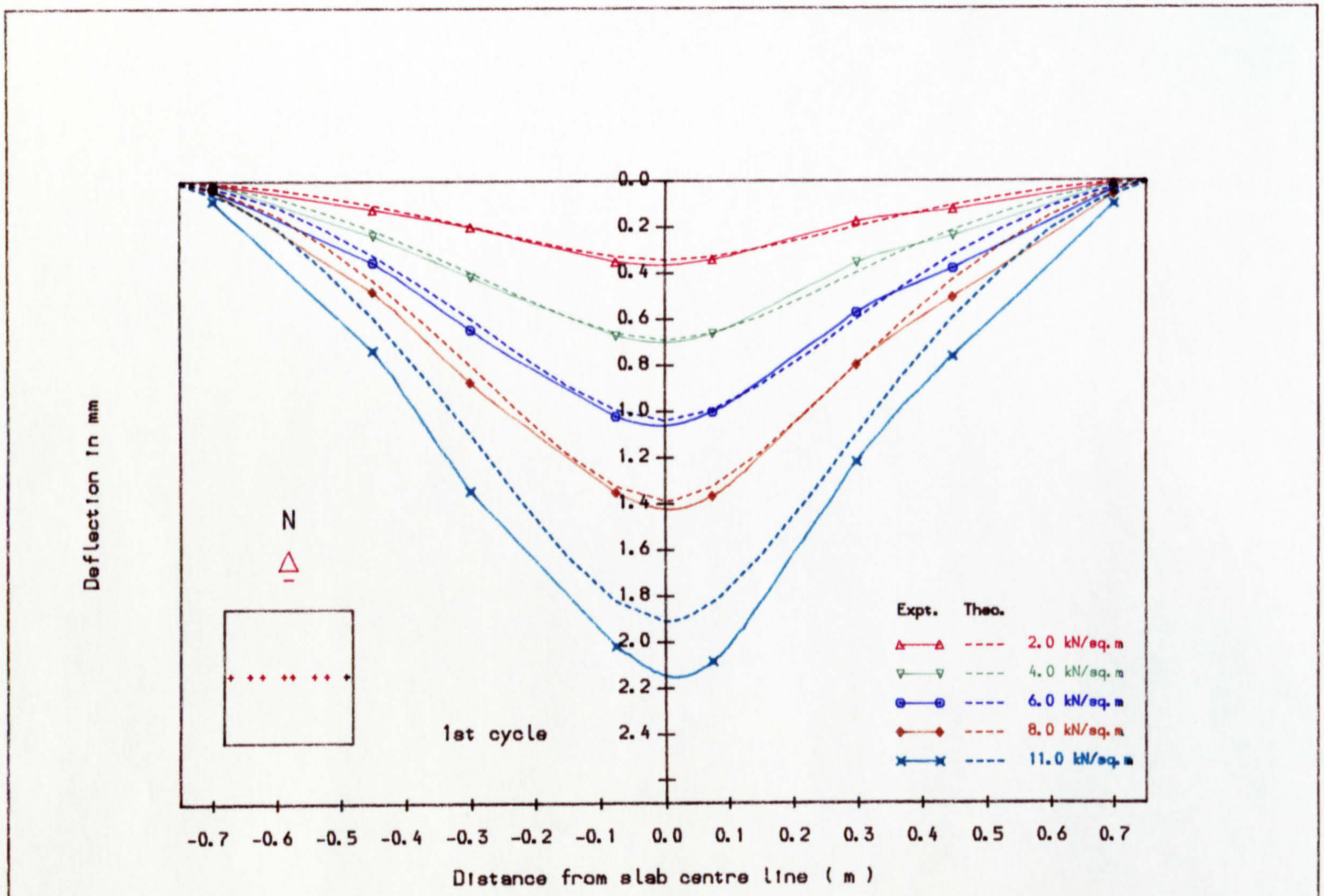

Fig. 8.24 Experimental and Theoretical deflected profiles along slab centre line, Slab A3

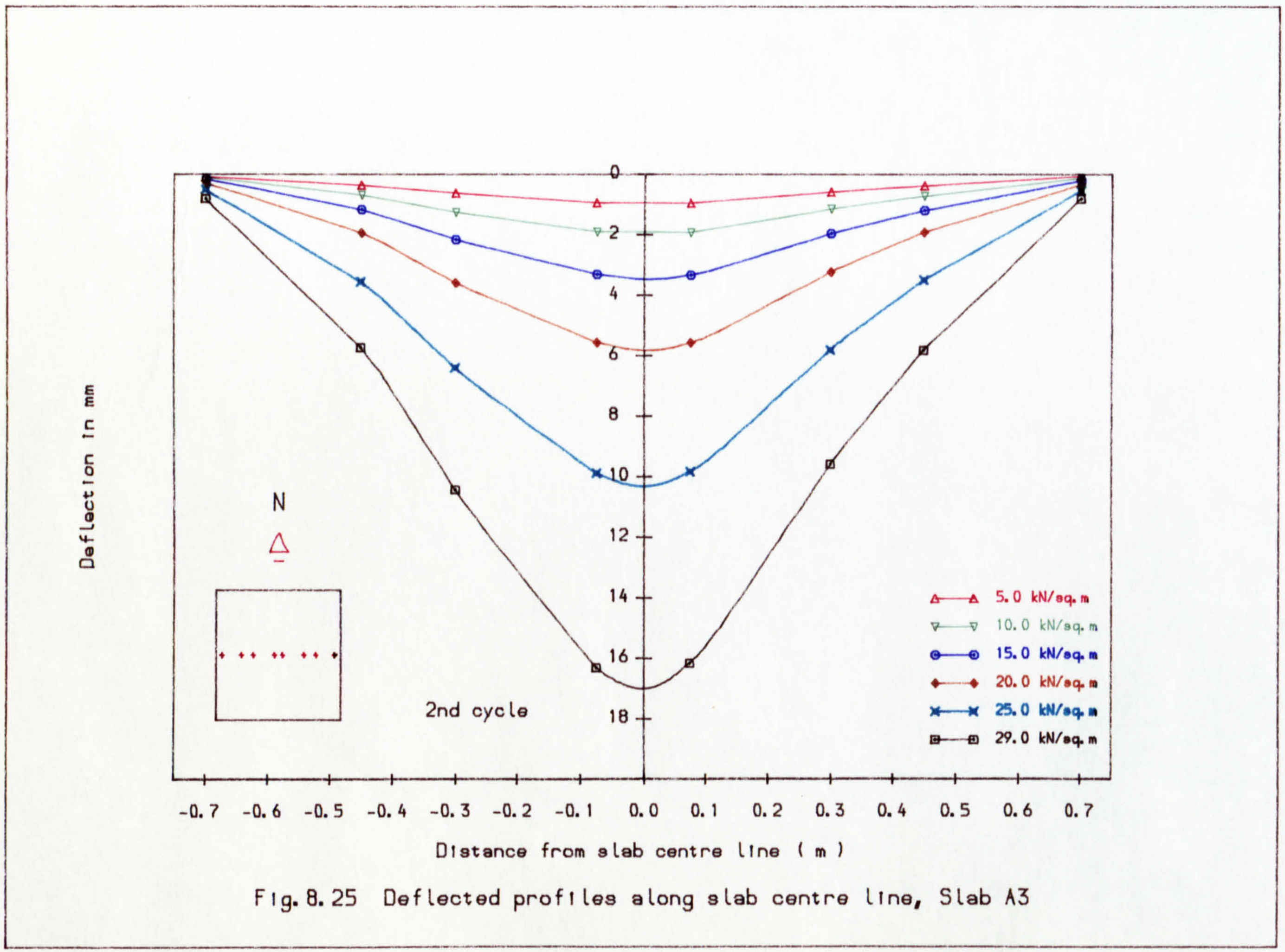

Fig. 8.25 Deflected profiles along slab centre line, Slab A3

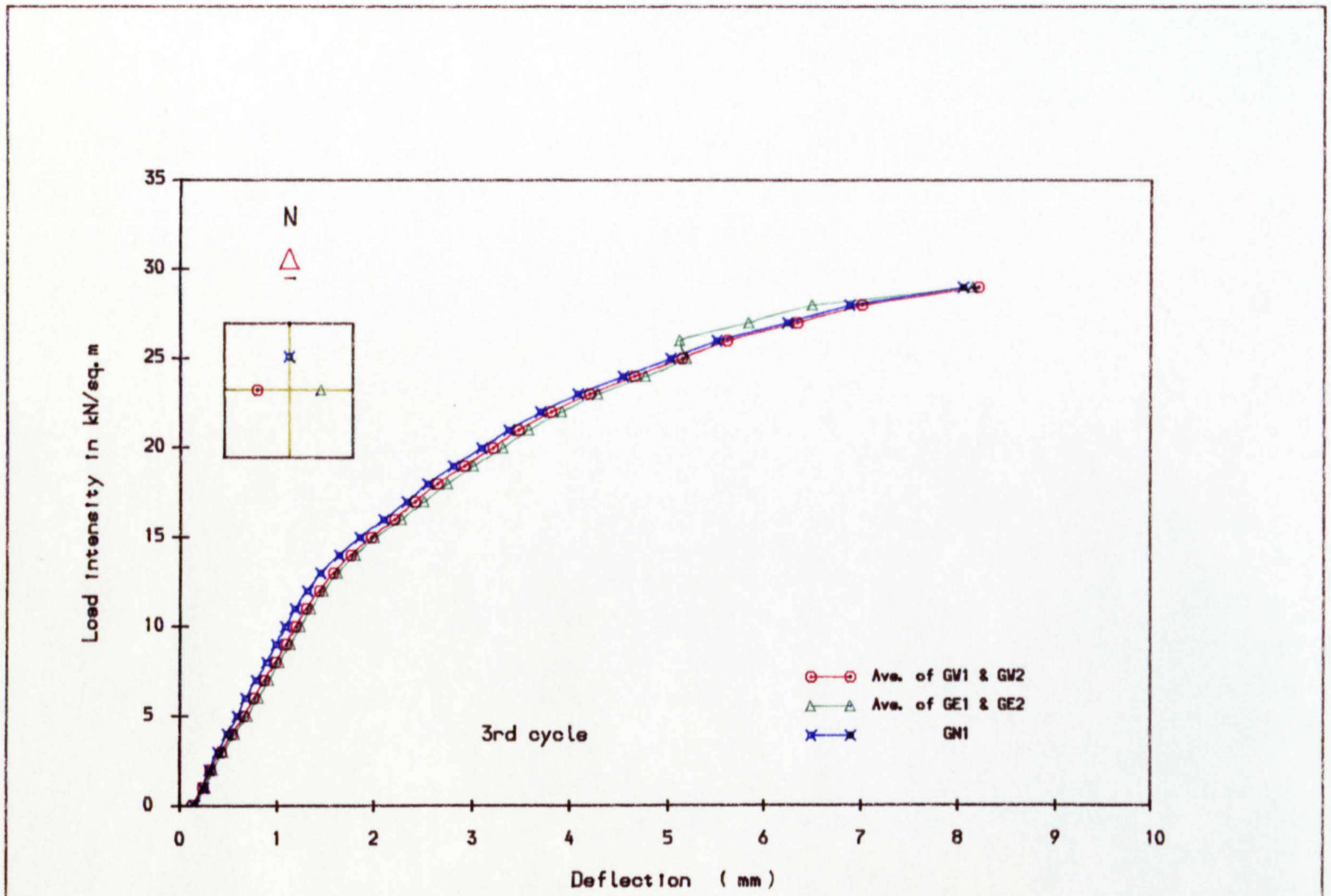

Fig. 8.26 Load-Deflection response at symmetrical points (1/4 span from column centre lines), Slab C1

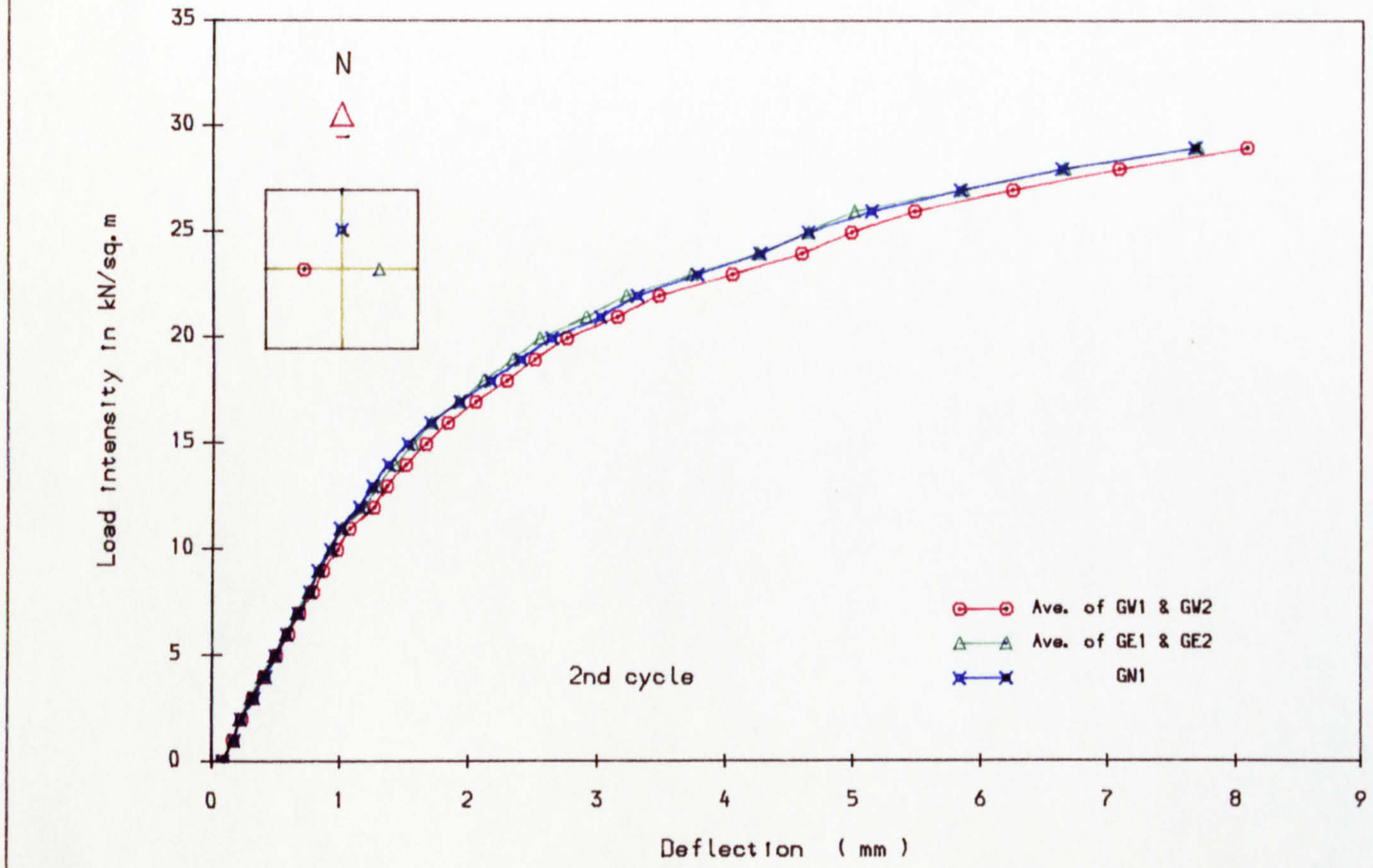

Fig. 8.27 Load-Deflection response at symmetrical points (1/4 span from column centre lines), Slab A3

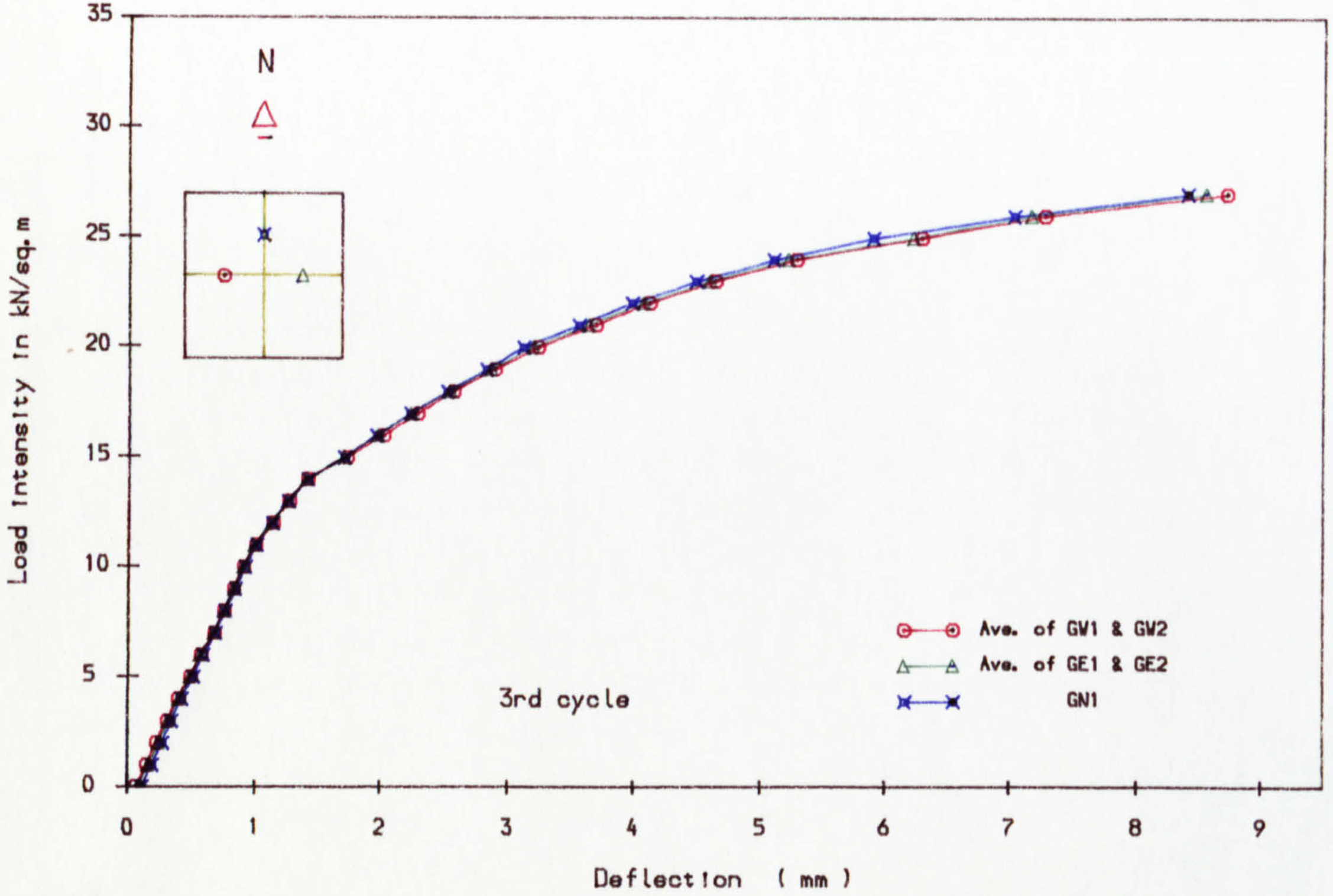

Fig. 8.28 Load-Deflection response at symmetrical points (1/4 span from column centre lines), Slab B3

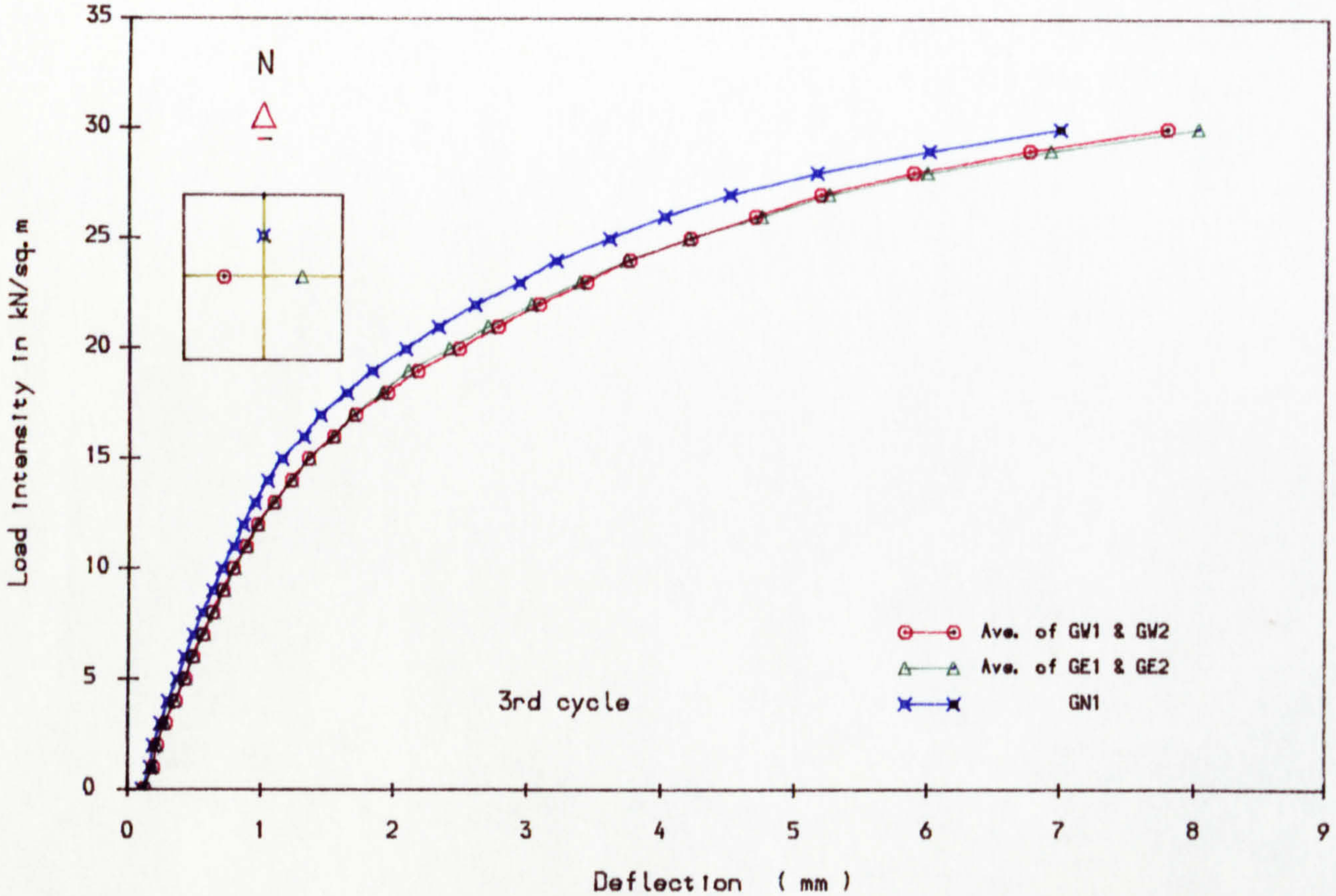

Fig. 8.29 Load-Deflection response at symmetrical points (1/4 span from column centre lines), Slab C2

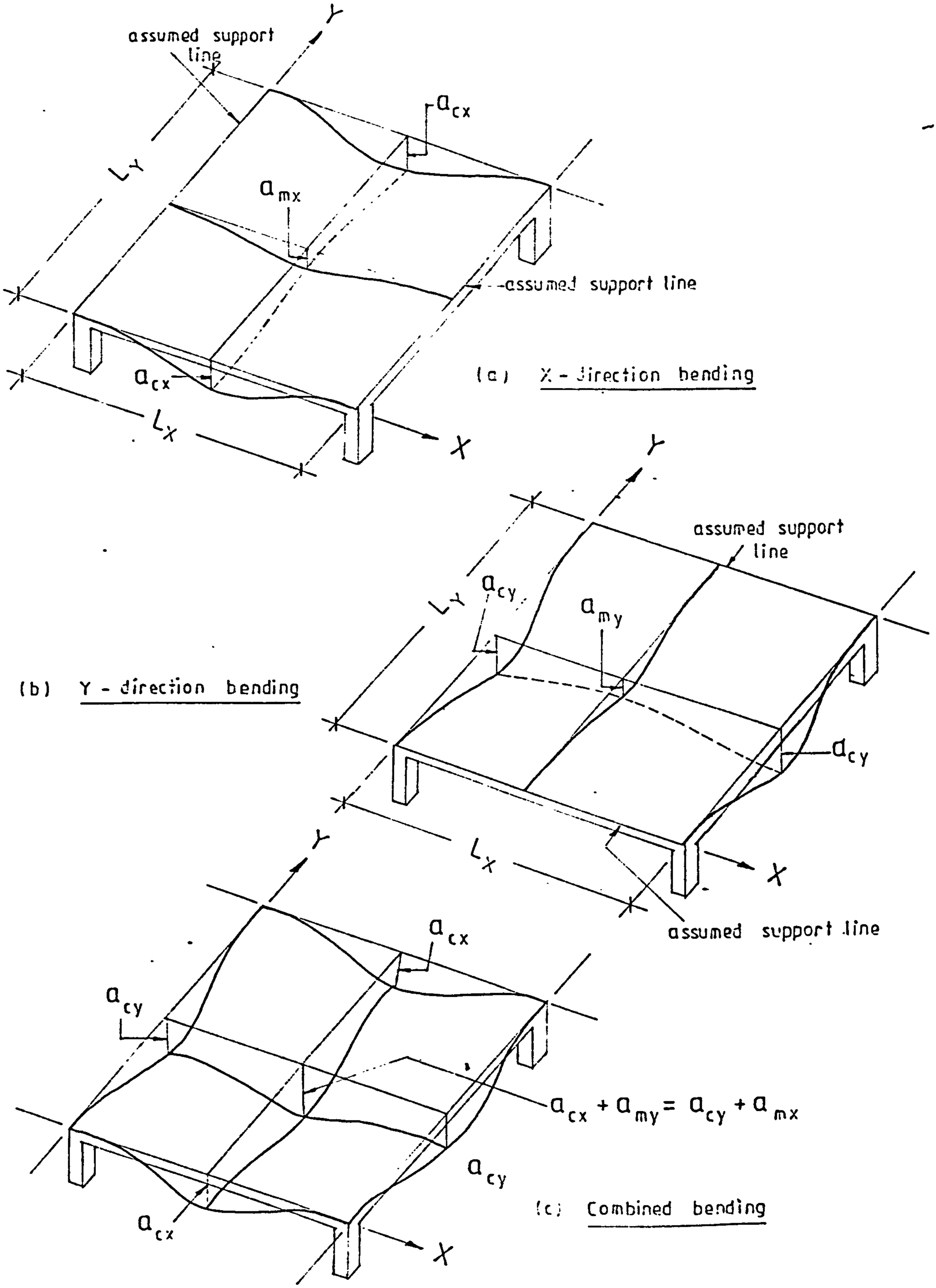

Fig. 8.30 Schematic representation of mid-panel deflection computations for square panel

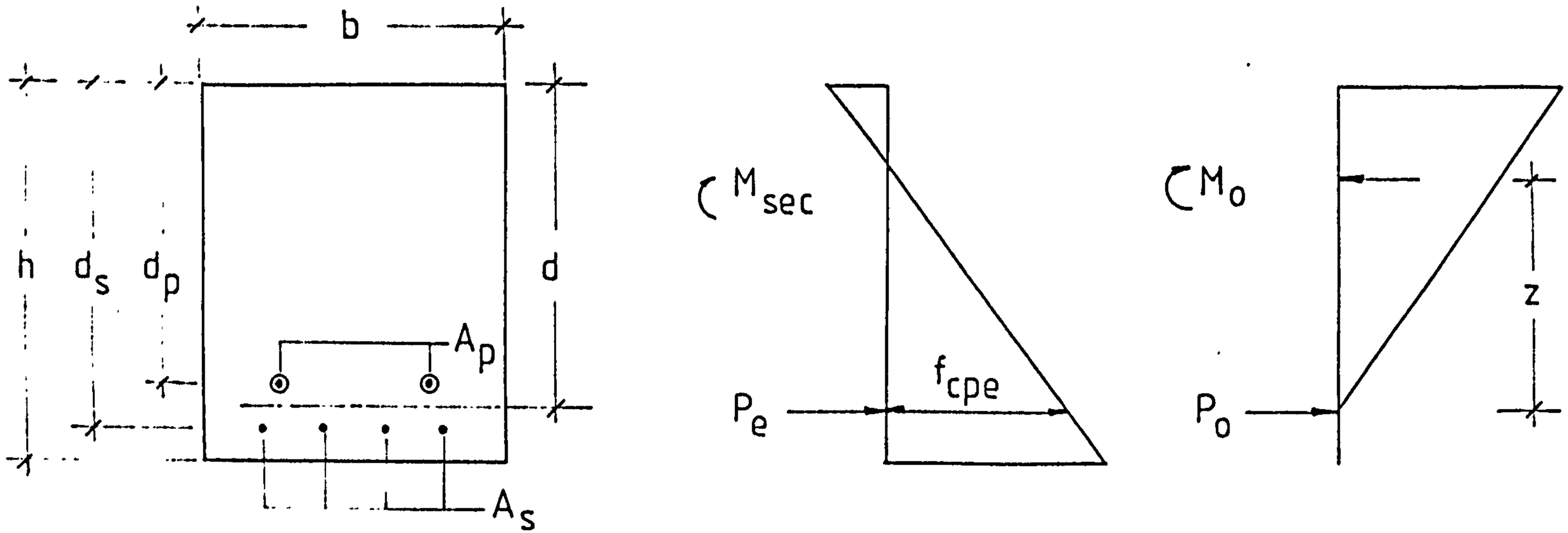

Effective prstress Stresses at reference load

$$d = \frac{A_p\, d_p + A_s\, d_s}{A_p + A_s}$$

Fig. 8.31 Reference force in the analysis of cracked section

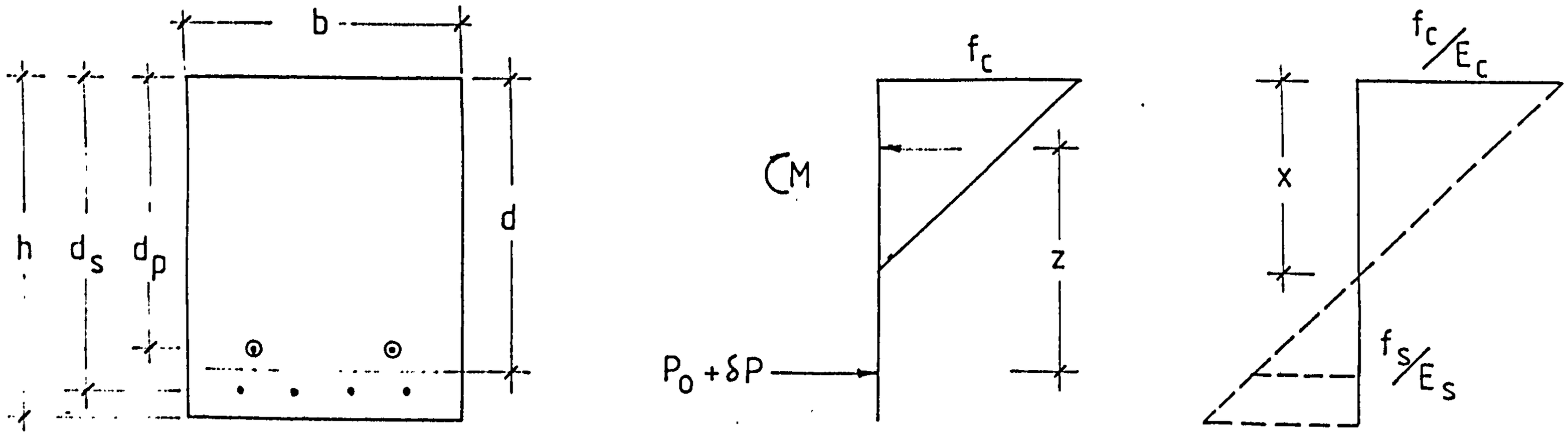

Fig. 8.32 Stress and strain distribution in cracked section

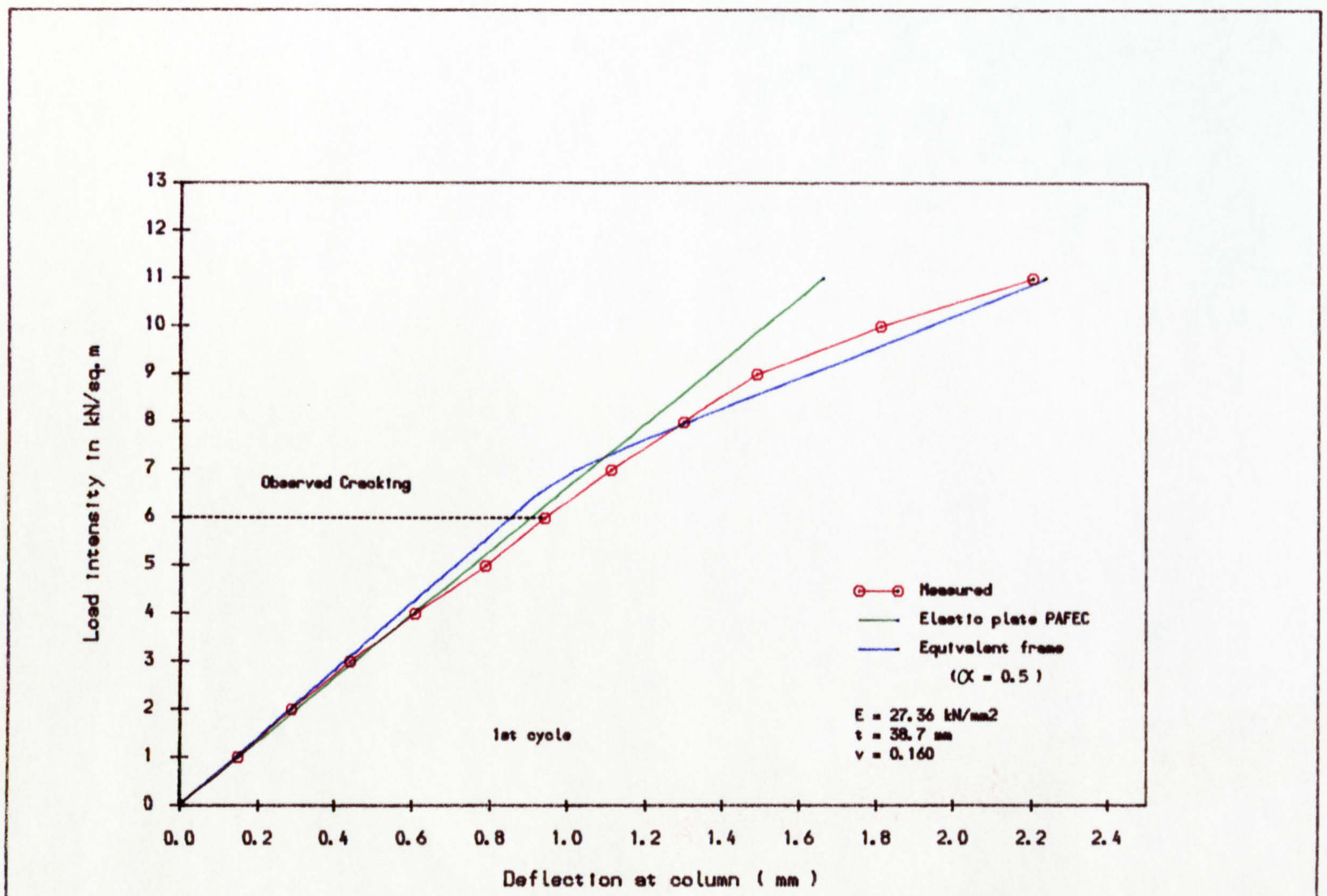

Fig. 8.33 Measured and Computed Load-Deflection curve, Slab A4

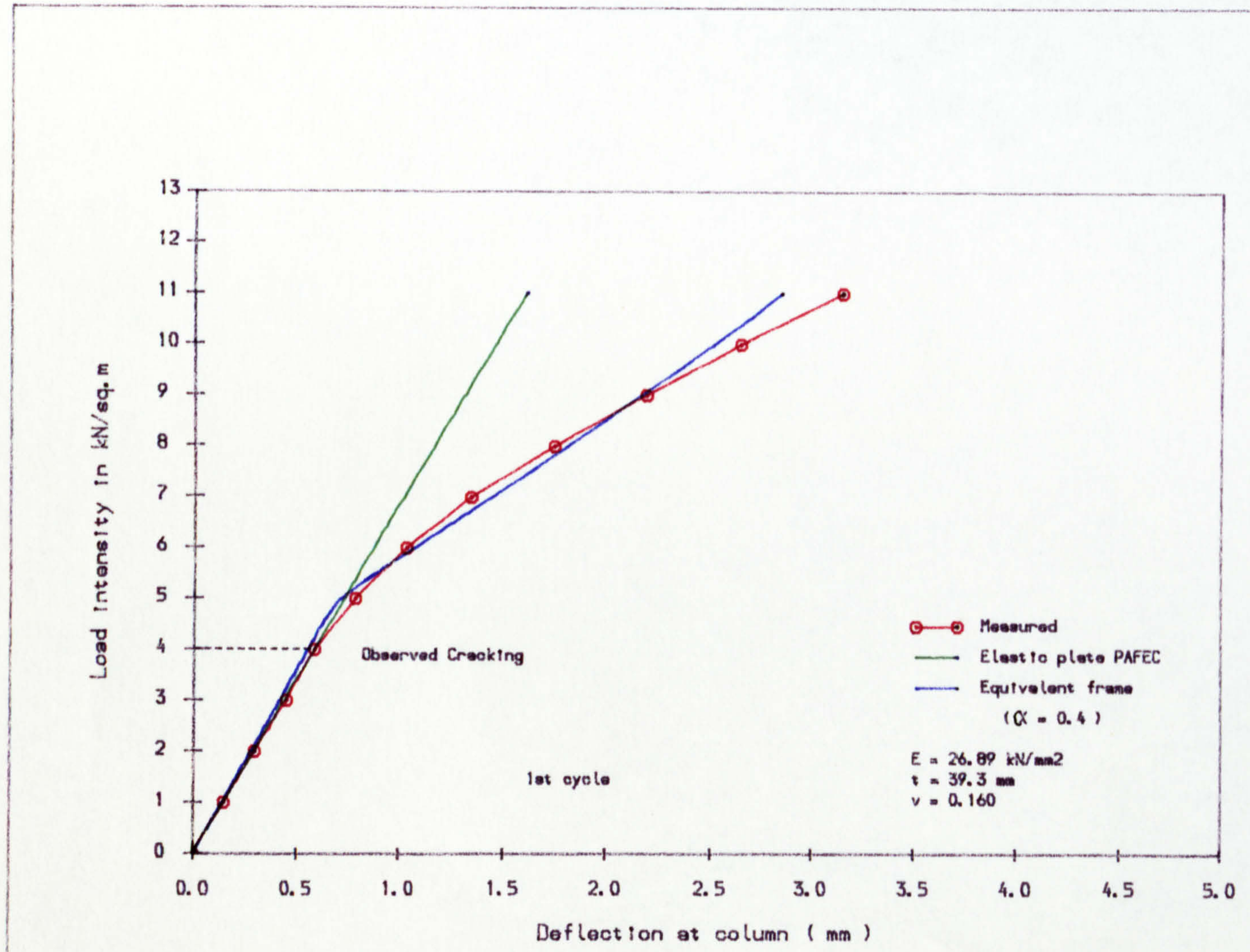

Fig. 8.34 Measured and Computed Load-Deflection curve, Slab B4

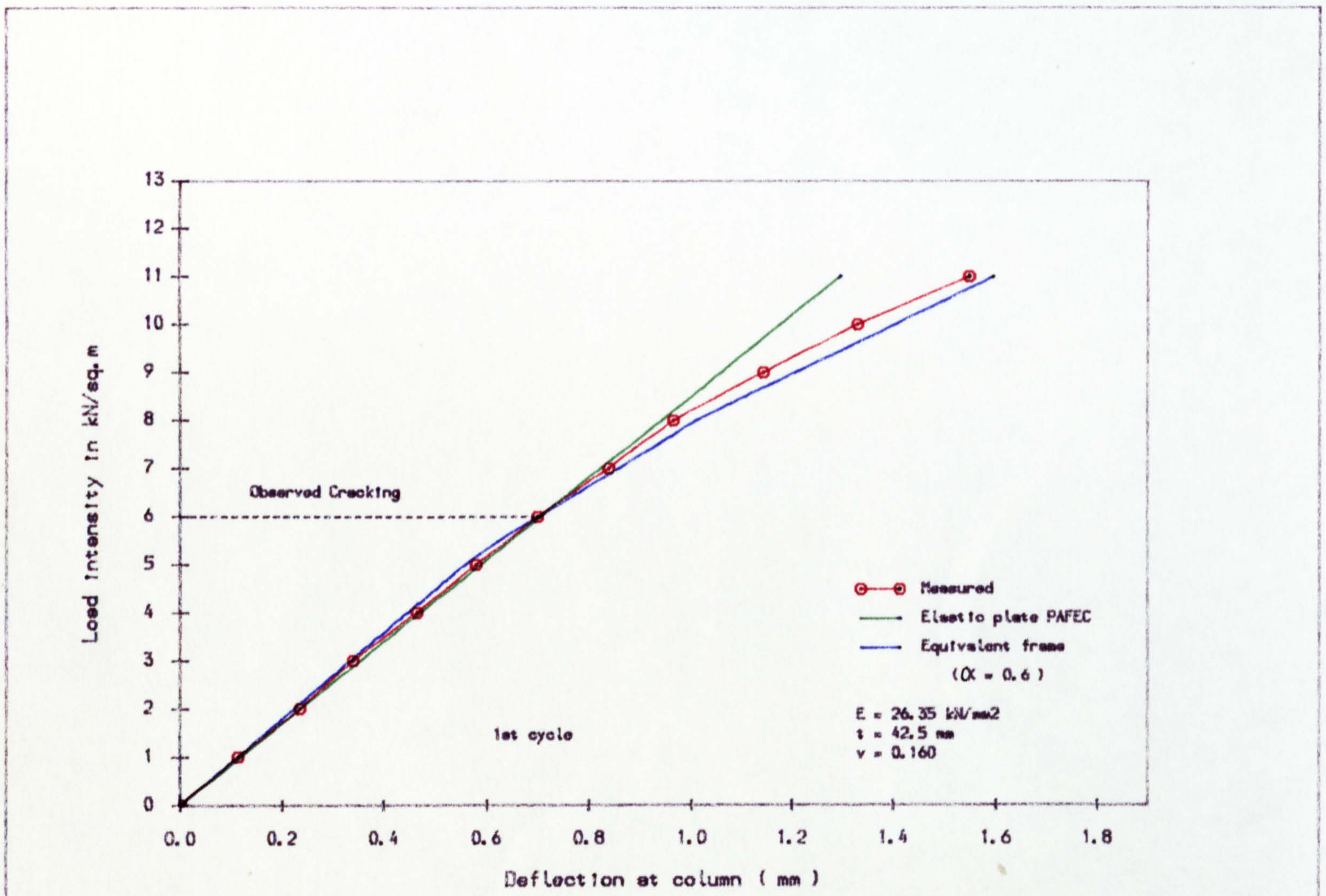

Fig. 8.35 Measured and Computed Load-Deflection curve, Slab C2

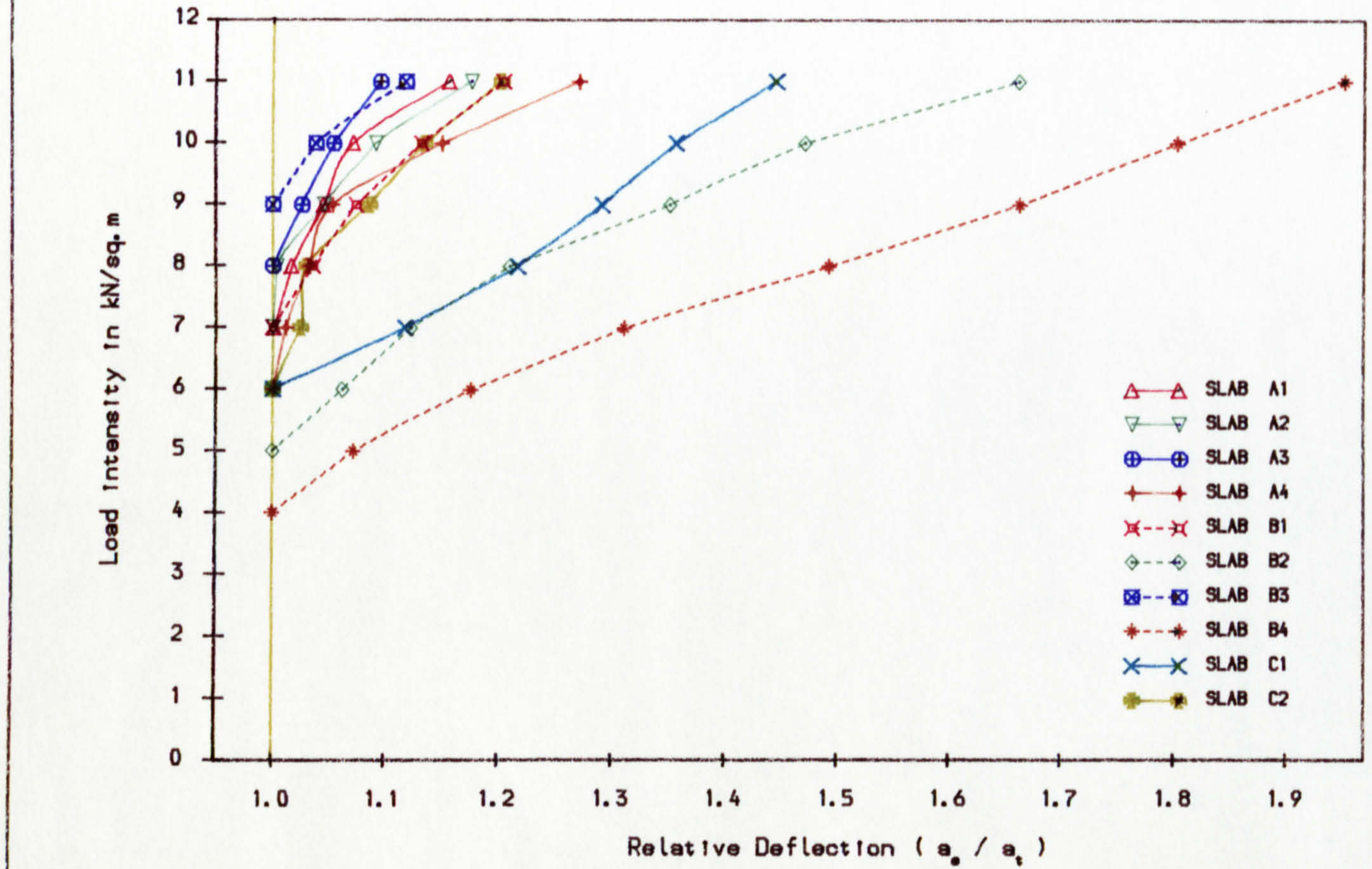

Fig. 8.36 Load against Relative Deflection

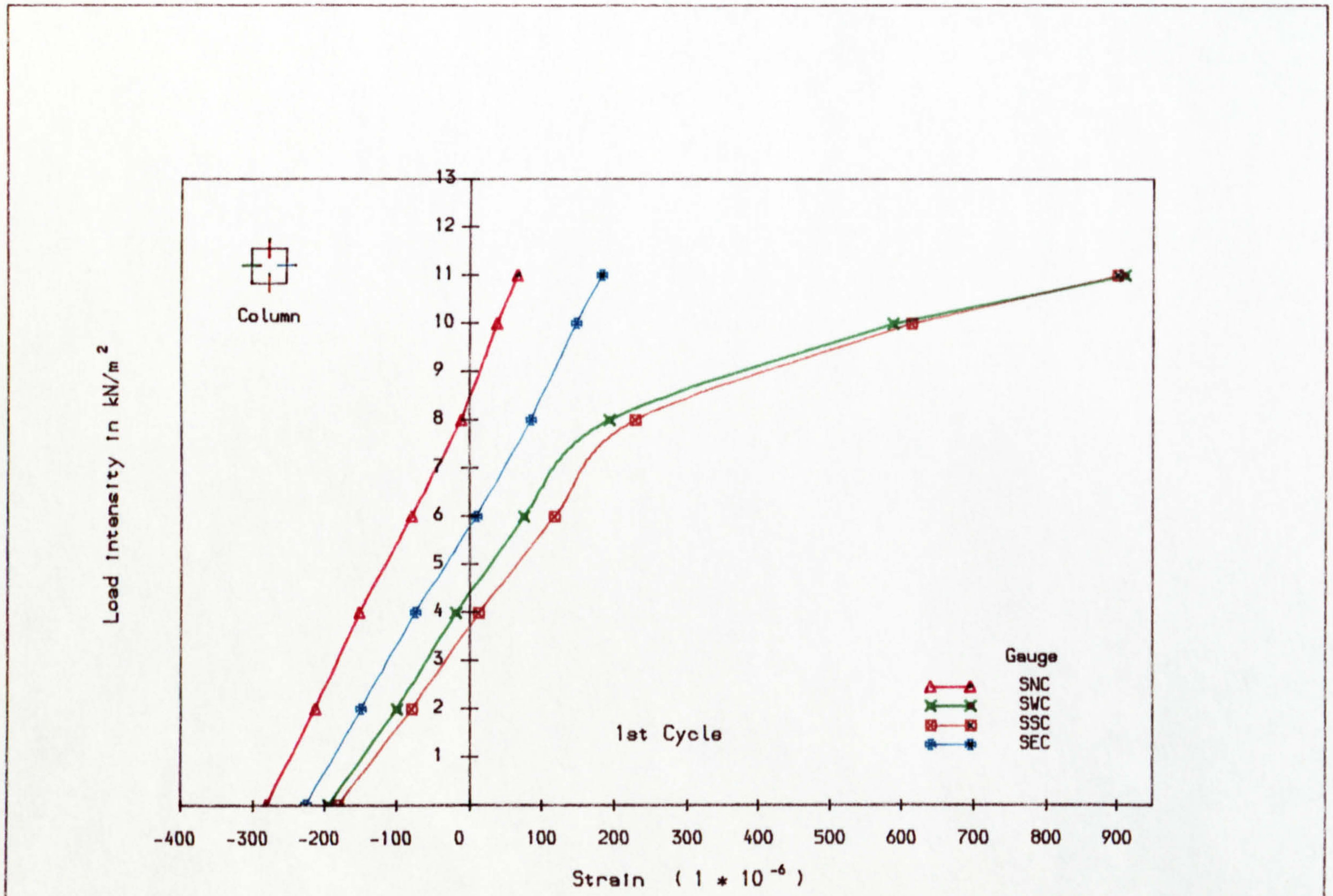

Fig. 8.37 Tensile concrete strain at column face due to applied load, Slab A1

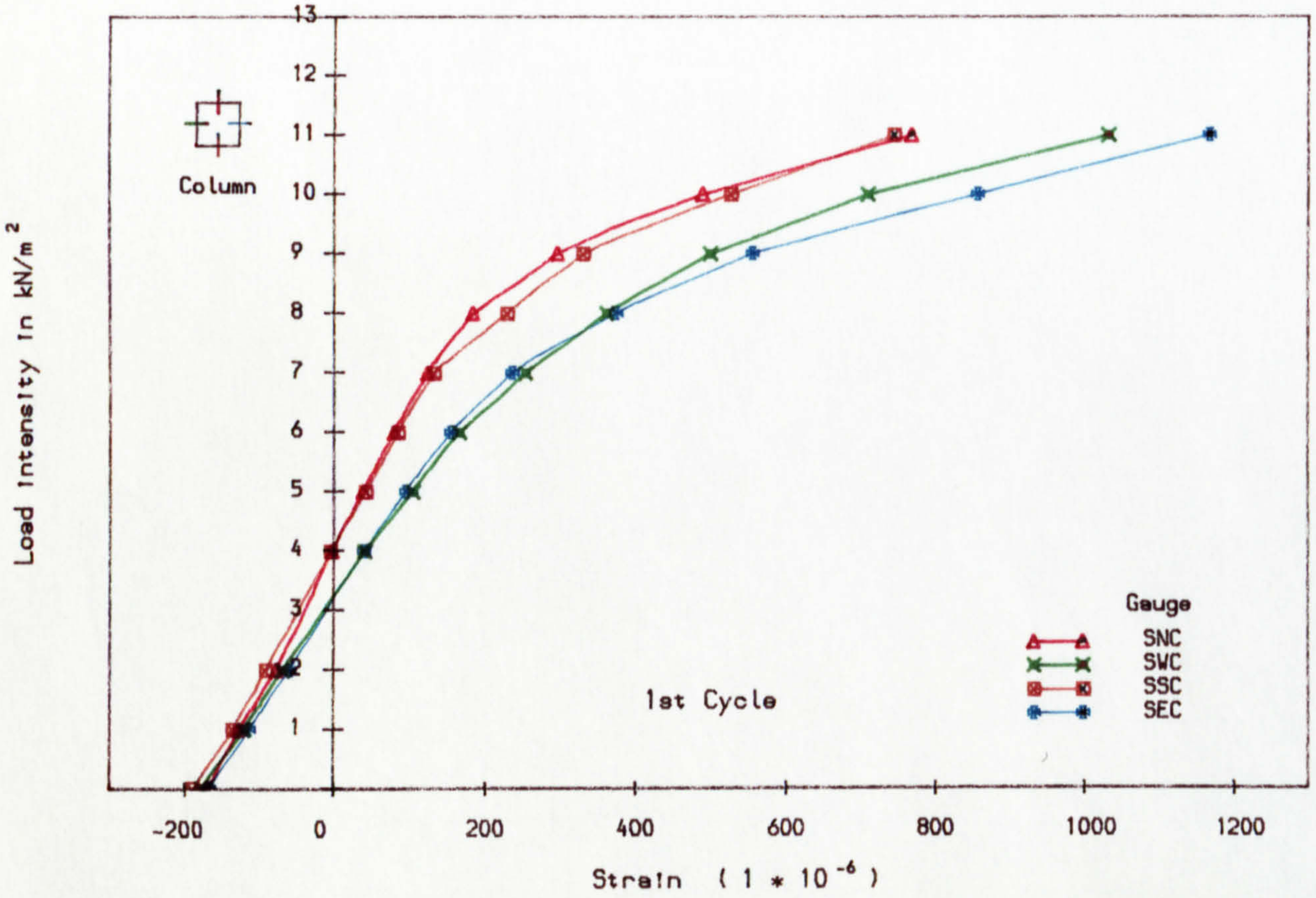

Fig. 8.38 Tensile concrete strain at column face due to applied load, Slab A4

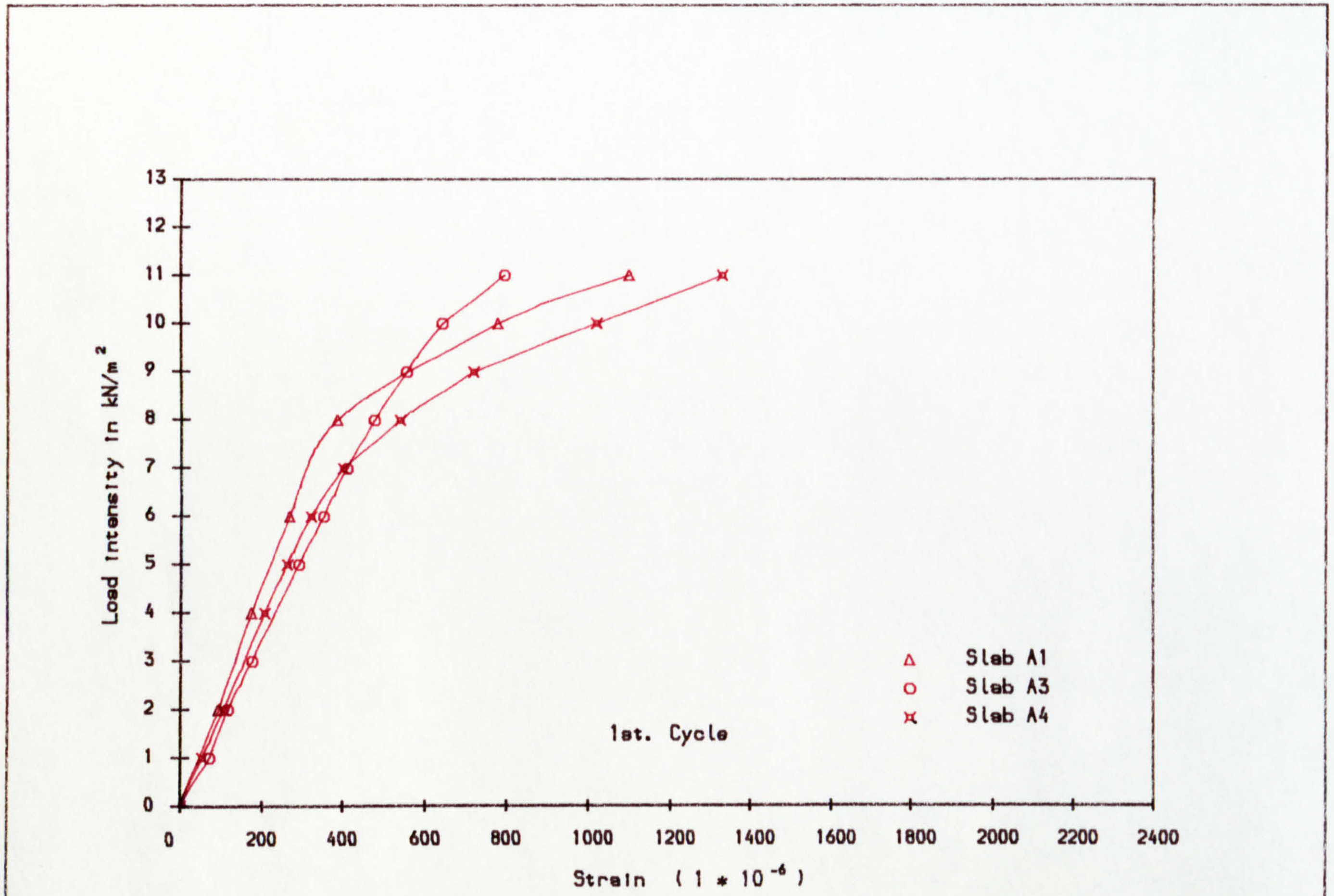

Fig. 8.39 Tensile concrete strain at column face due to applied load in series A slabs

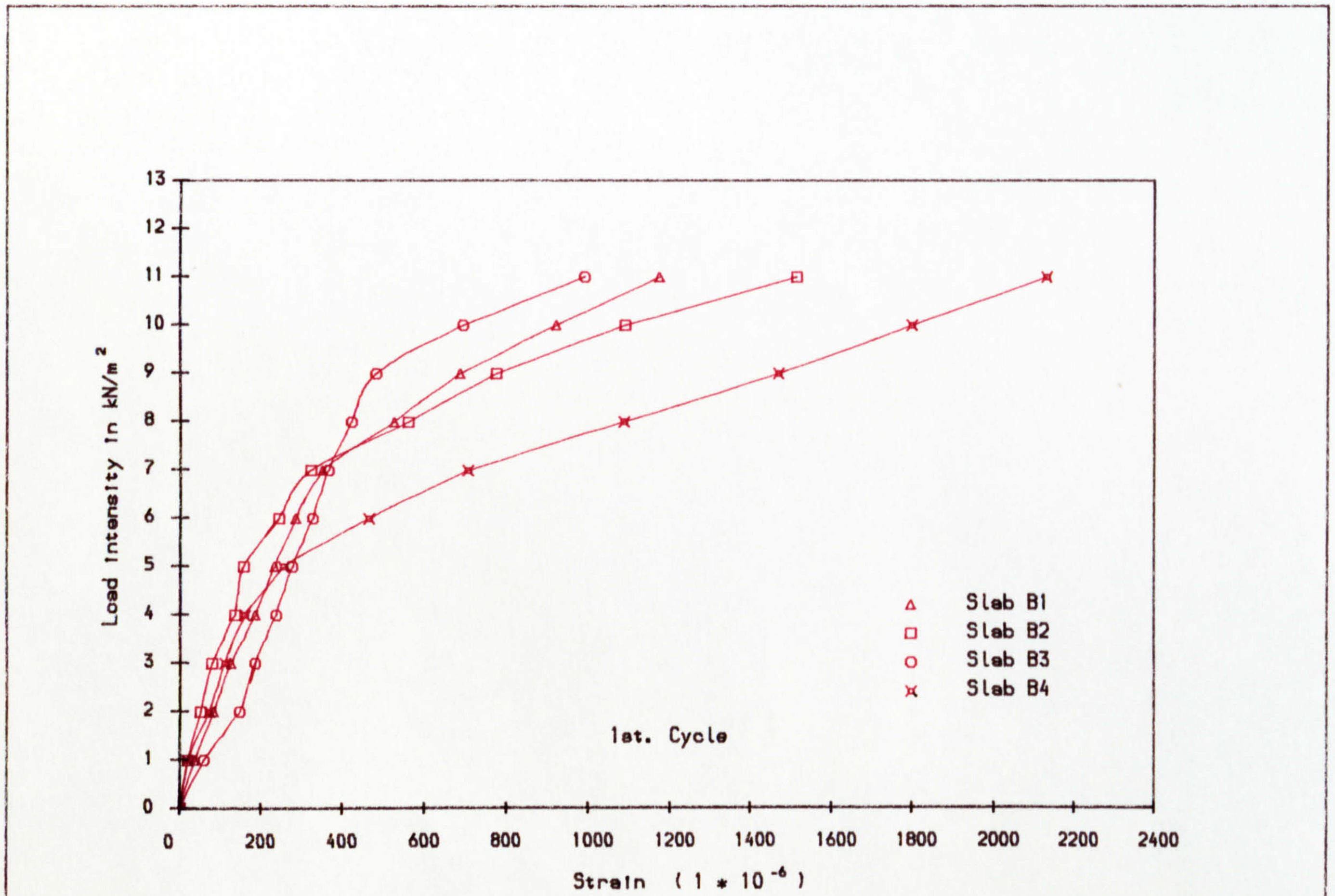

Fig. 8.40 Tensile concrete strain at column face due to applied load in series B slabs

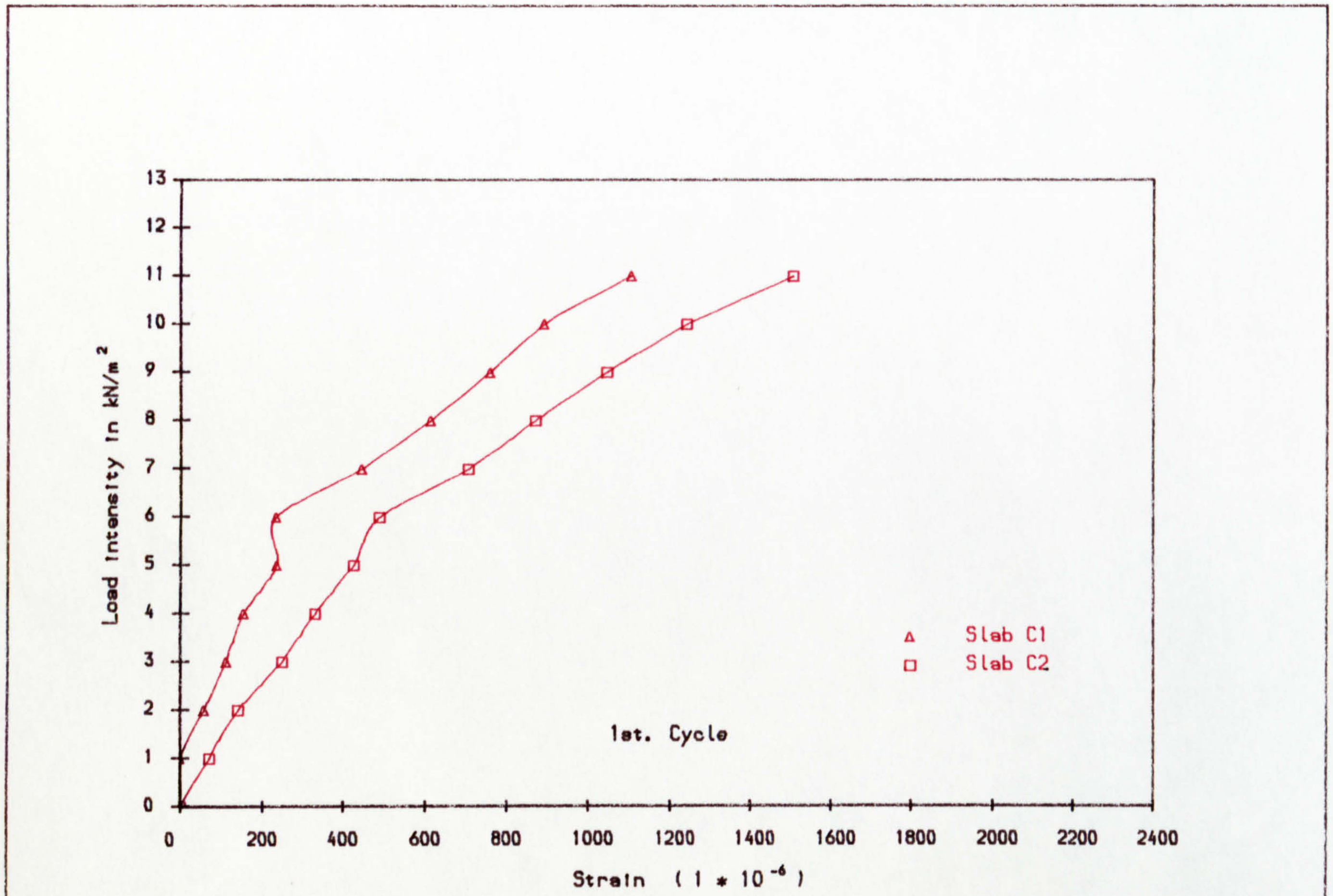

Fig. 8.41 Tensile concrete strain at column face due to applied load in series C slabs

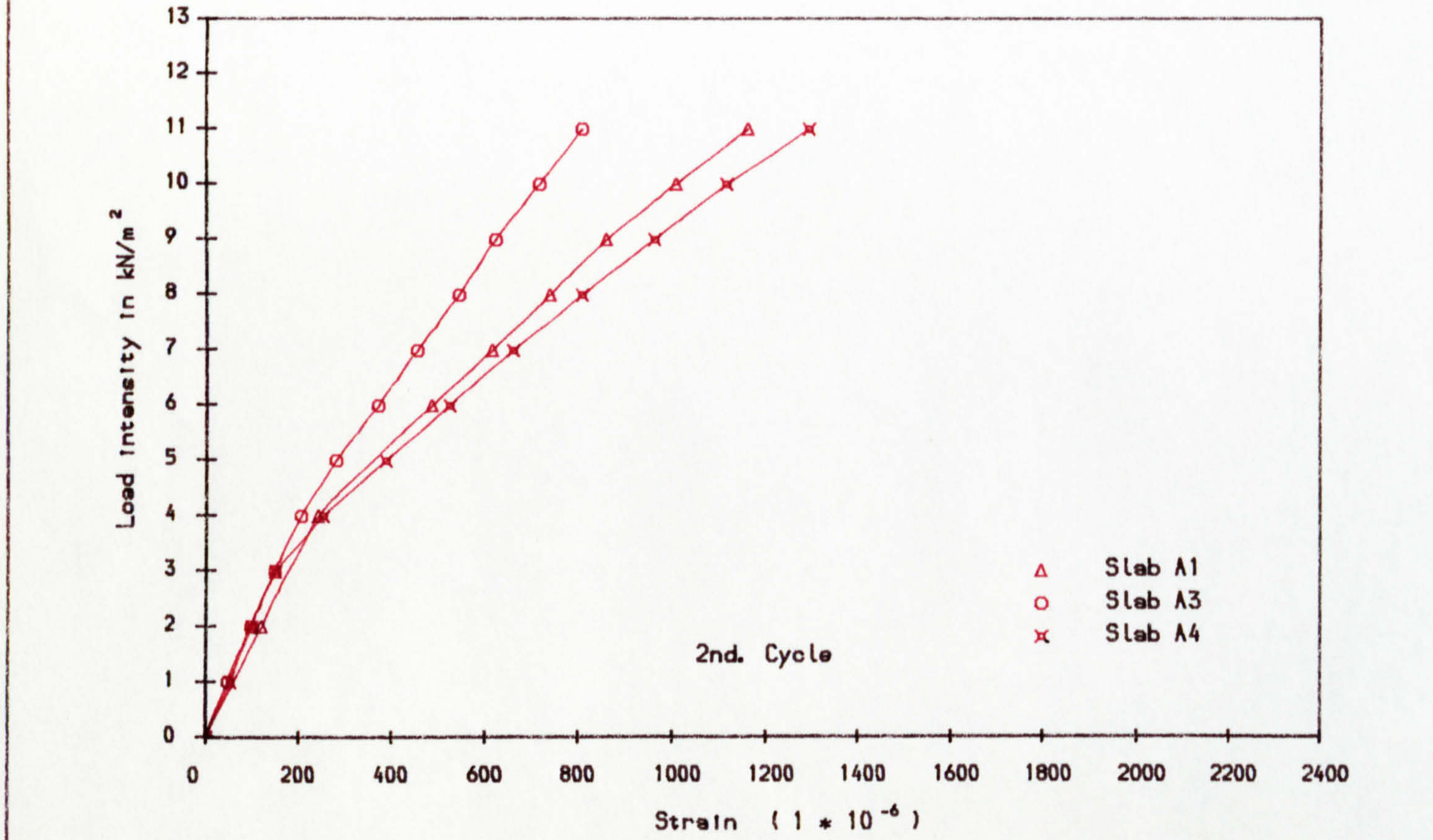

Fig. 8.42 Tensile concrete strain at column face due to applied load in series A slabs

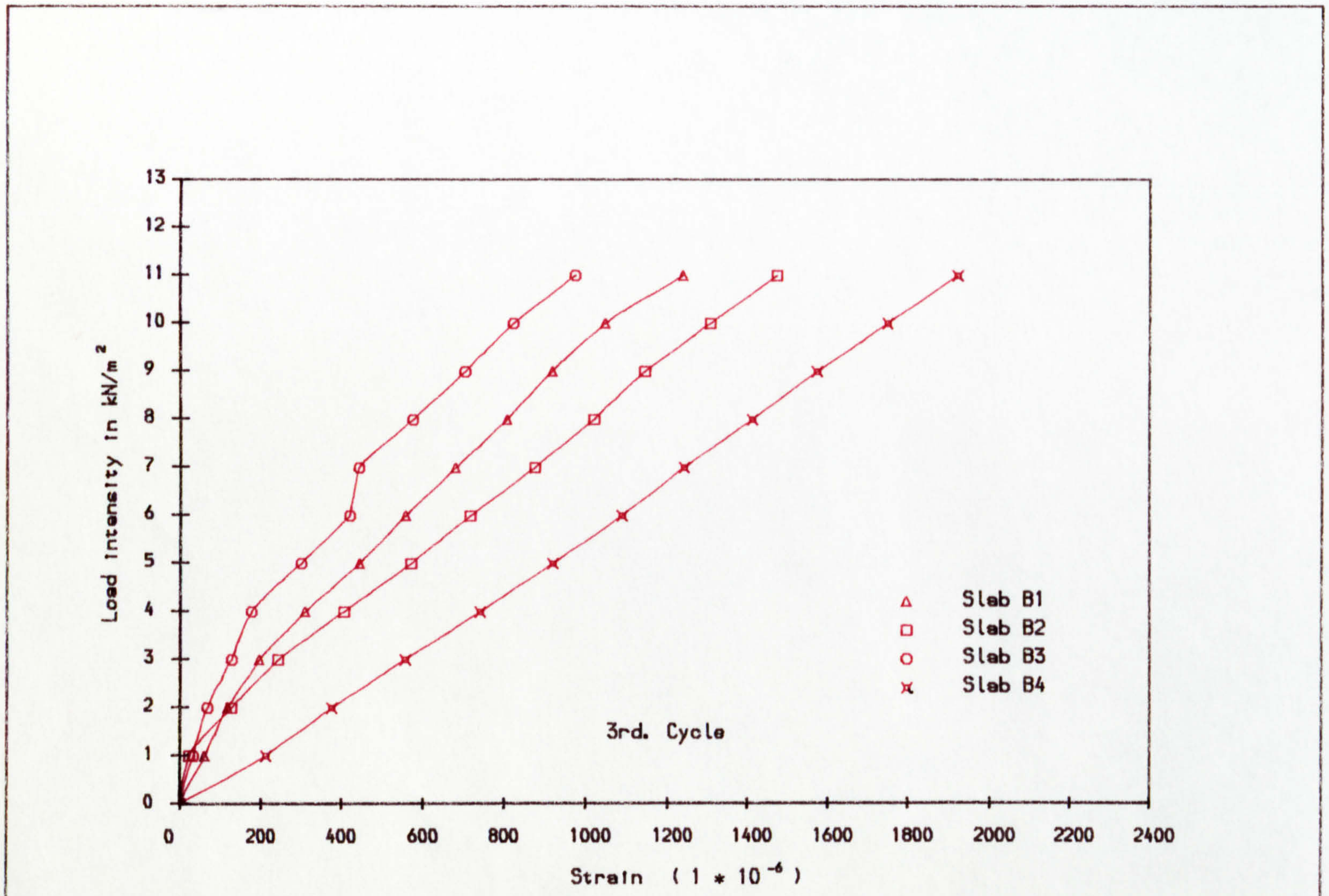

Fig. 8.43 Tensile concrete strain at column face due to applied load in series B slabs

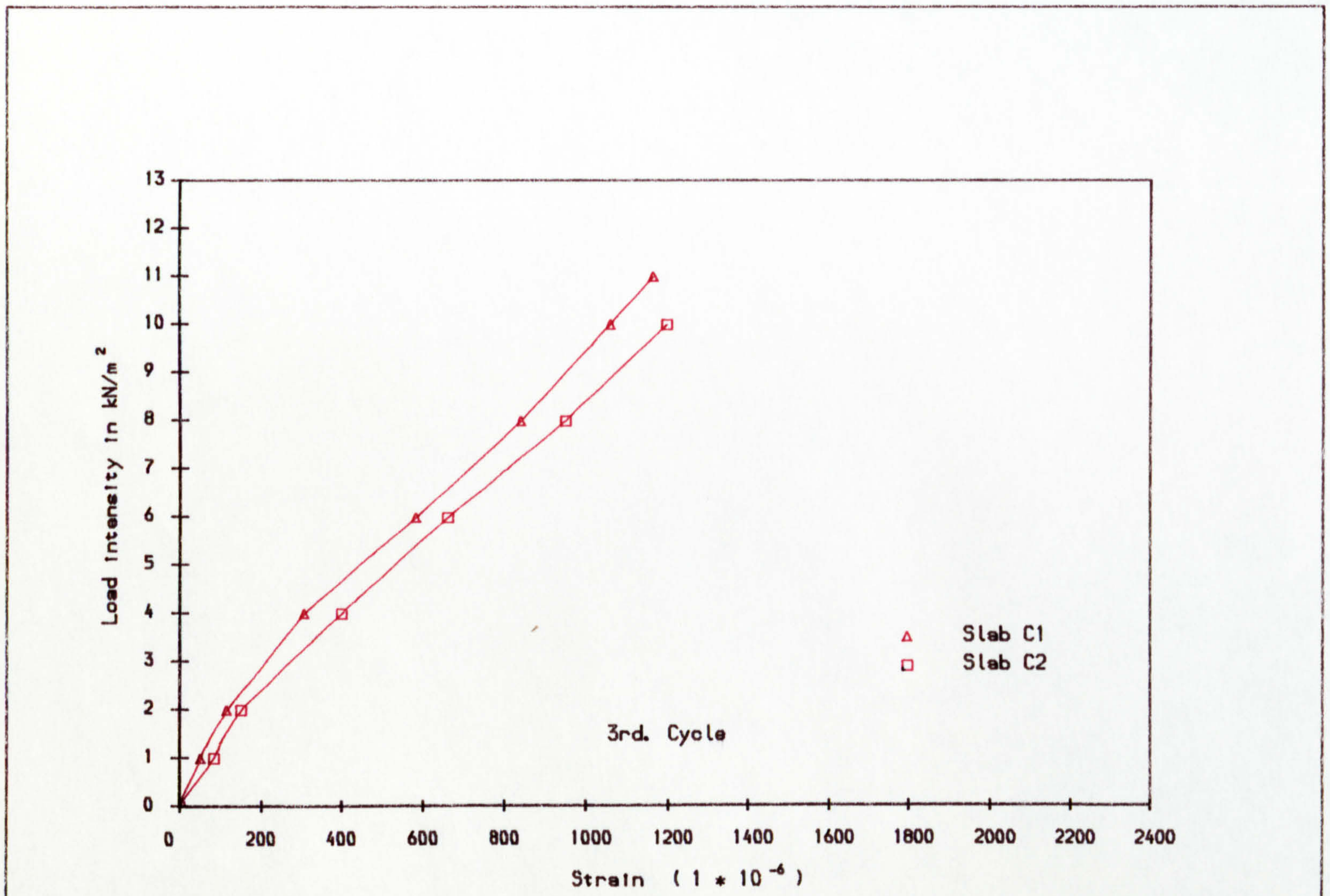

Fig. 8.44 Tensile concrete strain at column face due to applied load in series C slabs

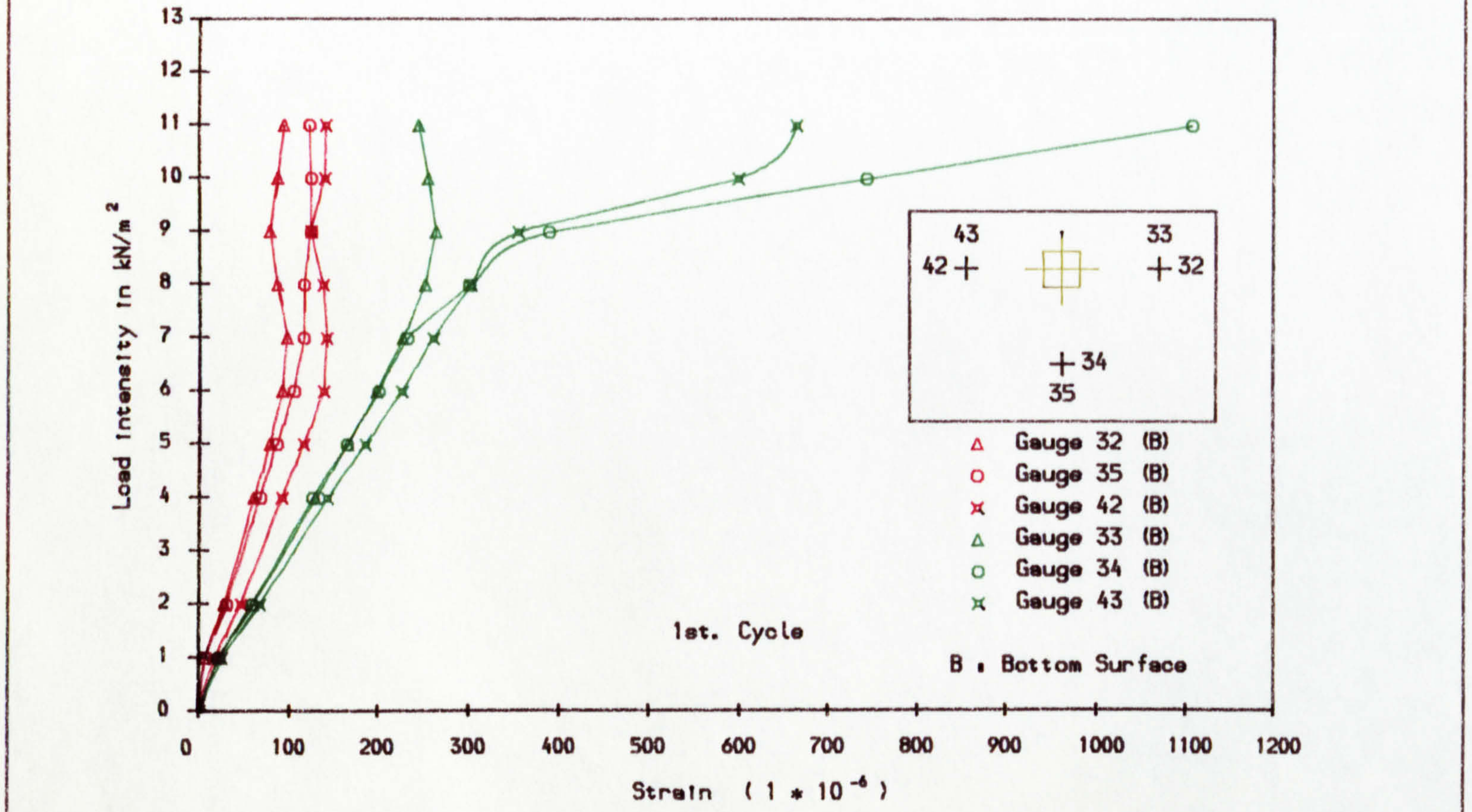

Fig. 8.45 Concrete strain at 100mm from panel centre lines, Slab A4

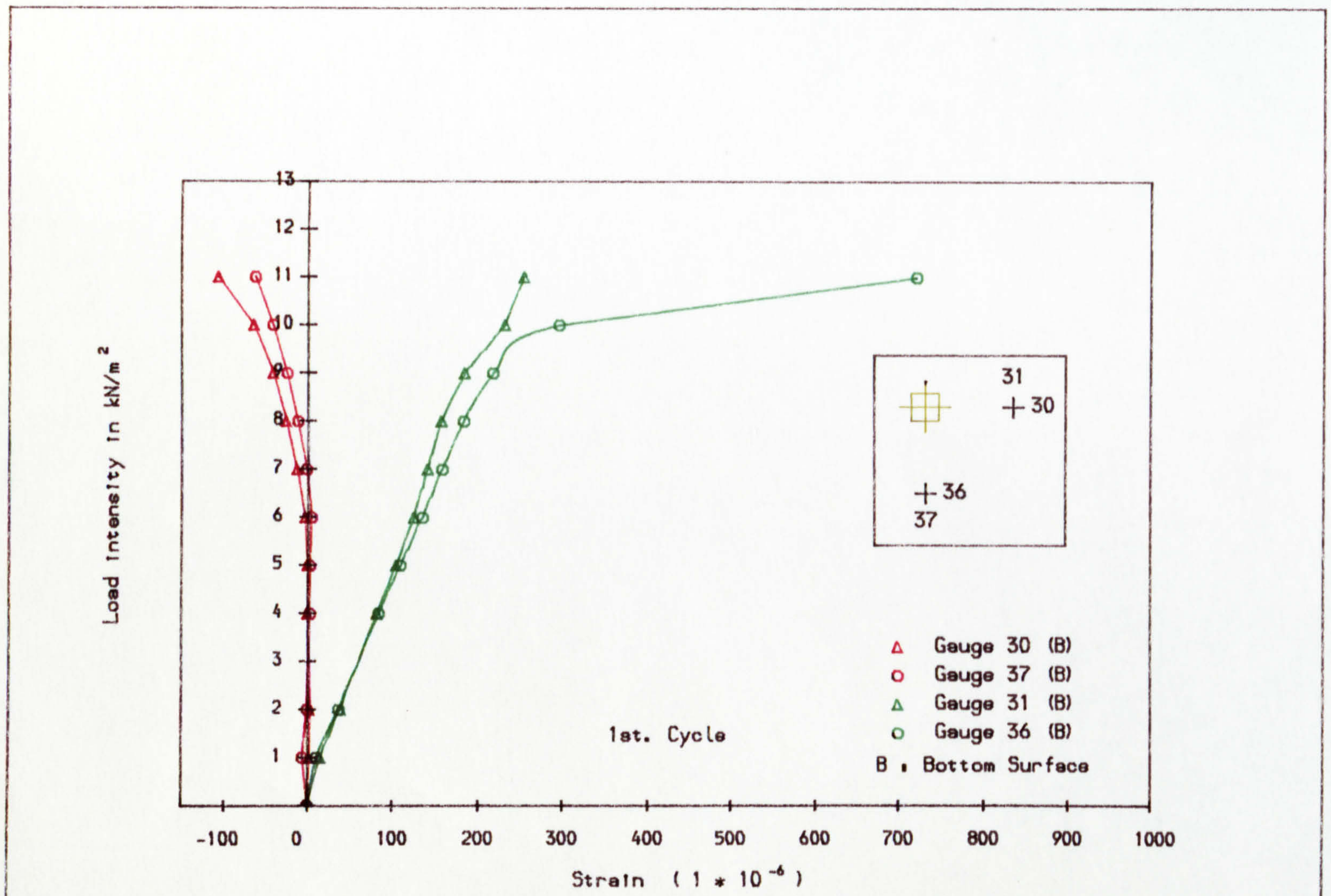

Fig. 8.46 Concrete strain at 225mm from panel centre lines, Slab A4

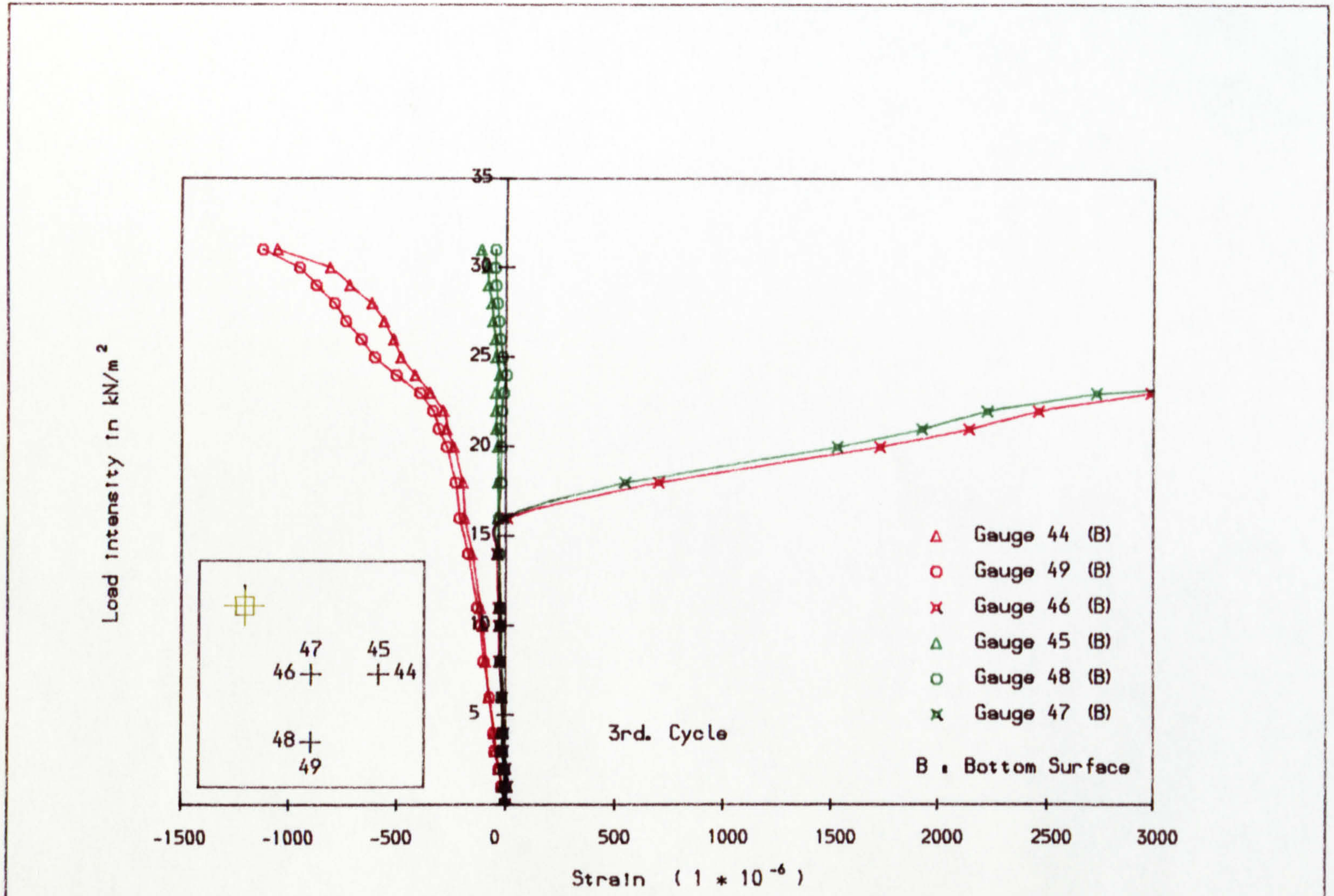

Fig. 8.47 Concrete strain at 375mm from panel centre lines, Slab B1

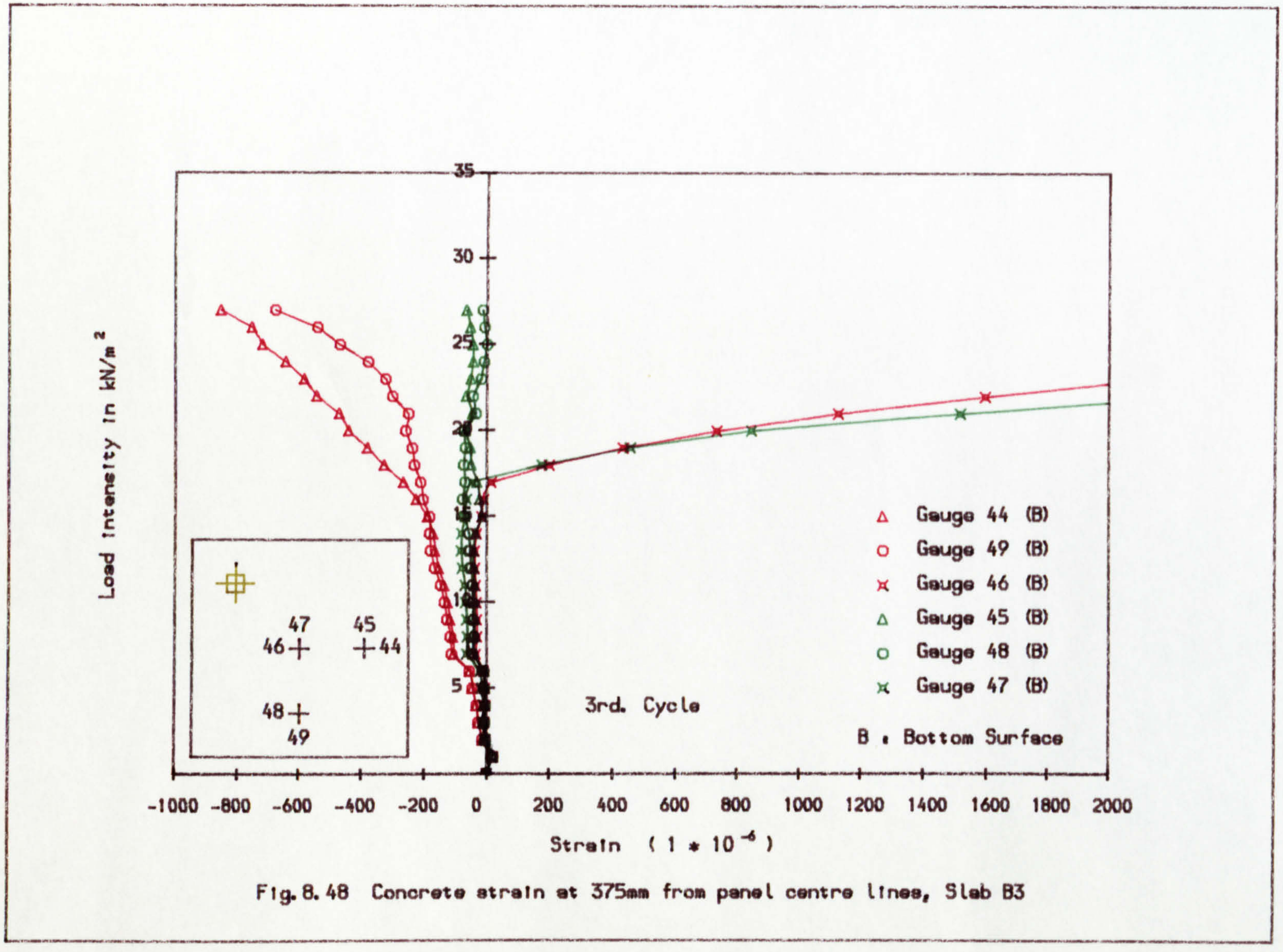

Fig. 8.48 Concrete strain at 375mm from panel centre lines, Slab B3

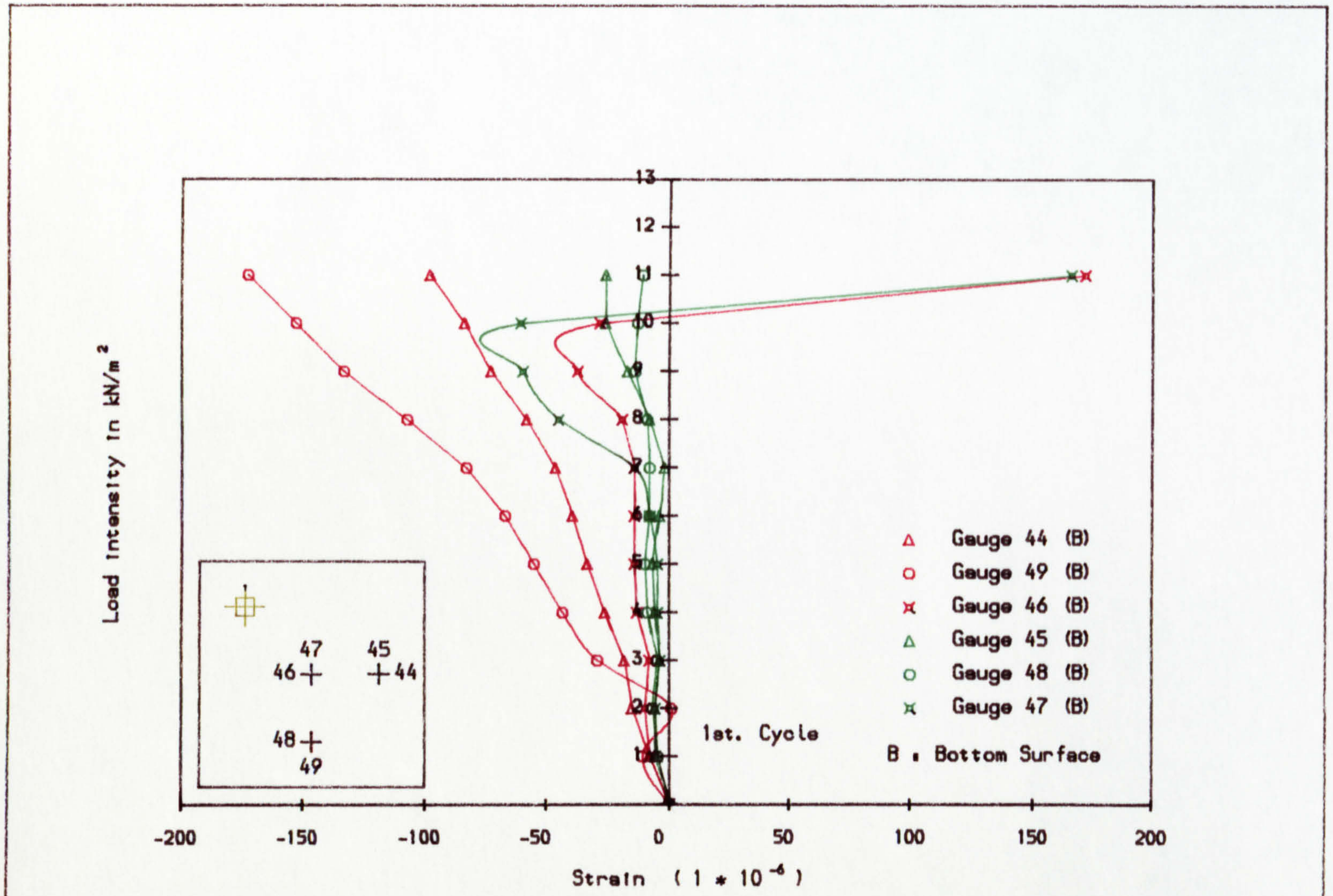

Fig. 8.49 Concrete strain at 375mm from panel centre lines, Slab B4

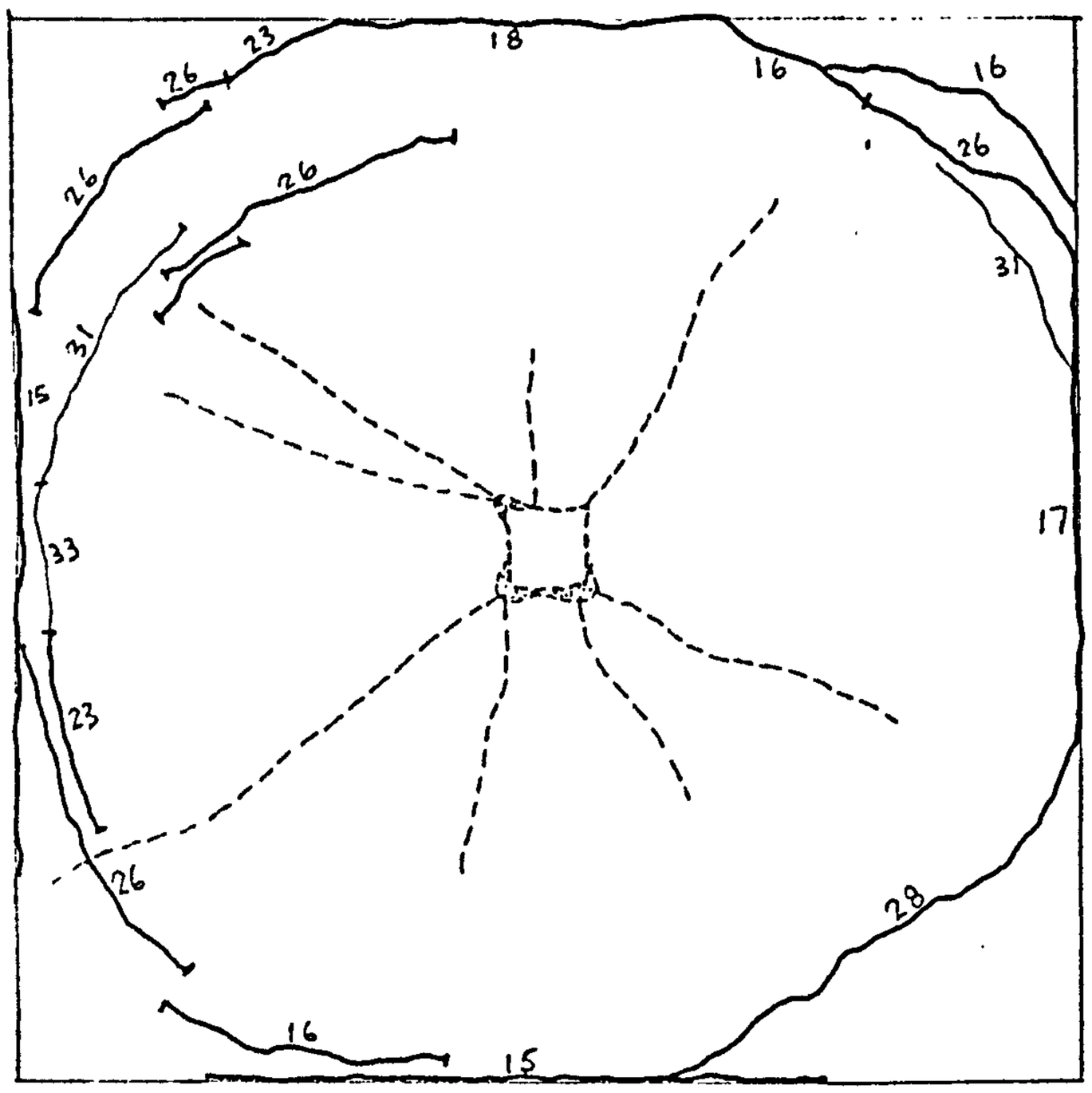

(a) Top surface

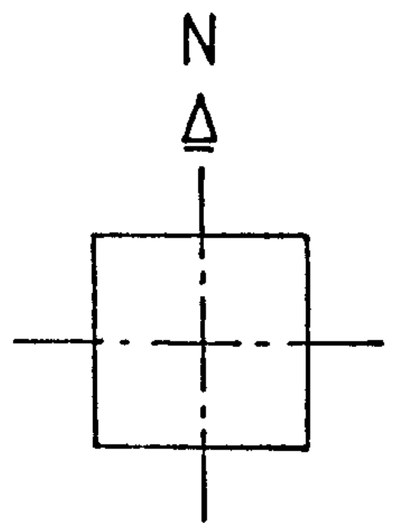

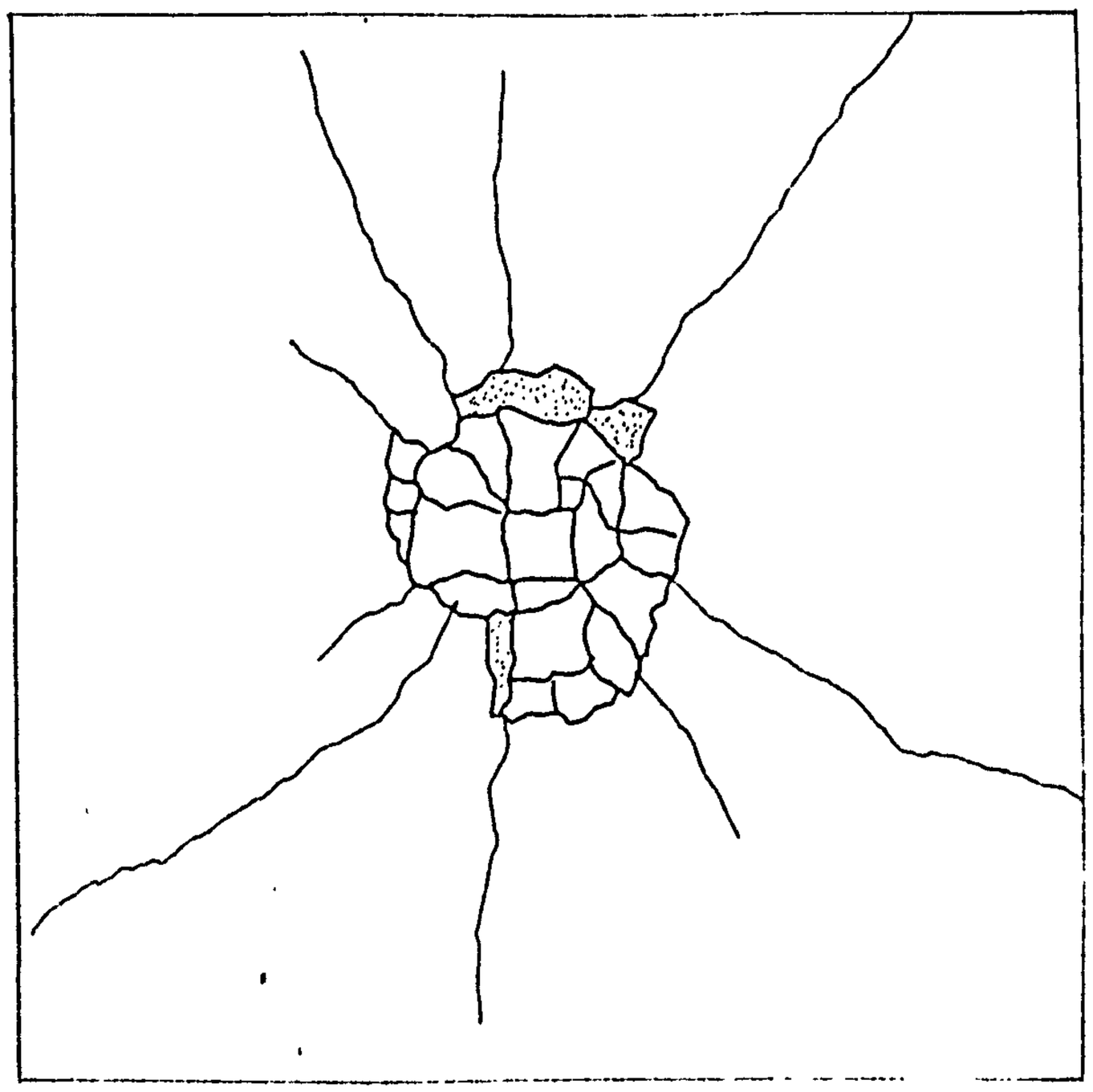

(b) Bottom surface

Fig. 8.50 Plans of crack pattern, A1

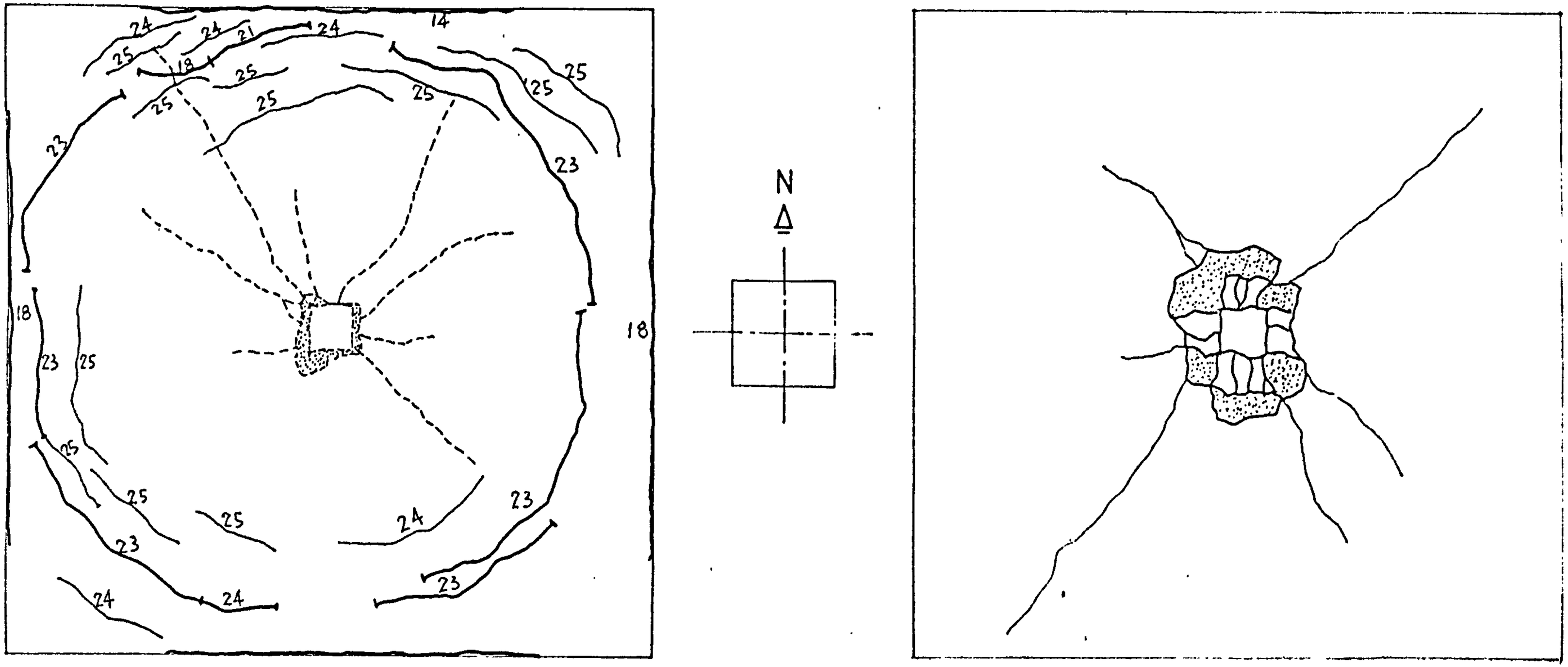

(a) Top surface

(b) Bottom surface

Fig. 8.51 Plans of crack pattern, A2

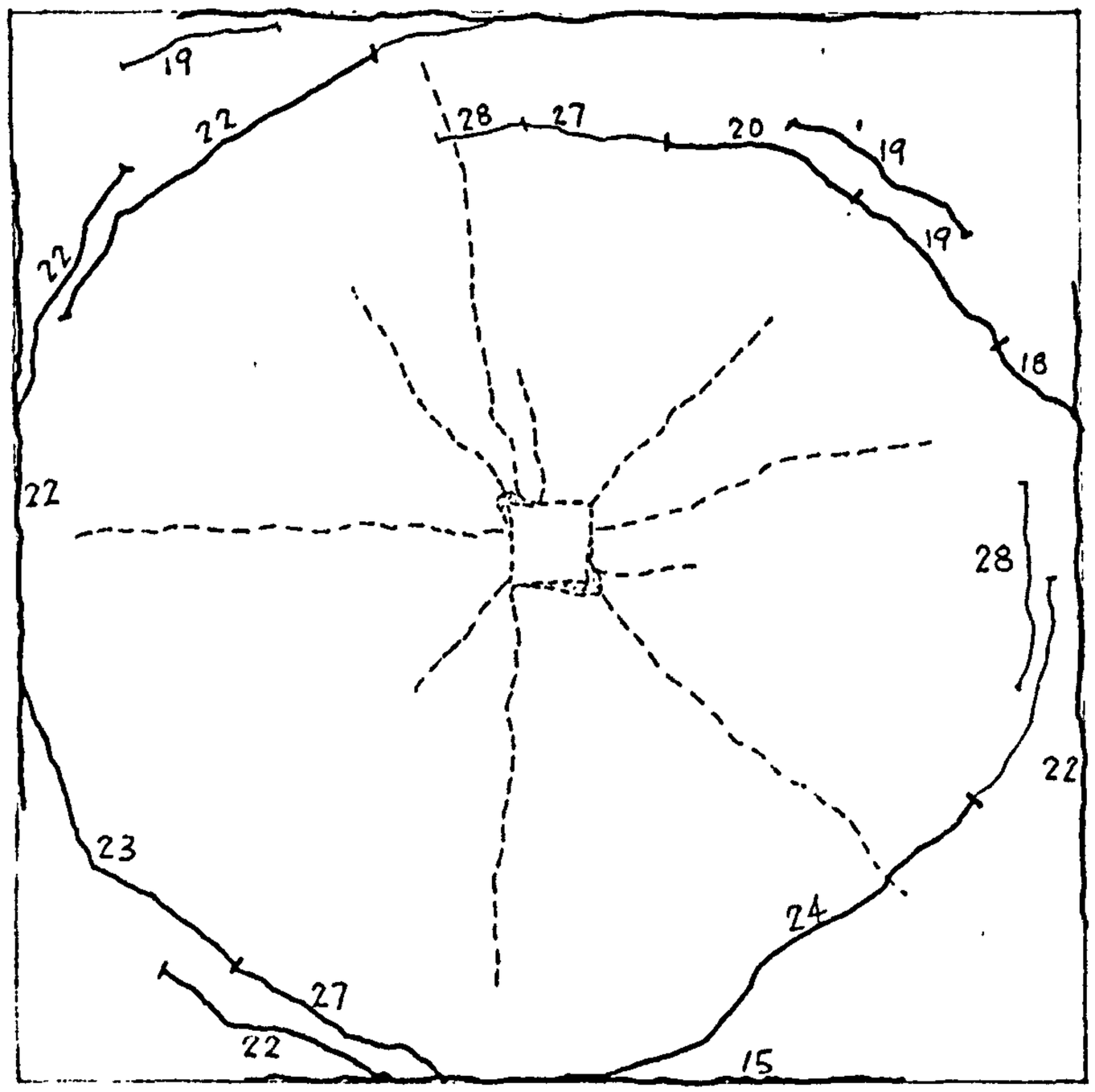

(a) Top surface

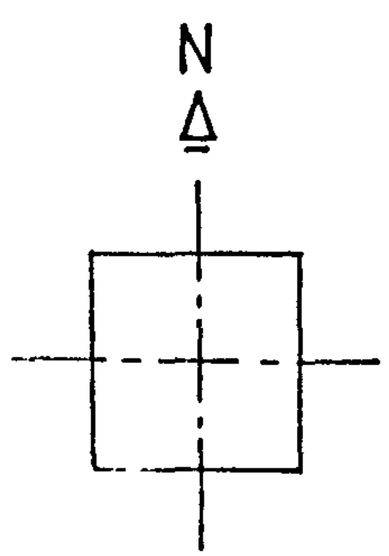

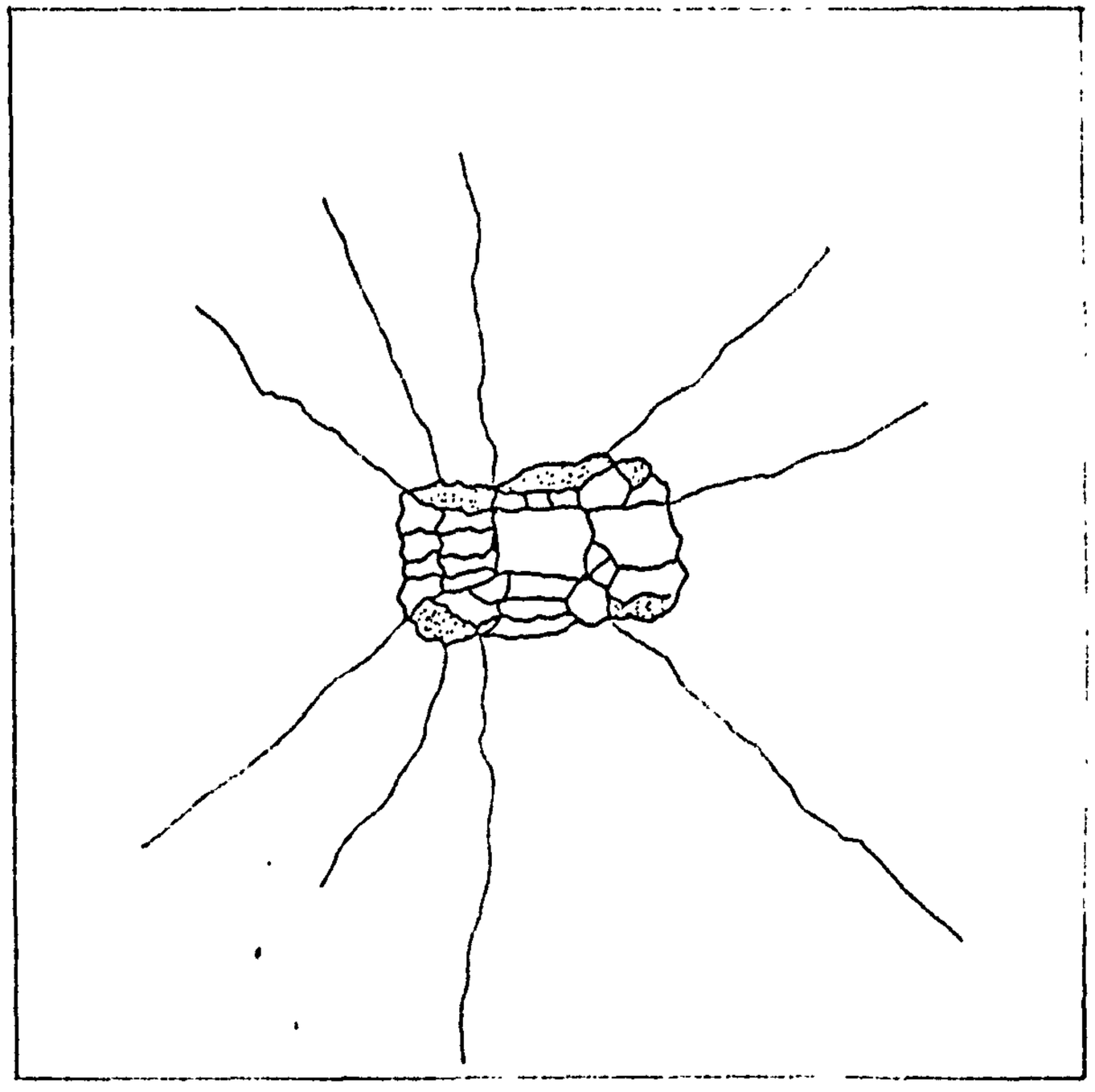

(b) Bottom surface

Fig. 8.52 Plans of crack pattern, A3

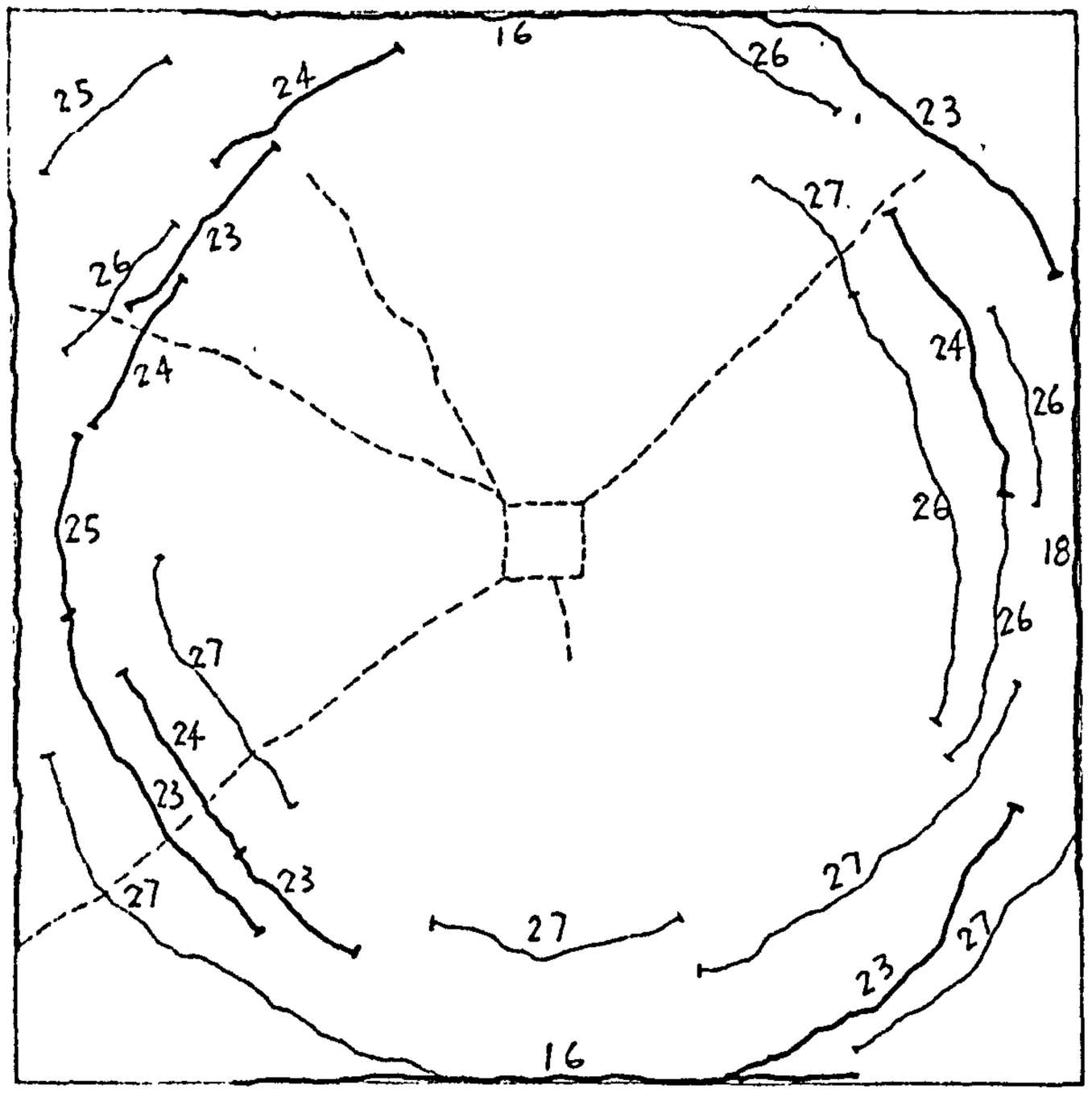

(a) Top surface

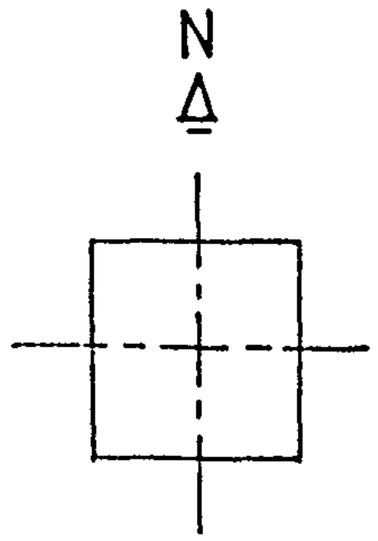

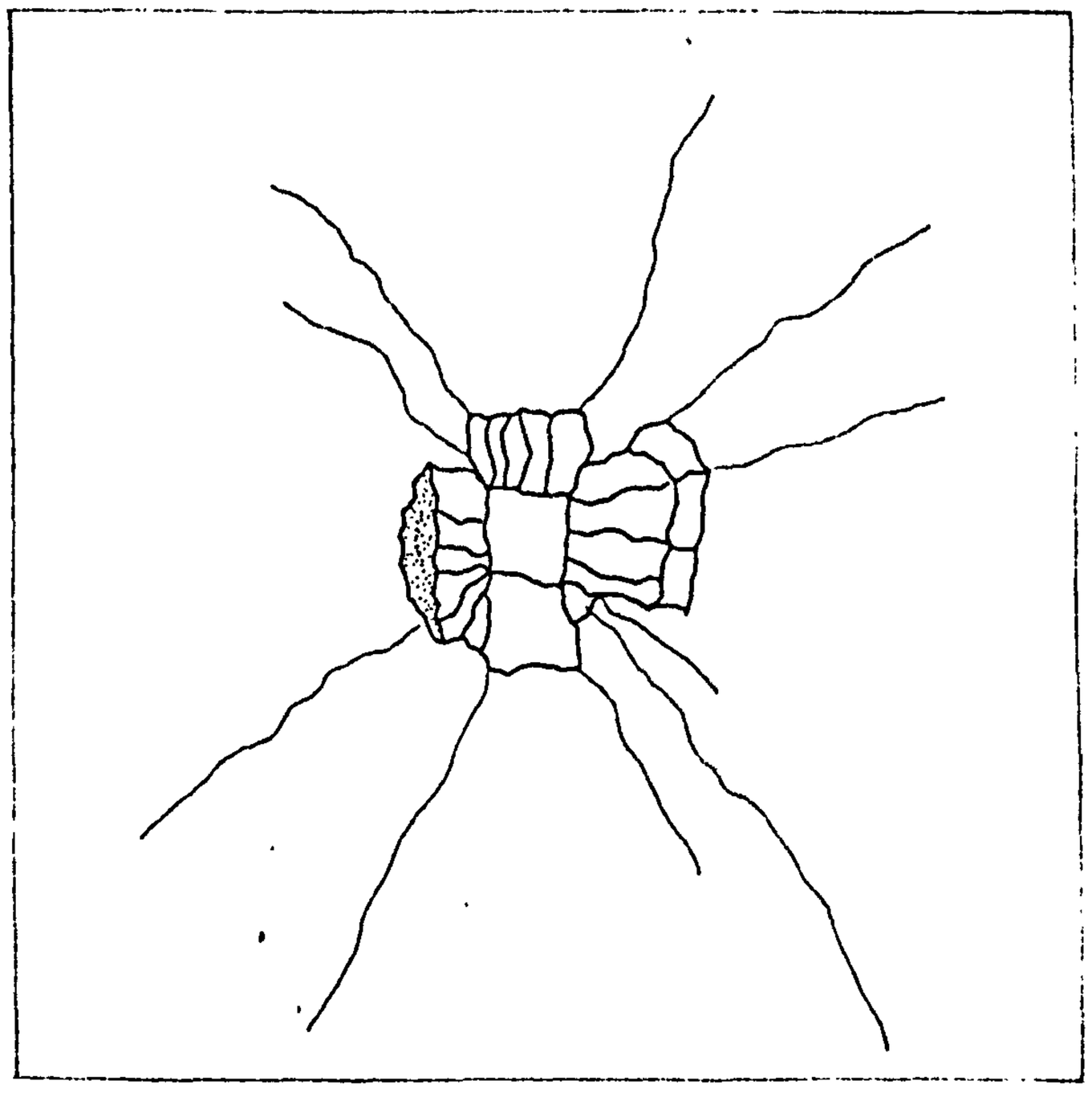

(b) Bottom surface

Fig. 8.53 Plans of crack pattern, A4

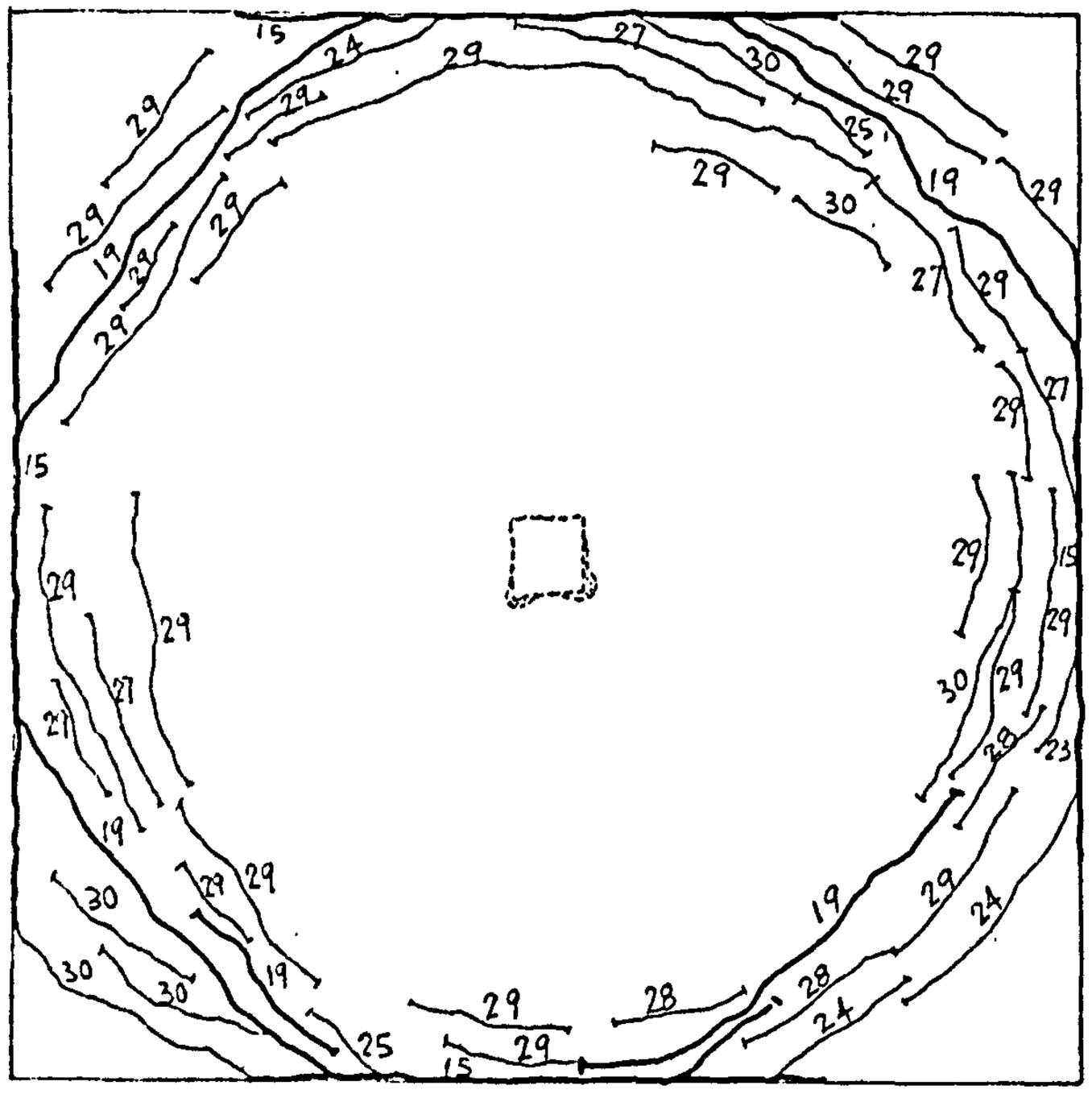

(a) Top surface

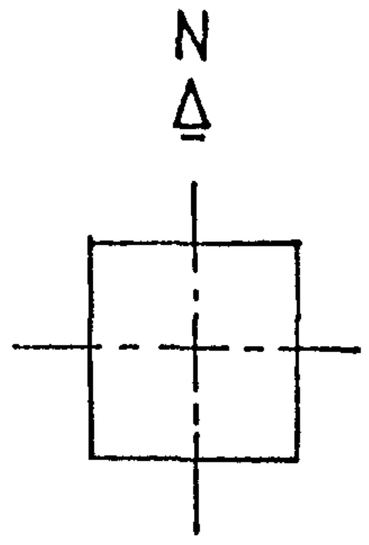

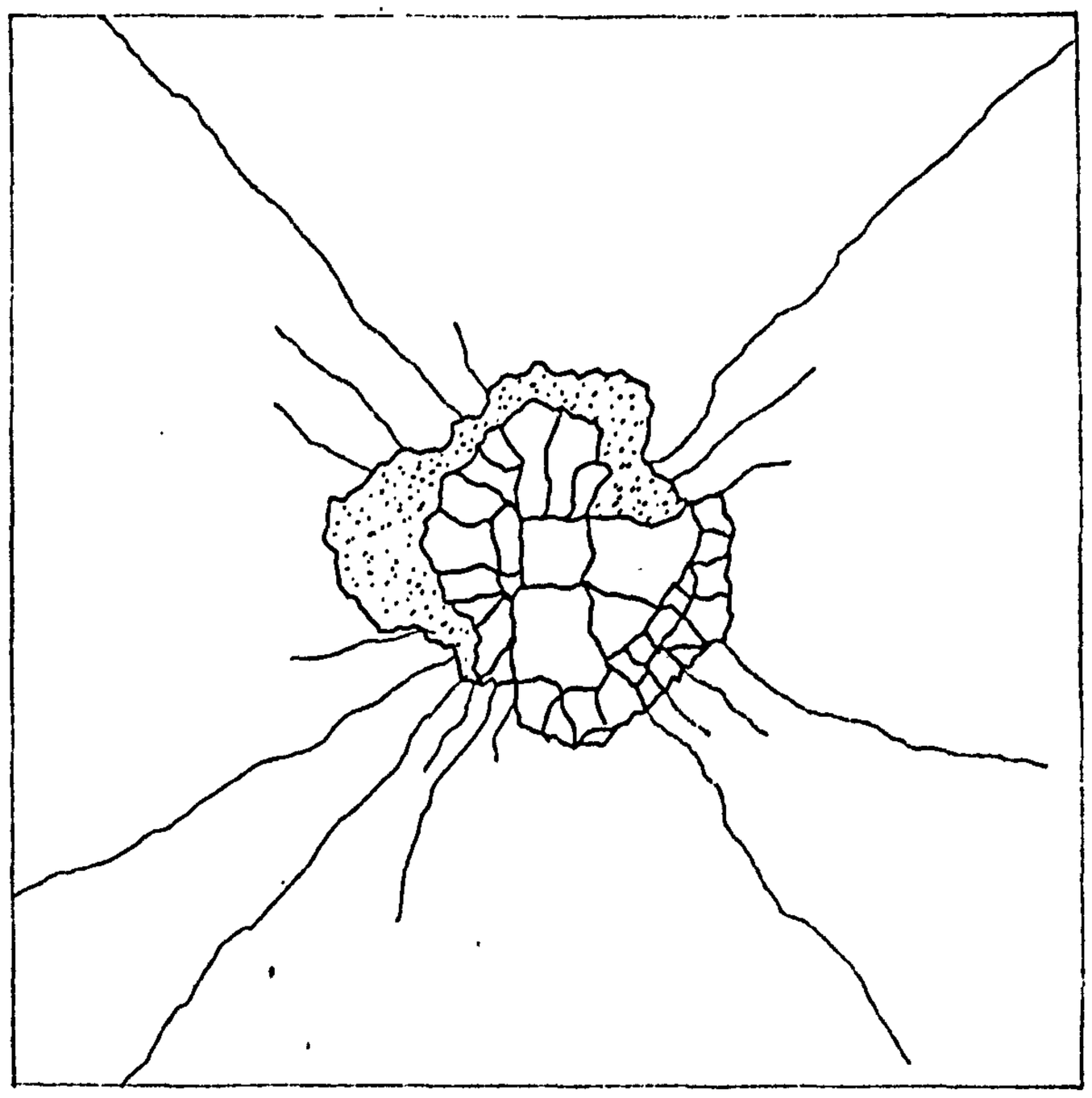

(b) Botton surface

Fig. 8.54 Plans of crack pattern, B1

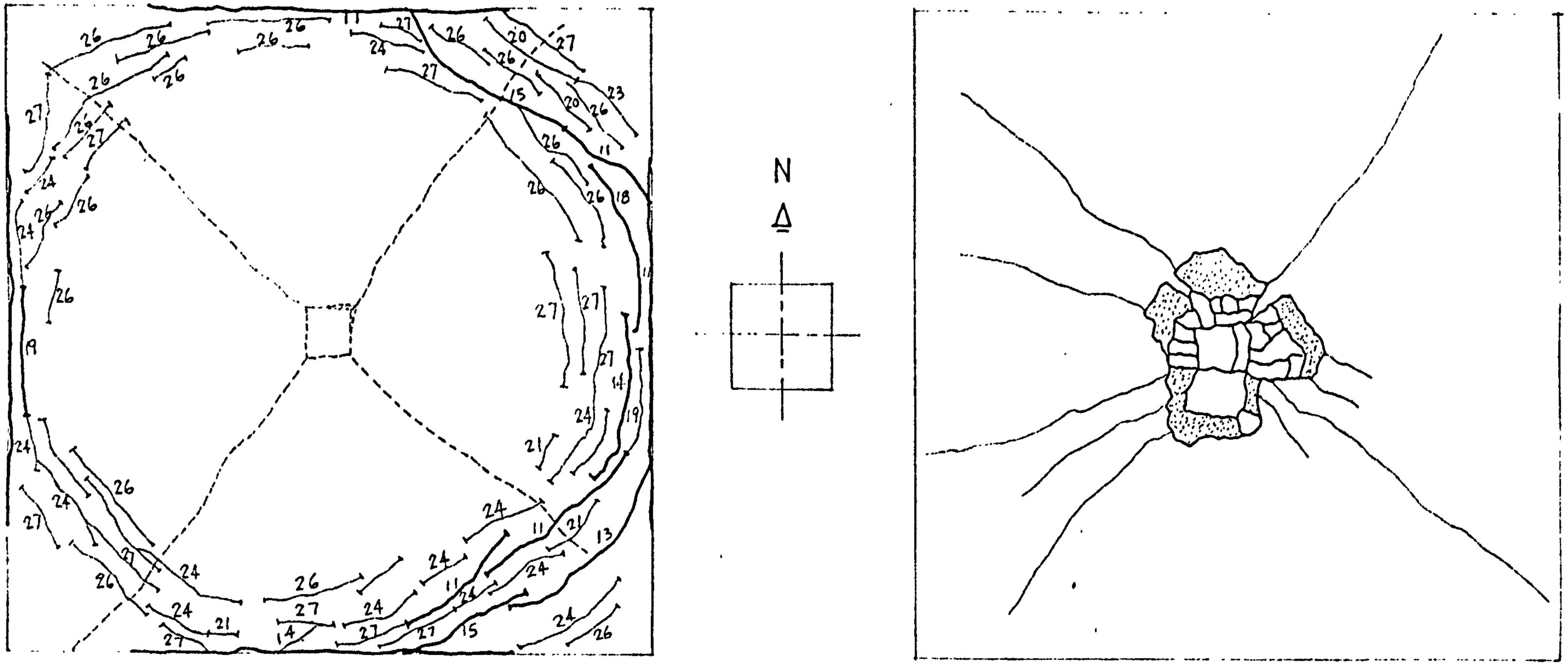

(a) Top surface

(b) Bottom surface

Fig. 8.55 Plans of crack pattern, B2

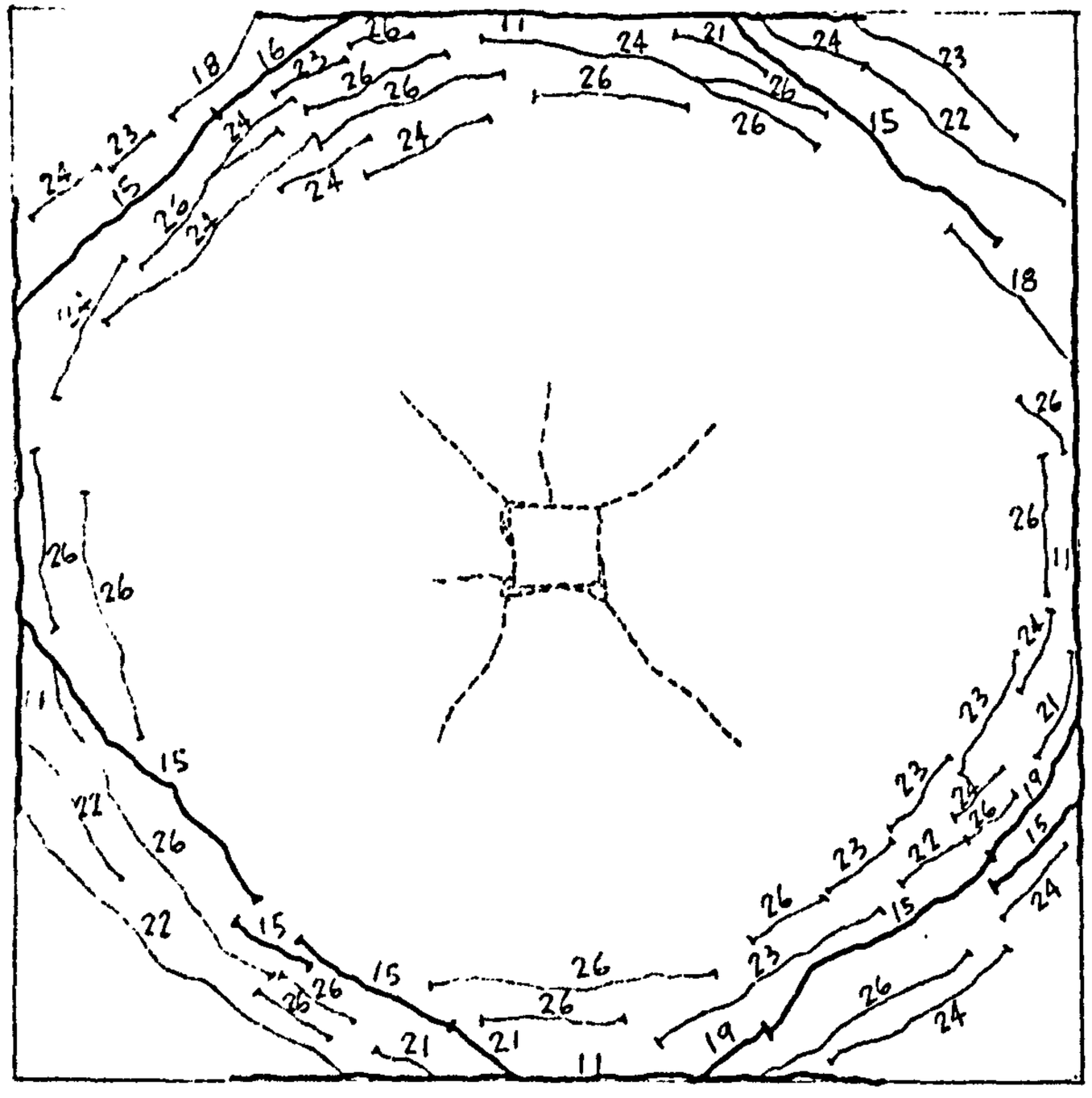

(a) Top surface

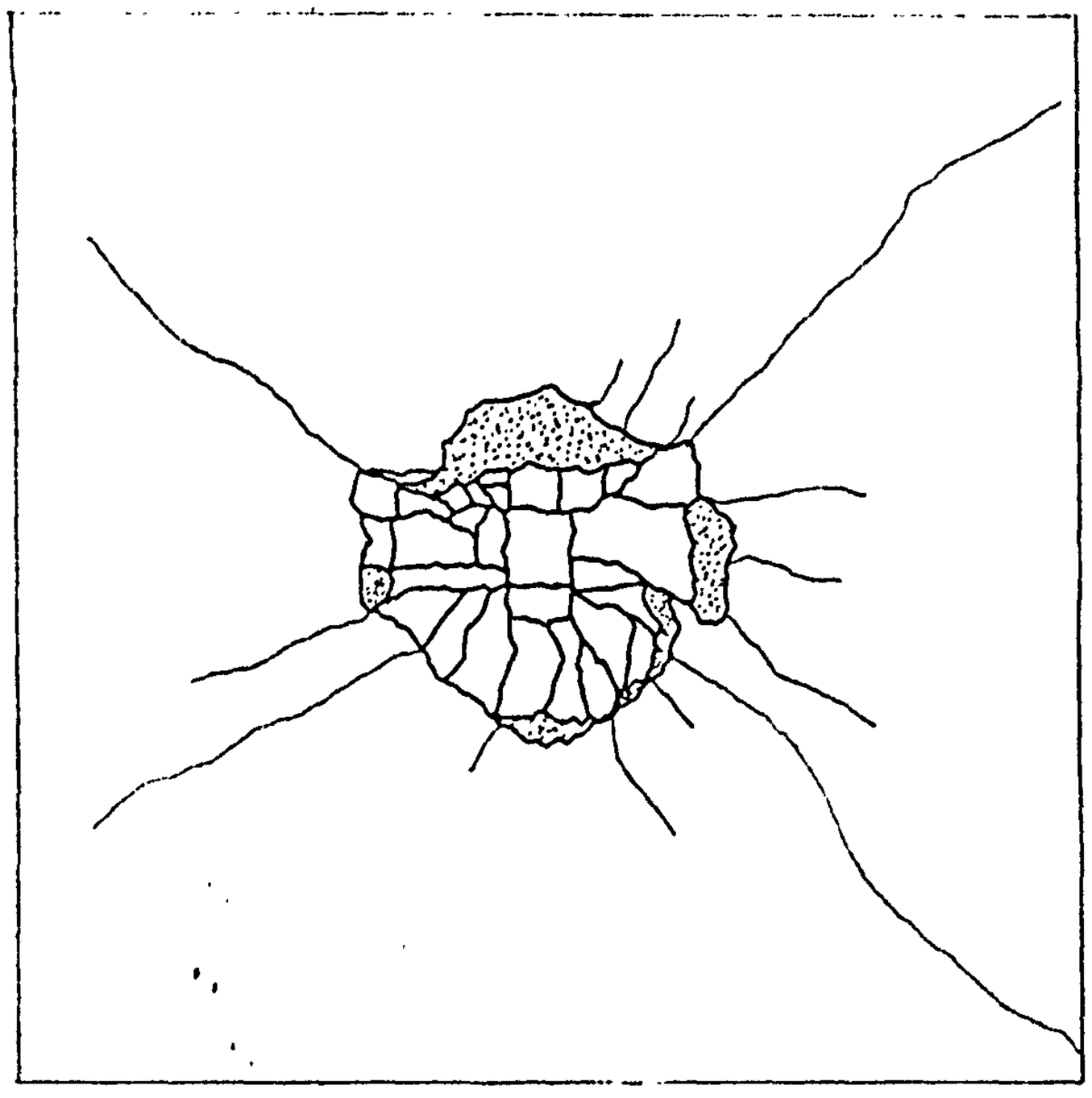

(b) Bottom surface

Fig. 8.56 Plans of crack pattern, B3

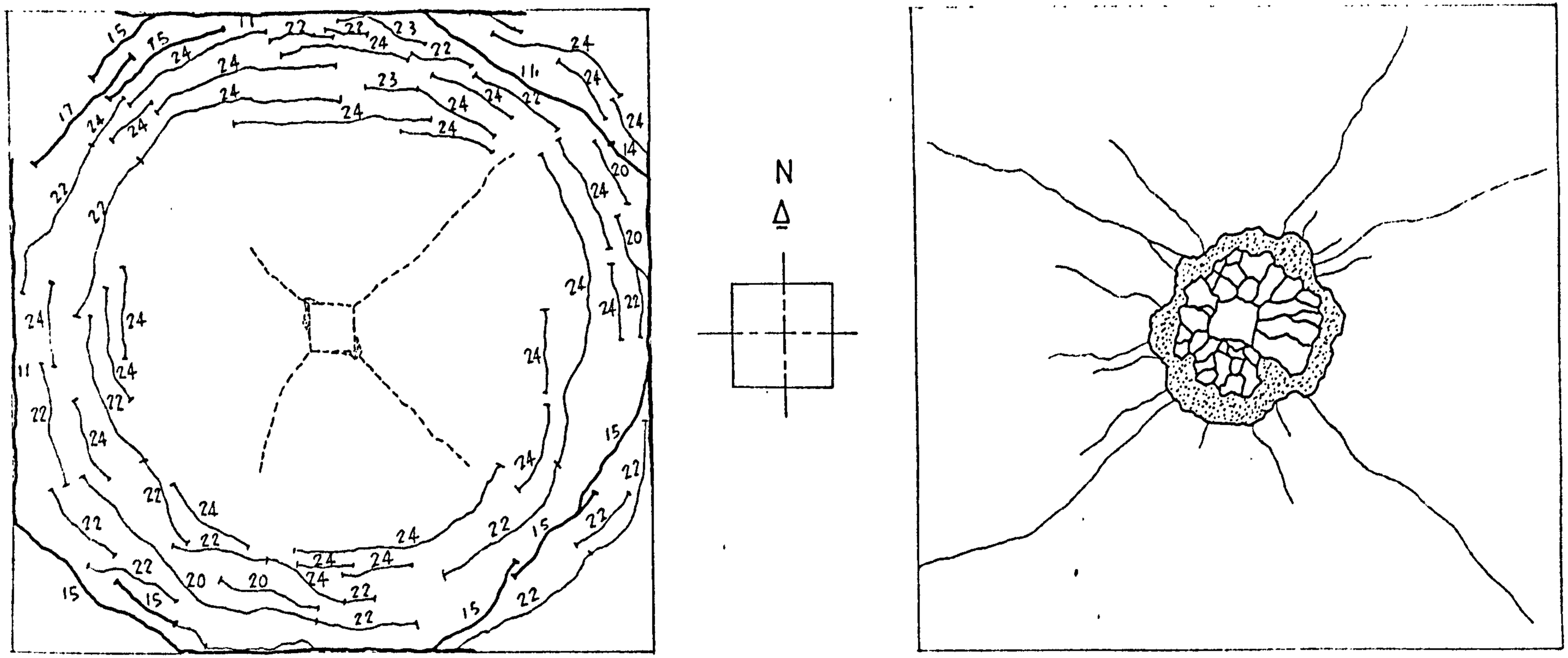

(a) Top surface

(b) Bottom surface

Fig. 8.57 Plans of crack pattern, B4

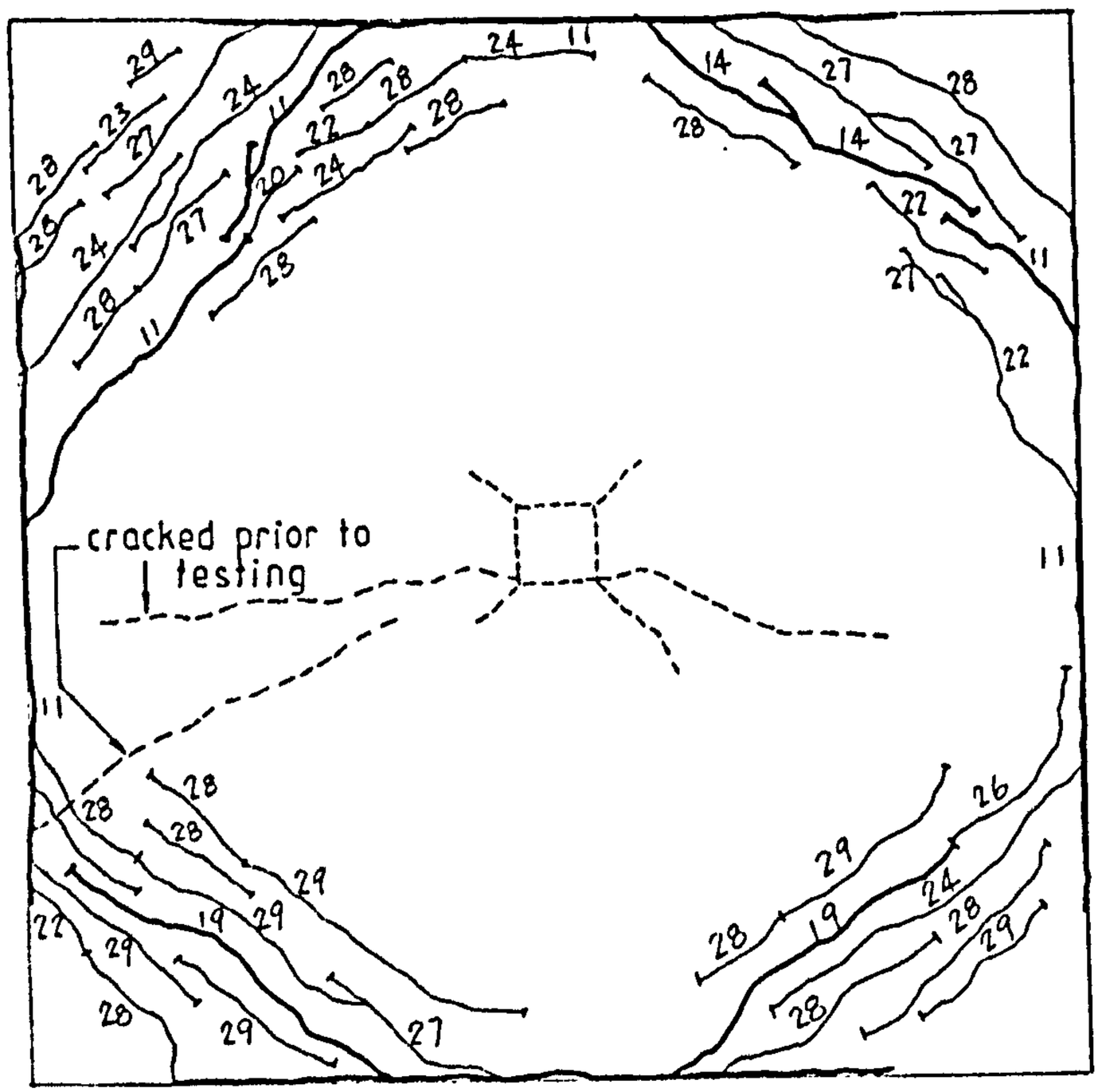

(a) Top surface

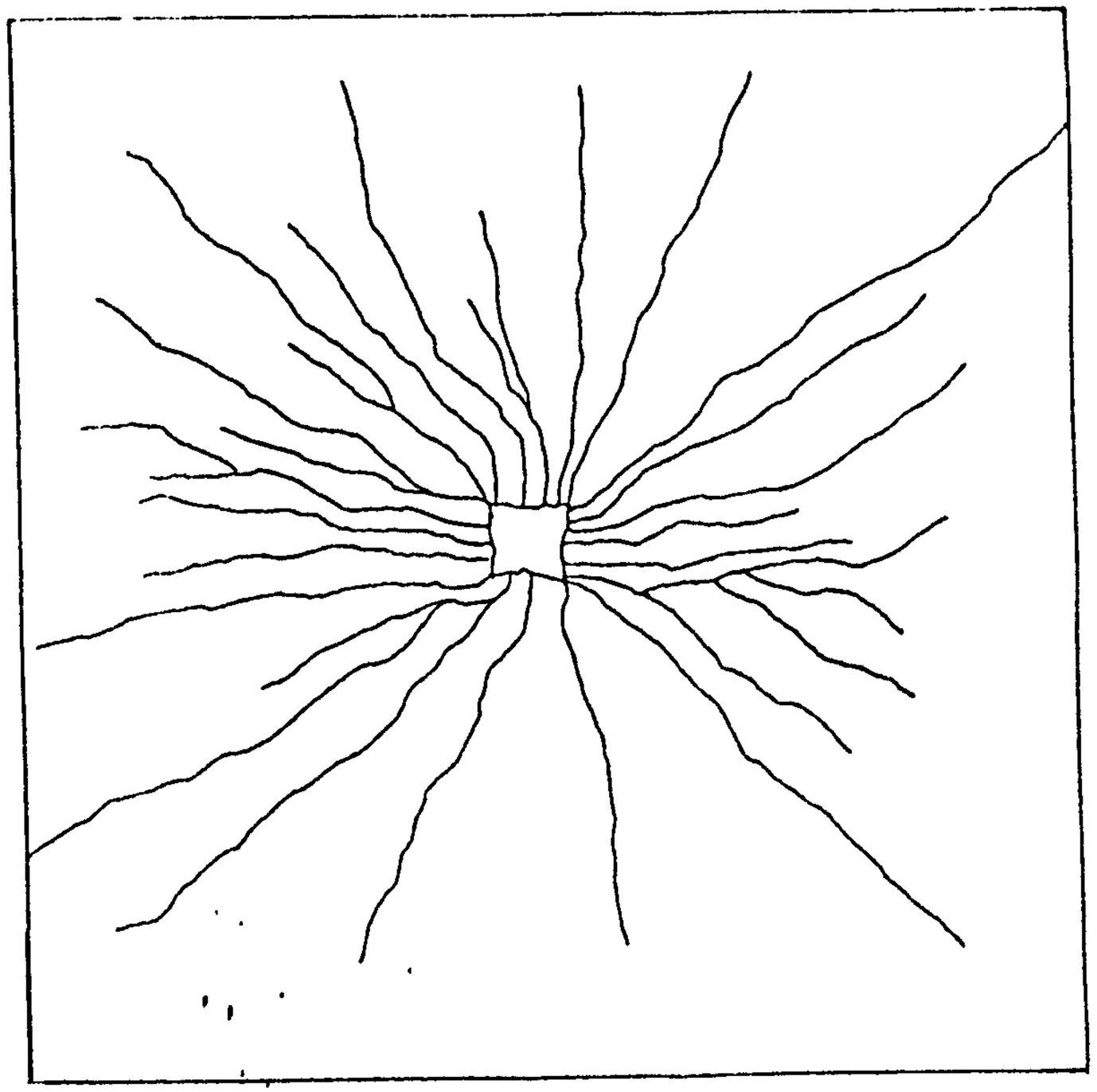

(b) Bottom surface

Fig. 8.58 Plans of crack pattern, C1

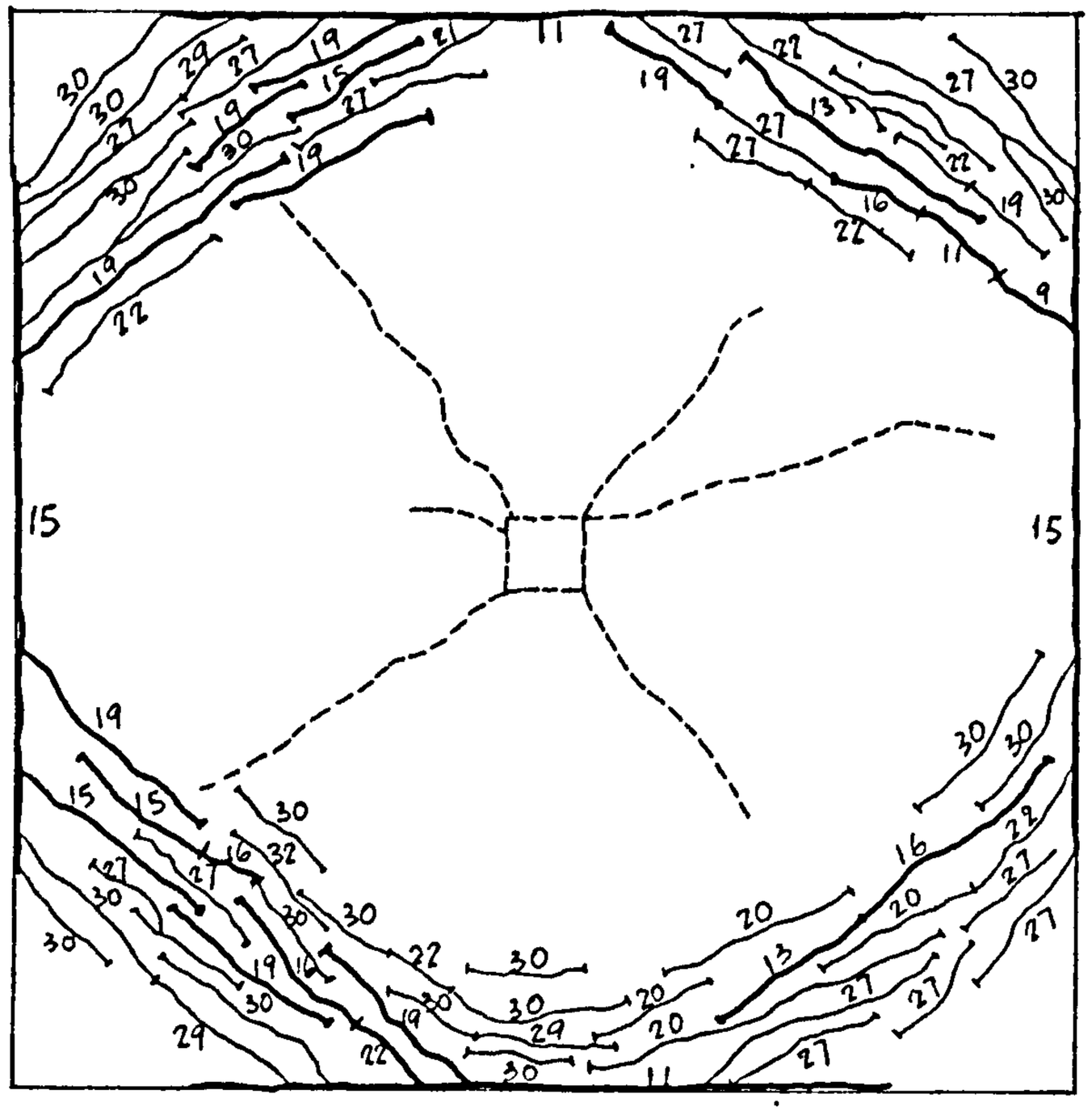

(a) Top surface

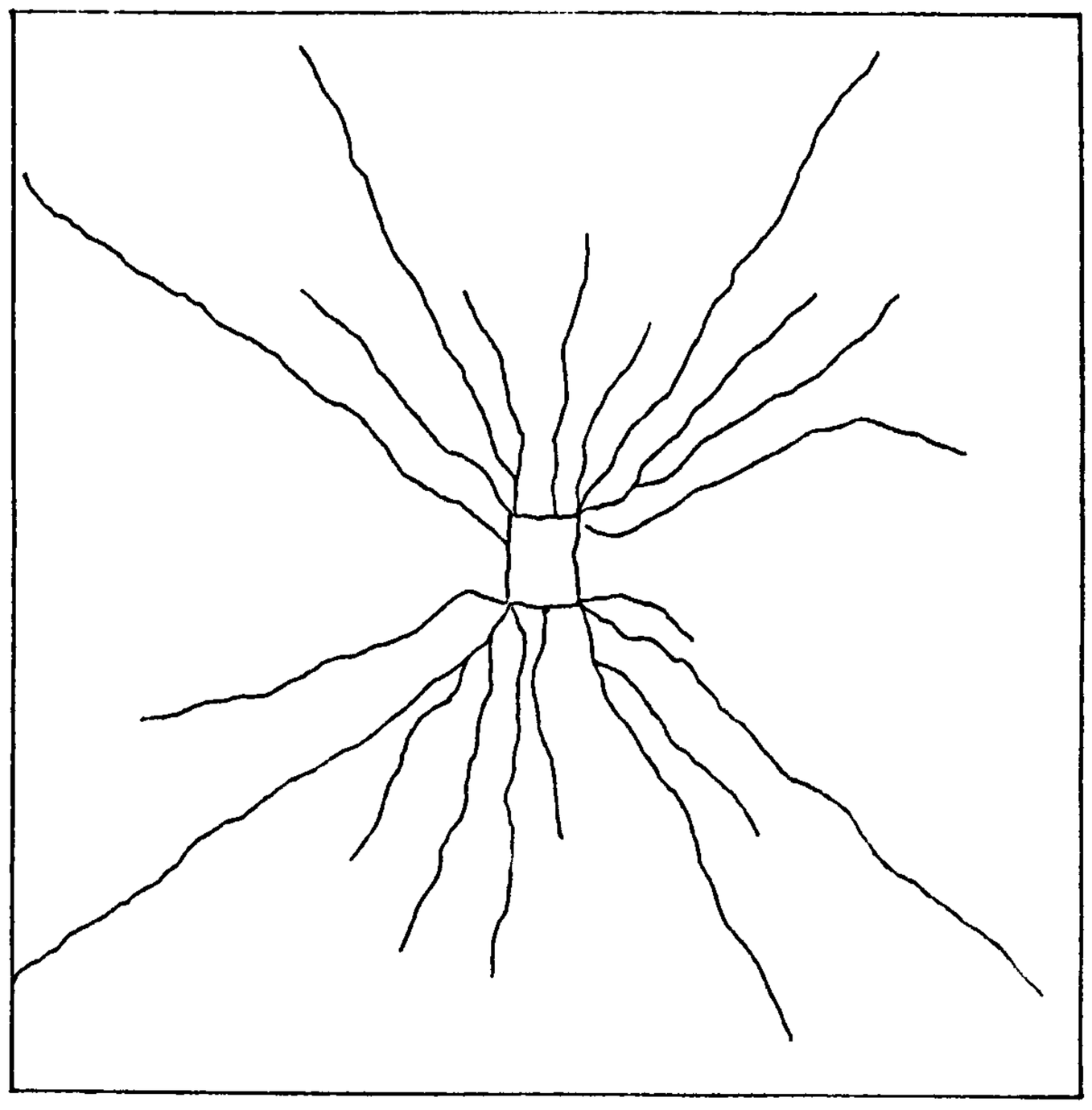

(b) Bottom surface

Fig. 8.59 Plans of crack pattern, C2

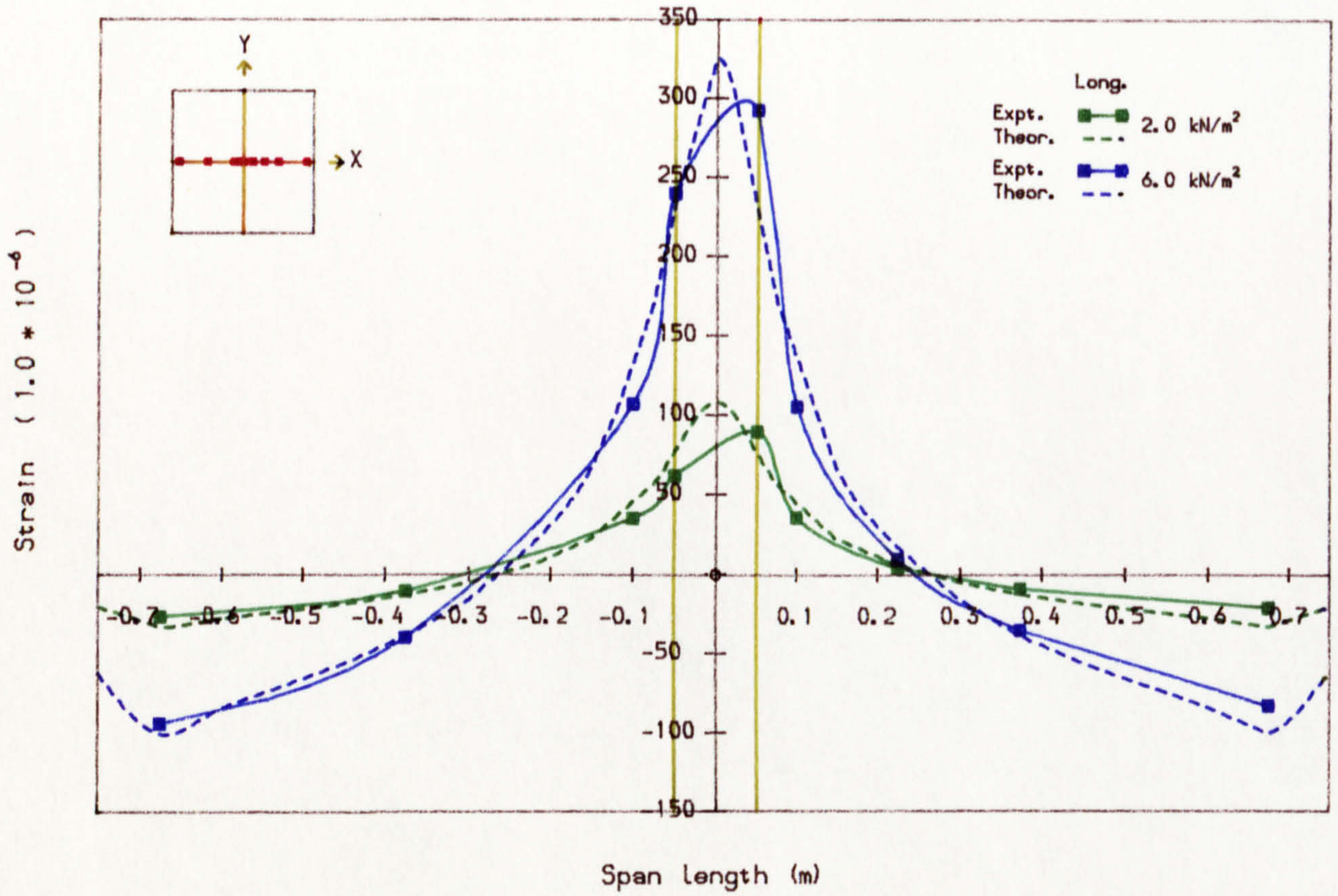

Fig. 8.60 Measured and theoretical longitudinal bending strain along slab centre line, Slab B1

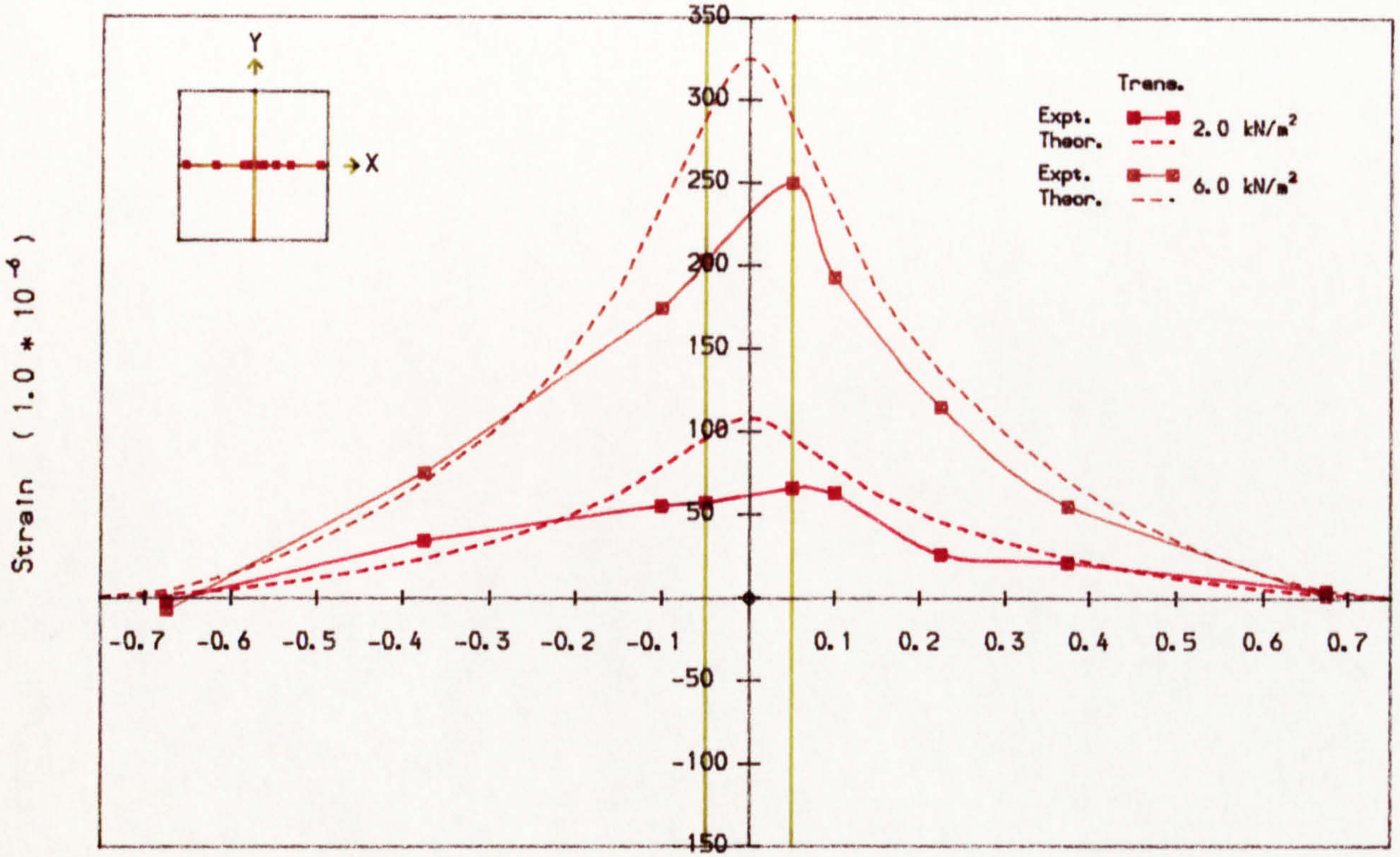

Fig. 8.61 Measured and theoretical transverse bending strain across slab centre line, Slab B1

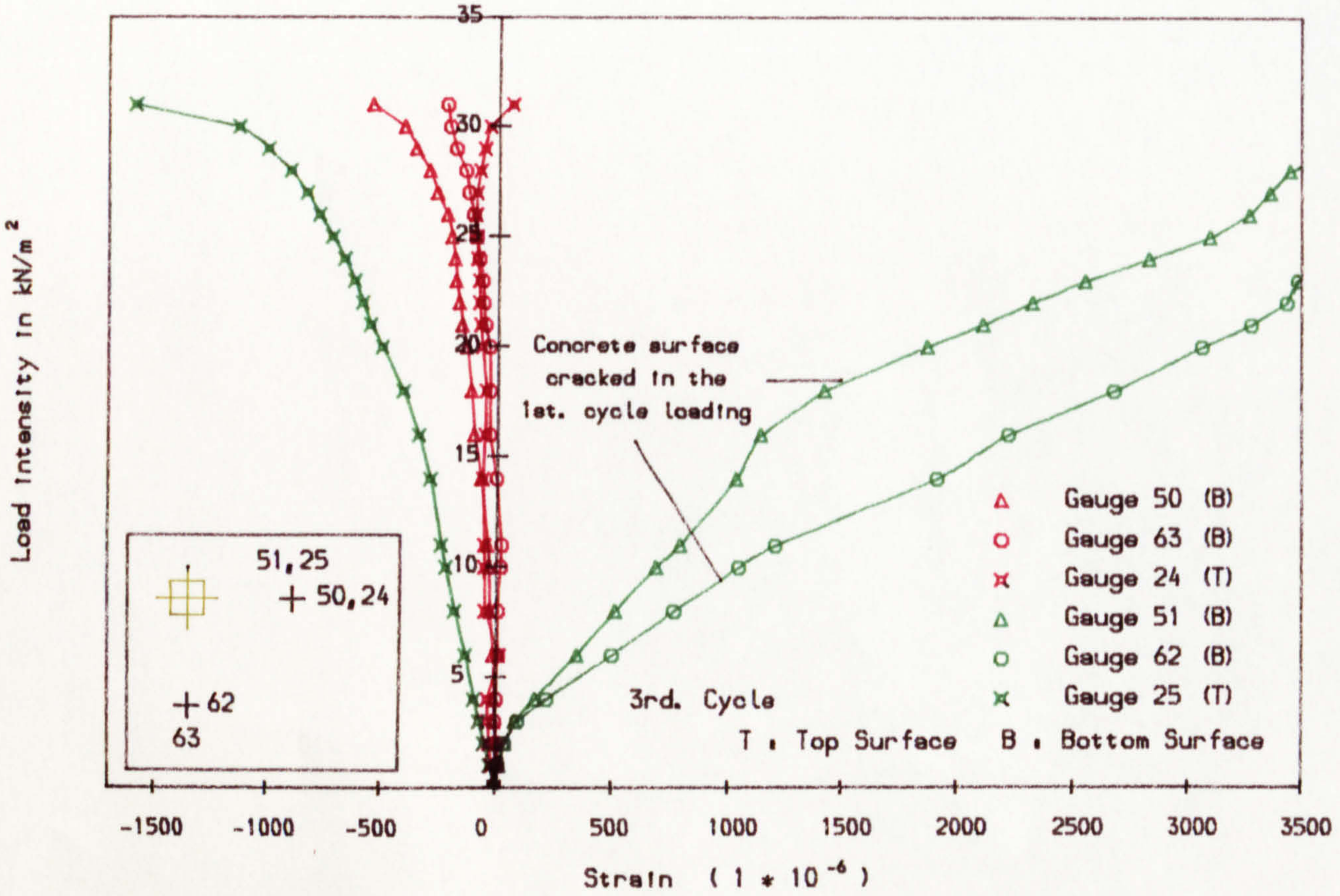

Fig. 8.62 Concrete strain at 225mm from panel centre lines, Slab B1

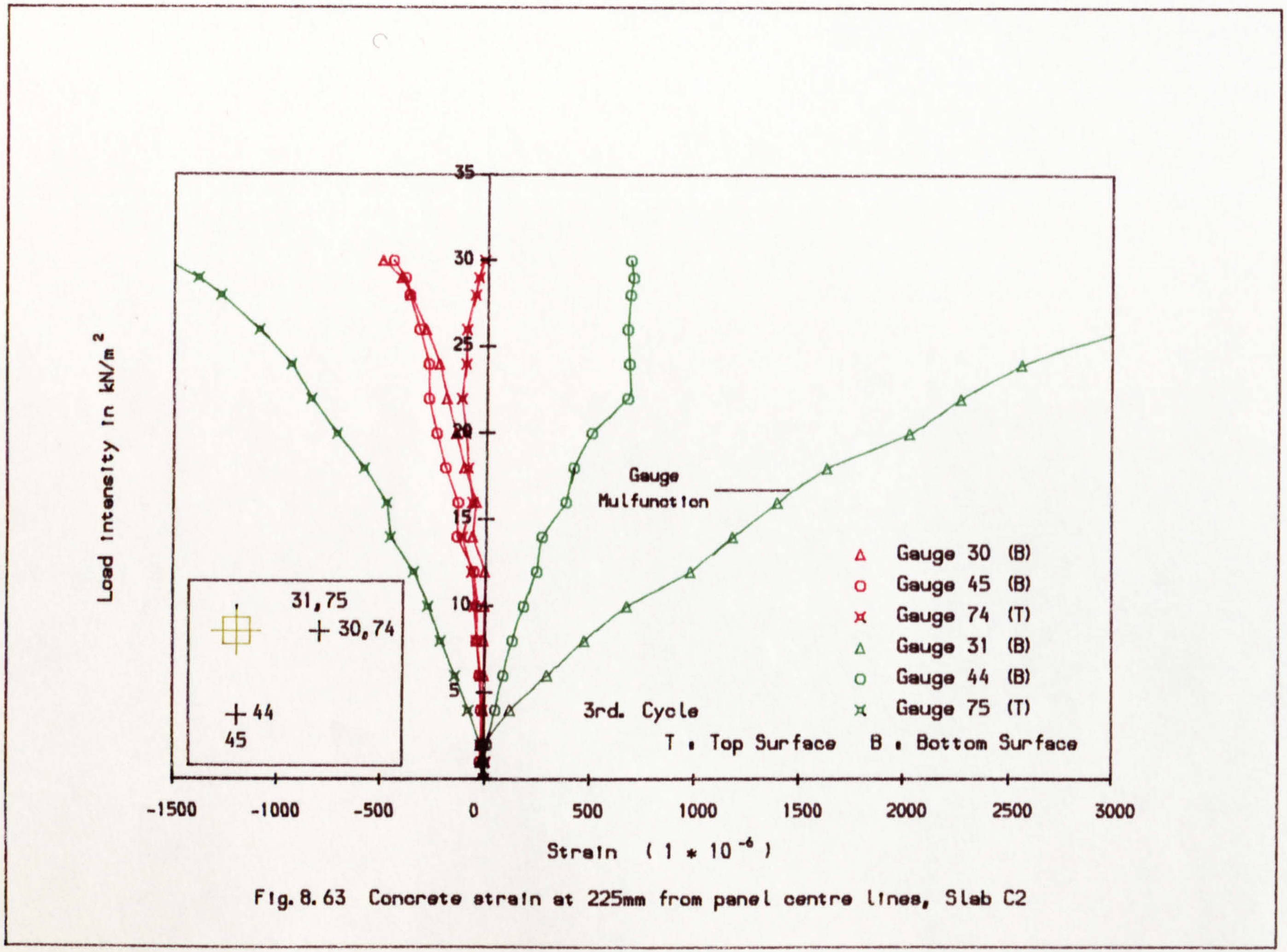

Fig. 8.63 Concrete strain at 225mm from panel centre lines, Slab C2

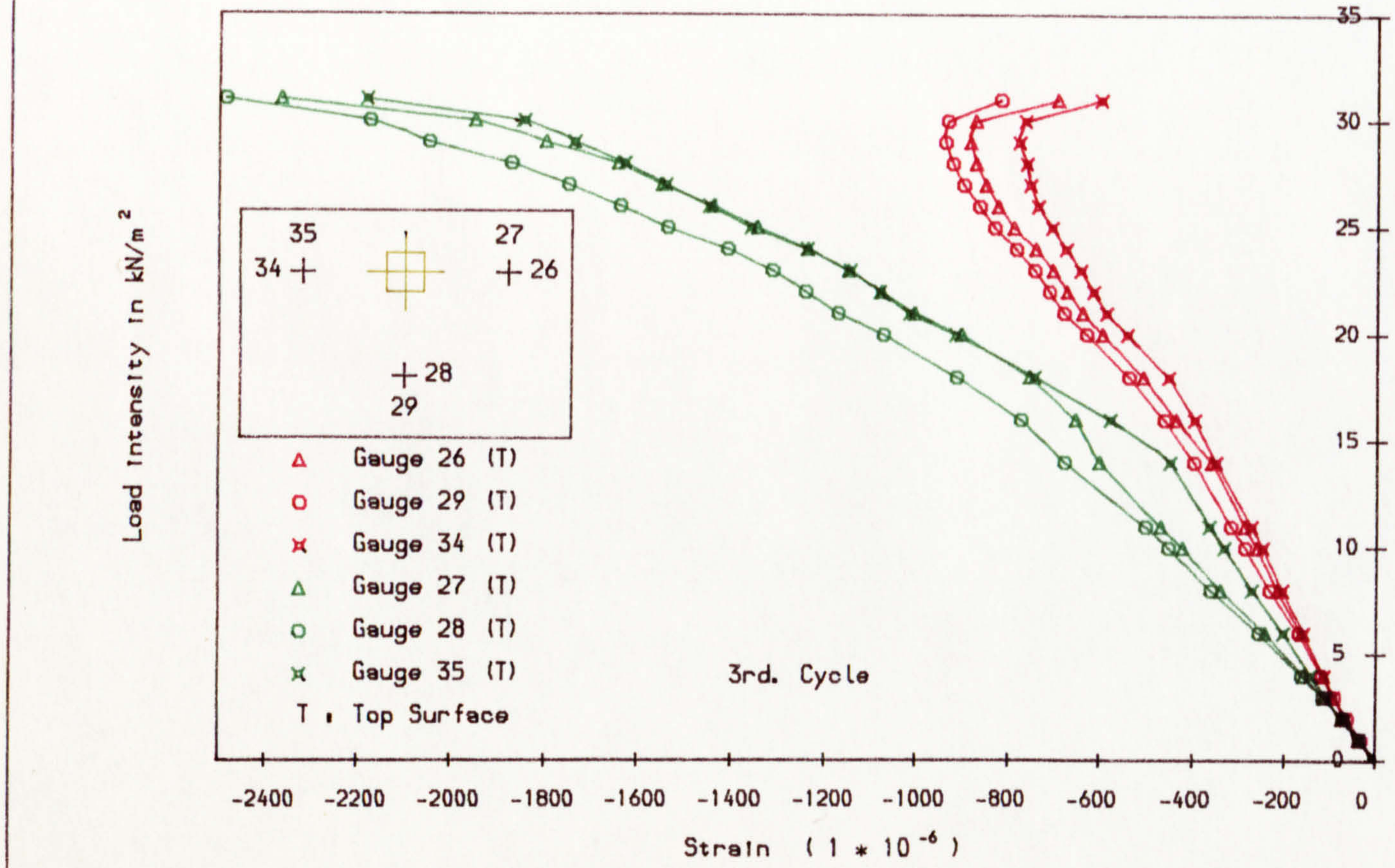

Fig. 8.64 Concrete strain at 100mm from panel centre lines, Slab B1

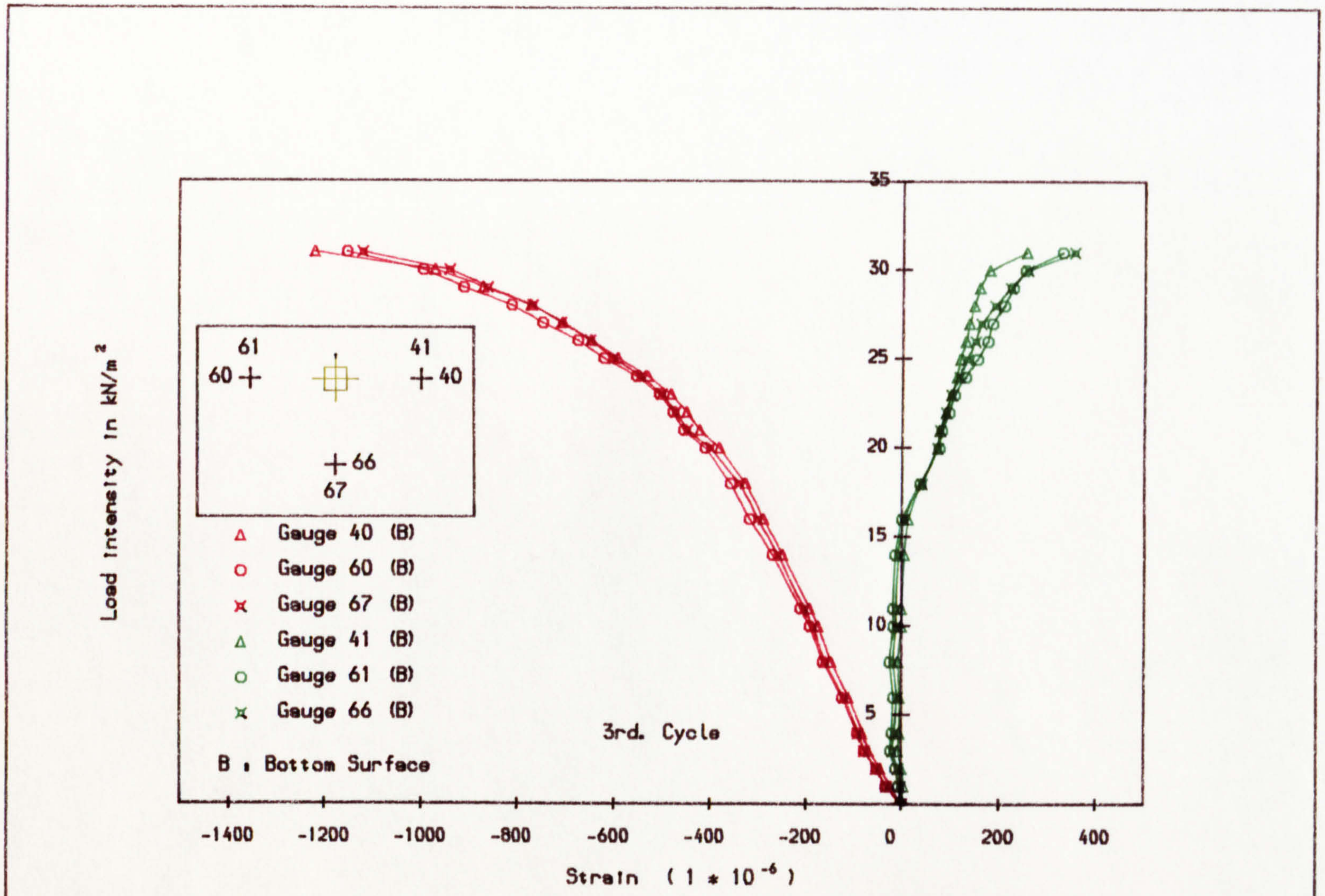

Fig. 8.65 Concrete strain at 675mm from panel centre lines, Slab B1

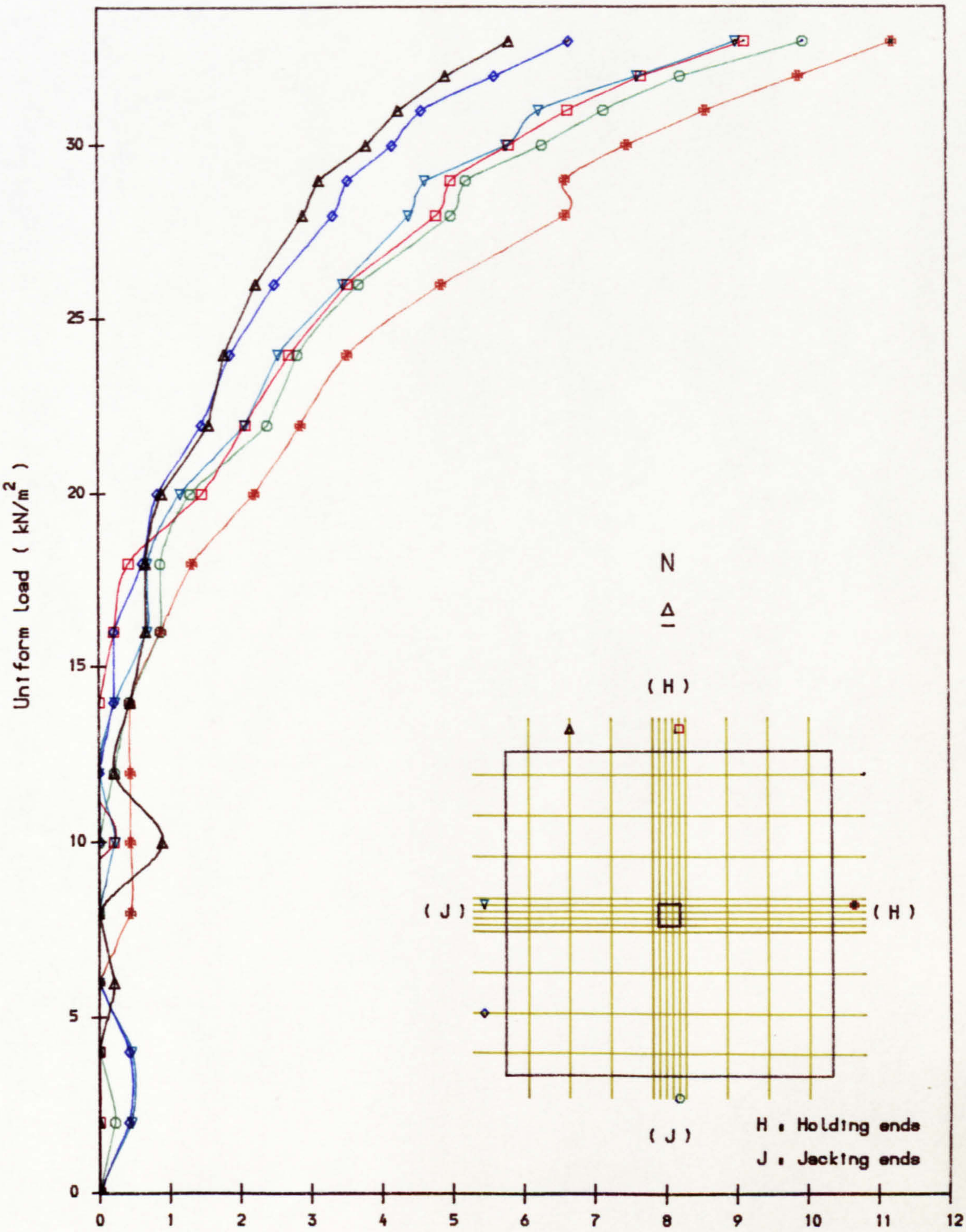

Fig. 8.66 Changes of tendon stress under uniform loading, Slab A1

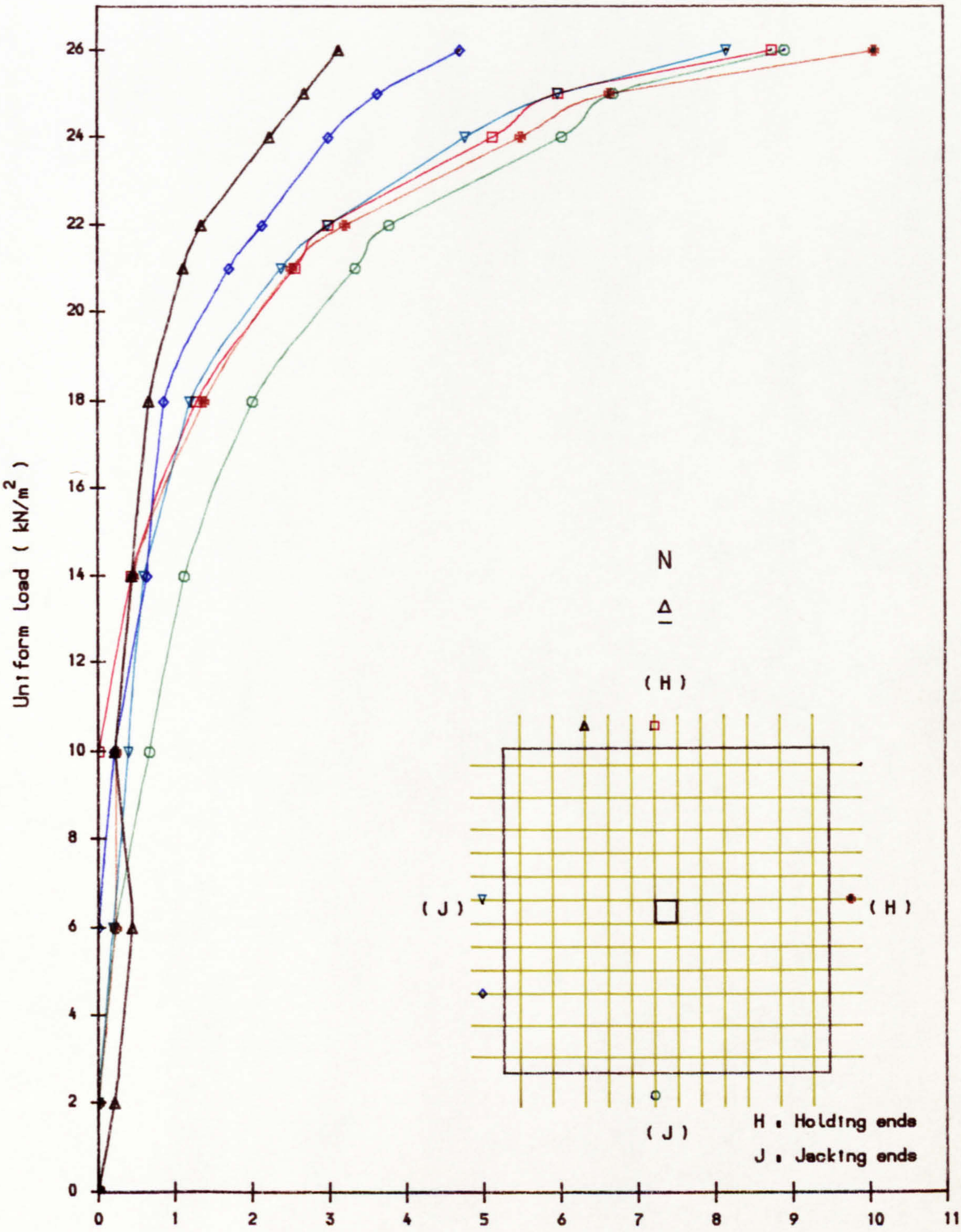

Fig. 8.67 Changes of tendon stress under uniform loading, Slab A2

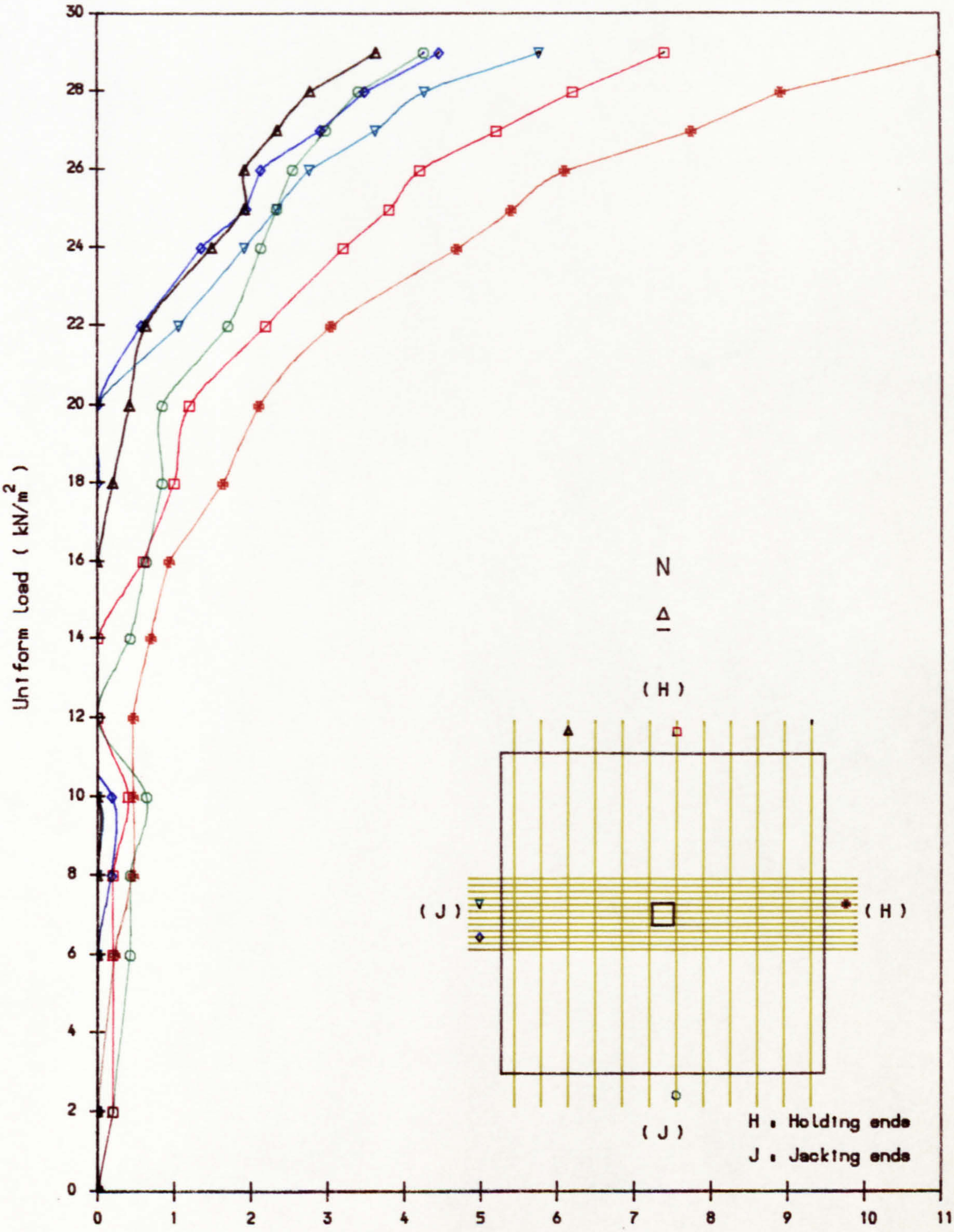

Fig. 8.68 Changes of tendon stress under uniform loading, Slab A3

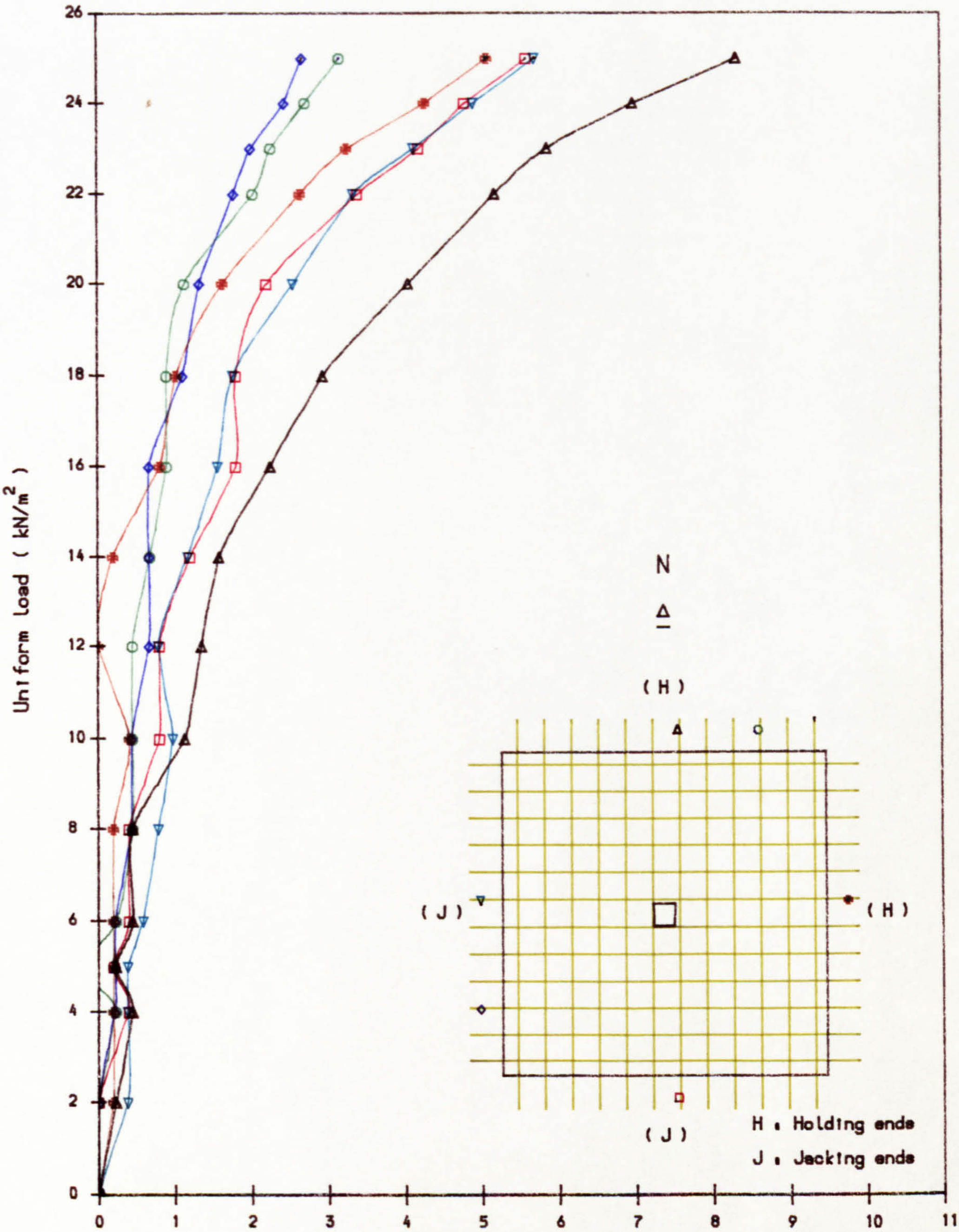

Fig. 8.69 Changes of tendon stress under uniform loading, Slab A4

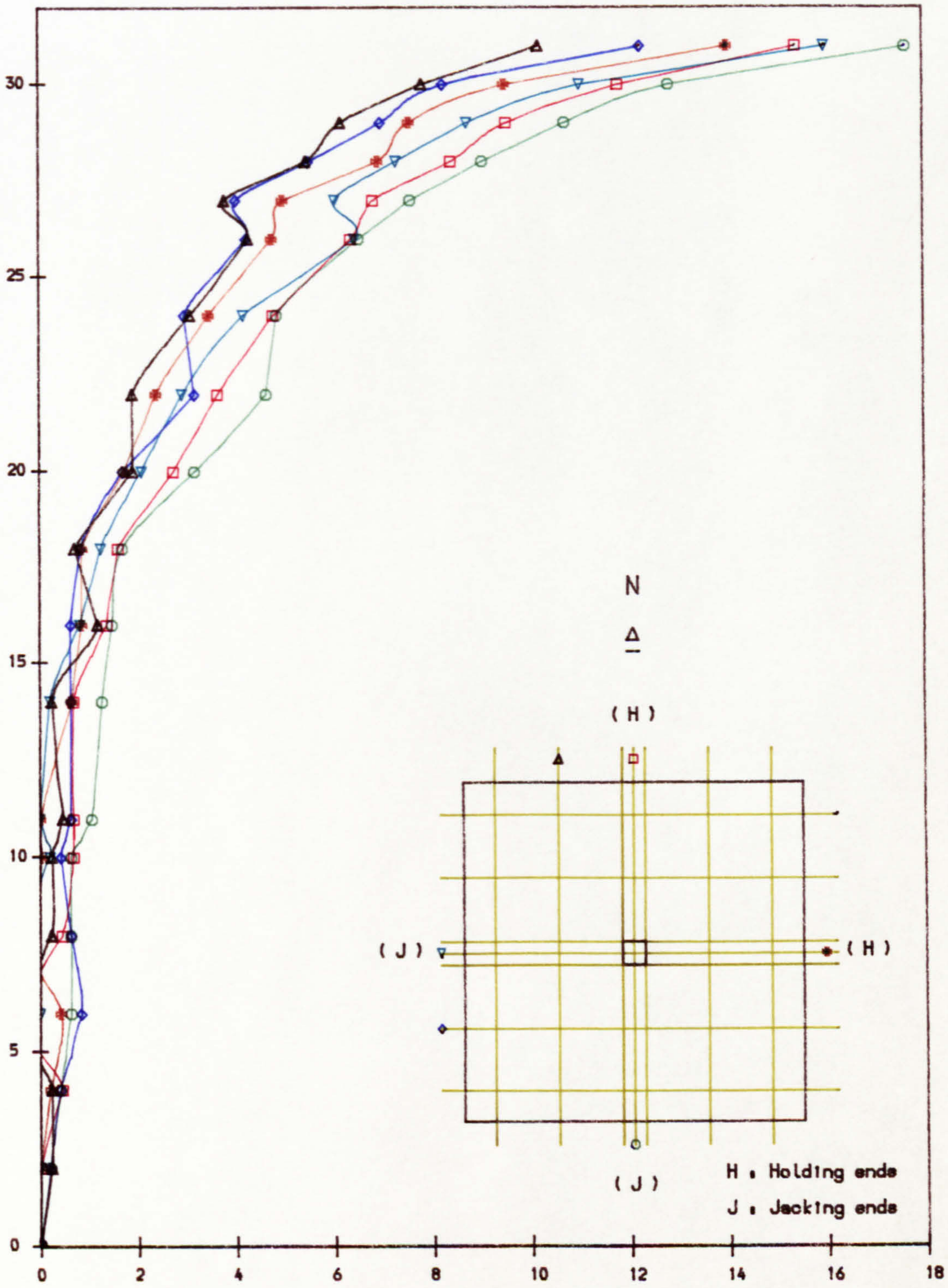

Fig. 8.70 Changes of tendon stress under uniform loading, Slab B1

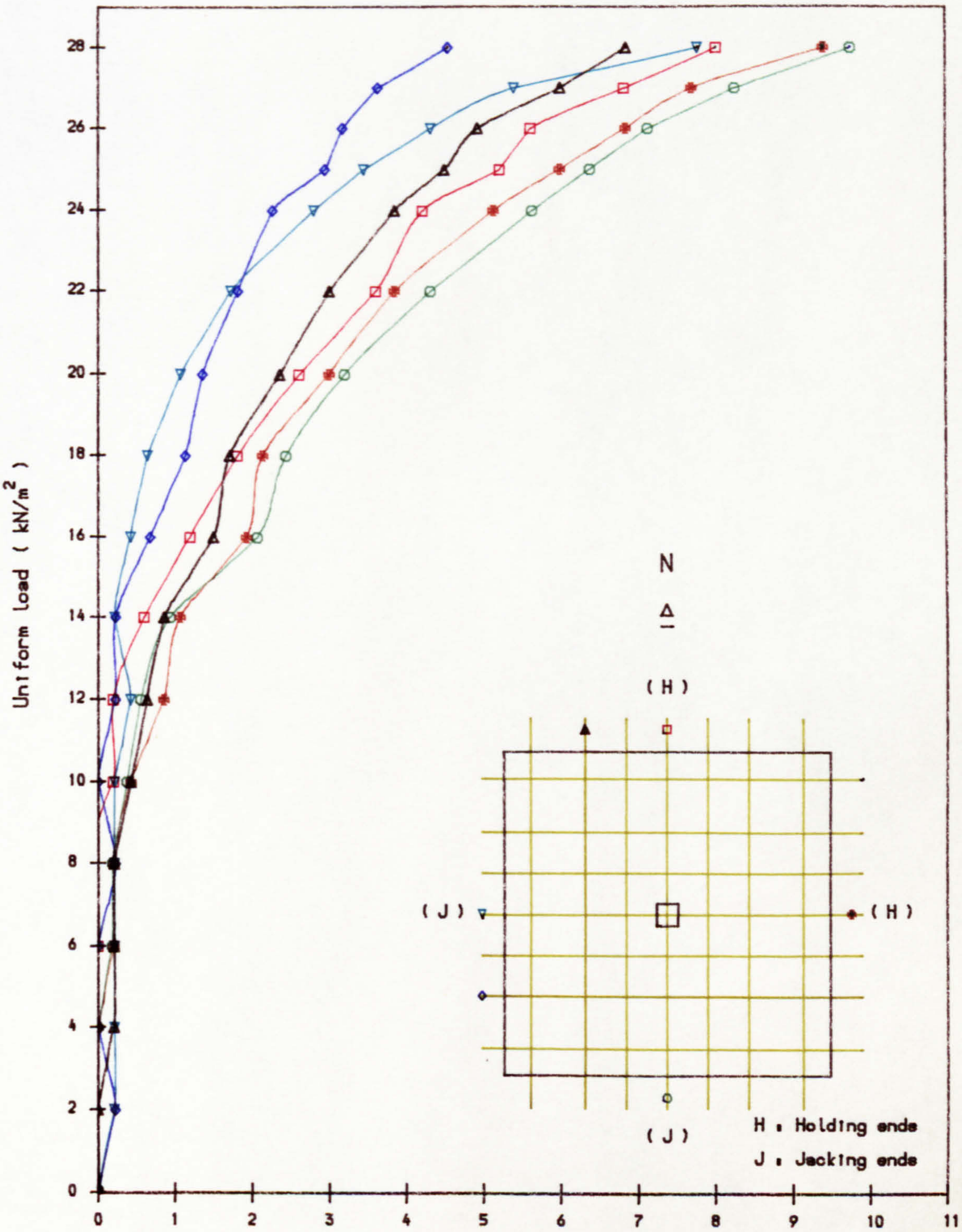

Fig. 8.71 Changes of tendon stress under uniform loading, Slab B2

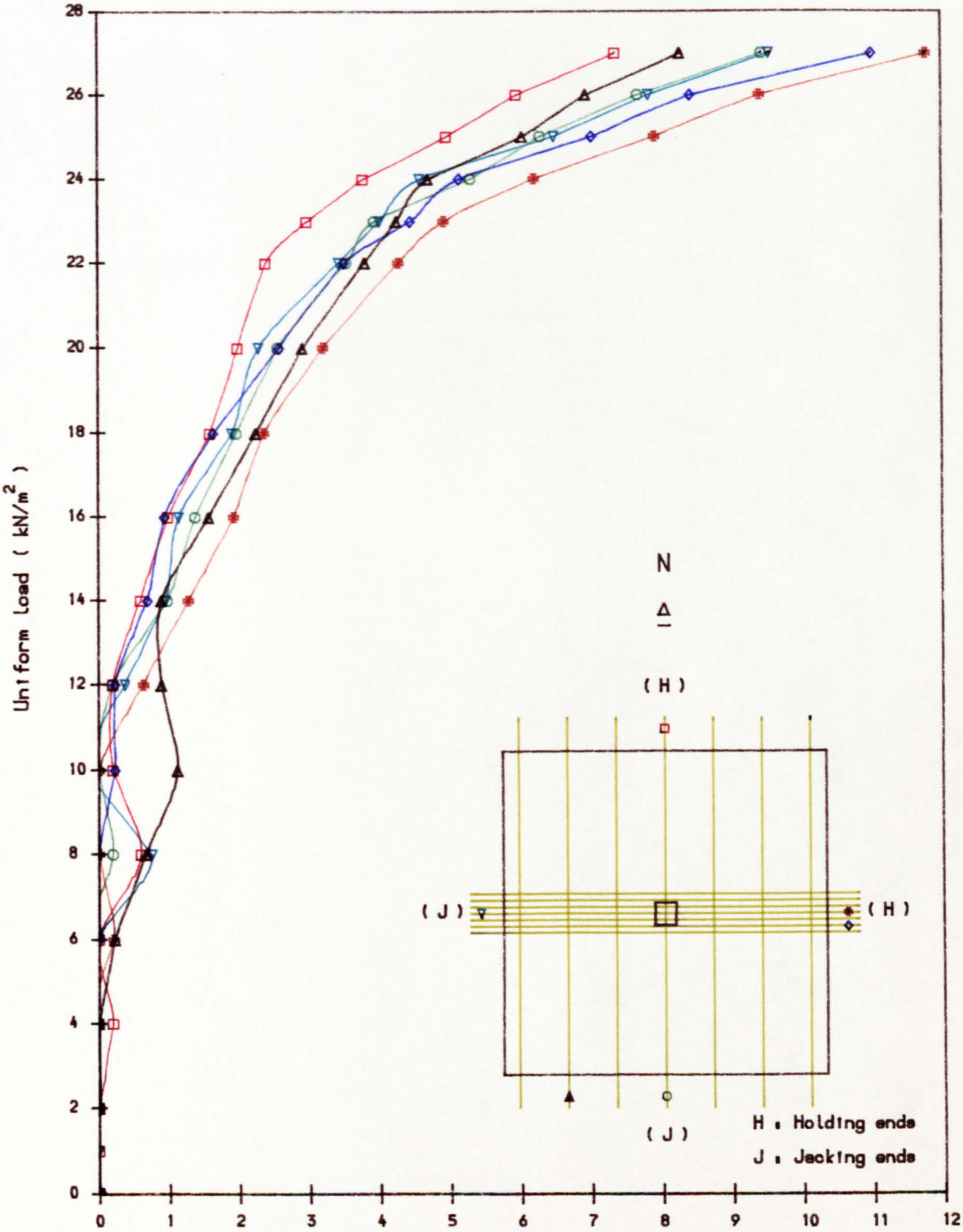

Fig. 8.72 Changes of tendon stress under uniform loading, Slab B3

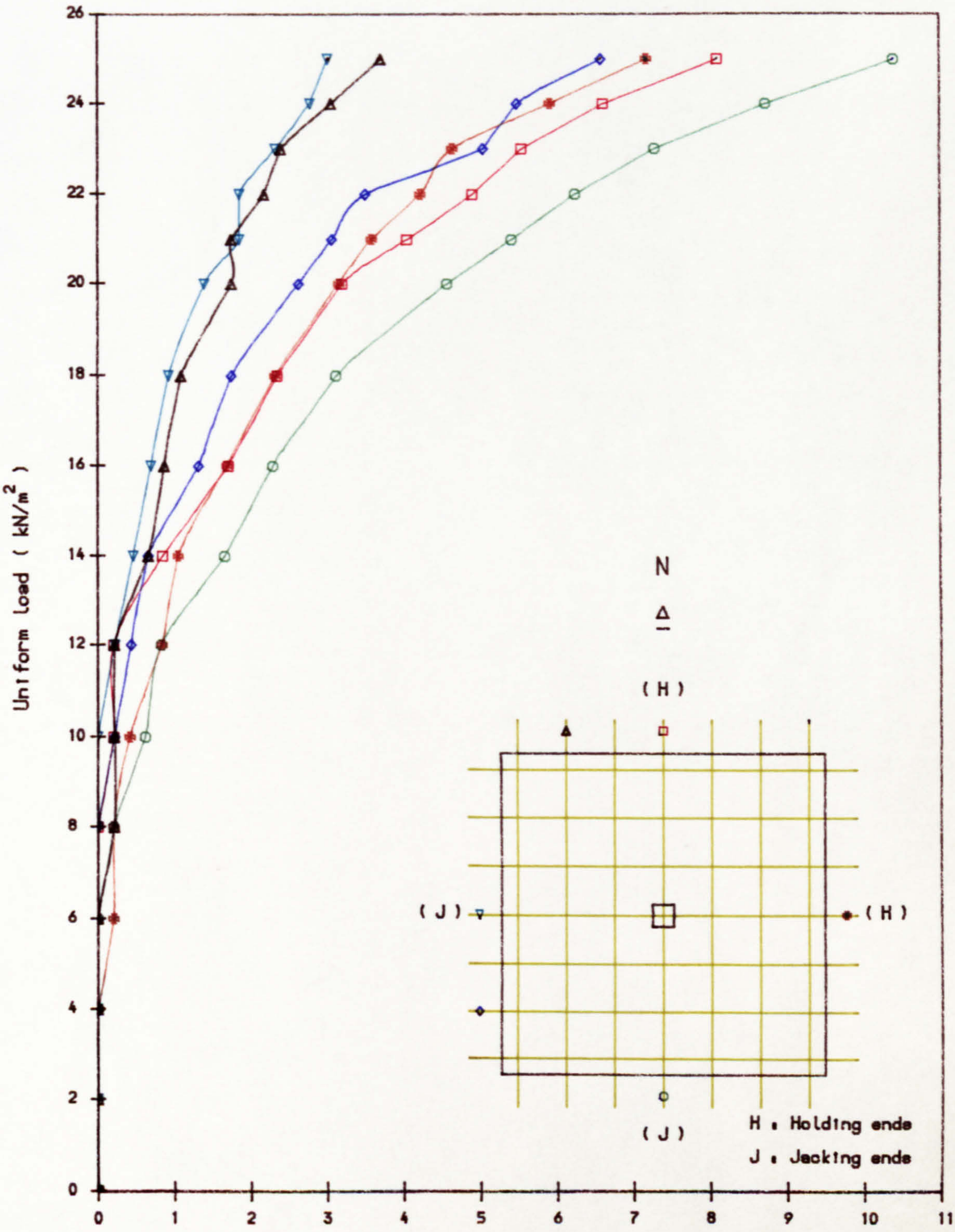

Fig. 8.73 Changes of tendon stress under uniform loading, Slab B4

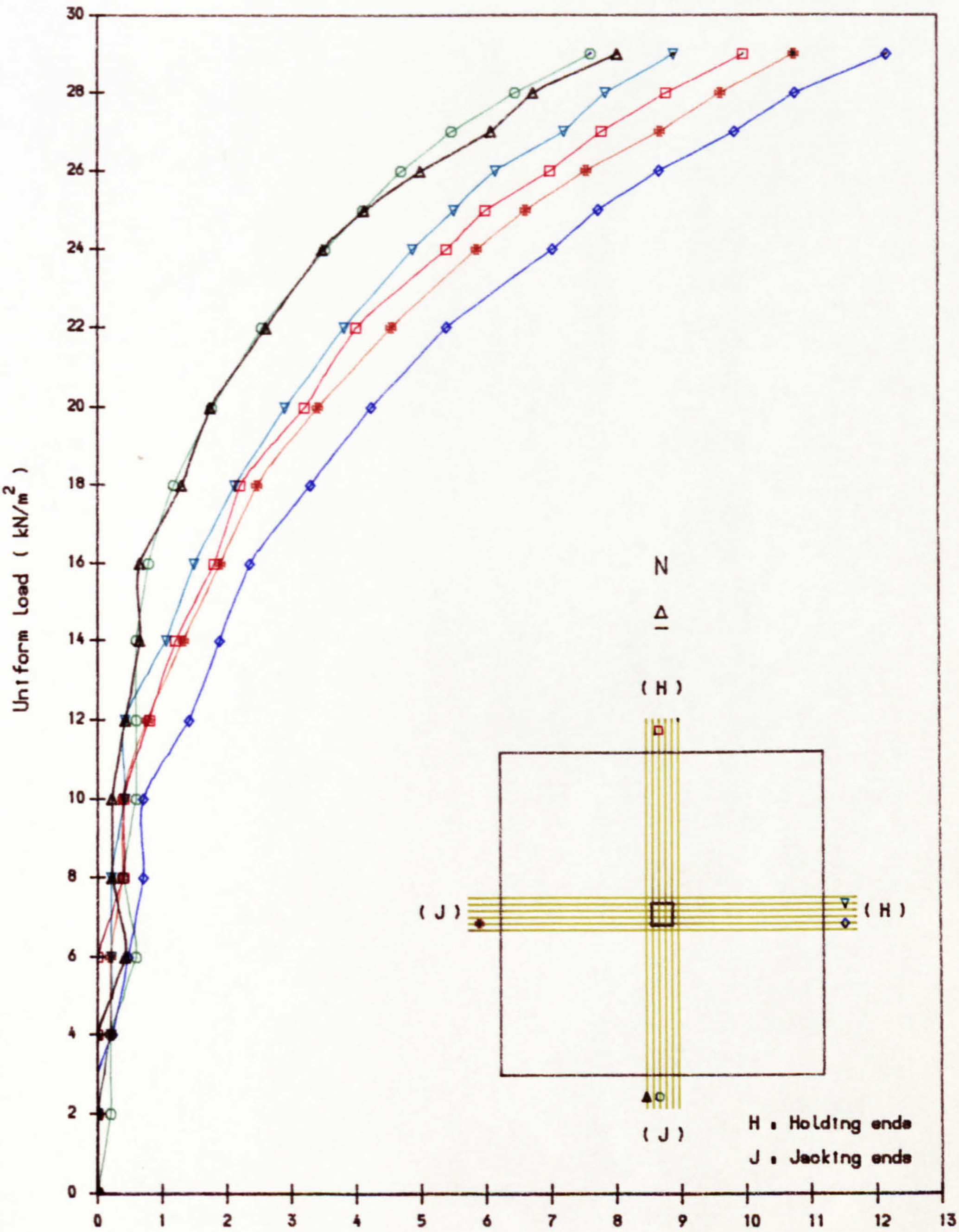

Fig. 8.74 Changes of tendon stress under uniform loading, Slab C1

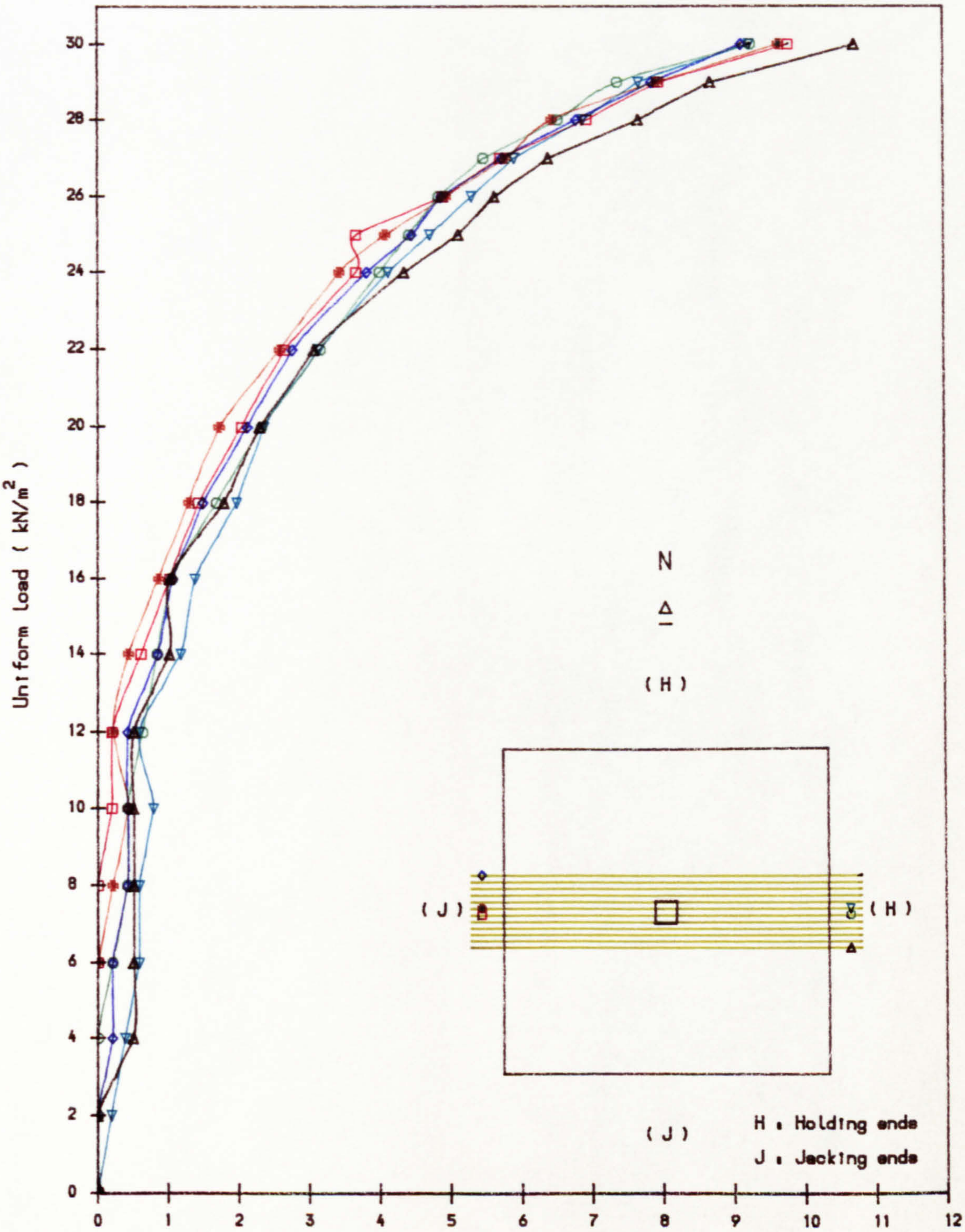

Fig. 8.75 Changes of tendon stress under uniform loading, Slab C2

PLATES

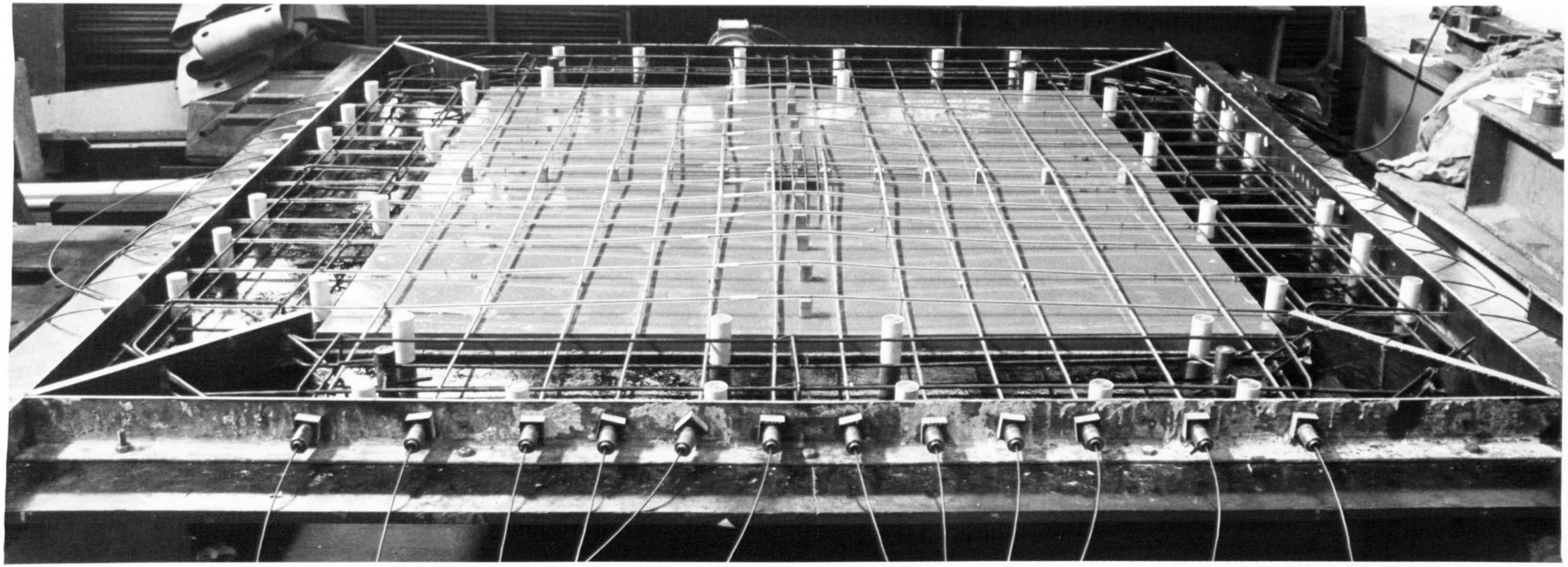

Plate 1 Prestressed reinforcement frame in Slab A 2

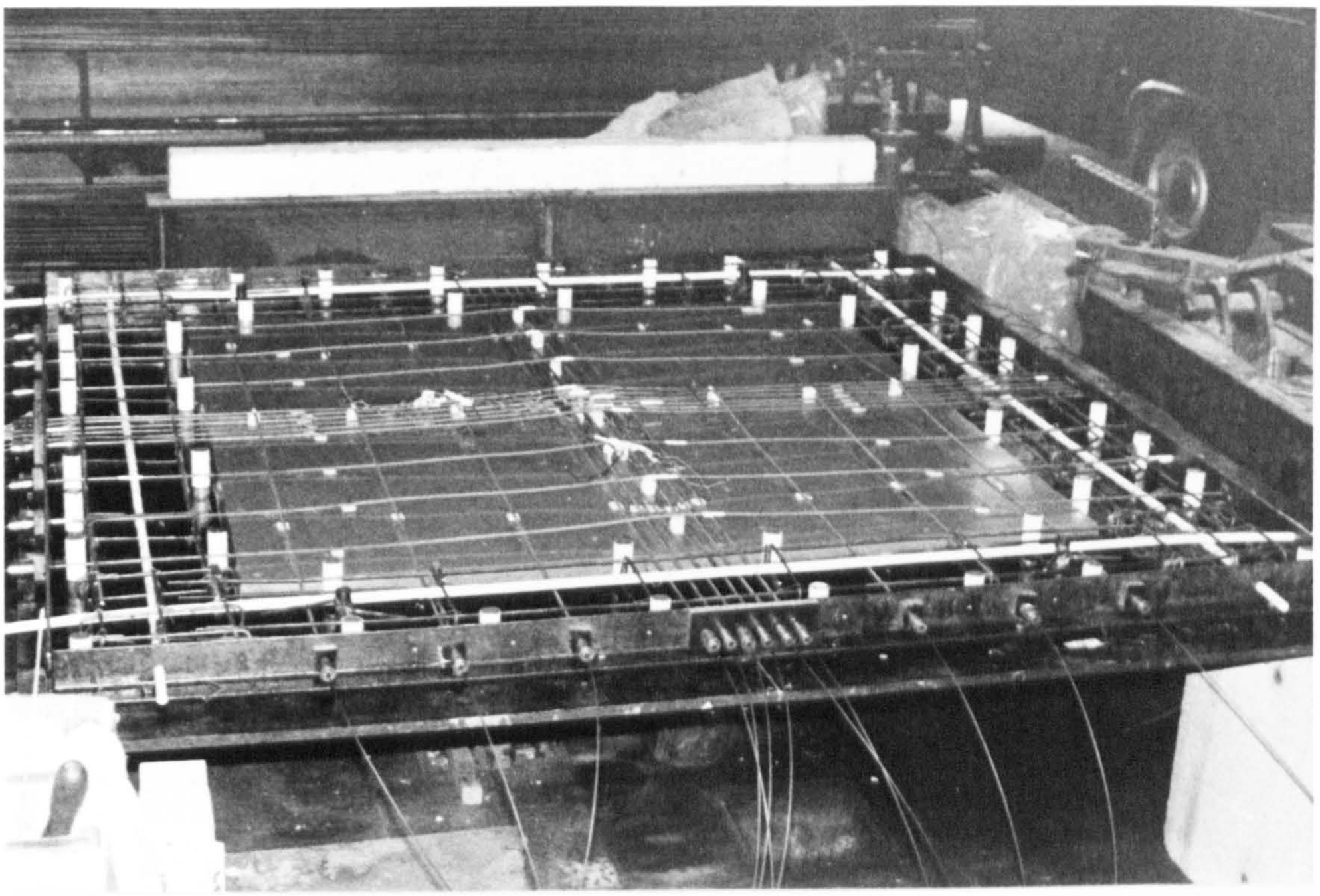

Plate 2 Prestressed reinforcement frame in Slab A1

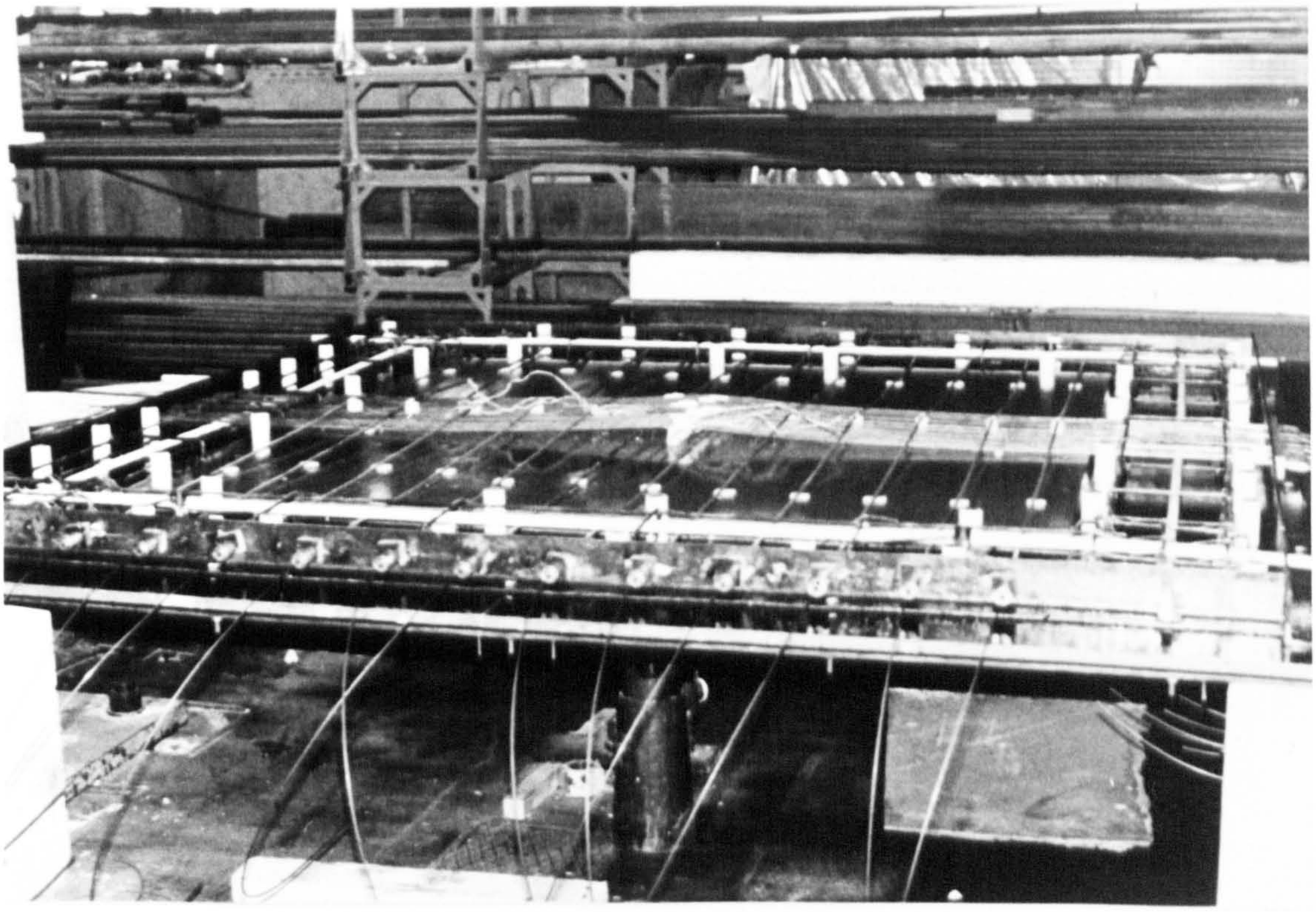

Plate 3 Prestressed reinforcement frame in Slab A3

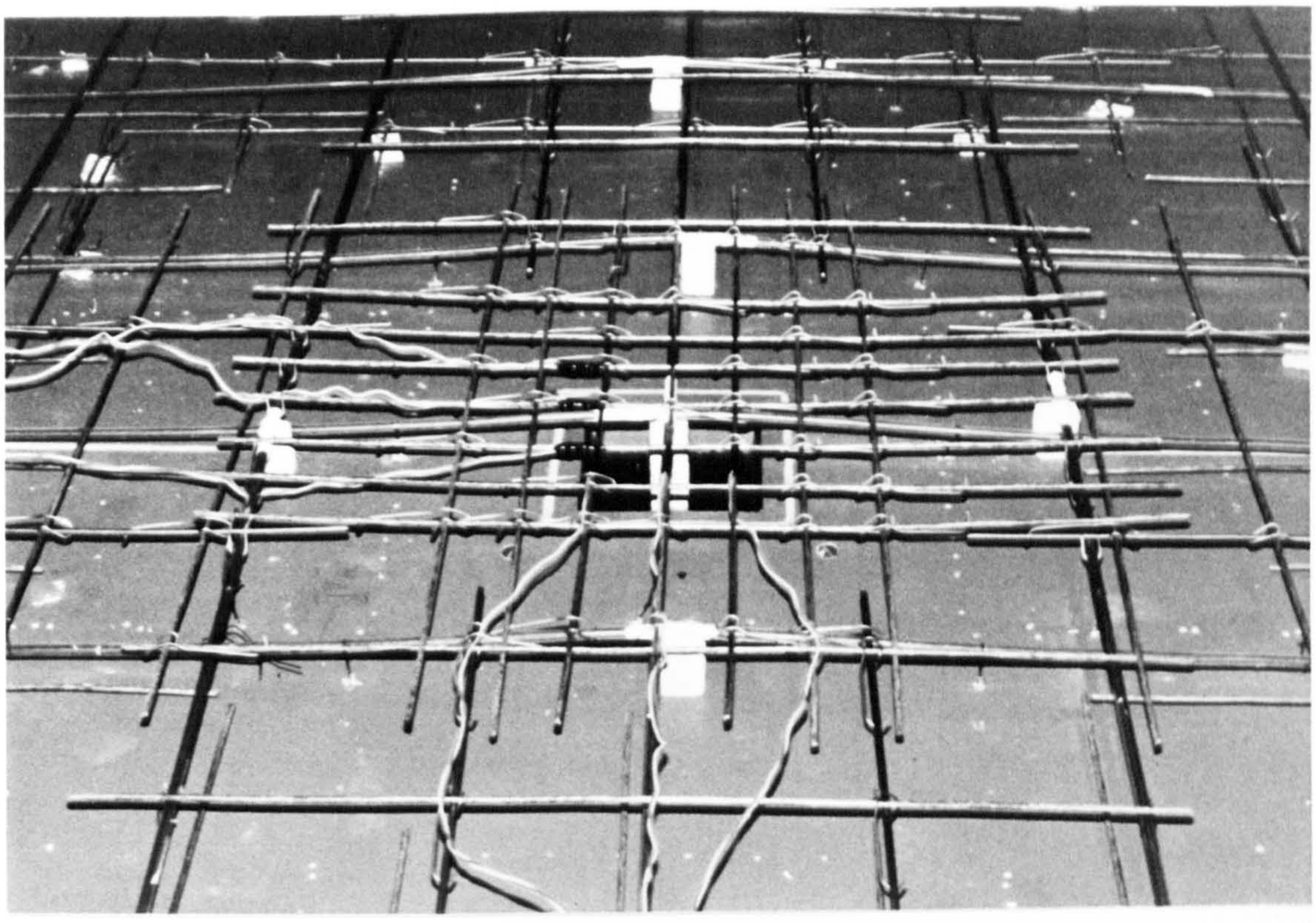

Plate 4 Column non-prestressed reinforcement (B 1 to C 1)

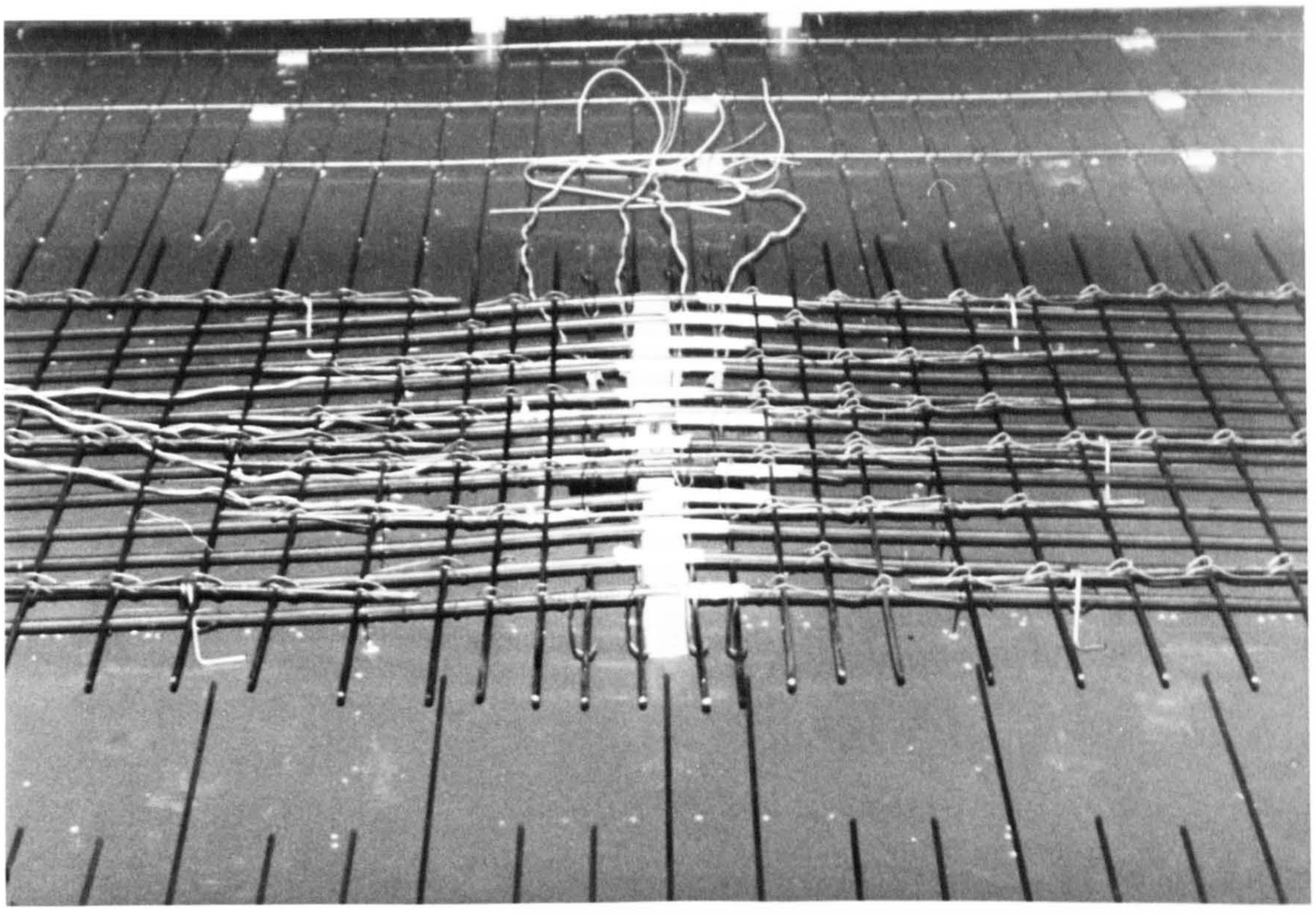

Plate 5 Column non-prestressed reinforcement (C 2)

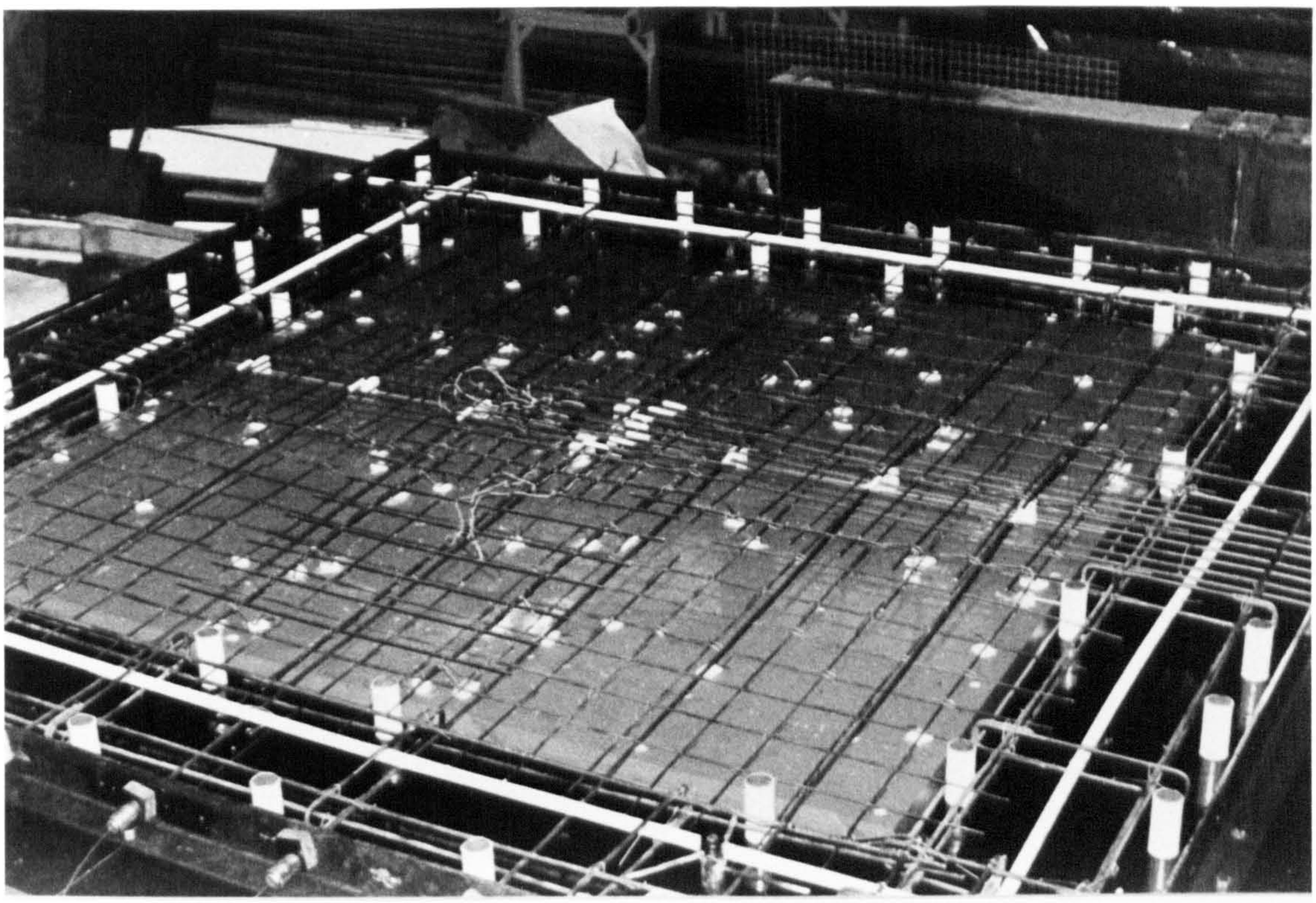

Plate 6 Bottom non-prestressed reinforcement (B1 to C1)

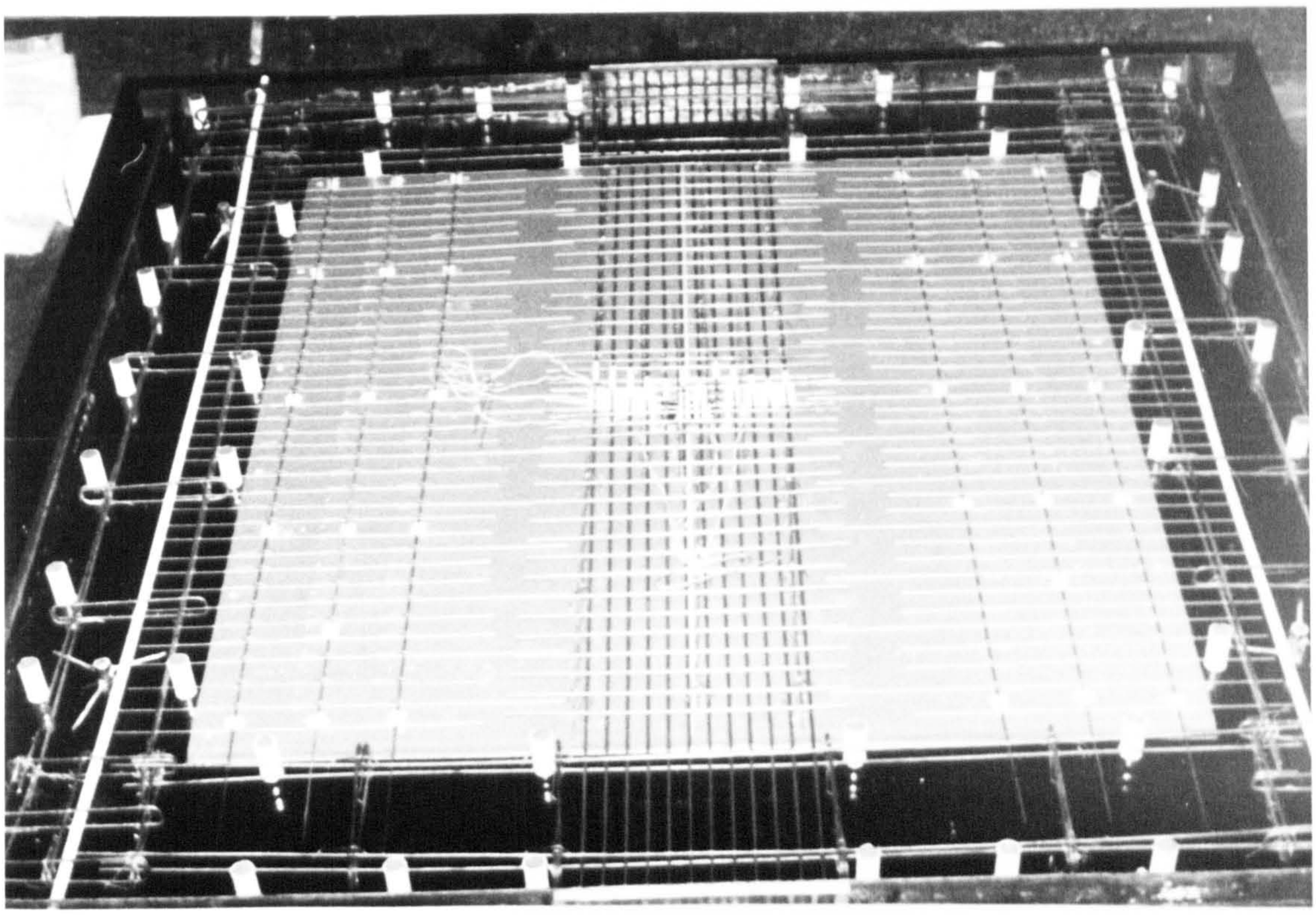

Plate 7 Bottom non-prestressed reinforcement (C 2)

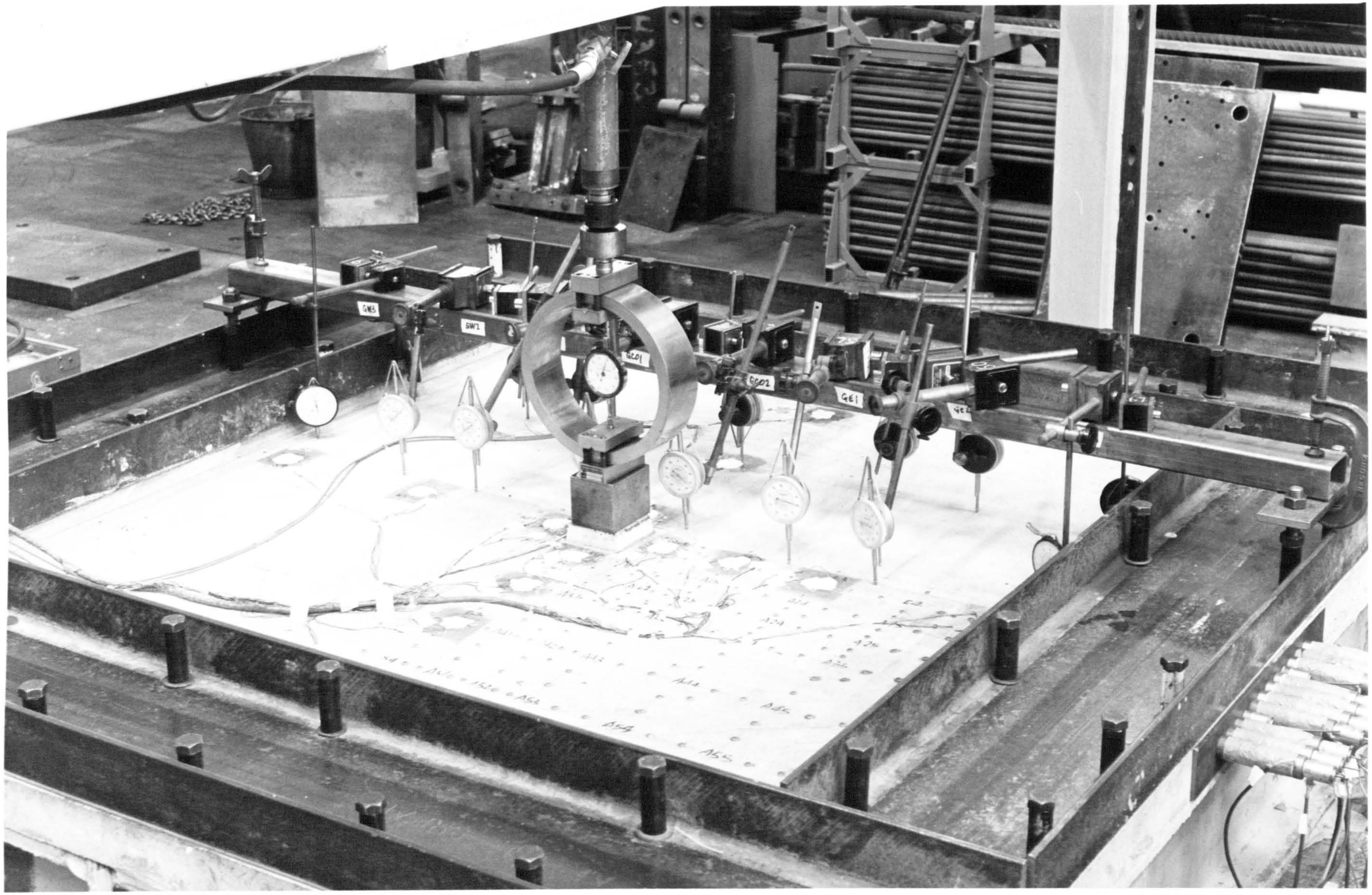

Plate 8 General test setup

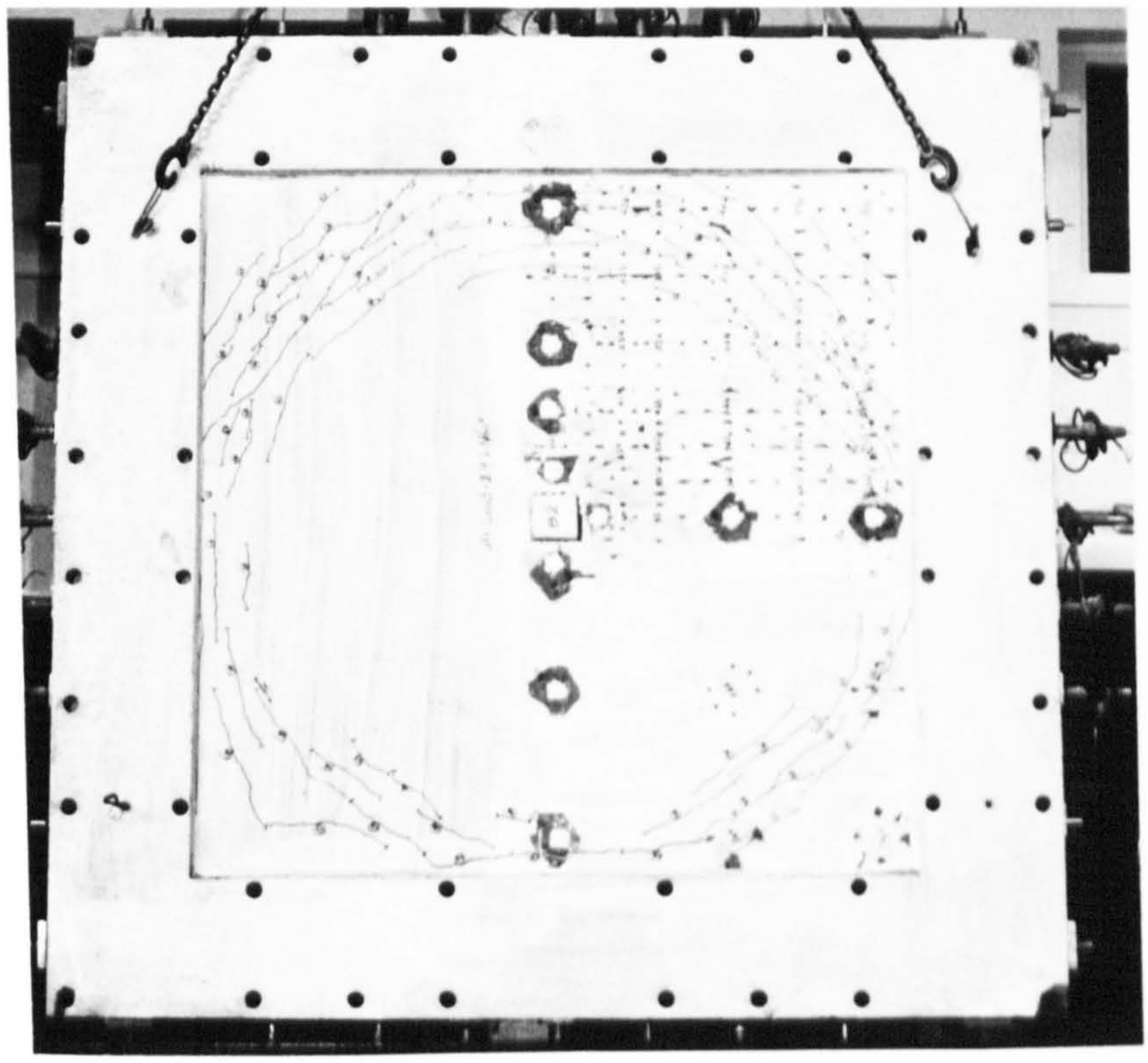

(a) Top surface

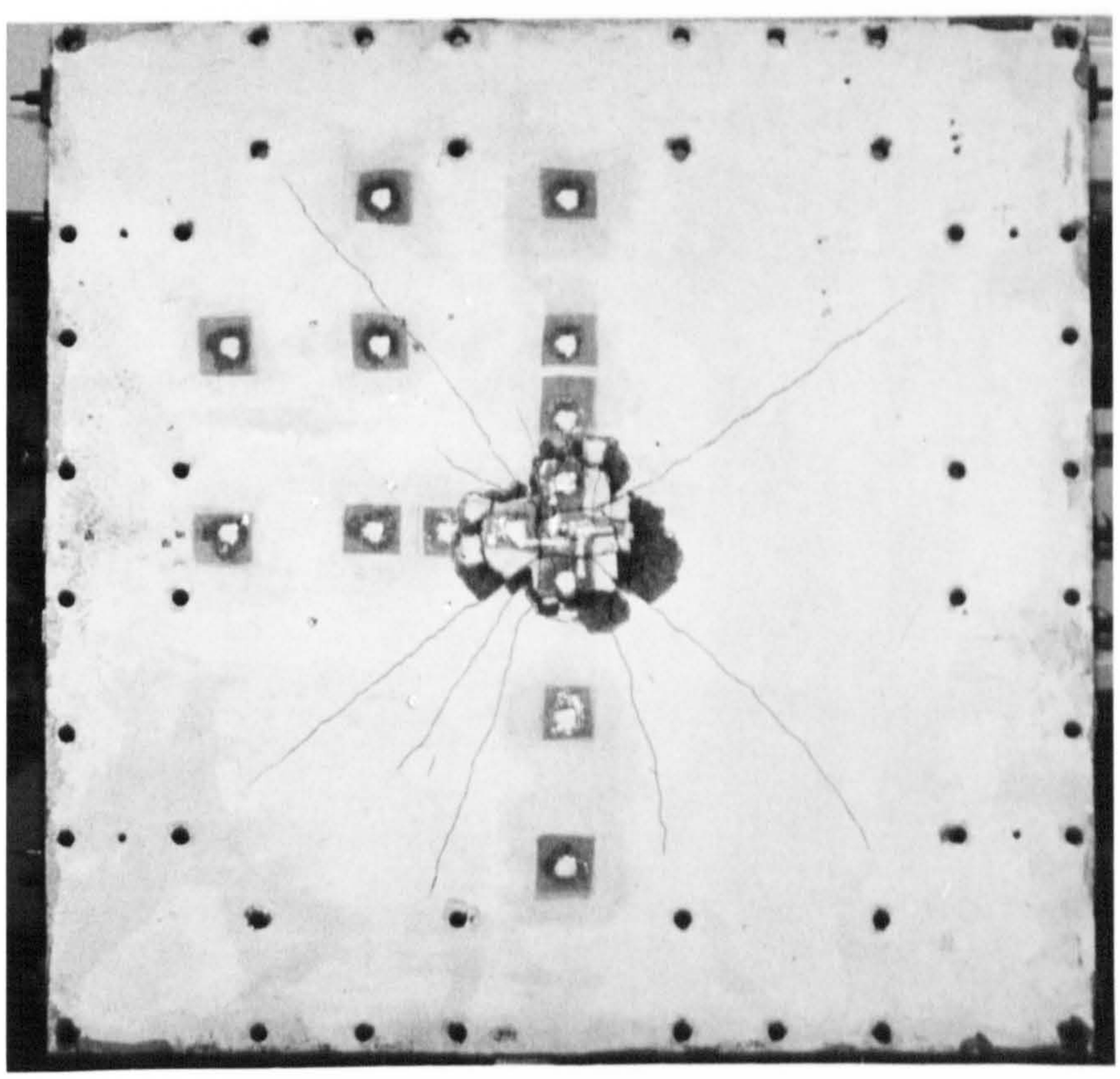

(b) Bottom surface

Plate 9 Typical crack patterns (B2)

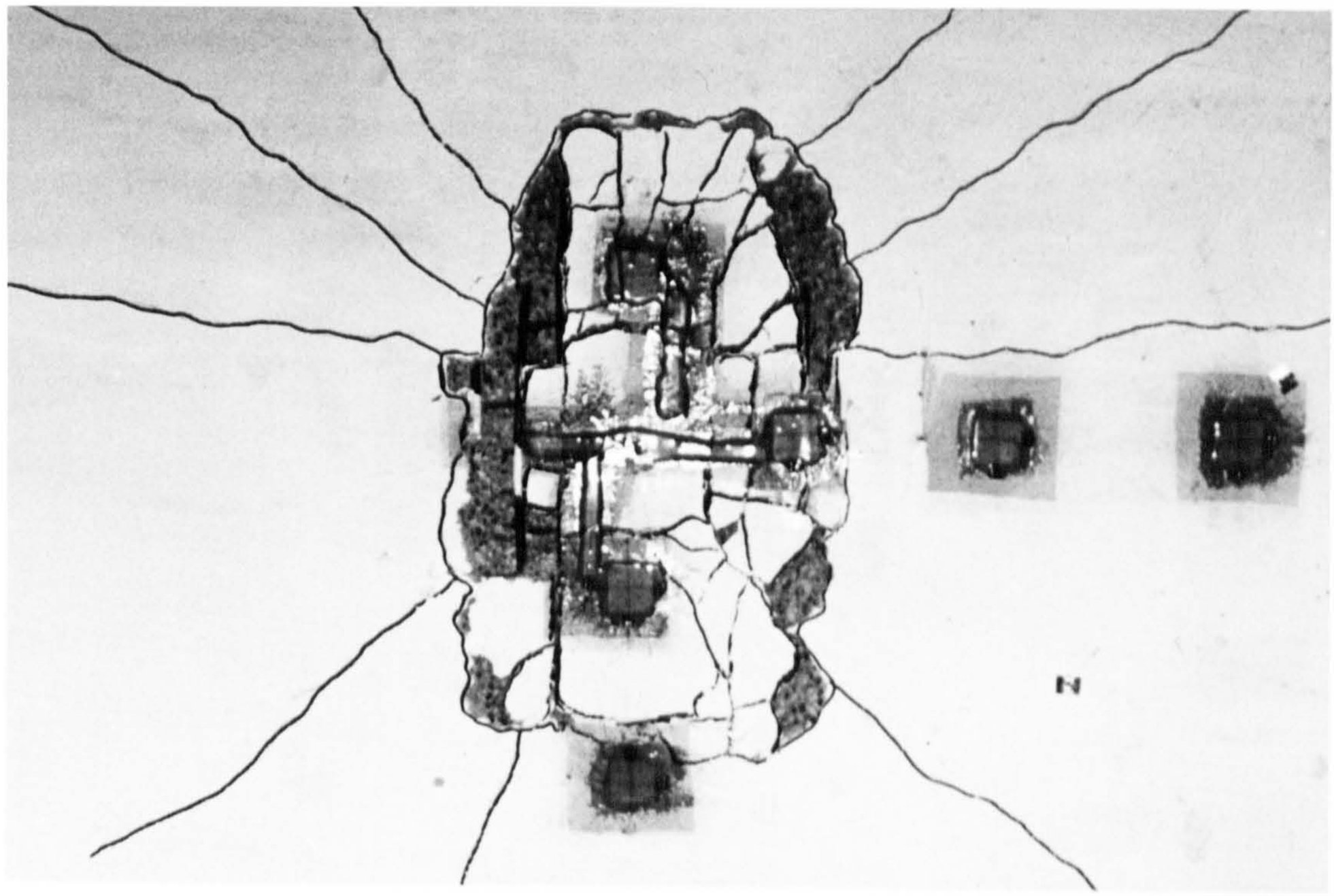

(a) Slab A3 (Unsymmetrical tendon arrangement)

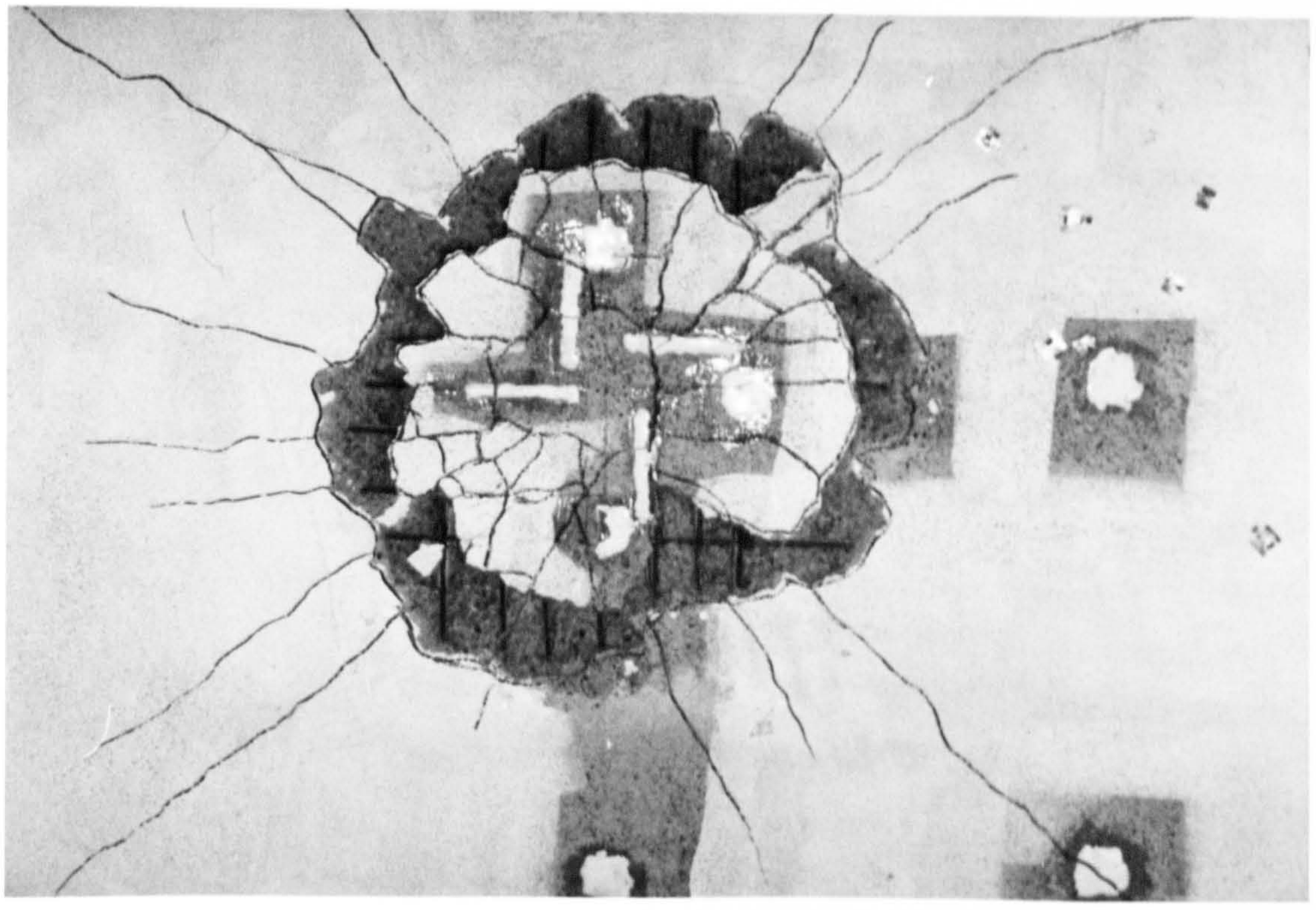

(b) Slab B4 (Symmetrical tendon arrangement)

Plate 10 Typical punching shear failure

APPENDICES

APPENDIX 1

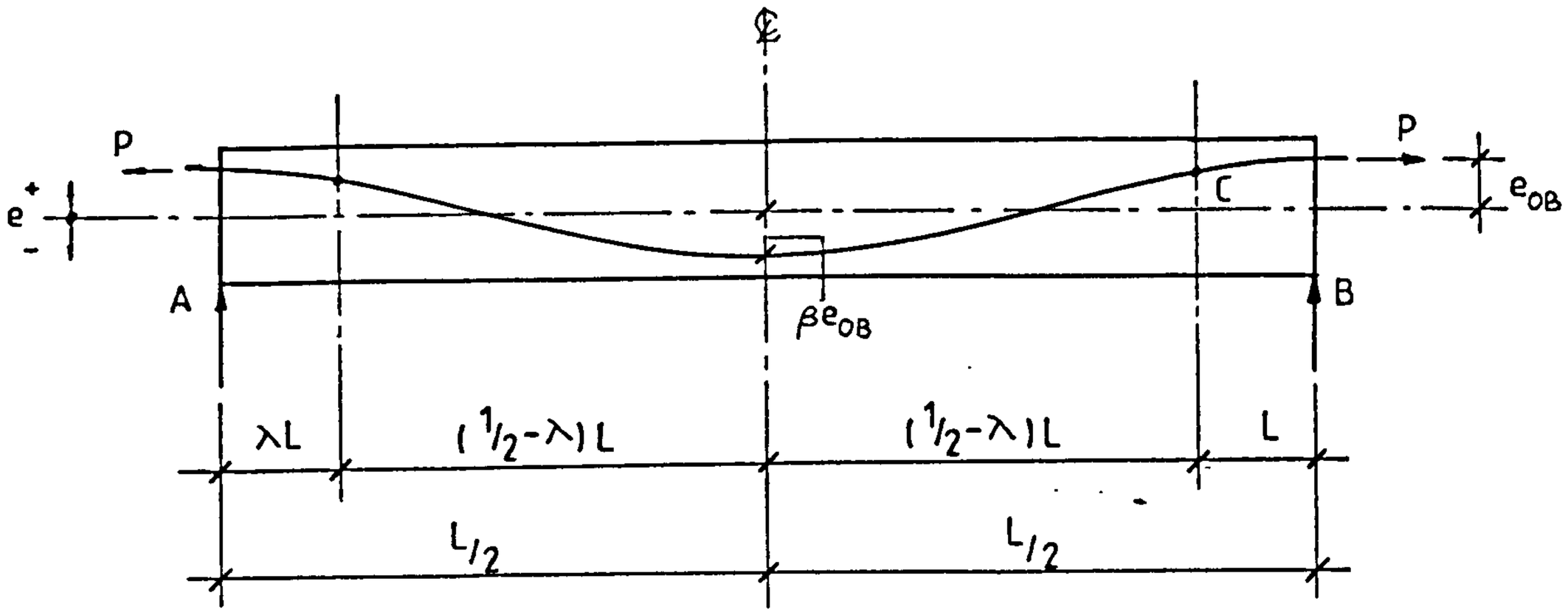

Fig.A1: Idealised Tendon Profile

(a) Tendon Profile:

The tendon profile in an internal span of a continuous structure consists of two segments of a second degree parabola. The position of common tangent is located at C, a distance λL from the centre-line of the supports. The maximum eccentricities of the tendon at the support and mid-span are e_{OB} and βe_{OB} respectively.

General equation of the parabola of each segment of the profile is

$$e_x = \ell x^2 + mx + n$$

Referring fig.A1.

(i) $0 \leq x \leq (\frac{1}{2} - \lambda)L$

Boundary conditions:

At $x = 0$ $\qquad e_x = \beta e_{OB}$

$$\frac{de_x}{dx} = 0$$

$x = (\frac{1}{2} - \lambda)L$ $\qquad$ slope $= \frac{de_{x1}}{dx}$

(ii) $(\frac{1}{2} - \lambda)L \leqslant x \leqslant L/2$

Boundary conditions:

At $x = (\frac{1}{2} - \lambda)L$ $\qquad$ slope $= \frac{de_{x2}}{dx}$

$x = L/2$ $\qquad e_x = e_{OB}$

$$\frac{de_x}{dx} = 0$$

(iii) At point C

$$\text{slope} = \frac{de_{x1}}{dx} = \frac{de_{x2}}{dx}$$

Solving: $\qquad 0 \leqslant x \leqslant (\frac{1}{2} - \lambda)L$

$$e_x = e_{OB}\left[\frac{2(1 - \beta)}{(\frac{1}{2} - \lambda)}\left(\frac{x}{L}\right)^2 + \beta\right] \qquad \ldots\ldots\ldots\ldots \text{(A1.1)}$$

$$(\tfrac{1}{2} - \lambda)L \leqslant x \leqslant L/2$$

$$e_x = e_{OB}\left[-\nu\left(\frac{x}{L}\right)^2 + \nu\left(\frac{x}{L}\right) - \frac{\nu}{4} + 1\right] \qquad \ldots\ldots\ldots\ldots \text{(A1.2)}$$

where $\nu = \dfrac{2(1 - \beta)}{\lambda}$

(b) Idealisation of prestressing forces by Equivalent Load Method

In a shallow member of span L, a parabolic tendon subjected to a constant tension P′ and having a maximum drape a, will create an equivalent uniform load given approximately by

$$W_{bal} = \frac{8Pa}{L^2} \qquad \ldots\ldots\ldots\ldots \text{(A1.3)}$$

(i) $0 \leq x \leq (\frac{1}{2} - \lambda)L$

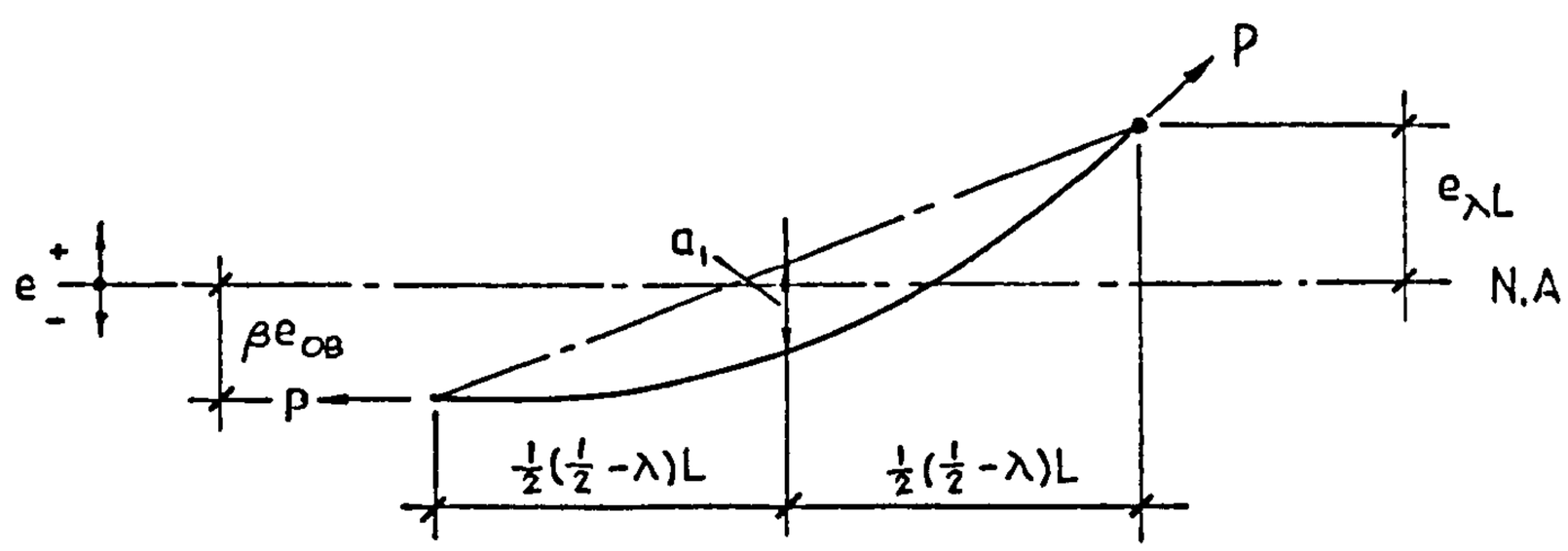

Fig.A2: Sagging Tendon Segment

From equation A1.1 and referring to fig.A2,

$$a_1 = \tfrac{1}{2}e_{OB}\,(1 - \beta)(\tfrac{1}{2} - \lambda)$$

From equation A1.3, the transverse upward load is given in the span between the points of inflection by

$$W_{1_{bal}} = 4\,\frac{Pe_{OB}}{L^2}\,\frac{(1 - \beta)}{(\frac{1}{2} - \lambda)} \qquad \ldots\ldots\ldots\ldots \text{(A1.4)}$$

(ii) $(\frac{1}{2} - \lambda)L \leqslant x \leqslant L/2$

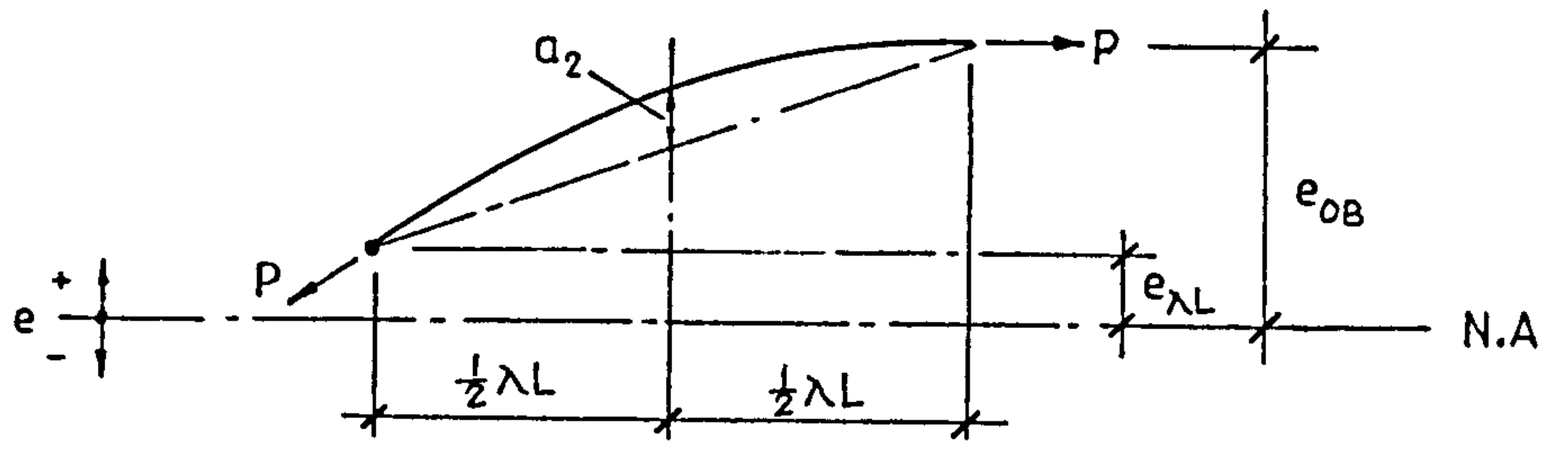

Fig.A.3: Hogging Tendon Segment

From equation A1.2 and referring to fig.A3

$$a_2 = e_{OB} \frac{\nu\lambda^2}{4}$$

The transverse downward load over the support between the points of inflection is given by

$$W_{2_{bal}} = -4 \frac{Pe_{OB}}{L^2} \frac{(1 - \beta)}{\lambda} \quad \ldots\ldots\ldots\ldots \text{(A1.5)}$$

(iii) Summary

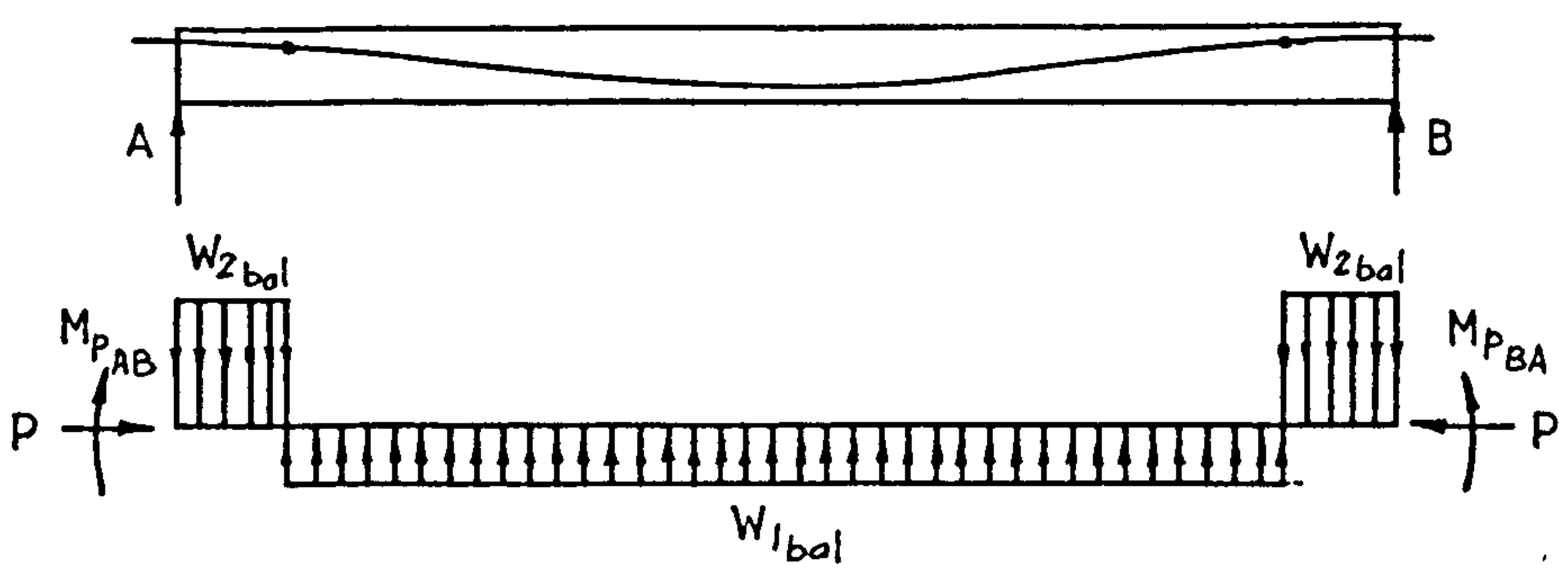

Transverse loads:

Upwards: $$W_{1_{bal}} = 4 \frac{Pe_{OB}}{L^2} \frac{(1 - \beta)}{(\frac{1}{2} - \lambda)}$$

Downwards: $$W_{2_{bal}} = -4 \frac{Pe_{OB}}{L^2} \frac{(1 - \beta)}{\lambda}$$

Fixed-end prestressing moments:

$$M_{P_{AB}} = M_{P_{BA}} = -\frac{2}{3} Pe_{OB} (1 - \beta)(1 - \lambda)$$

..... (A1.6)

APPENDIX 2

Computation of Slab Instantaneous Deflection Using Equivalent Frame Method

A.2.1 Computation Procedures

Following the moment analysis by either the equivalent frame approach or the direct design method, the mid-span deflection of the slab is computed as the sum of the deflection at mid-span of the column strip in one direction and the deflection at mid-span of the middle strip between columns in the other direction, as shown in Fig.8.30. For rectangular panels, or other panels that have different characteristics in the two directions, an average is taken of the deflection calculated by the two alternative methods viz, column strip in X-direction with middle strip in Y-direction and vice versa.

Under uniform vertical loads, the mid-span deflection of a panel can be considered (55) as the sum of three parts, that of a panel assumed to be fixed at both ends of its span, plus that due to the known rotation at each of the two support lines. The mid-span 'reference' deflection of a uniformly loaded member of an equivalent frame (full width) having fixed ends is

$$a_{f,ref} = \frac{WL^4}{384E_c I_{frame}} \qquad \text{--- Eqn. A2.1}$$

where W is the load per unit length in the direction of the frame and I_{frame} is the moment of inertia of the full width of the frame.

The calculation of the mid-span deflection of the column or middle strip under fixed end conditions is based on the M/EI ratio of the strip to that of the full panel width

$$a_{f,strip} = a_{f,ref} \times \frac{M_{strip}}{M_{frame}} \frac{E_c I_{frame}}{E_c I_{strip}} \quad \text{--- Eqn. A2.2}$$

The ratio, M_{strip} / M_{frame} can be considered as a lateral distribution factor (LDF) for the strip (56).

If the ends of the column at the floor above and below are assumed fixed (as is usual for equivalent frame analysis), then the rotation of the column is equal to the net applied moment divided by the stiffness of the equivalent column. (*)

$$\theta = \frac{M_{net}}{K_{ec}} \quad \text{--- Eqn. A2.3}$$

(*) The equivalent column is assumed in the ACI 318-83 Building Code to consist of the actual column above and below the slab-beam plus an attached torsional member transverse to the direction of the span and extending to the bounding panel center lines on each side of the column. Specific guidelines for determining the torsional stiffness of this member are given in the ACI Code.

The mid-span deflection of the slab-beam experiencing an end rotation of θ radians, the far end of the beam being fixed is

$$a_\theta = \frac{\theta L}{8} \qquad \text{--- Eqn. A2.4}$$

The total mid-span deflection for the column and middle strip is then the sum of the parts

$$a_{strip} = a_{f,strip} + a_{\theta L} + a_{\theta R} \qquad \text{--- Eqn. A2.5}$$

where θ_L , θ_R , refer to the left and right column rotations respectively.

For a square internal panel, referring to Fig.8.30, the mid-span deflection is obtained from

$$a_m = a_{cy} + a_{mx} = a_{cx} + a_{my} \qquad \text{--- Eqn. A2.6}$$

For a rectangular panel, the mid-span deflection is given by the following equation

$$a_m = \frac{[(a_{cx} + a_{my}) + (a_{cy} + a_{mx})]}{2.0} \qquad \text{--- Eqn. A2.7}$$

A.2.2 Effect of Cracking

The effect of cracking is to reduce the second moment of area and hence the flexural stiffness of the slab and to increase the deflection at any load level, even though the uncracked concrete between the cracks continues to have a stiffening influence. Prior to cracking, deflection calculations are generally based on the

uncracked gross concrete section (CP110 and ACI 318-83 Codes) neglecting the contribution due to reinforcement and no significant error is introduced. Under cracking conditions, however, because of the varying degree and extent of the cracking, the moment of inertia is not constant over the whole slab and calculations based on the fully cracked transformed section can seriously overestimate the deflection.

To account for the effect of cracking in the computation of deflection, the ACI Code recommends the use of a weighted moment of inertia or the I-Effective method originally proposed by Branson (57),

$$I_e = \left(\frac{M_{cr}}{M_{max}}\right)^3 I_g + \left[1 - \left(\frac{M_{cr}}{M_{max}}\right)^3\right] I_{cr} \quad \text{---} \quad \text{Eqn. A2.8}$$

where I_g = moment of inertia of gross uncracked concrete section

I_{cr} = moment of inertia of the cracked transformed concrete section

M_{cr} = cracking moment

M_{max} = maximum value of bending moment in the span

Equation A2.8 was devised on the basis of simply supported rectangular and T-section beams; its use for two-way slabs was, however, permitted under the 1971 as well as the present 1983 ACI Code. There are, however, few experimental data to demonstrate its applicability to partially prestressed flat slabs.

To comply with the ACI (1971) Code for the effect of cracking in a multi-panel slab system, Kripanarayanan and Branson (56)

suggested that equation A2.1 should be modified as follows:

$$a_{f,ref} = \frac{WL^4}{384E_c I_{a,frame}} \quad \text{--- Eqn. A2.9}$$

where $$I_{a,frame} = \alpha I_e^+ + (1 - \alpha) I_c^- \quad \text{--- Eqn. A2.10}$$

and α = an empirical constant whose value is less than 1

I_e^+ = effective moment of inertia for slab width at mid-span (from Eqn A2.8)

I_e^- = effective moment of inertia for slab width at supports (from Eqn A2.8)

For continuous members, the ACI (1983) Code (section 9.5.2.4) suggests a 'simple average' of I_e values for the positive and negative moment region, and equation A2.10 can be written as

$$I_{a,frame} = \tfrac{1}{2}[I_e^+ + \tfrac{1}{2}(I_e^- + I_e^+)] \quad \text{--- Eqn. A2.10(i)}$$

with $\alpha = 0.5$

A somewhat improved deflection may be made by using a 'weighted average' section properties. For members with both ends continuous, ACI Committee 435 (58) recommends that the average effective moment of inertia should be

$$I_e = I_e^+ \left[\left(1 + \left(\frac{M_{e1}+M_{e2}}{2M_{tot}}\right)^{\phi}\right)\right] + \frac{I_{c1}^- + I_{e2}^-}{2}\left(\frac{M_{e1}+M_{e2}}{2M_{tot}}\right)^{\phi}$$

--- Eqn. A2.10(ii)

where I_{e1}^-, I_{e2}^- = effective moments of inertia of the ends of the span

M_{tot} = total statical moment

ϕ = positive number

From equation A2.10 and A2.10(ii), the empirical constant can also be expressed as

$$\alpha = 1 + \left(\frac{M_{e1} + M_{e2}}{2M_{tot}}\right)^{\phi}$$

Equation A2.10(ii) generally gives increasing accuracy in computing the deflection by varying the value of ϕ. The Committee 435 recommends a minimum value of $\phi=2$. In the range of $0.1 < \frac{M_{e1} + M_{e2}}{2M_{tot}} < 0.6$, a value of $\phi=4$ is suggested. With $\phi=4$ and $\frac{M_{e1} + M_{e2}}{2M_{tot}} = 0.6$, the calculated value of α is 0.7. In computing the deflections of the present test slabs, other values of α than the ones mentioned above will be considered.

A.2.3 Second Moment of Area

The effect of cracking on the deflection of a column-supported slab is likely to be less than the deflection of a beam because the maximum moments occur over only a fraction of the total width of the critical section. Tests on flat slabs (prestressed and non-prestressed) have shown that most cracking occurs in the negative bending regions close to the column. At service load, the mid-span positive moment regions generally have limited cracking or remain uncracked. For this reason, it has been suggested in the ACI 318-83 Commentary that, the deflection of flat slabs under dead load I_g should be used in equation A2.10 and with dead plus live load I_g should be used for the middle strip and I_e for the column strip.